

Physicochemical
Problems
of Mineral Processing
40 (2006)

Instructions for preparation of manuscripts

It is recommended that the following guidelines be followed by the authors of the manuscripts:

- Original papers dealing with the principles of mineral processing and papers on technological aspects of mineral processing will be published in the journal which appears once a year
- The manuscript should be sent to the Editor for reviewing before February 15 each year
- The manuscript should be written in English. For publishing in other languages an approval of the editor is necessary
- Contributors whose first language is not the language of the manuscript are urged to have their manuscript competently edited prior to submission.
- The manuscript should not exceed 10 pages
- Two copies of the final manuscript along with an electronic version should be submitted for publication before April 15
- There is a 80 USD fee for printing the paper. No fee is required for the authors participating in the Annual Symposium on Physicochemical Problems on Mineral Processing
- Manuscripts and all correspondence regarding the symposium and journal should be sent to the editor.

Address of the Editorial Office

Wrocław University of Technology
Wybrzeże Wyspiańskiego 27, 50-370 Wrocław, Poland
Institute of Mining Engineering
Laboratory of Mineral Processing

Location of the Editorial Office:

pl. Teatralny 2, Wrocław, Poland
phone: (071) 320 68 79, (071) 320 68 78
fax: (071) 344 81 23

zygmunt.sadowski@pwr.wroc.pl
andrzej.luszczkiewicz@pwr.wroc.pl
jan.drzymala@pwr.wroc.pl

<http://www.ig.pwr.wroc.pl/minproc>

Physicochemical
Problems
of Mineral Processing
40 (2006)

www.ig.pwr.wroc.pl/minproc

WROCLAW 2006

Editors of the journal

Zygmunt Sadowski – editor-in-chief, Jan Drzymała, Andrzej Łuszczkiewicz

Editorial Board

Wiesław Blaschke, Marian Brożek, Stanisław Chibowski,
Witold Charewicz, Tomasz Chmielewski, Beata Cwalina, Janusz Girczys,
Andrzej Heim, Jan Hupka, Andrzej Krysztafkiewicz, Janusz Laskowski,
Kazimierz Małyś, Paweł Nowak,
Andrzej Pomianowski (honorary chairman), Stanisława Sanak-Rydlewska,
Jerzy Sablik, Kazimierz Sztaba (chairman)

Reviewers

W. Apostoluk, W. Charewicz, J. Drzymała, W. Janusz, T. Jesionowski, A. Heim,
J. Hupka, A. Krysztafkiewicz, A. Lutyński, A. Łuszczkiewicz, I. Maliszewska,
P. Nowak, Z. Sadowski, W. Walkowiak

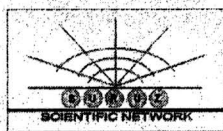
Technical assistance

Stefan Zawadzki

The papers published in *Physicochemical Problems of Mineral Processing* are abstracted
in *Chemical Abstracts*, *Metals Abstracts*, *Реферативный Журнал* and other sources

This publication was supported in different forms by:

Komitet Górnictwa PAN
(Seksja Wykorzystania Surowców Mineralnych)
Akademia Górnictwo-Hutnicza w Krakowie
Politechnika Śląska w Gliwicach
Politechnika Wroclawska
Scientific Network SURUZ



ISSN 0137-1282

OFICyna WYDAWNICZA POLITECHNIKI WROCLAWSKIEJ, WYBRZEŻE WYSPIAŃSKIEGO 27,
50-370 WROCLAW, POLAND

CONTENTS

55 Years of Scientific Work of Professor Kazimierz SZTABA	I
J. Grodzka, A. Pomianowski, Wettability versus hydrophilicity	5
J. Drzymała, Atlas of upgrading curves used in separation and mineral science and technology	19
M. Brożek, A. Młynarczykowska, Application of the stochastic model for analysis of flotation kinetics with coal as an example	31
T. Dang-Vu, J. Hupka, J. Drzymała, Impact of roughness on hydrophobicity of particles measured by the Washburn method	45
D. Szyszka, J. Drzymała, J. Łuczyński, K.A. Wilk, J. Patkowski, Concentration of α -terpineol and (2-dodecanoyloxyethyl)trimethylammonium bromide required for prevention of air bubble coalescence in aqueous solutions	53
A.M. Amer, Kinetics of alkaline pressure leaching of mechanically modified zircon concentrate	61
W. Mulak, A. Szymczycha, A. Leśniewicz, W. Żyrnicki, Preliminary results of metals leaching from a spent hydrodesulphurization (HDS) catalyst	69
A. Muszer, A. Łuszczkiewicz, Mineralogical characteristics of accessory minerals from Osiecznica deposit, SW Poland	77
A. Muszer, Petrographical and mineralogical characteristics of the metallurgical slag from the Dörschl furnace (Głogów Foundry, Poland)	89
T. Szymura, Research on incrustation in a model evaporative cooler	99
A. Jarosinski, Comparative properties study of products of chromite sintering ...	109
G. Özbayoğlu, N. Ataman, Evaluation of Turkish industrial wastes as blasting abrasives	117
J. Girczys, I. Kupich, Reduction of sulphate ions concentration in discharge waters from Zn-Pb mines	125
P. Nowak, R. P. Socha, Oxidation and dissolution of metal sulfides from flotation wastes in circulating water – the fate of sulfide sulfur	135
E. Skwarek, W. Janusz, Adsorption of Ni(II) ions at the Fe_2TiO_5 /electrolyte solution interface – the electrical double layer structure	149
W. Janusz, A. Gałgan, M. Reszka, Electrical double layer at the Cu_2O /aqueous solution of alkali metal chlorides interface	161
St. Chibowski, M. Paszkiewicz, Polyacrylic acid (PAA) adsorption on alumina (Al_2O_3) surface. Influence of sodium dodecyl sulfide (SDS) on adsorption in PAA-SDS- Al_2O_3 system	175
M, Ulewicz, W. Walkowiak, Removal of Zn(II), Cd(II) and Pb(II) using polymer inclusion membrane transport with proton ionizable DB-16-C-5 crown ethers	185
B. Gajda, M.B. Bogacki, Laboratory simulation of nickel(II) and cobalt(II) ion separation in a continuous counter-current extractor	195
R. Kucerova, P. Fecko, Biodegradation of PAU, PCB, and NEL soil samples from the hazardous waste dump in Pozd’átky (Czech Republic)	203

A. Szubert, Z. Sadowski, Application of shrinking core model to bioleaching of black shale particles	211
R. Modrzewski, P. Wodziński, A method of designing membrane	227
A. Heim, T. Gluba, A. Obraniak, E. Gawot-Młynarczyk, M. Błaszczuk, The effect of wetting parameters on mechanical strength of granulated..... material	237
T.P. Olejnik, Grinding kinetics of selected minerals with reference to the number of contact points	247
F. Ciesielczyk, A. Krysztafkiewicz, T. Jesionowski, Sedimentation and wettability of synthetic magnesium silicates	255
W. Malewski, A. Krysztafkiewicz, T. Jesionowski, Preparation of polysilic acid sols by ion exchange method	265
K. Siwińska-Stefańska, A. Krysztafkiewicz, T. Jesionowski, Physicochemical analysis of silicas coated with natural latex milk	275
M. Janczarek, J. Hupka, H. Kisch, Hydrophilicity of TiO ₂ exposed to UV and VIS radiation	287
M. Krasowska, K. Terpiłowski, E. Chibowski, K. Malysa, Apparent contact angles and time of the three phase contact formation by the bubble colliding with Teflon surfaces of different roughness	293
A. Heim, T. Gluba, A. Obraniak, E. Gawot-Młynarczyk, M. Błaszczuk, The effect of wetting on silica flour granulation	307
T. Farbiszewska J. Farbiszewska-Kiczma, E. Jażdżyk, Z. Sadowski, A. Szubert, Kinetic study of biodegradation of organic matter extracted from black shale ore	317

55 Years of Scientific Work Professor Kazimierz SZTABA



Professor Kazimierz Stanisław Sztaba was born on the 17th day of July, 1931 in teachers family in Krakow. In 1949 he passed the maturity exam and then entered the Mining Faculty of the University of Science and Technology (AGH) in Krakow. At the beginning of 1953 he passed, with a distinction, his diploma exam of the 1st degree basing on a thesis entitled *Analysis of performance of "Zloty Stok" mechanical processing plant* gaining a title of mining engineer. In 1955 he passed his diploma exam of the 2nd degree based on the *Analysis of wet classification process* thesis, and gained the title of master of mining engineering science with specialization in mechanical processing.

In December 1952 he was employed at then the Department of Mechanical Mineral Processing as a tutor. On March 2, 1960 he became a philosophy doctor of technical sciences after defending his thesis on *Influence of feed grain characteristics on homogeneous material wet classification results*. On June 24, 1964 he became a mineral processing doctor of science on the basis of his scientific activity and work on *Some geometrical features of mineral grains sets*. Later Professor Sztaba was appointed associate professor in 1968 and professor in 1977.

From October 1, 1968, for one year, he had been a head of the Mineral Mechanical Processing Department of the Mining Faculty of AGH. Since October 1, 1969, until 1985, he had been a director of the Mineral Processing Institute of AGH (in 1974 named Mineral Processing and Utilization Institute).

In the period of 1969-1972 he was the Personnel Development Deputy Rector of AGH. Because of his position, he led at that time, *inter alia*, a newly-introduced system of postgraduate and doctoral studies, making their status one of the greatest in Poland. During his initial work at the University of Science and Technology - AGH he dealt mainly with fine grains technology issues (micromeritics), particularly with flow classification and basic geometrical features of mineral grains. However, always the

main and, in some way, personal mineral process in scientific work of Professor Sztaba was, widely understood, grained materials classification and also identification and evaluation of materials and dressing processes.

Among 291 published works, which author or co-author is Professor Sztaba, about 50 concern, widely understood, grain classification (flow and mechanical classification), as well identification methods and separated materials features evaluation (not only geometrical).

So a great number of papers concerning classification processes proves that the particular interest of Professor Sztaba is this topic. Already in his 2nd degree thesis he introduced, for the first time in science, separation numbers and curves to describe and evaluate flow classification processes. An effect of this was two important publications, initiating his publishing activity.

- *Statistical method of wet classification process investigation*. Archiwum Górnictwa t. I, z.1, 1956, pp. 33-54.
- *Separation curves in wet classification process*. Archiwum Górnictwa t. I, z.2, 1956, pp. 167-197.

A kind of summary of Professor Sztaba ideas regarding classification processes is the paper on *Directions and development trends of model descriptions of flow processes*, Archiwum Górnictwa, 38, 2 (1993) and a book entitled *Przesiewanie*, Śląskie Wyd. Techniczne, Katowice 1993.

In 1969, apart from classification processes, he started also to deal with control and dressing problems in technological processes as well with liquid-slurry economics in processing plants.

He defined the task of a complex control of dressing technological processes, control on the basis of mathematical models of the processes. In consequence, he formulated a thesis on useless character of actually possible to achieve mathematical deterministic models to evaluate and optimize real dressing processes. To justify this thesis he studied necessary stochastic models and determined the possibilities of their application in a widely understood technological processes control, with output to their automation.

These works created certain style of solving industrial dressing processes by mathematical modeling. The methods of description represented various versions of multiple regression and correlative theory of stochastic processes. The models form evolved with time, taking into consideration some elements of heuristic approach to the industrial dressing processes modeling. Concrete scientific effects of these works were presented, *inter alia*, during the International Mineral Processing Congresses in Cagliari, Sydney, Donieck, Cannes, and Stockholm.

A review of the most important achievements of Professor Sztaba in mathematical modeling of dressing processes shows that he played a very important role as a research moderator of the mentioned issues, creating directions and purposes for investigations and proposing some concrete solutions. The results of this research were works on widely understood dressing processes control and mineral raw

materials processing, and technological processes automation. Within the latter activity, there were works connected with both individual technological values of regulation and control of processes or whole mineral processing plants.

Personal works of Professor Sztaba on the micromeritics topic were concentrated mainly on mineral grain geometric features and their sets (thesis of the associate professor title and several papers), possibilities of grain characteristics generalisation methods, dependence between space compaction and grains geometric features, as well as efficiency of grained materials mixing. A general direction of these works concerned a possibly general presentation of the mentioned phenomena and dependencies with application of statistical methods. In particular, he pointed to great possibilities of application of the term *segregation* to identify processing objects, proposing, *inter alia*, original methods of such applications.

The range of scientific works of Professor Sztaba of flow classification and dewatering processes, being a part of the liquid-slurry economics issue, is recently concentrated on application of these processes to fine or very fine grains with concrete practical application, for example, to clayey raw materials.

In the area of complex raw materials utilization, Professor Sztaba presented many analyses and papers (beginning from announced in 1970 first article in Poland proposing the idea of complex raw materials utilization and its conditions and then during next years developed the bases of rational utilization of wastes being created in the subsequent stages of the raw materials processing) and also other scientific works making possible to realize organizational and productive purposes, being done by various, selected institutions. Thanks to development of this issue, an enlargement of the Mineral Processing Institute of AGH investigations range was possible.

Apart from mentioned issues, Professor Sztaba dealt with widely understood mineral processing, for example he led and cooperated in many scientific works, being done as research-scientific activity of the Institute, in diploma works and many publications, reviews, opinions and norm projects. In particular, during the last years he presented and justified a thesis of gradual vanishing of mineral processing technological limitations and transforming it into highly complex mineral engineering.

After retirement (2002), Professor Sztaba did not stop his scientific activity and still leads research projects and helps younger workmates. The effect of this is, *inter alia*, a monography on *Identification and evaluation of selected mineral raw materials and theirs dressing processes features*, Wyd. IGSMiE PAN, Krakow 2003; of which he is the editor and main author.

It is worthy to underline that he has supervised 27 Ph.D. students, among them two are presently professors of AGH and one gained the title of professor. He reviewed many Ph.D., associate professor, and professorship theses.

Janina GRODZKA*, Andrzej POMIANOWSKI**

WETTABILITY VERSUS HYDROPHILICITY

Received June 28, accepted July 3, 2006

Basing on recent works we discuss the issue relating wetting and hydrophilicity pointing out the topics enabling a fast progress in this area. Wetting is a phenomenon that is still the subject of intensive studies, both pure and applied. However, precise definitions of its molecular basis are still lacking and the static and dynamic macroscopic parameters should also be defined. An important role seems to be played by profound investigation on relaxation times of the primary elemental steps of the joined chemical and mechanical processes.

Key word: wettability, hydrophilicity, hydrophobicity, water clusters, flotation, interfacial phenomena, contact angle

INTRODUCTION

Wettability and hydrophilicity are closely related phenomena. Most research groups working on surface activity use these terms in their every-day practice. The wettability and hydrophilicity phenomena are useful in solving practical issue as well as scientific concerns on both molecular and macroscopic scales under static (at thermodynamic equilibrium) and dynamic conditions. During the last few years interest in a better understanding of wettability is systematically growing. For instance discussions at a recent SURUZ (2006) meeting encouraged us to summarize the recent state of knowledge concerning wetting utilizing numerous original and review articles, especially those of Guillot (2002) and Verdaguer et al. (2006).

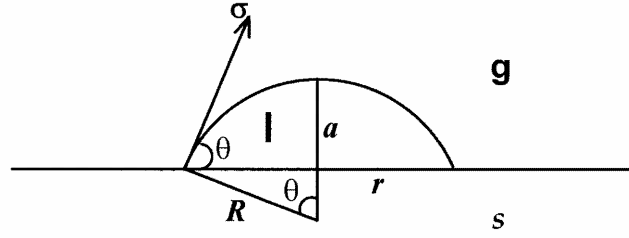
FROM MACROSCOPIC TO MOLECULAR DIMENSIONS

Not long ago Platikanov (Toshev and Platikanov, 2004) remind us a precise thermodynamic analysis of the wetting process. He showed that the simplest model of a wetting system consist of a plane homogeneous surface of an ideally hard and

* Medical Center of HCP Poznań, Poland

** Professor Emeritus of Polish Academy of Sciences, Tenczynek, Poland,
izabela.pomianowska@neostrada.pl

practically insoluble solid being at equilibrium with a liquid or solution and either saturated vapor of the liquid or insoluble neutral gas. The number of conditions concerning the nature of the considered phases directly indicates the number of sources of error and problems in delineation of wetting processes.



$$(d\Omega)_{T,\mu_i} = -\Delta p dV + \sigma dA_{lg} + (\omega_{ls} - \omega_{gs}) dA_{ls}, \quad d\Omega = 0$$

$$V = \frac{1}{6} \pi a (3r^2 + a^2); \quad A_{lg} = \pi (r^2 + a^2); \quad A_{ls} = \pi r^2$$

Fig.1. The state of thermodynamic equilibrium of a wetting system

Figure 1 presents the state of a thermodynamic equilibrium in a system of already mentioned properties. We assume a lack of any external forces, including gravity, even though their introduction to the system is simple. However, it complicates the final formulas resulting from the system geometry and equilibrium of the “surface forces”. Figure 1 shows a drop placed on a flat surface, cut with a plane perpendicular to the diameter of the fragment of the sphere drop. The equations inserted in Fig.1 describe the condition of thermodynamic equilibrium ($d\Omega = 0$). The radius of the sphere is denoted with R , the drop volume V , drop-solid surface area A_{ls} , drop-gas surface area A_{lg} , radius of the “perimeter” (spherical perimeter of wetting) r , and the height of the drop a . We have shown also the vector of force σ , which is tangent to the drop and results from the interfacial tension (gas-liquid) γ , and the angle θ between the tangent and the surface of the solid.

The angle θ observed on a macroscopic scale is commonly called the wetting angle. It is agreed to measure the angle through the liquid phase. It can be seen in the figure that the wetting angle for well wetting liquids (up to a complete, “ideal” wetting) must tend to zero. For the non-wetting liquids the drop contacting the liquid remains spherical and the wetting angle is 180° . In Fig.1 symbols g , l , and s denote the gas, liquid, and solid phases, respectively. The interfacial regions are denoted as l - g , g - s , and l - s , or shortly by lg , gs , and ls .

Equilibrium in this “open” system having $T = \text{const}$, and constant composition ($m_i = \text{const}$) means that the minimum of the free energy Ω of the system can be calculated

for $-pV = \text{const}$ providing $d\Omega = 0$. We omit here mathematical derivation of the equilibrium of open systems based on the Gibbs thermodynamics giving only the sense of symbols and conclusions based on authors considerations. It should be stressed here that there is an essential difference between the nature of a system composed of two liquid phases and a gas and that composed of two solids and a gas, or a system composed of a solid, gas, and liquid. In contrast with the liquid phases, the solid phases (ideally hard and elastic) cannot change their macroscopic shape after a contact with gas, i.e. they cannot change the shape. Practically non-compressible liquids do not show the elasticity of their "form". For a solid body in contact with gas or liquid we must distinguish components of its excess free energy appearing due to interactions with molecules of the gas or liquid of the interfacial region and its "own surface tensions" $_{gs}\gamma$ and $_{gl}\gamma$. We define them using the following formulas: $_{gs}\gamma = _{gs}\omega_s - _s\omega_s$ and: $_{ls}\gamma_s = _{ls}\omega_s - _s\omega_s$. It is worth to notice the question of a wide variation of the names that we come across in the area of the "surface phenomena". An excuse for a lack of precision in theoretical descriptions of surface phenomena is the argument that precise measurements of certain parameters, even those which are very well defined, is often not possible. Large deviations result from both the nature of the "real" phases, the variety of the measuring methods, and from inappropriate conditions of the experiments.

PRECISE NOMENCLATURE AND SYMBOLS

The excess specific (or molar) free energies of the surface are denoted in the following way for one-component condensed phases:

for fixed T and V : $_{l}f_1$ and: f_s (for a liquid and solid phases),

for fixed T and p : $_{l}g_1$ and: g_s

for fixed T and m_i : $_{l}\omega_1$ and: $_{s}\omega_s$.

Strictly speaking the definitions are limited only to the condensed phases at an equilibrium with their saturated vapor, or as we say "in vacuum". However, often we assumed the presence of the so-called inert gas, instead of the vacuum, having a finite volume or pressure. The gas is not soluble in the phases forming the system and is not absorbed at the interfacial regions. So, there is no doubt that for the contact of phases the symbols $_{gs}f_s$, $_{gs}g_s$, and $_{gc}\omega_s$ can be applied along with indication of the type of gas or the vapor, though determination of their values is not always possible. Due to mentioned above inaccuracies of the measurements, as a rule simplifications for "pure" liquids are commonly applied:

$$g^0 \approx _{gl}f_1 \approx _{gl}g_1 \approx _{gl}\omega_1,$$

and for the solutions:

$$_{gl}\omega_1 \approx g = g^0 - \Pi \text{ (for: } T = \text{const.}, \text{ and: } m_i = \text{const}).$$

The "surface pressure" $\Pi = \gamma - \gamma^0$ is obviously a function of the composition of solution, and γ^0 denotes "pure solvent".

A fast development of measuring equipment and a tendency to get more precise results lead us to the conclusion that the technique of measuring the interfacial tensions from the shape of pending or sessile drops is one of the best. The apparatuses make possible the control of the composition of the gas phase, enables thermostating the measuring chamber and does not require the use of any corrections. A precise thermodynamic description based on the equilibrium of forces resulting only from the interfacial tensions and gravity forces makes also possible to determine the contact angles during the same measurement. A maximum precision of the results requires, however, optimization of the drop volume depending on the density of liquid and the value of measured interfacial tension. In the case of solids, because of their hardness and elasticity, their excess specific values of the free energies cannot be replaced with the tensions. In addition, even during unlimitedly slow recrystallization, they do not achieve spherical shape, though they minimize the free energy by the formation of walls. The quasi-static final state depends on cooling conditions. The amorphous solids are usually overcooled liquids or as composition of microcrystalline patches. Only close to the melting temperature, the excess free energies can be determined from the measurements of the interfacial tensions of the saturated liquid phase extrapolated to the melting point. It gives the possibility of determining the $(_{gs}\gamma^0)_{top}$ component. We take here advantage of the fact that the derivatives of the chemical potential are continuous at the temperature of the phase transitions, which however is not the same as the precise determinations of the $_{gs}\omega_s$ values. A rigorous use of appropriate definitions of the considered parameters is important only for accurate understanding of wetting.

A proper form of the Young formula is:

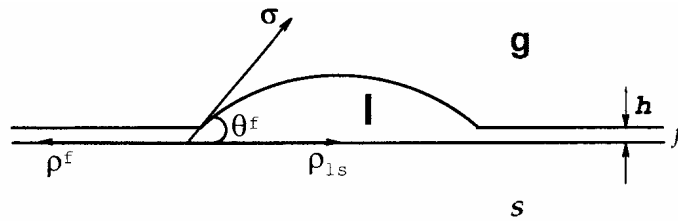
$$\gamma \cos \theta = {}_{gs}\omega_s - {}_{ls}\omega_s = \Delta {}_{ls}\gamma$$

because both the contact with gas and liquid modifies ${}_s\omega_s$ function of the state defined for vacuum, and therefore is only for the gaseous phase, characterized by the vapor pressure of the solid. We must remember that: ${}_{gs}\omega_s = {}_s\omega_s + {}_{gs}\gamma$.

The components of γ are the tensions that are localized in the Gibbs “tension plane” and act in the interfacial region due to the modification of the interparticle bonds of liquid and solid. Sometimes this region contains an aqueous film of thickness h . It should be remembered that for a direct contact between the solid and liquid is not necessary to attain the equilibrium between saturated vapor of a liquid or solvent and the solid surface. Unfortunately, the process of attaining the equilibrium indirectly by the gaseous phase is usually very slow. In the case of a drop of an aqueous solution, a very important issue is the equilibrium sorption of the saturated vapor of the solution on the initially dry solids at the same temperature. A particularly important is the question of the modification by the water vapor of the surface of such solids as quartz, mica, silica, and silicates because of a particular nature of the bonds with water. The process depends on temperature, pressure, and time. These substances immersed in

water form gel layers, more or less slowly, and depending on the pH. It is worth to remember a remark of Platikanov (Toshev and Platikanov, 2004) who stressed that strictly speaking the assumption of the identity of the excess free energies and interfacial tensions is never true, while it is often used in practice. Only rarely this is nearly true. From very rich Platikanov's material (Toshev and Platikanov, 2004) we have chosen only one fragment, no doubt, a very important one, describing the thermodynamic equilibrium in systems having complete wettability. We limit here the considerations to the situation, in which the volume, size of the plane surface of the solid, and the volume of liquid are such that they allow the formation of the „equilibrium” aqueous interfacial film.

All interested in the description of the „free liquid films” in the form of bubbles or being in the equilibrium with „black films” should consult the Platikanov (Toshev and Platikanov, 2004) lecture.



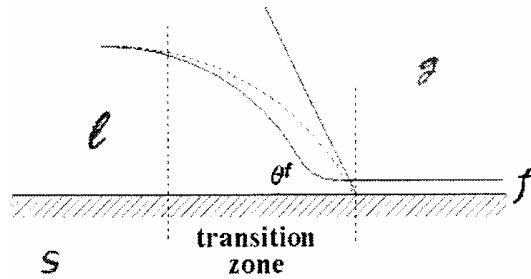
$$\Pi = p_N - p_l = p_g - p_l = \Delta p_c$$

$$\rho^f = \rho_{ls} + \sigma \cos \theta^f = \rho_{ls} + \sigma + \int_h^{\infty} \Pi dh + \Delta p_c h$$

ρ^f is the superficial tension of the film in contact with the solid.

Fig. 2. A scheme of a sessile drop on a plane surface covered with a thin liquid film. $p_g - p_l = \Delta p_c$ is the pressure difference between the gas phase and the liquid in the drop

Figure 2 shows a scheme of the system consisting of a drop sitting on a plane surface covered with a thin liquid film. The macroscopic wetting angle is also shown. The macroscopic view is not able to reveal the presence of an equilibrium aqueous film because its usual thickness is about $0.5 \mu\text{m}$. The formula given in Fig.2 represents a dependence of the wetting angle θ^f in the vicinity of the drop perimeter on the film thickness changing from its equilibrium value h to the “ ∞ ” thickness beneath the drop. The surface tension of the equilibrium film ρ^f is balanced by the sum: $\rho_{ls} + \sigma \cos \theta^f$. The surface pressure Π depends on the solution composition and balances the pressure increase Δp_c caused by the drop surface curvature. dh is the change of the local film thickness.



$$\cos \theta^f = 1 + \frac{1}{\sigma} \int_h^{\infty} \Pi dh + \frac{\Delta p_c h}{\sigma}$$

Fig. 3. Enlarged Platikanov's picture of the "transition region"

Figure 3 presents an enlarged Platikanov's picture of a "transition region", in which the microscopic shape of the interfacial layer is changing within the nanometric scale. Only beyond this region the surface of the drop becomes „identical” with the macroscopic one. The wetting angle, determined macroscopically θ^f , is the wetting angle characteristic for the border of a drop, gaseous phase, and a film covering a well wetted surface of a solid with a thin layer of thickness h . The thickness h is also an important and characteristic feature of well wetted surfaces. Equation given in Fig. 3 was confirmed experimentally by Platikanov (Toshev and Platikanov, 2004). It should be remembered that wettable bodies, beside a visible macroscopic wetting angle, differ in the thickness of the invisible equilibrium surface film.

At this point we would like to make some remarks concerning the measurements of the macroscopic wetting contact angles. It is possible to perform very precise measurements only for a system consisting of two very little mutually soluble phases. An ideal model of such a system is mercury in contact with an aqueous solution having a well defined redox potential. Measurements of macroscopic wetting angles on solid surfaces is a very difficult task due to problems with the nature and preparation of surfaces. These problems sum up and lead to a hysteresis of the wetting angles. This phenomenon is a result of low reproducibility of the results and their variation with time. As for any other phenomenon in which hysteresis appears, we look for the reasons of dependency on the direction of performing the experiments. When a liquid is propagating over the surface, we observe advancing angles. In the contrary to that, withdrawing the liquid creates receding angles. These processes depend not only on direction of medium movement but also on the speed of the process, which always is related to the slow-attaining equilibrium state, and results from the energetic barrier which depends on the nature of the process. Usually, the height of the barriers is related to the sample history, its surface preparation and usually not well known final micro-state inhomogeneity, roughness, contaminations,

etc. The course of a very slow quasi-static detachment of air bubble from selected surfaces was presented by Pomianowski (1960). The fixed wetting angles on galena and mercury in xanthate solutions and on paraffin, called the equilibrium contact angles, assumed 46, 62, and 107 degrees. The investigations were initiated by a hot, at that time, discussions concerning the scale of wetting and its applicability in describing the flotation processes. The nonwetting scale, as other ones applied in thermodynamics, is arbitrary. It may start from zero, but there were also the arguments for 90 degrees as the initial value of nonwetting. The thermodynamic arguments favor zero degree as the starting point of the scale since it represent an ideal wetting. On such surfaces the thickness of a surface wetting film tends to infinity. In practice, the thickness of the film is about 7 water molecules thick, because at this distance the structure of the vicinal water, as is now called the interfacial water, has the structure practically identical with the bulk water. As the hydrophobicity increases, the thickness of the interfacial film h decreases, and finally water takes the form of dynamic "flickering clusters" containing from about 20 to 280 molecules. Water in interfacial regions raises recently more and more interest (Paul and Chandra 2003, 2004; Liu et al., 2005; Tombari et al., 2005; Koga and Tanaka, 2005; Ju and Yang, 2006; Ewing, 2006).

A characteristic feature of flotation systems are dynamic conditions of the contact of air bubbles with mineral particles which are usually significantly lower in dimensions in relation to the bubble. It raises a question to what degree the static wetting angles, measured on plane macroscopic surfaces, can be used for estimating the degree of "hydrophilicity". A setup, consisting of a tensiometer combined with a camera (Pomianowski and Para, 1988) made it possible to record variations in the wetting angle and the perimeter of wetting under the conditions of a slowly increasing force of detachment of a bubble from the surface. The technical equipment at that time allowed to draw only one important, no doubtful, conclusion: it is not the value of the wetting angle itself but its hysteresis is determining floatability. There are two behaviors of the "wetting perimeter". It may easily slide over the surface due to the influence of the external forces acting in the system, or it tends to be rather stably localized. The static angles being below 90° cause that the force needed to detach the bubble results from its perimeter of adhesion and the surface tension of the solution. For larger angles at the moment of detachment the force must be greater. However, it should be remembered that for small grains the so-called "angle of shape" plays an important role. Most easily these relationships can be observed on render, to a different extent, hydrophobic drops of mercury on which the variations in the angle and wetting perimeter caused by an external force are large and easily measurable with modern equipment. The most recent works of Verdaguer et al. (2006) carried out with STM, under precisely controlled conditions (temperature increasing from 4° K) showed that irrespective of the degree of macroscopic hydrophobicity of the metals the two first layers of water have the structure of hexagonal ice. Using a modified AFM technique it was also shown (SIRGHI et al., 2006) that within the nanometric

molecular scale the speed of wetting process is determined by a mechanical equilibrium, because other processes are significantly slower, and under dynamic conditions the system does not gain the minimum of the thermodynamic potential.

A combination of studies of wetting with modern electro- and spectrochemical techniques such as STM, AFM, and the time resolved sum frequency generation, together with a computerized equipment recording variations of wetting angles with time, should lead in the nearest future to a significant development in the theory and practice of wetting.

During the recent SURUZ (2006) workshop, two basic ways of approaching this problem has been presented, that is an “applied” aspect of the investigation of the macroscopic wettability and a typical basic description derived from the principal electrical interactions. Adamczyk (2006) has shown in a systematic and suggestive way that present possibilities of a precise description of the behavior of systems in the interfacial regions are limited by a simple and rarely recognized by many other scientists fact that the interaction of charges is dependent on their distance. There is no doubt about the validity of the Coulomb law. However, a precise formulation of the rules and the values of interactions becomes difficult when the distances between ions, dipoles, and systems of many charges become comparable with the atomic sizes.

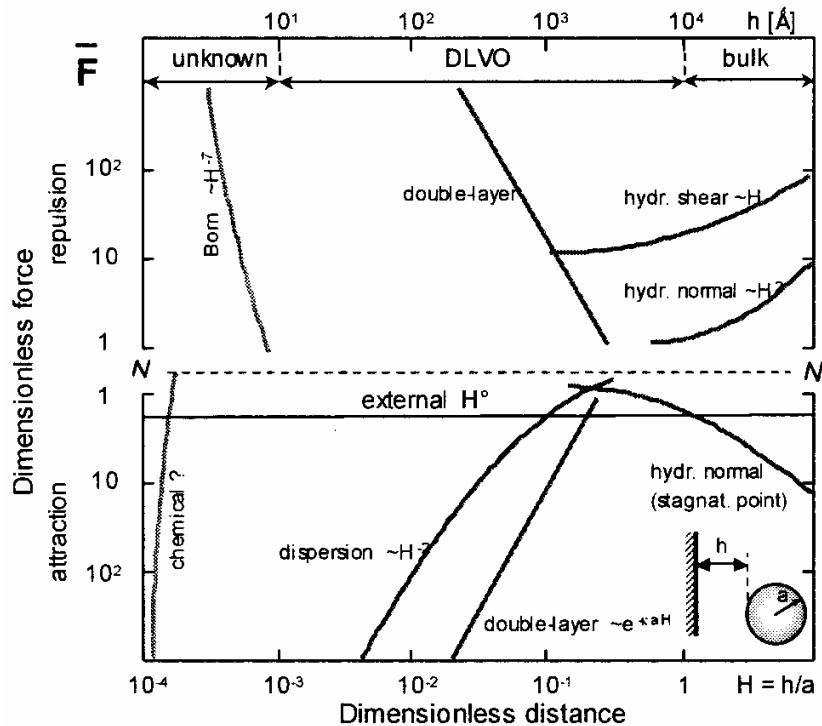


Fig. 4. Relative significance of forces affecting particle adsorption. After Adamczyk, 2006

The data presented in the diagram show clearly, as it has been mentioned in numerous publications recently, that it is not possible to apply strictly the DLVO theory and the resulting from the theory formulas containing the Hamaker parameter (Grasso et al., 2002; Grodzka and Pomianowski, 2005). It becomes more and more commonly recognized that for molecular considerations on a nanometric scale a more precise definition of hydrophobicity, as well as interrelation of "hydrophobic interactions" with changes in the structure of water in the vicinity of the groups and bonds of the dissolved in water foreign molecules, is necessary. These phenomena are, in certain systems, „observed" by the presence in the solutions of dissolved gases and small hydrophobic molecules, as well as by large area of the walls of laboratory vessels (Wennerstrom, 2003; Yang et al., 2003; Attard, 2003; Meyer et al. 2005; Ju and Yang, 2006). There exists a well documented evidence that at low temperatures fluctuating aggregates of water molecules (known - in professional works - as "flickering clusters") contain a measurable contribution of dynamic, bound with hydrogen bonds, "clusters" of a nanometric size.

No later than several years ago it was realized that the hydrogen bonds have the energy of the order of 10 kT, and the London dispersive forces cannot disturb the internal structure of water clusters of a high symmetry. These dynamic structures, based on a characteristic for liquid water pentamer structure (Haraker et al., 2005) are formed at the contacts of water with hydrophobic fragments of systems and they remain statistically stable in the ensemble, with some analogy to the "stability" of micellar aggregates.

WHAT CAN WE PRESENTLY SAY ABOUT WETTING AND TO WHAT EXTENT IS IT TRUE?

The wettability by water, a liquid of a special structure, requires definition of the concept of the hydrophilicity both in a molecular and macroscopic sense. We have to remember that every definition is introduced for a special case. Therefore, it must appropriately broad and detailed. The philosophical school of Vienna positivists assumed that in natural sciences the definitions should be particular recipes for a precise measurement of the value of the defined feature. Therefore, the most difficult task is to formulate cognitive scientific definitions. For instance *natural water* means water of an average isotopic composition containing smaller or greater concentrations of substances with which it either has been or is in contact. *Pure water* means natural water which is free of all substances dissolved in it. *Chemically pure water* means an isotopic mixture of molecules of H₂O, D₂O, and T₂O with prevailing O¹⁶ isotope. Different, though equally rigorous requirements are formulated for applied systems, and still different and rigorous for pure research. Therefore, the most difficult and requiring the best knowledge combined with common sense are works involving both theory and practice.

The Polish Workshop (Suruz, 2006) is an ideal illustration of the necessity of both close contact and a good co-operation between representatives of both approaches to the studied systems. Drzymala (2006) stressed a tendency of accumulation of such information on the nature of complex flotation systems which would allow a good prediction of the results of separation. Adamczyk (2006) presented a primary source of all interactions, including the most complex, considered on atomic as well as macroscopic levels. Both lecturers presented systems for which we are close to describe precisely and quantitatively the occurring there phenomena, but at the same time they showed difficulties in generalization of the conclusions. It is important to stress here that the origin of difficulties is different in applied research and in pure studies. We used this dichotomic classification only to more clearly present our point of view. In reality both types of the investigations are interwoven, and they are distinguished only by their aim formulated by a particular author. Drzymala (2006) revealed a correct ambition to organize and define the concept of the „key role” of the process played by the mineralization of bubbles in a set of primary single processes in the global mechanism of flotation. On the contrary, Adamczyk (2006) showed the source of present limitations, conceptual and mathematical, in calculation of particular interactions appearing in the systems containing particles of various sizes. Such a characteristic gap results from a lack of theoretical delineation of interactions in nano-dispersed systems. It is the largest dynamic clusters of water, being a part of an ensemble of molecules differing in the structure resulting from the existence of hydrogen bonds, which are nanometric in diameter. In applied studies of systems in which the local dynamic conditions (in space and time) fluctuate, the phenomenological thermodynamic predictions are not sufficient. The data on the energy barriers for elemental processes are very difficult to estimate. A very tedious way of the progress seems to be created by computer simulations of these processes and studying the systems that are sufficiently simple and are subjected to the same processes which takes place in real, more complex, systems. Drzymala (2006) gave an example of such simple process. It is for instance the behavior of mercury in the solutions of flotation agents. A.N. Frumkin, an internationally renowned scientist, pointed to this system before the Second World War (Frumkin, 1927). He also pointed out the role of the so-called generalized electrocapillary effect (Frumkin, 1979). It represents a thermodynamic relationship between molecular as well as macroscopic wetting and electrical potential, generated on the surface of the condensed matter by appropriate composition of the solution. Mercury is particularly suitable for studying such effect because only mercury allows to measure precisely the values of all parameters necessary for calculations. The measurement of some isolated surface properties is not possible on solids and studying of some others is more difficult as well as less accurate and less precise than on mercury.

Due to diversity of problems we are dealing with, we shall start from the discrimination between various descriptions of systems on a molecular and macroscopic scale. Here we should return to the fact that there is not possible to make

strictly dichotomous classification, which causes a necessity to apply arbitrary definitions. For instance in the field of strongly dispersed systems, the name of colloid is given to a set of particles or macromolecules of at least one dimension smaller or equal to 1 micron (μm). Even more troublesome is the definition of the difference of a true and colloidal solution. If we take as the criterion the fact that the solution does not disperse the light, also the nature and way of illumination must be taken into account. Due to this fact, the nanometric systems occupy a special place. Depending on the used definition, they may belong either to the colloidal system or to true solution. As a consequence, their equilibrium state may be described as the transition of phases or chemical equilibrium. This is in analogy to the discussion on the nature of light. The difference is only the way of description, not the essence of the question. We always try to choose a simpler description for a particular situation, for obvious reasons. Davies (1957) paved the way leading to the quantitative molecular definition of the degree of hydrophilicity, showing which way the hydrophilic-lipophilic (HLB) equilibrium index should be ascribed not only to the particular substances, but also to the functional groups and types of bonds, in a given system. He showed how these values result from the phase distribution equilibrium constants of substances or their fragments, between water and a desired oil (hydrophobic) phase. We consider it natural to extend the concept of a hydrophobic phase also to gases that are poorly soluble, and first of all to vacuum. In the case of aqueous solutions, it means a space filled with saturated vapors of water and of the studied substance. Furthermore, making use of the additivity rule of the free energies, it is possible to define in the modeling works the functionals of density and the local values as properties of inhomogeneity regions both on free surface and in particulate fine systems, for instance colloidal systems (Meng et al., 2003; Jaqaman et al., 2004). Having numerical data characterizing the degree of hydrophilicity consistent with the generalized HLB index, one could macroscopically define the hydrophilicity through wetting investigations.

The theory and practice of wetting is simple in the systems of two liquids unless (as it was discussed earlier) we do not enter the nanometric level in which the degree of hydrophilicity needs a precise theoretical descriptions using local values of the parameters. Enormous difficulties are met during a precise description of wettability of "real" solids.

We can expect in the nearest future a breakthrough in the theoretical model description of two border type systems, molecularly smooth, practically non-oxidizable, monocrystals of metals in two extreme cases:

- 1: "practically" hydrophobic metals, and
- 2: ideally hydrophilic metals.

In recent years, techniques of synthesis, purification, and observation of deposition of single water molecules and formation of first few layers of water on selected walls of monocrystals have been developed. Also directly an increase in the surface mobility, starting with a single molecule up to the pentamer of water molecules, has

been observed. The already quantitatively known fact that the free energy of sorption of water molecules on many metals are of the same order of value as the free energy of the hydrogen bond between the water molecules has been already confirmed. It was correlated with the results of the above mentioned studies showing that on various metals the structure of water remains similar only in two first molecular layers. The next layers differ more and more, depending on the degree of hydrophilicity of the metal, determined by the structure of water. More hydrophilic metals bind strongly water, competing for its hydrogen bonds, changing their number, structure and energies. It is commonly described as breaking the structure of water, favoring more dense CS structure. More hydrophobic metals favor the formation of an open, more ordered structure of ES water. The speed of a spontaneous self-diffusion motion of interfacial ad-atoms of metal in water and its solutions was also studied deeply. The role of electrical potential in the process has also been reported (Dutkiewicz, 2002).

Metals, similarly to other substances, may behave in solutions in two very different ways. They can be practically non-polarizable semi-cells or be ideally polarized. In both cases their wettability may be theoretically described using the “generalized theory of the electrocapillarity” of Frumkin. Until now, it was not possible to describe the intermediate cases in a strict thermodynamic way. There is only one preliminary work of Para (Pomianowski and Para, 1988), pointing to a possible utilization of the above mentioned phenomena to show the influence of solution red-ox potential on surface tension of mercury. Such investigations, however, have never been popular. They require a tedious preparation of water, very pure mercury (purified and distilled) and very good anaerobic environment of work. Nowak (2006) has spent many years attempting to show a quantitative relationship between oxidation of the surface of mineral particles and their ability to bind thiol collectors.

We would like to end the paper with a remark concerning the complexity of transferring pure studies into industrial applications. A good example of such difficulty was for us a close observation of implementation works being carried out for many years at the Institute for Non-Iron Metals in Gliwice, Poland.

ACKNOWLEDGEMENTS

The authors wish to thank Janka Rodakiewicz-Nowak for her involvement and valuable help in preparation of the paper.

The support of the SURUZ program and its managers as well inclusions of our papers and lectures into programs of the Physicochemical Problems of Mineral Processing conference and SURUZ activities, especially Young Scientists Forums, are gratefully acknowledged.

REFERENCES

- ADAMCZYK, Z., (2006), *Dynamic aspects of surfactants and particle adsorption, lecture for Young Scientists Workshop on Surfactants in the Environment*, SURUZ 2006, Sudomie near Koscierzyzna, Poland, May 19-25.
- ATTARD P., (2003), *Nanobubbles and hydrophobic attraction*, Adv. Colloid Interface Sci. 104, 75.

- DAVIES J.T., (1957), Proc. 2-nd Intern. Congr. Surface Activity, 1 (1957) 426.
- DRZYMALA, J., (2006), Surfactants in flotation, lecture for *Young Scientists Workshop on Surfactants in the Environment*, SURUZ 2006, Sudomie near Koscierzyna, Poland, May 19-25.
- DUTKIEWICZ E., (2002), *Dynamics of electrochemical surface processes at the monocrystalline electrode/electrolyte solution interface and the theory of structure and properties of the interface*, *Facultatis Chemiae, Universitatis Studiorum Mickiewiczianae Posnaniensis, Annales I*, p. 67-102, Wyd. Nauk. UAM Poznan, Poland.
- EWING G.E., (2006), *Ambient thin film water on insulator surfaces*, *Chem. Rev.* 106, 1511.
- FRUMKIN A.N., (1932), *Physicochemical principles of flotation theory*, *Trudy Uralsko - Kuznieckoj Sesji AN SSSR*, izd. A.N. (1932) Leningrad (in Russian).
- FRUMKIN A.N., (1979), *Potential of zero charge*, *Izdat. Nauka*, (in Russian).
- GRASSO D., SUBRAMANIAM K., BUTKUS M., STREVETT K. and BERGENDAHL J., (2002), *A review of non DLVO interactions in environmental colloidal systems*, *Rev. Environ. Sci. and Biotechn.* 1, 17.
- GRODZKA J. and POMIANOWSKI A., (2005), *On the necessity of modifying the DLVO theory (in equilibrium systems)*, *Physicochem. Problems Min. Proc.* 39, 11.
- GUILLOT B., A., (2002), *Reappraisal of what we have learnt during three decades of computer simulations on water*, *J. Mol. Liq.* 101, 219.
- HARKER H.A., VANT M.R., KEUTCH F.N., MICHAEL E.A., Mc LAUGHLIN R.P. and SAYKALLY R.J., (2005), *Water pentamer: Characterization of the torsional - puckering manifold by tetrahertz VRT spectroscopy*, *J. Phys. Chem. A* 109, 6483.
- JAQAMAN K., TUNCAY K. and ORTOLEVA P.J., (2004), *Classical density functional theory of orientational order at interfaces: Application to water*, *J. Chem. Phys.* 120, 926.
- JU S., YANG S. and LIAO M., (2006), *Study of molecular behavior in a water nanocluster: Size and temperature effect*, *J. Phys. Chem. B* 110, 9286.
- KOGA K., and TANAKA H., (2005), *Phase diagram of water between hydrophobic surfaces*, *J. Chem. Phys.* 122, 104711.
- LIU P., HARDER E. and BERNE B.J., (2005), *Hydrogen bond dynamics in the air - water interfaces*, *J. Phys. Chem. B* 109, 2949.
- MENG S., WANG E.G. and GAOS S., (2003), *A molecular picture of hydrophilic and hydrophobic interactions from ab initio density functional theory calculations*, *J. Chem. Phys.* 119, 7616.
- MEYER E.E., LIN Q. and ISRAELACHVILI J.N., (2005), *Effect of dissolved gas on the hydrophobic attraction between surfactant - coated surfaces*, *Langmuir* 21, 256.
- NOWAK P., (2006), D.Sc. monograph (habilitation), Institute of Catalysis and Surface Chemistry, Polish Academy of Science, Kraków, Poland.
- POMIANOWSKI A. and PARA G., (1988), *Electrocapillarity in the model mercury flotation*, *Materials Sci. Forum* 25-26, 447.
- POMIANOWSKI A., 1960. *Abreisskräfte und Randwinkelhysterese in den Systemen: Lösung / Luftblase / Quecksilber - oder Festkörperoberfläche*, III Intern. Congress of Surface Activity, 4, 435.
- PAUL S. and CHANDRA A., (2003), *Dynamics of water molecules at liquid - vapor interfaces of aqueous ionic solutions: effect of ion concentration*, *Chem. Phys. Lett.* 373, 87.
- PAUL S. and CHANDRA A., (2004), *Hydrogen bond dynamics at vapour - water and metal water interfaces*, and: *Binding of hydrogen bonding solutes at liquid - vapour interfaces of molecular fluids*, *Chem. Phys. Lett.* 386 (2004) 218, and: 400, 515.
- SIRGHI L., SZOSZKIEWICZ R. and RIEDO E., (2006), *Volume of a nanoscale water bridge*, *Langmuir* 22, 1093.
- SURUZ, (2006), *Young Scientists Workshop: Surfactants in the environment, Sudomie near Koscierzyna, Poland, May 19-25*. Organized by Dept. of Chem. Techn., Gdańsk University of Technology
- TOMBARI E., SALVETTI G. and FERRARI C., (2005), *Thermodynamic functions of water and ice confined to 2nm radius pores*, *J. Chem. Phys.* 122, 104712.
- TOSHEV B. and PLATIKANOV D., 2004. *A new approach in the wetting thermodynamics: superficial tension of the film in the contact with solid*, SURUZ Workshop (2004) - Kraków.

- VERDAGUER A., SACHA G.M., BLUHMH. and SALMERON M., (2006), *Molecular structure of water at interfaces: Wetting at the nanometer scale*, Chem. Rev. 106, 1478.
- WENNERSTRÖM H., 2003. *Influence of dissolved gas on the interaction between hydrophobic surfaces in water*, J. Phys. Chem. B 107, 13772.
- YANG J., DUAN J., FORNASIERO D. and RALSTON J., (2003), *Very small bubble formation at the solid - water interface*, J. Phys. Chem. B 107, 6139.

Grodzka J., Pomianowski A., *Zwilżanie a hydrofilność*, Physicochemical Problems of Mineral Processing, 40 (2006), 5-18 (w jęz. ang.).

Opierając się na najnowszych pracach oryginalnych i przeglądowych, omówiliśmy podstawowe zagadnienia hydrofilowości i zwilżalności. Wskazaliśmy problemy, których rozwiązanie umożliwi szybkie postępy w tej dziedzinie. Zwilżalność należy do zjawisk o dużym znaczeniu, zarówno poznawczym, jak i praktycznym. Potrzebne jest sprecyzowanie definicji stosowanych pojęć i skali ich wartości. Należy dokładnie określić skalę zmian struktury wody, zarówno w pobliżu rozpuszczonych w niej cząsteczek, jak też w nanometrycznych oraz mikroskopowych obszarach granic międzyfazowych.

Jan DRZYMAŁA*

ATLAS OF UPGRADING CURVES USED IN SEPARATION AND MINERAL SCIENCE AND TECHNOLOGY

Received March 3, 2006; reviewed; accepted April 28, 2006

The atlas presents the existing in scientific and technical literature upgrading curves relating quality and quantity of products of separation for a given feed quality. The upgrading curves were classified into groups including A_r (α -insensitive curves, triangle area accessible for plotting), A_o (α -insensitive curves, square area available for plotting), B_r (α -sensitive curves with triangle plotting area), B_o (α -sensitive curves, having square plotting area), C_r (α -insensitive curves, for $\beta > \alpha$ or $\beta < \alpha$ triangle area), and C_o (α -insensitive curves, for $\beta > \alpha$ or $\beta < \alpha$, square area). Other classifications are also possible. It was presented in the atlas that the shape of the upgrading curve depends on the upgrading parameters used for plotting but they contain and reflect the same information given in a specific, for each curve, way. The applicability of each upgrading curve depends on the needs of the user and personal preferences. An appropriate matching an upgrading curve with a set of separation results allows to approximate the curve with a simple mathematical formula which can be used in other applications. Since the possible number of separation curves is infinite, there is a need for collecting known upgrading curves and creating new ones. The readers are kindly asked to report, not mentioned in this atlas, upgrading curves to jan.drzymala@pwr.wroc.pl

Key words: separation, upgrading, enrichment, recovery, yield, effectiveness, efficiency

INTRODUCTION

Separation relies on splitting an initial material (feed) into two or more smaller portions in a real or virtual way. The final separation takes place due to splitting forces operation in the system. The separation can be real or virtual, selective or non-selective, etc. During the separation additional forces such as ordering, disordering, neutral, etc. can operate in the system (Fig. 1).

The separation systems may contain one or more components. The components of a separation system have numerous features such as size, density, hydrophobicity,

* Wrocław University of Technology, Wybrzeże Wyspińskiego 27, 50-370 Wrocław, Poland,
jan.drzymala@pwr.wroc.pl.

magnetic susceptibility, etc. Certain features of the components are utilized for separation. The features and components of a separation system are interrelated and form a fractal-like structure (Fig.2).

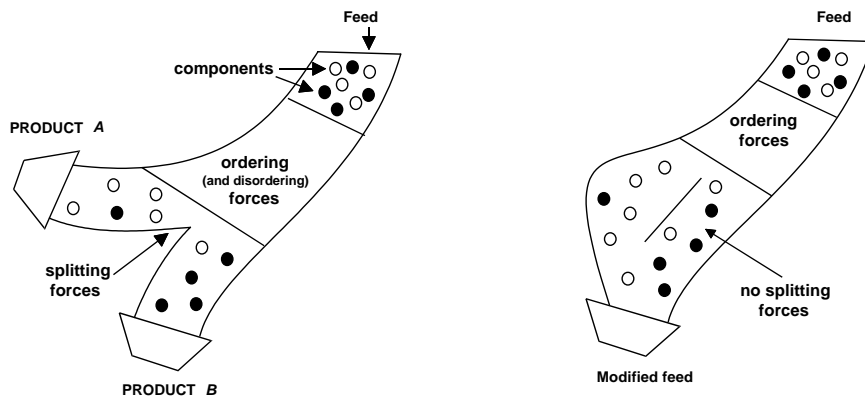


Fig. 1. Elements of separation process. Real separation (a) and virtual separation (b)

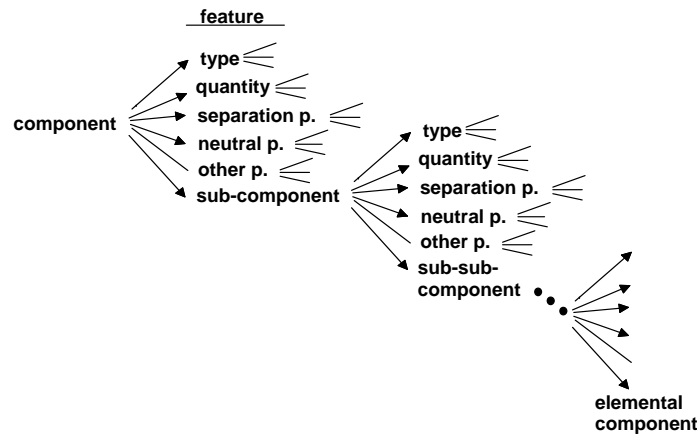


Fig. 2. Fractal-like structure of components and their features

Combining the features of a separation system into pairs provides different approaches that can be used for analyzing separation systems (Fig. 3) including for instance upgrading, classification, sorting, etc. The upgrading takes into account the quality and quantity of products. They can be considered either alone or combined together as well as combined with the feed quality. In other words the upgrading utilizes quantity of products (γ_j), and qualities expressed as content of components in products (β_{ij}), and the content of components in the feed (α_i) where i stands for component and j for product and they assume values 1,2,3,... Combinations of α , β , γ . can also be used. Thus, the starting parameters for analyzing separation as upgrading

are α , β , γ . These parameters can be combined to form new parameters which equally well, as the original ones, characterize the process. New parameters created with α , β , γ are for instance recovery ($\varepsilon = \gamma\beta/\alpha$) or enrichment ratio $K = \beta/\alpha$. The number of parameters resulting from combinations of α , β , γ is infinite. Therefore, the number of possible upgrading curves is also infinite. They represent the same data but in a different esthetical and graphical form. Their usefulness depends to a great extent on personal preferences. Thus, there is a need to create an atlas of the upgrading curves and classify the upgrading curves. Such an attempt was undertaken and the results are presented in this work.

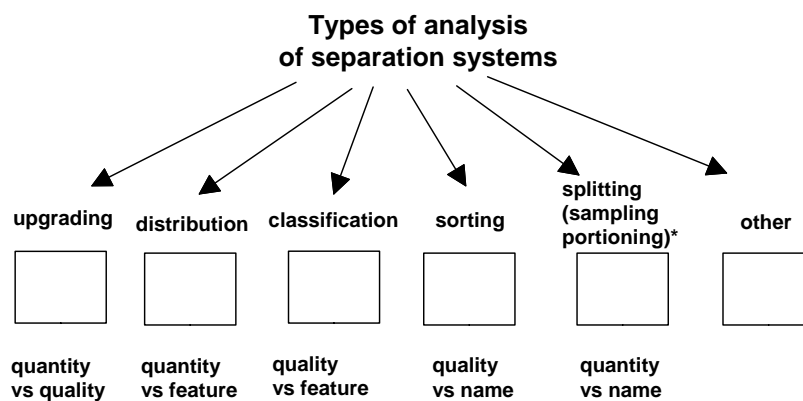


Fig. 3. Possible ways of analyzing separation results

Customarily, the upgrading curves are named after the person who first used the curve. In this atlas only the most known separation curves will be presented. Other curves will be collected in a second part of this atlas in the future. Their arrangement is based on a classification given below. It is recommended to plot in an upgrading curves not only the results of real separation as the real separation line but also the ideal separation (for a complete liberation), ideal mixing, and no upgrading lines (or points). Other lines, for instance the upgradeability that is the maximum possible upgrading for a given liberation, are also possible. The upgrading curve can be given either in a non-cumulative or cumulative way. In this atlas only cumulative upgrading curves, as being more universal, are considered. When the shape of the curves is identical, they bear the same with different Latin numerals.

CLASSIFICATION OF UPGRADING CURVES

Since there is an infinite number of upgrading parameters and curves, their classification can be accomplished in a great number of ways. Tentatively, until a more sophisticated way is designed, in this atlas we will use classification given in Table 1.

Table 1. Classification of upgrading curves utilized in this work

Group symbol	Description, sensitivity to variation of α and area available for plotting	Examples
A_j	α -insensitive curves, triangle area	Fuerstenau, Luszczkiewicz
A_o	α -insensitive curves, square area	not known
B_j	α -sensitive curves, triangle area	Henry I, II, III Mayer I, II, III (Dell) Holland-Batt (β) Holland-Batt H (Hancock) beta-beta
B_o	α -sensitive curves, square area	Halbich, Stepiński I, II, III, IV,
C_j	α -insensitive curves, for $\beta > \alpha$, triangle area	not known
C_o	α -insensitive curves, for $\beta > \alpha$, square area	Stepiński V, Hall

UPGRADING BALANCE

For plotting the upgrading curves hypothetical results of separation were considered. The balance of upgrading is given in Table 2. Only the principal parameters, that is γ , β , α and some selected combined upgrading parameters ($K=\beta/\alpha$, and $\varepsilon=\gamma\beta/\alpha$) are included in the table. If no subscripts i, j at symbols γ , β , α in the table and in the figures are given, it means that the subscript is either 1 or 1,1 ($i=1$ means component 1; $j=1$ means product 1). Sometimes instead $\beta_{1,2}$ symbol ϑ is used which denotes ϑ_1 that is remaining (2) product (tailing).

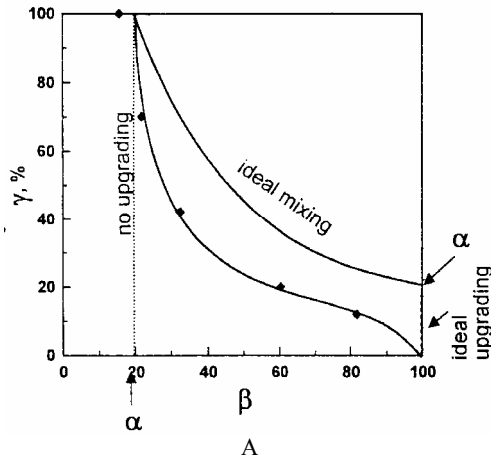
Table 2. Upgrading balance of a hypothetical separation

Product	Yield, γ (%)	Content, β , %	Upgrading ratio $K = \beta/\alpha$	Recovery $\varepsilon = \gamma\beta/\alpha$, %
Concentrate K_1	12.06	81.70	5.305	63.98
Concentrate K_2	20.14	60.40	3.922	79.01
Concentrate K_3	42.27	32.44	2.106	89.07
Concentrate K_4	70.14	21.73	1.411	98.93
Tailing	29.86	0.52	0.0338	1.01
Feed	100.00	15.40= α	1	100.00

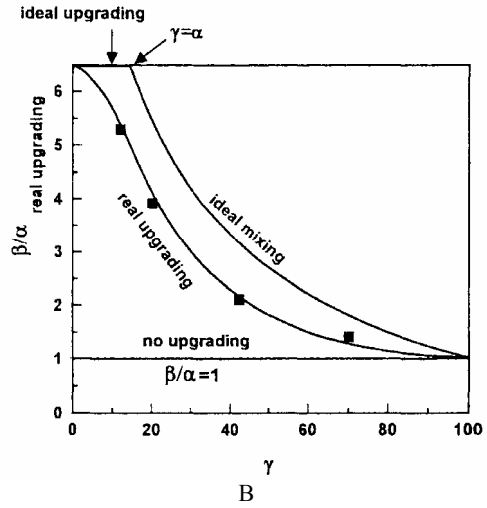
ATLAS OF UPGRADING CURVES

Upgrading curves that can be encountered in technical and scientific papers on separation are given in Figs 4-6. They are presented in groups according to the classification given in Table 1. The upgrading curves belonging to group B are presented in Fig. 4.

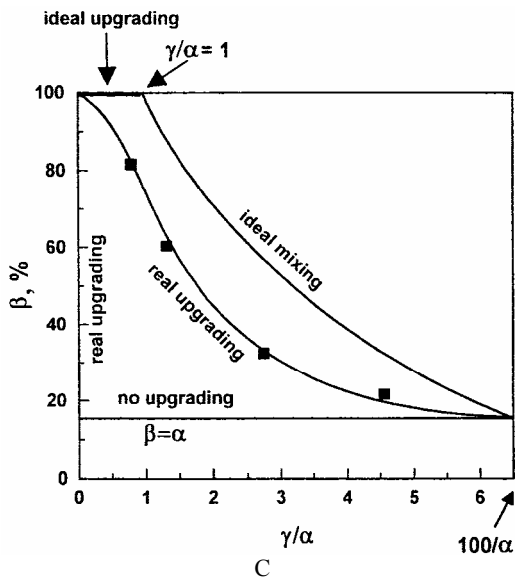
Henry curve
Henry, 1905; Reinhardt, 1911



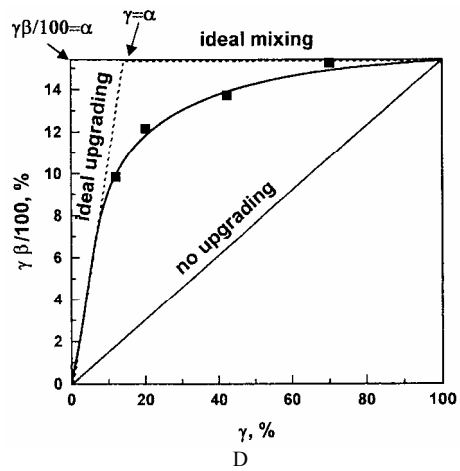
Henry II (enrichment ratio) curve
Holland-Batt, 1985



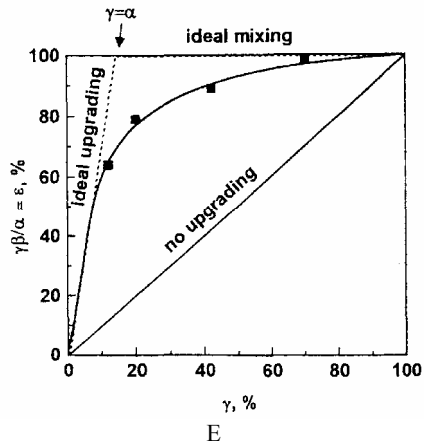
Henry III curve
(no references available)



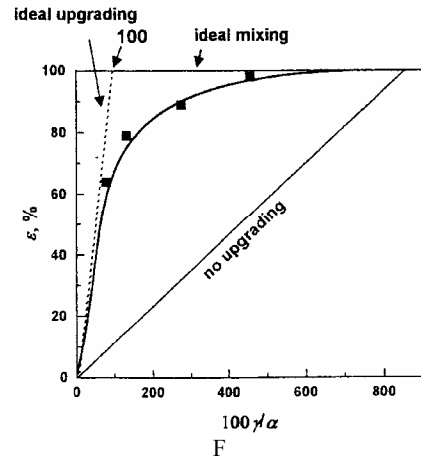
Mayer I (original) curve
(Mayer, 1950, 1951, 1952a, 1952b; Stepiński, 1952, 1964, 1965; Tarjan 1981)



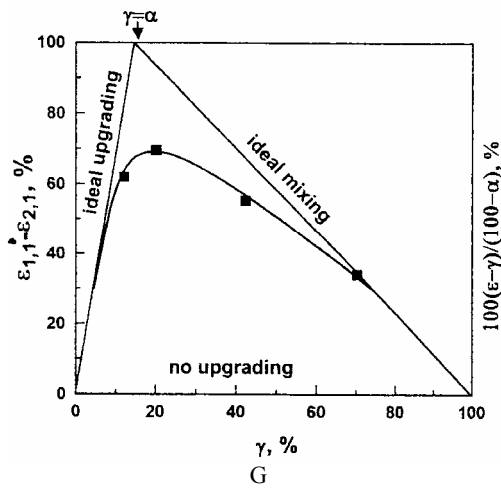
Mayer II curve
(Stępiński, 1952, 1964, 1965,
Nixon and Moir, 1956/7)



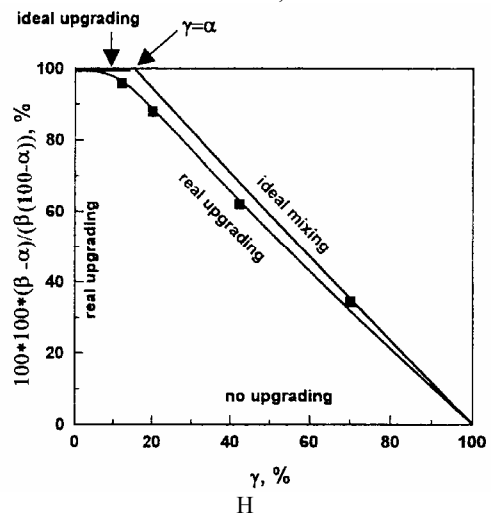
Mayer III (Dell curve)
Dell, 1953, 1961, 1969, 1972



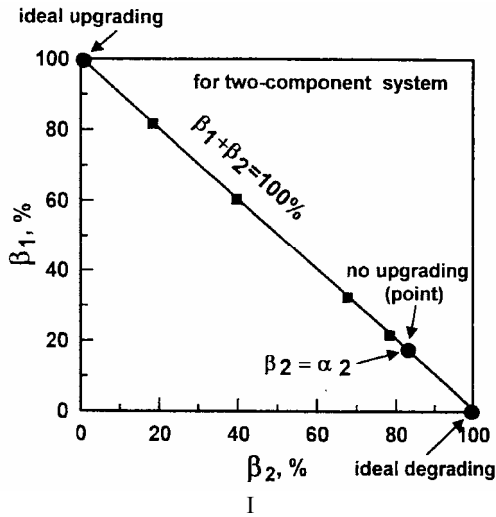
Holland-Batt (Hancock parameter) curve
Holland-Batt, 1985



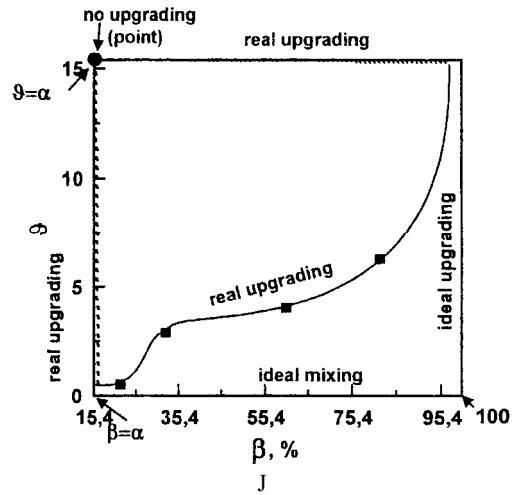
Holland-Batt (β) curve
Holland-Batt, 1985



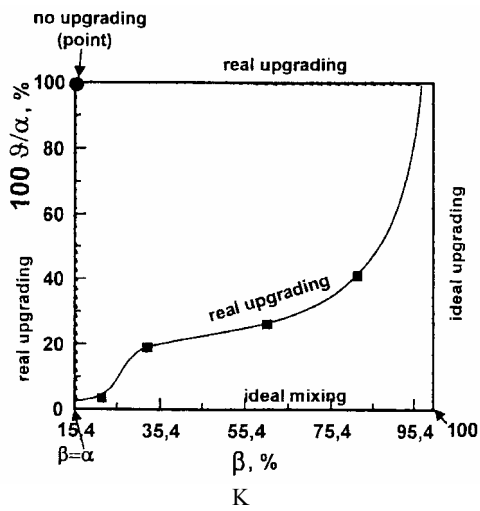
beta-beta curve
Hall, 1971



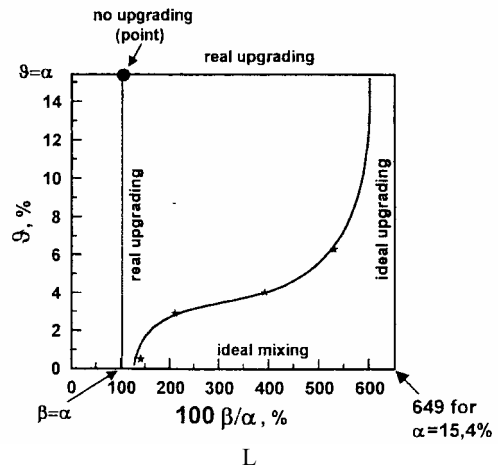
Stepiński I curve
Stepiński, 1955, 1958; Pudło, 1957



Stepiński II curve
(this work, based on Pudło I curve)



Stepiński III curve
(this work, based on Stepiński I)



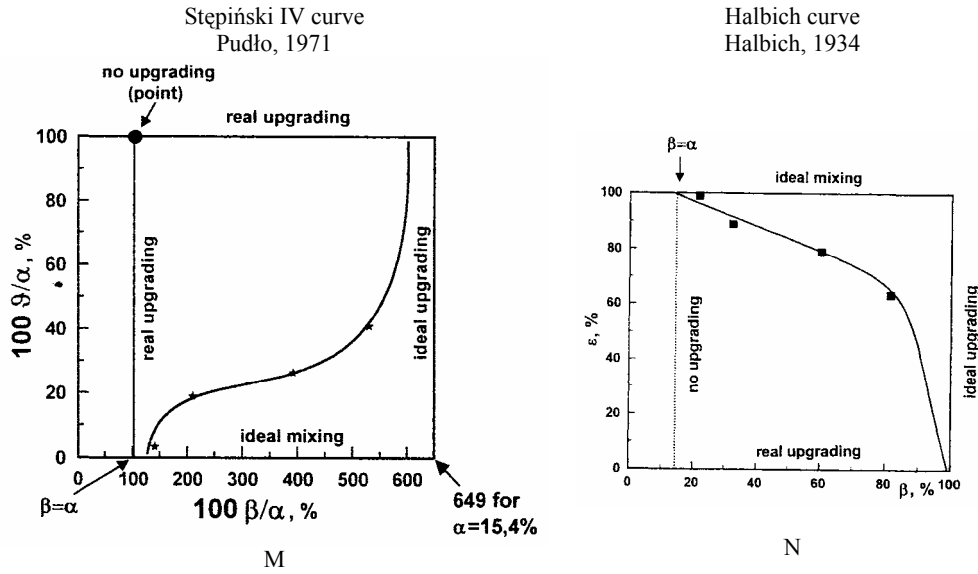


Fig. 4. Type B_l (α -sensitive with triangle or near triangle area available for plotting) upgrading curves (A-I and type B₀ upgrading curve which are α -sensitive curves, square area, J-N)

The upgrading curves belonging to group A are presented in Fig. 4.

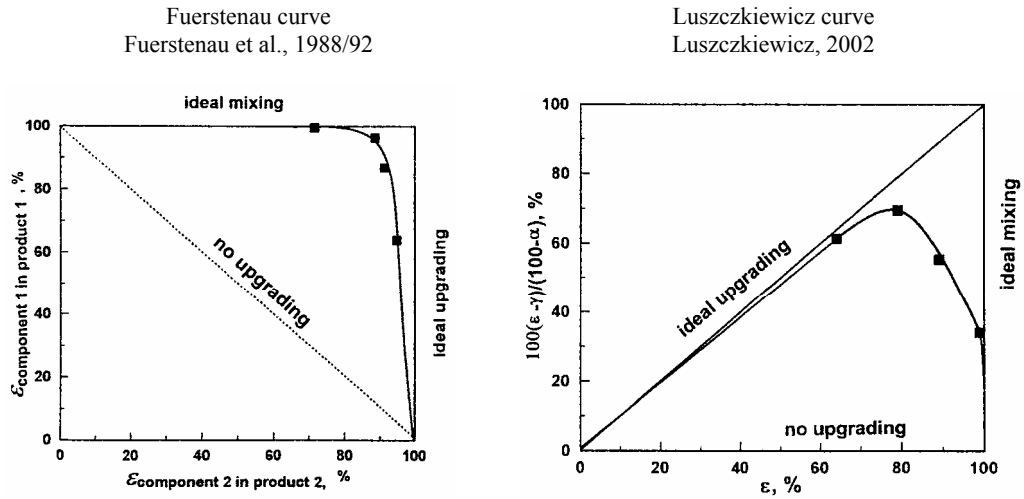


Fig. 5. Type A_l upgrading curves which are α -insensitive curves and offer a triangle area for plotting

The upgrading curves belonging to group C are presented in Fig. 6.

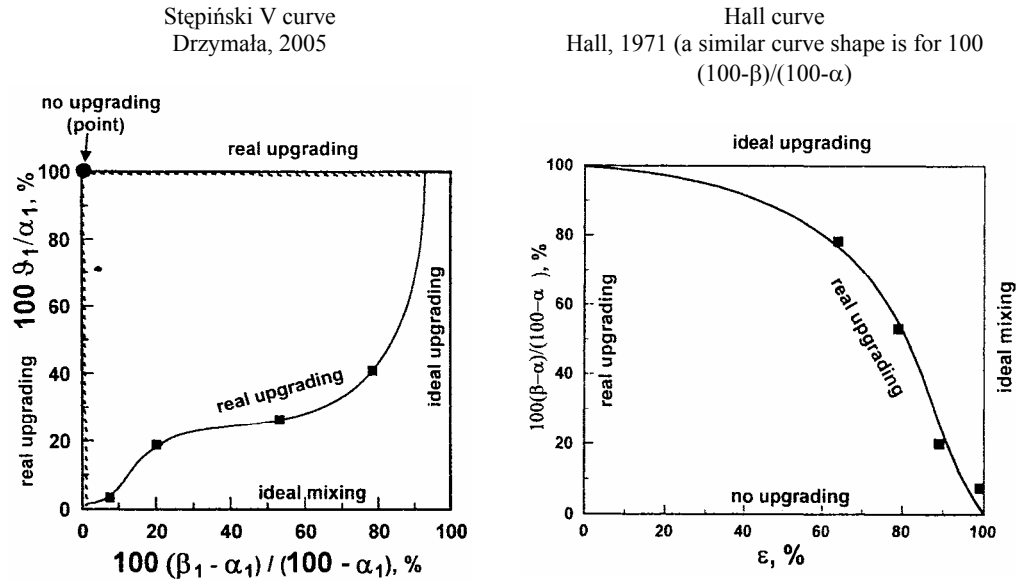


Fig. 6. C_0 type of upgrading curve (α -insensitive curves, for $\beta > \alpha$, square area)

The presented in this atlas upgrading curves represent a small number of all possible plots. In a next publication additional upgrading curves created to extend the list of available plots will be offered.

The author of this atlas asks all interested in a further development of the atlas to submit new and omitted upgrading curves to make the list more complete. The curves will be collected and published as a next part of this publication and later on the internet. The upgrading curves should meet the following standards: be cumulative and contain lines (or points) of real, no, and ideal separation lines, and if possible, the ideal mixing line. The curve will be named after the author of the curve. The propositions can be submitted either by e-mail to jan.drzymala@pwr.wroc.pl or sent by post service to Jan Drzymała, Wrocław University of Technology, Mining Engineering Department, 50-370 Wrocław, Poland.

CONCLUSIONS

There are many available upgrading curves. Their shape depends on the upgrading parameters used for plotting but they contain and reflect the same information, though in a specific for each curve way. Their applicability seems to depend on the needs of the user and personal preferences. The possible number of separation curves is infinite. They characterize well separation process in contrast to single separation parameters which do not fulfill that role.

LIST OF SYMBOLS

- γ - yield of a product; yield of product 1; yield of concentrate, %,
 γ_j – yield of product j , where j is 1, 2, 3 ..., %,
 β - content of a component in a product; content of component 1 in product 1, content of useful component in concentrate, %,
 $\beta_{i,j}$ - content of component i in product j , where i is 1, 2, 3 ... and j is 1, 2, 3 ..., %,
 α - content of a component in the feed; content of component 1 in the feed, content of useful component in the feed, %,
 α_i - content of component i in the feed, where i is 1, 2, 3 ..., %,
 ϑ - content of component 1 in product 2 (tailing or rest of material), same as $\beta_{1,2}$, %,
 K - enrichment (upgrading) ratio ($K=\beta/\alpha$), 100K gives enrichment ratio in %,
 ε - recovery ($\varepsilon=\gamma\beta/\alpha$) of a component in a product, recovery of component 1 in product 1, recovery of component 1 in concentrate, %,
 $\varepsilon_{i,j}$ – recovery of component i in product j , where i is 1, 2, 3 ... and j is 1, 2, 3 ..., %

REFERENCES

- DELL, C.C., (1953), *Release analysis - a new tool for ore-dressing research*, w: Recent developments in mineral dressing, London, IMM, 75-84.
- DELL, C.C., (1961), *The analysis of flotation test data*, Quarterly of the Colorado School of Mines, v. 56, No.3, 113 .
- DELL, C.C., (1969), *An expression for the degree of liberation of an ore*, Trans. Inst. Min. Metal., Sec., C, Mineral Process Extr. Metal., 78, C152.
- DELL, C.C., (1972), *Release analysis - a comparison of techniques*, Trans. Inst. Min. Metal., Sec., C, Mineral Process Extr. Metal., 81, C89.
- DRZYMALA, J., (2005,) *Evaluation and comparison of separation performance for varying feed composition and scattered separation results*, Int. J. Miner. Process., 75, 189-196.
- FUERSTENAU D.W., et al., (1988-1992), *Coal surface control for advanced fine coal flotation*, Final Report, University of California, Berkeley, DOE/PC/88878-T13, DE92 015625, see also: Jia, R., Harris, G.H., Fuerstenau, D.W., 2002. Chemical reagents for enhanced coal flotation, Coal Preparation, 123-149; Sotillo, F.J., Fuerstenau, D.W., Harris, G., 1997. Surface chemistry and rheology of Pittsburgh No.8. coal-water slurry in the presence of a new pyrite depressant, Coal Preparation, 18, 151-183.
- HALBICH, W., (1934), *Über die Anwendungsmöglichkeiten einiger Netzmittel in der Flotation*, Kondrad Triltsch, Würzburg.
- HALL, W.B., (1971), *The mathematical form of separation curves based on two known ore parameters and a single liberation coefficient*, Trans. IMM., Sec.C, 80, C213-C222.
- HENRY, (1905), *Le lavage des charbons*, Revue Universelle, ser. 4, vol. V, p.274 (Information after H. Czeczott, Przeróbka mechaniczna użytecznych ciał kopalnych, Kraków, 1937).
- HOLLAND-BUTT, A.B., (1985), *Analysis of mineral separation system by means of recovery functions*, Trans. IMM, Section C., 94, C17-29.
- LUSZCZKIEWICZ, A., (2002), *Evaluation of efficiency of separation of multi-component concentrates of disseminated elements*, Prace Naukowe Instytutu Politechniki Wrocławskiej, nr 101, Konferencja 35, 87-103 (in Polish).
- MAYER, F.W., (1950), *Die Mittelwertkurve, eine neue Verwackungskurve*, Glückauf, 26, 498-509.

- MAYER, F.W., (1951), *Krzywe średniej wartości (krzywe „M”)*. Część I. *Metoda krzywych średniej wartości w przeróbce mechanicznej*, Przegląd Górniczy, 11, 446-452.
- MAYER, F.W., (1952a), *Przemysłowe badania przeróbcze krzywymi „M”*. A. *Mieszanina dwu węgli*, Przegląd Górniczy, 3, 109-111.
- MAYER, F.W., (1952b), *Przemysłowe badania przeróbcze krzywymi „M”*. B. *Mieszanina trzech i więcej węgli*, Przegląd Górniczy, 4, 148-153.
- NIXON, J.C., Moir, D.N., (1956/7), *The assessment of flotation results*, Bull IMM, London, Trans. IMM, 66, 453-469.
- PUDŁO, W., (1957), *Zależność między średnią zawartością metalu w odpadach a średnią zawartością metalu w koncentracie*, Rudy i Metale Nieżelazne, 1, 1-6.
- PUDŁO, W. (1971), *O pewnej metodzie aproksymacji krzywych wzbogacalności*, Zeszyty Problemowe Górnictwa PAN, Zeszyt 2, Vol., 9, 83-103.
- REINHARDT K., (1911), *Charakteristik der Feinkohlen und ihre aufbereitung mit Rücksicht auf der grösste Ausbringen*, Glückauf, 47(6-7), 221, 257-64.
- STĘPIŃSKI W., (1952), *Krzywe średniej wartości w zastosowaniu do wzbogacania rud*, Przegląd Górniczy, VIII (XXXIX), no. 10(657), 377-380.
- STĘPIŃSKI W., (1955), *Teoria Przeróbki Mechanicznej Kopalni*, cz.II.
- STĘPIŃSKI W., (1958), *Ekonomika przeróbki rud i węgla*, Kraków, 1958.
- STĘPIŃSKI W., (1964), *Krzywe średnich wartości jako miernik oceny dwustadialnej flotacji*, R9, nr 10, 532-535.
- STĘPIŃSKI W., (1965), *Krzywe średnich wartości dwustadialnej flotacji rudy ubogiej*, Rudy i Metale Nieżelazne, R10, nr 3, 117-120.
- TARJAN, G., (1981). *Mineral Processing*, vol. 1., Akademiai Kiado, Budapest.

Drzymala J., *Atlas krzywych wzbogacania do opisu separacji stosowanych w nauce i przemyśle mineralnym*, Physicochemical Problems of Mineral Processing, 40 (2006), 19-29 (w jęz. ang.).

Atlas zawiera znane z literatury naukowej i technologicznej krzywe wzbogacania przedstawiające zależność jakości produktów separacji od ich ilości dla danej jakości nadawy. Krzywe wzbogacania zostały sklasyfikowane na grupy: A_1 (nieczułe na zawartość składników w nadawie z trójkątnym obszarem dostępnym do kreślenia krzywych), A_0 (nieczułe na zawartość składników w nadawie z kwadratowym obszarem dostępnym do kreślenia), B_1 (czułe na zawartość składników w nadawie z trójkątnym obszarem dostępnym do kreślenia), B_0 (czułe na zawartość składników w nadawie z kwadratowym obszarem dostępnym do kreślenia), C_1 (nieczułe na zawartość składników w nadawie dla $\beta > \alpha$ oraz $\beta < \alpha$, obszar trójkątny), oraz C_0 (nieczułe na zawartość składników w nadawie α dla $\beta > \alpha$ oraz $\beta < \alpha$, obszar kwadratowy), gdzie β oznacza zawartość składnika w koncentracie a α w nadawie. Istnieją jeszcze inne możliwe podziały krzywych wzbogacania. W pracy pokazano, że kształt krzywych wzbogacania zależy od parametrów wzbogacania użytych do ich kreślenia i zawierają one te same informacje lecz w innej specyficznej dla danej krzywej formie graficznej, a stosowalność wybranej krzywej wzbogacania zależy od potrzeb użytkownika i osobistych preferencji. Odpowiednie skojarzenie krzywej wzbogacania z danymi pomiarowymi pozwala na aproksymację krzywych odpowiednimi równaniami matematycznymi, które mogą być użyteczne do innych aplikacji. Ponieważ liczba możliwych krzywych separacji jest nieskończona, istnieje potrzeba zebrania znanych krzywych wzbogacania i scharakteryzowania nowych. Czytelnicy tej publikacji proszeni są o nadsyłanie nieopisanych dotąd krzywych wzbogacania pod adres: jan.drzymala@pwr.wroc.pl

Marian BROŻEK*, Anna MŁYNARCZYKOWSKA**

APPLICATION OF THE STOCHASTIC MODEL FOR ANALYSIS OF FLOTATION KINETICS WITH COAL AS AN EXAMPLE

Received March 15, 2006; reviewed; accepted May 15, 2006

Flotation as a random process, in which the random variable representing the number of particles raised to the froth layer during a fixed time t depends on time, is a stochastic process. As a result of turbulence of the medium in the flotation chamber, apart from the process of particles adhesion to bubbles, a reverse process occurs whose intensity depends on the ash content. This is the process of detachment the particles from bubbles. Such a situation is described best by the stochastic process of birth and death.

The paper briefly presents the assumption and differential equation of the model as well as its solution in the form of the equation of flotation kinetics. The authors have presented the interpretation of equation parameters. According to the empirical dependences of recovery of floating particles in the froth product on time for several coal samples, differing by the ash content, the following parameters of the kinetics equation were calculated: the resultant adhesion rate constant and permanent adhesion rate constants. The resultant adhesion rate constant, being the sum of permanent adhesion and detachment rate constants, is independent on the ash content whereas the permanent adhesion rate constant decreases with the increase of ash content.

Key words: flotation kinetics, stochastic process, model of birth and death, adhesion rate constant, detachment rate constant

INTRODUCTION

Flotation, as any technological process in which the results are determined by many random factors, is the process occurring in time. In order to form a permanent attachment between a particle and a bubble there must be, first of all, a collision between a particle with a bubble and the kinetic energy must be contained in a certain range of values, on the one hand large enough to overcome the barrier of the potential

* AGH University of Science and Technology, Faculty of Mining and Goeengineering, Department of Mineral Processing, Environment Protection and Waste Utilization, Al. Mickiewicza 30, 30-065 Kraków, Poland, tel/fax(48-12)617-21-98, e-mail: brozek@agh.edu.pl; ** mindziu@agh.edu.pl.

of the particle-bubble interaction and, on the other, little enough to make this connection stable. In other words, not to detach the particle from the bubble. Both the particle-bubble collision and the value of particle kinetic energy are of random character.

As it can be seen, the permanent particle-bubble connection is determined by a set of random events whose probabilities affect the velocity of the process course. The higher probability, the faster is the flotation process.

Kinetics, i.e. the course of the process in time, results not only from the statistical character of phenomena occurring on the phase boundaries but also from the successive inflow of free surface into the flotation system on which the adhesion of mineral particles in the form of air bubbles occurs and which, among others, limits the velocity of the process course.

Many authors dealt with the problem of flotation kinetics: (Zuniga 1935, Schuhmann 1942, Sutherland 1947, Beloglazov 1947, Pogorelyj 1961a,b, 1962, Bushell 1962, Imaizumi and Inoue 1963, Melkich 1963a, 1963b, 1964, Tomlinson and Fleming 1963, Bogdanov et al., 1964, Bogdanov et al., 1964, Volin and Swami 1964, Zeidenberg et al., 1964, Harris and Rimmer 1966, Loveday 1966, Tille and Panu 1968, Inoue and Imaizumi 1968, Kapur and Mehrotra 1973, 1974, Mehrotra and Kapur 1974, Mehrotra and Kapur 1975, Trahar and Warren 1976, Collins and Jameson 1976, Harris 1978, Maksimov and Jemeljanov 1983, Xu Changlian 1985, Szatkowski and Freyberger 1985, Vanangamudi and Rao 1986, Laskowski et al., 1991, Varbanov et al., 1993, Lazic and Calic 2000).

In a way, there is an analogy between the mechanism of chemical reaction and the mineralization of the air bubble in the flotation process. Therefore, the flotation kinetics is described by the equation analogical to the equation of kinetics of chemical reaction.

Zuniga (1935) was the first who applied the differential equation of kinetics of chemical reaction to the description of kinetics of batch flotation. It can, in its general form, be written as follows:

$$\frac{dC}{dt} = -kC^n \quad (1)$$

where: $C(t)$ – concentration of floating particles remaining in the flotation chamber up to the moment t ; k – flotation rate constant; n – constant characterizing the order character of the process (order of flotation kinetics).

The flotation rate constant, occurring in this equation, is a macroscopic parameter which should contain information about the process affecting factors. This information is recorded by the models of flotation rate constant which determines the process kinetics.

Equation (1) is the equation of flotation kinetics of particles which are homogeneous in their surface properties, i.e. equal-floating particles which possess the

same value of the flotation rate constant. After solving equation (1) for $n = 1$ and calculating the recovery of floatable particles to the froth product, the following expression is obtained:

$$\varepsilon(t) = 1 - \exp(-k t) \quad (2)$$

As it results from equation (2), after long flotation time (theoretically infinitely long), all floating particles in the given physicochemical conditions will have been floated out. It is known from experience that flotation is a kinetic and thermodynamic phenomenon (Drzymala, 2001). It means that the value of recovery after a long time of flotation, especially for larger and difficult to float particles, is smaller than 1. There are no analogical cases in the kinetics of chemical reaction.

After imposing the following boundary condition upon equation (2):

$$\lim_{t \rightarrow \infty} \varepsilon(t) = \varepsilon_{\infty} \quad (3)$$

the dependence of recovery on time is expressed by the function:

$$\varepsilon(t) = \varepsilon_{\infty} [1 - \exp(-k t)] \quad (4)$$

Formula (4) represents a general form of kinetics equation of the 1st order. In such a concept this is a determinist model. The parameters of this model are empirical constants. The notion of equilibrium recovery ε_{∞} was introduced into the model of chemical reaction as a second parameter to readjust the model to empirical dependences. There were no theoretical premises in the construction of the basic equation of kinetics which could justify such a step. The equation of the process of birth and death is such an equation of kinetics, known in the theory of stochastic processes (Bailey 1964), the solution of which comprises all the subprocesses present in mineralization of bubbles.

STOCHASTIC MODEL OF KINETICS OF BATCH FLOTATION

In the stochastic model the number of particles $N(t)$ raised to the froth level up to time t is the random variable depending on time. From the point of view of theory of stochastic processes the model based on the kinetics of chemical reaction is a pure birth process. The particles which were subjected to adhesion to bubbles are not able to return to the phase of suspension.

As a result of turbulence of medium in the flotation chamber, despite the process of adhesion of particles to bubbles, there is a reverse process of lower intensity, i.e. the process of detachment the particles from the air bubbles (Mika and Fuerstenau 1968, Schulze 1977, Woodburn et al., 1971, Schulze 1992, Maksimov and Emelianov 1983,

Geidel 1985, Honaker and Ozsever 2003). The process of birth and death is a model which describes such a process.

The model of the process of birth and death was applied and solved mathematically by Litwiniszyn (1966) for the description of kinetics of the colmatage process. In this process the particles of solids, present in the liquid, are being caught in the porous medium as a result of surface interactions of this medium with particles. Here two sub-processes may appear: adhesion to the porous body and detachment resulting from interactions with the flowing liquid.

The process of ion flotation (Stachurski 1970) and the process of wet magnetic separation (Siwiec 1982) run according to the model of birth and death. If the state of system in which l particles are attached to bubbles is marked as E_l and the state in which $l+1$ particles are attached is marked as E_{l+1} , in the process of birth and death, the transitions from E_l to E_{l+1} and E_l to E_{l-1} are possible.

For the transition from E_l to E_{l+1} the function of intensity of the adhesion process $\lambda(l)$ is formed whereas for the transition from the state E_l to E_{l-1} the function of intensity of the detachment process $\mu(l)$ is formed, according to the following formulas:

$$\lambda(l) = \lambda_o (n_o - l) \quad (6a)$$

$$\mu(l) = \mu_o l \quad (6b)$$

where: n_o – number of particles floating in the floatation chamber in the moment $t = 0$; λ_o and μ_o – certain constants. Thus the intensity of the adhesion process is proportional to the number of particles remaining in the free state ($n_o - l$), while the intensity of the process of detachment is proportional to the number of particles attached to bubbles (l). Probability $P_l(t)$ that at the moment t there are l particles attached to bubbles is fulfilled by the following system of differential equations (Litwiniszyn 1966):

$$\frac{dP_l(t)}{dt} = -[\lambda_o(n_o - l) + \mu_o l]P_l(t) + \lambda_o(n_o - l + 1)P_{l-1}(t) + \mu_o(l + 1)P_{l+1}(t) \quad (7)$$

while $l = 1, 2, \dots, n_o$.

Equations (7) has the following solution:

$$P_l(t) = \binom{n_o}{l} \frac{l}{(\lambda_o + \mu_o)^{n_o}} [(\mu_o + \lambda_o)e^{-(\lambda_o + \mu_o)t}]^{n_o - l} [1 - e^{-(\lambda_o + \mu_o)t}]^l \quad (8)$$

The average value of the random variable $N(t)$ is:

$$E[N(t)] = \sum_{l=0}^{n_o} l P_l(t) = \frac{n_o \lambda_o}{\lambda_o + \mu_o} [1 - e^{-(\lambda_o + \mu_o)t}] \quad (9)$$

Accordingly, the recovery of particles raised to the froth layer is expressed by the formula:

$$\varepsilon(t) = \frac{E[N(t)]}{n_o} = \frac{\lambda_o}{\lambda_o + \mu_o} [1 - e^{-(\lambda_o + \mu_o)t}] \quad (10)$$

The form of this formula is analogical to formula (4) while $\varepsilon_\infty = \frac{\lambda_o}{\lambda_o + \mu_o}$ and $k = \lambda_o + \mu_o$. It can be said that the constants λ_o and μ_o are, respectively, the constants of the process of adhesion and detachment of particles from the air bubbles. These constants can be calculated from formula (10) because:

$$\lim_{t \rightarrow \infty} \varepsilon(t) = \frac{\lambda_o}{\lambda_o + \mu_o} = \varepsilon_\infty \quad (11)$$

$$\left. \frac{\partial \varepsilon(t)}{\partial t} \right|_{t \rightarrow 0} = \lambda_o \quad (12)$$

Matching the empirical dependence to the model one it is possible to evaluate the values of the processes of adhesion and detachment under given physicochemical and hydrodynamic conditions in the flotation chamber.

A PHYSICAL INTERPRETATION OF THE BIRTH AND DEATH MODEL CONSTANTS

It results from formula (4) of recovery of a useful mineral in the froth product for $\varepsilon_\infty = 1$ that after the appropriately long time (theoretically infinitely long) the whole floatable mineral will be transferred to the froth product (all particles connected with the air bubbles will find their way to the froth product). The flotation rate constant is:

$$\left. \frac{d\varepsilon}{dt} \right|_{(t=0)} = k \quad (13)$$

A comparison of this formula to formula (12) leads to the conclusion that in the case of flotation without detachment the flotation rate constant is equivalent to the resultant adhesion rate constant. All the particles attached to the air bubbles will pass to the froth product. None of them will be detached from the flotation aggregate.

From formula (4) for $\varepsilon_\infty = 1$ the flotation rate constant and, at the same time, the resultant adhesion rate constant is:

$$k = \frac{1}{1 - \varepsilon} \frac{d\varepsilon}{dt} \cong \frac{1}{1 - \varepsilon} \frac{\Delta\varepsilon}{\Delta t} \quad (14)$$

Since

$$\varepsilon = \frac{l}{n_o} \quad \text{and} \quad \Delta\varepsilon = \frac{\Delta l}{n_o} \quad (15)$$

then

$$k = \frac{\Delta l}{\Delta t(n_o - l)} = S_b \frac{l_c}{\Delta t(n_o - l)} \frac{\Delta l}{S_b l_c} = S_b P_c P_a \quad (16)$$

where : n_o – initial number of floatable particles in the flotation chamber; l - number of particles attached to the air bubbles up to the time t ; Δl - number of particles attached to the bubbles in the time Δt ; l_c - number of particles colliding with the bubble in the unit time; S_b -total surface of bubbles passing through the surface unit of the cross-section of the flotation machine in the time unit; P_c and P_a – probabilities of collision and adhesion, respectively,;

$$P_c = \frac{l_c}{\Delta t(n_o - l)} \quad P_a = \frac{\Delta l}{S_b l_c} \quad (17)$$

The condition of adhesion to occur is the collision between a particle and a bubble. Thus, the resultant adhesion rate constant is the product of probability of collision and probability of adhesion on the surface of air bubbles flowing through the surface unit of the cross-section of the flotation chamber in the time unit. Resultant adhesion is therefore a number of all particles which were instantaneously or permanently attached to the bubbles surfaces. A part of them will be detached as a result of turbulent movements of the medium. Consequently, the number of particles attached permanently to the bubble surface is the difference between the total number of particles attached to bubbles and the number of particles detached from them. The particles attached permanently will be raised to the froth product. Therefore, in the case of the model of flotation, with respect to the process of particle detachment from the bubble surfaces, the following scheme of the process of adhesion (in the sense of balance of the number of particles) can be assumed:

$$\text{Permanent adhesion} = \text{resultant adhesion} - \text{detachment} \quad (18)$$

As it results from the above scheme and formula (10), the constant λ_o denotes the permanent adhesion rate constant whereas the flotation rate constant k is the resultant adhesion rate constant.

It is an obvious fact that such particles are detached which were previously subjected to adhesion to the bubble. Therefore the detachment rate constant will be the product of the resultant adhesion rate constant k and probability of detachment, P_d :

$$\mu_o = k P_d = S_b P_c P_a P_d \quad (19)$$

On the other hand, according to scheme (18), the constant of permanent adhesion rate constant is :

$$\lambda_o = k - \mu_o = S_b P_c P_a - S_b P_c P_a P_d = S_b P_c P_a (1 - P_d) \quad (20)$$

Applying formulas (20) and (19) it is possible to calculate the value of equilibrium recovery,

$$\varepsilon_\infty = \frac{\lambda_o}{\lambda_o + \mu_o} = \frac{S_b P_c P_a (1 - P_d)}{S_b P_c P_a} = 1 - P_d \quad (21)$$

Thus, P_d , λ_o and μ_o can be determined from the empirical dependence $\alpha(t)$. This fact creates an additional tool for studying the basis of the process of mineralization of air bubbles in the mass process.

EXPERIMENTAL

METHOD OF SAMPLES PREPARATION

Coal of the special seam (type 33) of the Piast Mine was used which was crushed in the roller crusher below 0.5 mm. The wet screen analysis was applied, obtaining the particle size fractions (0.5-0.4), (0.4-0.315), (0.315-0.2), (0.2-0.1) mm. After drying, each size fraction was subjected of float and sink analyses. The analysis was carried out in the solution of zinc chloride. Narrow density fractions (-1.35), (1.35-1.5), (1.5-1.7), (1.7-1.8), (1.8-2.0) and (+2.0) Mg/m³ of size fraction were obtained as products of separation. The narrow size fraction-density fractions were stored in vacuum to limit the oxidation of coal surface and next then were used for research. Ash content was determined in every sample.

DETERMINING THE FLOTATION KINETICS

Flotation experiments for coal were performed at room temperature in the Denver laboratory apparatus of 1 dm³ capacity with the constant rotor speed 2020 rpm and the fixed air flow-rate (Mlynarczykowska, 2004). The content of solids was the same in all experiments and was 80 g/dm³. Such conditions ensured the constant amount and size of air bubbles in the chamber with limited turbulence of flotation pulp caused by the rotor. Low concentration of flotation pulp was used for practical reasons because

at low pulp density it is possible to obtain favourable results of coal flotation (Sablik 1998).

The weighed portion was wetted for 15 min in the solution of the flotation agent of predetermined concentration, next stirred for 5 min without air. The aqueous solution of butanol was used as a collecting and frothing agent which does not change pH of pulp but only decreases the surface tension at the gas – liquid interface which causes the air dispersion in the suspension to increase. Also its adsorption on the surface of air bubbles follows which ensures their stabilization and prevents coalescence (Malysa 2000a,b, Krzan and Malysa 2002). On the basis of initial investigations, proper concentrations of the reagent were selected ensuring the formation of froth of appropriate structure and durability.

In the performed series of investigations the fractionated flotation was carried out in which the concentrates were collected in the following time intervals: 15, 15, 30, 30, 30 s and every 1 min. The time of carrying out the flotation depended on particle sizes and fraction density. As a rule the last froth product was collected after 6 minutes of flotation. The samples were weighed after drying and the ash content was determined.

RESULTS AND DISCUSSION

The investigations of flotation kinetics of respective densimetric fractions of size fraction 0.2-0.315 mm were performed at butanol concentration of $2 \cdot 10^{-3}$ mol/dm³ and the corresponding surface tension 68.5 mN/m. Its measurements were made by means of the ring method with the digital K9 KRUSS tensometer at room temperature (about 22°C). The measurement accuracy was 0.1 mN/m.

The curves of flotation kinetics were drawn according to the results of empirical tests of this sample. The empirical dependences were approximated by model equations of flotation kinetics of the 1st order (Eq. (4)). The parameters of this equation, ε_{∞} and k , were calculated in the following way. For the given value ε_{∞} equation (4) can be transformed to the form:

$$\ln \frac{\varepsilon_{\infty}}{\varepsilon_{\infty} - \varepsilon} = k t = y \quad (22)$$

Next, the constant k was calculated by the least square method. The rate of agreement of the model dependence with empirical courses was evaluated by means of the curvilinear correlation coefficient R :

$$R = \sqrt{1 - \frac{\sum_{i=1}^n (\varepsilon_i - \hat{\varepsilon}_i)^2}{\sum_{i=1}^n (\varepsilon_i - \bar{\varepsilon})^2}} \quad (23)$$

in which: $\bar{\varepsilon}$ – average value of recovery; $\hat{\varepsilon}_i$ – value of recovery calculated from the model in the i -th point; ε_i – experimental value of recovery in the i -th point; n – number of experimental points. The value ε_∞ was changed every 0.01 to reach the maximum value of the curvilinear correlation coefficient.

Figure 1 shows the model curves of flotation kinetics. Empirical values are marked by circles. In all cases the curvilinear correlation coefficient is larger than 0.96. Model dependences $\varepsilon(t)$ are given by each figure. The permanent adhesion rate constant was calculated on the basis of model dependences $\varepsilon(t)$, according to formulas (12), (11) and (4):

$$\lambda_0 = \lim_{t \rightarrow 0} \frac{d\varepsilon(t)}{dt} = k \varepsilon_\infty \quad (24)$$

The calculated values of the permanent adhesion rate constant are given by each model dependence. As it can be seen in the quoted results, the resultant adhesion rate constant k is practically independent from the ash content.

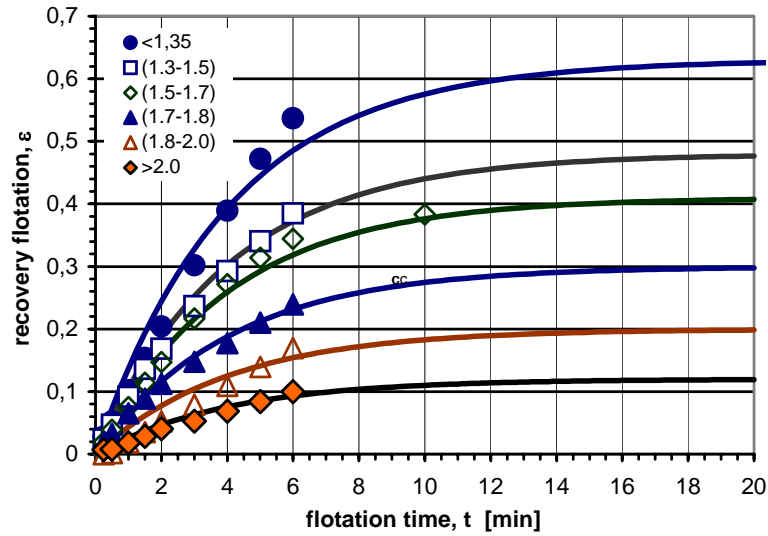


Fig.1. Flotation kinetics:

density fraction <1.35 [Mg/m^3], $A=1.06\%$, $\varepsilon=0.63(1-e^{-0.245t})$, $\lambda_0=0.154$ [1/min],
 density fraction $(1.35-1.5)$ [Mg/m^3], $A=7.91\%$, $\varepsilon=0.48(1-e^{-0.249t})$, $\lambda_0=0.12$ [1/min],
 density fraction $(1.5-1.7)$ [Mg/m^3], $A=23.18\%$, $\varepsilon=0.41(1-e^{-0.25t})$, $\lambda_0=0.102$ [1/min],
 density fraction $(1.7-1.8)$ [Mg/m^3], $A=36.32\%$, $\varepsilon=0.30(1-e^{-0.246t})$, $\lambda_0=0.074$ [1/min],
 density fraction $(1.8-2.0)$ [Mg/m^3], $A=48.71\%$, $\varepsilon=0.20(1-e^{-0.245t})$, $\lambda_0=0.079$ [1/min],
 density fraction >2.0 [Mg/m^3], $A=77.63\%$, $\varepsilon=0.12(1-e^{-0.249t})$, $\lambda_0=0.03$ [1/min].

This constant, according to formula (16), is proportional to the product $P_c P_a$. The probability of adhesion is expressed by the following formula (Yoon and Mao 1966, Schimmoler et al. 1993).

$$P_a = \exp\left(-\frac{E}{E_k}\right) \quad (25)$$

where: E – size of energy barrier of the particle-bubble interaction; E_k – kinetics energy of the particle, necessary to form the bubble-particle aggregate. Energy barrier E grows with the increase of ash content. Also the particle kinetic energy increases because is proportional to particle density which grows with the increase of ash content. Accordingly, the value of the expression under the exponent may change slightly (i.e. increase) with the growth of ash content. If we take into consideration the fact that with the growth of particle density also the probability of collision increases (Nguyen Van and Kmet 1992), then the product of both probabilities may remain constant. On the other hand, the constant of permanent adhesion decreases with the growth of ash content.

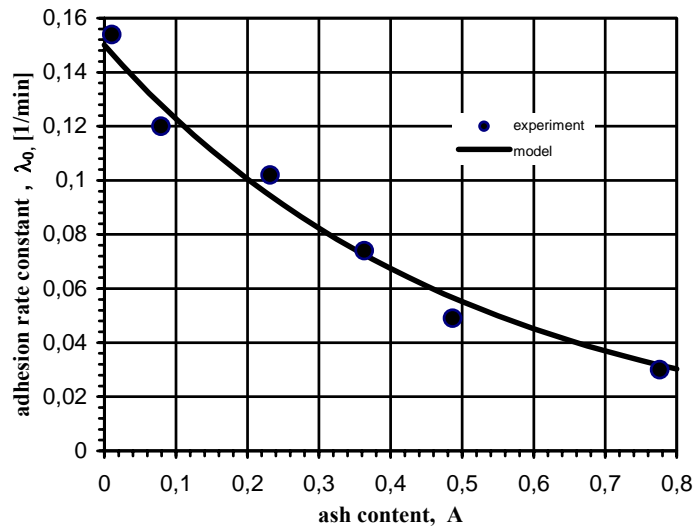


Fig. 2. The permanent adhesion rate constant as a function of ash content in the sample of particle size distribution (0.2-0.315) mm; $\lambda_0 = 0.15 e^{-2A}$

Figure 2 presents the dependence of permanent adhesion rate constant on ash content in the sample under flotation. The following empirical model was proposed:

$$\lambda_o(A) = a e^{-b \cdot A} \quad (26)$$

where: a and b – empirical constants while $a = \lambda_o(0)$ is the permanent adhesion rate constant for the ash free coal. It will depend on the coal type, its petrological composition, surface oxidation rate, particle size, etc. and physicochemical and dynamic conditions in the flotation chamber. The constant b , with the above factors, will depend first of all on the composition of coal mineral matter. For the sample tested here, the dependence $\lambda_o(A)$ is expressed by the formula:

$$\lambda_o(A) = 0.15 e^{-2A} \quad (27)$$

The index of curvilinear correlation is 0.99990 which proves good compatibility of the proposed model dependence with experimental values.

CONCLUSIONS

The deterministic model of kinetics of batch flotation of coal of the 1st order with 2 parameters (Eq. 4) does not comprise quantitatively all sub-processes present in bubbles mineralization. The experiment showed that the resultant flotation rate constant in this model is practically independent from the ash content. This fact can be explained by means of the stochastic model of birth and death. The flotation rate constant in the stochastic model achieves the interpretation of the resultant adhesion rate constant which is the sum of the permanent adhesion rate constant and detachment rate constant. With the growth of ash content the permanent adhesion rate constant decreases and the detachment rate constant increases so that their sum remains constant. It can be assumed that all particles of the non-zero rate of exposition of the coal substance on the particle surface are subjected to adhesion to bubbles. Yet, on the surface of particles of low ash content, i.e. high content of the coal substance, the three-phase contact is formed with a large perimeter and it will be, consequently, a permanent connection. At a low content of coal substance and a low rate of exposition, this connection will be less permanent because of the smaller perimeter of the three-phase contact. Therefore the process of particles detachment will be more intense.

ACKNOWLEDGEMENTS

The paper has been written within the European Union grant “Scientific Network - Surfactant and Dispersed Systems in Theory and Practice”. Contract no INCO-CT-2003-003355, and supported by a grant of the National Research Committee no 4 T12A 035 30

REFERENCES

- BAILEY N.T.J., (1964), *The Elements of Stochastic Processes with Application to the Natural Sciences*. John Wiley & Sons, New York, London, Sydney.
- BELOGLAZOV K.F., (1947), *Principles of flotation process*. Metallurgizdat (in Russian).
- BOGDANOV O.S., HAINMAN V.J., MAXIMOV I.I., (1964), *On certain physical-mechanical factors determining the rate of flotation*, Proc. VII IMPC, New York, Gordon & Breach, p.169 – 174.
- BUSHELL C.H.G., (1962), *Kinetics of flotation*. Trans. AIME 223, 266-278.
- COLLINS G.L., JAMESON G.J., (1976), *Experiments on the flotation of fine particles. The influence of particle size and charge*, Chem. Eng. Sci., 31, 985-991.
- DRZYMALA J., (2001), *Podstawy mineralurgii*, Oficyna Wydawnicza Politechniki Wrocławskiej.
- GEIDEL T., (1985), *Probability of attachment between mineral grains and air bubbles and its relation to flotation kinetics*, Aufber. Technik 26, 287-294.
- HARRIS C.C., RIMMER H.W., (1966), *Study of two-phase model of the flotation process*, Trans. IMM, 75, 153-162.
- HARRIS C.C., (1978), *Multiphase model of flotation machine behaviour*, Int. J. Miner. Process., 5, 107-129.
- HONAKER R.Q., OZSEVER A.V., (2003), *Evaluation of the selective detachment process in flotation froth*, Minerals Engineering, 16, 975-982.
- IMAIZUMI T., INOUE T., (1963), *Kinetic consideration of froth flotation*, Proc. VI IMPC, Cannes 1963, pp. 581-593.
- INOUE T., IMAIZUMI T., (1968), *Some aspects of flotation kinetics*, Proc. VIII IMPC, Leningrad, vol. II, p.386-398.
- KAPUR P.C., MEHROTRA S.P., (1973), *Phenomenological model for flotation kinetics*, Trans. IMM, 82, 229-234.
- KAPUR P.C., MEHROTRA S.P., (1974), *Estimation of the flotation rate distributions by numerical inversion of the Laplace transform*, Chem. Eng. Sci., 29, 411-415.
- KRZAN M., MALYSA K., (2002), *Profiles of local velocities of bubbles in n-butanol, n-hexanol and n-nonanol solutions*, Coll. Surfaces. A: Physicochemical and Engineering Aspects, 207, 279-291.
- LASKOWSKI J.S., Xu Z, Yoon R.H., (1991), *Energy barrier in particle-to-bubble attachment and its effect on flotation kinetics*, Proc. XVII IMPC, Dresden, vol.2, 237-249.
- LAZIC P., CALIC N., (2000), *Boltzman's model of flotation kinetics*, Proc. XXI IMPC (Rome), vol.B, p.B8a 87-93.
- LITWINISZYN J., (1966), *Colmatage – scouring Kinetics in the Light of Stochastic Birth – Death Process*, Bull. Pol. Acad. Sci., XV, 907-911.
- LOVEDAY B.K., (1966), *Analysis of froth flotation kinetics*. Trans. IMM, 75, 219-225.
- MAKSIMOV I.I., EMELJANOV I.I., (1983), *The effect of turbulence on detachment process in the flotation pulp*. Obogascenie rud, no 2, 16-19.
- MALYSA E., (2000a), *Wpływ uziarnienia na wyniki flotacji węgla kamiennego*. Gosp. Surowcami Mineralnymi, 16, 29-41.
- MEHROTRA S.P., Kapur P.C., (1974), *The effects of aeration rate, particle size and pulp density on the flotation rate distribution*. Powder Technology, 9, 213-219.
- MEHROTRA S.P., KAPUR P.C., (1975), *The effect of particle size and feed rate on the flotation rate distribution in a continuous cell*, Int. J. Miner. Process., 2, 15-28.
- MELKICH V.I., (1963a), *A statistical theory of the flotation process*, Obogascenie rud, no 6, 17-20 (in Russian).
- MELKICH V.I., (1963b), *The equation of statistical dynamics of the flotation process*, Obogascenie rud. no 4, 26 – 28 (in Russian).
- MELKICH V.I., (1964), *Experimental verification of statistical model of the flotation process*. Obogascenie rud, no 5, 42-43 (in Russian).
- MIKA T., Fuerstenau D., (1968), *A microscopic model of the flotation process*, Proc. Proc. VIII IMPC, Leningrad, vol. II, pp.246-269.

- MLYNARCZYKOWSKA A., (2004), *Wpływ parametrów fizycznych i fizykochemicznych na kinetykę flotacji surowców na przykładzie węgla*, Praca doktorska, Biblioteka Główna AGH, Kraków, Poland
- NGUYEN VAN A., KMET S., (1992), *Collision efficiency for fine mineral particles with single bubble in a countercurrent flow regime*, Int. J. Miner. Process., 35, 205-223.
- POGORELYJ A.D., DEMIDO N.M., MATVEJEV I.I., (1961a), *The certain principles of performance of multi-cell flotation machine*, Izv. VUZ Tsvetnaja Metallurgia, no 6, 16-25 (in Russian).
- POGORELYJ A.D., (1961b), *On flotation characteristic of industrial pulp*, Izv. VUZ Tsvetnaja Metallurgia, no 5, 59-68 (in Russian).
- POGORELYJ A.D., (1962), *The range of application of Beloglazov equation of the flotation kinetics*, Izv. VUZ Tsvetnaja Metallurgia, no 1, 33-40 (in Russian).
- RADDOEV B.P., ALEXANDROVA L.B., TCHALJOVSKA S.D., (1990), *On the kinetics of froth flotation*, Int., J. Miner. Process., 28, 127-138.
- SABLIK J., (1998), *Flotacja węgla kamiennych*. Główny Instytut Górnictwa, Katowice, Poland.
- SCHIMMOLLER B.K., Luttrell G.H., Yoon R.H., 1993. *A combined hydrodynamic – surface force model for bubble – particle collection*, Proc. XVIII IMPC, Sydney, vol.3, p.751-756.
- SCHUHMANN R., (1942), *Flotation kinetics I. Methods for steady-state study of flotation problems*, J. Phys. Chem. 46, 891 – 902.
- SCHULZE H.J., (1977), *New theoretical and experimental investigations on stability of bubble particle aggregates in flotation: a theory on the upper particle size of floatability*, Int. J. Miner. Process., 4, 241-259.
- SCHULZE H.J., (1992), *Interface actions in mineral processes*, Aufber. Technik, 33, 434-443.
- SIWIEC A., (1982), *Models of selected treatment processes*, Sci. Bull. University of Mining and Metallurgy no. 884, 51-56 (in Polish).
- STACHURSKI J., (1970), *The Mathematical Model for the Ion-Extraction Flotation Process*, Archiwum Górnictwa, 15, 219-229.
- SUTHERLAND K.L., (1948), *Physical chemistry of flotation – XI kinetics of the flotation process*, J. Phys. Chem. 52, 394-425.
- SZATKOWSKI M., FREYBERGER W.L., (1985), *Kinetic of flotation with fine bubbles*, Trans. IMM, 94, 61-70.
- TILLE R., PANU G., (1968), *Some considerations on flotation kinetics*, Proc. VIII IMPC, Leningrad, vol. II, p.487-499.
- TOMLINSON H.S., FLEMING M.G., (1963), *Flotation rate studies*. Proc. VI IMPC, Cannes, Pergamon Press, Oxford – New York, pp. 563-579.
- TRAHAR W.J., WARREN L.J., (1976), *The flotability of very fine particles – a review*. Int. J. Miner. Process., 3, 103-131.
- VANANGAMUDI M., RAO T.C., (1986), *Modelling of batch coal flotation*. Int. J. Miner. Process., 16, 231-243.
- VARBANOV R., FORSSBERG E., HALLIN M., (1993), *On the modeling of the flotation process*, Int. J. Miner. Process., 37, 27-43.
- VOLIN M.E., SWAMI D.V., (1964), *Flotation rates of iron oxides*, Proc. VII IMPC, New York, Gordon & Breach, p.193-206.
- WOODBURN E.T., KING R.P., COLBORN R.P., (1971). *The effect of particle size distribution on the performance of a phosphate flotation process*, Metall. Trans., 2, 3163-3174.
- XU CHANGLIAN, (1985), *Kinetic models for batch and continuous flotation in a flotation column*, Proc. XV IMPC, Cannes, vol. III, p.16-27.
- YOON R.H., MAO L., (1996), *Application of extended DLVO theory, IV. Derivation of flotation rate equation from first principles*, J. Coll. Int. Sci. 181, 613-626.
- ZAIDENBERG I. S., LISOVSKIJ D.I., BUROVOJ I.A., (1964), *On certain approach to mathematical modelling of the flotation process*, Tsvetnye Metally, no 7, 24-29 (in Russian).
- ZUNIGA H.G., (1935), *Flotation recovery is an exponential function of its rate*, Bol. Soc. Nac. Min., Santiago 47, 83-86.

Brożek M., Młynarczykowska A., *Zastosowanie modelu stochastycznego do analizy kinetyki flotacji na przykładzie węgla*, Physicochemical Problems of Mineral Processing, 40 (2006), 31-44 (w jęz. ang).

Flotacja jako proces losowy, w którym zmienna losowa przedstawiająca liczbę ziaren wynoszonych do warstwy piany do określonego czasu t zależy od czasu, jest procesem stochastycznym. Na skutek turbulencji ośrodka w komorze flotacyjnej oprócz procesu adhezji ziaren do pęcherzyków zachodzi proces odwrotny o intensywności zależnej od zawartości popiołu, czyli proces odrywania ziaren od pęcherzyków. Tego typu sytuację najlepiej opisuje stochastyczny model procesu narodzin i giniecia. W artykule przedstawiono pokrótce założenia oraz równanie różniczkowe modelu jak również jego rozwiązanie w postaci równania kinetyki flotacji. Podana została interpretacja parametrów równania. Na podstawie empirycznych zależności uzysku ziaren flotujących w produkcie pianowym od czasu dla kilku próbek węgla, różniących się zawartością popiołu, wyliczono parametry równania kinetyki: stałą prędkości adhezji wypadkowej oraz stałą prędkości adhezji trwałej. Stała prędkości adhezji wypadkowej będąca sumą stałych prędkości adhezji trwałej i prędkości odrywania jest niezależna od zawartości popiołu, natomiast stała prędkości adhezji trwałej maleje ze wzrostem zawartości popiołu.

Trong DANG-VU*, Jan HUPKA*, Jan DRZYMALA**

IMPACT OF ROUGHNESS ON HYDROPHOBICITY OF PARTICLES MEASURED BY THE WASHBURN METHOD

Received March 15, 2006; reviewed; accepted May 15, 2006

Wettability and penetration kinetics of liquid into porous material were studied by the capillary rise method. The mass gain of the penetrating liquid in a tube filled with glass beads was measured vs. time. Two types of glass beads surfaces: unmodified (smooth), modified (rough), were used to investigate the influence of porous material surface on wettability and penetration kinetics. It was found that the surface roughness has a significant effect on the penetration kinetics but not on the contact angle. The penetration rate of liquids into porous material with the rough surface was found to be over two-fold greater than that for porous materials with unmodified (smooth) surface. It is well known that the surface roughness has a significant effect on the macroscopic contact angle for flat surfaces. Our experiments showed that the contact angle of a collection of particles does not depend on their surface roughness. It may suggest that the surface roughness does not influence the microscopic contact angle.

Key words: roughness, capillary rise, penetration kinetics, porous media, flotation

INTRODUCTION

The wettability of surfaces is an important property in many applications including flotation and washing. The wettability is generally characterized by the contact angle between liquid, solid surface, and gaseous environment. The contact angle has been mostly studied for flat surfaces as a function of liquid drop size, heterogeneity and roughness of the surface (Kwok and Newmann, 1991; Miller *et al.*, 1996; Drelich and Miller, 1994; Adamson, 1967). For particulate materials, particles forming a bed and for porous material, however, the contact angle has not received the same attention.

The roughness has a significant effect on the macroscopic contact angle of flat surfaces (Adamson, 1967). However, no study on surface roughness of particles

* Department of Chemical Technology, Gdansk University of Technology, 80-952 Gdansk, Poland.

** Department of Mining Engineering, Wroclaw University of Technology, 50-370 Wroclaw, Poland.

forming porous materials was found in the literature. The present study is an extension of the effort (Dang-Vu and Hupka, 2005; Dang-Vu et al., 2005) to investigate the contact angle of porous materials and penetration kinetics using the capillary rise method.

EXPERIMENTAL

The characteristics of the glass beads used to form a bed of particles resembling porous material is presented in Table 1. The glass beads were provided by the Interglass Ltd. Walbrzych, Poland.

Table 1. Characteristics of bed of particles

Symbol	Pore size [μm]	Porosity [m^3/m^3]	Bulk density [kg/m^3]	Surface property	Source
A	60 – 110	0.34	1589	smooth (unmodified)	*
B	150 – 250	0.33	1619	smooth (unmodified)	*
C	150 - 250	0.30	1678		*
D	150 – 250	0.36	1556	rough (modified)	this work

* - Dang-Vu and Hupka, 2005; Dang-Vu et al., 2005

Bed D was obtained after performing a surface modification, which can be summarized as follows (Dang-Vu, 2005):

1. Glass beads were dipped in 10 % hydrofluoric acid for 5 min
2. Then, they were dipped in etching solution for 10 min. The etching solution consisted of distilled water (35%), 40%-hydrofluoric acid (30%), potassium hydrofluoride (KHF_2) (35%)
3. Glass beads were again dipped in hydrofluoric acid for 3 minutes
4. Modified glass beads were then washed with distilled water and dried over night at 120°C

The characteristics of the wetting liquid used in this study is shown in Table 2.

Table 2. Characteristics of liquids used for capillary rise experiments (20°C)

Wetting liquid	Density [kg/m^3]	Viscosity [$\text{mPa}\cdot\text{s}$]	Surface tension [mJ/m^2]
Water	997	1.01	72.3
Toluene	862	0.55	27.8
Ethanol	785	1.20	22.0
Heptane	684	0.41	20.3
Octane	703	0.55	21.8
Decane	730	0.92	23.9

The capillary rise experiment, also called the Washburn method, was used to study the impact of surface properties of porous materials on wettability and penetration rate. The penetration height of the liquid in a 0.7 cm diameter glass tube filled with glass beads was measured vs. time. The increase of the penetrating liquid in glass beads bed was recorded every two seconds using an electronic balance. Details of the experimental apparatus and procedures are given elsewhere (Dang-Vu and Hupka, 2005).

RESULTS AND DISCUSSION

Electron scanning microscope images of the glass bead before and after surface modification are presented in Fig. 1. A dull surface of the glass bead after modification was clearly observed. The depth of the groove of the modified surface roughness is in the range of 5 to 15 μm . It is worth to note that after the surface modification the mass of particle decreased, however, its radius remained unchanged.

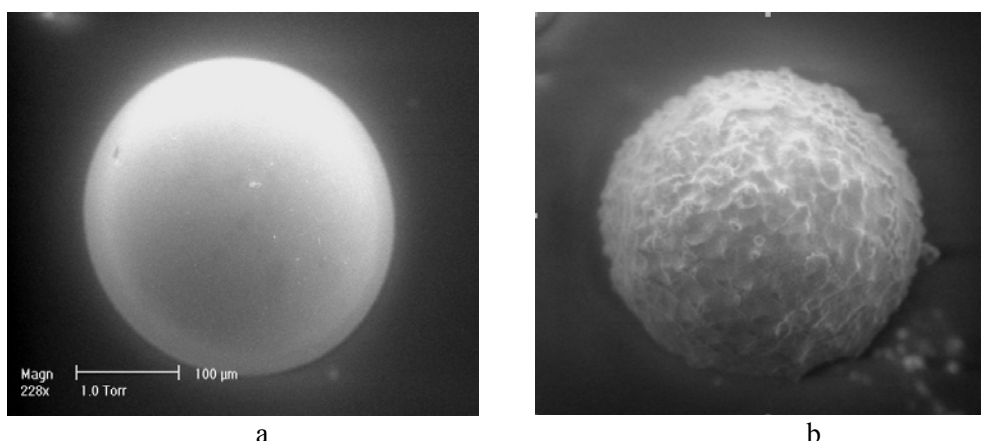


Fig. 1. The surface of glass beads before (a) and after (b) modification

The relationships between the square of liquid mass and penetration time for particles with the modified surface are shown in Fig. 2. As can be seen for all the wetting liquids, the relationships are linear and in good agreement with the Washburn equation. Water was the fastest penetrating liquid while ethanol was the slowest. The same relationships for beds A, B, and C have been presented previously elsewhere (Dang-Vu and Hupka, 2005).

It is worth note that in our previous report (Dang-Vu and Hupka 2005) in the case of the unmodified glass beads with mean radius of 60 – 110 μm the relationship between the squared mass of liquid and penetration time was linear, but for that with mean radius of 150 – 250 μm the relationship between the squared mass vs. time was parabolic for the some wetting liquids. In the present study, although the particles

have large mean radius (150 – 250 μm), the relationship m^2 vs. t is linear for all tested liquids, indicating the effect of surface roughness on the penetration kinetics. This can be explained by the fact that an intergranular space between particles with rough surface is more even than that of unmodified surface. The penetration of liquid becomes more even resulting in a linear relationship between the squared liquid mass and penetration time.

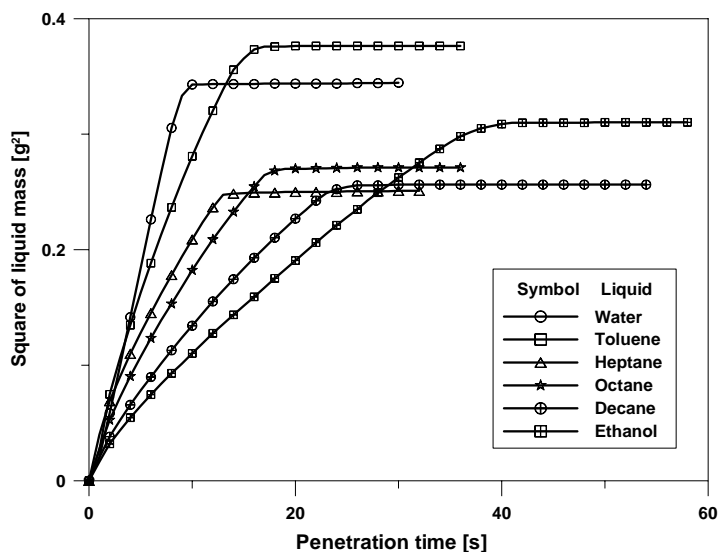


Fig. 2. Relationship between the square of liquid mass and penetration time for bed D

Pictures showing penetration of liquids into beds D and B are presented in Fig. 3. As can be seen in Fig. 3 the liquid penetrated more evenly into bed D than bed B. In the case of bed D (rough surface), liquid penetrated to the top of the bed surface and wetted the whole top surface at the same time. However, in the case of bed B (smooth surface), the liquid penetration is not even. In the top of the bed surface only some wetting regions were observed.

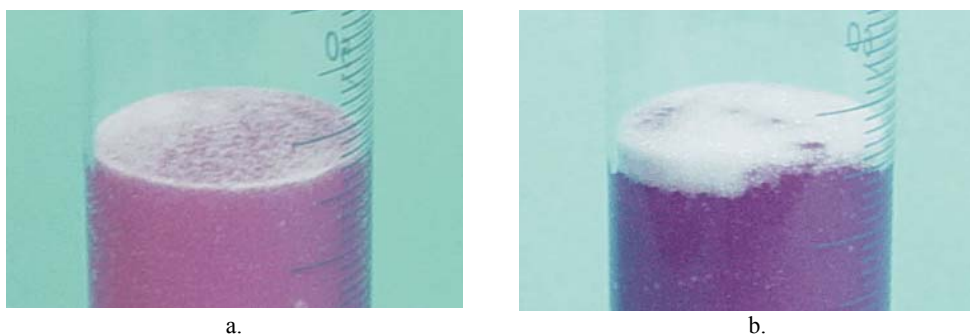


Fig. 3. Penetration of liquid into bed D (a) and B (b)

The effect of surface roughness of particles on penetration rate can be also observed in Fig. 4, which presents the slope of the m^2 vs. t curve for different beds. The results for unmodified particles (bed A, B, and C) were from our previous report (Dang-Vu and Hupka, 2005). As can be seen, the order of the slope for the wetting liquid in bed D is the same as that in bed A, B, and C. However, the value of the slope for bed D is over two-fold greater than that for the rest of the beds. Liquid penetrates into bed D over two-fold faster than beds A, B, C, indicating a significant effect of the surface roughness on the penetration rate.

As shown in Fig. 4 for alkane hydrocarbon, the penetration rate decreases with the chain length (number of carbon atom in the chain). A similar result has been reported in literature (Dang-Vu *et al.*, 2002; Gonzalez-Martin *et al.*, 2001; Prestidge and Tsatouhas, 2000, Hupka *et al.*, 2003)

It can be concluded from Fig. 2 that water penetrates the beds faster than toluene. The slope for toluene was calculated and used for determination of the contact angles of the studied liquid in relation to the toluene which was arbitrarily taken as the reference liquid due to its largest product of $\frac{m^2}{t} \cdot \frac{\eta}{\rho^2 \gamma}$ (Dang-Vu, 2005). The results of calculations are presented in Table 3.

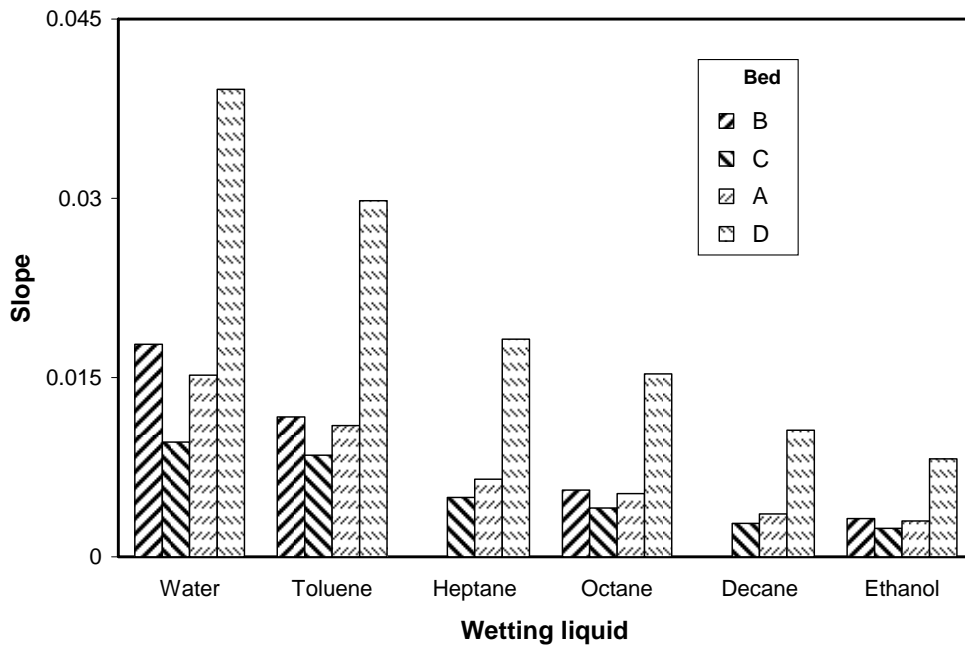


Fig. 4. The slope of m^2 vs. t curve for glass beads: A - unmodified small particles with pore size of 60 – 110 μm ; B - unmodified large particles with pore size of 150 – 250 μm , C - unmodified particles with pores size of 60 – 250 μm ; and D - large particles with pore size of 150 – 250 μm and modified surface (rough)

Table 3. Slope and contact angles for bed D

Wetting liquid	Slope of m^2 vs. t curve	Contact angle [deg]
Water	0.039	47
Toluene	0.030	* (0)
Heptane	0.018	13
Octane	0.015	15
Decane	0.011	18
Ethanol	0.008	26

* Toluene was assumed to be the reference wetting liquid

As shown in Table 3, for alkane hydrocarbon the contact angle decreases with the chain length. Similar result has been reported in literature (Dang-Vu *et al.*, 2002; Gonzalez-Martin *et al.*, 2001; Prestidge and Tsatouhas, 2000).

Similarly to the penetration kinetics study, in order to observe the effect of surface roughness on the contact angle, the calculated contact angle for bed D was plotted together with that for bed A, B, and C in Fig. 5. As can be seen there, the relative contact angle of liquids on the modified rough surface is comparable to that of unmodified particles. In contrary to penetration kinetics, the effect of surface roughness on the contact angle is insignificant.

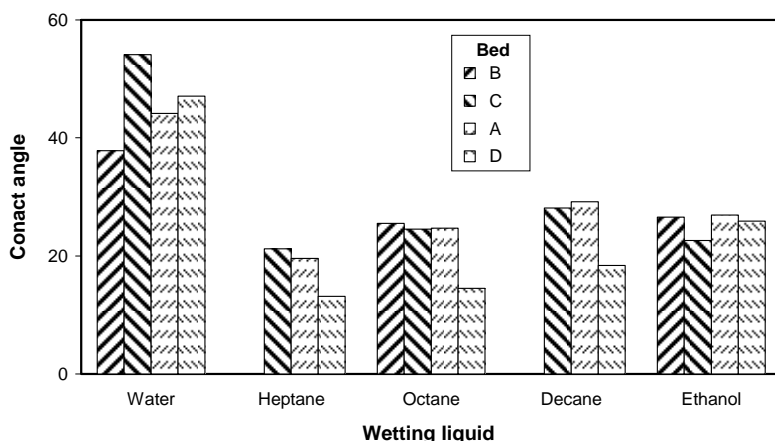


Fig. 5. Contact angle for beds A, B, C, D. A - unmodified small particles with pore size of 60 – 110 μm ; B - unmodified large particles with pore size of 150 – 250 μm , C - unmodified particles with pores size of 60 – 250 μm ; and D - large particles with pore size of 150 – 250 μm and modified surface (rough)

In the capillary rise (Washburn) method, the contact angles are calculated from the ratio of penetration rate of the reference wetting liquid and the studied liquid (Dang-Vu, 2005). The surface roughness of the particles increases the penetration rate of all liquids, i.e. the studied and reference liquid. Therefore, the variation in the penetration rate of the reference wetting and studied liquid is small, resulting in small variation in contact angle value of both liquids.

CONCLUSIONS

This investigation shows that the roughness of surface has a significant effect on the kinetics of liquid penetration of a collection of particles but not on the contact angle. The penetration rate of a liquid into porous material with a rough surface is over two-fold greater than that for smooth surfaces. This finding may have a significant importance in various phenomena, especially flotation of particles. The results of this investigation indicate that the hydrophobicity of flotation, in contrary to kinetics of flotation, should not be influenced by the roughness of particles.

ACKNOWLEDGEMENTS

The authors wish to thank the European Union SSA FP6 SURUZ project for support.

REFERENCES

- ADAMSON, A.W., (1967), *Physical Chemistry of surfaces*, Wiley.
- CRAWFORD R., KOOPAL L. K., RALSTON J., (1987), *Contact angles on particles and plates*, *Colloids Surf.* 27, 57-64.
- DANG-VU T., (2005), *PhD dissertation*, Gdansk University of Technology, Gdansk, Poland,
- DANG-VU T., HUPKA J., NALASKOWSKI J., (2002) *Important of time evaluation in capillary rise method*, *Proceedings of The Third International Conference Environmental Technology for Oil Pollution*, 08-11.09.2002, Gdańsk, 2, 139-145.
- DANG-VU T., HUPKA J., (2005), *Characterization of porous materials by capillary rise method*, *Physicochem. Problems Min. Process.* 39 47-65.
- DANG-VU T., HUPKA J., ARANOWSKI R., MISIUK S., (2005), *Analysis of different approaches of capillary rise method for characterization of porous materials*, *Proceedings of the 4th International Conference "Oils & Environment" AUZO 2005*, June 23-23, 2005, Gdansk, Poland, p. 184-191.
- DRELICH J., MILLER J. D., (1994), *The effect of solid surface heterogeneity and roughness on the contact angle/drop (bubble) size relationship*, *Colloid Interface Sci.*, 164, 252-259.
- GONZALEZ-MARTIN M. L., JANCZUK B., LABAJOS-BRONCANO L., BRUQUE J. M., GONZ C. M., (2001), *Analysis of the silica surface free energy by the imbibition*, *J. Colloid Interface Sci.*, 240, 467-472.
- HUPKA J., DANG-VU T., WERSOCKI S., (2003), *Badanie osadu czynnego jako sorbentu oleju*, *Inżynieria Ekologiczna*, 9, 145-153.
- KWOK D. Y., NEWMANN A. W., *Contact angle measurement and contact angle interpretation*, *Adv. Colloid Interface Sci.*, 81 (1999) 167-249.
- MILLER J. D., VEERAMASUNENI S., DRELICH J., YALAMANCHILI M. R., YAMAUCHI G., (1996), *Effect of roughness as determined by atomic force microscope on the wetting properties of PTFE thin films*, *Polym. Eng. Sci.*, 36, 1849-1855.
- PRESTIDGE C. A., TSATOUHAS G., (2000), *Wettability studies of morphine sulphate powders*, *Int. J. Pharm.*, 198, 201-212.

Trong Dan-Vu, J. Hupka, J. Drzymala, *Wpływ szorstkości powierzchni ziarn na ich hydrofobowość mierzona metodą Washburna*, *Physicochemical Problems of Mineral Processing*, 40 (2006), 45-52 (w jęz. ang.).

Badano zwilżalność oraz kinetyka penetracji cieczy w warstwie ziarn mineralnych metodą wzniesienia kapilarnego (metoda Washburna). Mierzono wzrost masy jako funkcję czasu dla układu w którym następowała penetracja cieczy w rurkę wypełnioną kulkami szklanymi. Użyto dwóch typów kulek szklanych: niemodyfikowanych o gładkiej powierzchni oraz modyfikowanych o szorstkiej powierzchni. Stwierdzono, że szorstkość powierzchni znacząco wpływa na szybkość penetracji cieczy w rurkach z ziarnami, ale nie wpływa na wyliczony kąt zwilżania, który jest miarą hydrofobowości układu. Szybkość penetracji cieczy w układ z kulkami o szorstkiej powierzchni był dwukrotnie większy niż z ziarnami w postaci niemodyfikowanych gładkich kulek. Wiadomo, że chropowatość powierzchni ma wpływ na makroskopowy kąt zwilżania płaskich powierzchni. Jednakże nasze eksperymenty wykazały, że dla materiałów ziarnistych tworzących warstwę kąt zwilżania nie zależy od porowatości ziarn. Może to sugerować, że mikroskopowy kąt zwilżania mało zależy od kształtu powierzchni.

Danuta SZYSZKA*, Jan DRZYMALA*, Jacek ŁUCZYŃSKI**,
Kazimiera A. WILK**, Jacek PATKOWSKI***

CONCENTRATION OF α -TERPINEOL AND (2-DODECANOYLOXYETHYL)TRIMETHYL AMMONIUM BROMIDE REQUIRED FOR PREVENTION OF AIR BUBBLE COALESCENCE IN AQUEOUS SOLUTIONS

Received May 15, 2006; reviewed; accepted June 30, 2006

Flotation is a widely used process in mineral processing. It utilizes different reagents including, collectors and frothers. It was proposed by Cho and Laskowski to use the so-called critical coalescence concentration (CCC) for characterization of flotation frothers. In this paper the CCC values were determined for α -terpineol, which is widely used as a frother in laboratory flotation tests, and for (2-dodecanoyloxyethyl)trimethylammonium bromide (DMM-11) which represents a broad family of reagents known as chemodegradable cationic surfactants. The CCC for α -terpineol was found to be 0.16 mmol/dm³ while for DMM-1, depending of the procedure of approximation, between 0.06 and 0.14 mmol/dm³.

Key words: critical coalescence concentration, flotation, bubbles, surfactants

INTRODUCTION

In 2002 Cho and Laskowski (2002a,b) introduced a concept of CCC which seems to be an important parameter characterizing surface active reagents. CCC is the concentration of a reagent which prevents bubbles in aqueous solutions from coalescence. The CCC, coupled with the dynamic frothing index (DFI) (Małysa *et al.*, 1978, 1982; Czarnecki *et al.*, 1982) is a good base for assessment of surfactants for flotation. According to Laskowski (2004), Grau and Heiskanen (2003) and Grau *et al.*

* Wrocław University of Technology, Department of Geoengineering, Mining and Geology,
Wybrzeże Wyspińskiego 27, 50-370 Wrocław, Poland.

** Wrocław University of Technology, Department of Chemistry, Wybrzeże Wyspińskiego 27,
50-370 Wrocław, Poland.

*** UMCS, Department of Radiochemistry and Colloid Chemistry, ul. M.C. Skłodowskiej 3,
20-031 Lublin, Poland.

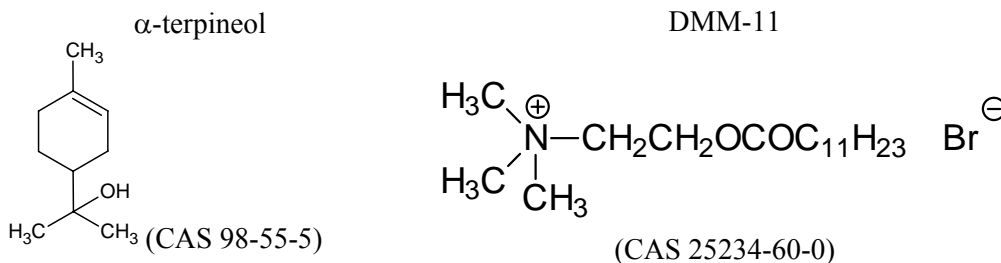
(2005), selective surfactants are those which have high CCC and low DFI while powerful frothers assume high DFI and low CCC values.

Table 1. CCC for different surfactants (after Laskowski, 2004)

Surfactant	CCC, mmol/dm ³
MIBC (methylisobutylcarbinol)	0.11
(PO)1 (oxypropylene methyl ether)	0.52
(PO)2 (dioxypropylene methyl ether)	0.17
DF-200 (trioxypropylene methyl ether)	0.089
DF-250 (tetraoxypropylene methyl ether)	0.033
DF-1012 (polyoxypropylene methyl ether, n=6.3)	0.015

Thus, the CCC is a useful parameter, but only several surfactants have been investigated so far in order to establish their CCC (Cho *et al.*, 2002a,b; Laskowski (2003, 2004). They are presented in Table 1. The goal of this research is to determine the CCC for two reagents, which represent two different families of surfactants. The first one is α -terpineol which is widely used as frother in laboratory flotation tests for ores and raw materials. The other surfactant is (2-dodecanoyloxyethyl) trimethylammonium bromide (denoted as DMM-11) and it represents a broad family of reagents known as chemodegradable cationic surfactants (Wilk *et al.*, 1994). The structures of the investigated surfactants are given in Table 2.

Table 2. Structures of the investigated surfactants



EXPERIMENTAL

MATERIALS

α -terpineol (C₁₀H₁₈O or dl-p-menth-1-en-8-ol) and DMM-11 (C₁₇H₃₆BrNO₂ or (2-dodecanoyloxyethyl)trimethylammonium bromide) were tested. α -terpineol was purchased from Fluka while the DMM-11 surfactant was synthesized in the Department of Chemistry of Wrocław University of Technology starting from N,N-dimethylaminoethyl ester of dodecanoic acid (Łuczyński, 2000) and then by quaternization in an ethereal solution using methyl bromide (Obląg *et al.*, 2001). The t_m of DMM-11 is 135 – 140 °C while the CMC is 5.9·10⁻³M. Then, the obtained salt was purified by a repeated crystallization, first from the CHCl₃ – n-hexane mixtures,

and next from the methanol–diethyl ether mixtures. A high purity of DMM-11 was proved by elementary analysis, surface tension measurements, and NMR data.

The stock solution of α -terpineol contained 0.05 wt.% of the frother while DMM-11 was used from daily prepared aqueous solutions.

α -terpineol was dissolved in distilled water by applying vigorous stirring for 16 h at 40°C while no special procedure of dissolution was applied for DMM-11 which easily dissolves in water. Some additional properties of the surfactants used in the experiments are given in Table 3. Double distilled water was used in all experiments.

Table 3. Selected properties of surfactants used in this study (at 25°C)

Property	α -terpineol	DMM-11
Chemical formula	$C_{10}H_{18}O$	$C_{17}H_{36}BrNO_2$
Supplier	Fluka	Chemistry Department of The Wroclaw University of Technology
Molecular weight (g/M)	154.25	326.00
Physical state	solid	solid
Solubility, g/dm ³	1.987	no limit
Density, g/cm ³	0.948	not determined

Methods

Bubbles have been generated in an open rectangular cell of 89 cm³ in volume (Fig. 1). They have been generated with a small plastic tube at an airflow rate of about 5 dm³/min. This procedure was applied for different concentrations of the surfactants. The process of bubble formation along with the bubbles approaching the water-air interface was photographed and recorded with a digital camera. Six frames containing at least 50% of well shaped and visible bubbles were chosen from each recorded experiment. The photographs were later used for bubble diameter measurements. The average size of the bubbles was calculated as an arithmetical mean for all (usually ~200) bubbles seen in the photograph.

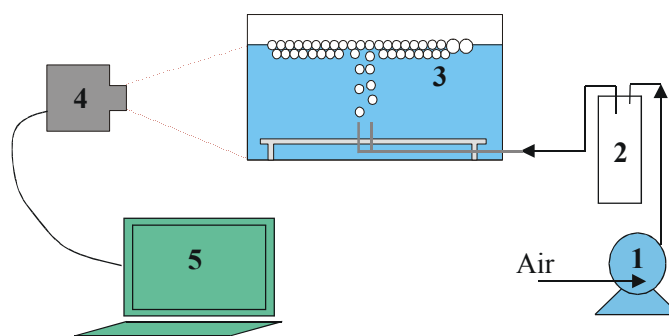


Fig. 1. Experimental set-up for CCC measurements:
1) peristaltic pump, 2) equalizing tank, 3) cell, 4) digital camera, 5) computer

RESULTS AND DISCUSSION

Figures 2 and 3 show the size of bubbles as a function of surfactant concentration for α -terpineol and DMM-11, respectively. Figures 2a and 3a present the bubble in distilled water. At higher frother concentrations ($c \gg CCC$) the size of bubbles becomes constant and equal to the size of the original, newly formed, bubbles. Near and below the CCC, the bubbles undergo coalescence, their size increases and the foam formed by the surfactants is very unstable. The foam exists only during the bubbling the gas through the solution and collapses when the percolation is stopped. Figures 4 and 5 provide the critical coalescence concentration (CCC) determined by a graphical method similar to that used for the CMC determination.

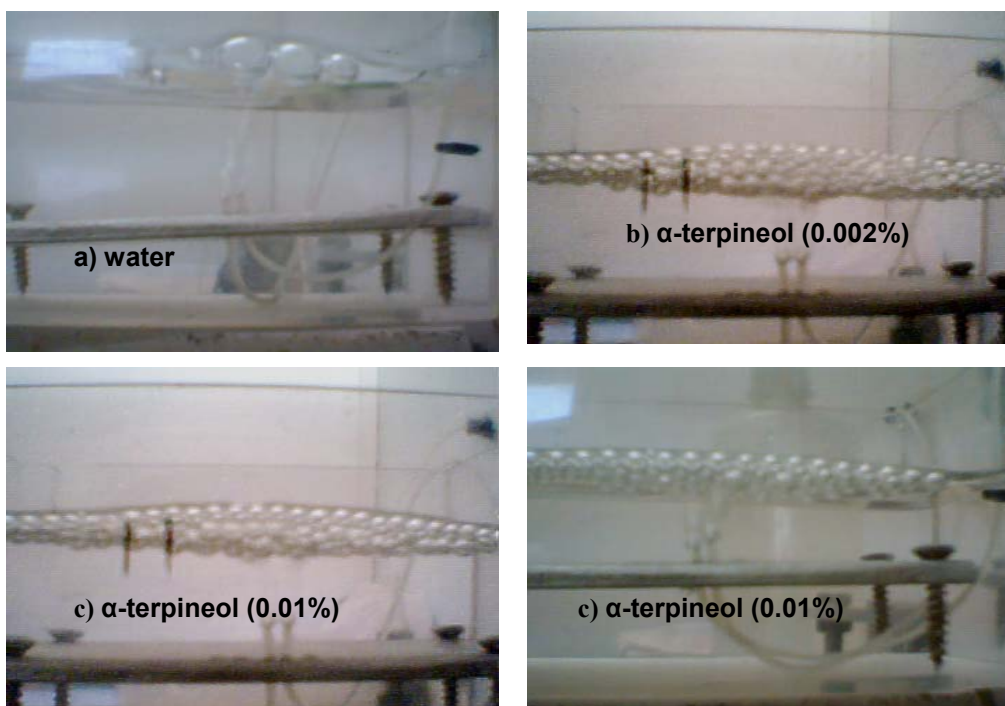


Fig. 2. Bubbles formed in aqueous solutions containing α -terpineol: a) 0%, b) 0.002%, c) 0.01%, and d) 0.05% (wt %)

According to Figs 4 and 5, the CCC value for α -terpineol is about 0.16 mmol/dm^3 while for DMM-11 is above 0.05 mmol/dm^3 , that is, depending on the procedure of approximation, somewhere between 0.06 and 0.14 mM . A comparison of the CCC values of the investigated here surfactants with those characterized by Laskowski *et al.* (2004) shows, that the CCC for α -terpineol is closed to that of MIBC, while for DMM-11 is similar to that of polyoxypropylene methyl ether frothers with n between two ((PO)2) and three (DF-200).

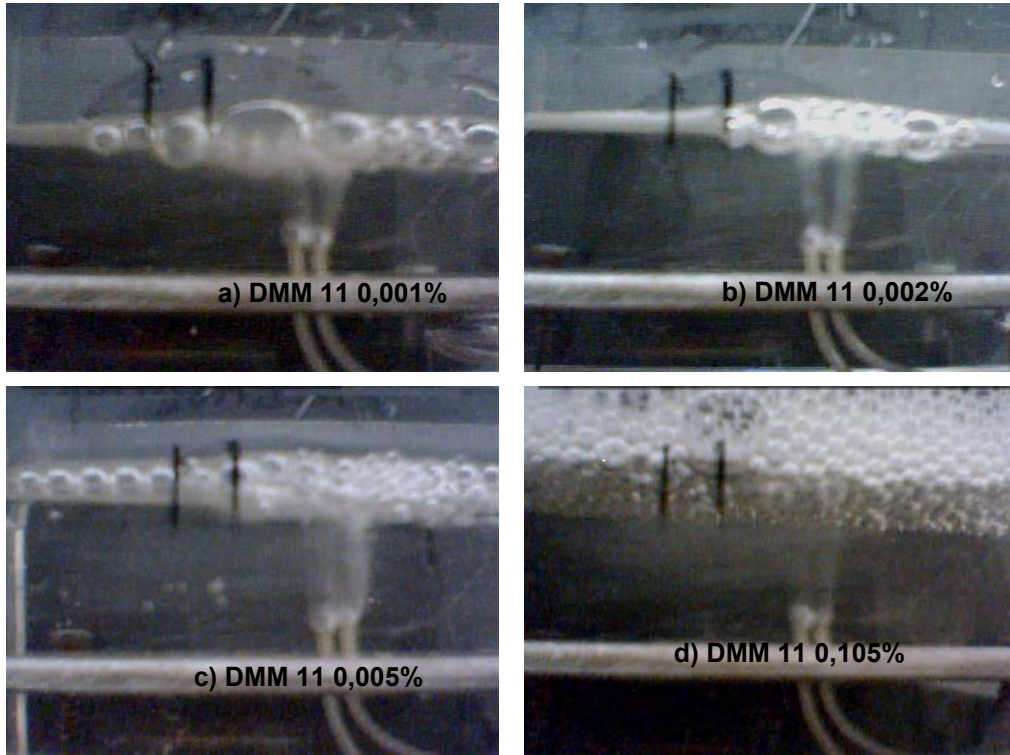


Fig. 3. Bubbles formed in aqueous solutions containing DMM-11: a) 0%, b) 0.002%, c) 0.005%, and d) 0.105%

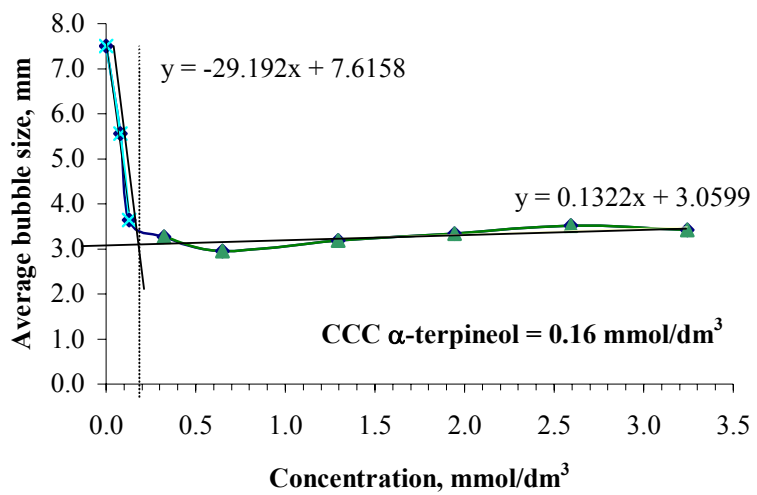


Fig. 4. Critical coalescence concentration (CCC) for α -terpineol

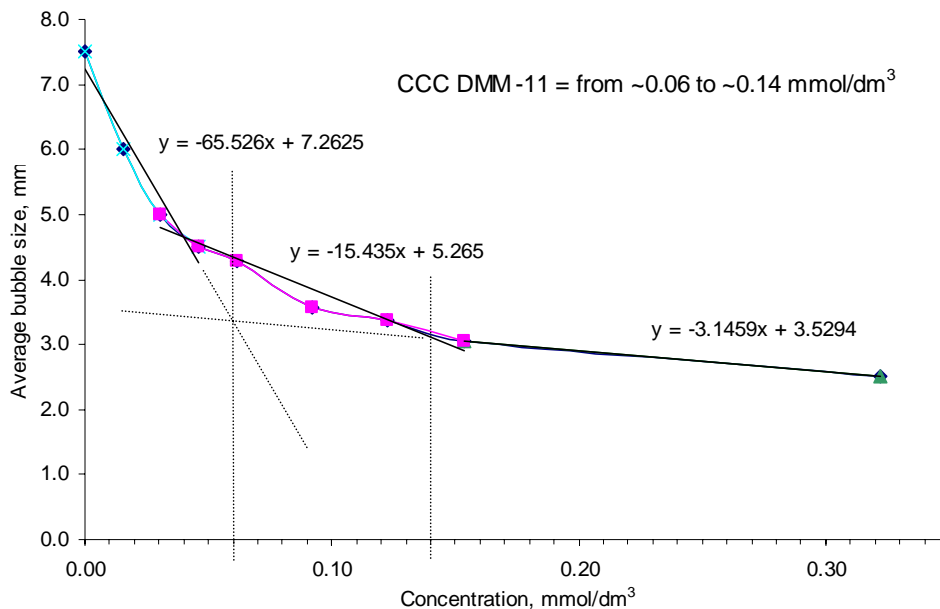


Fig. 5. Critical coalescence concentration (CCC) for DMM-11

CONCLUSION

The CCC of α -terpineol is about 0.16 mmol/dm³ and the CCC of DMM-11 is somewhere between 0.06 and 0.14 mmol/dm³.

ACKNOWLEDGEMENTS

This work was partially financed by a grant from the Wrocław University of Technology (W-6/I-11, zlec. 342 773, 2006/7). The authors wish to thank the European Union SSA FP6 SURUZ project for support.

REFERENCES

- CHO, Y.S., LASKOWSKI, J. S., (2002a), *Effect of Flotation Frothers on Bubble Size and Foam Stability*, Int. J. Min. Proc. Vol. 64, pp. 69-80.
- CHO, Y.S., LASKOWSKI, J. S., (2002b), *Bubble Coalescence and Its Effect on Bubble Size and Foam Stability*, Canadian J. Chem. Eng. Vol. 80, pp. 299-305.
- CZARNECKI, J., MAŁYSA, K., POMIANOWSKI, A., (1982), *Dynamic Frothability Index*, J. Coll. Interface Sci. Vol. 86, pp.570-572.
- GRAU, R., HEISKANEN, K., (2003), *Gas Dispersion Measurements in a Flotation Cell*, Minerals Engineering, 16(11), 1081-1089
- GRAU, R., LASKOWSKI J. S., HEISKANEN, K., (2005), *Effect of Frothers on Bubble Size*, Int. J. Mineral Process, pp. 225-233

- LASKOWSKI, J. S., (2003). *Fundamental Properties of Flotation Frothers*, Proc 22nd INT. Mineral Processing Congress, Cape Town, Vol. 2, pp. 788-797.
- LASKOWSKI, J. S., (2004), *Testing Flotation Frothers*, Physicochemical Problems of Mineral Processing, Vol. 38, pp. 13-22.
- ŁUCZYŃSKI, J., (2000), *Aminoethylesters of Fatty Acids as Lysosomotropic Substances*, Ph.D. Thesis, Politechnika Wroclawska, Wrocław, Poland
- MAŁYSA, K., CZUBAK-PAWLIKOWSKA, J., POMIANOWSKI, A., (1978), *Frothing Properties of Solutions and Their Influence on the Floatability*, Proc. 7th Int. Congress Surface Actives Substances, Moscow, Vol. 3, pp.513-520.
- OBLĄK, E., LACHOWICZ, T.M., ŁUCZYŃSKI, J., WITEK, S., (2001), *Comparative Studies of the Biological Activities of Lysosomotropic Aminoesters and Quaternary Ammonium Salts on the Yeast *Saccharomyces cerevisiae**, Cell. Mol. Biol. Lett., 6, 871-880
- WILK, K. A., BIENIECKI, A., BURCZYK, B., SOKOŁOWSKI, A., (1994), *Synthesis and Hydrolysis of Chemodegradable Cationic Surfactants Containing the 1,3- Dioxolane Moiety*, J. Am. Oil Chem. Soc., Vol. 71, 81.

Szyska D., Drzymała J., Luczyński J., Wilk K.A., Patkowski J., *Stężenie α -terpinolu i bromku (2-dodekanoyloksyetylo)trimetyloamoniowego wymagane dla zapobiegania koalescencji pęcherzyków powietrza w roztworach wodnych*, Physicochemical Problems of Mineral Processing, 40, (2006) 53-59 (w jęz. ang.).

Flotacja jest jednym z najczęściej stosowanych procesów w mineralurgii. Wśród najważniejszych czynników flotacji są reagenty, a w szczególności stosowane odczynniki pianotwórcze (spieniacze). W celu charakteryzowania spieniaczy flotacyjnych Cho i Laskowski wprowadzili pojęcie krytycznego stężenia koalescencji (CCC). W pracy wyznaczano CCC dla typowego spieniacza stosowanego w procesie flotacji, jakim jest α -terpineol oraz dla DMM-11 reprezentującego surfaktanty z grupy chemodegradowalnych estrów kationowych. Stwierdzono, że CCC dla α -terpineolu wynosi 0.16 mmol/dm³, podczas gdy dla DMM-11, w zależności od sposobu aproksymacji, wynosi ono od 0.05 do 0.15 mmol/dm³.

Ashraf M. AMER*

KINETICS OF ALKALINE PRESSURE LEACHING OF MECHANICALLY MODIFIED ZIRCON CONCENTRATE

Received March 15, 2006; reviewed; accepted May 15, 2006

Hydrometallurgical processing of zircon concentrate separated from Egyptian black sands is attained through leaching with sodium hydroxide of mechanically pretreated zircon concentrate under relatively high temperature (260°C). The effects of temperature, sodium hydroxide concentration, grinding time, grain size, and leaching time were studied as well as the kinetics of the leaching process.

Key words: zirconium, zircon, mechanical activation, pressure leaching

INTRODUCTION

Zirconium is present fairly abundantly in the earth's crust but it is difficult to remove and has limited use outside the nuclear industry. The industrially important zirconium minerals are baddelyite (ZrO_2) and zircon ($ZrSiO_4$). Baddeleyite is relatively scarce, but zircon is available in abundant quantities in concentrated form and is the most important raw material for producing metallic zirconium, its alloys, and its compounds. Main occurrence of zircon in Egypt is a constituent of beach sands along with ilmenite and monazite. Zircon concentrate is separated from its heavy minerals by a gravity concentration followed by magnetic and electrostatic processing. (El-Hinawi, 1964).

Pyrometallurgical methods are used for processing of zircon concentrate which include fusion with caustic soda with the formation of acid soluble zirconate (MacDonald, et al 1982), sintering with lime or chalk and formation of calcium zirconate (Krisham et al, 1986; Mohammed and Daher, 2002). Thermal dissociation by plasma are commonly used for the production of technical and pure grade ZrO_2 in addition to the chlorination of a mixture of zircon and carbon to produce $ZrCl_4$ and has

* Environmental Science Dept., Faculty of Science, Alexandria Univ., Egypt

become the most popular method for producing $ZrCl_4$ (Abdel-Rehim and Khalil, 1975; Staumbaugh and Miller, 1983).

The aim of this work is to discuss a new process for extraction of zirconium from zircon concentrate instead of pyrometallurgical processing using mechanochemical treatment where grinding is carried out in the presence of sodium hydroxide and is followed by pressure leaching in autoclave.

Mechanical activation, usually done via energetic milling, has been demonstrated to accelerate the leaching of sulphide minerals (Welham 2001a) as well as of non sulphide minerals (Amer, 2000; 2001; 2002).

EXPERIMENTAL

The studied zircon concentrate was separated from black sands. The chemical analysis of studied concentrate is given in Table 1.

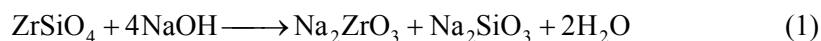
Table 1. Chemical analysis of zircon concentrate

Component	%
ZrO_2	64.50
SiO_2	32.58
Fe_2O_3	1.14
Al_2O_3	0.22
K_2O	0.03
TiO_2	0.9

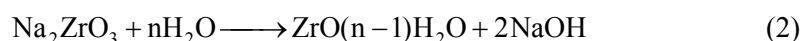
APPARATUS AND PROCEDURE

A stirred ball mill with a vertical attritor (PE 0.75, Netzsh, Selb) was used with steel balls of 2.0 mm diameter. The rotation rate was maintained at 1200 min^{-1} . Grinding was carried out in the presence of sodium hydroxide solution. The pulp from the attritor was charged into the autoclave and agitated by an impeller at 1200 min^{-1} . A complete description of the leaching system was given elsewhere (Levenspiel, 1972).

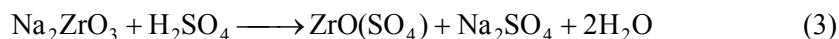
The reaction of zircon with caustic soda solution lead to formation of sodium zirconate and sodium silicate.



With dilution, sodium silicate is removed while sodium zirconate is hydrolysed to hydrated zirconia.



The resultant hydrated cake is dissolved in sulphuric acid as given in the following reaction:



After the complete dissolution of the cake, sulphate solution was filtered off and the impurities (Fe, Cu, Mg, Ti, Al, Na and Si) were analyzed in the solution by atomic spectrometry while zirconium was gravimetrically analyzed using mandelic acid as precipitant.

Effects of the following factors on the course of leaching of zircon concentrate were studied:

Temperature	200°-260°C
Concentration of sodium hydroxide	0.1-0.8M
Grinding time	0-5 hrs
Leaching time	30-300 min
Grain size	12-58 μm

RESULTS AND DISCUSSION

EFFECT OF TEMPERATURE

Figure (1) shows leaching results of zircon at the temperature ranging from 200 to 260°C. Temperature has a significant effect on the dissolution of zirconium. About 85% of zirconium present in zircon concentrate is leached at 260°C after 90 min. The surface reaction model was applied to determine the activation energy. Data presented in Figure (1) are plotted according to the following equation:

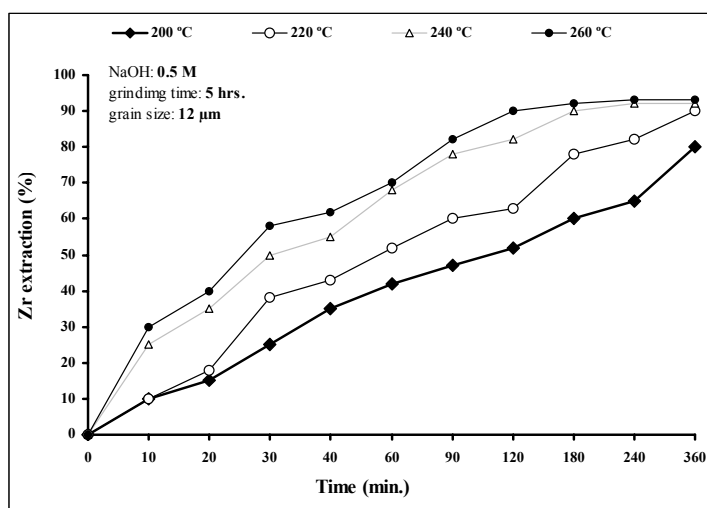


Fig. 1. Course of zirconium leaching at different temperatures

$$1 - (1 - \alpha)^{1/3} = k t \quad (4)$$

where:

- k – the apparent reaction rate constant,
- α – the fraction of zirconium leached,
- t – leaching time in sec^{-1} .

and presented in Figure (2). Slopes of curves in Figure 2 according to $d[1 - (1 - \alpha)^{1/3}] / dt$ represent the apparent rate constants (k). These constants as plotted according to the Arrhenius equation are shown in Figure (3). The activation energy was found to be equal to 72 kJ/mole. Its magnitude confirms a surface reaction-control mechanism.

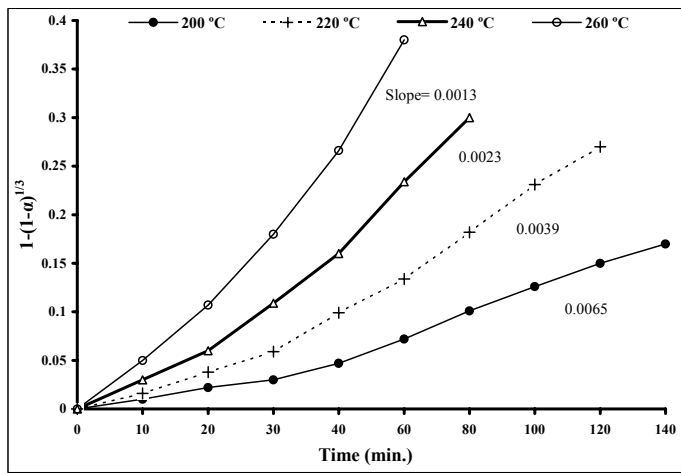


Fig. 2. A plot of $1-(1-\alpha)^{1/3}$ versus time for various temperatures

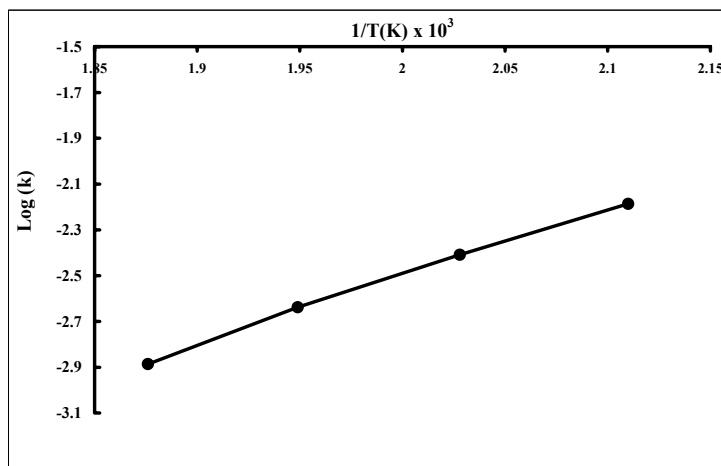


Fig. 3. Arrhenius plot for determination of activation energy

EFFECT OF PARTICLE SIZE

Figure (4) shows the experimental results obtained for particle size fractions of mean diameter: 12, 36, and 58 μm . The particle size effect is clearly seen since the first leaching stage consists of a series of straight lines.

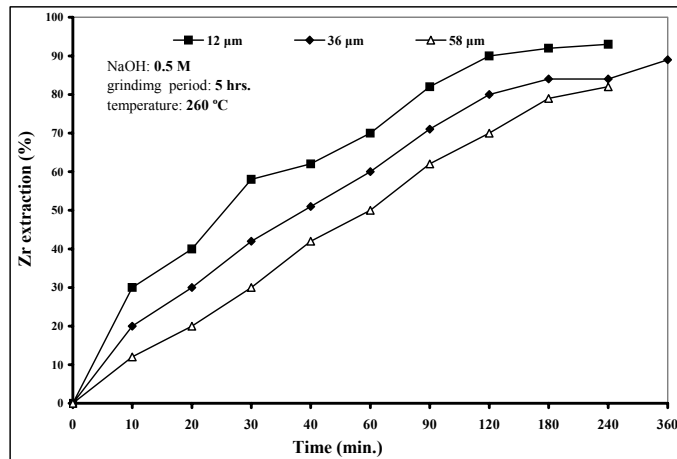


Fig. 4. Course of zirconium extraction at different particle sizes

The apparent rate constants (k) were calculated according to Eq. (1) and the external surface areas were calculated for different particle sizes using the following equation:

$$S = \frac{6m}{\rho D} \quad (5)$$

where:

S – the external surface area for the particles (see Table 2),

m – the mass of the leached sample,

ρ – the density of the sample 4.6 g/cm^3 ,

D – the particle mean diameter.

The specific apparent rate constants k/S were calculated and are shown in Table (2) which shows that the smaller the particle size the smaller the specific apparent rate constant. It is known that smaller particle size makes the boundary layer surrounding a particle thinner. Therefore under chemical control, the values of specific apparent rate constant increased with the decrease of particle size. So, the controlling step of leaching process seems to be chemically controlled.

Table 2. Rate constants for various particle sizes in the first leaching stage

D(μm)	S (cm^2)	K (min^{-1})	K/S
12	1786	0.1326	7.43×10^{-5}
36	595	0.0558	9.38×10^{-5}
58	369	0.0383	10.39×10^{-5}

EFFECT OF SODIUM HYDROXIDE CONCENTRATION

Figure (5) shows results of experiments with sodium hydroxide concentration varying from 0.4 to 0.8 M. The increase in sodium hydroxide concentration from 0.1 to 0.5 M led to an increase of zirconium leaching but further increase (>0.5M) gave no practical increase.

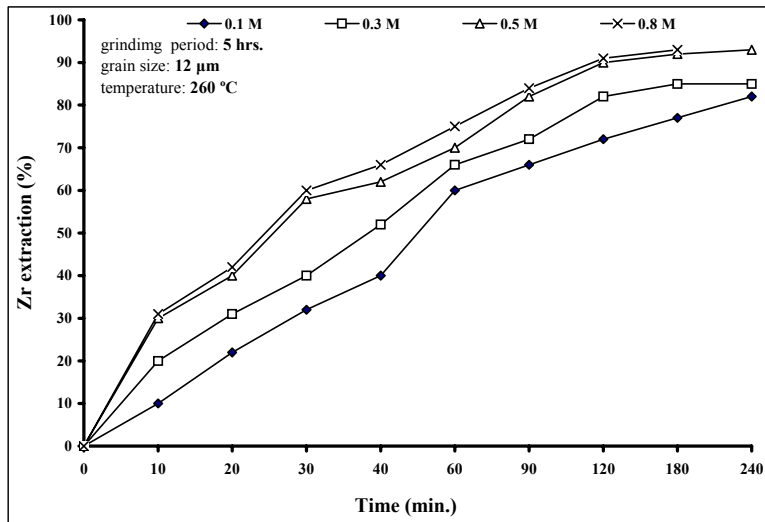


Fig. 6. Course of zirconium extraction at different grinding periods

The Langmuir-Hinshelwood equations may be used to evaluate the effect of sodium hydroxide concentration on leaching of zircon concentrate:

$$\Theta = \frac{KC_A}{1 + KC_A} \quad (6)$$

and

$$\Theta = C_A / C_{\max} \quad (7)$$

where:

Θ is the fraction of grain surface of zircon occupied by sodium hydroxide molecules.

C_A – the concentration of sodium hydroxide in the bulk solution (mol/L)

C_{\max} – the hydroxide adsorbed on zircon interface (mole/m²). Effect of grinding time.

The dependence of zircon leaching on grinding time is illustrated in Fig. (6). The apparent rate constant is directly proportional function of grinding time varying from 0 to 5 hrs. Such a dependence is consistent with the theory of leaching (Levenspiel, 1972).

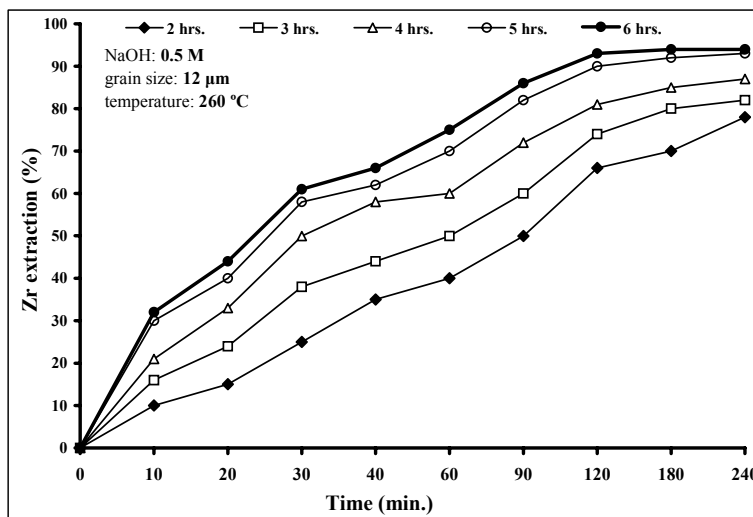


Fig. 5. Course of zirconium extraction at different sodium hydroxide concentrations

CONCLUSIONS

A new possibility of intensive zirconium removal from zircon concentrate is the mechanochemical activation which integrates mechanical and chemical processing operations in one step.

Results of investigation reveal that even a short leaching time (90 min) at 260°C led to removal of over 85% of zirconium after 5 hrs of grinding in the attritor using sodium hydroxide of 0.5 M zircon concentrate with particle size of 12 μm. The overall leaching reaction was found to be chemically rate controlled.

REFERENCES

- ABDEL-REHIM, A.M., KHALIL, S.O. (1975), *Sintering of Rosetta Zircon with calcite*, Acta Mineralogica, Petrographica, Szeged XX 11 / 1, 147-55.
- AMER, A.M. (2000), *Investigation of the direct hydrometallurgical processing of mechanically activated low-grade wolframite concentrate*, Hydrometallurgy, 58, 251-259.
- AMER, A.M. (2001), *Kinetics of acid pressure leaching of mechanically activated cassiterite concentrate*, Erzmetall, 54 (a) 446-449.
- AMER, A.M. (2002), *Processing of Egyptian boilerash from extraction of vanadium and nickel*, Waste Management, 22, 515-520.
- EL-HINAWI, E.E.; (1964), *Mineralogical and geochemical studies in Egyptian black sands*, Beitrage Zur Mineralogie and petrographic, 9, 519.
- KRISHNAN, T.S.; BABU, R.S., CAPTA, C.K. (1986), *Extended abstract*, Zirconia 86, Ceram. Soc. Jpn, 200-201.
- LEVENSPIEL, O. (1972), *Chemical reaction engineering*, New York (Wiley).
- MacDONALD, D.J.; GUIDOTT, R.A., HENRG, H.G. (1982), U.S. Bur Mines. Rep. Invest., 8718.
- MOHAMMED, N.A., DAHER, A.M. (2002). *Preparation of high purity zirconia from Egyptian zircon: an anion-exchange purification process*, Hydrometallurgy, 65, pp. 103-107.

- STAUMBAUGH, E.P., MILLER, J.F. (1983), Proceedings of 1st Int. Symposium on hydrothermal Research, p. 859.
- WELHAM, N.J. (2001), *Effect of extended grinding on the dissolution of Ta/Nb concentrate*, Can. Metall. Q, 40(2), 143-154.

Amer A.M., *Kinetyka alkalicznego ciśnieniowego ługowania mechanicznie modyfikowanego koncentratu cyrkonowego*, Physicochemical Problems of Mineral Processing, 40 (2006), 61-68 (w jęz. ang.).

Przeprowadzono hydrometalurgiczną przeróbkę koncentratów cyrkonowych wydzielonych z czarnego piasku pochodzącego z Egiptu poprzez ługowanie za pomocą wodorotlenku sodu przy względnie wysokiej temperaturze (260 °C). Koncentraty były mechanicznie aktywowane przed ługowaniem. Badano wpływ temperatury, stężenia wodorotlenku sodu, czasu mielenia, rozmiaru ziaren i czasu ługowania jak również kinetykę procesu ługowania.

Władysława MULAŁAK*, Anna SZYMCZYCHA*, Anna LEŚNIEWICZ*,
Wiesław ŻYRNICKI*

PRELIMINARY RESULTS OF METALS LEACHING FROM A SPENT HYDRODESULPHURIZATION (HDS) CATALYST

Received March 15, 2006; reviewed; accepted May 15, 2006

A spent industrial HDS catalyst Ni,Mo/ γ -Al₂O₃ used for reducing sulphur in petroleum products was physically and chemically characterized by X-ray diffraction, scanning electron microscope, electron microprobe and chemical analysis. The leaching efficiency of Mo, Ni, V and Al from the spent catalyst in oxalic acid solution with hydrogen peroxide addition was investigated. The effects of oxalic acid and hydrogen peroxide concentrations and the stirring speed on the rate of metal leaching were studied. The results revealed that addition of hydrogen peroxide to oxalic acid up to 3.0M H₂O₂ concentration enhanced leaching of metals remarkably, and thereafter remained relatively constant. The highest extraction of metals from the spent catalyst (at 50°C in solution of 0.5M H₂C₂O₄ with 3.0M H₂O₂) was found to be 90% Mo, 94% V, 65% Ni and 33% Al in 4 hour leaching.

Key words: spent hydrodesulphurization catalyst, metal foulants, acidic leaching

INTRODUCTION

The petroleum refining industry makes extensive use of catalysts for desulphurization of various fractions. The most common hydrodesulphurization (HDS) catalysts are Ni,Mo and Co,Mo on the γ -alumina support. During hydrodesulphurization the catalysts are deactivated by compounds of S, C, V, Fe, Ni, Si and traces of As and P (Furimsky and Massoth, 1999). As a result, the spent catalysts are classified as hazardous materials. However, such waste materials containing high metal concentrations may be considered as "artificial ores", since they can serve as secondary raw materials with a consequent reduction in the demand for primary mineral resources. Recycling of spent catalysts became an unavoidable task

* Wrocław University of Technology, Chemical Department, Wybrzeże Wyspiańskiego 27,
50-370 Wrocław, Poland, e-mail: wladyslawa.mulak@pwr.wroc.pl

not only for lowering catalysts costs but also for reducing their waste to prevent the environmental pollution. A variety of processing approaches for recovering metals from the spent catalysts has been proposed and most of the literature in this field is patented (Furimsky, 1996; Yoo, 1998). The spent catalysts are subjected to hydrometallurgical or hydro-pyrometallurgical treatment for metals recovery. In both cases the metals are recovered as mixed solutions and then separated by conventional separation techniques (solvent extraction, selective precipitation, ion-exchange). Hydrometallurgical processes involve leaching with alkaline or acidic solutions. Many reagents, such as NaOH, H₂SO₄, NH₃, (NH₄)₂SO₄ and oxalic acid with H₂O₂ and Fe(NO₃)₂, have been tested (Queneau et al., 1989; Rabah et al., 1997; Siemens et al., 1986; Stanislaus et al., 1993; Marafi et al., 1994; Marafi and Stanislaus, 2003). Hydro-pyrometallurgical processes involve roasting with Na₂CO₃, NaCl or Cl₂ gas (Kar et al., 2004; Biswas, 1985; Gaballah et al., 2002). The main aim of the present research work was to investigate the possibility and efficiency of leaching of the spent hydrodesulphurization catalyst in oxalic and sulphuric acids with oxidizing agents addition.

EXPERIMENTAL

CHARACTERIZATION OF SPENT CATALYST

The spent HDS catalyst was in the form of cylindrical extrudates of approximate diameter 0.3-0.4 mm and length 4-6 mm. It contained residual oil and was washed with hot toluene by Soxhlet process and dried at 110°C before experiments. The surface of the deoiled catalyst has been determined by nitrogen adsorption (BET method) and is equal to 80.0 m²/g. Powder XRD analysis of the spent catalyst showed that its main phase is γ -Al₂O₃, but V₅S₈ compound was also detected. Chemical analysis of the spent catalyst confirmed its partial composition as follows: 5.08% Mo, 5.26% Ni, 5.36% V and 24.57% Al. In turn, CHNS analysis showed that the spent catalyst contained (wt. %) carbon 17.6, hydrogen 1.14, nitrogen 0.38 and sulphur 9.64. The most interesting microscope evidence found in this study is provided by the cross-section of the spent catalyst extrudate. Electron microprobe analysis of the edge extrudate cross-section proved a high content of vanadium (23.37%), iron (4.12%) and sulphur (22.56%), but low content of nickel (2.71%) and molybdenum (3.42%). The middle extrudate cross-section did not evidence vanadium and iron. The results of microprobe analysis at the edge and middle part of the cross-section of the spent catalyst extrudate are given in Table 1 and in Fig. 1.

Table 1. Microprobe analysis of the cross-section of the spent catalyst extrudate

Part of the cross-section	Element content, %										
	C	O	Na	Al	Si	S	Ca	V	Fe	Ni	Mo
(1) edge	5.31	21.35	0.84	15.94	0.28	22.58	0.11	23.37	4.12	2.31	3.42
(2) middle	17.62	36.25	0.18	32.39	0.16	7.01	0.13	0.11	0.00	2.25	3.89

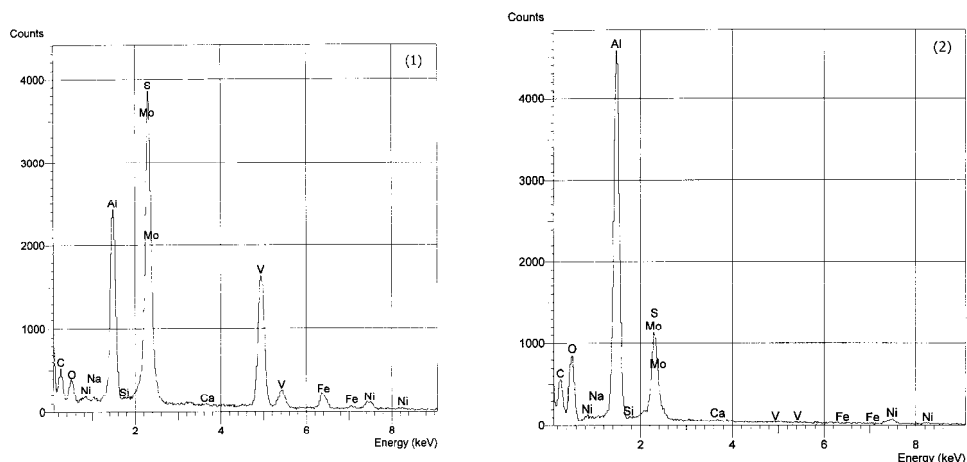


Fig. 1. Microprobe analysis of the cross-section of the spent HDS catalyst extrudate: (1) edge, (2) middle

It is clearly shown that metal foulants such as vanadium, nickel and iron are concentrated near the outer surface of the catalyst extrudate, blocking the pore mouths and retarding the access of the reactants to the active sites of the catalyst with the pores.

LEACHING EXPERIMENTS

In each experiment a flask containing 200 ml of leaching solution of the desired concentration was submerged in a tank the temperature of which was kept constant to within 0.1°C . When the required temperature had been reached a charge of 0.5 g of the spent catalyst was added and the stirring was started. A mechanical glass agitator of L shape with 25 mm impeller was applied. Its tip speed converted from 600 m^{-1} was equal to 0.785 m/s . The leaching was carried out for 3 and 4 hours during which nine 1 ml samples of the solution were taken for determination of the molybdenum, nickel, vanadium and aluminium concentration by the atomic emission spectrometry with inductively coupled plasma as the excitation source. The reproducibility of the leaching experiments was determined to be of order of $\pm 2\%$ by repeating selected experiments under identical conditions.

RESULTS AND DISCUSSION

SELECTION OF THE PROPER LEACHING SOLUTION

In order to choose a suitable leachant the solutions of sulphuric and oxalic acids were tested with H_2O_2 , NaNO_3 , NH_4NO_3 and $(\text{NH}_4)_2\text{S}_2\text{O}_8$ addition. The leaching was performed at 70°C with the constant stirring speed of 600 min^{-1} . The results of the leaching efficiencies at various solutions after three hour leaching are shown in Fig. 2 and Fig. 3.

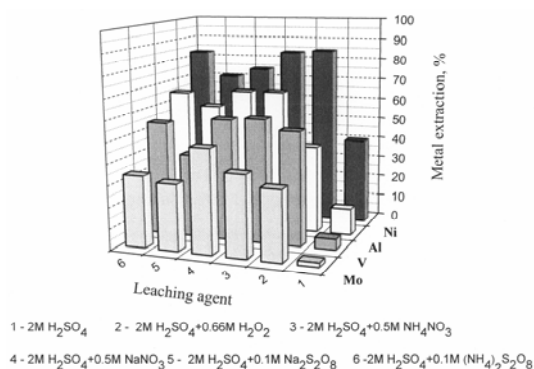


Fig. 2. Effect of adding various oxidizing agents to sulphuric acid solution on metal extraction

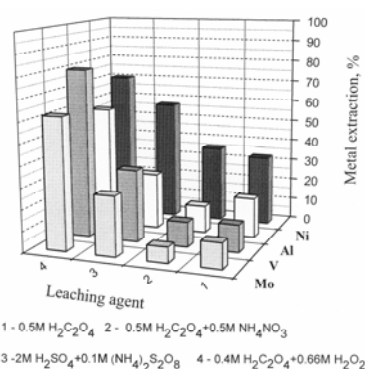


Fig. 3. Effect of adding various oxidizing agents to oxalic acid solution on metal extraction

From these figures it can be seen that oxalic acid as a chelating agent forms soluble metal complexes with molybdenum and vanadium (Marafi and Stanislaus, 1989), causing that the extraction of Mo and V is higher than that in the leaching with H₂SO₄ in the presence of H₂O₂. Leaching of the spent HDS catalyst in oxalic acid as well as in sulphuric acid with H₂O₂ addition is followed by the loss of the alumina catalyst support (about 40%). Leaching efficiency of nickel and vanadium in sulphuric acid solution with (NH₄)₂S₂O₈ and then with H₂O₂ is comparable for nickel (82.8%), vanadium (53.9%) and molybdenum (33.5%), but the extraction of aluminium was about 24.0% lower in the presence of H₂O₂ than (NH₄)₂S₂O₈.

EFFECT OF STIRRING SPEED

The effect of stirring speed on the metal leaching efficiency from the spent catalyst was investigated in solution containing 0.5M H₂C₂O₄ and 3M H₂O₂ at 50°C in the range of speed from 300 to 1200 min⁻¹.

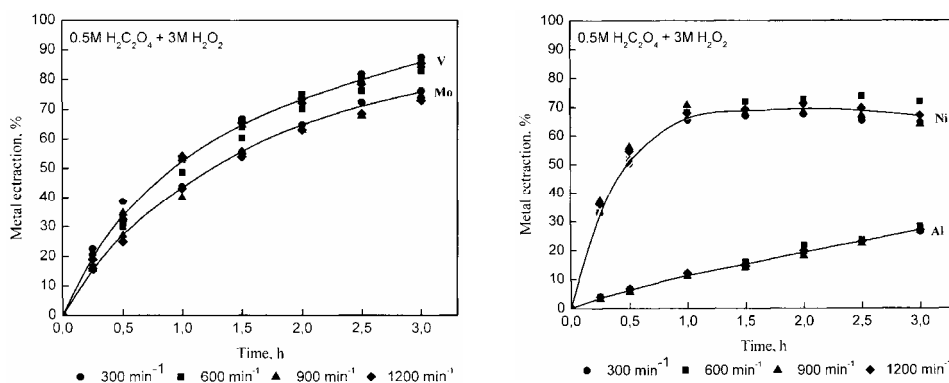


Fig. 4. Effect of stirring speed on metal extraction as a function of time at 50°C in solution containing H₂C₂O₄ and H₂O₂ after 3 hour leaching

The results presented in Figs 4a and 4b show that the leaching of molybdenum, nickel, vanadium and aluminium is independent of the stirring speed. This indicates that the diffusion of the reactants from the solution towards the surface of a catalyst particle, and the products away from the surface of the particle was fast, and hence did not control the leaching rate within the range of the stirring speeds tested. All subsequent experiments were carried out at a stirring speed of 600 min⁻¹ to assure the invariance of this parameter.

EFFECT OF HYDROGEN PEROXIDE CONCENTRATION

The influence of H₂O₂ concentration on the leaching of molybdenum, nickel, vanadium and aluminium from the spent HDS catalyst was determined by varying the initial concentration of H₂O₂ from 0.5 to 3.0M at 50°C in 0.5M H₂C₂O₄ solution. Fig. 5 shows summarized metals extraction after 4 hour leaching. Generally, the extraction of Mo, Ni, and V gradually increased up to 3.0M and then remained constant. The extraction of Al was practically not affected by the concentration of H₂O₂ within the whole range. The highest extraction of molybdenum (90%), vanadium (94%) and nickel (65%) was observed in 0.5M H₂C₂O₄ solution with 3.0M H₂O₂ at 50°C during 4 hour leaching.

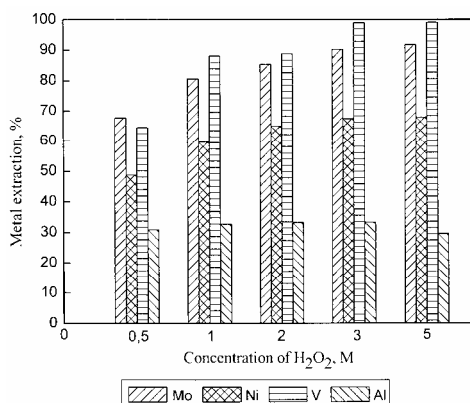


Fig. 5. Effect of H₂O₂ concentration on metal leaching efficiency at 50°C in 0.5M H₂C₂O₄ solution after 4 hour leaching

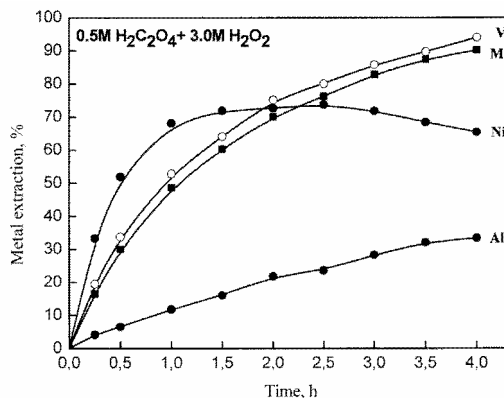


Fig. 6. Influence of leaching time on metal extraction from the spent HDS catalyst at 50°C in solution containing oxalic acid and hydrogen peroxide

Figure 6 depicts the kinetics of leaching of Mo, Ni, V and Al at 50°C in 0.5M H₂C₂O₄ solution with 3.0M H₂O₂ addition. As is seen the extraction of vanadium is quite similar to that of molybdenum and gradually increases with time. It was also found, that the extraction of nickel increased with time up to about two hours (74%) and then gradually decreased to about 65% after 4 hour leaching. This unexpected decrease is due to the precipitation of nickel as nickel oxalate (Santhiya and Ting, 2005).

EFFECT OF OXALIC ACID CONCENTRATION

The experiments were carried out at a leaching temperature of 50°C. The concentrations of $H_2C_2O_4$ used were 0.25, 0.375, 0.50 and 0.70M. The effect of $H_2C_2O_4$ concentration on the extraction of molybdenum, vanadium, nickel and aluminium at 50°C in 3.0M H_2O_2 solution after 4 hour leaching is presented in Fig. 7. These experimental results showed that the change in concentration of $H_2C_2O_4$ solution within the range 0.25-0.70M causes a gradual increase of the extraction of Mo (90%), V (94%), Ni (65%) and Al (33%) up to 0.5M $H_2C_2O_4$ and then it slowly falls down to 76% Mo, 84% V, 49% Ni and 28% Al in 0.7M $H_2C_2O_4$ solution. The kinetics of leaching of Mo, Ni, V and Al from the spent HDS catalyst at 50°C solution containing 0.7M $H_2C_2O_4$ and 3.0M H_2O_2 is illustrated in Fig. 8.

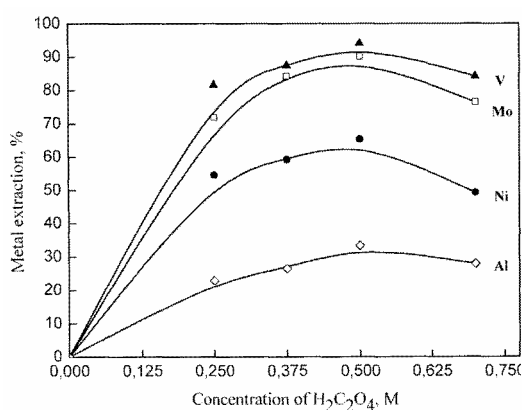


Fig. 7. Effect of $H_2C_2O_4$ concentration on metal leaching efficiency at 50°C in 3.0 M H_2O_2 solution after 4 hour leaching

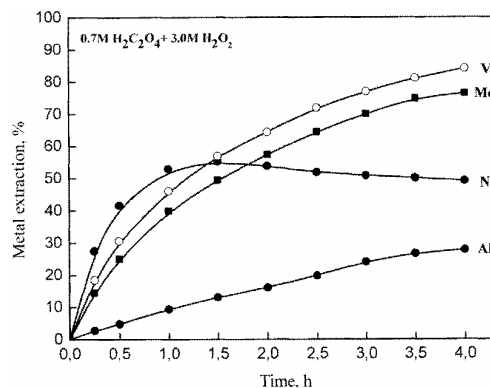


Fig. 8. Influence of leaching time on metal extraction from the spent HDS catalyst at 50°C in solution containing oxalic acid and hydrogen peroxide

The leaching plots in Figs 6 and 8 are generally similar although those for more concentrated solution of $H_2C_2O_4$ are lowered. Especially the decrease of nickel extraction is the deepest (only 75% of the optimal value) and the downfall begins already after 1.5 hours of the process.

CONCLUSION

1. X-ray diffraction analysis of the spent hydrodesulphurization (HDS) catalyst shows that its main phase is $\gamma-Al_2O_3$, however V_5S_8 compound was also detected.
2. Scanning electron microscopy and microprobe analysis of the spent catalyst extrudate cross-section revealed that vanadium, nickel, iron and sulphur are deposited near the outer surface of the catalyst extrudate.

3. Leaching rate of molybdenum, nickel, vanadium and aluminium from the spent HDS catalyst in oxalic acid with H₂O₂ addition is independent of the stirring speed. That indicates that the reaction is not controlled by the diffusion in the liquid phase.
4. Rise in H₂O₂ concentration up to 3.0M gradually increases the extraction of Mo, V and Ni, but thereafter it remains constant. The extraction of Al is practically not affected by H₂O₂ concentration within the range from 0.5 to 5.0M.
5. The change in the concentration of H₂C₂O₄ solution from 0.25 to 0.5M increases metals extraction, and thereafter gradually decreases it.
6. The highest leaching efficiency of the metals was obtained after 4 hour leaching in the solution containing 0.5M H₂C₂O₄ and 3.0M H₂O₂. The extraction of metals at the above conditions are: 90% Mo, 94% V, 65% Ni and 33% Al in 4 hours of leaching.

ACKNOWLEDGEMENTS

The authors wish to thank the Polish Committee for Scientific Research for financial support (grant No 3T09B 05428).

REFERENCES

- BISWAS R.K., (1985), *Recovery of vanadium and molybdenum from heavy oil desulphurization waste catalyst*, Hydrometallurgy, 14, 219-230.
- FURIMSKY E., (1996), *Spent refinery catalysts: environment, safety and utilization*, Catalysis Today 30, 223-286.
- FURIMSKY E., MASSOTH F.E., (1999), *Deactivation of hydroprocessing catalysts*, Catalysis Today , 52, 381-495.
- GABALLAH J., KANARI N., DJONA M., (2002), *Use of chlorine for mineral processing, metal extraction and recycling via synthesis of new reagent*, in: Chloride Metallurgy 2002, vol. 1. 32nd Annual Hydrometallurgy Meeting. Peek E., G. van Weert (Editors), Metallurgical Society of the Canadian Institute of Mining, Metallurgy and Petroleum, Montreal, pp. 203-225.
- KAR B.B., DATTA P., MISRA V.N., (2004), *Spent catalyst: secondary source for molybdenum recovery*, Hydrometallurgy, 72, 87-92.
- MARAFI M., STANSILAU A., (1989), *Regeneration of spent hydroprocessing catalysts: metals removal*, Applied Catalysis 47, 85-96.
- MARAFI M., STANSILAU A., ABSI-HALABI M., (1994), *Heavy oil hydrotreating catalyst rejuvenation by leaching of foulant metals with ferric nitrate-organic acid mixed reagents*, Applied Catalysis B: Environmental, 4, 19-27.
- MARAFI M., STANSILAU A., (2003), *Options and processes for spent catalyst handling and utilization*, Journal of Hazardous Materials B101, 123-132.
- QUENEAU P.B., HOGSETT R.F., BECKSTEAD L.W., BARCHERS D.E., (1989), *Processing of petroleum coke for recovery of vanadium and nickel*, Hydrometallurgy, 22, 3-24.
- RABAH M.A., HEWAIDY I.F., FARGHALY F.E., (1997), *Recovery of molybdenum and cobalt powders from spent hydrogenation catalyst*, Powder Metallurgy, 40 (4), 283-288.
- SANTHIYA D., TING Y.P., (2005), *Bioleaching of spent refinery processing catalyst using Aspergillus niger with high-yield oxalic acid*, Journal of Biotechnology, 116, 171-184.
- SIEMENS R.E., JONG B.W., RUSSELL J.H., (1986), *Potential of spent catalysts as a source of critical metals*, Conservation & Recycling, 9(2), 189-196.

STANISLAUS A. MARAFI M. ABSI-HALABI M., (1993), *Studies on the rejuvenation of spent catalysts: effectiveness and selectivity In the removal of foulant metals from spent hydroprocessing catalysts In coked and decoked forms*, Applied Catalysis A: General, 105, 195-203.

YOO J.S., (1998), *Metal recovery and rejuvenation of metal-loaded spent catalysts*, Catalysis Today, 44, 27-46.

Mulak W., Szymczycha A., Leśniewicz A., Żyrnicki W., *Wstępne wyniki badań nad ługowaniem metali z zużytego katalizatora hydroodsiarczania*, Physicochemical Problems of Mineral Processing, 40, (2006), 69-76 (w jęz. ang.).

Katalizatory hydroodsiarczania HDS o składzie Ni,Mo/Al₂O₃ oraz Co,Mo/Al₂O₃ należą do najszerszej stosowanych w procesach rafineryjnych. Ich dezaktywacja następuje głównie na skutek osadzenia się na powierzchni związków węgla i siarczków metali. Tego typu zużyte katalizatory zaliczane są do niebezpiecznych odpadów: są one łatwopalne, wybuchowe, toksyczne, korozyjne, a w kontakcie ze środowiskiem naturalnym wydzielają trujące gazy. Recykling tych katalizatorów jest konieczny ze względów ekologicznych i ekonomicznych. Do badań stosowano zużyty katalizator Ni,Mo/Al₂O₃ uprzednio odolejony toluenem. Jego charakterystykę fizykochemiczną wykonano na podstawie wyników analizy chemicznej, elementarnej, rentgenowskiej oraz skaningowym mikroskopem elektronowym z mikrosondą rentgenowską. Analiza chemiczna katalizatora wykonana metodą ICP-OES po uprzednim przeprowadzeniu próbki do roztworu wykazała następujące zawartości metali: 5,08% Mo, 5,26% Ni, 5,36% V oraz 24,57% Al. Wyniki analizy skaningowym mikroskopem elektronowym wykazały obecność wanadu, niklu, żelaza oraz siarki głównie na powierzchni katalizatora. W celu ustalenia optymalnego czynnika ługującego metale z katalizatora wykonano ługowania testujące w czasie trzech godzin w temperaturze 70°C w roztworach kwasu siarkowego (VI) oraz kwasu szczawiowego z dodatkiem takich utleniaczy jak: H₂O₂, NaNO₃, NH₄NO₃ oraz (NH₄)₂S₂O₈. Wykazano, że najlepszym czynnikiem ługującym molibden i wanad jest roztwór kwasu szczawiowego z dodatkiem ditlenku diwodoru, natomiast najlepszym czynnikiem ługującym nikiel jest roztwór zawierający kwas siarkowy (VI) z dodatkiem H₂O₂ lub (NH₄)₂S₂O₈. Określono wpływ stężenia H₂C₂O₄ oraz H₂O₂ na wydajność ługowania Mo, Ni, V oraz Al. Najwyższe wydajności wylugowania metali wynoszące 90% Mo, 94% V, 65% Ni oraz 33% Al uzyskano w roztworze zawierającym 0,5M H₂C₂O₄ z dodatkiem 3,0M H₂O₂ w temperaturze 50°C po 4 godzinach ługowania.

Antoni MUSZER*, Andrzej ŁUSZCZKIEWICZ**

MINERALOGICAL CHARACTERISTICS OF ACCESSORY MINERALS FROM OSIECZNICA DEPOSIT, SW POLAND

Received March 15, 2006; reviewed; accepted May 15, 2006

The composition of the heavy mineral fraction from the glass sand in Osiecznica (Lower Silesia, SW Poland) was described. Accessory minerals are present in the gravity concentrate mainly as individual grains, whereas lower amounts occur as vein rocks debris, inclusions in quartz grains and heavy minerals. The sample under study contained the following minerals: rutile, anatase, hematite-goethite, ilmenite-leucosene, zircon, monazite, xenotime, kyanite, pyroxenes, and quartz with inclusions of chalcopyrite, pyrite, pyrrhotite, sphalerite, pentlandite, arsenopyrite, and tetrahedrite-tennantite. Moreover, the presence of native gold and silver was determined. Major components of the concentrate are rutile, anatase, quartz with inclusions of ore minerals, zircon, and goethitized hematite. The other minerals occur in the amount below 2-3 vol. %. The content of native gold in the concentrate sample (0.11%) may be indicative of a significant concentration (around 1.5 g/Mg) of this metal in the Osiecznica deposit.

Key words: glass sand, heavy minerals, gravity concentration

INTRODUCTION

Deposits of glass sands (sandstones) near Osiecznica belong to the largest in Poland. According to the new Resources Balance (2005) the resources of the currently exploited deposit Osiecznica II amount to 22.43 Tg. The sandstones in this area belong to the northern part of the North-Sudetic Basin, the so called Bolesławiec syncline (Fig. 1). The basin comprises Cretaceous sediments overlain with sedimentary rocks of the Neogene. Cretaceous sandstones outcrops are very sparse (Milewicz 1967).

* University of Wrocław, Department of Geological Science, pl. Maksa Borna 1, Wrocław, Poland, amuz@ing.uni.wroc.pl.

** Technical University of Wrocław, Institute of Mining Engineering, Wybrzeże Wyspiańskiego 27, 50-370 Wrocław, Poland, andrzej.luszczkiewicz@pwr.wroc.pl.

The raw materials for glass production are Cretaceous sandstones of the Coniacian age and certain parts of the Santonian sandstones. Coniacian and Santonian beds are stretched along the axis of the basin from the NW to the SE and dip in the direction of its centre at 20–45° to the SW. The sandstones were subject to weathering (weakening) and parting in the zones of tectonical engagement. The Coniacian sandstones and some parts of the Santonian sandstones are characterized by expressed homogeneity. These are most of all fine-grained quartz sandstones in which the basic grain fraction (0.100 to 0.315 mm) prevails. The average amount of this fraction is around 80% (Milewicz 1967; Błaszak and Grodzicki 1979). The sandstones contain only trace amounts of heavy minerals.

Accessory minerals (heavy minerals) in the glass sands form a significant impurity (they may colour industrial semi-products). On the basis of the accessory minerals content a classification of deposits of sands (sandstones) has been prepared and a purity class of these sediments has been determined (classes from 1 to 6, and the best class S).

Glass sandstones (quartz well-sorted sandstones) contain no traces of micro- or macro-fossils. Such deposits are very difficult to correlate stratigraphically. The main aim of the investigations consisted of checking whether these stratigraphically ‘silent’ beds may contain some components that would allow lithostratigraphical correlation. Moreover, the authors decided to take an attempt and apply a technique called ore minerals analysis in the study of very well sorted quartz sandstones. The authors’ idea was also to check whether it is possible to determine a possible source area of the rocks in question on the basis of accessory minerals.

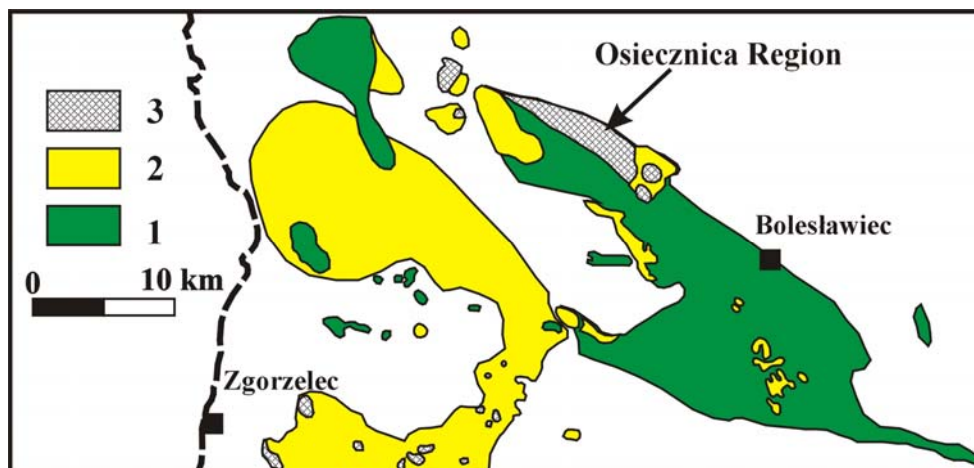


Fig. 1. Cretaceous and Neogene glass sandstones occurrence near Bolesławiec. 1 – Cretaceous sediments: sands and sandstones, clays and marls; 2 – Neogene sediments: sands and clays with lignite beds; 3 – areas of glass sand deposits

DEPOSIT DESCRIPTION

The deposit series is characterised by high homogeneity of mineral and chemical composition. The content of silica in the deposit reaches up to 98.0 wt. % and no more than 0.02 wt. % of iron oxides. After washing and removing clay matrix silica content reach up to 99.8 wt. % (Kozłowski 1986). The moist sand is grey, and after drying it is mainly white and in some cases yellow. The dominant mineral is quartz, and such components like feldspars, glauconite, heavy minerals and vein rocks debris are sparsely present. Heavy minerals have the form of individual grains and occur also as veinlets and inclusions in quartz and in other heavy minerals.

The deposit series is characterised by high homogeneity of chemical composition. A relatively low concentration of iron compounds in the sands (max. 0.02 Fe₂O₃) makes it possible to regard them as one of the best quality glass sands in Poland and Europe (Kozłowski 1986). The sands (sandstones) in question meet requirements of class 2, 3, 4 and 5 from which after adequate processing material of class 1, 2 and 3 is obtained (Poręba 1968).

An average thickness of the deposit is around 38 m (Osiecznica II). The overburden contains Cretaceous sediments younger than the Coniacian (clays, clay-shales and some sandstones), Miocene (sands, quartzites, and in some parts also gravels) and Pliocene-Holocene sediments (clayey sands and muds). An average thickness of the overburden is varied and ranges from 1.25 to 21 m (Błaszczak 1973).

METHODS

Fifty kilograms of preliminary purified glass sand from the Osiecznica II deposit were collected for the study. This sand was concentrated with the use of a concentration table of the Wilfey type (made by the British company Denver) at the Institute of Mining Engineering of the Wrocław University of Technology (Fig. 2). The resulting mass balance of this operation is shown in Table 1. Tailing 1 presented in this table as the purified glass sand was separated earlier on a commercial scale in a spiral separator at the Osiecznica Plant.

Table 1. Mass balance of heavy mineral fraction (HMF) of tabling of the glass sand

#	Product	Yield, %	HMF content, %	HMF recovery, %
1.	Concentrate 1	0.28	29.12	54.89
2.	Concentrate 2	0.45	8.15	24.41
3.	Middlings 1	1.09	0.63	4.61
4.	Tailings 2	3.34	0.12	2.69
5.	Tailings 1	94.85	0.02	13.39
6.	Calculated feed	100.00	0.15	100.00
7.	Feed assay		0.13	

In the products separated the contents of heavy mineral fraction was determined with the use of tetrabromoethane (heavy liquid $\rho=2950 \text{ kg/m}^3$). The heavy mineral fraction obtained from concentrate 1 (Table 1) was divided in the magnetic field of a permanent magnet into two fractions: magnetic and non-magnetic. Polished sections for reflected light microscopic studies and microchemical analyses were prepared from the heavy mineral fraction samples of the both concentrates. The polished sections were prepared with the use of a standard technique for metal ore samples (Muszer 2000). Polishing of the study material was performed on polishing cloths Struers DP-Mol, DP-Dur and DP-Nap while applying strictly defined grain sizes of diamond polishing pastes. The polished sections were investigated under the microscope in the Laboratory of Mineral Raw Materials at the Institute of Geologic Studies of the Wrocław University. The studies of samples were performed with Nikon binocular and investigated in reflected light with the use of Nikon Optiphot 2-Pol microscope.

Planimetric analysis and the Lucia M programme were used in the quantitative analysis of heavy minerals. The distribution of metals in sulphides was determined with the use of microchemical analysis. The elemental composition of minerals was studied with the use of scanning microscope SEM 515 (Philips) equipped with an X-ray spectrum analysis attachment. These investigations were carried out at the Institute of Low Temperature and Structure Research (Polish Academy of Sciences) in Wrocław.

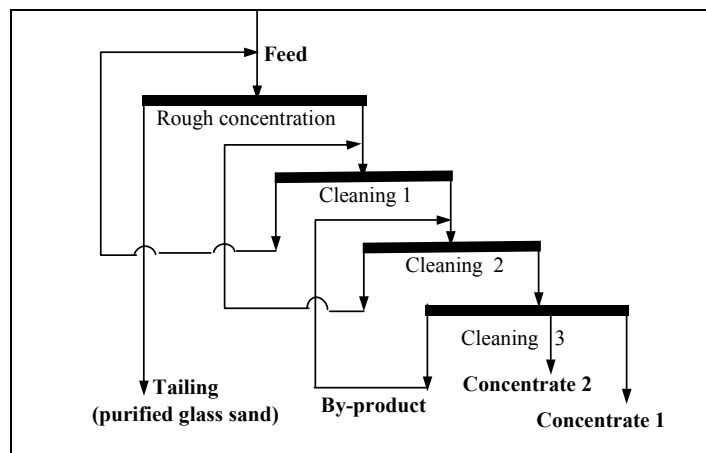


Fig. 2. Flowsheet of gravity separation with the use of a laboratory concentrating table

DESCRIPTION OF HEAVY MINERAL FRACTION

The concentration of heavy minerals in the Osiecznica deposit varies from 0.2 to 2.5 vol. % depending on the part of the deposit (Błaszak and Grodzicki 1979; Łuszczkiewicz 1987, 2002). The investigations revealed the presence of the following minerals in the sample: oxides, represented by rutile, anatase, magnetite, hematite-

goethite, ilmenite-leucoxene; quartz with inclusions of sulphides and oxides; phosphates (monazite, xenotime); silicates (zircon, disthene, pyroxenes) and sulphides (chalcopyrite, pyrite, pyrrhotite, sphalerite, pentlandite), sulphoarsenides and sulphoantimonides (arsenopyrite, tetrahedrite-tennantite). Moreover, native gold and silver were determined in the sample.

During the process of purification of glass sands (sandstones) heavy mineral fraction is concentrated mostly in the finest grain size fraction. In the Osiecznica deposit heavy mineral fraction is concentrated mainly in the fraction below 0.071 mm (Table 2). According to the investigations' results, the heavy mineral fraction concentration in the grain size fraction <0.1 mm is 3-4-fold greater than in the fraction >0.1 mm (Łuszczkiewicz 1987, 2002).

Table 2. Particle size composition and the distribution of heavy mineral fraction (HMF) in gravitational tailing from the purification of glass sands of the Osiecznica Plant (Łuszczkiewicz 1987, 2002)

Particle size, mm	Yield, %	Concentration of HMF, %	Recovery of HMF, %
+0.5	7.50	0.00	0.00
0.5 – 0.2	19.80	0.022	1.79
0.2 – 0.071	47.10	2.55	49.28
- 0.071	25.60	4.66	48.93
Calculated feed	100.00	2.44	100.00
Assay feed		2.35	

The main component of the heavy mineral fraction is rutile with anatase (TiO₂). These two minerals of titanium make up for 50.1 % of the concentration of all heavy minerals. Rutile and anatase grains are medium or poorly rounded. It is possible to observe columnar or acicular crystals which are frequently crushed. Rutile is characterised by red, brown and yellow internal reflexes, while the typical reflexes of anatase are white-yellowish. These both minerals are easy to polish. The most widespread rutile crystals are those with red - brown internal reflexes. Rutile grains contain inclusions of pyrrhotite and pyrrhotite-chalcopyrite aggregates. The inclusions may reach 25 µm in diameter.

An important component of the volumetric composition of the heavy mineral fraction separated from the gravitational concentrate is quartz. Its concentration amounts to around 18 % of all minerals in the heavy mineral fraction (Table 3). This quartz was separated from the sample with a permanent magnet. Macroscopic investigation of the magnetic fraction under reflected light revealed that individual quartz grains contain numerous inclusions of magnetite or magnetite with hematite, as well as inclusions of pyrrhotite with other ore minerals (Fig. 3). Quartz grains are colourless and have strong lustre, whereas in certain cases may be matted. The majority of quartz grains are semi-rounded or angular. The product under study contained very few well-rounded grains. The surface of individual grains is scratched and rough which implies rapid transport of these grains.

Table 3. The composition of the heavy mineral fraction from the Osiecznica deposit

Mineral	Concentration in % vol.
Rutile, anatase	50.10
Zircon	16.65
Monazite	1.99
Xenotime	0.56
Quartz	18.38
Magnetite	0.20
Hematite (goethite)	9.30
Ilmenite-leucoxene	2.30
Kyanite	0.10
Pyroxenes	0.10
Native gold	0.11
Pyrrhotite, pyrite, arsenopyrite, chalcopyrite, sphalerite	0.21
Total	100.00

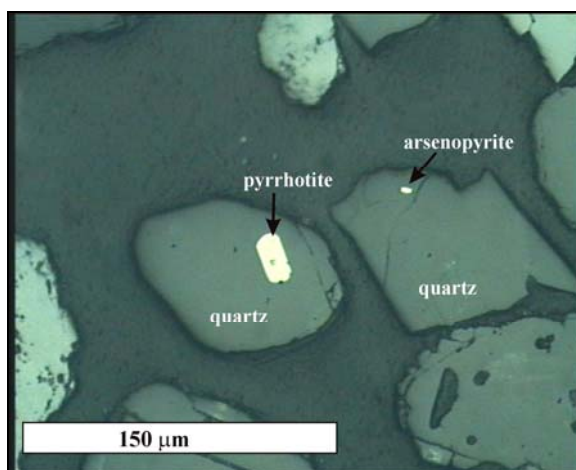


Fig. 3. Ore minerals (pyrrhotite, arsenopyrite) in quartz grains from Osiecznica. Reflected light, plane polarized light

The third most important component of the heavy mineral fraction is zircon. Its quantity is almost 3-fold lower than the amount of rutile-anatase (Tab. 3). The diameter of zircon crystals ranges from 50 to 200 μm . The concentrate contains two zircon varieties, i.e. zonal zircon and zircon without the zonal structure. Individual zircon grains are very well or poorly rounded. Zircons have a well defined structure of the tetragonal prism. Zircon crystals contain inclusions of pyrrhotite, chalcopyrite, pyrite and magnetite (Fig. 4). The diameter of inclusions ranges from 1 to 25 μm . The inclusions are idiomorphic and xenomorphic.

Hematite occurs in the concentrate in the form of separate grains. The diameter of grains ranges from 60 to 150 μm . This mineral reveals strong anisotropy and red internal reflexes. The majority of hematite grains contain substitution structures. Along cracks and from the boundaries of grains hematite was subjected to goethitization (substitution by goethite).

The concentration of other minerals in the heavy mineral fraction ranges from 0.1 % (kyanite) to 2.3 % (ilmenite-leucoxene). Ilmenite, monazite, xenotime, magnetite, kyanite, pyroxenes, native silver, and native gold are present in the concentrate as individual grains. The other minerals, i.e. sulphides (chalcopyrite, pyrite, pyrrhotite, pentlandite, sphalerite), arsenopyrite and tetrahedrite-tennantite form tiny inclusions in silicate or phosphate minerals.

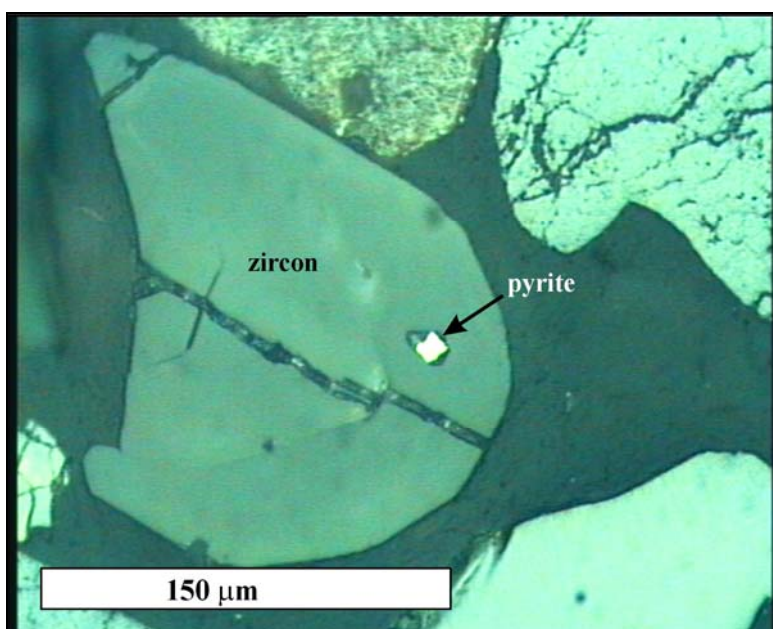


Fig. 4. Pyrite in a zircon grain from Osiecznica. Reflected light; plane polarized light

Ilmenite (ilmenite-leucoxene) forms grains from 70 μm to 0.2 mm in diameter. Most ilmenite grains contain substitution structures, i.e. traces of leucoxenization. Ilmenite grains are tabular with rounded corners. Their optical features are typical of this mineral. Ilmenite may form individual grains and was observed also in structures from the decomposition of solid solution in several magnetite grains. These structures univocally point to magmatic origin of these magnetite grains.

Monazite and xenotime are distinct from other grains in the concentrate. Monazite has white-yellow-brown internal reflexions and xenotime has yellow-brown internal reflexions. Monazite shows poor cleavage when compared with xenotime and is difficult to polish when compared with zircon.

Magnetite present in the concentrate very rarely forms grains. Most of these grains are martitized. Their characteristic feature is a magnetite-hematite grid structure typical of the process of substitution of magnetite by hematite. Most of magnetite grains occur as inclusions in quartz and are responsible for its magnetic properties. Quartz with magnetite inclusions is poorly rounded. Magnetite in quartz has the form of cubic crystals or oval-shaped exsolutions. Oval inclusions of magnetite are frequently accompanied by hematite inclusions of identical shape.

Pyrrhotite was observed in poorly rounded quartz grains, and in zircons and monazite. Pyrrhotite is present in the form of xenomorphic grains, oval shaped forms or as crystals. All zircons containing pyrrhotite inclusions are very well rounded and do not have zonal structure. The well rounded grains of quartz contain pyrite-pyrrhotite inclusions. These aggregates have xenomorphic structure and their diameter does not exceed 10 μm . Several zircon grains contain pyrrhotite with flame structures of pentlandite (structures from the decomposition of a solid solution). Moreover, hexagonal-monoclinical structures observed in pyrrhotite point to high temperature of its crystallization.

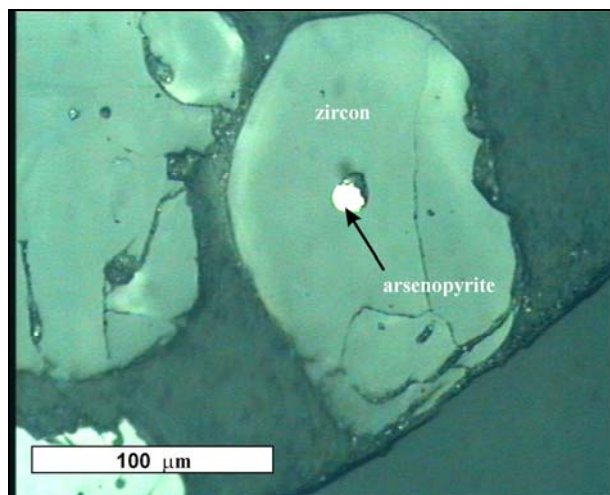


Fig. 5. Arsenopyrite in zircon grain from Osiecznica. Reflected light; plane polarized light

Chalcopyrite was observed in poorly rounded quartz grains and in a grain of a vein aggregate. In quartz grains chalcopyrite occurs in intergrowths with pyrrhotite, forming a shapeless xenomorphic aggregate. Chalcopyrite grains do not exceed 5 μm in diameter. Chalcopyrite grain is always smaller than pyrrhotite grain attached to it.

Arsenopyrite was observed as inclusions or veinlets in quartz or zircon. In quartz grains this mineral occurs as individual inclusions up to 10 μm in diameter or is intergrown to form pyrrhotite-arsenopyrite aggregates or aggregates of pyrrhotite-arsenopyrite-chalcopyrite. The diameter of these aggregates does not exceed 15 μm . The diameter of arsenopyrite in zircon grains does not exceed 15 μm (Fig. 5). The

microchemical analysis of elemental composition did not reveal the presence of any additions in this mineral. Both native gold and native silver are very rare in the concentrate. The concentration of native gold amounts to 0.11 vol. % of the heavy mineral fraction. This mineral is frequently intergrown with hematite. Native gold was also determined in the magnetic fraction separated from the heavy mineral fraction. Gold occurs in the form of scales and irregular clusters. The scales are up to 150 μm long and 25 μm thick (Fig. 6). Gold has distinct golden-yellow colour. In gold grains analysed microchemically an addition of Ag was determined in the amount ranging from 0.1 to 2.5 wt. %.

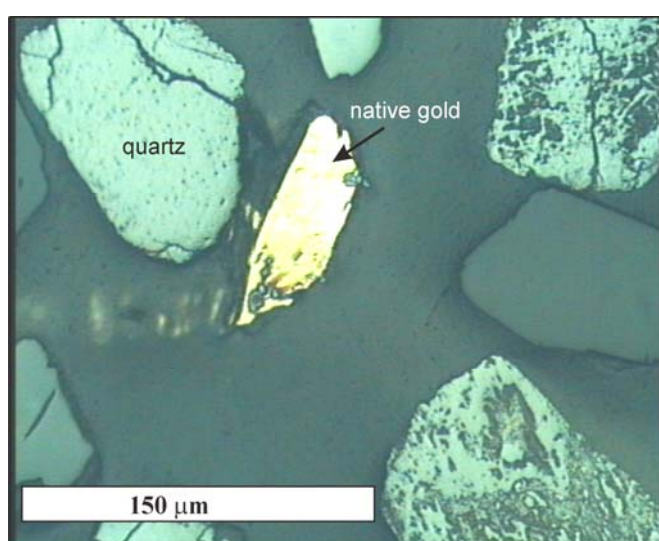


Fig. 6. Native gold with hematite from Osiecznica. Reflected light; plane polarized light

Pyrite is present in the heavy mineral fraction in the form of inclusions in grains of quartz and zircon (zonal zircon and zircon without the zonal structure). Quartz grains containing pyrite are poorly rounded. Grains of non-zonal zircon with pyrite are also poorly rounded. Grains of zonal zircons are on the other hand very well rounded and pyrite occurs in the external rim of zircon growth. Its diameter ranges from 1 to 5 μm .

Tetrahedrite-tennantite in the material from Osiecznica is very rare (Fig. 7). It was observed in two grains of the concentrate which consisted of quartz-calcite aggregates with sulphides and also in three inclusions in quartz grains. In the first example tetrahedrite-tennantite occurs in the concentrate grains in the form of intergrowths with chalcopyrite (Fig. 7).

This grain is a product of mechanical destruction of a hydrothermal vein. Apart from these two sulphides the aggregate from the vein contains also pyrite and sphalerite. In the second example tetrahedrite-tennantite has a form of an inclusion

intergrown with chalcopyrite inside quartz grains. The diameter of the tetrahedrite-tennantite-chalcopyrite ranges from 10 to 15 μm . The same quartz grains contain small inclusions of sphalerite (5 μm in diameter) intergrown with chalcopyrite.

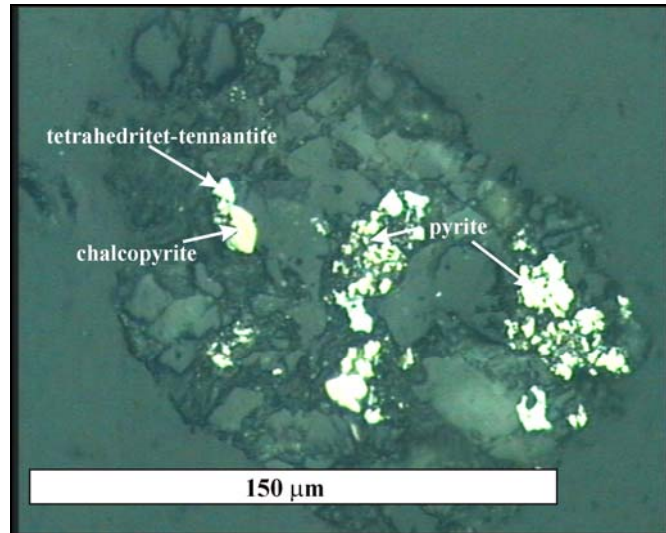


Fig. 7. A grain from a quartz-calcite vein (grey minerals) containing sulphide minerals from Osiecznica. Reflected light, plane polarized light

CONCLUSIONS

Although the glass sands from Osiecznica are very well sorted, they contain abundant ore minerals which have not been described earlier from this deposit. The minerals are simple sulphides of Cu, Fe and Zn, i.e. chalcopyrite, pyrite, pyrrhotite, sphalerite, pentlandite, and complex sulphides, i.e. arsenopyrite and tetrahedrite-tennantite. The sulphides may be a source of increased content of unwanted elements such as Zn, Cu, Ni, As, Sb in products and half-products, in industries in which purity of material is of utmost importance (e.g. glass production, pharmaceutical and chemical industry).

The sample contains also native gold and silver. Native gold concentration in the concentrate sample reaching 0.11 vol. % may be indicative of a high content of this metal in the Osiecznica deposit (around 1.5 g/Mg).

Accessory minerals described from Osiecznica glass sands point to the Sudetic area (S or SE of Osiecznica) as the source area. The composition of the main minerals in the heavy mineral fraction is different in relation to other occurrences of such sands in Poland (e.g. Biała Góra (Łuszczkiewicz 1987, 2002)). On the basis of major components in the heavy mineral fraction it is very difficult to define the source area of the glass sands under study. Accessory minerals, i.e. rutile, anatase, quartz, zircon

or monazite with xenotime occur in various magmatic or metamorphic rocks. Most mountain massifs in the Sudetes Mts are composed of such rock types. However, ore minerals present in the minerals mentioned earlier provide a source of univocal information regarding the origin of these ore minerals and at the same time information on the origin of the host mineral.

All of the ore minerals mentioned earlier (sulphides, sulphide analogues) observed as grown together or intergrown are a result of crystallisation in mesothermal conditions or under boundary conditions between mesothermal and catathedral. The presence of these minerals and the presence of the eroded hydrothermal vein point to the origin of the material from eroded rock massifs which contained hydrothermal quartz and quartz-feldspar veins. The rocks of such type are common in the Góry Kaczawskie Mts and the Pogórze Kaczawskie Foreland in the area between Zagrodno and Wojcieszów. It is plausible that gold and the main component of the glass sand, i.e. quartz did not originate from the region of Karkonosze Mts - Góry Izerskie Mts, which is indicated by the geographical position, but from an area located farther to the SE, i.e. the Kaczawskie Góry Mts.

REFERENCES

- Bilans zasobów kopalin i wód podziemnych w Polsce na 31 XII 2004 r.*, (2005), Wyd. Ministerstwo Środowiska.
- BŁASZAK M., (1973), *Atlas litologiczno-surowcowy Polski 1: 2 000 000*. Surowce skalne. I. Surowce okruchowe. Piaski kwarcowe przedczwartorzędowe. Wyd. Geol. Warszawa.
- BŁASZAK M., GRODZICKI A., (1979), *Piaski szklarskie*. W: Surowce mineralne Dolnego Śląska. Wyd. PAN. Wrocław-Warszawa-Kraków-Gdańsk.
- KOZŁOWSKI S., (1986), *Surowce skalne Polski*. Wyd. Geol. Warszawa.
- ŁUSZCZKIEWICZ A., (1987), Odzysk minerałów ciężkich z piasków szklarskich Kopalni „Osiecznica”. *Fizykochemiczne Problemy Mineralurgii*. nr. 19, 309-319.
- ŁUSZCZKIEWICZ A., (2002), *Poznawcze i technologiczne aspekty występowania minerałów ciężkich w surowcach okruchowych*. Prace Naukowe Instytutu Górnictwa Politechniki Wrocławskiej Nr 99, Monografie Nr 36. Wrocław
- ŁUSZCZKIEWICZ A., MUSZER A., (1999), *Złoto ze złoża naturalnych Rakowice koło Lwówka Śląskiego*. *Fizykochemiczne Problemy Mineralurgii*. nr. 33, 99-106.
- MILEWICZ (1967), *Kreda depresji północnosudeckiej w świetle nowych badań*. W: Przewodnik XL Zjazdu PTG. Warszawa.
- MUSZER A., (2000), *Zarys mikroskopii kruszców*. Wyd. Uniwersytetu Wrocławskiego, Wrocław.
- PORĘBA E., 1968, *Wykorzystanie złóż piasków szklarskich w Polsce*. I Konf. Nauk.-Tech. „Surowce skalne Polski”. Wyd. Geol. Warszawa.
- Muszer A., Łuszczkiewicz A.,** *Charakterystyka mineralogiczna minerałów akcesorycznych ze złoża w Osiecznicy na Dolnym Śląsku*, *Physicochemical Problems of Mineral Processing*, 40, (2006) 77-88 (w jęz. ang.).

Scharakteryzowano skład minerałów ciężkich w złożu piasków szklarskich z Osiecznicy na Dolnym Śląsku. W wydzielonym koncentracyjnym minerały akcesoryczne występują głównie jako samodzielne ziarna, w mniejszej ilości jako okruchy skał żyłowych oraz w postaci wrostków w ziarnach kwarcu i w samych minerałach ciężkich. W badanej próbce stwierdzono obecność rutylu, anatazu,

magnetytu, hematytu-goethytu, ilmenitu-leukoksenu, cyrkonu, monacytu, ksenotymu, cyanitu, piroksenów oraz kwarcu z wrostkami chalkopirytu, pirytu, pirotynu, sfalerytu, pentlandytu, arsenopirytu i tetraedrytu-tennantytu. Ponadto w badanej próbce stwierdzono obecność złota i srebra rodzimego. Głównymi składnikami w badanym koncentracie są rutil, anataz, kwarc z wrostkami kruszców, cyrkon oraz zgoethytowany hematyt. Pozostałe minerały występują w ilości mniejszej niż 2-3 % objętościowych. Zawartość złota rodzimego w badanej próbce koncentratu (0,11 %) może świadczyć o znaczącej zawartości tego metalu w złożu w Osiecznicy w ilości rzędu 1,5 g/Mg.

Antoni MUSZER*

PETROGRAPHICAL AND MINERALOGICAL CHARACTERISTICS OF THE METALLURGICAL SLAG FROM THE DÖRSCHL FURNACE (GŁOGÓW FOUNDRY, POLAND)

Received March 15, 2006; reviewed; accepted May 15, 2006

Lead metallurgical slag from the Dörschl furnace resembles magmatic rocks with respect to the mineral composition and petrographic structure. The majority of mineral phases in lead metallurgical slag are not 'stoichiometric' chemical compounds present in natural conditions. The slag studied contains Cu and Cu+Fe sulfides, i.e. cubanite, covellite, bornite and chalcopyrite. The most Cu-rich phase in the lead metallurgical slag is cubanite (16 - 20 % wt.). Cu is present also in the form of inclusions of metallic copper in silicates. Zinc is mostly present in the form of sulfides (sphalerite) and silicates (willemite). Iron occurs mainly as metallic iron of various composition, magnetite, phayalite and pyrrhotite. Magnetite forms tiny inclusions in silicates of phayalite type and in rhombic pyroxenes. Lead is mostly present in the form of Pb alloys with Ag, Cu, Zn. Arsenic present in the slag was captured by the crystallizing metallic iron and incorporated in its crystal lattice. The slag contains also a minor quantity of metallic silver and molybdenite. The knowledge of mineral phases composed of non-ferrous metals, i.e. Zn, Cu and Pb may facilitate the design of methods for their recovery. Thus a waste product that is arduous to the environment and deposited on a heap may become a valuable anthropogenic source of these metals.

Key words: metal alloys, ore minerals, metallurgical slag, furnace Dörschl, industrial waste, petrography and mineralogy of lead metallurgy slag

INTRODUCTION

Lead metallurgical slag from the Dörschl furnace resembles magmatic rocks with respect to the mineral composition and petrographic structure. The slag is an analogue of magmatic rocks present in the Earth's crust. The majority of mineral phases in the lead metallurgical slag are not 'stoichiometric' chemical compounds present in natural conditions. Due to their fast crystallization process these mineral phases may be regarded as unstable. The elemental composition of the chemical compounds under study is much different from that of their analogues present in ores. Due to their

* University of Wrocław, Department of Geological Science, Poland, amus@ing.uni.wroc.pl

physical and optical properties, the metal-bearing mineral phases will be referred to in this paper as ore mineral by analogy to mineral present in ores.

The studies were concentrated on the description of ore minerals and metal compounds in slag from the Dörschl furnace in the “Głogów” Foundry (copper metallurgy), and on the determination of crystallographic forms in which the main chemical elements are concentrated in the process of lead smelting. The knowledge of mineral phases composed of non-ferrous metals, i.e. Pb, Zn and Cu may facilitate the design of uncomplicated methods for their recovery. Thus a waste product that has been deposited on a heap may become a valuable anthropogenic source of these metals. The transition from waste to a component of anthropogenic deposit shall reduce negative impact on the environment and decrease the related cost of waste disposal.

METHODS

Samples of these slags were obtained for investigations in 2002 and 2003, during the study of metallurgic dusts in the vicinity of “Głogów” Foundry (Grech 2002, Wójcik 2003, Muszer 2004). Samples from 2002 and 2003 years were mixed in the proportion of fifty to fifty per cent. Also 1.5 kg sample of the lead metallurgical slag was taken to petrographical and mineralogical investigations.

Table 1. Outputs of a lead metallurgical slag sample

Fraction	γ %	non-magnetic fraction	γ % 0.6 T	γ % 0.9 T
>0.125	63.83	14.61	11.65	73.74
<0.125	36.17	----	4.52	95.48
total	100,00			

In order to prepare the lead metallurgical slag for the investigations it was ground in a crush mill (Fritz’s Mill) and separated into two grain-size fractions: >0.125 mm and < 0.125 mm (Tab. 1). In order to determine the character of ore minerals that reveal magnetic properties, magnetic concentration was carried out (in dry state; 5 cycles of concentration). The enrichment was performed with the use of permanent magnets with magnetic induction 0.6 T and 0.9 T. After separation with the magnet of components revealing strong and weak magnetic properties, polished sections for microscopic investigations in the reflected light were prepared from individual grain-size fractions, i.e. >0.125 mm and <0.125 mm, from five products received for the study. The sections were prepared according to the standard method for metal ore samples (Muszer 2000). Polishing of the study material was performed on polishing cloths (Struers DP-Mol, DP-Dur and DP-Nap) while applying strictly defined grain sizes of diamond polishing pastes.

The polished sections were investigated under the microscope in the Laboratory of Mineral Raw Materials at the Institute of Geologic Studies of the Wrocław University.

The studies in reflected light were performed with the use of Nikon Optiphot 2-Pol microscope. Planimetric analysis and the Lucia M programme was used in the quantitative analysis of ore minerals. The proportion of metals in sulfides and orthosilicates was determined with the use of microchemical analysis. The elemental composition of minerals was studied with the use of scanning microscopes SEM 515 (Philips) and JOEL JSM-55800LV equipped with an X-ray spectrum analysis attachment. These investigations were carried out at the Institute of Low Temperature and Structure Research (Polish Academy of Sciences) in Wrocław and at the Wrocław University of Technology.

THE QUALITATIVE AND QUANTITATIVE CHARACTERISTICS OF THE LEAD METALLURGICAL SLAG

The charge for lead smelting consists of lead slag from the shaft process, converter ashes, electro-furnace ashes, converter slag and lead slag from Kaldo furnace (Table 2). The per cent share of individual components in the smelting process varies in relation to the quantity of the furnace charge.

Table 2. The contents of metals in metallurgical waste (Pluciński et al. 1996)

Component	Slag from shaft furnaces	Converter ashes	Electro-furnace ashes	Converter ashes	Slag from Kaldo furnace
Pb	44.4	46.37	44.58	64.24	56.4
Cu	1.67	0.87	1.72	1.01	1.06
Zn	6.1	8.17	16.34	1.82	-
As	3.22	2.59	0.98	6.67	1.24
Sb	0.03	0.01	0.052	0.09	4.9
Bi	0.034	0.02	0.0078	0.021	0.24
S _{og}	10.9	11.3	1.85	4.58	-
Fe	0.7	0.2	0.23	0.06	-
SiO ₂	4.4	0.2	4.72	2.56	9.04
Na ₂ O	0.4	0.4	1.2	0.23	-
K ₂ O	1.9	0.4	12.7	0.18	-
C _{org}	13.55	-	1.83	0.22	-
C _{org}	11.27	-	-	-	-
Cl	1.5	-	0.03	0.1	0.2
Cd	0.015	-	0.12	-	-
Ag	0.012	0.045	0.007	0.007	0.21
Hg	0.001	-	-	-	-
Re	0.013	0.003	0.0006	-	-
Main Pb-bearing component	PbS	PbSO ₄	PbO	PbO	PbO · SiO ₂ /2PbO · SiO ₂

During the process of smelting of crude lead, there forms a slag characterized by varied elemental and mineralogical composition (Bielankin et al. 1957; Ptak, Nowakowski 1978).

The lead metallurgical slag composition depends on the share of individual components in the furnace charge (Table 2). The proportion of shaft furnace slags in the charge amounts to 30-60%, converter ash 10-40%, oxide ash and slag 5-20%, and of the 'own' slag from the foundry 0-10% (Pluciński et al. 1996). The slag formed in the Dörschl furnace (lead metallurgy slag) is a mixture of slag, copper-lead matte and waste from Ni-Co refining. The proportion of individual metals varies strongly (Tab. 3).

Table. 3. An average composition of the lead metallurgy slag, after Pluciński et al. (1996)

Component	Contents [%]
Pb	4.2-8.0
Cu	2.2-4.3
Ag	0.004-0.008
Fe	15.0-25.0
Zn	6.0-12.0
SiO ₂	10.0-18.0
S _{og}	10.0-12.0

The following mineral phases were determined in the lead metallurgy slag sample: metallic iron, cubanite, covellite, bornite, chalcopyrite, metallic copper, sphalerite-willemitite, Pb alloys, magnetite (+hematite), pyrrhotite, cuprite and trace amounts of metallic silver and molybdenite. The major transparent constituents are phayalite (Fe₂SiO₄), silicates and silicate alloy. The majority of ore minerals of the tabular or scaly morphology (covellite, cubanite) are strongly structurally intergrown with other copper sulfides or silicates parallel or perpendicular to the crystallization planes.

Almost total amount of metallic iron present in the sample was taken out with a weak magnet (magnetic induction 0,6 T). A characteristic feature of the alloy is its high reflectance and isotropism. The size of iron grains in the slag ranges from several to several tens of μm in diameter. The shape of this mineral is frequently irregular; intergrowths with phayalite are common.

Metallic iron contains high proportion of As. Its quantity is within a range from 1 to 24 % wt. Iron contains also high amounts of sulphur - up to 2.5 % wt. Metallic iron forms growths with pyrrhotite, silicates and silicate alloy. In places continuous transition from metallic iron to iron-lead alloy is observed (Fig. 1).

Cubanite has physical properties typical of its natural counterpart. It forms tabular crystals very strongly intergrown with silicate minerals and silicate alloy. The size of individual crystals does not exceed 100 μm in diameter. Its optical properties depend

on the Cu content in the ore mineral and vary within wide limits. A particular feature is its brownish-yellow to brass-brown colour and strong anisotropy related with the elemental composition. Cu content in natural cubanite is around 23.4% In the Cu sulfide under study it amounts to 16 - 20% wt. of Cu (Fig. 2).

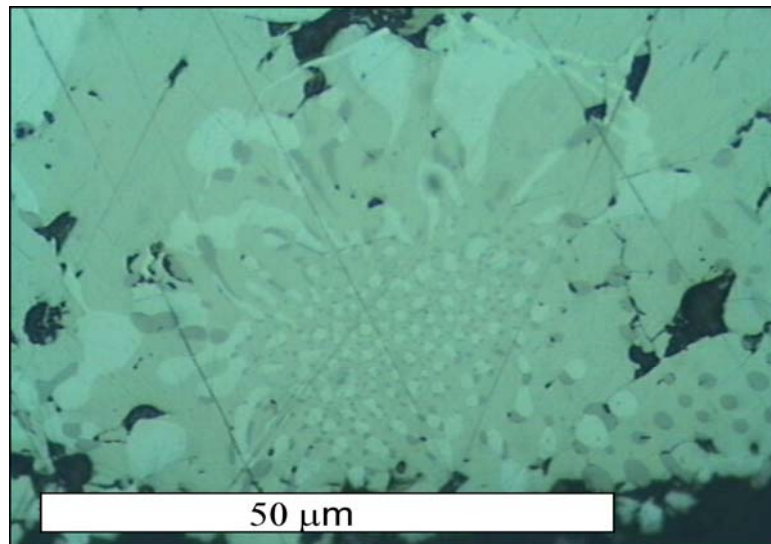


Fig. 1. Metallic iron with variable elemental composition (Fe-As to Fe-Pb). Reflected light; plane polarized light

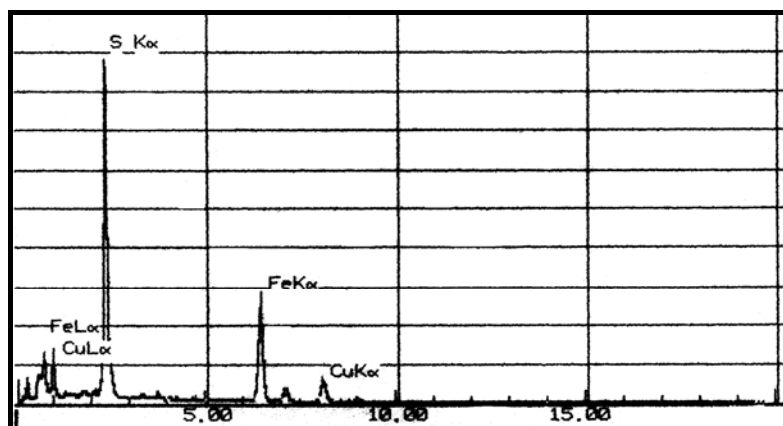


Fig. 2. Characteristic X-ray spectrum of "cubanite"

This is a feature indicative of sulphur deficiency and fast crystallization of this mineral. Cubanite is most commonly present in the form of tabular intergrowths with covellite, bornite or silicates (Figs. 3, 4).

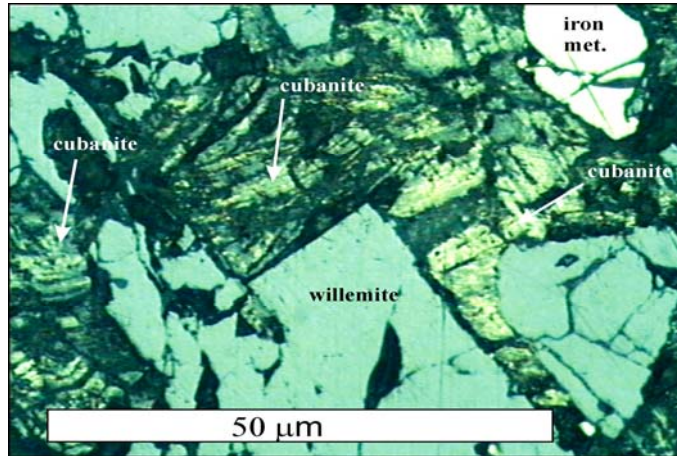


Fig. 3. Cubanite structure in lead metallurgy slags. Reflected plane polarized light.

Covellite is a common sulfide in the slag under investigation. Its physical and optical properties are so distinct that it is difficult to mistake it for any other chemical compound. It is characterized with a typical tabular morphology and fiery-orange-red anisotropy. In individual covellite grains one may observe continuous transitions from ‘cubanite’ to ‘semi-bornite’ (Fig. 4). Along crystallization planes of covellite alloys and silicates of Fe-Na are frequently encountered.

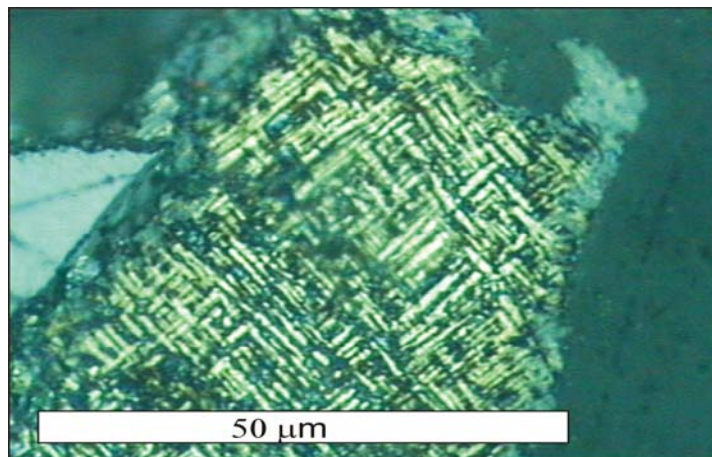


Fig. 4. Cubanite-bornite-covellite structure in lead metallurgy slag. Reflected plane polarized light

The content of copper in covellite under study is different from Cu proportion in natural covellites. Covellite present in copper ores contains around 66.5% Cu. In the samples analyzed the copper content is much lower and ranges from 46 to 53% wt.

Cu. This varied Cu content is related with the presence of Fe ions in the structure of covellite. Iron content may in places reach up to 18.5% wt. On the basis of observation of grains and crystals one may state that they have optical and physical properties of covellite, but their chemical composition shows phase transitions from bornite to cubanite (Fig. 4).

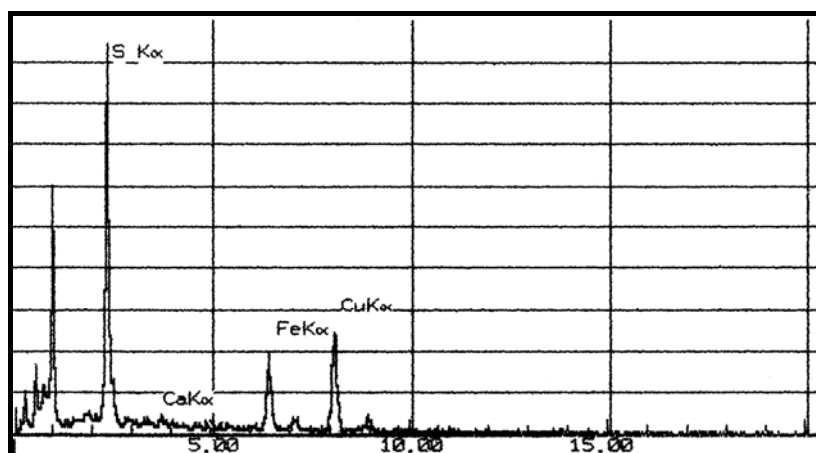


Fig. 5. X-ray spectrum of 'covellite'

Bornite is characterized by a varied colour from brown to blue-heather colour. It reveals very weak anisotropy and its chemical composition is different from the one of the natural bornites. Bornite does not form a uniform crystalline phase. Microchemical analyses confirmed that most commonly it is a mixture of transition phases from semi-bornite to covellite-cubanite with an addition of chalcopyrite (Fig. 6). In places bornite contains small oval forms of 'pure' metallic copper. The Cu concentration varies in individual grains from 31.5 to 59.5 % wt. Cu and never reaches the proportion observed in natural bornites 63.3 % wt. Cu. Its chemical composition is more similar to that of the compound Cu_3FeS_3 or CuFeS_6 , than the one of Cu_5FeS_4 .

Chalcopyrite is a very rare ore mineral constituent of the samples. It is very distinctly visible at the background of grey silicates and sphalerite. Its yellow colour is typical of natural chalcopyrite and its anisotropy is very weak. It forms intergrowths with other copper sulfides. The grain sizes do not exceed several tens of μm in diameter.

Metallic copper in the lead metallurgy slag is rare. It is most frequently present in the form of oval or round inclusions in bornite and metal silicates. The copper exsolutions reach up to a dozen or so micrometers in diameter. Bigger forms of a wire type are not grown with silicates but they are covered with a thin coat of cuprite. The copper grains analyzed are of an extraordinary 'purity'. The proportion of other metals' additions is below 0.5% wt.

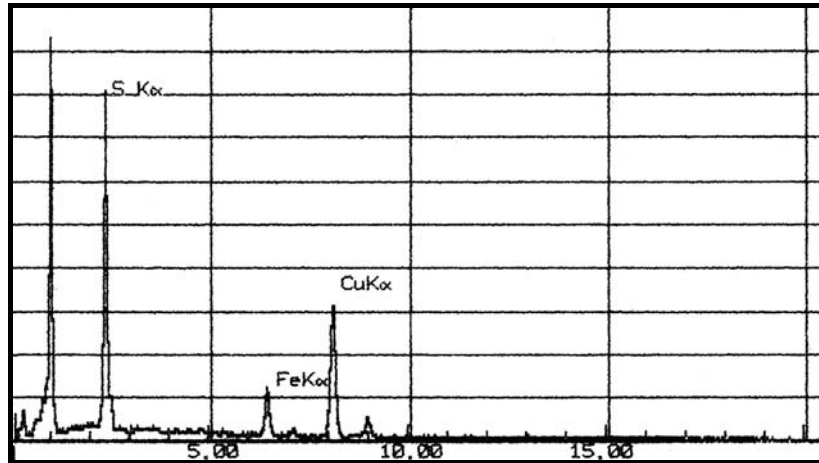


Fig. 6. X-ray spectrum of 'bornite'

Sphalerite present in the material under study contains high amounts of Fe. It is characterized with a low reflectance and grey colour which is a feature distinguishing it clearly from natural sphalerites. The surface of sphalerites studied is easy to polish - this is yet another difference from their natural counterparts. The mineral colour is uniform grey on the whole surface. It forms irregular shapes or grains intergrown with phayalite, willemite and Mg-Ca silicates. Their physical and optical properties are typical of sphalerite. Its chemical composition could be expressed with a formula $(\text{Zn,Fe})\text{S}$. The content of Fe ranges from 9 to 17.1% wt. of Fe. Sphalerite is accompanied by willemite that forms growths and intergrowths with it. Because of difficulty in separation of these two minerals from one another they have been treated together in the course of the quantitative analysis.

Pb alloys are easy to distinguish in the material as they have very high reflectance when compared with the other ore minerals. The reflectance points to a low amount of metal admixtures in the alloys. Pb alloys have various complicated forms: drop-like, vermicular and oval. In places there are transitions from a pure Pb alloy to the alloy containing Pb and Fe. The majority of Pb alloys grains are grown-together with other metal compounds or silicates.

Magnetite is most commonly present in the form of tiny crystals within phayalite or silicate alloy. The size of individual crystals ranges from 0.2 μm to 60 μm in diameter. This mineral forms automorphic or hypautomorphic crystals. It also forms inclusions in sphalerite. Large magnetite grains bear traces of martitization (hematite formation). This process advanced from the outer rim of the grains. Microchemical analyses revealed no presence of admixtures in this mineral.

Pyrrhotite is present in the samples mainly in the form of growths with metallic iron, cubanite or phayalite. This mineral has typical optical parameters, distinct anisotropy and brown-creamy colour.

Table. 4. Quantity of main ore minerals in % vol

Cubanite	Metallic iron	Metallic copper	sphalerite- willemite	Bornite	Covellite
19.07	19.60	0.67	26.72	1.37	3.52
Chalcopyrite	Magnetite	Pb alloy	Pyrrhotite	Cuprite	Covellite-cubanite
0.40	13.04	8.52	4.60	0.07	2.42

The main useful mineral in the slags is sphalerite, which is most frequently intergrown with willemite. These both minerals constitute 26.72% vol. of all ore minerals (Tab. 4). The second most common mineral is cubanite. Its quantity amounts to 19.07% vol. The third one is metallic iron of varied elemental composition. These four minerals make up 65.39% vol. of the ore minerals in the slag. The quantity of the other ore minerals ranges from 0.07 % vol. (cuprite) to 13.04% vol. (magnetite). Apart from the ore minerals mentioned earlier, the sample contained accessory amount of molybdenite and tiny exsolutions of metallic silver.

CONCLUSIONS

The lead metallurgy slags from the Dörschl furnace from the ‘Głogów’ Foundry contain Cu and Cu+Fe sulfides, i.e. cubanite, covellite, bornite and chalcopyrite. The first mineral is the main Cu carrier in the lead metallurgy slag. Its optical and physical properties resemble the properties of natural cubanite present in metal ores. The copper concentration in cubanite ranges from 16 to 20%. The rest of copper occurs in the form of metallic Cu. Zinc is mainly concentrated in the sulfide (sphalerite) and silicate (willemite) forms. These both minerals frequently form intergrowths. Iron is present mostly as metallic iron, magnetite and pyrrhotite. Iron alloy grains have irregular shapes and form gradual transitions to alloys of Fe-Pb-As. Magnetite is present in the form of tiny inclusions in silicates of phayalite type and in rhombic pyroxenes. The main Pb carriers are lead alloys with various admixtures such as Fe, Ag, Cu, Zn. Arsenic in the slag was intercepted by metallic iron during crystallization. The microchemical analyses revealed no presence of arsenic in other minerals of the lead metallurgical slag.

The determination of mineral phases composed of non-ferrous metals (Zn, Cu, Pb) may help in designing of a recovery technology. Thus a waste material, regarded as arduous to the environment, may become a valuable anthropogenic source of these metals.

REFERENCES

- BIELANKIN D.S., IWANOW B.W., LAPIN W.W., (1957), *Petrografia kamieni sztucznych*. Wyd. Geol. Warszawa.
- GRECH G., (2002), *Analiza antropogenicznych pyłów powstających w rejonie Huty Miedzi „Głogów”* M.Sc. Thesis, Arch. Uni. Wroc.
- KUCHARSKI M., (2003), *Pirometalurgia miedzi*. Wyd. Nauk.-Dydak. Kraków
- MUSZER A., (2000), *Zarys mikroskopii kruszców*. Wyd. Uniw.Wroc.Wrocław.
- MUSZER A., (2004), *Mineralogical characteristics of metallurgical dust in the vicinity of Głogów*. Physic. Probl. of Min. Proces.38, 329-340.
- PLUCIŃSKI S., Cis W., Gargul J., Olewiński L., Wroński W., Zakrzewski J., (1996), *Technologia odzysku metali towarzyszących*. in: Monografia KGHM Polska Miedź S.A.. Kraków.
- PTAK W., Nowakowski J., (1978), *Wykorzystanie rud i koncentratów ołowiu*. in: Surowce mineralne świata. Cynk, Ołów, Kadm. Wyd. Geol. Warszawa.
- WÓJCIK R., (2003), *Charakterystyka pyłów atmosferycznych pomiędzy LGOM a Wrocławiem na podstawie badań w świetle odbitym*. M.Sc. Thesis, Arch. Uni.Wroc.
- Muszer A.**, *Charakterystyka petrograficzno-mineralogiczna metalurgicznych żużli poolowiowych z pieca wahadłowego Dörschla. Huta Głogów. Polska*, Physicochemical Problems of Mineral Processing, 40, (2006) 89-98 (w jęz. ang.).

Głównym celem niniejszych badań było scharakteryzowanie kruszców i związków metali w żużlach pochodzących z pieca „Dörschla” z huty miedzi „Głogów” oraz określenie, w jakich formach krystalograficznych gromadzą się najważniejsze pierwiastki przechodzące podczas wytopu ołowiu. Znajomość faz mineralnych złożonych z metali kolorowych, tj. Pb, Zn, Cu może przyczynić się do opracowania łatwego sposobu ich odzysku i zminimalizowania negatywnego skutku oddziaływania ich na środowisko, a tym samym obniżenia kosztów jego składowania. W próbce żużła poolowiowego stwierdzono obecność: żelaza metalicznego, kubanitu, kowelinu, bornitu, chalkopirytu, miedzi metalicznej, sfalerytu-willemitu, stopów Pb, magnetytu (+ hematytu), pirotynu, kuprytu oraz śladowe ilości srebra met. i molibdenitu. Dominującym składnikiem przezroczystym jest fajalit (Fe_2SiO_4), krzemiany oraz stop krzemianowy (szkliwo). Większość kruszców o budowie tabliczkowej lub łuseczkowej (kowelin, kubanit) są silnie przerośnięte strukturalnie z innymi siarczkami miedzi lub krzemianami zgodnie z powierzchniami krystalizacyjnymi lub prostopadle do nich. Głównym nośnikiem Cu w żużlach poolowiowych jest kubanit w którym ilość miedzi waha się w zakresie od 16 do 20 % wag. Ponadto Cu gromadzi się w formie miedzi metalicznej w postaci wrostków w krzemianach. Cynk zgromadzony jest głównie w formie siarczkowej (sfaleryt) i krzemianowej (willemit). Żelazo koncentruje się głównie w żelazie metalicznym o różnym składzie, magnetycie, fajalicie oraz pirotynie. Magnetyt obecny jest w formie drobnych wrostków w krzemianach typu fajalit i w piroksenach rombowych. Głównym nośnikiem Pb są stopy ołowiu z domieszkami Ag, Cu, Zn. Arsen obecny w żużlu został przechwycony przez krystalizujące żelazo metaliczne i w budowany w sieć krystaliczną. Żużle poolowiowe, uciążliwe dla środowiska a obecnie składowane na hałdzie, stać się mogą cennym złożem antropogenicznym.

Teresa SZYMURA *

RESEARCH ON INCRUSTATION IN A MODEL EVAPORATIVE COOLER

Received March 15, 2006; reviewed; accepted May 15, 2006

The paper presents research on scale formation performed in a laboratory model of an evaporative cooler. Such type heat exchangers are often applied in industrial cooling systems. As a heat carrier they usually use raw water, which despite its numerous advantages is also a source of many problems like corrosion and incrustation. The elaborated model makes possible to perform qualitative and quantitative testing of crystalline deposits that form on heating surfaces. The following tests performed with the application of the mentioned cooler model have been presented in the paper:

1. phase crystallization of calcium carbonate,
2. ammonium sulfate effect on incrustation in a model heat exchanger.

Diffractometric tests have shown differences in phase composition of calcium carbonate deposits, which have formed at different temperatures and in the presence of ammonium sulfate. At 40°C calcium carbonate has formed as anhydrous calcite and monohydrate while at 55-60°C additionally as aragonite. An addition of ammonium sulfate has inhibited scale accretion and even caused its insignificant dissolution.

Key words: cooling water, scale water, treatment, ammonium salts

INTRODUCTION

A continuous social and economic developments involve ever-increasing demand for water of adequate quality. Meeting of the demand requires many actions of various kinds and in that number shutdowns of water-based cooling systems that are applied in many industry branches.

In recirculating cooling systems the cooling effect is mainly obtained by evaporation of a part of water (high heat of evaporation). It is the reason why in such systems a fraction of the water volume gets consumed as compared to once-through cooling systems. However, water evaporation brings about its condensation, which causes exceeding the solubility product, especially of the main component of raw

* Lublin University of Technology, Institute of Building Engineering, 20-618 Lublin, ul. Nadbystrzycka 40, Poland, T.Szymura@pollub.pl.

water i.e. calcium carbonate, which in turn results in the precipitation of deposits called scale. There are also other problems that occur in water-based systems such as corrosion of construction materials, sludge formation, and biological fouling (Kowal, 1980). The presence of deposits on heat exchanger surfaces is of significant effect as it impedes heat flow and then the installations operate at a reduced efficiency.

Calcium carbonate deposits can form for the following reasons:

- susceptibility to deposit formation under the influence of temperature changes, which has an effect on the CaCO_3 solubility,
- changes in the solution pH, which disturbs carbonate-calcium equilibrium and causes CaCO_3 precipitation or its dissolution.

Calcium carbonate can crystallize in three forms: calcite, aragonite and vaterite. Conditions for the formation of individual phases have been discussed in many publications (Xu, et al. 1999; Turner, et al. 1998; Wray and Daniels, 1957). The present paper presents a research on calcium carbonate formation in a laboratory model of a spray-evaporative cooler.

QUALITY OF COOLING WATER

The basic requirement for cooling water is the so-called stability (Gomółkowie, 1994). Water stability can be defined as property that there is neither precipitation nor dissolution of calcium carbonate. In the case of spray-evaporative condensers it is practically impossible to maintain the stability as the cooling water temperature is about 30°C while the temperature of hot coil pipes in extreme cases can reach even $50\text{--}60^\circ\text{C}$. In such a case the conditions for the formation of dense scale deposits occur, especially that water gets condensed as a result of partial evaporation.

Considering various anti-scaling methods that are in use, two directions can be distinguished:

- introduction of supplementary water with most of the scale-generating pollutants removed,
- treatment of the circulating water by the addition of incrustation inhibitors.

Sometimes both approaches are jointly applied - preliminary treatment at first and then stabilization to inhibit scale formation in the course of water condensation. The application of inhibitors is simple and efficient as compared to other methods commonly used for the protection of industrial water-based systems. Modern inhibitor programs for cooling water treatment can be classified into three extensive groups (Ascolese, 1998):

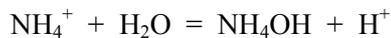
- acid method where pH of water is maintained between $6.0 \div 6.7$,
- neutral programs at the water pH of $6.8 \div 7.8$,
- alkaline programs when the water pH is $7.8 \div 9.0$.

Working with acid or neutral pH usually consists in maintaining the pH at an adequate level with the use of acid - usually HCl or H_2SO_4 - which is called acid grafting. Alkaline programs do not need pH correction but their disadvantage is that

there is a hazard of massive deposit formation, mainly of carbonates and that is why it is necessary to maintain low coefficient of water condensation, which increases water treatment costs.

Acid action is an efficient way to inhibit scaling and remove already-formed deposits but there is a risk of its overdosing and causing corrosive damage to the installation. Additionally, for economical reasons, acid grafting is not recommended when carbonate hardness of water exceeds $100 \text{ mg CaCO}_3/\text{dm}^3$ (Gomółkowie, 994).

Instead of acid, it is suggested to apply a salt of weak base (ammonium) and strong acid (hydrochloric, sulfuric). The salt hydrolyzes and safely acidifies the environment (Zagórski, et al. 1978):



The equilibrium constant is ca. $2 \cdot 10^{-5}$, so the cooling water pH does not drop below 6 when such salt is added. A total lack of prevention can lead to the formation of thick scale deposits, which dramatically decreases heat exchange efficiency (Fig. 1).

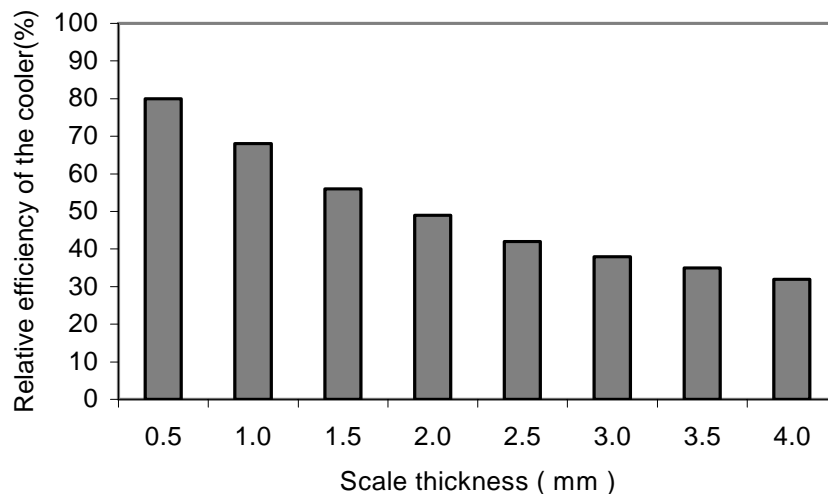


Fig. 1. Efficiency of an evaporative cooler vs. scale thickness

INDUSTRIAL STANDARD OF AMMONIA EVAPORATIVE CONDENSERS

Exchangers of the discussed type are often applied in the industry and especially in cold stores and plants of the fruit-and-vegetable processing branch. Operation of an evaporative condenser consists in pumping refrigerant vapor (ammonia) with a compressor to the cooling system. The vapor gets condensed under constant pressure and temperature. Heat gets absorbed by air and water at the external side of pipes. Application of the both media is thermodynamically and economically justified, as

they are easily available. For air there is practically no limit of availability although from the thermodynamic point of view water is much better applicable. However, water resources are limited and water treatment costs should also be considered, both of which make its availability worse than it is in the case of air.

Figure 2 presents a diagram of a typical spray-evaporative industrial condenser (Zalewski, 1998). Coils made of smooth pipes make its principal part. Cooled ammonia flows in the pipes in the downward direction. A spray system is installed above the coils to uniformly distribute water over the coil pipes. A catch-drop composed of adequately shaped elements meant to catch water drops carried with the air stream is mounted above the spray system. Outer surface of coils is sprayed with water that gravitationally flows down the warm pipes. Water evaporates into the air stream and gives up the heat received through the pipe walls from the condensing ammonia.

Cooling water works in a recirculating system. It is fed from a water tank and transferred by means of pumps to the spray system. A constant addition of fresh makeup water is required because of the water bulk losses resulting from its evaporation, being carried away by the air stream, leaks, and also from sludge removal performed to maintain optimal condensation level of water.

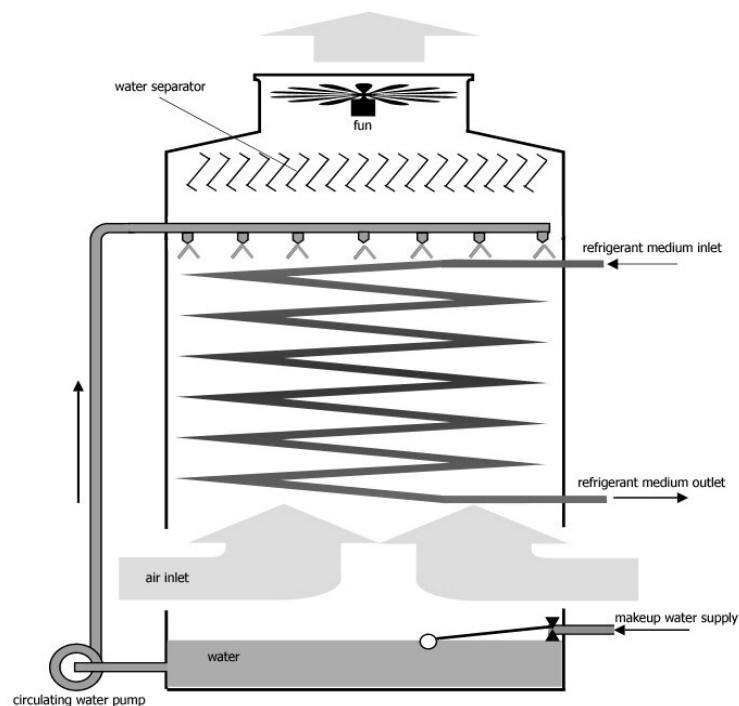


Fig. 2. Diagram of an industrial evaporative cooler

TESTS ON SCALE FORMATION PERFORMED IN A MODEL HEAT EXCHANGER

A model of a heat exchanger of the spray-evaporative type has been elaborated for the testing purposes. The model makes possible to perform simulation of processes that run in an industrial installation at the water-air side, where conditions for scale formation occur. Figure 3 presents a diagram of the model. The model consists of:

1. a tank of circulating water with a valve for its partial drain to perform sludge removal,
2. a set of steel pipes that serve as a coil with water inside and a thermostat connected to the water circulation system,
3. perforated troughs that distribute water at the exchanger top to uniformly spray the pipes,
4. water pump that makes water circulating,
5. air chamber to realize free airflow from the bottom of the pipes upwards,
6. drain valve to control condensation level of recirculating water,
7. inlet for air stream directed counter-current to the gravitationally flowing water.

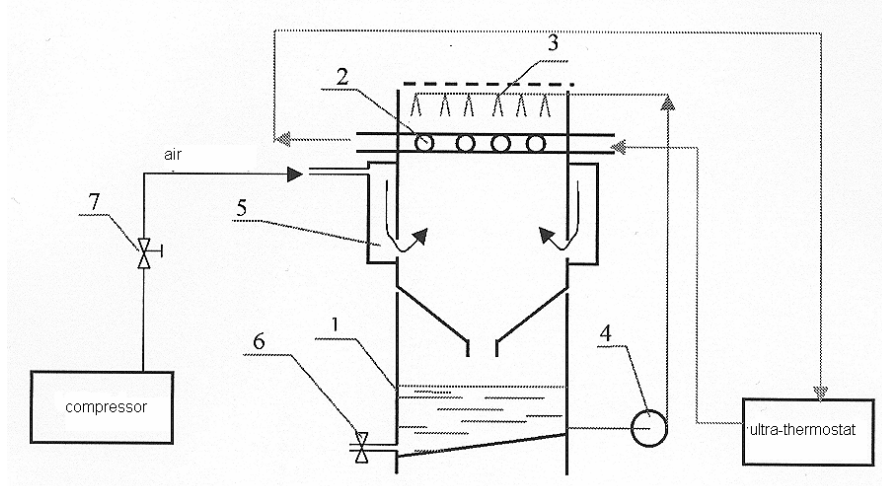


Fig. 3. Model of a spray-evaporative cooler : 1 – water tank, 2 – water coil, 3 – water distributor with a catch-drop, 4 – water pump, 5 – air chamber, 6 – drain valve, 7 – control valve with a rotameter

The following tests have been performed with the application of the discussed model:

1. calcium carbonate crystallization on pipes at 40 - 60°C,
2. effect of ammonium sulfate on incrustation processes in the model.

Tests have been performed under following conditions: temperature of the pipes 40 and 50-60 °C, feeding water parameters (calcium hardness 350 mg CaCO₃/dm³, carbonate hardness 350 mg CaCO₃/dm³, pH 7,2). The deposit has been tested chemically and with the application of a HZGA 2 Carl Zeiss Jena diffractometer.

EXPERIMENT 1. CRYSTALLIZATION OF CALCIUM CARBONATE

The system has been filled with 10 dm³ of feeding water. A thermostat has been connected to the water circulation system and a pump of circulating water has been switched on. Air stream of 500dm³/h intensity has been let in. Operation time of the installation has been 5 hours per 24 hours, over the period of 240-hours in total. Makeup water has been supplied as circulating-water losses have been occurring. As the experiment has proceeded a deposit has crystallized and it has been subdued to detailed testing. Photographs of the following crystals: rhombohedral crystals of calcite of the size of a few micrometers, which have crystallized in the temperature of 40°C and sharp-edged rhombic crystals of aragonite, which have crystallized at the temperature of 60°C are presented in Figs 4-5.

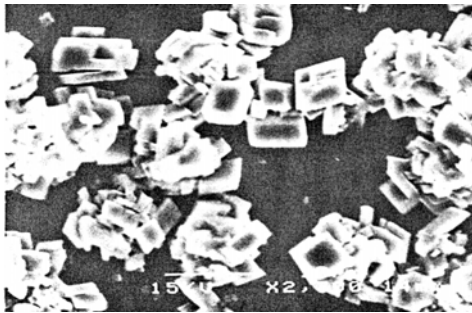


Fig.4. Crystals of calcite

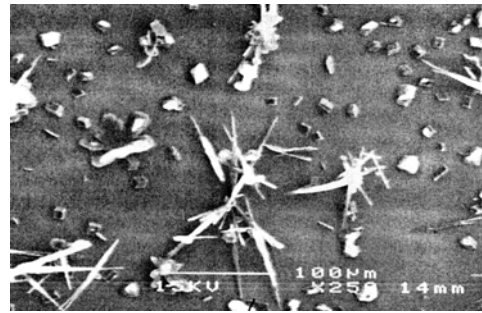


Fig.5. Crystals of aragonite

Figure 6 presents a diffraction pattern of scale that has formed at 40°C. A distinct calcite peak can be seen at 26.9° and many other peaks also indicate that the formed deposit is calcite. Other peaks as 20.5°, 29.2°, 41.5° indicate the presence of monohydrate.

Figure 7 presents a diffraction pattern of scale that has formed at 60°C. A distinct calcite peak can be seen at 29.5° as well as numerous aragonite peaks at 26°, 27°, 32.8° and also monohydrate peaks e.g.. 20.5°C.

Recirculating water has been tested once in 24 hours with determining contents of calcium and chlorides in it. Condensation degree n of water has been calculated on the basis of the obtained results:

$$n = \frac{\text{concentration of chlorides in circulating water}}{\text{concentration of chlorides in feeding water}},$$

as well as the calcium hardness ratio t :

$$t = \frac{\text{calcium hardness in circulating water}}{\text{calcium hardness in feeding water}}$$

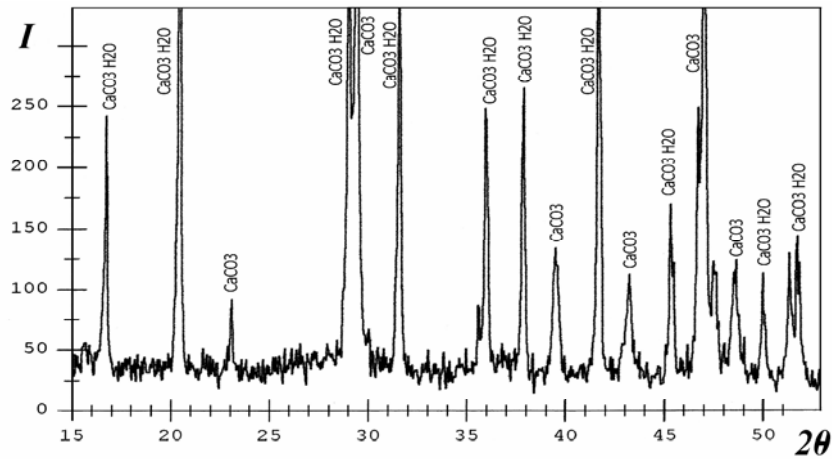


Fig. 6. Diffraction pattern of scale that has crystallized at 40°C

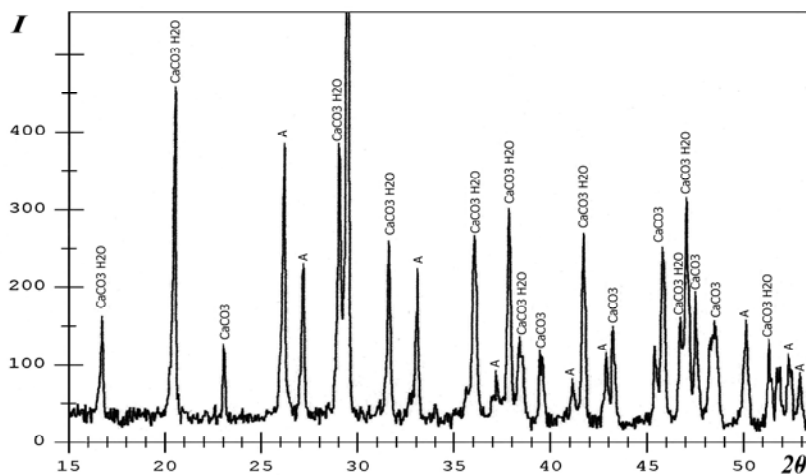


Fig. 7. Diffraction pattern of scale that has formed in the model at 60°C

The $t/n < 1$ ratio shows a loss of Ca^{2+} ions in circulating water as compared to the chloride content and indicates the presence of calcium ions in another form, which means that a solid phase has crystallized (curves 1 in Fig. 8). The pH value of water has increased up to 8.4.

EXPERIMENT 2. EFFECT OF AMMONIUM SULFATE ON INCRUSTATION PROCESSES

Exactly 4.25 mol/dm^3 of $(\text{NH}_4)_2\text{SO}_4$, has been added to feeding water, which is equivalent to 150% of a stoichiometric dose with respect to the hardness. Pipes of the heat exchanger have been partially covered with scale that formed during the previous experiment performed at 40°C (crystallized calcite).

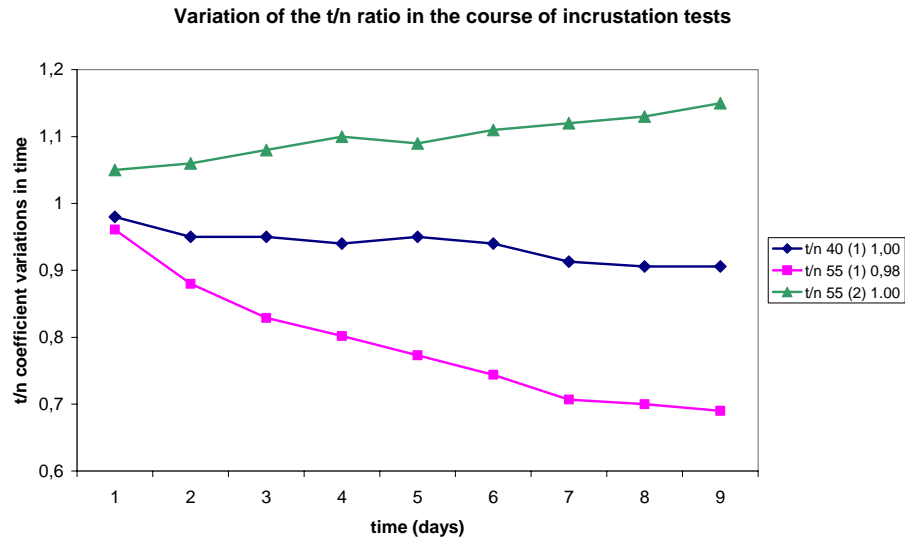


Fig. 8. Variations of the t/n ratio in the course of incrustation tests

The testing duration has been 5 hours per 24 hours over the period of 240 hours. Temperature of the pipes has been 60°C . The formed scale has been subdued to diffractometric tests.

Figure 9 shows a diffraction pattern of a scale sample taken when experiment 2 has been completed. The graph shows peaks that are characteristic for calcite, while there are no peaks indicating the presence of aragonite. Calcium sulfate crystals have not been found although the solubility product has been exceeded. When the testing has been completed at the bottom of the circulating water tank tiny chips of scale have been found and they have shown to be calcite.

Recorded values of the condensation coefficients n and t have shown that the t/n ratio has remained contained within the range from 1 to 1.15 (curve 2 in Fig. 8), which means that no further scale buildup has occurred. Calcium ion concentration has been a little higher than it should follow from the condensation level, which indicates that some insignificant chemical dissolution of the scale deposited on the exchanger pipes has occurred. The pH of circulating water has remained at the level of 6.9.

DISCUSSION

Design of the model makes possible to simulate conditions of an industrial spray-evaporative condenser. An important feature of the model is water recirculation. Temperature of the circulating water differs by ca. $20\text{-}25^{\circ}\text{C}$ from the temperature of the heat exchanger pipes. Air blow cools the water and also makes its evaporation easier by smashing water drops into smaller ones

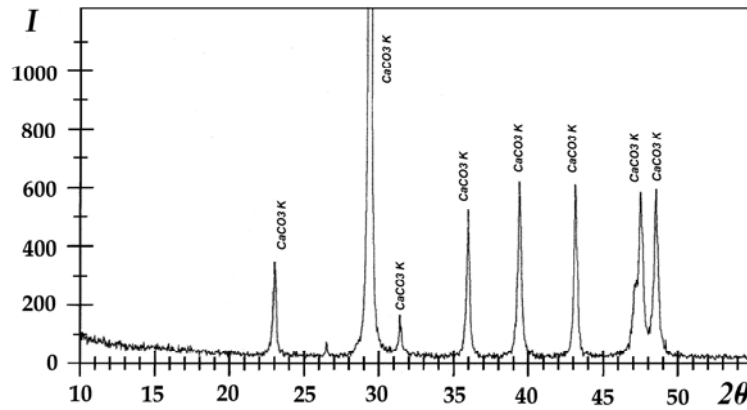


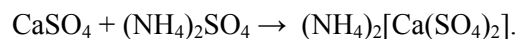
Fig.. 9. Diffraction pattern of scale subdued to the action of $(\text{NH}_4)_2\text{SO}_4$ at 60°C .

Results of tests performed in the model agree with the literature data (Gomółkowie, 1994; Kowal, 1980; Lipiec and Szmal, 1976). In cooling installations the forming deposit is chiefly calcium carbonate in the form of calcite and monohydrate, while at above 50°C - 60°C a considerable part of the deposit is an unstable aragonite that in some time re-crystallizes into calcite. Crystallization of calcite or aragonite can also be influenced by over-saturation of the solution as well as by the presence of magnesium ions.

The other part of the discussed experiment proves that an addition of ammonium sulfate brings about some insignificant dissolution of the scale ($t/n > 1$), which decisively enhances heat exchange conditions in cooling systems. The selection of an ammonium salt of a strong acid, which hydrolyzes and lightly acidifies the environment, is not accidental, as it eliminates acid, whose overdosage can bring serious corrosive consequences.

An addition of ammonium ions as a biogenic factor is not any shocking in this specific case, as the ammonia presence in a system that includes an ammonia condenser is a obvious because of its leaks to the cooling water resulting from the system leak-tightness faults. The selection of ammonium sulfate to be applied in industrial installations is economically justified, as it is the cheapest of all strong-acid ammonium salts.

In the other experiment calcium sulfate has not crystallized even though the solubility product has been exceeded. According to manuals on chemical analysis calcium sulfate dissolves in the solution of $(\text{NH}_4)_2\text{SO}_4$, because of the formation of complex compounds according to the following reaction (Lipiec and Szmal, 1976):



The reaction runs better under hot conditions and that is why the formation of gypsum on hot walls of a heat exchanger and in the presence of ammonium sulfate is rather unlikely.

CONCLUSIONS

1. As far as the formation of CaCO_3 deposits is concerned, the results of testing performed in the discussed model agree with those given in the pertinent literature. Calcite forms at lower temperatures and aragonite occurs when the temperature exceeds 50°C .
2. The model testing has confirmed what has been observed in other laboratory or industrial installations when ammonium salts have been applied for cooling water treatment purposes (Szymura and Pomianowski, 2005). The dissolution of CaCO_3 , scale crumbling, and no further formation of new solid phases of calcium sulfate or calcium carbonate is observed, even though the solubility products is exceeded.

REFERENCES

- ASCOLESE CHR., BAIN D.J. (1998), *Take Advantage of Effective Cooling-Water –Treatment Programs*, Chemical Engineering Progress, 3, 49-54.
- GOMÓLKOWIE E. i B. (1994), *Technologia wód przemysłowych z ćwiczeniami*, Wrocław.
- KOWAL A.L. (1980), *Technologia wody*, Warszawa, Arkady.
- LIPIEC T., SZMAL Z. (1976), *Chemia analityczna z elementami chemii instrumentalnej*, W-a, PZWL
- SZYMURA T., POMORSKA K. (2005). *Zastosowanie soli amonowych w układach wody chłodniczej*, Chłodnictwo, 1-2.
- TURNER C.W., SMITH D.W. (1998), Calcium Carbonate Scaling Kinetics Determined from Radiotracer Experiments with Calcium- 47 Ind. Eng. Chem. Res. 37, 439-448.
- WRAY J.L., DANIELS F. (1957), *Precipitation of calcite and aragonite*, J.Am.Chem.Soc. 79, 2031-2034.
- XU S., MELENDRES C.A., PARK J.H., KAMRATH M.A. (1999), *Structure and Morphology of Electrodeposited CaCO_3 : X-Ray Diffraction and Microscopy Studies*, Journal of the Electrochemical Society, 146 (9), 3315-3323.
- ZAGÓRSKI K., WARSZAWA Z., SZYMURA T. (1978), *Sposób usuwania węglanowego kamienia kotłowego i zapobiegania jego powstawaniu w wodno-chłodniczych instalacjach przemysłowych*, Patent Polski nr 102517.
- ZAŁEWSKI W., LITWIN M., PACZESNA J. (1998), *Wyparne chłodnice cieczy. Charakterystyki cieplne i metoda doboru*, Chłodnictwo, 12, 37-40.
- Szymura T.**, *Badania powstawania kamienia kotłowego w modelowej chłodnicy wodno-powietrznej* Physicochemical Problems of Mineral Processing, 40 (2006), 99-108(w jęz. ang.)

Przedstawiono badania powstawania kamienia kotłowego w laboratoryjnym modelu chłodnicy wodno-powietrznej. Wzorzec takiego wymiennika ciepła jest często spotykany w przemysłowych instalacjach chłodniczych. Wykorzystywana tam nieuzdatniona woda jako nośnik ciepła, pomimo wielu zalet, jest sprawcą wielu problemów, takich jak korozja i inkrustacja. Powstały kamień kotłowy na ściankach wymiennika ciepła powoduje spadek wydajności chłodzenia. Trzymilimetrowa warstwa kamienia obniża wydajność nawet o 60%. Opracowany model pozwala na badania jakościowe i ilościowe powstających na powierzchniach grzejnych krystalicznych osadów. W tym artykule zaprezentowano następujące badania z użyciem modelu chłodnicy; 1. krystalizację fazową węglanu wapnia w temperaturze $30-60^\circ\text{C}$. 2. wpływ siarczanu amonu na procesy inkrustacji w modelowym wymienniku ciepła. Badania dyfraktometryczne wykazały różnice w składzie fazowym osadów węglanu wapnia, powstałych w różnych temperaturach i w obecności siarczanu amonu. W temperaturze $30-40^\circ\text{C}$ powstawał węglan wapnia w postaci kalcytu bezwodnego i monohydratu, w temperaturze $55-60^\circ\text{C}$ dodatkowo jako aragonit. Dodany siarczan amonu w dawkach ponad stechiometrycznych powodował, że kamień nie narastał, a nawet nieznacznie się rozpuszczał.

Andrzej JAROSINSKI*

COMPARATIVE STUDY OF PROPERTIES OF CHROMITE SINTERING PRODUCTS

The aim of the work was to compare the properties of chromite sintering products derived from the industrial process of sodium chromate winning. The investigations were carried out on two kinds of products. The first sample was obtained in a modified process of sodium chromate production relying on sintering chromite ore with soda, calcium oxide, and chromium waste. The second sample was derived from the dolomitic process which is commonly used in industrial practice.

The phase (microscope observations, X-ray diffraction, infrared spectrophotometry) and chemical analyses were applied. In accordance with the assumption, the main component of the obtained sinter was sodium chromate being a soluble phase. The content of this compound was from 0.175 to 0.236 kg CrO₃/kg of charge. The constituents of the insoluble fraction of tested sinters were periclase (MgO), calcium oxychromite (9CaO·4CrO₃·Cr₂O₃), chromopicotite ((Fe,Mg)(Cr,Al,Fe)₂O₄) and dicalcium silicate (2CaO·SiO₂).

It was found that both materials have similar phase composition but different contribution of the above mineral phases. The sinters derived from the dolomite process contained additionally brownmillerite. The tested sinters differ in softening points. Other physicochemical properties of the sinters derived from the modified process of sodium chromate production are similar with the ones for the sinters derived from the dolomite method.

Keywords: sodium chromate(VI), modified process, chromium compounds winning

INTRODUCTION

Sodium chromate is the main intermediate product used in manufacturing of all other chromium compounds. The winning of this compound from chromite ores or its concentrates has been traditionally achieved by a roasting process of mixture containing ore, soda-ash and diluent. The kind and amount of diluent influence essentially the working load of the blend rotary kiln as well as the amount of chromium waste material (so called chromic mud) in the blend. An improper choice of the blend leads to the formation of accretions in the hot part of the rotary kiln, which is

* Instytut Chemii I Technologii Nieorganicznej Politechniki Krakowskiej, 31-155 Krakow
ul. Warszawska 24, e-mail - ajar@chemia.pk.edu.pl.

a result of lowering of the softening and melting points of sinter. This influences the efficiency of the chromate extraction. The residue – chromic mud generated during this process is commonly dumped at special heaps. This mud contains hexavalent chromium Cr(VI) and for this reason the residue has become a major problem from the industry connected with the chromium compounds production. The technological aspects of utilization of chromic mud were presented for example by Jarosiński and Maczka, 2001 as well as Kowalski and Wzorek, 2002.

Until 1999 sodium chromate was produced with the use of the classic dolomite method, which generated large amounts of the chromic mud. This year in Poland a modified process was implemented based on substitution of the chromite ores by a chromic waste derived from the chromium compounds winning. In the process of sodium chromate production such materials as e.g. chromic mud, waste consisting of hydrated chromium oxides and various kinds of recycling (in-process and off-process) materials (Kowalski, 2002; Kowalski and Walawska, 2002) are applied. The modified method is more efficient in material and energy consumption in relation to the dolomite process. Moreover, the amount of generated residue in the modified process is significantly lower than that in the dolomite process.

A comparative study of properties of sinters derived from the dolomite and the modified processes of sodium chromate production is conducted in this paper. The obtained results should contribute to our understanding of the dependence of the physicochemical properties of the sinter on its structure.

EXPERIMENTAL

The following materials were used for the studies. Sinter derived from the dolomite process and sinters obtained by the modified process of sodium chromate winning. The analysis of chemical composition of all investigated samples was conducted according to the classical analytical methods. Alkalis were determined with the AAS (Perkin Elmer 370) method. The diffraction patterns were obtained employing a Philips diffractometer. The spectrophotometrical analysis in the infrared region was carried out with the use of a DIGITAL AB Scimitar Series apparatus with the application of pressed pellets containing KBr and the sample.

Microscopic examination of the tested sinters was carried out using an optical microscope and scanning electron microscope “JEOL”. The sintering and softening points of the investigated samples were determined using a hot-stage microscope (Leitz). The observations of samples in the range 20 - 1500°C in an oxidizing atmosphere were conducted.

RESULTS AND DISCUSSION

The chemical analysis of the investigated samples is presented in Table 1. As can be seen in Table 1, the amount of soda-ash in charges was for all mixtures lower than the stoichiometric quantity of this compound needed to association of chromium with

sodium chromate. In the case of sinter 3, the molar ratio M_{Na} was higher in relation to the other sinters. According to the technological assumptions, the quantity of lime was enough to chemically bind silica by dicalcium silicate. Particularly, a large excess of lime was in sinter 3.

Table 1. The chemical composition of the investigated sinters [%]

Component	Sinters*		
	1	2	3
CrO ₃	24.4	22.6	25.1
Cr ₂ O ₃	2.16	1.7	5.1
Al ₂ O ₃	9.4	4.8	4.8
Fe ₂ O ₃	9.7	5.5	5.5
CaO	15.8	18.0	19.9
MgO	22.0	19.3	23.6
SiO ₂	7.0	6.6	4.4
Na ₂ O	12.9	11.4	17.5
Molar ratio:			
M_{Na} [Na ₂ O/CrO ₃]	0.76	0.74	0.89
M_{CaO} {CaO/SiO ₂ }	2.42	2.92	4.84

*1,2 – sinters obtained by the modified process - samples taken at one month intervals from the plant sodium chromate production, 3 – sinter derived from the dolomite process

The physicochemical properties of the tested samples are given in Table 2. It should be pointed out that degree of chromium oxidation for sinter obtained in the new process is higher than that for sinters derived from the dolomite process. Moreover, softening point for all tested samples amounted to $\geq 1200^{\circ}\text{C}$. The results indicate that under industrial conditions melted sinters and buildups practically did not form because the maximal temperature in the rotary kiln used in the process of sodium chromate winning amounted to $1150\text{-}1200^{\circ}\text{C}$. The sinters from the modified process feature a higher sintering point than sinters obtained by the dolomite process. These parameters influence the degree of chromium oxidation. The obtained productivity are comparably with the values presented by Kowalski et al., 2002.

On the basis of microscopic studies, it has been found that the mean particle diameter was 0,005 mm. In all tested samples the presence of fine crystalline irregular crystals forming numerous aggregates was observed. These aggregates are connected with a micro or fine crystalline structure or independent phase (Fig.1). The surface of grains was well developed. Part of particles had shape closed to spherical. The size of some sinters components is in the range of 0.005-0.04 mm in size.

An example of a microscopic image of thin shallows of the sinter is presented in Fig. 2. In all cases, fine microcrystalline and partly isotropic background with yellow colouring derived from sodium chromate was observed.

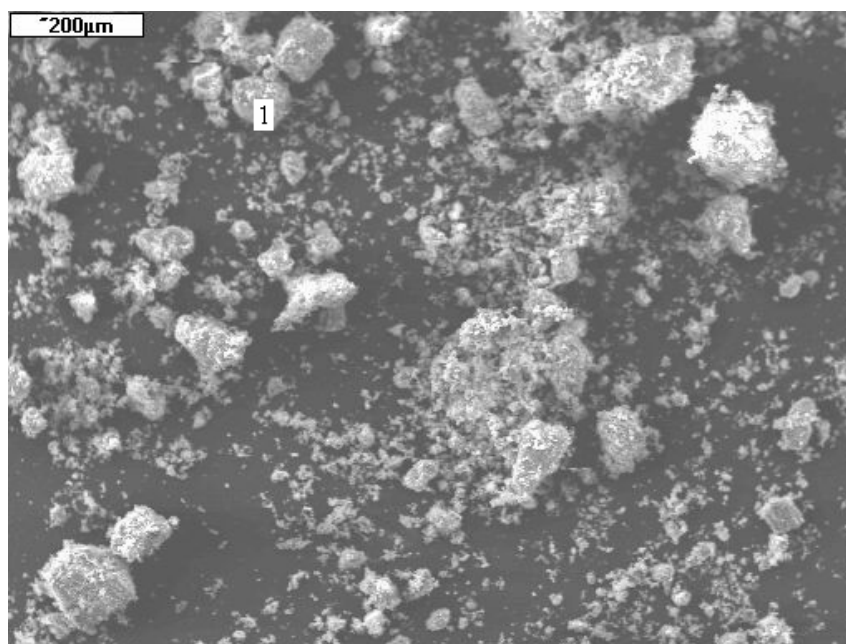


Fig.1. SEM micrograph of the tested sinter (sample 1)

Table 2. The physicochemical properties of investigated sinters

Property	Dimension	Kind of sinter*		
		1	2	3
Specific gravity	kg m ⁻³	2950	3000	2990
Degree of Cr oxidation	%	89,7	91,1	78,9
Productivity	kg CrO ₃ /kg of charge	0.214	0.236	0.175
Sintering point	° C	1100	950	900
Softening point	° C	1280	1250	1200

*1,2 – sinters obtained in the modified process - samples taken at one month intervals from the plant sodium chromate production, 3 – sinter derived from the dolomite process

Moreover, the chromium minerals associated with calcium and iron phases were calcium oxchromite and chromopicotite. Especially, the later chromium phase appeared in small quantities. Among other minerals, the presence of colourless, turning into gray, isotropic periclase of high refractive index was observed. The sinter derived from the dolomite process contained also brownmillerite. Brownmillerite was not found in samples 1 and 2. The other iron phase in the above two sinters was hematite.

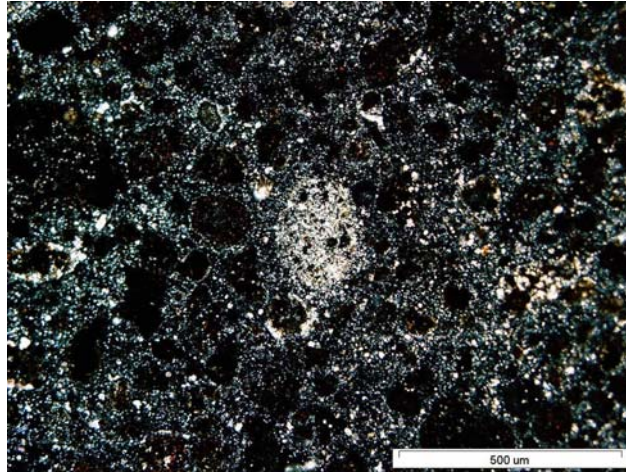


Fig. 2. Image of sinter after leaching of sodium chromate (sample 3)

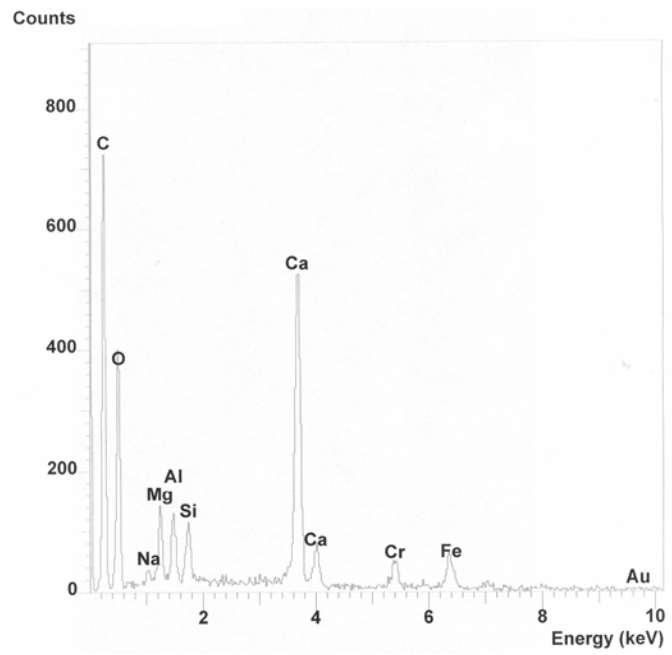


Fig.3. Results of EDS analysis (sample 1 – grain area No. 1)

Table 3. Results of X-ray analysis of tested sinters

Kind of sinter				Mineral phase
1		3		
d(nm)	I	d(nm)	I	
		7.34	20	B.
4.96	20	4.96	20	S.C.
4.05	65	4.06	65	S.C.
3.90	100	3.90	100	S.C.
		3.67	30	B.
3.57	40	3.57	40	S.C.
2.90	100	2.90	100	S.C., C.S., CP.
		2.78	30	S.C., C.S.,
2.73	70	2.73	70	S.C.,C.S.
		2.66	60	B.
2.615	85			C.S.
2.510	96			H.
		2.466	30	S.C.
		2.44	20	B.,P.
2.170	13			S.C.,C.S.
		2.106	100	P., C.S.,CP.
2.100	100			P.,CP., H., C.S.
1.983	24			C.S.
1.941	60			P.,H.
1.780	20			S.C.
1.490	90			P.

S.C.-sodium chromate, C.S. – dicalcium silicate, B – brownmillerite, CP- chromopicotite, P- periclase, H- hematite

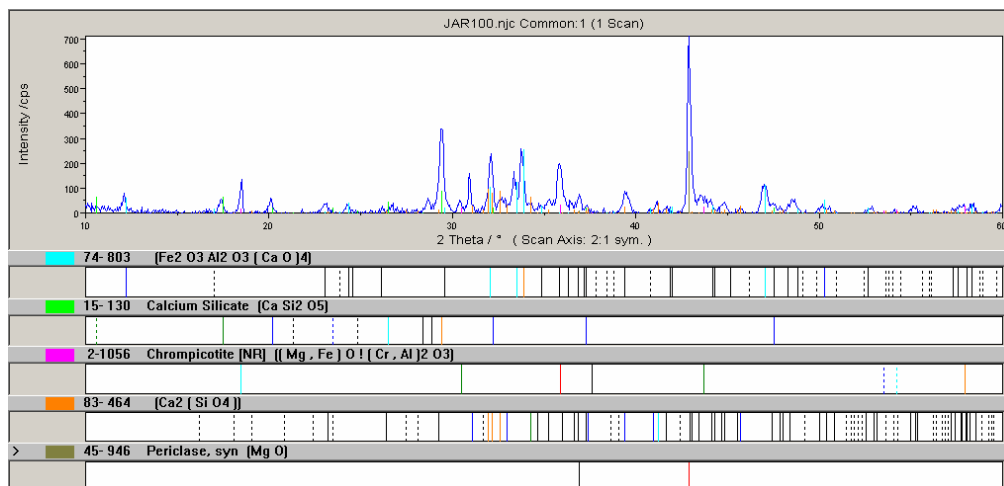


Fig. 4. X-ray diffraction pattern of sinter after leaching sodium chromate (sample 1)

Results of EDS analysis are presented in Fig. 3. The X-ray analysis confirmed the presence of the discussed minerals in the tested samples (Table 3 and Fig. 4.). The spectrophotometric analysis of the soluble phase showed a clear absorption band coming from chromates ($850-950\text{ cm}^{-1}$).

CONCLUSION

The obtained results make it possible to determine quantitatively individual forms of chromium during the process. This is important for practical purposes. The carried out investigations proved that the degree of chromium oxidation was higher for charge containing chromium waste than for the blend prepared with dolomite diluent. According to a technological assumption, sodium chromate was a dominant mineralogical phase. Moreover, chromium is also present in the form of calcium oxychromite in all tested sinters. Chromopicotite occurred there as traces. In the insoluble fraction, the main phase was periclase. Moreover, dicalcium silicate was part of the phase composition of this fraction. Hematite was identified in sinters derived from the modified process. The presence of this phase in the sinter derived from the dolomite process was observed. The physicochemical properties of both investigated materials were similar, except the softening and sintering points.

REFERENCES

- JAROSIŃSKI A., MAĆZKA W., (2001), *Technologiczne aspekty wykorzystania błota pochromowego*, Gospodarka Surowcami Mineralnymi, 17, 89-96.
- KOWALSKI Z., WZOREK Z., (2002): *Utilisation of chromic waste in sodium chromate(VI) production process*, J. Loss Prevention in Process Industr., 15, 169-178.
- KOWALSKI Z., (2002), *Technologie związków chromu*, Kraków.
- KOWALSKI Z., WALAWSKA B., (2002), *Research on the utilisation of waste chromic materials in the sodium chromate production process*, Waste Management & Research 20, 99-107.
- KOWALSKI Z., FELA K., WIECZOREK-CIUROWA K., (2002), *The role of grain size of chromite ore in the sodium chromate production*, Pol. J. Appl. Chem., 2, 121-133.
- Jarosiński A.**, *Badania porównawcze właściwości produktów spiekania chromitu*, Physicochemical Problems of Mineral Processing, 40 (2006), 109-115 (w jęz. ang.).

Celem pracy było porównanie właściwości fizykochemicznych produktów spiekania chromitów otrzymanych w procesie wytwarzania chromianu sodu w warunkach przemysłowych. Badania prowadzono dla dwóch rodzajów produktów. Pierwszy otrzymano w zmodyfikowanym procesie wytwarzania chromianu sodu, w którym wsad stanowiły takie składniki jak chromit, soda, tlenek wapnia oraz odpady tzw. błoto pochromowe. Drugi rodzaj spieku został pobrany z procesu wytwarzania tego związku metodą powszechnie stosowaną w praktyce przemysłowej – metoda dolomitowa. Ocenę składu mineralnego badanych próbek oparto na obserwacjach mikroskopowych oraz analizie spektrofotometrycznej w podczerwieni i rentgenograficznej. Wskaźniki produktywności, wyrażone jako masa CrO_3 przypadająca na jednostkę masy wsadu, kształtowały się na poziomie 0,175-0,236. Zgodnie z założeniami technologicznymi fazę rozpuszczalną stanowił chromian sodu, natomiast w skład frakcji nierozpuszczalnej wchodziły takie fazy jak peryklaz, oksychromit wapnia czy krzemian dwuwapniowy. Spieki pochodzące z procesu dolomitowego zawierały dodatkowo brownmilleryt. Również inne właściwości fizykochemiczne badanych spieków były podobne, z wyjątkiem temperatur spiekania i mięknięcia.

Gülhan ÖZBAYOĞLU*, Nihat ATAMAN**

EVALUATION OF TURKISH INDUSTRIAL WASTES AS BLASTING ABRASIVES

Received March 15, 2006; reviewed; accepted May 15, 2006

Surface preparation is the key factor in determining the success of a protective coating system. Failure to ensure high standards of surface preparation will eventually have a detrimental effect on the life and performance of the coating system applied. Preparation of steel is best achieved by the use of abrasive blast cleaning to remove millscale and rust and provide a suitable surface profile for application of the coating system. Materials from different origins can be used as a blasting medium including coal slag, smelter slag, mineral abrasives, metallic abrasives, and synthetic abrasives.

This paper represents evaluation of Turkish industrial wastes as abrasives in blast cleaning operations. Three different slag samples of two sources were investigated. The samples were prepared by crushing, screening and washing. The chemical composition and physical characteristics of the samples were determined. All the samples were tested on industrial scale.

Test results showed that converter slag meet all the specifications for abrasives and it can be used in blast cleaning operations. However, coal furnace slag and granulated blast furnace slag are not suitable for use as blasting abrasive.

Key words: industrial waste, surface preparation, abrasive, blast cleaning, slag

INTRODUCTION

An essential preliminary to any coating operation is proper surface preparation and its importance cannot be overemphasized. It is believed that of the cost of a coating job, as much as two-thirds goes for surface preparation and labor (NACE, 2000). There are no coatings which will provide long term protection when applied over a poorly prepared surface.

Abrasive blasting is the most widely used method of surface preparation. It is the process of propelling abrasive particles from a blast machine, using the power of compressed air (Hansel, 2000). Its importance has long been known and several

* Prof. Dr., Middle East Technical University, Department of Mining Engineering, 06531, Ankara.

** Res. Asst., Middle East Technical University, Department of Mining Engineering, 06531, Ankara.

researches on blasting pre-treatment have been conducted (Wingen, 1988; Momber and Wong, 2005; Kambham et al., in press; Rosenberg et al., in press) and its effects on adhesiveness of coating systems have been investigated (Amada et al., 1999; Griffiths, 1996; Mellali et al., 1994; Amada et al., 1998; Harris and Beevers, 1999; Çelik et al., 1999; Staia, 2000).

A vital component in successful preparation of surfaces by abrasive blasting is the blasting media (Robinson, 2000). Copper slag, coal slag, garnet, steel grit, and steel shot are common blasting abrasives. Traditionally sand was used, but metallic grit and slag abrasives have replaced it due to the adverse health and environmental effects of silica dust associated with sand. Besides environmental and health concerns, there are numerous considerations in selection of suitable media. While quality and performance of an abrasive is determined by its physical properties and chemical cleanliness, availability and cost mainly determine the economics of abrasives. Although there exists well known blasting abrasives in market, local supply restricts their usage. This situation has led the authors to conduct such a research. The objective of this research is to produce blasting abrasives from Turkish industrial wastes and investigate the usability of produced abrasives in surface preparation technologies.

EXPERIMENTAL

MATERIALS

Three different slag samples of two sources were investigated and tested. A coal furnace slag sample from Çayırhan thermal power plant (Ankara), a granulated blast furnace slag and a converter slag sample from Ereğli Iron and Steel Works.

Coal slag is a coarse, granular, gray colored waste-product that is collected from the bottom of the furnace that burn coal for the generation of steam. It contains white and brownish particles and porous granules of 1.5 cm maximum size. Granulated blast furnace slag is water-quenched, glassy, yellowish, sand-like granules with a top size of about 5-6 mm. Converter slag is the air-cooled steel furnace slag, sometimes called as steel slag, and the sample contains brownish grey vesicular lumps with a top size of about 15-20 cm.

MATERIAL CHARACTERIZATION

Physical characteristics and chemical cleanliness of the materials was evaluated in accordance with Turkish standard TS EN ISO 11126 (2002) which is adopted from ISO standards. Samples were assessed from the aspects of size distribution, apparent density, hardness, moisture content, water soluble contaminants and water-soluble chlorides. Those specifications are determined by the methods described in TS EN ISO 11127 Part 2 to 7 (2002). Chemical composition of the materials was determined by X-ray fluoresce method.

SAMPLE PREPARATION

Since original samples have different physical characteristics, pretreatments of test samples before sizing were performed in different ways. Converter slag sample were first crushed in a jaw crusher to below 3 mm - the maximum allowable size for blasting abrasives - because of its lumpy nature. On the other hand, coal furnace and granulated blast furnace slag samples were air-dried before sizing due to their high moisture content. Samples were sieved for specified sizes, 1.2 mm – 0.3 mm. Oversize materials were re-crushed and undersize materials were rejected.

INDUSTRIAL APPLICATION

Prepared samples were tested in Sedef Shipyard (İstanbul) from performance and quality aspects using industrial scale blasting machine. Blasting conditions are given in Table 1. Rusted steel surfaces were selected from the plates of a ship in maintenance. Plates were blasted until all of the samples were consumed and the surfaces were evaluated. In order to assess the surface cleanliness, Turkish standard TS EN ISO 8501-1 (2000) was used. Surface profile pattern of blasted surfaces were evaluated using Rugotest No. 3 surface profile comparator.

Table 1. Blasting conditions during industrial application

Stand-off distance	~ 60 cm
Blasting angle	60-90°
Air Pressure	700 kPa
Nozzle diameter	10 mm

RESULTS AND DISCUSSION

CHEMICAL COMPOSITION

Coal slag is mainly an aluminum silicate material. Chemical analysis of the coal furnace slag sample and Eurogrit coal slag abrasive is given in Table 2.

Table 2. Chemical analysis of coal furnace slag sample and eurogrit coal slag abrasive

Components	SiO ₂	Al ₂ O ₃	CaO	Fe ₂ O ₃	MgO	Na ₂ O	K ₂ O	Other	LOI
Eurogrit* (%)	45-52	24-31	3-8	7-11	2-3	0-1	2-5	traces	-
CFS (%)	48.1	10.5	13.7	7.4	6.2	1.6	1.6	0.9	9.6

* source: http://www.eurogrit.nl/temp/uk_us/index.html.

Chemical compositions of two coal slags showed that aluminum content of coal furnace slag is quite lower than that of coal slag abrasive used in industry. However, its calcium and magnesium content is higher compared to Eurogrit coal slag abrasive.

Those differences are possibly due to the petrographical and mineralogical compositions of coal and its associated mineral matter. Chemical analysis of coal furnace slag also reveals that there is almost 10 % loss of ignition, which is possibly the indication of unburned coal.

Results of the chemical analysis of granulated blast furnace slag sample and typical slag composition obtained from National Slag Association (USA) is given in Table 3. Apart from the little variations, granulated blast furnace slag seems to be a typical calcium silicate slag.

Table 3. Chemical analysis of granulated blast furnace slags

Components	FeO	SiO ₂	MnO	Al ₂ O ₃	CaO	MgO	S	Other
NSA (%)	0.2-1.6	27-38	0.15-0.76	7-12	34-43	7-15	1.0-1.9	-
GBFS (%)	0.09	36.82	0.56	15.38	40.80	4.91	1.20	0.15

The chemical composition of Turkish converter slag and its counterparts from South Africa (Lieuw Kie Song and Emery, 2001), Taiwan (Li, 1999) and USA (NSA, 2005) is given Table 4. High iron and CaO contents of converter slag sample draw attention. The reason may be originated from higher scrap and lime addition to produce a strongly basic slag. Although most of calcium exists in bound crystalline form with the other constituents, converter slag can also contain free lime.

Table 4. The major components of converter slags

Components	Total Fe (%)	FeO (%)	SiO ₂ (%)	MnO (%)	Al ₂ O ₃ (%)	CaO (%)	MgO (%)
Converter Slag (Turkey)	21.87	9.36	9.62	4.66	0.89	49.48	2.39
South Africa	19.2	12.1	12.5	4.8	4.1	36.4	8.9
Taiwan	1-8	5-20	13-16	4-7	0.9-1.7	45-52	4-6
USA	-	24	15	5	5	42	8

STANDARD SPECIFICATIONS

Turkish standard TS EN ISO 11126 evaluates the materials from the aspects of size distribution, apparent density, hardness, moisture content, water soluble contaminants and water-soluble chlorides.

According to this standard, abrasive particles should not be coarser than 3.15 mm and amount of particles finer than 0.2 mm and coarser than 2.8 mm should not be higher than 5 %. Particle size distributions of coal furnace slag and granulated blast furnace slag samples showed that original materials can not be used as an abrasive in

blast cleaning without sizing. However, more than 70 % of original coal furnace slag and almost 90 % of original granulated blast furnace slag can be utilized as abrasive after only a proper sizing. On the other hand, lumpy nature of converter slag necessitated a crushing stage before sizing. After successive crushing and sizing it is also seen that more than 90 % of converter slag can be used in blast cleaning operations from the point of size distribution. However, they should meet the other requirement in order to be used in industry.

Measured apparent densities of investigated materials and specifications stated by related standards are given in Table 5.

Table 5. Apparent densities of materials

Material	Coal Furnace Slag	Granulated Blast Furnace Slag	Converter Slag
TS EN ISO 11126 (kg/dm ³)	2.4-2.6	3.0-3.3	-
Sample (kg/dm ³)	2.1	2.4	3.8

As it is seen from Table 5 coal furnace slag and granulated blast furnace slag samples do not meet the specifications. Both of them are below the required values. Lower apparent density of coal furnace slag is attributed to its chemical composition. Low aluminum content and unburned coal possibly reduces its apparent density. As to granulated blast furnace slag, its apparent density is much lower than specified values. This might point out a porous structure possibly due to cooling regime. Converter slag has the highest apparent density among studied materials. It might be due to high iron content in the slag and possibly occur with scrap metal additions during steel production.

Specifications of non-metallic abrasives covered in TS EN ISO 11126 with the investigated slag samples are compared in Table 6.

Table 6. Specifications of Turkish (ISO) standards with investigated slag samples

Specification	TS EN ISO 11126	CFS	GBFS	CS
Hardness (Mohs)	Min. 6	< 6	> 6	> 6
Moisture Content (%)	Max. 0.2	0.03	0.02	0.03
Conductivity (mS/m)	Max. 25	-	15.7	811
Water Soluble Chloride (%)	Max. 0.0025	-	0.0004	0.0013

Hardness of granulated blast furnace slag and converter slag are obviously greater than 6 in Mohs scale. On the other hand, different particles of coal furnace slag sample scratches the glass slide in different levels, therefore the exact hardness value of coal furnace slag is doubtful and it is considered to be low to be used in blast cleaning. Conductivity of coal slag and its water soluble chloride content were not determined

because of its failure in industrial application. While converter slag meets most of the criteria, its conductivity value exceeds the maximum allowable limit. This problem may be overcome by thorough washing with river water. Pre-treatment of washing not only removes the water soluble contaminants but may also prevent dusting generated by adhering fines. Granulated blast furnace slag seems to be appropriate to be used as abrasive from standard specification aspects. However, industrial application determines the final decision.

INDUSTRIAL APPLICATION

Industrial application of converter slag showed that the tested sample cleaned the work surface from most of the mill scale, rust, and foreign matter providing “Sa 2” degree of cleanliness. “Sa 2” is considered, in many cases, satisfactory. However, applied pressure should be high enough and enough cleaning time should be given, up to the point of the best achievable cleanliness. The slag sample also provided surface roughness of B N9a on Rugotest No.3, which is sufficient for general purpose blast cleaning operations. It was also noticed that the tested sample did not leave residues on the work surface preventing contamination. Additionally, it appeared to be a low dusting material, which may otherwise hinder the blasting operation. Therefore, the tested sample was accepted to be a promising candidate, especially with some improvements in its physical properties.

The application of granulated blast furnace slag on the work surface revealed some interesting results. At the first look, it seemed to provide “Sa 2½” degree of cleanliness and created brighter, near to white, surface than does the converter slag. However, the appearance of blasted surface was misleading. When the worked surface was viewed with magnification, it was realized that the sample left local traces of contamination in the form of white spots. The residues smear the surface and gave an extra brightness and white look. Comparison of the worked surface with the surface profile comparator showed that the sample provides surface roughness between the mid point of B N9 and B N10 on Rugotest No.3, which is suitable for all purpose blast cleaning operations. In addition, it appeared to be a low dusting material and this provided a superior feature to that sample. As a result, although granulated blast furnace slag has a good cleaning performance, it can not be utilized as an abrasive due to left residues on the blasted surface.

Industrial application of coal furnace slag showed that it was not able to clean the surface from mill scale, rust and paint coatings. Visual assessment of surface cleanliness revealed that the tested sample is not applicable in blast cleaning operations. It did not fulfill even the requirements of the “Sa 1” degree of cleanliness which is the lowest degree in blast cleaning. In addition, it was not able to provide the lowest degree of roughness, which is B N6 on Rugotest No.3. Hence it does not meet the surface profile requirement by the industry, which is commonly in the range of B N9a-B N10a.

CONCLUSIONS

The chemical composition and physical characteristics of alternative blasting abrasives were determined in the light of ISO standards and they were tested in industry. Converter slag meets the hardness, moisture content and water soluble chloride criteria of the standards. However, its conductivity value is above the maximum allowable limit. But it is considered to easily be overcome with thorough washing. Industrial application of converter slag showed that it provides “Sa 2” degree of cleanliness and surface roughness of B N9a, which is accepted as satisfactory in many cases for surface preparation of steel works.

Aluminum content of coal furnace slag is quite lower than that of coal slag abrasive used in industry. However, its calcium and magnesium content is higher and it possibly contains unburned coal. Those differences in its chemical composition are considered to be adversely effective in its physical properties, i.e., toughness, density, etc. The coal furnace slag does not meet the most of ISO specifications and it failed during industrial application. Consequently, it can not be used as abrasive in blasting.

Granulated blast furnace slag meets all of the requirements of ISO standards, except for its lower apparent density, which is attributable to its porous structure. Although the granulated blast furnace slag has a good cleaning performance and provides required surface profile it can not be utilized as an abrasive in preparation of the steel since it leaves local traces of contamination in the form of white spots on the worked surface. Converter slag is mainly utilized as pavements, road construction material and railway ballast. In the literature, there is limited information about the utilization of those materials as blasting abrasive. This study showed that converter slag can be a good candidate after a pre-treatment consisting of crushing, sizing and washing as the same requirement for most of the other blasting abrasives. It is also noticed that any material that meets the specifications of standards may not necessarily be utilized as an abrasive. Industrial application determines the final decision.

In this study only degree of surface cleanliness and roughness are studied. Cleaning rate and consumption of blasting abrasives should also be investigated in order to determine their feasibility to be usable in industry.

ACKNOWLEDGEMENT

Financial support from Middle East Technical University (BAP- 2005-07-02-00-84) is gratefully acknowledged.

REFERENCES

- AMADA, S., HIROSE, T., (1998), *Influence of grit blasting pre-treatment on the adhesion strength of plasma sprayed coatings: fractal analysis of roughness*, Surface and Coatings Techn., 102, 132-137.
- AMADA, S., HIROSE, T., SENDA, T., (1999), *Quantitative evaluation of residual grits under angled blasting*, Surface and Coatings Technology 111, 1-9.
- ÇELİK, E., DEMIRKIRAN, A. Ş., AVCI, E., (1996), *Effect of grit blasting of substrate on the corrosion behaviour of plasma-sprayed Al_2O_3 coatings*, Surface and Coatings Technology 116-119, 1061-1064.
- GRIFFITHS, B.J., GAWNE, D.T., DONG, G., (1996), *The erosion steel surfaces by grit blasting as a preparation for plasma spraying*, Wear 194, 95-102.

- HANSEL, D., (2000), *Abrasive Blasting Systems*, Metal Finishing, V98 (7).
- HARRIS, A.F., BEEVERS, A., *The effect of grit blasting on surface properties for adhesion*, Int. Jour. Adhesion and Adhesives 19 (1999) 445-452.
- KAMBHAM, K., SANGAMESWARAN, S., DATAR, S.R., KURA, B., *Copper slag: optimization of productivity and consumption for cleaner production in dry abrasive blasting*, Journal of Cleaner Production, in press.
- LI, Y.S., (1999), *The use of waste basic oxygen furnace slag and hydrogen peroxide to degrade 4-chlorophenol*, Waste Management 19, 495-502.
- LIEUW KIE SONG, E.R., EMERY, S., (2001), *Preliminary development of slag as a stabilised material for labour intensive construction of roads*, in: Proc. First International Conference on Employment Creation in Development, South Africa.
- MELLALI, M., GRIMAUD, A., FRAUCHAIS, P., (1994), *Parameters Controlling The Sand Blasting of Substrates for Plasma Spraying*, Proc. of the 7th National Thermal Spray Conf., Boston, 227-232.
- MOMBER, A.W., WONG, Y.C., (2005), *Overblasting effects on surface properties of low-carbon steel*, JCT Research 2 (6) 453-461.
- NACE International Basic Corrosion Course Handbook, (2000), Houston, chp 14, 7-14.
- National Slag Association (NSA), (2005), Steel Slag, available at http://www.national-slagassoc.org/PDF_files/SSPremAgg.PDF.
- ROBINSON, J. (Ed.), (2000), *What lies beneath – surface preparation, the key to coating performance*, Corrosion Management, 16-22.
- ROSENBERG, B., YUAN, L., FULMER, S., *Ergonomics of abrasive blasting: A comparison of high pressure water and steel shot*, Applied Ergonomics, in press.
- STAIA, M.H., RAMOS, E., CARRAQUERO, A., ROMAN, A., LESAGE, J., CHISOT, D., MESMACQUE, G., (2000), *Effect of substrate roughness induced by grit blasting upon adhesion of WC-17% Co thermal sprayed coatings*, Thin Solid Films 377-378, 657-664.
- TS EN ISO 11126, (2002), *Preparation of steel substrates before application of paints and related products - Specification for non - metallic blast cleaning abrasives*, Turkish Standards Institution.
- TS EN ISO 11127, (2002), *Preparation of steel substrates before application of paints and related products - Test methods for non-metallic blast cleaning abrasives*, Turkish Standards Institution.
- TS EN ISO 8501-1, (2000), *Preparation of steel substrates before application of paints and related products-Visual assessment of surface cleanliness Part 1: Rust grades and preparation grades of uncoated steel substrates after overall removal of previous coatings*, Turkish Standards Institution.
- WINGEN, J., (1988), *Technical note: Grit blasting as surface preparation before plasma spraying*, Surface and Coatings Technology 34, 101-108.
- G. Özbayoğlu, N. Ataman**, *Ocena tureckich odpadów przemysłowych jako ścierniwo*, Physicochemical Problems of Mineral Processing, 40 (2006), 117-124 (w jęz. ang.).

Właściwości powierzchniowe są bardzo ważnym parametrem, który determinuje utworzenie efektywnej warstwy ochronnej na powierzchni ciała stałego. Zaistniałe uchybienia w przygotowaniu powierzchni mogą mieć negatywny wpływ na długość czasu funkcjonowania i jakość powstałego pokrycia powierzchniowego. W procesie otrzymywania wyrobów ze stali, istotną rolę odgrywa użycie odpowiedniego ścierniwa w celu usunięcia rdzy i zgarów, co gwarantuje otrzymanie czystej powierzchni, na którą można nałożyć warstwę ochronną. Materiały, o różnych źródłach pochodzenia, można wykorzystać jako ścierniwo. Do tej grupy materiałów można zaliczyć: żużel węglowy, żużel hutniczy, ścierniwo mineralne, ścierniwo metaliczne i ścierniwo syntetyczne.

W pracy przedstawiony został rozwój tureckiej gałęzi przemysłu, która wykorzystuje odpady jako ścierniwo w operacjach czyszczących. Badaniom poddano trzy żużle pochodzące z dwóch miejsc. Otrzymane próby zostały odpowiednio przygotowane przez zmielenie, klasyfikację na sitach i odmycie drobnej frakcji. Określony został skład chemiczny i właściwości fizyczne badanych próbek ścierniwa. Wszystkie trzy ścierniwa były testowane w warunkach przemysłowych. Wyniki otrzymane z tych testów wskazują, że badane ścierniwa można użyć do operacji czyszczenia. Jednak, żużel węglowy i granulowany żużel wielkopiecowy nie były odpowiednim materiałem dla produkcji past polerskich.

Janusz GIRCZYS, Iwona KUPICH*

REDUCTION OF SULPHATE IONS CONCENTRATION IN DISCHARGE WATERS FROM Zn-Pb MINES

Received March 15, 2006; reviewed; accepted May 15, 2006

The paper presents a technological concept of limiting the concentrations of SO_4^{2-} ions in discharge waters from ore mines. It is based on authors' research performed for waters of Bytom trough, discharged on the surface in the volume of 30 thousand m^3/day . The method applied has been based on transferring SO_4^{2-} ions into a slightly soluble alkaline calcium-aluminium sulphate.

The technological concept assumes the following:

- use of the waste from anodic oxidation of aluminium (AUA) as a basic reagent in the process,
- conducting the reaction with AUA in a heterogeneous system,
- economic utilisation of post-process slime.

The results of laboratory tests indicate that the process will be feasible in practical use, and water will reach, after treatment, the quality corresponding with, at least, class III purity of surface waters.

Key words: calcium-aluminium sulphate, precipitation, environment, oxidation, surface water

INTRODUCTION

In the peak period of development of the mining industry in Poland, the mining-produced drainage was a source of water discharge amounting to 3 million m^3/day (GUS, Ochrona Środowiska, 1992). Such a scale of the phenomenon cannot be without consequence to the environment. The largest contribution to the stream of underground water discharged to surface water comes from hard coal mines. That is why in relation to them actions have been taken aimed at minimising the damages in the environment. The programme comprising research, design and development work resulted in the construction of two industrial installations for utilisation of underground water, functioning on the basis of different, original technological solutions (Motyka, Magdziorz, 1991). However, the diversified characteristics of waters from drainage of the extractive industry mining various minerals, makes

* Technical University of Częstochowa, Institute of Environmental Engineering, Brzeźnicka 60 a, 42-200 Częstochowa, E-mail: iis@is.pcz.czyst.pl, Tel : (034) 3250 -917, Fax: (034)37 21-304.

impossible to transfer, in a simple way, the experience gained by the hard coal mining industry into other branches of mining.

The ore mining industry, whose water discharge is considerably smaller, must search for other, own solutions. In this case, the discharge waters have their characteristics similar to the leaching solutions from waste storage yards produced by extractive or metallurgical industries. The fact should be emphasised that the abandonment of mining does not solve the problem of water discharge from the existing drainage.

From the Bytom trough, where there are no active zinc and lead mines any more, but yet the volume of 30 thousand m³/day of water discharge resulting from ore mining is pumped up to the surface (Kropka et al. 1994; Hydrolog S.C. Operat 2000). The management of these waters had not been included in the R&D programmes, and still it is an open problem. The specificity of the applied technologies is a result of the properties of underground water and objectives to be obtained using the utilisation technologies. They are different than in the case of desalination of sea water, and in the case of water and sewage management.

The main pollution source of the Bytom trough discharge waters are the processes occurring in the rock mass and in the waste placed on the surface. In these processes, the ions of heavy metals and sulphates are mainly leached. Their concentrations exceed many times the level considered admissible for discharge into surface water courses. As far as the removal of heavy metal ions to the degree enabling to meet the admissible concentrations is solved using simple means of precipitation of hydroxides, then the reduction of sulphate concentration demands applying complicated technologies. In this material, the results are presented aimed at developing a technology for removal of SO₄²⁻ ions from water solutions through precipitating them in the form of basic calcium-aluminium sulphate. The process was realised with the use of the waste product from anodic oxidation produced in the plants manufacturing the elements of the so-called aluminium joinery.

It was assumed that, by using aluminium compounds in an alkali environment, it is possible to precipitate SO₄²⁻ ions through changing their concentration to a level legally acceptable for surface waters. To use this process in the discharge water utilisation technology, it must fulfil the following conditions:

- low cost of the principal reagent,
- non-complicated method of batching, conducting the reactions and separating their products,
- possibility to integrate the proposed process into the existing system.

It was assumed that the process is to be conducted in heterogeneous conditions, with the use of fine Al(OH)₃ sediment, being a waste from the electrochemical processing of aluminium elements. The investigations were aimed at elaborating the technological guidelines for the process of reducing SO₄²⁻ ions concentration in the discharge waters from the Bytom trough to a level enabling to discharge the treated water into the receiver.

METHODOLOGY OF TESTING AND DETERMINATION

MATERIALS

The underground water samples were randomly collected at the inflow to the pumping chamber located at Bolko shaft in Bytom, during the operation of pumps forcing water from water heading to the surface. These are waters coming entirely from natural inflow.

Table 1. Characteristic quality indices of raw underground water- Bolko shaft

Index	Unit	Concentration range
pH	-	7.05 – 7.39
SO ₄ ²⁻	mg/dm ³	930 -1150
Zn	mg/dm ³	8.34- 15.0
Pb	mg/dm ³	< 0.010- 0.098

The waste in the process of anodic oxidation of aluminium is further on called the AUA waste. The remainder, after the process of electrochemical processing of aluminium, is a used electrolyte, which is subject to neutralisation by means of NaOH up to pH = 7.0. The originating sediment containing, first of all, aluminium hydroxide is being dewatered in a filtration press up to the water content of 75%. Yearly, about 500 Mg of the sediment is produced, considered to be waste, for which one seeks for the possibility of use. In the natural and alkali conditions, this waste is insoluble in water. The waste samples collected from the filter were dried at 105⁰C, after that they were crushed in a mechanical mortar. After crushing, the material was obtained having the grain size of less than 200µm. The derivatographic analyses of the AUA dried at 105⁰C have shown that that its main component is Al(OH)₃. The concentration of aluminium in the AUA was 290 g/kg of dry matter.

In the tests, analytically pure calcium hydroxide was also used.

METHOD OF CONDUCTING THE TESTS

The experiments were conducted in the FLOCCULATOR 2000 apparatus, designed to carry out tests in the laboratory conditions. Six glass containers with individually controlled mixers have time control elements mounted on them. These are the timers and speed control units. This enables to set exact values of rotational velocity and duration of individual phases of the process. The volume of water samples was constant and equalled 1dm³. The time of contact of reagents with water and their dose varied.

The process was conducted in three phases:

- fast mixing, up to pH = 11.5,
- slow mixing,
- sedimentation and crystallisation.

The cleaning efficiency of discharge water was determined on the basis of SO_4^{2-} concentration in the over-sediment water.

The analyses of the sediment originating in the process of discharge water cleaning were performed only in selected cases. The principal criterion of selection was the obtainment of satisfactory purity of the treated water.

RESULTS OF THE TESTS

The tests on sulphate precipitation, performed with the use of an AUA waste sample of $0.7\div 0.9 \text{ g/dm}^3$, and time of contact of the sediment with the solution of ca. 1 h, gave no satisfactory results (Fig. 1).

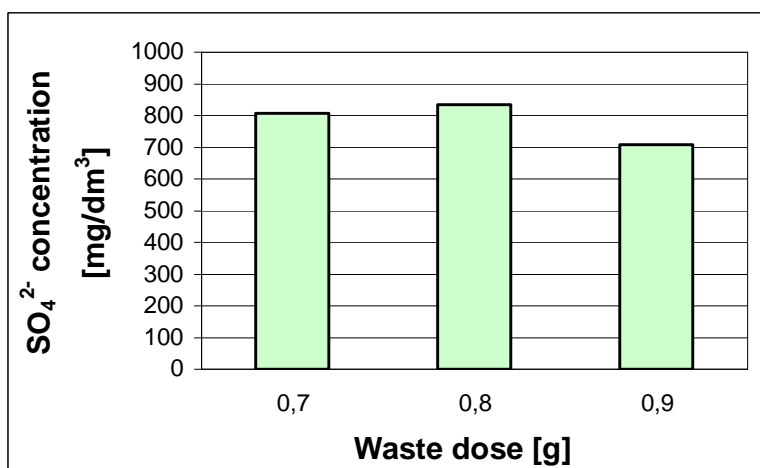


Fig. 1. Relationship between the dose of waste and final sulphate concentration. Initial sulphate concentration was 1034.3 mg/dm^3

The extension of used doses and time of contact leads to the results presented in Fig.2. The solid line in the figure correspond to linear correlation of measurement results.

In both tests performed, the 2 h time of free mixing was used. Of importance was the value of pH reached by the reaction mixture after fast mixing. It was found that the reaction is conditioned by reaching the value of pH of ca. 11.5. This condition is fulfilled when the Ca(OH)_2 dose equal to 4 g/dm^3 is used. It ensures effective precipitation of sulphate ions, while no effect of fast mixing time on the results of reaction are observed.

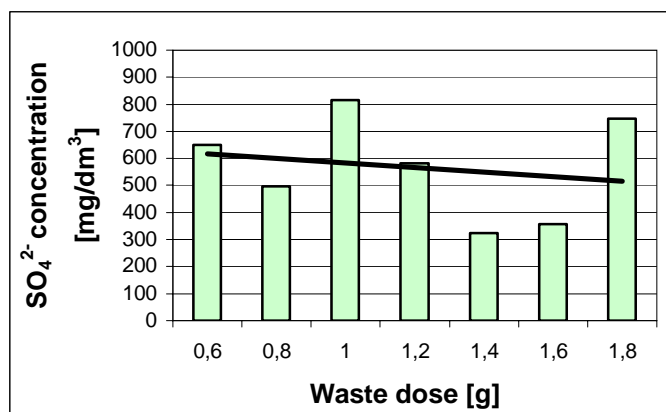


Fig. 2. Relationship between AUA dose and final sulphate concentration. Initial sulphate concentration was 930.6 mg/dm³; time of contact 48 h

On the basis of multiple tests of precipitation of alkali calcium sulphate, the optimal doses of reagents being 4g Ca(OH)₂ and 1.6g AUA waste were confirmed. For such doses, the effectiveness of the process of SO₄²⁻ removal from discharge waters proved to be the best.

The next parameter that affects the effectiveness of sulphate ions removal is the time of slow mixing. By using the most advantageous doses and extending the time of slow mixing, the results were obtained as shown in the diagram of Fig. 3.

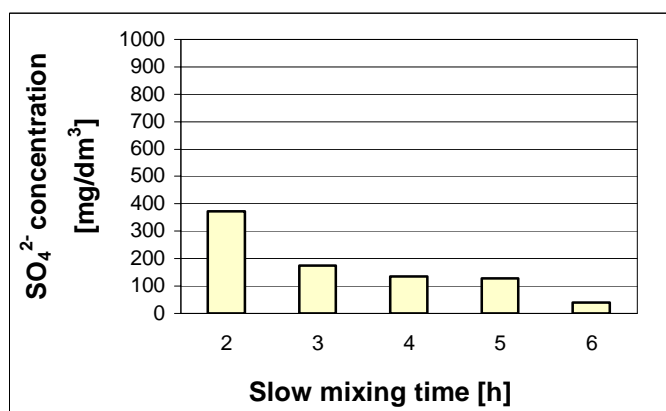


Fig. 3. Relationship between time of slow mixing and final sulphate concentration. 4 g/dm³ Ca(OH)₂; AUA - waste 1.6 g/dm³; initial sulphate concentration was 1045.0 mg/dm³

The extension of slow mixing time to 6 h enabled to obtain an effective process of SO₄²⁻ precipitation, without the need to apply a long time of contact of the sediment with over-sediment water. The time was shortened to 1 h.

Using the 1.6 g AUA dose and extending the slow mixing time up to 6 h makes it possible to reduce the Ca(OH)_2 dose to 3.5 g/dm^3 without worsening the effectiveness of the process of water cleaning from sulphates (Fig. 4).

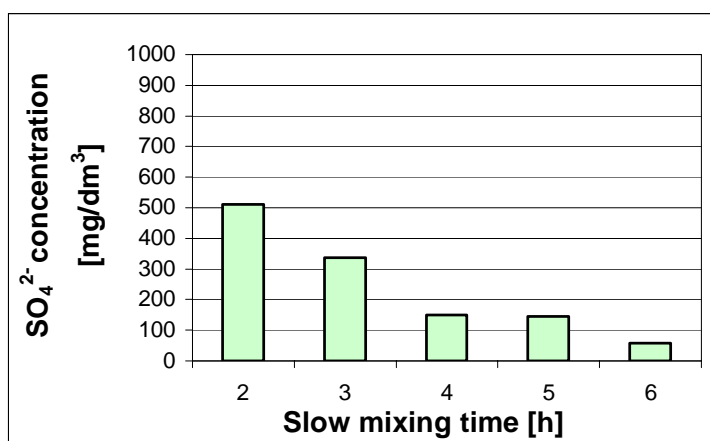


Fig. 4. Relationship between time of slow mixing and final sulphate concentration. $3.5 \text{ g/dm}^3 \text{ Ca(OH)}_2$; AUA - waste 1.6 g/dm^3 ; initial sulphate concentration was 1045.0 mg/dm^3

The properties of the AUA waste, which is insoluble in the process conditions, allow supposing that the reaction proceeds close to its surface. The scanning picture of the originating solid product (Fig. 5) confirms the existence in it of hexagonal forms of aluminium-calcium monosulphate.

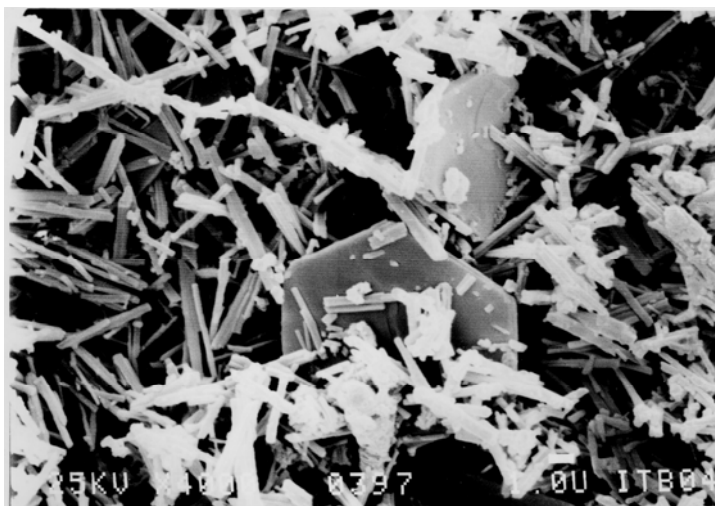


Fig. 5. Scanning photograph of process sediment; magnification x 1000

The thermo gravimetric analysis (Fig.6) has revealed three characteristic decrements of mass. The first, in several stages, in the temperature range of 120 to 630 °C, is connected with the presence of crystalline water. It exists both in monosalt structures and ettringite, in the amounts greater than determined. The decrement of mass and endothermic curve in the temperature range of 660÷760 °C are the diagnostic features of calcite. Its presence in the amount of ca. 20% confirms the fact that the creation of CaCO_3 is, in the process conditions, a competitive reaction to bonding of sulphate ions. The third peak, in the temperature range of 1200 ÷ 1300 °C, is connected with decomposition of CaSO_4 . The weight content of this component indicates that the SO_4^{2-} bond results mainly from creation of ettringite. In ettringite ($3\text{CaO}\cdot\text{Al}_2\text{O}_3\cdot3\text{CaSO}_4\cdot32\text{H}_2\text{O}$), the mass ratio of CaSO_4 to $3\text{CaO}\cdot\text{Al}_2\text{O}_3$ is 1.51. In the monosalt ($3\text{CaO}\cdot\text{Al}_2\text{O}_3\cdot\text{CaSO}_4\cdot12\text{H}_2\text{O}$) it is much lower, being 0.50. The result of thermo gravimetric analysis has revealed that in the tested material, the ratio of CaSO_4 to anhydrous remainder without calcite, is 0.93. Therefore, this is a proof for the question stating that the process proceeds mainly towards creation of ettringite.

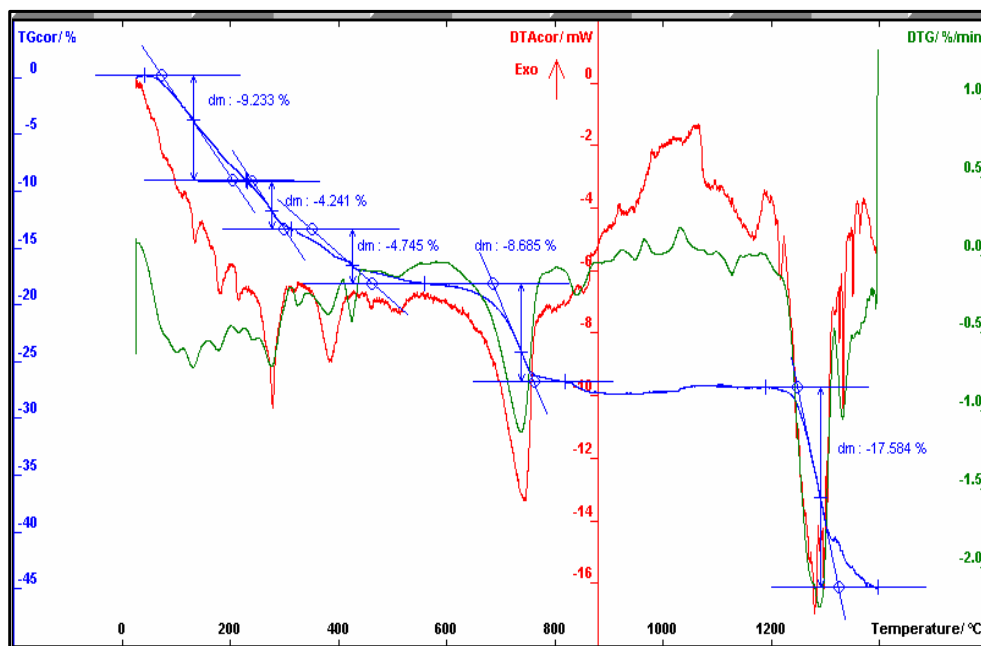


Fig.6. Derivatogram of a sediment sample after the process of discharge water cleaning with the use of AUA waste

By applying the dose of 1.6 g AUA (876 mg Al_2O_3), it is possible to remove from it of ca. 1000 mg SO_4^{2-} (Figs. 3 and 4). This means that 1 mole of Al_2O_3 binds 1.22 of mole SO_4^{2-} . Such a result can be obtained when a part of sulphate ions is built in the ettringite structure. For practical application of the process, it is important that, as

early as after 2 hours of slow mixing, 60% of sulphates taking part in the reaction are removed. The elimination of next 40% of SO_4^{2-} ions requires to extend the time of slow mixing up to 6 h. In the over-sediment water $30\div 100 \text{ mg SO}_4^{2-}/\text{dm}^3$ remains. This justifies good effectiveness of the process of binding sulphate ions. This leads to the degree of cleaning which enables to discharge it into surface waters.

The investigations performed may be summarised with a proposal of a schematic technological diagram of cleaning waters discharged by Zn-Pb ore mines. This scheme, presented in Fig. 7, in a simplified way, gives the guidelines of the proposed technology. Batching of AUA and calcium hydroxide introduces minor change in the presently used scheme for water treatment. In respect of pH value of over-sediment water exceeding the standard, the scheme was extended with adding a process of saturation with carbon dioxide. Such a process is used in the technologies of water and sewage cleaning (Kowal, 1990). A source of CO_2 can be the atmospheric air.

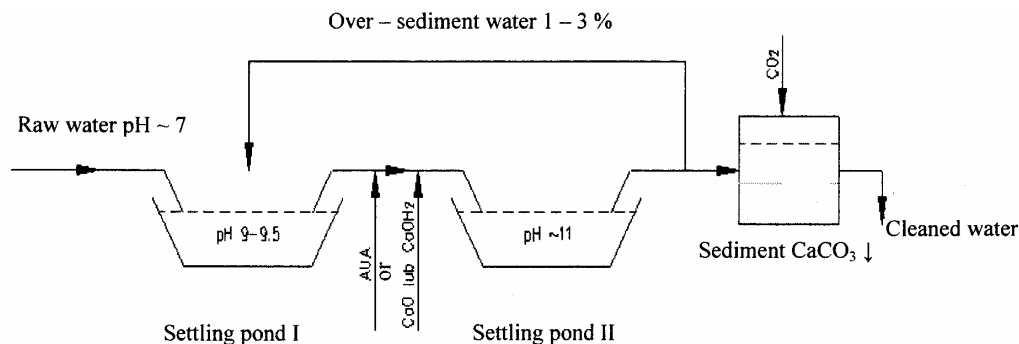


Fig. 7. Schematic technological diagram for cleaning water discharged from Zn- Pb mines located in Bytom trough, using AUA waste

Fast and slow mixing in the laboratory conditions are a model reproduction of batching the reagents directly into the pipeline, under turbulent flow conditions, and then laminar flow in the settling pond.

Running the process of water utilisation in accordance with the technology presented schematically in Fig. 7 needs solving the question of management of the originating post - reaction sediment. For the sediment obtained in the investigations, the reactivity tests were performed (Szymanek, 2000) by determining the material capability of binding SO_2 from flue gas, presented in grams of S per kilogram of sorbent (Bis and Radecki, 2002). The obtained average result $\text{CI}=136.6 \text{ gS/kg sorbent}$ with the standard deviation of the average value $\sigma_n= 19.2$ points to excellent sorptive properties of the post-reaction sediment.

CONCLUSIONS

1. In the process of cleaning of underground water discharged from the Zn-Pb ore mines from SO_4^{2-} ions, it is possible to use, as an active reagent, the waste obtained after electrochemical treatment of aluminium (AUA) for which there is, so far, no idea of management.
2. The effectiveness of the process depends chiefly on bringing the reaction mixture to the required pH and time of slow mixing.
3. The process with the use of AUA waste is based on a heterogeneous reaction between the $\text{Al}(\text{OH})_3$ sediment and water solution, and leads to origination of alkali calcium-aluminium sulphate, mainly ettringite.
4. The properties of sediments produced in the course of cleaning of underground water discharged from ore mines, with the use of AUA waste, point to the possibility of their management as sorbents by dry methods of sulphur removal from flue gas.
5. The process water, because of its alkali character and high aluminium content, must be brought to the quality condition corresponding with the legal requirements, which demands applying individual technological solutions for each investment.

REFERENCES

- BIS Z., RADECKI M., (2002), *Alternatywne sorbenty wapniowe do odsiarczania spalin w kotłach fluidalnych*, IX Konferencja Kotłowa nt.: Aktualne problemy budowy i eksploatacji kotłów, 59-72.
- HYDROLOG S.C., (2000), *Operat wodnoprawny na odprowadzenie wód kopalnianych z nieczynnych wyrobisk porudnych Zakładu Górniczego – Centralnej Pompowni „Bolko” w Bytomiu do rzeki Brynicy w km 20+100*, Katowice.
- KOWAL A.L. (red.), (1990), *Odnowa wody Podstawy teoretyczne procesów*, Wyd. Politechniki Wrocławskiej, Wrocław.
- KROPKA J., DALIBÓG J., ZDYBIEWSKA K., (1994), *Zawodnienie i likwidacja kopalń rud cynku i ołowiu w niecce bytomskie*, Przewodnik LXV Zjazdu PTG Sosnowiec, Wyd. Uniw. Śląskiego, Katowice, s. 253-262.
- MOTYKA J., MAGDZIORZ A., (1991), *Zagospodarowanie zasolonych wód z kopalń węgla kamiennego poprzez ich utylizację metodami chemicznymi*, Konferencja n.t. Kierunki zagospodarowania zasolonych wód z KWK, 23 lipiec 1991, GIG – Katowice.
- OCHRONA ŚRODOWISKA 1992, (1992), *Materiały i opracowania statystyczne GUS*, Warszawa.
- SZYMANEK A., (2000), *Badania modyfikowanych sorbentów wapniowych do suchego odsiarczania spalin*, Ph. D. Thesis, Politechnika Wroclawska, Wydział Mechaniczno-Energetyczny.

Girczys J., Kupich I., *Redukcja stężeń jonów siarczanowych w wodach zrzutowych kopalń Zn-Pb*, Physicochemical Problems of Mineral Processing, 40 (2006), 125-134 (w jęz. ang.).

W artykule zawarto założenia technologiczne procesu ograniczania stężeń jonów SO_4^{2-} w wodach zrzutowych kopalń rudnych. Oparto je na badaniach własnych wykonanych dla wód kopalń niecki bytomskiej, wyprowadzanych na powierzchnię w ilości do 30 tys. m^3/d . Zastosowano metodę polegającą na przeprowadzaniu jonów SO_4^{2-} w słabo rozpuszczalny alkaliczny siarczan wapniowo-glinowy.

Opracowana koncepcja technologiczna zakłada:

- użycie odpadu z anodowego utleniania aluminium (AUA) jako podstawowego reagenta w procesie,
- prowadzenie reakcji z AUA w układzie heterogenicznym,
- wykorzystanie gospodarcze osadu poprocesowego.

Rezultaty badań laboratoryjnych wykazują, że proces będzie możliwy w praktycznym stosowaniu, a woda po oczyszczeniu uzyska jakość odpowiadającą, co najmniej klasie III czystości wód powierzchniowych.

Paweł NOWAK*, Robert P. SOCHA*

OXIDATION AND DISSOLUTION OF METAL SULFIDES FROM FLOTATION WASTES IN CIRCULATING WATER – THE FATE OF SULFIDE SULFUR

Received March 15, 2006; reviewed; accepted May 15, 2006

Dissolution of Zn, Pb, and sulfate ions in water from flotation lead-zinc ore tailings was investigated by passing water through columns filled with the waste. Conductivity, pH and concentration of selected ions in the effluent were measured and expressed as a function of exchange ratio of pore water (ER). Samples collected from the tailing after the experiments were investigated by X-ray photoelectron spectroscopy (XPS). Due to high concentration of carbonate minerals, which saturate the flowing water with hydrocarbonate ions, the concentration of both lead and zinc ions in the effluent is very low, below the standard for industrial waste water (except the very initial period). At the same time sulfide sulfur oxidizes partially to elemental sulfur, not to sulfates. For that reason the transfer of sulfates from the flotation wastes is rather limited.

Key word: flotation waste, sulfide oxidation, pyrite oxidation, sulfide minerals

INTRODUCTION

Modern industry uses significant amount of non-ferrous metals. Ores of non-ferrous metals, rich enough to be processed directly by pyrometallurgical methods, are practically exhausted and mainly low-grade ores are processed now. In the case of copper, processing of ores containing as low content of copper as 1% is still economically profitable. So, the production of non-ferrous metals is accompanied by the appearance of huge amounts of wastes. For example, the Polish copper industry, during 50 years of its activity, deposited 600 000 000 Mg (tones) of wastes on a depository place, occupying 2300ha of land (Łuszczkiewicz, 2000). The impact of the industrial wastes on the environment in Poland has been reviewed by Helios-Rybicka (1996). Non-ferrous metals appear in ores mainly as metal sulfides and the principal technology used for removal of valuable sulfide minerals from ores is froth flotation (Leja, 1982). Besides, the sulfides of the recovered metals ore may contain sulfide and

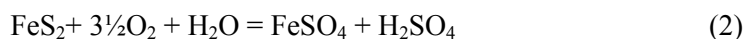
* Polish Academy of Sciences, Institute of Catalysis and Surface Chemistry, Kraków, Poland

non-sulfide minerals of other metals. These minerals are present in flotation tailings, creating a real danger for the environment, when the tailings are deposited in a field.

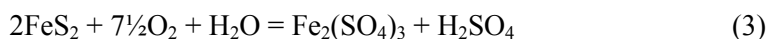
Special position in that respect occupies pyrite. Pyrite is the most abundant sulfide mineral (Craig and Vaughan, 1990) accompanying almost all sulfide and many non-sulfide minerals, including coal. At the same time pyrite has no application and in flotation process pyrite is directed to tailings. So, flotation tailings may contain as much as 60-70% of pyrite. Pyrite oxidizes relatively easily, and contrary to mono-sulfides, which oxidize to neutral sulfates according to the reaction:



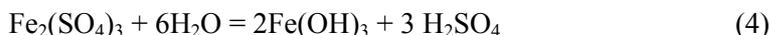
pyrite generates sulfuric acid during its oxidation



in the quantity of one mole of acid per one mole of pyrite. The amount of acid may be lower when pyrite iron oxidizes to trivalent state.



On the other hand, when pH of the surrounding aqueous phase increases above approximately 5.5, ferric sulfate hydrolyses according to the reaction:



creating additional amount of sulfuric acid. That sulfuric acid, together with dissolved trivalent iron are the main components of so-called acid mine drainage (AMD), i.e. waters flowing from worked-out mines, flotation waste deposits and sometimes from natural rocks containing pyrites (Doyle, 1990; Evangelou, 1995). Strongly acidic and oxidizing (due to the presence of trivalent iron) waters solubilize rocks containing otherwise insoluble minerals, causing contamination of the environment and sometimes leading to catastrophes of buildings (Moore and Luoma, 1990). At natural conditions (free access of CO_2) and circumneutral pH, most of sulfide minerals oxidize to insoluble carbonates (Salter and Jones, 1986; Banks et al., 1997). These carbonates create protective layers on the surface of sulfide grains and protect them from dissolution. When the rock contains minerals that have neutralizing properties (mainly carbonates of calcium and magnesium), waters outgoing from mines and depository places may be so pure that in many places they are used as the pot water for the surrounding localities (Banks et al., 1997). Therefore, lime and limestone are commonly used to decrease the concentration of iron and non-ferrous metal ions in water and wastes (Schwartz and Ploethner, 1999). The presence of carbonates not only decreases the rate of oxidation of sulfides and causes the precipitation of the metal ions as insoluble carbonates and trivalent iron as iron hydroxide, but also stabilizes pH at approximately 8 and decreases the activity of sulfide-oxidizing bacteria (Gleisner

and Herbert, 2002). On the other hand, the grains of limestone, when contacted with the acidic solutions containing dissolved iron, aluminium and non-ferrous metal ions may be covered by coatings composed mainly of complex Fe and Al sulfates and gypsum, sealing the surface of the grain from the contact with the solution and lowering their reactivity. The influence of carbonates on pyrite oxidation is complex. The presence of HCO_3^- ions increases the initial rate of pyrite oxidation, but this rate drops later on due to the formation of protective hydroxide coatings (Nicholson et al., 1988, 1990; Moses and Herman, 1991.). Sulfide minerals, including pyrite, may oxidize to elemental sulfur:



both in industrial leaching processes (Buban et al, 2000) as well as in wastes left in natural conditions (Byerley and Scharer, 1992). Naturally, from the point of view of the environment protection, that way of sulfide minerals oxidation is much more preferable. Unfortunately, ever-present bacteria usually oxidize sulfide sulfur to sulfates.

The oxidation of sulfide minerals is a very important problem not only from the point of view of environment protection and it was the object of a countless number of studies. However, most of the published papers are devoted to the oxidation of pure minerals. The papers concerning the oxidation of sulfide minerals in complex mixtures, like flotation tailings, are rather scarce. The present paper is devoted to the oxidation of sulfide minerals in flotation wastes from the flotation plant at the ZGH Bolesław metallurgical complex. The ores processed there contain galena and sphalerite as the main valuable minerals and some oxidized lead and zinc minerals as well as significant amount of pyrite and marcasite. Oxidized lead and zinc minerals are much better soluble than respective sulfides and may dissolve to some extent even in the absence of oxidizing factors and the oxidation of pyrite may induce the solubilization of sulfides. On the other hand these ores contain high concentration of calcite and dolomite, which should depress the emission of lead and zinc ions from the wastes. Another problem is the possible emission of sulfates, which not always is depressed by carbonates of calcium and magnesium because the sulfates of both metals are relatively well soluble. So, the course of sulfides' oxidation and emission of potential contaminants from the mentioned tailings has been investigated experimentally with the special attention to the oxidation of sulfide sulfur.

EXPERIMENTAL

Flotation wastes were collected from flotation tailing pond where they had been left in a wet state and had the consistency of a dense suspension. The phase composition of the wastes was determined by X-ray diffraction, using the Siemens D 5005 (Bruker) instrument. Figure 1 presents the diffraction pattern of the wastes. It is

to be seen that the main minerals constituting the wastes were: dolomite, ca 40 mol%, calcite, ca 20 mol%, pyrite + marcasite, ca 30 mol%, and quartz, ca 10 mol%. Thorough diffraction analysis revealed also the presence of minor quantities (below 1%) of sphalerite, galena, cerusite and smithsonite. Particle size distribution of the wastes was measured by sieving through a set of laboratory sieves (Fritsch). As usually in flotation tailings, the particles size distribution was rather broad: 50 weight % of the grains had the diameter below 0.15 mm and 10 weight % below 0.05 mm. The sample (several tenths of kilograms) was homogenized and placed in tightly sealed plastic cans. Most of the experiments were performed with the wastes as received, however part of the sample was dried at 105°C to constant weight and used in the experiments in a dry state.

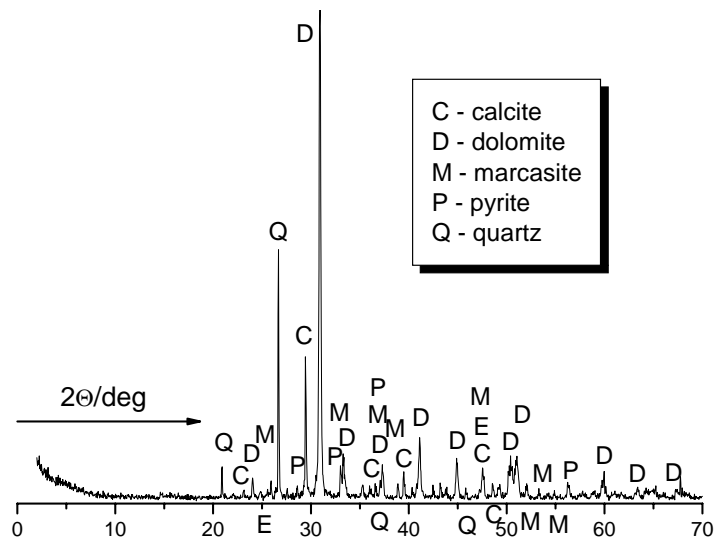


Fig. 1. X-ray diffraction pattern of investigated flotation tailings

Emission of metal ions and sulfates to the water flowing through the wastes was investigated by placing the wastes in a column made of organic glass depicted in Fig. 2 and passing distilled water from the top of the column to its bottom. Water being in equilibrium with air was used, but in one experiment water before the introduction to the column was bubbled with argon to remove oxygen. The internal diameter of the column was 5 cm. The height of the wastes in the column ranged from 9 to 42 cm, the weight (dry state) from ca 360 g to ca 1600 g, respectively. In the case of loading the wet wastes to the column, the bottom part of the column (between the outlet and the gilded mesh supporting the wastes) was first filled with water and then the wastes, in the form of dense suspension, were poured from the top to a predetermined high. Finally, the top of the column was filled with water and connected to the Mariotte

bottle supplying the inlet water and stabilizing the hydrostatic pressure. In the case of dried samples the column was filled with water to the height of a few centimeters above the gilded mesh supporting the wastes and the dry wastes were poured from the top to water portion by portion. After each portion of wastes water was added to keep all the time the level of water over the top of the wastes. Finally, the top of the column was filled with water and connected to the Mariotte bottle.

The porosity of the wastes in the column was calculated from the known volume, weight, and specific density of dry wastes. For the wet wastes the porosity amounted to 0.31 – 0.35 and it was relatively constant during the experiment. Only two experiments were performed with the dried wastes, the porosity in both experiments was changing from approximately 0.52 at the beginning to approximately 0.46 at the end. The amount of water that has flown through the column was expressed as the exchange ratio (ER) of the pore water. Constant hydrostatic pressure was kept during the experiment and expressed as the hydraulic gradient (ratio of the difference between the level of outlet and inlet and the height of the column (see Fig. 2). Hydraulic gradient was different in different experiments and in particular experiment it was between 0.25 and 5. Samples of outlet solution were collected regularly, weighted, and then pH, conductivity, and concentration of selected ions were determined. Conductivity and pH were measured using a CX551 multifunction meter (Elmetron). In one experiment the concentration of oxygen in the outlet solution was measured with the use of CTN-9202S Clark-type electrode (ZTP Elsent). Concentration of selected ions in the outlet solution was measured with the NOVA 60 photometer (Merck). The concentration of following ions was controlled in the outlet solution: Ca^{2+} , Cd^{2+} , Cl^- , CrO_4^{2-} , Cu^{2+} , Fe^{2+} , Fe^{3+} , K^+ , Mg^{2+} , Mn^{2+} , Mo(VI) , Na^+ , Ni^{2+} , Pb^{2+} , SO_4^{2-} , Ti^{3+} , Zn^{2+} but only Ca^{2+} , Cl^- , Fe^{2+} , Fe^{3+} , Mg^{2+} , Na^+ , Pb^{2+} , SO_4^{2-} , and Zn^{2+} appeared in measurable quantity. The experiments were conducted in the thermostated room at $24.5 \pm 0.5^\circ\text{C}$.

In several cases, at the end of the experiment wastes were carefully removed from the column in a way not to mix them, and small samples from the top, middle and bottom of the column were collected. The samples were tightly closed in plastic containers and transferred to the XPS (X-ray photoelectron spectroscopy) laboratory at the University of Turku (Finland) where the XPS spectra of the samples were measured. Each wet sample was firmly pressed to the surface of a special conducting carbon foil and mounted in the forechamber of the spectrometer. During pumping-off

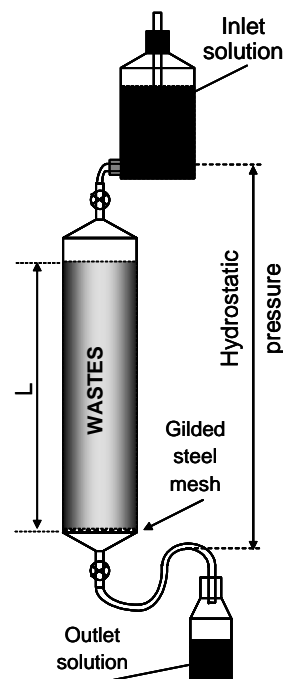


Fig. 2. Column used in the experiments

the forechamber the samples naturally dried. When the pressure in the forechamber dropped to the appropriate level the sample was introduced to the measuring chamber and the spectrum acquired. Photoelectron spectroscopic investigations were performed using the Perkin-Elmer ESCA 5400 spectrometer with monochromatized Al K_{α} X-ray source. More information on the measuring system and the spectra interpretation may be found in previous papers (Nowak et al., 2000 a,b). Investigated wastes were composed mainly of non-conducting substances. Measuring the XPS spectra of such substances presents a real problem due to so-called charging. That was eliminated by applying flood-gun. Such procedure introduces however some uncertainty in the recorded binding energy (BE) values. It was overcome by applying correction. Two lines were chosen as reference for correction: Si 2p of quartz (103.3 eV) and C 1s of so-called carbon contamination (285 eV). Both lines were sufficiently strong – quartz appeared in the wastes in the quantity of approximately 10 mol%, as stated by XRD analysis, and carbon contamination appear in any sample contacted with atmospheric air. The position of both lines is known with good precision (Moulder et al., 1992). Weighted (versus the distance from both reference lines) mean position between the lines chosen as reference lines was assumed as the position of the analyzed line. However, such correction was valid only for those emission lines that were placed either between the above mentioned lines or very close to one of them. Fortunately, the most important lines, namely S 2p (162 - 168 eV), Pb 4f (~142 eV), Mg $KL_{23}L_{23}$ (Auger, ~301 eV), Ca $2p_{3/2}$ (~347 eV) fulfilled those conditions. However, neither Fe $2p_{3/2}$ (~707 eV) nor Zn $2p_{3/2}$ (1022 eV) may have been properly corrected. So, only shape of the band and their intensity was analyzed in such a case.

RESULTS

The best way to estimate the total concentration of ionic species in a solution is to measure its conductivity (Evangelou, 1998). Naturally conductivity is a non-specific quantity and it cannot replace the chemical analysis of the solution but if the qualitative composition of the solution is constant, conductivity gives a quick measure of the concentration.

Table 1. The concentrations of the selected ions in consecutive stages of one of the experiments with wastes loaded as wet to the column. Exchange ratio (ER), pH and conductivity (κ) of the effluent are also given. Weight of the wastes in the column was 1600 g (in the dry state), height 39 cm, and hydraulic gradient 5.0. All concentrations are given in mgdm^{-3} , conductivity in mScm^{-1}

Stage	ER	pH	κ	Ca^{2+}	Mg^{2+}	SO_4^{2-}	Na^+	Cl^-	Pb^{2+}	Zn^{2+}
I	0.64	7.90	3.88	620	302	2980	41	74	1.6	3.1
II	3.12	8.02	2.41	660	36.5	1600	<10	<5	0.9	2.3
III	5.58	8.00	0.37	51	13.4	44	<10	<5	0.09	0.25

Figure 3 presents the changes of conductivity and pH of the outlet of the column as a function of exchange ratio (ER) of the pore water in two experiments performed at identical conditions. The repeatability of the results of the experiments was rather good, as may be seen. The course of the dependence of both κ and pH on ER in all experiments was similar to that presented in Fig. 3. The experiment may be divided into three stages (marked in Roman numerals in the figure). Typical concentrations of the most important ions present in the effluents from the column in consecutive stages of one of the experiments are presented in Table 1.

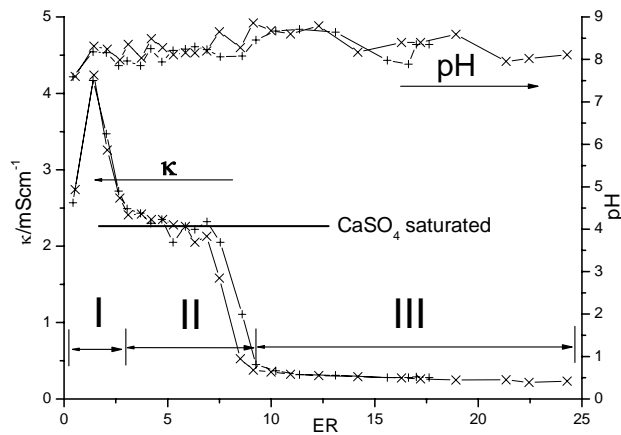


Fig. 3. The change of pH and conductivity of the outlet solution of the column in two experiments performed at identical conditions: height of the wastes 16 cm, weight of wastes (dry state) 660 g, hydraulic gradient 5.0

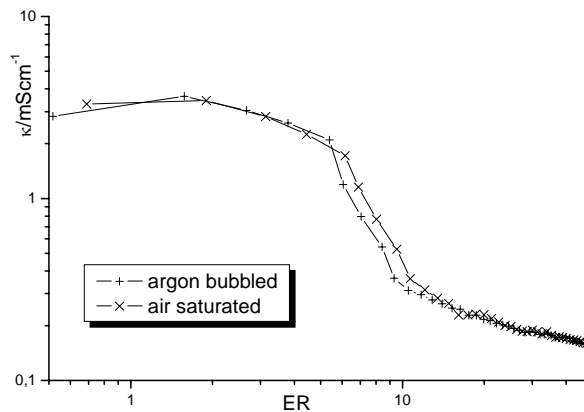
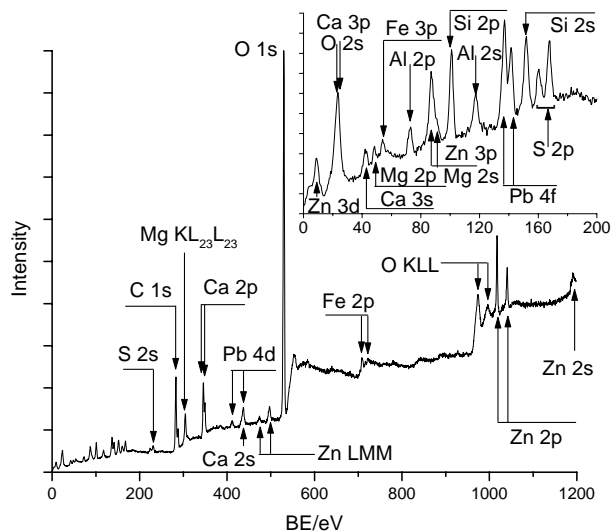


Fig. 4. Conductivity changes in two experiments: in one of them water in equilibrium with atmospheric air was used, in the other experiment water was bubbled with argon to remove oxygen before introduction to the column. All other parameters of the experiments were identical: hydrostatic gradient = 4.0, mass of the sample = 350 g, height of the waste layer 9.0 cm

The first stage was always short ($ER \leq 3$) and characterized by a high concentration of dissolved substances, these substances being magnesium and calcium sulfates. The second stage was longer and the main ionic component of the effluent was calcium sulfate. The conductivity in this stage was equal to the conductivity of saturated solution of gypsum. Third stage lasted to the end of the experiment and the composition of the solution during that stage of the process was dominated by carbonate complexes of calcium. The most pronounced difference between different experiments appeared in stages I and II, depending on the state of the wastes before the start of the experiment (wet or dry). When the wastes were dried before the experiment, pH in stage I was much lower (~ 5.5 at the beginning) and quite a lot of Fe^{2+} appeared in the effluent. No iron in the effluent of the column was ever observed in the case of wastes loaded to the column in the wet state. In the case of wastes loaded to the column in the dry state, the duration of stage II was much longer than in the case of wastes loaded as wet. In the later case, when the layer of the wastes in the column was rather short, stages I and II were not so clearly resolved. Starting from the beginning of stage III the concentrations of ions were continuously diminishing and the conductivity of the effluent was diminishing too (see Fig. 4) in parallel to the concentration of calcium. The maximum value of ER for which the data in Fig. 4 are showed is 50, but the conductivity (and in parallel the concentration of Ca^{2+} , Pb^{2+} and Zn^{2+}) continued to decrease as long as the experiment was conducted (the same was observed for all experiments). The longest experiment lasted 146 days; the highest ER value attained was 145 (not in the same experiment). The conductivity in the third stage of the process was determined mainly by the dissolution of carbonate minerals present in the wastes, so it is not surprising that the conductivity did not depend on the presence of oxygen in the influent water (see Fig. 4). However, the concentrations of both lead and zinc, in two parallel experiments with oxygen free water in one of them (Fig. 4) was also the same within the limit of the analysis accuracy up to the $ER = 50$ (then the experiment with oxygen free water was stopped). Table I presents the concentrations at the very beginning of stage III of the experiment. In all experiments, after 10 – 30 exchanges of pore water the concentration of both SO_4^{2-} and Mg^{2+} dropped below the limit of detectability (5 mgdm^{-3} in the case of both ions). In one of the experiments the concentration of oxygen in the effluent of the column was measured. A short column (9 cm) and relatively high hydraulic gradient (3.0) were applied, but after 41 exchanges of pore water the concentration of oxygen in the effluent was still below the limit of detectability.

Figure 5 presents the survey XPS spectrum of the wastes after dismantling the column. Except the emission lines of Ca, Mg, O, C, Fe, Pb, Zn, S and Si, relatively strong Al line appeared in the spectrum. Aluminium occurs in the wastes probably as several different aluminosilicates, having different diffraction patterns. For that reason they have not appeared in the XRD analysis. Both Pb and Zn emission lines were stronger than may be expected basing on the composition of the wastes.

Fig. 5. Survey XPS spectrum of the wastes after 21 exchanges of pore water and dismantling off the column. Sample taken from the bottom part of the column. Hydraulic gradient during experiment 5, weight of the wastes in column 660 g (in dry state), height of the wastes in the column 16 cm



The obvious explanation is that most of lead and zinc appeared in the adsorbed state, on the surface of calcite, dolomite and iron hydroxides produced by oxidation of pyrite. The BE of the Pb $4f_{7/2}$ line was approximately 0.7 eV higher than that for lead carbonate. Contrary to lead and zinc, the emission line of iron (Fe 2p) was weaker than might be expected. At pH that was inside the column, the concentration of trivalent iron in the solution is extremely low (Dyer et al., 1998). So, the concentration of iron species in the solution was too low to cause the adsorption of iron at the surface of carbonates. On the other hand iron hydroxides and hydrated oxides are very good adsorbents and their surfaces was probably covered by adsorbed ions. XPS is a surface-sensitive method and even monolayer coverage may decrease significantly the emission of electrons from the background. Figure 6 presents the S 2p line of the XPS spectra of the samples collected from different parts of the column. For the sake of comparison the S 2p line of the XPS spectrum of a pyrite sample fractured and then exposed to atmosphere is presented in Fig. 7.

Despite some uncertainty, connected with the procedure of BE correction, the interpretation of the S 2p spectra of waste samples is straightforward. Both sulfide sulfur and oxidized sulfur may be easily discriminated in the spectrum. Most of the emission at the BE of sulfide sulfur may be unequivocally ascribed to pyrite (~162.6 eV), but a weak shoulder at the position close to either the sulfur in galena (161 eV) or sphalerite (161.5) (Laajalehto et al., 1994) may be visible too. Note further, that the spectrum for the sample collected from the top of the column differs strongly from those of both the samples collected from the middle and the bottom of the column as well as from the spectrum of wastes before loading to the column.

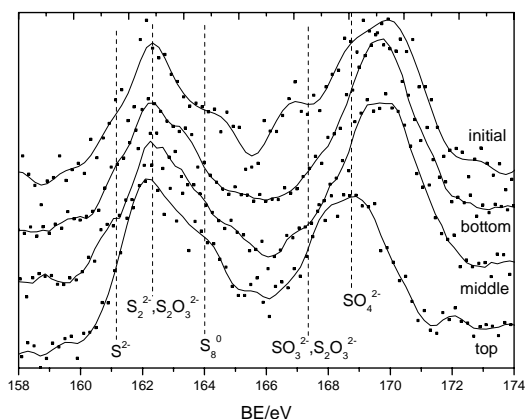


Fig. 6. S 2p region of the XPS spectra of the wastes after dismantling off the column. Samples taken from different parts of the column, as described in figure. Spectrum of the wastes before loading to the column (initial) is presented too. Parameters of the experiment like in Fig. 5. Thiosulfate appear twice at two different BEs, because thiosulfate ion has two different sulfur atoms that give the emission at different binding energies. Points – measured data. Continuous lines – data smoothed by the ORIGIN program

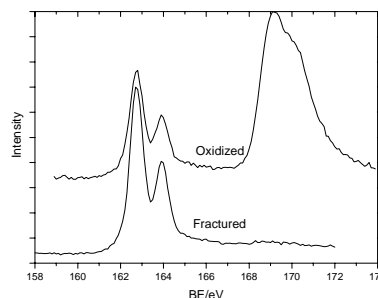


Fig. 7. Example of the S 2p line of the XPS spectrum of the freshly fractured and oxidized surface of pyrite. Coal pyrite from the coal mine Jastrzębie in Poland. After fracturing pyrite was oxidized 10 days in air

The obvious reason is that the concentration of dissolved ions (Fe^{2+} , HCO_3^- , and SO_4^{2-}) at the top of the column is the lowest and the concentration of oxygen the highest. So, the top of the column is best “cleaned off” the soluble and desorbable species and at the same time the conditions for pyrite oxidation are the best there. The position of the emission line that may be ascribed to sulfates in the case of that sample is similar to the case of oxidized pyrite (compare Fig. 6 and 7) and may be ascribed to sulfate on the surface of pyrite. However, the sulfate line in both the samples from the middle of the column and from the bottom of the column is shifted towards higher BE by approximately 1 eV. It may be postulated that down the column sulfate ions appear mainly in the adsorbed state, at the surface of the carbonate minerals and iron hydroxides. The lead line, which was ascribed to the lead ions on the surface of calcite, also showed the shift in the direction of higher BE. Note, that the proportion of sulfate sulfur is lowest at the top of the column and highest at the bottom. In the case of initial sample both sulfate at the surface of pyrite and adsorbed sulfate appear. It also seems that the intermediate-valence sulfur (sulfite? thiosulfate?) appear in the initial sample and, to the less extent at the top of the column. Interesting question is the possible presence of elemental sulfur. A shoulder at the position expected for elemental sulfur evidently appears in the spectrum of initial sample and to a lesser extent in the spectrum of the sample from the top of the column. Note that neither elemental sulfur nor intermediate-valence sulfur are visible in the spectrum of

oxidized pyrite (Fig. 7). In the spectrum (not showed) of the sample collected from the experiment where ER ratio was much higher (61), the emission at the BE characteristic for elemental sulfur was much higher (in comparison to other forms of sulfur).

DISCUSSION

The following picture of the process of oxidation of metal sulfides and generation of contaminants in the flotation wastes from the ZGH Bolesław may be presented, basing on the column tests and the XPS spectra. The main source of sulfates in the water flowing through the wastes is the dissolution of sulfates formed by oxidation of metal sulfides (mainly pyrite) during the storage of the wastes. After dissolution of the sulfates (stage I and II of the experiment) the concentration of sulfates transferred to the flowing (air-saturated) water was rather low, below the standards for industrial waste waters. The degree of oxidation of the wastes may be estimated from the total amount of sulfates liberated from the wastes during stages I and II of the experiment. In accordance with commonly accepted opinions the oxidation of sulfides is much faster when waste is kept in the dry state as compared to the wastes kept under the surface of water. In the case of the waste kept as dry, ferrous sulfate and sulfuric acid formed in reaction (2) rest at the surface of pyrite. When the wastes are poured into water, both H_2SO_4 and FeSO_4 dissolve and the pH of the solution drops. Sulfuric acid reacts with calcite and dolomite inside the column according to the reactions:



Well soluble ferrous sulfate appears in the effluent of the column. When the wastes are kept under the water, both sulfuric acid and ferrous sulfate dissolve immediately after their formation. Sulfuric acid react with calcite and dolomite according to reactions (6) and (7) and ferrous sulfate oxidize to ferric sulfate:



When pH of the pore water grows up the hydrolysis of ferric sulfate occurs (reaction 4). So, no ferrous sulfate is present in pore water. Magnesium sulfate is very well soluble and it leaves column in stage I of the process. The solubility of gypsum is limited - part of it precipitates already during the storage of the wastes and is removed during stages I and II of the experiment. So, wastes kept as wet contain sulfate ions in the form of gypsum both precipitated and dissolved in pore water, and in the form of dissolved magnesium sulfate. When the experiment starts, the incoming water first replaces water containing dissolved sulfates in pores, and then dissolves gypsum so the only sulfates that may be observed by XPS in the sample collected from the top of the column are those from the oxidation of sulfides by oxygen (reactions 1 and 2).

However, when water flows down the column the concentration of sulfates grows up and sulfate ions adsorb at the surface of carbonate mineral grains and iron hydroxides. As a result the ratio of sulfates grows up down the column.

Part of sulfide sulfur evidently oxidizes to elemental sulfur, as may be inferred from the XPS spectra. The formation of elemental sulfur may be supported by following reasoning. If all oxygen, present in the influent water (saturated with air) had oxidized sulfide sulfur to sulfates according to reactions (1) and/or (2) the concentration of sulfates in the effluent would have been 13.7 mgdm^{-3} , as may be easily calculated. However in all performed experiments the concentration of sulfates dropped down below 5 mgdm^{-3} soon after the end of stage II of the experiment and no oxygen was found in a control experiment after 41 exchanges of pore water. That is in apparent contradiction with the relatively high amount of sulfates observed by XPS, especially because both Mg and Zn sulfates are very well soluble in water, the solubility of CaSO_4 is relatively (comparing to carbonate) high and even lead sulfate is orders-of-magnitude better soluble than lead carbonate. The best explanation is that the sulfate observed by XPS appears mainly as adsorbed on the surface of carbonates. Note, that even very small amount of a substance dispersed homogeneously on the surface may contribute very strongly to the XPS spectrum. Formation of elemental sulfur is a very important aspect of the process. If the oxidation of sulfides present in wastes proceeded completely to elemental sulfur there would be no formation of sulfuric acid and the emission of contaminants to the environment would be much lower. In the literature concerning the oxidation of pyrite by dissolved oxygen at circumneutral pH no formation of elemental sulfur was reported (Nicholson et al., 1988, 1990; Moses and Herman, 1991) and other sulfides (galena and sphalerite) were present in the investigated wastes in minor quantity as compared to pyrite + marcasite, so they could not be the source of elemental sulfur observed by XPS. The formation of elemental sulfur on the surface of sulfide minerals is now extensively studied in our laboratory.

Similar situation, like in the case of sulfate ions, occurs in the case of zinc and lead ions. The concentrations of both metals in the effluent during stage III of the experiment were low and below the standard for industrial waste water, obviously kept at such low level by low solubility of cerussite and smithsonite (or hydrocerussite and hydrozincite). High and constant concentration of HCO_3^- ions is due to the presence of high amount of calcite and dolomite that saturate the solution. Note, that higher concentration of zinc and lead ions in stage I and II of the experiment may be ascribed to very high concentration of Ca^{2+} and Mg^{2+} ions that cause lowering the concentration of carbonate ions according to the solubility product of calcite and dolomite. Rather high ratios of lead and zinc dissolution as indicated by the XPS spectra is obviously due to the sorption of the ions of both metals at the surface of carbonate minerals and iron hydroxides. That sorption is well documented in the literature (Zachara et al., 1991; Rimstidt et al., 1998; Godelitsas et al., 2003; Rouff et al., 2004).

CONCLUSIONS

The dissolution of zinc, lead, and sulfate ions in water from the flotation wastes containing relatively high concentration of pyrite and marcasite (~30 mol%) and minor quantities of sulfide and oxidized minerals of zinc as well as lead is strongly suppressed due to beneficial influence of carbonate minerals present in the wastes (calcite and dolomite). Concentration of zinc and lead is kept low due to the saturation of the flowing water by the carbonate ions from the dissolution of calcite and dolomite. Calcite and dolomite are much better soluble than carbonates of zinc and lead and, according to the solubility product, the concentration of zinc and lead species in the presence of calcite and dolomite is much lower than in the saturated solution of pure zinc and lead carbonates. At the same time the sulfide sulfur of metal sulfides present in the wastes is oxidized partly to elemental state, which diminished the amount of sulfate ions generated during the contact with air-saturated water. Altogether, it makes the investigated wastes relatively safe to dispose, providing that they are placed below the surface of water.

REFERENCES

- BANKS D., YOUNGER P.L., ARNESON R.-T., IVERSON E.R. AND BANKS S.B., 1997, *Mine-water chemistry: the good, the bad and the ugly*, Environmental Geology, **32**, 157 - 174.
- BUBAN K.R., COLLINS M.J., MASTERS I.M. AND TRYTTEN L.C., 2000, *Comparison of direct pressure leaching with atmospheric leaching of zinc concentrates*, in: Lead-zinc 2000, Proceedings of the Lead-Zinc Symposium, Pittsburgh, USA, (J.E. Dutrizac, J.A. Gonzalez, D.M. Henke, S.E. James and A.H-J. Siegmund, editors), The Minerals, Metals and Materials Society, Warrendale, 727 - 738.
- BYERLEY J.J. AND SCHARER J.M., 1992, *Natural release of copper and zinc into the aquatic environment*, Hydrometallurgy, **30**, 107 - 126.
- CRAIG J.R. AND VAUGHAN D.J., 1990, *Compositional and textural variations of the major iron and base-metal sulfide minerals*, in: Sulfide deposits – their origin and processing (P.M.J. Gray, G.J. Bowyer, J.F. Castle, D.J. Vaughan and N.A. Warner - editors), The Institution of Mining and Metallurgy, London, 1 - 16.
- F.M. DOYLE, 1990, *Acid mine drainage from sulfide ore deposits*, w: Sulfide deposits – their origin and processing (wydawcy - P.M.J. Gray, G.J. Bowyer, J.F. Castle, D.J. Vaughan i N.A. Warner), The Institution of Mining and Metallurgy, Londyn, 301 - 310.
- DYER J.A., SCRIVNER N.C. AND DENTEL S.K., 1998, *A practical guide for determining the solubility of metal hydroxides and oxides in water*, Environmental Progress, **17**, 1 - 8.
- EVANGELOU V.P., 1995, *Pyrite Oxidation and Its Control*, CRC Press, Boca Raton, USA.
- EVANGELOU V.P., 1998, *Environmental Soil and Water Chemistry. Principles and Application*, J. Wiley&Sons, Nowy Jork
- GLEISNER M. AND HERBERT R.B. JR., 2002, *Sulfide mineral oxidation in freshly processed tailings batch experiments*, Journal of Geochemical Exploration, **76**, 139 - 153.
- HELIOS-RYBICKA E., 1996, *Impact of mining and metallurgical industries on the environment in Poland*, Applied Geochemistry, **11**, 3 - 11.
- GODELITSAS A., ASTILLEROS J.M., HALLAM K., HARISSOPOULOS S., PUTNIS A., 2003, *Interaction of calcium carbonates with lead in aqueous solutions*, Environ.Sci.Techl., **37**, 3351-3360.
- LAAJALEHTO K., KARTIO I. AND NOWAK P., 1994, *XPS Study of Clean Metal Sulfide Surfaces*, Applied Surface Science, **81**, 11-15.
- LEJA J., 1982, *Surface Chemistry of Froth Flotation*, Plenum Press, Nowy Jork.

- LUSZCZKIEWICZ A., 2000, *Koncepcja wykorzystania odpadów flotacyjnych z przeróbki rud miedzi w regionie Legnicko-Głogowskim*, Inżynieria Mineralna, **1**, 25 – 35.
- MOORE J.N. AND LUOMA S.N., 1990, *Hazardous wastes from large-scale metal extraction*, Environmental Science and Technology, **24**, 1278 - 1285.
- MOSES C.O. AND HERMAN J.S., 1991, *Pyrite oxidation at circumneutral pH*, Geochimica et Cosmochimica Acta, **55**, 471 – 482.
- MOULDER J.F., STICKLE W.F., SOBOL P.E. AND BOMBEN K.D., 1992, *Handbook of X-ray photoelectron spectroscopy*, Perkin Elmer, Eden Prairie, USA.
- NICHOLSON R.V., GILLHAM R.W. AND REARDON E.J., 1988, 1990, *Pyrite oxidation in carbonate-buffered solutions: 1. Experimental kinetics. 2. Rate control by oxide coatings*, Geochimica et Cosmochimica Acta, **52**, 1077-1085, **54**, 395-402.
- NOWAK P. AND LAAJALEHTO K., 2000a, *Oxidation of Galena Surface – an XPS Study of the Formation of Sulfoxy Species*, Applied Surface Science, **157**, 101-111
- NOWAK P., LAAJALEHTO K. AND KARTIO I., 2000b, *A Flotation Related X-Ray Photoelectron Study of the Oxidation of Galena Surface*, Colloids and Surfaces A, **161**, 147-160
- RIMSTIDT J.D., BALOG A. AND WEBB J., 1998, *Distribution of trace elements between carbonate minerals and aqueous solutions*, Geochimica et Cosmochimica Acta, **62**, 1851-1863.
- ROUFF A.A., ELZINGA E.J., REEDER R.J. AND FISHER N.S., 2004, *X-ray absorption spectroscopic evidence for the formation of Pb(II) inner-sphere adsorption complexes and precipitates at the calcite - water interface*, Environ. Sci. Technol., **38**, 1700 - 17007.
- SALTER J.D. AND JONES M.P., 1986, *Galena alteration in bicarbonate environment*, Trans. Inst. Min. Metal., **95**, C95 - C106.
- SCHWARTZ M.O., PLOETHNER D., 1999, *Removal of heavy metals from mine water by carbonate precipitation in the Grootfontein-Omatako canal, Namibia*, Environmental Geology, **39**, 1117 - 1126.
- SIMÓN M., MARTIN F., GARCIA I., BOUZA P., DORRONSORO C. AND AGUILAR J., 2005, *Interaction of limestone grains and acid solutions from the oxidation of pyrite tailings*, Environmental Pollution, **135**, 65 – 72.
- ZACHARA J.M., COWAN C.E. AND RESCH C.T., 1991, *Sorption of divalent metals on calcite*, Geochimica et Cosmochimica Acta, **55**, 1549 – 1562.

ACKNOWLEDGEMENTS

All experiments on leaching the wastes with water were performed in the Strata Mechanics Research Institute of PAS in Kraków, on the laboratory stand constructed there. Kind collaboration and helpful discussions with Professor Jakub Bodziony and helpful technical assistance of Mr. Jarosław Aksamit from that Institute are kindly acknowledged. The XPS spectra were performed at the Laboratory of Materials Science of Turku University (Finland) during a visit in the framework of exchange program between PAS and Academy of Finland. The work was financially supported by State Committee for Scientific Research of Poland through the grant number 5T12A-038-23.

Nowak P., Socha R.P., *Utlenianie minerałów siarczkowych w odpadach flotacyjnych – przemiany siarki siarczkowej*, Physicochemical Problems of Mineral Processing, 40, (2006) 134-148, (w jęz. ang.).

Badano rozpuszczalność jonów Zn i Pb oraz siarczanowych z odpadów flotacyjnych rud cynkowo-olowiowych przepuszczając wodę przez kolumny wypełnione odpadami. Odcieki z kolumn badano oznaczając ich pH, przewodnictwo oraz stężenia wybranych jonów jako funkcję krotności wymiany wody porowej (ER) w odpadach. Z odpadów po doświadczeniu pobrano próbki, które badano metodą spektroskopii fotoelektronów generowanych promieniowaniem X (spektroskopia XPS). Stwierdzono, że dzięki dużej zawartości minerałów węglanowych, które nasycają przepływającą wodę jonami wodorowęglanowymi stężenia jonów cynku i ołowiu, poza początkowym okresem, są znacznie poniżej normy dla ścieków przemysłowych. Równocześnie siarczkowa siarka w znacznej części utlenia się do siarki pierwiastkowej a nie do siarczanów, co powoduje, że emisja siarczanów z odpadów jest stosunkowo niewielka.

Ewa SKWAREK, Władysław JANUSZ*

ADSORPTION OF Ni(II) IONS AT THE Fe₂TiO₅/ELECTROLYTE SOLUTION INTERFACE – THE ELECTRICAL DOUBLE LAYER STRUCTURE

Received March 15, 2006; reviewed; accepted May 15, 2006

Physicochemical properties of Fe₂TiO₅ (pseudobrookite structure) surface was studied and basic properties of electrical double layer of the Fe₂TiO₅/NaCl+Ni²⁺ solution system were described. The adsorption of Ni (II) at the pseudobrookite/aqueous solutions interface was studied over the pH range of 3 to 11. The influence of ionic strength, pH, and presence of ions was researched. ζ potential, surface charge density, adsorption density, pH_{50%} and ΔpH_{10-90%} parameters for different concentrations of background electrolyte were presented. The adsorption constants of surface hydroxyl groups' reactions were determined using numerical optimization.

Key words: Fe₂TiO₅, electrical double layer, surface charge density, zeta potential, adsorption

INTRODUCTION

Titanium substituted iron oxides are widespread in nature and represent an important mineral resource for the commercial obtainment of both iron and titanium compounds. Pseudobrookite is recently considered as a non-terrestrial an oxygen source for lunar bases (Guo et al. 1999). Pseudobrookite, a natural mineral, is present in igneous and metamorphic rocks and has magnetic properties (Guo et al. 1999, Surowce 1985). Fe₂TiO₅ can be used as material for optical filters and for photo catalytic applications (Perkas et al. 2001, Misook 2003, Garcia et al. 2002).

In the resent years many papers been published that describe methods of preparation of Fe₂TiO₅ by means of the sol-gel method (Misook 2002, Kanga et al. 2001, Lee et al. 2001) or by mixing in stoichiometric amounts Fe₂O₃ and TiO₂ powders.

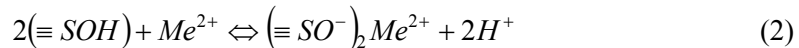
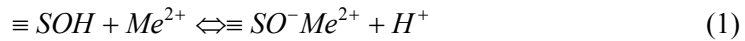
* Uniwersytet Marii Curie-Skłodowskiej, Wydział Chemii, Pl. M.C. Skłodowskiej 3, 20-031 Lublin, PL.

The surface charge at the $\text{Fe}_2\text{TiO}_5/\text{NaCl}$ aqueous solution interface results from similar reactions to the simple oxide/electrolyte interface e.g. acid-base dissociation of the amphoteric surface hydroxyl groups ($-\text{SOH}$) and reaction of complexation of hydroxyl groups.

The equilibrium constants that characterize these reactions according the site – binding theory are important physicochemical quantities that characterize structure of the electrical double layer. There are a few method of calculation of these constants e.g.: Davis et. al., modified Schwarzenbach’s method, and numerical optimization methods.

James and Parks reviewed electrical double layer models at the metal oxide interface and their suitability for estimating the surface charges and zeta potentials under a wide range of conditions including those with an adsorbing heavy metal species present in solution. They concluded that the simultaneous measurement of parameters such as surface charge, zeta potential and degree of heavy metal adsorption is desirable for precise description of edl at the metal oxide interface (James and Parks 1982).

According to the site binding theory of edl the divalent ions can be adsorbed specifically on the metal oxide surface by forming the coordinate bonds between the surface oxygen atoms and the adsorbed cation. Some of them are adsorbed so strongly that there are no water molecules between the adsorbed ion and the surface, so-called inner-sphere, complexes are formed. If a water molecule is present between the adsorbed ion and the surface, then the outer-sphere complex is formed (Hayes and Katz 1996). Divalent ions may adsorb at the metal oxide surface on one or two surface sites (Schindler 1981). It is assumed that the following reactions are responsible for the adsorption of divalent cations at the oxide/electrolyte interface:



As may be noticed from Eq 1, 2 and 3 the adsorption of cations releases hydrogen ions from hydroxyl groups, so the increase of pH in the system will favor the adsorption of cations at the metal oxide/electrolyte interface. Consequently, the sharp increase of the cation adsorption from 0% to 100%, with increase of pH of the electrolyte as much as 1, 2 units are observed. This relationship is called “edge of adsorption” and Robertson and Leckie (1997) have proposed very useful parameters to characterize it:

- $dp\text{Me}/dp\text{H}$ – parameter that shows the activity of cations; must vary when pH of the solution changes to maintain the constant adsorption of the cations,

- pH_{50%} - the value of pH when 50% of initial concentration of cations adsorbs, this parameter characterizes the position of adsorption edge on the pH scale,
- pH_{10-90%} - the range of pH where the adsorption changes from 10% to 90%, it characterizes the slope of the edge,

$$*K_1^S = \frac{[H^+][\equiv SO^-Me^{2+}]}{[Me^{2+}][\equiv SOH]} \frac{\gamma_H\gamma_1}{\gamma_{Me}\gamma_0} \times \exp\left(\frac{e(2\psi_1 - \psi_H)}{kT}\right), \quad (4)$$

$$*\beta_{21}^S = \frac{[H^+]^2[(\equiv SO^-)_2Me^{2+}]}{[Me^{2+}][\equiv SOH]^2} \frac{\gamma_H^2\gamma_2}{\gamma_{Me}\gamma_0^2} \times \exp\left(\frac{e(2\psi_2 - \psi_H)}{kT}\right), \quad (5)$$

$$*K_{MeOH}^S = \frac{[H^+]^2[\equiv SOMeOH]}{[Me^{2+}][\equiv SOH]} \frac{\gamma_H^2\gamma_1}{\gamma_{Me}\gamma_0} \times \exp\left(\frac{e(\psi_1 - \psi_H)}{kT}\right), \quad (6)$$

where:

γ_1, γ_2 – activity coefficients of $\equiv SOH^{(z-1)+}$ and $(\equiv SO)_2H^{(z-2)+}$ groups, ψ_1, ψ_2 – means potentials in the planes of adsorption of Me^{2+} bounded to $\equiv SOH^{(z-1)+}$ and $(\equiv SO)_2H^{(z-2)+}$ surface species respectively, γ_0 – activity coefficients of $\equiv SOH$ group, γ_H – activity coefficients of H^+ ions, γ_{Me} – activity coefficients of metal cation, k – Boltzman constant.

The value of reaction constants may be determined by numerical optimization procedures. Results of specific adsorption of ions at electrical double layer structure may be described by means of DLM (double layer model) and TLM (triple layer model).

The influence of ionic strength, pH and presence of ions on adsorption of Ni (II) on the electrical double layer structure – at the Fe₂TiO₅ (pseudobrookite structure)/electrolyte interface was investigated. This study can help to understand the distribution process of Ni (II) ions between the solid phase and a solution during the enrichment processes because Ni occurs in some titanium/iron ores. Their purpose was to describe the process of adsorption of Ni (II) ions at Fe₂TiO₅/electrolyte interface. Adsorption measurements were complemented by surface charge density and determinations of ζ potential. The effect of Ni (II) adsorption on the properties of the edl is discussed. To determine the constants of surface reaction by numerical optimization, the ion adsorption data were used following the triple layer model of the edl.

EXPERIMENTAL

Experiments were performed on a commercial Fe_2TiO_5 sample from Alfa Aesar. The specific surface of the Fe_2TiO_5 sample, determined by nitrogen desorption, was $1.45 \text{ m}^2/\text{g}$. BJH analysis of the isotherm obtained by adsorption-desorption of nitrogen did not reveal microspores, only mezopores of the size of 35 \AA in the examined Fe_2TiO_5 sample were detected. Roentgen diffraction analysis revealed that crystallographic structure of measured substance is pseudobrookite. Nickel ions adsorption was performed with ^{63}Ni isotope as a tracer. The specific adsorption of Ni (II) ions at Fe_2TiO_5 interface was investigated by the means of radioisotope method as a function of Ni (II) ions concentration, NaCl concentration and pH. The initial concentration of Ni (II) ions ranged from 1×10^{-6} to $1 \times 10^{-3} \text{ mol} \cdot \text{dm}^{-3}$, pH was changed from 3 to 10. As a background electrolyte NaCl solution was used of concentrations 0.1 , 0.01 , $0.001 \text{ mol} \cdot \text{dm}^{-3}$. The adsorption measurements were complemented by the potentiometric titration of Fe_2TiO_5 suspensions and electrophoresis measurements.

To remove ionic type contaminations, which might influence the ion adsorption measurements, the pseudobrookite was washed with double distilled water until constant conductivity about 2 \mu S/cm was achieved. Adsorption and surface charge measurements were performed simultaneously in the suspension of the same solid content, to keep the identical conditions of the experiments in a thermostated Teflon vessel in 25°C . To eliminate the influence of CO_2 all potentiometric measurements were performed under nitrogen atmosphere. pH values were measured using a set of glass REF 451 and calomel pHG201-8 electrodes with Radiometer assembly. Surface charge density was calculated from the difference of the amounts of added acid or base to obtain the same pH value of suspension as for the background electrolyte.

The zeta potential of the pseudobrookite dispersions was determined by electrophoresis with Zetasizer 3000 by Malvern. The measurements were performed at 100 ppm solid concentration ultrasonication of the suspension.

RESULTS AND DISCUSSION

Figure 1 presents the surface charge density of pseudobrookite as a function of pH for two concentrations of NaCl solution as a background electrolyte. Figure 2 presents the ζ potential of Fe_2TiO_5 vs. pH for three concentrations of NaCl solution.

One may see that the pH_{IEP} and pH_{PZC} values differ. The pH_{iep} value is below $\text{pH}=4.2$, whereas the pH_{PZC} for Fe_2TiO_5 is near 8.9 . The difference between pH_{PZC} and pH_{IEP} may results form different part of interacting surfaces of metal oxide that is accessible in potentiometric titration and electrophoresis experiments. A part of pores may be smaller then 3 nm and assuming that slipping plane is 1.5 nm away from the solid surface. Then, such pores might be blocked during electrophoresis and surface properties for this part of solid will not be reflected during electrophoresis.

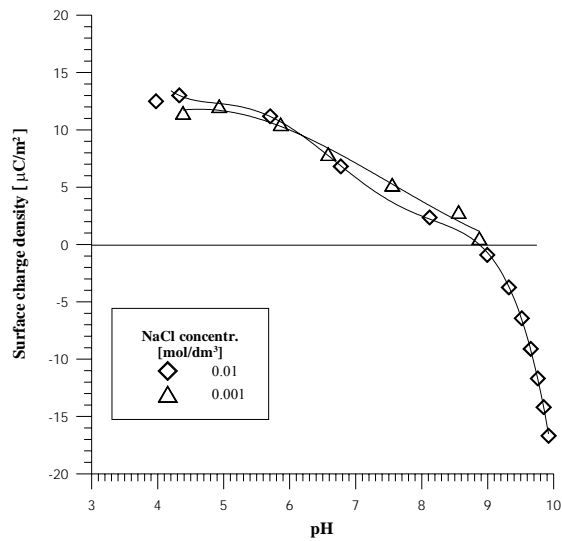


Fig. 1. Surface charge density at the Fe₂TiO₅/NaCl solution interface as a function of pH

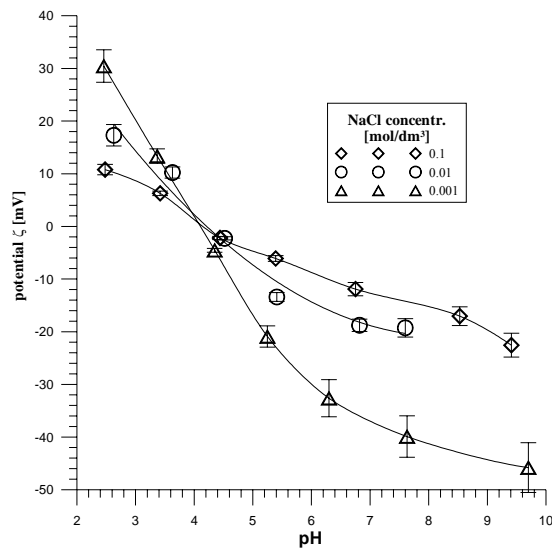


Fig. 2. The ζ potential as a function pH at the pseudobrookite particles in solution NaCl

Great part of surface charge may be compensated inside of particle pores and only the part created by ionized groups on the oxide surface is responsible for electrophoresis mobility. The difference in the position of pH_{IEP} and pH_{PZC} may also indicate the specific anion adsorption, because $\text{pH}_{\text{PZC}} > \text{pH}_{\text{IEP}}$. However, due to so low background electrolyte concentration this effect could not lead to such significant difference between pzc and iep.

The ionization and complexation constants of the surface hydroxyl groups were calculated according to the Davies *et al.* (1978), modified Schwarzenbach (Janusz 1991), and numerical optimization (Janusz 1994) methods, from surface charge density versus pH and electrolyte concentration data. The calculated values of the equilibrium constants are collected in Table 1.

Table 1. The values of surface ionization and complexation constants for $\text{Fe}_2\text{TiO}_5/\text{NaCl}$ solution system

Constants	Method		
	Davis <i>et al.</i>	Modified Schwarzenbach's	Numerical Optimization
pK_{a1}	5.99	5.66	5.50
pK_{a2}	10.31	9.86	10.57
pK_{Cl}	3.94	3.98	3.50
pK_{Na}	10.84	10.12	10.79

One can see a good agreement of the constants with the values calculated by various methods. $\text{Fe}_2\text{TiO}_5/\text{NaCl}$ system is characteristic for a relative big difference (ΔpK) between pK_{a1} and pK_{a2} ionization constants. Analysis of these constants indicates that there is a larger number of anionic surface groups than cationic ones, especially for the Fe_2TiO_5 system.

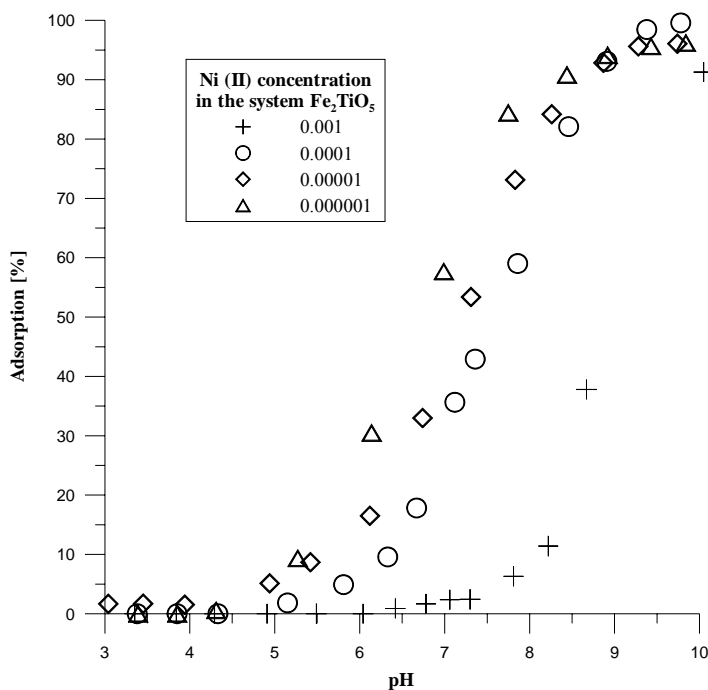


Fig. 3. Adsorption of Ni (II) ions at $\text{Fe}_2\text{TiO}_5 / 0.001 \text{ mol dm}^{-3} \text{ NaCl}$ interface vs pH

The adsorption density of Ni(II) ions as a function of pH in the Fe₂TiO₅/NaCl solution system is presented in Fig. 3. The adsorption edge of the nickel ion adsorption plot in the studied system is characteristic for adsorption of divalent cations on the oxides. With increasing initial concentration of nickel ions the adsorption edge shifts toward higher pH values. At pH≈10 the adsorption reaches 100% that means that almost all nickel ions are bound by solid phase.

Table 2. The values of pH_{50%} and ΔpH_{10-90%} parameters of Ni(II) adsorption edge for the system of Fe₂TiO₅/0.001 mol dm⁻³ NaCl solution

Parameters of adsorption edge	C _{Ni(II)} mol dm ⁻³			
	0.001	0.0001	0.00001	0.000001
pH _{50%}	8.93	7.49	6.94	6.66
ΔpH _{10-90%}	1.8	2.08	2.59	2.69

Characteristic parameters of adsorption edge, pH_{50%} and ΔpH_{10-90%} are listed in Table 2. These data show the shift of the adsorption edge towards higher pH values with the increase of starting concentration of nickel ions. The adsorption edge slope is characterized by the ΔpH_{10-90%} parameter. It increases when nickel ions initial concentration decreases in the system.

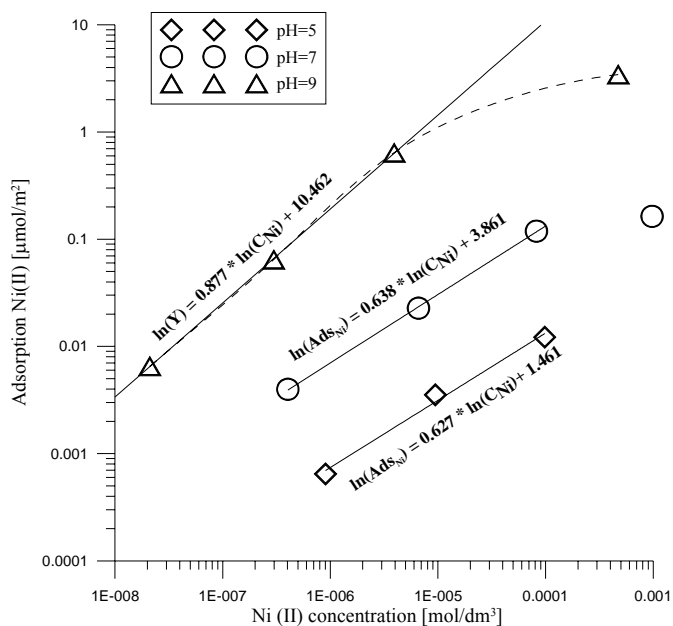


Fig. 4. Adsorption of Ni (II) at Fe₂TiO₅/0.001 NaCl solution interface as a function of equilibrium concentration for selected pH values (5, 7 and 9)

Figure 4 shows the adsorption isotherms of Ni(II) ions for selected pH values (pH=5.7 and 9). For the low concentrations of Ni ions the log-log plot of the isotherm is linear and is characterized by smaller than one slope coefficient. As can be noticed, increase of pH accompanies the increase the slope of the isotherms. Dependence: log number of adsorbed ions nickel vs. log concentration of these ions in solution is called the *Krurbatow plots*. For small concentration of ions it has a linear character, and it is usually described by the Freundlich isotherm.

The values of equilibrium constants of the adsorption reactions, calculated on the basis of the TLM model of edl, using numerical optimization procedure, are collected in Table 3.

Table 3. Values of the adsorption constants for Ni (II) ions for $\text{Fe}_2\text{TiO}_5/0.001 \text{ mol dm}^{-3}$ NaCl solution, Ni (II) ions

Constants	$C_{\text{Ni(II)}} \text{ mol dm}^{-3}$			
	0.001	0.0001	0.00001	0.000001
pK_1	7.80	5.45	7.27	7.70
$\text{p}\beta_2$	9.53	11.65	10.85	11.40

The results of the numerical optimization of Ni ions adsorption at the $\text{Fe}_2\text{TiO}_5/\text{NaCl}$ solution interface as a function of pH show that part of Ni ions is adsorbed by one or two hydroxyl groups.

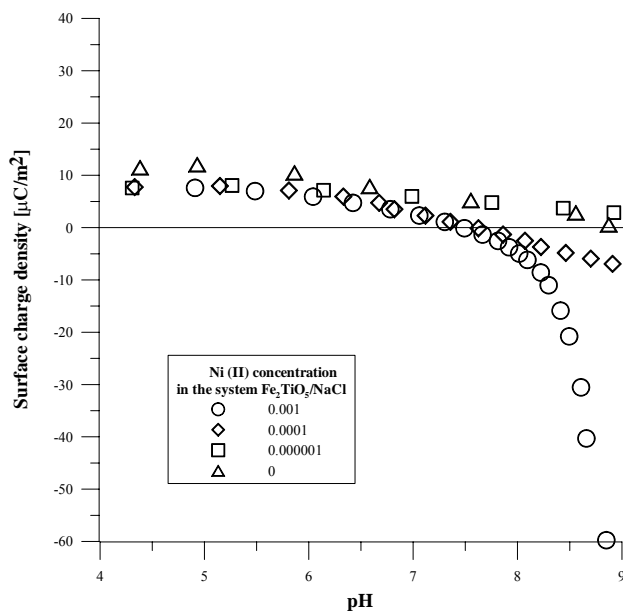


Fig. 5. The surface charge density $\text{Fe}_2\text{TiO}_5/\text{NaCl}$ solution interface as a function of pH

The surface charge density vs. pH in the presence and absence of Ni (II) ions is shown on Fig. 5. As it can be seen, the surfaces charge density plot for the lowest concentrations of Ni (II) is the same as for the system without nickel ions. The data in Fig. 5 shows that the value of pH_{pzc} is shifted towards lower pH values with the increase of initial concentration of Ni(II) ions. For 0.001 mol/dm³ concentration of Ni (II) of pH_{pzc} is about one pH unit lower than in Ni (II) free electrolyte solution. For this concentration the adsorption of Ni(II) produces the sharp increase of concentration of negatively charged groups above pH=8. This decrease of surface charge agrees with “adsorption edge” of nickel (II) ions in this pH range (Fig. 3). Assuming that one Ni²⁺ ion exchanges on Fe₂TiO₅ surface one hydrogen atom in one hydroxyl group, for pH=9 recorded adsorption of Ni²⁺ ions is 3.44 $\mu\text{mol}/\text{m}^2$ and should give surface charge density decrease by about 33.2 $\mu\text{C}/\text{cm}^2$. Adsorption of Ni²⁺ ions on two surface hydroxyl groups will cause the decrease twice higher and change of the surface charge density. Because the concentration of negatively charge groups increases about 60 $\mu\text{C}/\text{cm}^2$ as result of adsorption, that means that Ni ions adsorbs mainly on two hydroxyl groups.

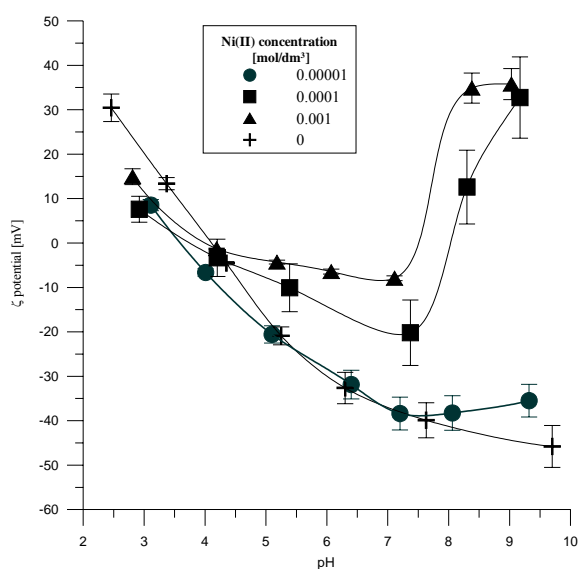


Fig. 6. ζ potential at Fe₂TiO₅ / NaCl solution interface as a function pH

Adsorption of Ni cations leads to the change of the surface hydroxyl group concentration onto the pseudobrookite surface and influences the ζ potential vs pH dependence (Fig. 6). As one can see, the ζ potential decreases with the increase of Ni(II) concentration. For 0.0001M Ni(II) concentration a charge reversal point (CR2) at pH=8.03 is observed. For the highest Ni(II) concentration (0.001M) the CR2 points shifts to pH=7.54.

CONCLUSIONS

1. The electrical double layer at the $\text{Fe}_2\text{TiO}_5/\text{NaCl}$ solution interface is characterized by $\text{pH}_{\text{PZC}}=8.9$ and $\text{pH}_{\text{IEP}}=4.2$. The values of surface ionization constants are $\text{pK}_{\text{a}1}=5.50$ and $\text{pK}_{\text{a}2}=10.57$ and surface complexation constants are $\text{pK}_{\text{Cl}}=3.50$ and $\text{pK}_{\text{Na}}=10.79$.
2. The adsorption of Ni(II) ions as a function of pH on Fe_2TiO_5 runs similarly as on simple metal oxides. The adsorption process can be characterized by the adsorption edge, which can be described by two parameters: $\text{pH}_{50\%}$ and $\Delta\text{pH}_{10-90\%}$. The parameter characterizing the position of adsorption edge ($\text{pH}_{50\%}$) shifts towards higher pH values with the increase of the initial metal concentration.
3. The adsorption isotherms of Ni(II) ions as a function of \log adsorption – \log concentration are linear. For pseudobrookite the metal adsorption can be fitted by a Freundlich isotherm.
4. The specific adsorption of divalent cations causes a shift of the pH_{IEP} towards alkaline pH values and an increase of the ζ potential. The high concentration of adsorbing Ni(II) cations causes the overcharging of the compact part of edl and position of CR2 point.

REFERENCES

- DAVIS J. A., R. O. JAMES, LECKIE J. O., (1978), *Surface Ionization and Complexation at the Oxide/Water Interface. I. Computation of Electrical Double Layer Properties in Simple Electrolytes*, J. Colloid Interface Sci. 63, 480.
- GRACIA F., HOLGADO J.P., YUBERO F., GONZÁLEZ-ELIPE A.R., (2002), *Phase mixing in Fe/TiO₂ thin films prepared by ion beam-induced chemical vapour deposition: optical and structural properties*, Surf. Coat. Technol., 158-159, 552-557.
- GUO W.Q., MALUS S., RYAN D.H., ALTOUNIAN Z., (1999), *Crystal structure and cation distributions in the FeTi₂O₅-Fe₂TiO₅ solid solution series*, J. Phys.: Condens. Matter 11, 6337-6346.
- JAMES R. O., PARKS G.A. A. (1989), *Characterization of Aqueous Colloids by Their Electrical Double-Layer and Intrinsic Surface Chemical Properties* in. Surface and Colloid Science vol.12, p.229, Wiley-Interscience, New York.
- JANUSZ W., (1989), *Adsorption of Sodium and Chloride Ions at the Rutile/Electrolyte Interface - Parameters of the Electric Double Layer*, Materials Chemistry and Physics, 24, 39-50.
- JANUSZ W., (1991), *Determination of Surface Ionization and Complexation Constants from Potentiometric Titration Data*, Polish J. Chem. 65, 799.
- JANUSZ W., (1994), *Electrical Double Layer in the System TiO₂ (Anatase)/Aqueous Solution of NaCl*, Polish J. Chem. 68, 1871.
- KANG M., (2003), *Synthesis of Fe/TiO₂ photocatalyst with nanometer size by solvothermal method and the effect of H₂O addition on structural stability and photodecomposition of methanol*, J. Mol. Catal. A: Chem.197, 173-183.
- KANG M., LEE S.Y., CHUNG C.H., CHO S.M., HAN G.Y., KIM B.W., YOON K.J., (2001), *Characterization of a TiO₂ photocatalyst synthesized by the solvothermal method and its catalytic performance for CHCl₃ decomposition*, J. Photochem. Photobiol., A. 144, 185.
- LEE S. H., KANG M., CHO S.M., HAN G.Y., KIM B.W., YOON K.J., CHUNG C.H., (2001), *Synthesis of TiO₂ photocatalyst thin film by solvothermal method with a small amount of water and its photocatalytic performance*, J. Photochem. Photobiol., A. 146, 121.

- PERKAS N., KOLTYPIN Y., PALCHIK O., GEDANKEN A., CHANDRASEKARAN S., (2001), *Oxidation of cyclohexane with nanostructured amorphous catalysts under mild conditions*. Appl. Catal., A 209, 125-130.
- ROBERTSON A. P., LECKIE J. O., (1997), *Cation binding predictions of surface complexation models: Effects of pH, ionic strength, cation loading, surface complex and model fit*, J. Colloid Interface Sci. 88, 444.
- SCHINDLER P.W., FURST, DICK B., WOLF R., (1976), *Ligand properties of silanol groups*, J. Colloid Interface Sci., 55-469.
- SUROWCE MINERALNE ŚWIATA, (1985), Wydawnictwo Geologiczne – Warszawa.

Skwarek E., Janusz W., *Adsorpcja jonów Ni(II) na granicy faz Fe₂TiO₅/roztwór elektrolitu – struktura podwójnej warstwy elektrycznej*, Physicochemical Problems of Mineral Processing, 40 (2006), 149-159 (w jęz. ang.).

Związki tytanu występujące w postaci dyspersji są stosowane w wielu gałęziach przemysłu. Wśród nich właściwości powierzchniowe zostały dobrze opisane dla ditlenku tytanu, natomiast niektórych związków tytanu są nieznane, należy do nich Fe₂TiO₅ występujący w przyrodzie jako pseudobrukite. Przeprowadzono pomiary adsorpcji jonów niklu, dla jego różnych stężeń początkowych, w funkcji pH dla układu Fe₂TiO₅/roztwór NaCl. Kształt krzywej adsorpcji w funkcji pH ma postać krawędzi adsorpcji. Wzrost stężenia początkowego jonów Ni(II), powoduje przesunięcie krawędzi w kierunku zasadowym skali pH. Wyznaczono charakterystyczne parametry krawędzi adsorpcji tj. pH_{50%} i ΔpH_{10-90%}. W oparciu o zależność adsorpcji od pH stosując model TLM, obliczono również stałe reakcji adsorpcji jonów Ni (II) metodą optymalizacji numerycznej. Zależność gęstości ładunku powierzchniowego od pH w obecności jonów Ni (II), jest w dobrej korelacji z zależnością adsorpcji jonów Ni (II) od pH. Adsorpcja jonów niklu na powierzchni Fe₂TiO₅ prowadzi do wzrostu stężenia grup ujemnie naładowanych.

Władysław JANUSZ, Anna GAŁGAN, Marek RESZKA *

ELECTRICAL DOUBLE LAYER AT THE Cu_2O /AQUEOUS SOLUTION OF ALKALI METAL CHLORIDES INTERFACE

Received March 15, 2006; reviewed; accepted May 15, 2006

Cuprite, copper oxide (I), is commonly found as an oxidation product of copper sulphides in the upper zones of copper deposits. This oxide in a dispersion form has found wide application. The structure of its double layer at copper oxide/electrolyte solution interface was not described yet because of its relatively high solubility and redox reactions. Experiments, presented in the paper, were performed on the copper oxide sample obtained by reduction of alkaline solution of copper(II) acetate by glucose. Surface charge density measurements were taken by potentiometric titrations taking into account solubility of the oxide. Zeta potential versus pH was calculated from electrophoretic measurements of the Cu_2O in 1:1 electrolyte solutions of alkali metal chlorides. Adsorption density of the background electrolyte was measured as a function of pH. To avoid CuCl precipitation all measurements were taken at concentrations lower than 0.001M of Cl^- . Basing on surface charge density versus pH dependence the ionization and complexation reaction constants were calculated.

Key words: electrical double layer, copper oxides/electrolyte interface, pzc, iep

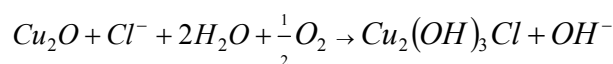
INTRODUCTION

Studies of electrical double layer (edl) at metal oxide/electrolyte solution have been performed for many years. Usually, they concern simple model systems of high thermodynamic stability and very low solubility that do not produce problems during experiments. Complex studies of surface properties of electrical double layer, comprising surface charge, zeta potential and adsorption of background electrolyte ions, were made for a few oxides such as silica, alumina, titania and iron oxides. The same properties for other oxides (mainly transition metals) are hardly known. It is also true for copper oxide. The oxide is used as a catalyst of partial oxidation of some alkenes. Being better catalyst of carbon monoxide oxidation than copper it may be

* Uniwersytet Marii Curie-Skłodowskiej, Wydział Chemii, Pl. M.C. Skłodowskiej 3, 20-031 Lublin

used in car combustion gas controlling devices. Moreover, Cu_2O is applied for protective paints for sea vessels, and pigment for glass and china. Its semi conductive properties may found application in solar cells. Cuprite (copper (I) oxide) is one of the most important copper minerals. Deposits of this mineral contain often Se, I, Pb, and sometimes also In, V, Cd, Sn, and Bi as admixtures (Surowce Mineralne Swiata 1977).

Cuprite is also presented in all patinas - that is copper or bronze covered objects, outdoor exposed for a long time. Usually, patinas formed on the objects exposed to atmosphere are brightly green. Surfaces, screened from atmospheric precipitation are dark. They are formed by copper hydroxychloride ($\text{Cu}_2(\text{OH})_4\text{Cl}$) and atacamite (Nassau et al. 1987, Selwyn et al. 1996). Copper hydroxychloride is also formed in reaction with cuprite (Strandberg 1998):



This reaction may take place on copper, bronze or brass covered surfaces at the sea coast as a result of interaction with salt water. Besides, the high concentration of chloride ions is produced by application of some salts as de-icers.

Depending on redox potential and pH, copper (I) ions in aqueous solutions containing chloride and hydroxide ions may form several insoluble compounds such as copper oxide (I), copper chloride (I) and copper oxide (II) (Pourbaix 1965, 1978). Figure 1. presents equilibrium diagram for three components system Cu-Cl-H₂O.

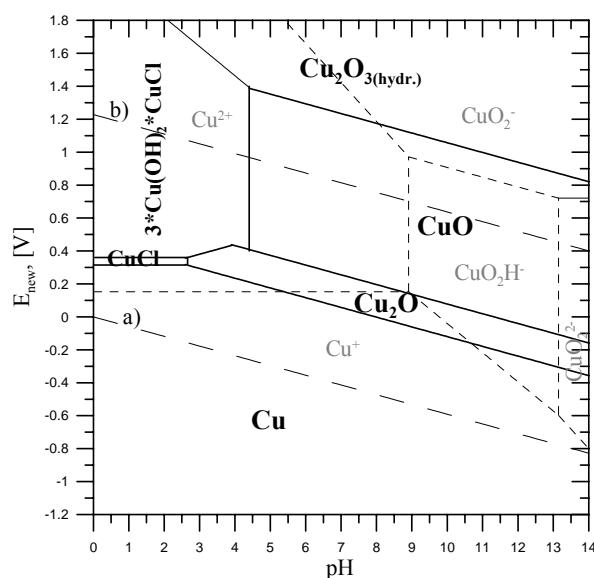
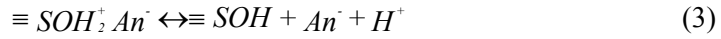
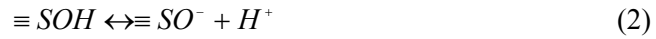


Fig. 1 Potential - pH equilibrium diagram for the system $\text{Cu}+0,001\text{M Cl}^-+\text{H}_2\text{O}$ at 25°C

It may be noticed that CuCl (nancotite) is not stable and in neutral environment hydrolyzes to Cu₂O. In oxidizing, acid environment a stable form is 3Cu(OH)₂·CuCl₂ (paratacamite).

The study of the electrical double layer (edl) structure at the solid/solution interface is useful in the explanation of the flotation reagents that adsorbs by electrostatic interaction as well as the interaction between particles and between particles and air bubbles. The formation of edl is due to presence of charge at mineral surface. The surface charge at the metal oxides /electrolyte solution interface, according to the site binding theory is created by of ionization (reactions 1 and 2) and complexation (reactions 1 and 2):



Above reactions (1-4) are described by thermodynamic constants:

$$K_{a_1} = \frac{[\text{H}^+][\equiv \text{SOH}]}{[\equiv \text{SOH}_2^+]} \cdot \frac{\gamma_H \gamma_0}{\gamma_+} \cdot \exp\left(\frac{-e\Psi_0}{kT}\right) \quad (5)$$

$$K_{a_2} = \frac{[\text{H}^+][\equiv \text{SO}^-]}{[\equiv \text{SOH}]} \cdot \frac{\gamma_H \gamma_-}{\gamma_0} \cdot \exp\left(\frac{-e\Psi_0}{kT}\right) \quad (6)$$

$$K_{An} = \frac{[\text{H}^+][\text{An}^-][\equiv \text{SOH}]}{[\equiv \text{SOH}_2^+ \text{An}^-]} \cdot \frac{\gamma_H \gamma_{An} \gamma_0}{\gamma_{\pm}} \cdot \exp\left(\frac{-e(\Psi_0 - \Psi_{\beta})}{kT}\right) \quad (7)$$

$$K_{Ct} = \frac{[\text{H}^+][\equiv \text{SO}^- \text{Ct}^+]}{[\equiv \text{SOH}][\text{Ct}^+]} \cdot \frac{\gamma_H \gamma_{\mp}}{\gamma_0 \gamma_{Ct}} \cdot \exp\left(\frac{-e(\Psi_0 - \Psi_{\beta})}{kT}\right) \quad (8)$$

where:

K_{a_1} - dissociation constant of surface group $\equiv \text{SOH}_2^+$; K_{a_2} - dissociation constant of surface group $\equiv \text{SO}^-$; K_{An} - anion complexation constant; K_{Ct} - cation complexation constant; [.] - concentrations of specific surface forms or ions in the solution; Ψ_0 - surface potential; Ψ_{β} - potential of Inner Helmholtz Plane (IHP); T- temperature; k-Boltzman constant ($1.38 \cdot 10^{-23} \text{ J} \cdot \text{K}^{-1}$), e- electron charge, γ_H - activity coefficient of H^+ ions, γ_0 - activity coefficient of $\equiv \text{SOH}$ groups, γ_+ - activity coefficient of $\equiv \text{SOH}_2^+$ groups, γ_- - activity coefficient of $\equiv \text{SO}^-$ groups, γ_{An} activity coefficient of

anions, γ_{Ct} - activity coefficient of cations, γ_{\pm} - activity coefficient of $\equiv\text{SOH}_2^+\text{An}^-$ groups, γ_{\mp} - activity coefficient of $\equiv\text{SO}^-\text{Ct}^+$ groups.

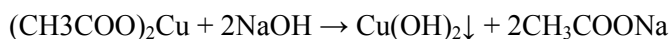
In the paper, some studies on electrical double layer at copper oxide (I)/electrolyte solution are presented. Measurements comprise surface charge, zeta potential and electrolyte ion adsorption. Alkali metal chlorides LiCl, NaCl, KCl, CsCl were used as background electrolytes to study influence of their cations on the electrical double layer properties. Experimental data were used to theoretical calculations of the ionization and complexation constants of reactions of the surface hydroxyl groups. The results of these calculations allowed estimate the shares of respective surface groups in the surface charge at the copper oxide (I)/electrolyte solution interface.

For calculations of ionization and complexation constants of surface hydroxyl groups the numerical optimization (Janusz 1994), Davies et al. 1978, modified Schwarzenbach's (Janusz 1991) and Sprycha (Sprycha and Szczypta 1984) methods were adopted.

EXPERIMENTAL

CU₂O PREPARATION

Copper (II) oxide, Cu₂O, may be precipitated from alkaline solutions of copper ions using reducing compounds such as hydrazine, hydroxylamine or saccharides with aldehyde groups. This method, widely applied for detection and quantitative determination of saccharides, was used in present research. Copper (II) acetate - 0.1M and glucose solutions were used as substrates. The procedure was as follows: 23 ml of NaOH solution was added to 250 ml of the copper (II) acetate solution to obtain blue precipitate of copper (II) hydroxide.



The sediment was ultrasonicated and obtained dispersion was heated to 30°C. Then, 500 ml of the glucose solution (180.1g/l) was added and reactor was heated to 98°C to reduce copper ions from Cu(II) to Cu(I). Obtained Cu₂O was quickly cooled with icy water then ultrasonicated again and left for a few hours to settle. Sedimented Cu₂O was washed with double distilled water till supernatant conductivity was below 2 μS/cm. Simultaneously, the fine particles were removed. Finally, the sediment was dried at 60°C. Applied concentration of the glucose was higher than calculated for side reactions of sugar molecules in alkaline environment as was noticed by Stanek et al. (1963).

METHODS

Potentiometric titration was performed in a Teflon thermostated vessel, in nitrogen atmosphere, free from CO₂, at 25°C. The pH of the solution was measured using PHM240 Research pH-meter (G202C and K401 electrodes). The whole titration

procedure (e.g. the addition of the titrant via Dosimat 6655 (Methrom) and data acquisition from the pHmeter was controlled by a computer. The surface charge density was calculated from the potentiometric titration data for blank (background) electrolyte solution and Cu₂O suspension. Copper (I) oxide is sparingly soluble oxide, so beside the charge formation reactions, the oxide dissolution reactions should also be considered in the hydrogen ion balance. The method of the Block and de Bruyn of surface charge determination, regarding the reaction of dissolution was used for investigated system (Block and de Bruyn 1970).

Adsorption densities of Na⁺, Cs⁺ and Cl⁻ ions were measured using a radiotracer technique with ²²Na, ¹³⁷Cs and ³⁶Cl radioisotopes supplied by Polatom (Świerk, Poland). The radioactive sources of respective isotopes, prepared from electrolyte solution before and after adsorption were measured using LS 5000 counter made by Beckman, USA. Adsorption of Li⁺ and K⁺ ions was calculated from uptake of concentration of these ions that was determined by ASA method.

Electrokinetic potential was measured using Zetasizer 3000, manufactured by Malvern (United Kingdom). Diluted Cu₂O suspensions containing 20 mg of solids in 200 cm³ of electrolyte solution were used. Before measurement the suspension were dispersed using Sonicator XL2020 made by Misonix.

OXIDE CHARACTERISTICS

Crystal structure of synthesized Cu₂O was determined by XRD analysis (X-ray diffraction). Made soon after sedimentation, it revealed minimal oxidation of copper oxide (I) to (II) as may be proved by peak at 2θ=38.65°. The oxidation took place mainly during drying that was manifested by darkening of the oxide surface. To avoid this reaction the oxide sample was washed with acetone immediately before drying. Such modification allowed obtains the oxide without CuO phase. Morphology and size of oxide particles was measured by electron microscopy (see Fig. 2.) One can see uniform (polydispersity equal 0.09), almost spherical particles of the mean diameter 296 nm determined by PCS method (Fig. 3.).

Table 1. Porosity and specific surface characteristic of Cu₂O sample.

Specific surface from BET isotherm [m ² /g]	6.15
Specific surface from Langmuir isotherm [m ² /g]	8.7
Summary pore volume from adsorption 1.7nm<d<300nm BJH method [cm ³ /g]	0.014198
Summary pore volume from desorption 1.7nm<d<300nm BJH method [cm ³ /g]	0.01778
Average pore radius from BET method [nm]	8.6
Average pore radius from adsorption - BJH method [nm]	8.3
Average pore radius from desorption - BJH method [nm]	8.8

Specific surface and porosity of the copper (I) oxide was determined by BET method. Obtained results are listed in Table 1.

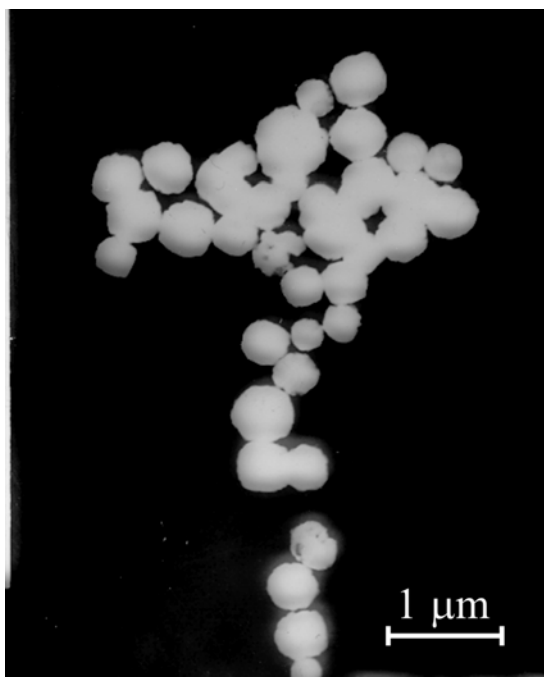


Fig 2. Transmission electron microscopy image of particles of Cu₂O sample

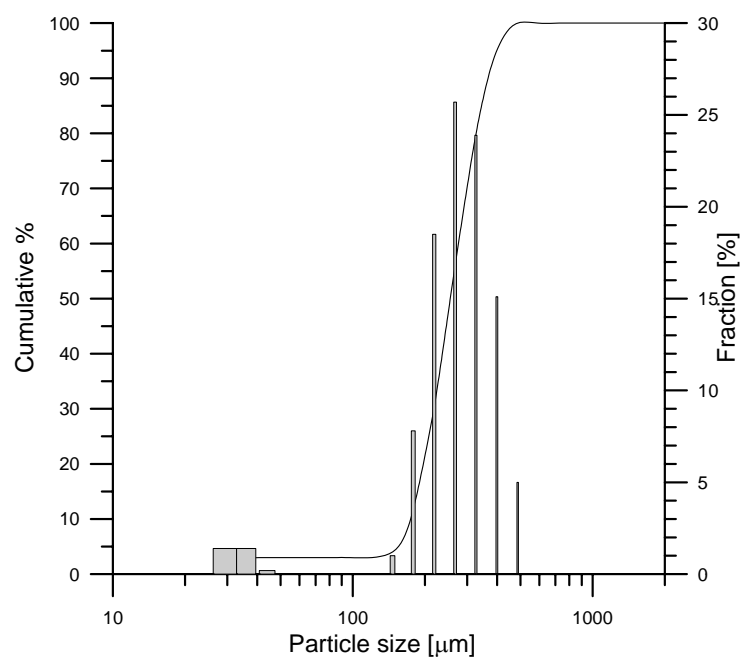


Fig. 3. Particle size distribution of Cu₂O sample

The very small volume of pores proves low porosity of the studied sample. The surface charge density calculations were carried out using BET specific surface area values.

ELECTRICAL DOUBLE LAYER AT Cu₂O/1:1 ELECTROLYTE SOLUTION INTERFACE

Electrical double layer at metal oxides/1:1 electrolyte solutions interface is in the *site binding* model characterized by following physicochemical properties: ionization and complexation constants, compact and diffuse layer capacity, pH_{pzc} and pH_{iep} . To calculate above values the surface density and zeta potential measurements were taken for Cu₂O/1:1 electrolyte solution (LiCl, NaCl, KCl, CsCl) systems. Basing on the relation the surface charge density versus pH the ionization and complexation reaction constants were calculated according to Davies et al. (1978) modified Schwarzenbach (Janusz 1991), and numerical optimization (Janusz 1994) methods. The ionization constants of surface hydroxyl groups were calculated from zeta potential versus pH dependence according to Sprycha (Sprycha and Szczypa 1984). To avoid CuCl_(s) formation (Fig. 1), all measurements were taken in chloride ion solutions of concentration below solubility product of CuCl i.e. $< 0.01 \text{ mole/dm}^3$

SURFACE CHARGE AND pH_{pzc}

Surface charge density as a function of pH and ionic strength of background electrolyte for Cu₂O/LiCl, Cu₂O/NaCl, Cu₂O/KCl, Cu₂O/CsCl systems is presented on Fig. 4a, 4b, 4c and 4d respectively.

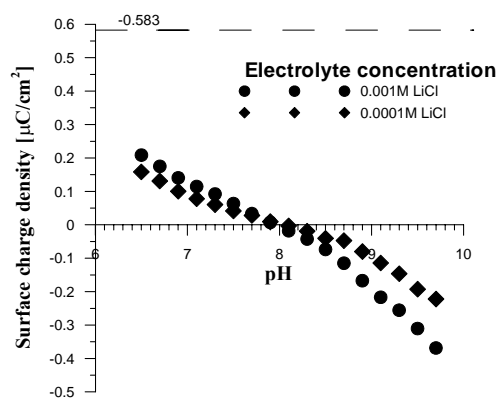


Fig. 4a. Surface charge density as a function of pH for Cu₂O/aqueous solution of LiCl

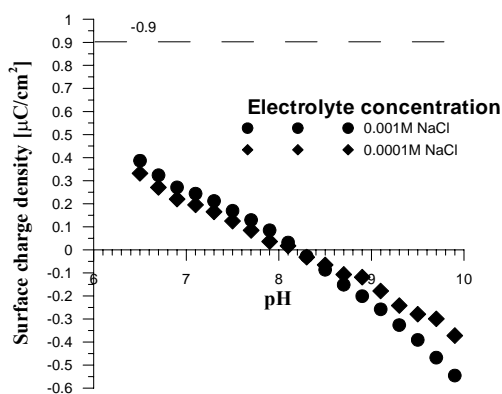


Fig. 4b. Surface charge density as a function of pH for Cu₂O/aqueous solution of NaCl

Relatively small values of surface charge density (below $2 \mu\text{C/m}^2$) in the whole studied pH range (6-10) may be observed for all systems. It is connected with substantial consumption of H⁺ ions in Cu₂O dissolution reactions that take place

beside adsorption of H^+ ions at the surface of the oxide. The original surface charge was negative in the whole pH range and the position of CIP (*common intersection point*) of surface charge density curves versus pH for various ionic strengths is close to pH_{iep} . For system with LiCl (Fig. 4a) CIP is at $pH=8.0$, for NaCl (Fig. 4b) at 8.3, for KCl (Fig. 4c) 8.15 and for CsCl (Fig. 4d) 8.2.

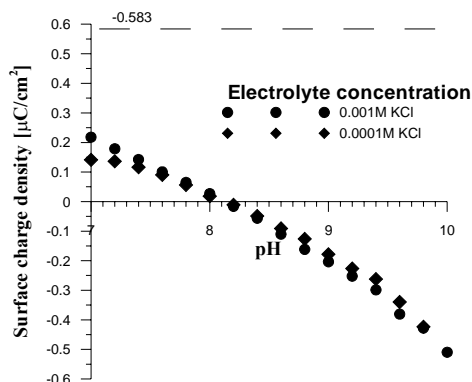


Fig. 4c. Surface charge density as a function of pH for Cu_2O /aqueous solution of KCl

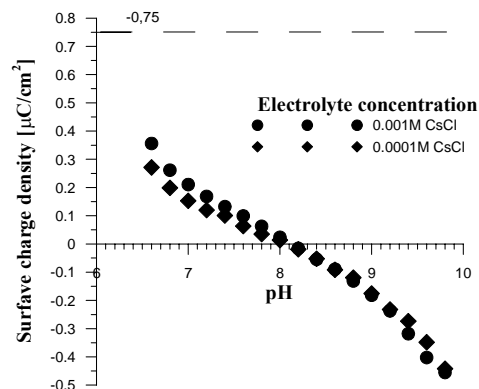


Fig. 4d. Surface charge density as a function of pH for Cu_2O /aqueous solution of CsCl

The position of CIP below pH axis may suggest presence of synthesis residues in the system as alkaline contaminations that are firmly bound to the Cu_2O surface. Considering above surface charge values were corrected for CIP value. The position of x-axis without correction is marked as dashed line. In all cases the influence of the ionic strength of the background electrolyte on the surface charge value is small. It is caused by previously mentioned compulsion - measurements at low concentration of electrolytes which gives low shares of complexation reactions in the surface charge. Basing on the surface charge values as functions of pH and concentration of the background electrolyte the ionization and complexation constants of surface hydroxyl groups on Cu_2O in solutions of alkali metal halides were calculated by Davie's et al. (Davis 1978) and modified by Schwarzenbach (Janusz 1991) methods. Obtained values of the constants are collected in Table 2.

As can be see from optimized data of Table 2 the most stable, positively charged groups are in CsCl solution and the least ones in LiCl. Stability of negatively charged groups, except LiCl, is almost the same for all solutions.

Surprising is the influence of the cation on the ionization and complexation reaction constants that leads to formation of positively charged groups. It may results from neglecting the activity coefficient of the surface groups and disregarding by *site binding* model some reactions at the interface. There is no accepted method of the above coefficient calculation till now. Ionization constants of both, negatively and positively charged groups, calculated by Davies method are comparable to these ones

obtained by Schwarzenbach. Analyzing complexation reaction constants of cations one may state the caesium cations as the most firmly adsorbed whereas lithium ions form the weakest bonding that is in agreement with Hoffmeister lyotropic series.

Table 2. Ionization and complexation reactions constants of surface hydroxyl groups for $\text{Cu}_2\text{O}/\text{Ct}(\text{Ct}=\text{Li, Na, K, Cs})\text{Cl}$ systems

Constant	Method		
	Optimization	Davis et al.	Schwarzenbach
$\text{Cu}_2\text{O}/\text{LiCl}$			
pK_{a1}	4.64	4.20	4.38
pK_{a2}	11.16	12.04	11.82
pK_A	5.50	5.73	7.25
pK_K	10.48	10.39	8.66
$\text{Cu}_2\text{O}/\text{NaCl}$			
pK_{a1}	4.72	4.9	5.2
pK_{a2}	11.69	11.45	11.4
pK_A	7.92	6.29	7.87
pK_K	8.12	10.99	8.71
$\text{Cu}_2\text{O}/\text{KCl}$			
pK_{a1}	4.69	5.19	5.16
pK_{a2}	11.63	11.49	11.49
pK_A	7.72	4.32	-
pK_K	8.33	10.48	8.62
$\text{Cu}_2\text{O}/\text{CsCl}$			
pK_{a1}	4.77	4.29	4.24
pK_{a2}	11.89	11.47	11.30
pK_A	7.23	6.23	7.87
pK_K	8.15	11.42	-

ZETA POTENTIAL AND pH_{iep}

Zeta potential versus pH and ionic strength of background electrolyte dependences for $\text{Cu}_2\text{O}/\text{LiCl}$, $\text{Cu}_2\text{O}/\text{NaCl}$, $\text{Cu}_2\text{O}/\text{KCl}$, $\text{Cu}_2\text{O}/\text{CsCl}$ systems are presented in Figs: 5a, 5b, 5c, and 5d.

In all cases, small differences (0.1-0.2 pH unit) may be observed for respective ionic strengths of background electrolytes. For LiCl solutions (Fig. 5a) pH_{iep} is 7.9 at concentration 0.001M and 8.0 for 0.0001M and 0.00001M. For systems with NaCl (Fig. 5b) 0.001M solution gives $\text{pH}_{\text{iep}}= 8.2$ whereas for 0.0001 and 0.00001M it reaches 8.0. In the case of KCl (Fig. 5c) pH_{iep} is equal to 8.2 for 0.001 and 0.0001M

solutions and 8.1 for concentration 0.00001M. The system with CsCl (Fig. 5d) pH_{iep} = 8.1 for 0.001M, 8.0 for 0.0001M and 8.2 for 0.00001M respectively. Shift of pH_{iep} connected with increase of the background electrolyte concentration is caused by specific adsorption of chloride ions on hydroxyl groups for all systems.

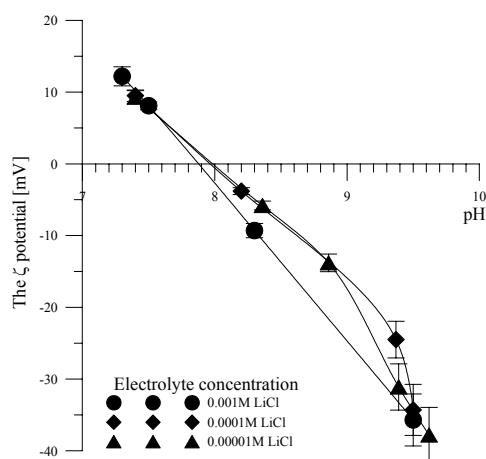


Fig. 5a. The ζ potential as a function of pH for Cu_2O in LiCl solutions

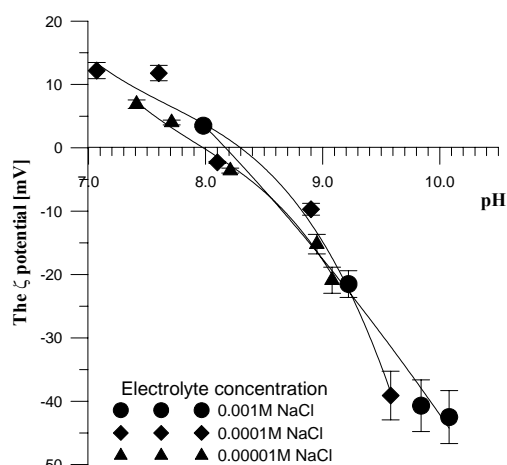


Fig. 5b. The ζ potential as a function of pH for Cu_2O in NaCl solutions

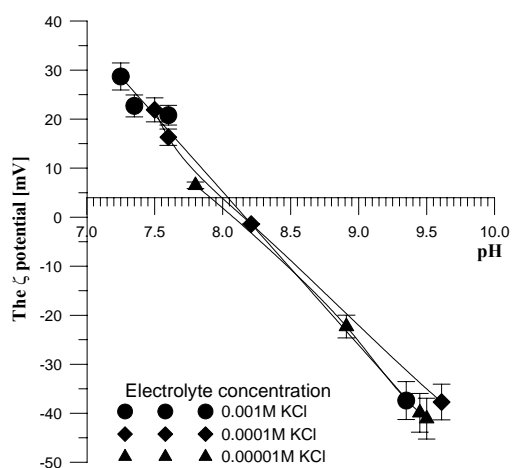


Fig. 5c. The ζ potential as a function of pH for Cu_2O in KCl solutions

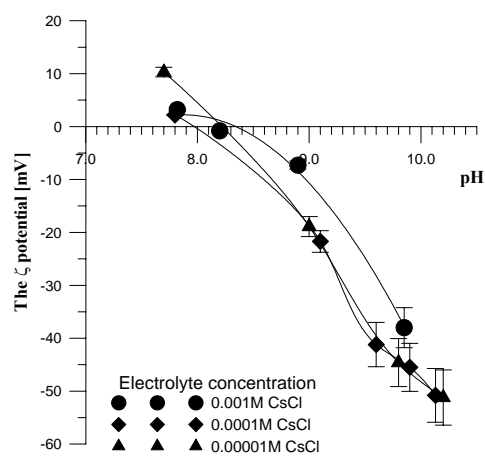


Fig. 5d. The ζ potential as a function of pH for Cu_2O in CsCl solutions

Increase of the concentration of the groups complexed by chlorides on copper oxide surface lowers concentration of ionized groups with positive charge that usually is manifested by small shift of pH_{iep} towards lower pH values. Because the

measurements were taken at low concentration of background electrolyte (to avoid CuCl formation) the lowering ζ potential value, accompanying the increase of the electrolyte concentration was not observed.

From potential zeta versus pH and background electrolyte concentration data the values of ionization constants of surface hydroxyl groups, on the surface of Cu_2O in alkali metal halides solutions were calculated following method proposed by Sprycha (Sprycha and Szczypa 1984). Obtained results are presented in Table 3.

Table. 3. Ionization constants of surface hydroxyl groups calculated according to Sprycha (Sprycha and Szczypa 1984)

Constant	Background electrolyte			
	LiCl	NaCl	KCl	CsCl
pK_{a1}	2.8	3.3	4.3	3.4
pK_{a2}	12.8	12.8	12.4	12.5

One may notice similar values for all constants connected with negatively charged group formation. Some unexpected differences, observed for the constants of positively charged groups may be connected with dissolution of the oxide and produced inaccuracy of pH measurements below pH_{iep} . Ionization constants, calculated from surface charge may differ from the ones obtained by Sprycha's method even by unit of pH.

Such big difference may arise from an error in determination of ionization and complexation constants from the surface charge and small dependence of σ_0 versus background electrolyte concentration. This weak dependence makes problems in determination of ionization and complexation constants by extrapolation acidity (complexation) quotients to electrolyte concentration.

BACKGROUND ELECTROLYTE ION ADSORPTION

Adsorption density of background electrolyte ions Li^+ , Na^+ , Cs^+ , and Cl^- is presented on Figures 6a, 6b, 6c, respectively. The adsorption of studied cations increases with pH rise that is in agreement with reaction of site binding model (Davis et al., 1978). Noticeable drop of adsorption at pH_{pzc} ($\text{pH}=8.0$) suggests that up to this value ionic exchange takes place. Li^+ adsorption (Fig. 6a) is nearly five-fold higher than Na^+ and Cs^+ ions adsorption. These last cations, as may be seen from Fig. 6b reveal the same adsorption (within error). Adsorption of Cl^- (Fig. 6c) decreases with growth of pH that is in agreement with reaction of site binding model (Davis et al. 1978). However, above pH_{iep} the adsorption of Cl^- ions do not decrease asymptotically to zero that proves specific adsorption of the anion as mentioned earlier.

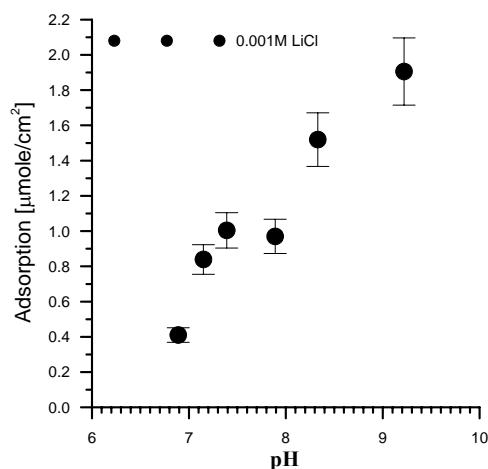


Fig. 6a. Li^+ ion adsorption as a function of pH at the $\text{Cu}_2\text{O}/0.001\text{M LiCl}$ interface

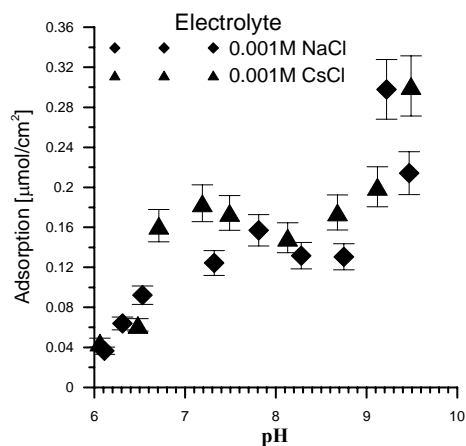


Fig. 6b. Na^+ (Cs^+) ion adsorption as a function of pH at the $\text{Cu}_2\text{O}/0.001\text{M NaCl}$ (CsCl) interface

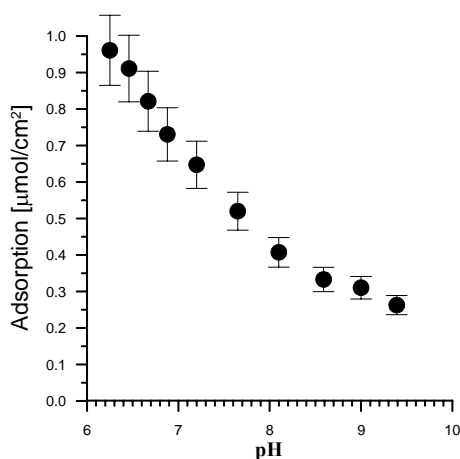


Fig. 6c. Cl^- ion adsorption as a function of pH at the $\text{Cu}_2\text{O}/0.001\text{M NaCl}$ interface

CONCLUSIONS

The study of electrical double layer structure at copper(I) oxide/aqueous solution interface of alkaline metal chlorides presented in this paper may be summarized as follows:

1. Density of the surface charge for Cu_2O in alkali metal chloride solutions changes by about $2 \mu\text{C}/\text{m}^2$ in pH 6-10 range due to dissolution of the oxide.
2. CIP was found in pH 8-8.2 range, depending on the system and agree with pH_{iep} for the same electrolyte. Position of CPI below x-axis suggests alkaline type

contamination, firmly bound to the surface that might remain after synthesis of the oxide.

3. According to calculated constants of electrolyte ions and adsorption measurements the studied cations may be arranged as follows: $\text{Li}^+ < \text{Na}^+ \approx \text{Cs}^+$ that is in agreement with Hofmeister lyotropic order.
4. In all studied systems pH_{iep} was found in pH 7.9 - 8.2 range.
5. Increase of adsorption of: Li^+ , Na^+ and Cs^+ cations below pH_{pzc} proves ion exchange in this range.
6. Adsorption density of Cl^- anions in pH_{pzc} is much higher than the adsorption density for studied cations that shifts insignificantly pH_{iep} with background electrolyte concentration change.

REFERENCES

- BLOK L., DE BRUYN P. L., (1970), *The ionic double layer at the ZnO/solution interface*, J. Colloid Interface Sci., 32, 527.
- DAVIS J. A., JAMES R.O., LECKIE J.O., (1978), *Surface Ionization and Complexation at the Oxide/Water Interface. I. Computation of Electrical Double Layer Properties in Simple Electrolytes*. J. Colloid Interface Sci., 63, 480.
- JANUSZ, W., *Electrical Double Layer in the System $\text{TiO}_2(\text{Anatase})/\text{Aqueous Solution of NaCl}$* , (1994), Polish J. Chem., 68, 1871.
- NASSAU K., GALLAGHER P.K., MILLER A.E., GRAEDEL T.E., (1987), *The characterization of patina components by X-ray diffraction and evolved gas analysis*, Corrosion Sci. 27, 669.
- POURBAIX H., (1965), *Atlas of Electrochemical Equilibria in Aqueous Solutions*, CEBELOR, Brussels, pp.385-392.
- POURBAIX M.; *Wykłady z korozji elektrochemicznej*; (1978), PWN; Warszawa.
- SELWYN L., BINNIE N.E., POITRAS J., LAVER M.E., DOWNHAM D.A, (1996), *Studies in Conservation* 1, pp. 2050-228.
- SPRYCHA R., SZCZYPA J., (1984), *Estimation of surface ionization constants from electrokinetic data*, J. Colloid Interface Sci., 102, 288.
- STANEK J., CERNY M., KOCOUREK J., PACAK J., (1963), *The Monosaccharides*, pp.180-181, Academic Press, New York.
- STRANDBERG H., *Reactions of copper patina compounds--II. Influence of sodium chloride in the presence of some air pollutants*, (1998), Atmospheric Environment, vol. 32, No.20, pp.3521-3526.
- SUROWCE MINERALNE ŚWIATA, *Miedź-Cu*, (1977), Wydawnictwa Geologiczne Warszawa

Janusz W., Galgan A., Reszka M., *Podwójna warstwa elektryczna na granicy faz tlenek miedzi(I)/wodny roztwór chlorków metali alkalicznych*, Physicochemical Problems of Mineral Processing, 40 (2006), 161-174 (w jęz. ang.).

Kupryt czyli tlenek miedzi (I) jest jednym z głównych minerałów miedzi. Występuje on również w tzw. strefie utleniania złóż zasobnych w siarczkowe minerały miedzi. Tlenek ten stosowany jest jako katalizator częściowego utlenienia niektórych alkenów, a także jest on lepszym od miedzi katalizatorem utleniania CO w związku z czym może być użyty do kontroli spalin samochodowych. Ponadto Cu_2O jest składnikiem farb do pokrywania dna statków, stosowany jest barwienia szkła i porcelany. Jako półprzewodnik, Cu_2O , jest także od kilkadziesiąt lat przedmiotem badań mających na celu wykorzystanie go w ogniwach słonecznych.

Badania przedstawione w pracy prowadzono na próbce otrzymanej przez redukcję glukoza zasadowego roztworu octanu miedzi (II). Przeprowadzono pomiary gęstości ładunku powierzchniowego metodą miareczkowania potencjometrycznego z uwzględnieniem rozpuszczalności tlenku. Metodą elektroforetyczną wyznaczono zależność potencjału zeta na granicy faz Cu_2O / roztwór elektrolitu 1:1 chlorków metali alkalicznych. Wyznaczono zależność adsorpcji jonów elektrolitu nośnego w funkcji pH. W celu uniknięcia wytrącania się CuCl pomiary prowadzono w roztworach o stężeniu nie wyższym niż 0,001M. W oparciu o zależność gęstości ładunku powierzchniowego od pH obliczono wartości stałych równowag reakcji jonizacji i kompleksowania.

Stanisław CHIBOWSKI, Małgorzata PASZKIEWICZ*

POLYACRYLIC ACID (PAA) ADSORPTION ON ALUMINA (Al₂O₃) SURFACE. INFLUENCE OF SODIUM DODECYL SULFIDE (SDS) ON ADSORPTION IN PAA-SDS-Al₂O₃ SYSTEM

Received March 15, 2006; reviewed; accepted May 15, 2006

Mutual interactions of ionic polymer with ionic surfactant on alumina surface in system PAA/SDS/Al₂O₃/NaCl solution system were studied. The research was preceded by studies of the polymer and surfactant in aqueous solution. Obtained data were used for explanation of adsorption equilibrium in the alumina - polymer solution system in SDS presence. Mechanism of polyacrylic acid - surfactant interaction on Al₂O₃ was explained basing on adsorption and surface tension changes measurements of pure and mixed PAA and SDS solutions in studied system. An influence of the polymer molecular weight and surfactant concentration on adsorption equilibrium at metal oxide-polymer-surfactant interface was considered. An essential role of carboxyl groups of the polymer chain was proved in these systems.

Key words: adsorption, polyacrylic acid, alumina, SDS

INTRODUCTION

Systems containing polymer and surfactant often reveal specific adsorption properties and demand research. Their properties find increasing application in many important industrial processes where stabilization or flocculation of high dispersed system takes place. Precise determination of important parameters for these processes demands many studies of these systems such as adsorption and its influence on electrokinetic properties of solid-solution interface, conformation changes of polymer under surfactant influence and mutual polymer-surfactant interactions.

It is well known from literature that ionic and nonionic surfactants behave differently in solution than in mixture with a polymer (Somasundaran et al. 1985,

* Department of Radiochemistry and Colloid Chemistry Faculty of Chemistry,
Maria Curie-Skłodowska University, M. Curie Skłodowska Sq. 3, 20-031 Lublin, Poland.

1997; Fleer et al. 1993, 1993A; Sastry et al., 1995). Knowledge of interaction responsible for adsorption mechanism in polymer-surfactant system is important from practical and theoretical point of view and needs intense research. In this paper authors aimed to investigate influence of anionic surfactant sodium dodecylsulphate (SDS) on adsorptive properties of anionic polymer, polyacrylic acid (PAA) on alumina surface.

MATERIALS AND METHODS

MATERIALS AND REAGENTS

As a surface-active compound, the sodium dodecyl sulphate $C_{12}H_{25}SO_4Na$ (SDS) was used and polyacrylic acid (PAA) (molecular weights: 2000 and 240,000) produced by Aldrich was used as a polyelectrolyte. NaCl was used as a background electrolyte.

Alumina, Al_2O_3 , produced by Merck was applied as an adsorbate. The specific surface area of aluminium oxide, calculated according to the Brunauer–Emmett–Teller method was $161\text{ m}^2\text{ g}^{-1}$. Before measurements, Al_2O_3 was washed with double distilled water until the conductivity of the supernatant was smaller than $2\ \mu\text{S cm}^{-1}$. The average diameter of the Al_2O_3 particles, estimated by scanning electron microscopy was 450 nm. All particles were spherical.

ADSORPTION STUDY

Adsorption of PAA on Al_2O_3 surface performed from the pure solutions of the polymers and mixed PAA-SDS solutions on the Al_2O_3 surface was carried out using the static method (Cibowski and Krupa, 1999, 2000) as follows. Al_2O_3 was added into the Erlenmeyer flask, which contained 10 cm^3 of the analyzed solution (specified pH, concentration of the polymer and electrolyte). The obtained suspensions were shaken for 24 h. Then alumina was centrifuged and 5 cm^3 of the supernatant were taken for the further analysis. The adsorption was calculated from the difference between the PAA concentration before and after the adsorption (c_{eq} , wt. ppm), using the reaction between polyacrylic acid and hyamine proposed by Crummett and Hummel (Crummett, Hummel 1963). The opacity which increases after hyamine addition to the solution was measured colorimetrically using a spectrophotometer (Specord M42, Carl Zeiss) with a special computer program M500. The used wavelength was 500 nm.

VISCOSITY MEASUREMENTS

The thickness of PAA adsorption layer (δ) was also measured by the viscosity method (Pandou and Siffert, 1987; Wang and Audebert, 1988), using a rotation rheometer. For this purpose, the Al_2O_3 suspensions of various volumetric fractions (Φ_0) were prepared. The volumetric fraction of the solid was determined from the formula:

$$\phi_0 = \frac{m}{dv}$$

where m is the solid mass, d the solid specific gravity and v is the reference solution volume.

Next, the suspensions were shaken for 24 h and their viscosity (η), as well as that of the reference solutions (η_0) were measured using a rotation rheometer. In this way, the dependence of η/η_0 on Φ_0 (volume fraction in the absence of the polymer) was plotted (calibration curve). In the same way, the viscosity of the suspensions with the adsorbed polymer (η_p) as well as that of the polymer solution (η_{p0}) was measured and the ratio η_p / η_{p0} was determined. Next, the volumetric fraction of the solid in the presence of the polymer (Φ_p) was estimated from the calibration curve. When the radius of the Al₂O₃ particles is known, the thickness of the adsorption layer can be calculated from the following formula:

$$\delta = r \left[\left(\frac{\phi_p}{\phi_0} \right)^{1/3} - 1 \right]$$

where r is the radius of a metal oxide particle.

The measurements of the thickness of the polymer adsorption layer were performed at volume fraction Al₂O₃ (ϕ_0) equal 0.0126.

SURFACE TENSION MEASURED

Mutual polymer-surfactant interaction was determined from measurements of the of the surface tension changes of water solutions containing constant concentration of the polymer (1×10^{-3} g/ml) and various concentrations of the surfactant. The surface tension of PAA-SDS system was measured with thermostated stalagmometer applied "free downfall of a drop" method [Lando Oakley 1967, Pierson Witaker 1976]. All these measurements were taken at 25°C.

RESULTS AND DISCUSSION

Due to mutual interaction of polymer and surfactant a complex is formed often of much different properties than those of pure substrates. Their interactions may be examined by measurements of surface tension, viscosity, adsorption and electrokinetic changes of solid-solution interface (Somasundaran et al. 1985, 1991, 1997).

ADSORPTION STUDIES OF PAA/Al₂O₃/NaCl SYSTEM

To explain an influence of SDS on sorptive properties of PAA on surface of Al₂O₃ one should examine adsorption equilibrium for PAA in the system. Adsorption of such compounds is measured from drop of their concentration from the solution contacted with a solid. Linear, elastic polymer macromolecules may attain various conformations at solid liquid interface therefore there may be various number of segments bound to the surface (Somasundaran et al., 1997).

Usually macromolecules tend to adopt conformation that enables maximal contact of polymer chain with the solid surface. For this reason bonding of the one segment increases probability of the other ones adsorption that results in multi bond formation. Fig. 1. presents adsorption isotherms of polyacrylic acid on alumina for two molecular weights of PAA.

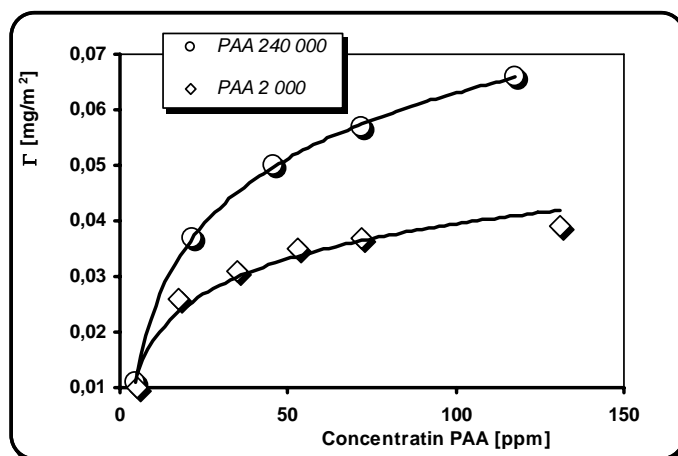


Fig. 1: Isotherms of PAA 2000 and PAA 240 000 adsorption onto Al₂O₃ at pH 6

One may notice marked influence of the polymer molecular weight on the size of its adsorption. The amount of adsorbed polymer is higher for its higher molecular weight. As mentioned previously polymer macromolecule is bond to the surface of the solid through some number of segments. This number may be the same for various molecular weights of the polymer but total amount of adsorbed polymer is higher for the one of bigger molecule. It may be explained by more loops and tails in interface conformation of the PAA of higher molecular weight. The amount of adsorbed polymer also increases with its concentration. Both effects lead to more compact layer of the polymer with many loops and tails structures of the polymer at the surface and thicker polymer layer.

Obtained adsorption data agree with calculated thickness of the adsorption layer (δ) formed on the surface of the oxide (Tab. 1.).

Table 1. Thickness of the adsorption layer of the polyacrylic acid on the surface of Al_2O_3 from the pure polymer and mixed PAA-SDS solutions

M_w PAA	PAA C_{PAA} [ppm]	PAA δ [nm]	PAA Γ [mg/m^2]	PAA-SDS δ [nm]	PAA-SDS Γ [mg/m^2]
2000	50	2.34	0.032	1.98	0.025
	100	2.62	0.04	2.14	0.028
240 000	50	8.71	0.05	2.01	0.026
	100	9.47	0.062	2.44	0.035

The extent of PAA adsorption on metal oxides depends distinctly on pH of the solution. This dependence is well illustrated by Fig.2.

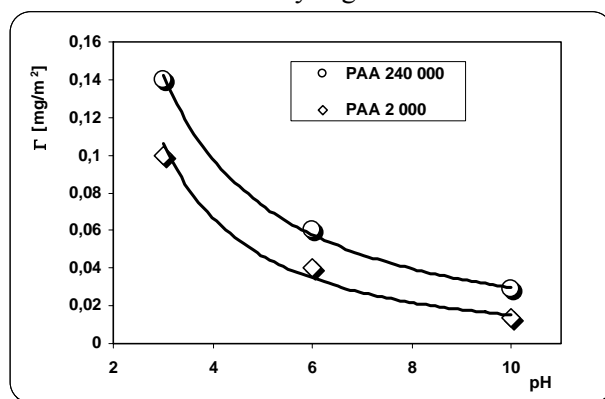


Fig. 2. Adsorption of PAA of various molecular weights as a function of pH of their solution

Generally, amount of adsorbed polymer as a function of pH of the solution depends on both: type of surface group of adsorbent and dissociation degree of carboxyl group of the PAA macromolecule. Total surface charge of the oxide depends on the number of surface forms i.e. $-MOH_2^+$; $-MOH$ and $-MO^-$. Along with pH change the dissociation degree of carboxyl groups is changing so is number and type of Al_2O_3 surface groups. In Table 2, the dissociation degree of PAA and calculated concentrations of various surface groups of alumina are listed for various pH of the system. Observed decrease of the amount of adsorbed polyacrylic acid produced by increase of pH of the solution is due to increase of the ionization degree of carboxylic groups in PAA chain.

PAA macromolecules, with $pK_a = 4.5$ (Gebhardt and Furstenau 1983), in acidic environment up to $pH=4.5$ have dominating, non-dissociated $-COOH$ groups. When pH increases these groups dissociate to $-COO^-$ ones that increases repulsion with also increasing negative charge on the surface of the solid. As a consequence the adsorption of PAA is decreasing. Noticed adsorption of PAA for pH higher than pH_{pzc} , (pH_{pzc} for $Al_2O_3 = 7.9$) proves specific interaction between polymer and solid in this

range because due to electrostatic repulsion physical bonding is impossible. This assumption may be supported by analysis of the concentration of various surface groups of alumina listed in table 2.

Table 2. [COOH]/[COO⁻] group concentration ratio in polyacrylic acid macromolecule and concentration of various surface groups of Al₂O₃ in [$\mu\text{C}/\text{cm}^2$], ($C_{\text{NaCl}}=1 \times 10^{-3} \text{ mole} \times \text{dm}^{-3}$) for various pH of the solution

pH	[COOH]/[COO ⁻] ^a	Concentration of groups ^b		
		- AlOH ₂ ⁺	- AlO ⁻	- AlOH
3	31	0.6	-1.1	105
4.5	1	0.4-	-1.9	112
6	0.031	0.28	-2.8	121.7
9	0.000031	0.1	-7.3	120.6

^a Values obtained from the classical relation $\text{pH} - \text{pK}_a = \log(\alpha/(1-\alpha))$ [Pettersen et al. 2000].

^b The data presented were obtained by numerical optimization of the electrical double layer model (Dawia and James, 1978).

Below pH_{pzc} , beside hydrogen bridge type interaction, electrostatic attraction between $-\text{AlOH}_2^+$ and dissociated $-\text{COO}^-$ groups may play important role. As a consequence the increase of PAA adsorption below pH_{pzc} is observed.

Because adsorption of PAA macromolecules takes place at pH range 3-10 and concentration of surface group $-\text{AlOH}$ is much higher than other ones and pH independent one may assume their dominant role in adsorption process on Al₂O₃ surface through hydrogen bridge. Such bonding between hydrolyzed surface of Al₂O₃ and polyacrylic acid macromolecule may exist because carboxyl group of the polymer may act as donors or acceptors of protons. A diagram below presents reaction between surface groups of alumina and non dissociated and dissociated carboxyl group of PAA macromolecule.

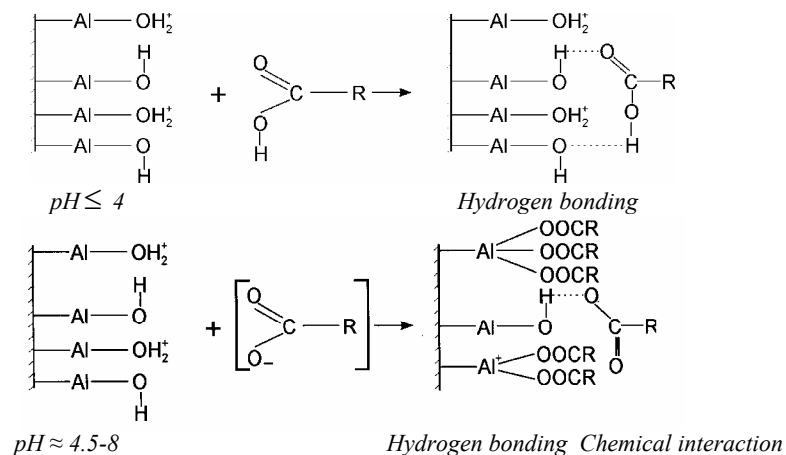


Fig. 3. PAA macromolecule - Al₂O₃ surface interaction (Santhiya et al., 19990)

Basing on literature (Somasundaran et al., 1985, 1997 1991, 1997A, Santhiya et al., 1999) and own studies concerning PAA adsorption on metal oxide surface we may propose following mechanism of the polymer adsorption on the alumina:

1. Below pH_{pzc} of Al_2O_3 (pK_a PAA = 4.5) for adsorption process of the polymer with carboxyl groups ($-COOH$, $-COO^-$) of PAA on positively charged alumina surface the hydrogen bonds and electrostatic interactions are responsible;
2. In pH 4.5 - 8 range (pH_{pzc} Al_2O_3 = 7.9) beside hydrogen bond a chemical interactions between ionized carboxyl groups and Al ions present on surface of the oxide (Fig. 3). Electrostatic interactions also take place in this pH range.
3. Above pH_{pzc} , for adsorption process of PAA (with almost completely ionized carboxyl groups) on alumina surface (covered predominantly with negatively charged AlO^- groups) only specific interactions are responsible (hydrogen bridge or chemical reaction between $AlOH$ and $-COO^-$ groups). In this pH range there is no electrostatic interactions and due to there is lowest adsorption of PAA.

ADSORPTION STUDIES OF PAA/SDS/ Al_2O_3 /NaCl SYSTEM

Described above adsorptive behavior of polyacrylic acid on alumina surface is helpful in understanding processes at solid/solution interface in a mixed polymer-surfactant system.

A characteristic feature of surfactants is their ability to decrease surface tension of water. This behavior may be modified by for example polymer addition. Variations of concentration of both polymer and surfactant may vary surface tension of such solution. Final changes depend mainly on mutual polymer-surfactant interactions i.e. type of substances and formation of complexes. Hydrophobic interactions, hydrogen bridge bonds and electrostatic interactions are responsible for behavior of such systems (Somasundaran et al., 1997, 1997; A Santhiya et al., 1999).

In the paper, surface tension measurements of PAA, SDS and their mixtures in aqueous solutions were undertaken to detect polymer-surfactant interaction.

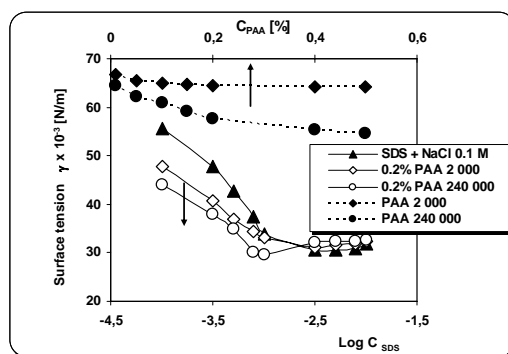


Fig. 4. Surface tension of PAA of various molecular weights versus polymer concentration [%] (dashed line) and surface tension of mixed PAA-SDS solutions versus SDS concentration (solid line) in 0.1 M NaCl solution

Figure 4 presents changes of the surface tension of solutions as a function of polymer concentration (dashed lines) and for mixed PAA-SDS solutions as a function of surfactant concentration (permanent line) at constant polymer concentration (0.2%). As may be seen, polymer almost does not change surface tension of its solutions. In mixed solutions, due to mutual interaction between molecules the polymer-surfactant complexes are formed (solid line in Fig. 4).

In mixed PAA-SDS system one may notice influence of the polymer molecular weight on lowering of the surface tension. It probably is caused by hydrophobic interactions between PAA and SDS chains, because electrostatic repulsion of negatively charged chains of both molecules makes complex formation impossible (Lang 1971).

Considered above adsorption measurements for mixed PAA/SDS solutions on alumina surface were used to explain described behavior of the system. As can be seen in Figs 5 and 6 the presence of anionic surfactant noticeably lowers the amount of adsorbed polymer on Al_2O_3 surface.

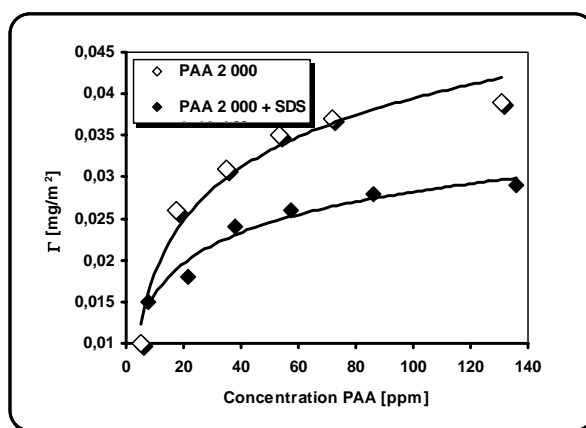


Fig. 5. Adsorption of PAA and PAA-SDS complexes ($M_w=2\ 000$) on Al_2O_3 surface for PAA/ Al_2O_3 /NaCl and mixed PAA/SDS/ Al_2O_3 /NaCl systems, $C_{\text{NaCl}}=1 \times 10^{-3}\text{M}$; $C_{\text{SDS}}=1 \times 10^{-4}\text{M}$

A dramatic lowering PAA adsorption in the presence of SDS may be attributed to competitive adsorption of PAA-SDS complexes and free SDS that blocks adsorption sites on the alumina surface. Additionally, spacial conformation of PAA-SDS complexes differs much from PAA macromolecules in solution. It results in greater number of interaction points of such complex molecule with functional groups of Al_2O_3 .

Adsorption of PAA from its solution leads to structure of polymer chain with numerous loops spread to the bulk of solution. Such conclusion may be proved by adsorption layer thickness measurements on Al_2O_3 for pure PAA and mixed PAA-SDS solutions (Tab. 1).

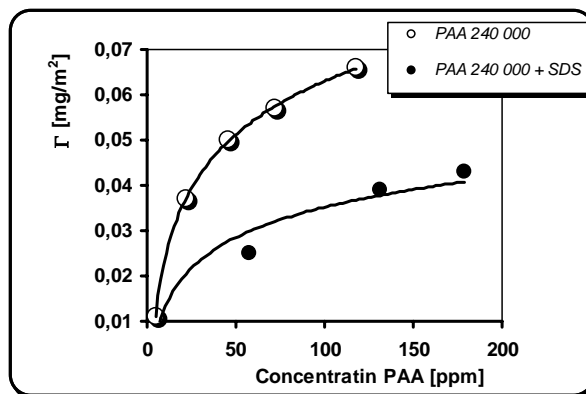


Fig. 6. Adsorption of PAA and PAA-SDS complexes ($M_w = 240\,000$) on Al_2O_3 surface for PAA/ Al_2O_3 /NaCl and mixed PAA/SDS/ Al_2O_3 /NaCl systems, $C_{NaCl} = 1 \times 10^{-3} M$; $C_{SDS} = 1 \times 10^{-4} M$

As a consequence, flat compact adsorption layer of PAA-SDS complexes decreases adsorption of PAA.

It leads to the mentioned earlier decrease of the adsorption layer thickness. Especially pronounced is this effect for PAA of higher molecular weight.

REFERENCES

- CHIBOWSKI S., KRUPA M., (1999), *Adsorpt. Sci. Technol.*, Volume: **17**, p. 813
 CHIBOWSKI S., KRUPA M., (2000), *J. Dispersion Sci. Technol.*, Volume: **21**, p. 761
 CRUMMETT W.B., HUMMEL R.A., (1963), *J. Am. Water Works Assoc.*, Volume: **55**, p. 209
 DAWIS J. A., JAMES R. O., (1978), *J. Colloid Interface Sci.* **63**, 480.
 FLEER G.J., COHEN STUART M.A., SCHEUTJENS J.M.H.M., COSGROVE T., VINCENT B., *Polymers at Interfaces*, (1993), Chapman & Hall, London.
 FLEER G.J., SCHEUTJENS J.M.H.M., DOBIAS B., (Ed.) *Coagulation and Flocculation; Theory and Applications*, (1993A), Marcel Dekker, New York. (Chapter 5)
 GEBHARDT J. E., FURSTENAU D. W., (1983), *Colloids Surf.*, **7**, 221.
 LANDO J. L., OAKLEY H. T., (1967) *J. Coll. Inter. Sci.* **25**, 526.
 LANGE H., (1971), *Kolloid-Z. Z-Polym.*, **243**, 101.
 PANDOU A.M., SIFFERT B., *Colloid Surf.*, Volume: **24**, (1987), p. 159
 PETERSON A., MARINO G., PURSIHEIMO A., ROSENHOLMO J.B., (2000), *J. Colloid Interface Sci.* **228**, 73.
 PIERSON E. W., WITAKER S., (1976), *J. Coll. Inter. Sci.* **54**, 203.
 SANTHIYA D., SUBRAMANIAN S., NATARAJAN K.A., MALGHAN S.G., (1999), *J. Colloid Interface Sci.* **216**, 143-153.
 SASTRY N.V., SEQUARIS J.M., SCHWUGER M.J., (1995), *Journal of Colloid and Interface Science* **171**, 224-233
 SOMASUNDARAN P., CLEVERDON J., (1985), *Colloids Surfaces*, **13**, 73.
 SOMASUNDARAN P., HUANG L., (1997), *J. Chem.*, **71**, 568-582.
 SOMASUNDARAN P., KRISHNAKUMAR S., (1997A), *Colloids Surfaces*, **123-124**, 491.
 Somasundaran P., SNELL E. D. AND Q. XU, (1991), *J. Coll. Inter. Sci.* **144**, 165-173
 WANG T.K. AUDEBERT R., (1988), *J. Colloid Interface Sci.* **121**, 32.

Chibowski S., Paszkiewicz M., *Adsorpcja kwasu poliakrylowego na powierzchni tlenku glinu Al_2O_3 . Wpływ dodecylowego siarczanu sodu (SDS) na adsorpcję w układzie PAA-SDS- Al_2O_3* , Physicochemical Problems of Mineral Processing, 40 (2006), 175-184 (w jęz. ang.).

Polimer i surfaktant oddziałując ze sobą tworzą kompleks, którego własności często różnią się znacznie od własności czystych składników. Te wzajemne oddziaływania można badać mierząc takie wielkości jak np.: napięcie powierzchniowe, lepkość, adsorpcję czy też zmiany elektrokinetyczne granicy faz ciało stałe-roztwór. W pracy podjęto próbę opisu mechanizmu adsorpcji kwasu poliakrylowego (PAA) na powierzchni tlenek glinu w obecności i pod nieobecność dodecylowego siarczanu sodowego (SDS). Opierając się na badaniach własnych oraz doniesieniach literaturowych dotyczących adsorpcji PAA na powierzchni tlenków metali zaproponowano mechanizm adsorpcji polimeru na powierzchni Al_2O_3 . Przeprowadzone pomiary adsorpcji w układzie mieszanym PAA-SDS na powierzchni Al_2O_3 wykazały, że w obecności anionowego surfaktantu następuje wyraźny spadek ilości zaadsorbowanego polimeru. Powodu wyraźnego obniżenia się adsorpcji PAA w obecności SDS należy szukać zarówno w konkurencyjnej adsorpcji niezwiązanego w formę kompleksów dodecylowego siarczanu sodu jak również utworzonych kompleksów PAA-SDS.

Małgorzata ULEWICZ*, Władysław WALKOWIAK

REMOVAL OF Zn(II), Cd(II) AND Pb(II) USING POLYMER INCLUSION MEMBRANE TRANSPORT WITH PROTON IONIZABLE DB-16-C-5 CROWN ETHERS

Received March 15, 2006; reviewed; accepted May 15, 2006

Competitive transport of Zn(II), Cd(II), and Pb(II) ions from aqueous nitrate source phase ($c_{Me} = 0.001$ M) through polymer inclusion membranes (PIMs) containing cellulose triacetate (as support), *o*-nitrophenyl pentyl ether (as plasticizer) and proton ionizable lariat ether derivatives (as ion carriers) has been investigated. The influence of varying the lipophilicity of *sym*(R)(hydroxy)dibenzo-16-crown-5 macrocycles with R groups such as hydrogen (in 1), decyl (in 2) and phenyl (in 3) on the selectivity and efficiency of Zn(II), Cd(II), and Pb(II) transport through polymer inclusion membranes is studied. The influence of HLB (hydrophile-lipophile balance) and V_x (molecular volumes) on the transport selectivity of metal ions was investigated. Relationship between the cation size and initial fluxes transport of metal cation was shown. The selectivity coefficients of Pb(II)/Zn(II) and Cd(II)/Zn(II) decrease with increase of carrier concentration in inclusion membrane.

Key words: polymer inclusion membrane, zinc(II), cadmium(II), lead(II), proton ionizable ethers

INTRODUCTION

Selective removal of metal ions from industrial and waste aqueous solutions is very important for the hydrometallurgical processing. Among the different methods used for removal and separations of the metal ions, such as solvent extraction, ion exchange, the transport across liquid membranes is very attractive. The transport through liquid membrane is used for selective separation and concentration of metal ions from source aqueous phase, in which the concentration of metal ionic species is above $1 \cdot 10^{-4}$ M. A variety of types of liquid membranes exists, i.e. bulk (BLMs),

* Department of Metal Extraction and Recirculation, Czestochowa University of Technology, 42-200 Czestochowa, Armii Krajowej 19 Street, e-mail: ulewicz@mim.pcz.czest.pl.

** Division of Chemical Metallurgy, Wroclaw University of Technology, 50-370 Wroclaw, Poland.

emulsion (ELMs), supported (SLMs) and polymer inclusion membranes (PIMs). A new type of membrane system, called polymer inclusion membrane (PIM), has been developed which provides metal ion transport with high selectivity, as well as easy setup and operation (Bond et al., 1999).

Macrocyclic compounds such as crown ethers were successfully used for metal ions separation in solvent extraction, transport through liquid membranes and in ion exchange systems. During last years several neutral crown ethers and lariat ethers were successfully used for separation transport of heavy metal ions. In competitive transport of zinc(II) and cadmium(II) across emulsion liquid membrane with dicyclohexane-18-crown-6, near quantitative selectivity for Cd(II) over Zn(II) and Hg(II) has been achieved (Izatt et al., 1987). This can be explained by the preferential transport of neutral cation-anion moieties of CdA_2 from Zn^{2+} and $[\text{HgA}_2]^{2-}$, where $\text{A} = \text{SCN}^-$, I^- , Br^- or Cl^- (Izatt et al., 1986). Cho et al., (1991, 1995) found out that a single transport of Cd^{2+} across emulsion liquid membranes by diazo-18-crown-6 (DA18C6) from 0.4 M SCN^- aqueous solutions is much more effective in comparison with Zn^{2+} . On the other hand, Dadfarnia and Shamsipur (1992) discovered quantitatively transport of zinc(II) and only 1 % of cadmium(II) across bulk liquid membrane with DA18C6 and palmitic acid.

The transport studies through cellulose triacetate membrane have been reported recently. Polymer inclusion membranes containing CTA and macrocyclic compounds such as dibenzo-18-crown-6, hexathia-18-crown-6, diaza-18-crown-6 and hexaaza-18-crown-6 were investigated by Gherrou et al., (2001, 2004, 2005). Comparison of carrier-facilitated transport of lead(II) across SLM and PIM has been reported by Aguilar et al., (2001). It was shown that ligands like 18-crown-6 provide high selectivity for lead(II) over cadmium(II) and zinc(II) ions. Competitive transport of trace radionuclide ions, i.e. Cs-137, Sr-90 and Co-60 from aqueous solutions through PIM's using dibenzo-21-crown-7 and dinonylnaphtalenesulfonic acid was studied by Kozłowski et al., (2000). Competitive alkali metal cation transport through PIM's containing alkyldibenzo-16-crown-5-oxyacetic acid carriers shown the excellent selectivity for sodium(I) transport with fluxes being strongly influenced by the length of the alkyl chain geminally attached to the functional side arm in the lariat ether molecule.

Hayashi et al., (2003) reported on the selective proton-driven transport of lead(II) ions across polymer inclusion membranes with proton diionizable polyethers bearing different alkyl chain lengths (from $-\text{C}_7\text{H}_{15}$ to $-\text{C}_{16}\text{H}_{33}$). The transport selectivity of PIM with polyether bearing $-\text{C}_8\text{H}_{17}$ alkyl chain was as follows $\text{Pb}^{2+} > \text{Cu}^{2+} > \text{Cd}^{2+} > \text{Zn}^{2+} > \text{Ni}^{2+}$. However Ulewicz et al., (2004) investigated competitive transport of Zn(II), Cd(II), and Cu(II) ions from aqueous chloride source phase through polymer inclusion membranes containing side-armed lariat ether-type derivatives of diphosphaza-16-crown-6 as ion carrier. It was found, that the initial fluxes of all investigated cations increase with acidity of the feed phase increase and the selectivity order was as follows: $\text{Cd(II)} > \text{Zn(II)} > \text{Cu(II)}$.

A few papers deal with the selective removal of metal ions with calix-crown ethers. Kim et al., (2001) studied calixcrown ethers for transport of alkali metal cations through PIM and SLM. The calix-crown-6 exhibited the best selectivity toward cesium cation over other alkali metal cations. The PIM's exhibited faster transport as well as higher durability than the SLM's. Also Levitskaia et al., (2002) studied competitive cesium(I) ions transport with calix[4]arene-crown-6 or calix[4]arene-biscrown-6 as ion carriers. Membrane containing calix-*monocrown* carriers exhibited less efficient but more selective cesium(I) transport than those with calyx-*biscrown* carriers. Ulewicz et al., (2005) also investigated competitive transport of Zn(II), Cd(II), and Pb(II) ions from aqueous nitrate source phase through polymer inclusion membranes with derivatives of calix[4]crown-6 as ion carriers. It was found, that type of groups (-OH, -OMe) attached to the calix[4]-crown-6 molecule has the influence on selectivity and efficiency of Zn(II), Cd(II), and Pb(II) transport through polymer inclusion membranes. The selectivity coefficient of Pb(II)/Zn(II) and Cd(II)/Zn(II) decreases with nitric acid concentration increase in receiving phase.

We now present the competitive transport of zinc(II), cadmium(II), and lead(II) ions from dilute aqueous solutions with lipophilic proton-ionizable lariat ethers. The selectivity of metal ions transport as a function of carrier concentration in membrane is studied. Also effects of structural modification of ionizable ethers derivatives upon the efficiency and selectivity of ions transport is now reported.

EXPERIMENTAL

REAGENTS

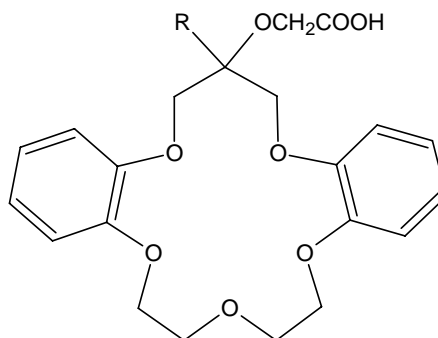
The inorganic chemicals, i.e. zinc(II), cadmium(II), lead(II) nitrates and hydrochloric acid were of analytical grade and were purchased from POCh (Gliwice, Poland). The aqueous solutions were prepared with double distilled water, which conductivity was 0.1 $\mu\text{S/m}$. The organic reagents, i.e. cellulose triacetate (CTA), *o*-nitrophenyl pentyl ether (ONPPE) and dichloromethane were also of analytical grade and were purchased from Fluka and used without further purification. The density of plasticizer, i.e. *o*-nitrophenyl pentyl ether was 1.085 g/cm^3 . Derivatives of proton-ionizable crown ethers 1 ÷ 3 were synthesized by Bartsch et al., (2000) and Brown et al., (1991).

POLYMER INCLUSION MEMBRANE PREPARATION

A solution of cellulose triacetate as the support, *o*-nitrophenyl pentyl ether as the plasticizer, and proton-ionizable crown ether 1 or 2 as the ion carrier in dichloromethane as the organic solvent were prepared. A specified portion of this organic solution was poured into a membrane mold comprised of a 9.0 cm glass ring attached to a plate glass with cellulose triacetate - dichloromethane glue. The dichloromethane was allowed to evaporate overnight and the resulting membrane was separated from the glass plate by immersion in cold water. Next, the membrane was

soaked in water for 12 hours. Two samples of membrane were cut from the same membrane film for duplicate transport experiments. The membrane contained 2.6 cm³ ONPPE /1g CTA, and 0.3 ÷ 1.0 M lariat ether based on plasticizer. The average PIM membrane thickness was 35 μm.

Crown ether -R:
 $\frac{1}{2}$ -H
 $\frac{2}{2}$ -C₁₀H₂₁
 $\frac{3}{2}$ -C₆H₅



TRANSPORT STUDIES

Transport experiments were conducted in a permeation cell in which the membrane film (at surface area of 4.9 cm²) was tightly clamped between two cell compartments. Both, i.e. the source and receiving aqueous phases (45 cm³ each), were mechanically stirred at 600 rpm. The receiving phase was 1.0 M HCl. The PIM transport experiments were carried out at the temperature of 20 ± 0.2 °C. Small samples of the aqueous receiving phase were removed periodically via a sampling port with a syringe and analyzed to determine zinc(II), cadmium(II) and lead(II) concentrations by atomic absorption spectroscopy method (AAS Spectrometer, Solaar 939, Unicam). The source phase pH was kept constant and controlled by pH meter (ph-meter, CX-731 Elmetron, with combine pH electrode, ERH-126, Hydromet, Poland).

The kinetics of PIM transport was described by a first-order reaction in metal ion concentration:

$$\ln\left(\frac{c}{c_i}\right) = -kt \quad (1)$$

where c is the metal ions concentration (M) in the source aqueous phase at some given time, c_i is the initial metal ions concentration in the source phase, k is the rate constant (s⁻¹), and t is the time of transport (s).

To calculate the k value, a plot of $\ln(c/c_i)$ versus time was prepared. The rate constant value for the duplicate transport experiment was averaged and standard deviation was calculated. The relationship of $\ln(c/c_i)$ vs. time was linear, which was confirmed by high values of determination coefficient (R^2), i.e., which were mostly from 0.980 to 0.998. The permeability coefficient (P) was calculated as follows:

$$P = -\frac{V}{A}k, \quad (2)$$

where V is volume of the aqueous source phase, and A is an effective area of membrane.

The initial flux (J_i) was determined as equal to:

$$J_i = P \cdot c_i. \quad (3)$$

The selectivity coefficient (S) was defined as the ratio of initial fluxes for $M1$ and $M2$ metal ions, respectively:

$$S = J_{i,M1} / J_{i,M2} \quad (4)$$

RESULTS AND DISCUSSION

It was previously found (Ulewicz et al., 2005) that competitive transport of Zn(II), Cd(II) and Pb(II) ions through PIM with calix[4]crown-6 derivatives as the ion carriers allow for removal of metal ions from acidic nitrate aqueous solutions. Now we applied ionizable lariat ether derivatives for zinc(II), cadmium(II), and lead(II) removal from nitrate aqueous solutions.

Table 1. The values of initial fluxes, selectivity orders and selectivity coefficients for competitive transport of Zn(II), Cd(II), and Pb(II) across PIM with ether **2** in membrane. Source phase: aqueous solution of Cd(II), Zn(II), Pb(II) at 0.001M concentration, pH = 7.0. Receiving phase: 1.0 M HCl. Membrane: 2.6 cm³ ONPPE / 1g CTA

Ether, M	Metal ions	Initial flux, J_i ($\mu\text{mol}/\text{m}^2\text{s}$)	Selectivity order and selectivity ratios
0.3	Zn(II)	0.47	Pb(II) > Cd(II) > Zn(II) 1.67 3.23
	Cd(II)	0.91	
	Pb(II)	1.52	
0.5	Zn(II)	0.68	Pb(II) > Cd(II) > Zn(II) 1.53 3.09
	Cd(II)	1.37	
	Pb(II)	2.10	
1.0	Zn(II)	1.68	Pb(II) > Cd(II) > Zn(II) 1.40 2.11
	Cd(II)	2.54	
	Pb(II)	3.55	

The transport kinetics of metal ions with **1** or **2** is presented in Fig. 1. As can be seen from this figure crown ether **1** is transported metal ions much slower than crown ether **2**. The initial fluxes and selectivity of metal ions transport through PIM with crown ether **2** from aqueous source phase containing equimolar mixture of all metals

is shown in Table 1. The selectivity order of metal ions fluxes transported with 2 is as follows: Pb(II) > Cd(II) > Zn(II). At pH equal 7.0 the percent molar contributions of uncomplexed cations (i.e. Zn²⁺, Cd²⁺ or Pb²⁺) of complex species for those metals with OH⁻ are over 99,5 % (Stability Constants of Metal-Ion Complexes, 1982).

As can be seen from this table, the initial fluxes of all investigated metal cations increase with concentration of crown ether 2 in membrane increase. On the other hand, the selectivity coefficients of Pb(II)/Cd(II) and Pb(II)/Zn(II) for PIM slightly decrease with crown ether 2 concentration increase in membrane.

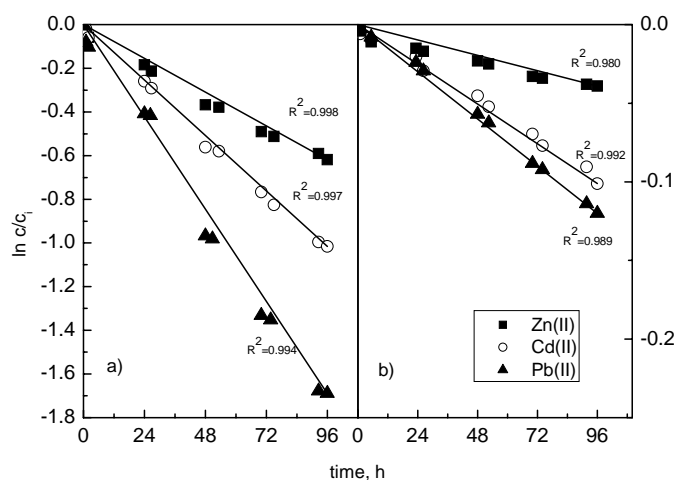


Fig. 1. Kinetics of Zn(II), Cd(II), and Pb(II) transport through PIMs containing 1.0 M ether 2 (a) and 0.5 M ether 1 (b). Source phase: $c_{Me} = 0.001$ M, pH = 7.0; receiving phase: 1.0 M HCl; membrane: 2.50 cm³ ONPPE / 1.0 g CTA

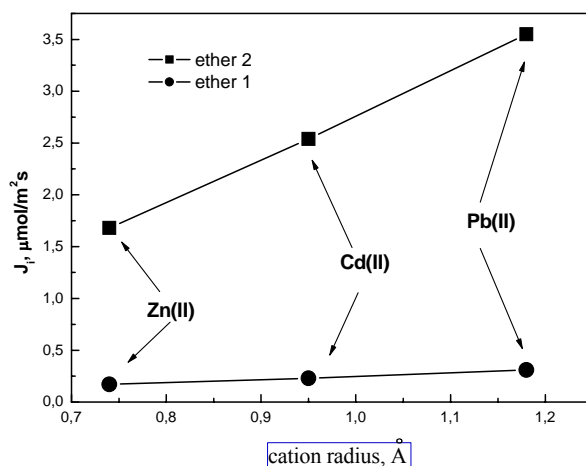


Fig. 2. Relationship of initial metal ions fluxes obtained from transport through PIM with ether 1 and 2 vs. metal cation radius. Experimental conditions as in Fig.1

Diameter of DB-16-crown-5 is estimated as $2.0 \div 2.4 \text{ \AA}$ (Vögtle and Weber, 1989). On the other hand, all metal cations studied processes diameters lower than crown ether cavity diameter (Matrel and Hancock, 1996). As can be seen from Fig. 2, the best transport cation is lead(II), which possess the highest diameter values.

The obtained results prove that the selectivity of zinc(II), cadmium(II) and lead(II) ions separation with the ionizable lariat ethers 1 \div 3 depends upon the nature of the substituents attached at the ring. The chemical behaviour of these lariat ethers with the same internal crown cavity size involving five oxygen atoms is affected by the external substituents (side arms). Therefore, the considered lariat ethers could be specifically characterized by means of their molar intrinsic volume, V_x (cm^3/mol), and hydrophile-lipophile balance (HLB), both calculated according to McGowan et al., (1990) and McGowan and Sowada (1993).

$$V_x = \sum n_i V_{x,i} - 6.56 \cdot B \quad (5)$$

where $V_{x,i}$ is a volume specific for the i -th kind of atom in the solute molecule, the number of which is n_i , and B are total bonds between the atoms (irrespective whether single or multiple). The number of bonds could be easily calculated with the following equation:

$$B = N - 1 + R \quad (6)$$

where N and R stand for the total number of atoms and rings in the molecule, respectively.

The HLB value was calculated as:

$$HLB = 7 - 0.337 \cdot V_x + 1.5 \cdot n \quad (7)$$

where n denotes the total number of oxygen and nitrogen atoms in the molecule. Calculated values of V_x and HLB are show in Table 2.

Table 2. Value of V_x and HLB for lariat ethers studied

Compounds	V_x , mol/cm^3	HLB
<u>1</u>	291.0	9.2
<u>2</u>	431.9	4.4
<u>3</u>	351.8	7.1

In Fig. 3 the relationship of hydrophile-lipophile balance (HLB) and molecular volumes (V_x) vs. the flux transport of metal ions is shown. As can be seen from this figure, the initial fluxes of all investigated metal cations increase with molecular volumes of lariat ether increase and decrease with hydrophile-lipophile balance value

increase. For compound 3, at the concentration of 0.5 M in membrane, the selectivity coefficients of Pb(II)/Cd(II) and Pb(II)/Zn(II) were 1.6 and 3.4, respectively. However, the selectivity coefficients of Pb(II)/Cd(II) and Pb(II)/Zn(II) for crown ether 1 at the concentration of 0.5 M were 1.4 and 1.8, respectively.

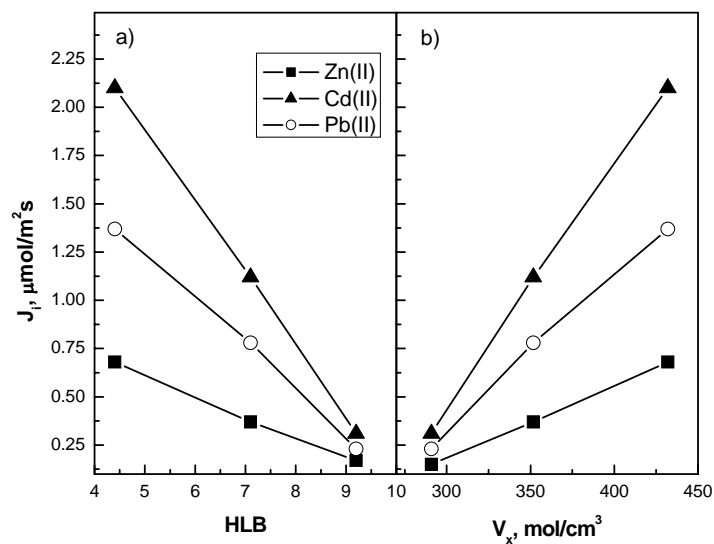


Fig. 3. Initial Zn(II), Cd(II) and Pb(II) transport fluxes through PIM vs. HLB and V_x . Source aqueous phase: solution of Cd(II), Zn(II), Pb(II) at 0.001 M concentration, pH = 7.0 Membrane: 2.6 cm³ ONPPE / 1g CTA, 0.5 M crown ethers 1, 2 and 3.

CONCLUSIONS

Lead(II), cadmium(II) and zinc(II) cations can be effectively removed from aqueous nitrate solutions in polymer inclusion membrane transport with derivatives of ionizable crown ethers as an carriers. The type of group attached (-H, -C₁₀H₂₁, and -C₆H₅) to the DB-16-crown-5 molecule has the influence on selectivity and efficiency of Zn(II), Cd(II), and Pb(II) transport through polymer inclusion membranes. The selectivity order of metal ions fluxes for crown ether 2 is as follows: Pb(II) > Cd(II) > Zn(II). The selectivity coefficients of Pb(II)/Cd(II) and Pb(II)/Zn(II) slightly decreases with lariat ether concentration increase in membrane. It was shown that the hydrophile-lipophile balance and molecular volumes of crown ethers influence on transport of metal ions. On the other hand, the relationship between the cavity diameter of ethers and initial fluxes was shown.

REFERENCES

- AGUILAR J.C., RODRIGUEZ E., GYVES J. De, BARTSCH R.A., KIM M. (2001), *Design, synthesis and evaluation of diazadibenzocrown ethers as Pb(II) extractants and carriers in plasticized cellulose triacetate membranes*, *Talanta*, 54, 1195-1204.
- BARTSCH R. A., BITALAC L. P., COWEY C. L., ELSHANI S., GOO M.J., HUBER V. J., IVY S. N., JANG Y., JOHNSON R. J., KIM J. S., LUBOCH E., McDONOUGH J. A., PUGIA M. J.; SON B., ZHAO Q. (2000), *Lariat Ether Alcohols Based on Dibenzo-16-crown-5*, *J. Heterocyclic Chem.* 37, 1337-1350.
- BOND H., DIETZ M. L., ROGERS R.D., Eds. (1999), *ASC Symposium Series 716*, Washington, DC.
- BROWN P. R., HALLMAN J. L., WHALEY L. W., DESAI D. H., PUGIA M. J., BARTSCH R. A. (1991), *Competitive, Proton-Coupled, Alkali Metal Cation Transport across Polymer-Supported Liquid Membranes Containing sym-(Decyl)-dibenzo-16-crown-5-oxyacetic Acid: Variation of the Alkyl 2-Nitrophenyl Ether Membrane Solvent*, *J. Membrane Sci.* 56, 195-206.
- CHO M. H., CHUN H. S., KIM J. H., RHEE Ch. H., KIM S. J. (1991), *Study on separation of heavy metal ions in a natural macrocycle-mediated emulsion liquid membrane system*, *Bull. Korean Chem. Soc.*, 12, 474 - 477.
- CHO M.H., SHIN S. Ch. (1995), *Studies on the macrocycle-mediated transport of divalent metals ions in a supported liquid membrane system*, *Bull. Korean Chem. Soc.*, 16, 33 - 36.
- DADFARNIA S., SHAMSIPUR M. (1992), *Highly selective membrane transport of zinc(2+) ion by a cooperative carrier composed of 1,10-diaza-18-crown-6 and palmitic acid*, *Bull. Chem. Soc. Jpn.*, 65, 2779 - 2783.
- GHERROU A., KERDJOU DJ H., MOLINARI R., DRIOLI E., (2001), *Facilitated transport of Ag(I), Cu(II) and Zn(II) ions by using DB18C6 and DA18C6 as carriers: Interface behavior on the ion transport*, *Sep. Sci. Technol.* 36, 2289-2304.
- GHERROU A., KERDJOU DJ H., MOLINARI R., SETA P., DRIOLI E., (2004), *Fixed sites plasticized cellulose triacetate membranes containing crown ethers for silver(I), copper(II) and gold(III) ions transport*, *J. Membr. Sci.*, 228, 194-157.
- GHERROU A., KERDJOU DJ H., MOLINARI R., SETA P., (2005), *Preparation and characterization of polymeric plasticized membranes (PPM) embedding a crown ether carrier application to copper ions transport*, *Material Sci. Eng.*, C25, 436-443.
- HAYASHI R., HAYSHITA T., YASHIKAWA T., ARATANI K., BARTSCH R.A., TERAME N. (2003) *Design of a polymer inclusion membrane having proton ionizable polyether carriers and their separation function for lead ion*, *Bunseki Kagaku*, 52, 755-762.
- IZATT R. M., BONALD R. L., GENG W., CHO M. H., CHRISTENSEN J. J. (1987), *Separation of bivalent cadmium, mercury and zinc in a natural macrocyclic-mediated emulsion liquid membrane*, *Anal. Chem.*, 59, 2405 - 2409.
- IZATT R. M., LINDCH G. C., BRUENING R. L., BRADSHAW J. S., LAM D. J. D., CHRISTENSEN J.J. (1986), *Design of cation selectivity into liquid membrane systems using macrocyclic carriers*, *Pure Appl. Chem.*, 58, 1453 - 1460.
- KIM, J. K.; KIM, J. S.; SHIL, Y. G.; LEE, K. W.; OH, W. Z. (2001), *Selective extraction of cesium ion with calix[4]arene crown ether through thin sheet supported liquid membranes*, *J. Membr. Sci.*, 187, 3-11.
- KOZŁOWSKI C., WALKOWIAK W., PELLOWSKI W., KOZIOŁ J. (2002), *Competitive transport of toxic metal ions by polymer inclusion membranes.*, *J. Radioanal. Nucl. Chem.*, 253, 389-394.
- LEVITSKAIA T. G.; LAMB J.D.; FOX K.L.; MOYER B.A., (2002), *Selective carrier-mediated cesium transport through polymer inclusion membranes by calix[4]arene-crown-6 carriers from complex aqueous mixtures*, *Radiochimica Acta*, 90, 43-52.
- MARTELL A.E., HANCOCK R.D. (1996) *Metal complexes in aqueous solutions*, Plenum Press, New York.
- STABILITY CONSTANTS OF METAL-ION COMPLEXES*, (1982) Part A: Inorganic Ligands, Pergamon Press, New York.

- ULEWICZ M., KOZŁOWSKI C., WALKOWIAK W. (2004), *Removal of Zn(II), Cd(II) and Cu(II) ions by polymer inclusion membrane with side-armed diphosphaza-16-crown-6-ethers*, Physicochemical Problems of Mineral Processing, 38, 131-138.
- ULEWICZ M., BOCHEŃSKA M., LESIŃSKA U., WALKOWIAK W. (2005), *Studies on removal of Zn(II), Cd(II) and Pb(II) ions in polymer inclusion membrane transport with calix[4]-crown-6 derivatives*, Physicochemical Problems of Mineral Processing, 38, 107-116.
- VÖGTLE F., WEBER E., *Crown ethers-complexes and selectivity* (1989) [In:] E. Weber, J. L. Toner, I. Goldgerg, F. Vögtle, D. A. Laidler, J. F. Stoddart, R. A. Bartsh, C. L. Liotta: Crown ethers and analogs, S. Patai (Ed.), New York.

Ulewicz M., Walkowiak W., *Wydzielanie jonów Zn(II), Cd(II) i Pb(II) przez polimerowe membrany inkluzyjne zawierające jonizowalne etery koronowe*, Physicochemical Problems of Mineral Processing, 40, (2006), 185-194 (w jęz. ang.).

Zbadano selektywność wydzielania jonów cynku(II), kadmu(II) i ołowiu(II) z wodnych roztworów azotanowych zawierających równomolową mieszaninę metali ($c_{Me} = 0,001$ M) w procesie transportu przez polimerowe membrany inkluzyjne (PIM) przy użyciu w roli przenośników jonów jonizowalnych eterów koronowych o koronie DB-16-C-5. Badane etery różniły się rodzajem grupy dołączanej do korony (-H, -C₁₀H₂₁, -C₆H₅). Polimerowe membrany inkluzyjne syntezowano z trójoctanu celulozy (nośnik), eteru *o*-nitrofenylopentylowego (pastyfikator) i jednego z eterów koronowych 1 ÷ 3 (przenośnik jonów); stężenie przenośnika jonów w przeliczeniu na plastyfikator zmieniano w granicach 0,3 - 1,0 M. Współczynniki separacji Pb(II)/Cd(II) i Pb(II)/Zn(II) przez PIM przy użyciu eteru 2 były nieznacznie wyższe niż przy użyciu eteru 3 i 1. Dla badanych eterów o stężeniu 0,5 M w membranie współczynniki separacji Pb(II)/Cd(II) i Pb(II)/Zn(II) wynosiły odpowiednio 1,4 i 1,8; 1,5 i 3,1 oraz 1,6 i 3,4 dla eterów 1, 2, i 3. Wykazano, że początkowe wartości strumienia transportu badanych jonów rosną ze wzrostem objętości molowej eteru koronowego, natomiast maleją ze wzrostem bilansu hydrofilowo-hydrofobowego (HLB) eteru koronowego. Ponadto stwierdzono, że niezależnie od zastosowanego eteru lariatowego o koronie DB-16-C-5 najlepiej transportowane są kationy o największej średnicy.

Bernadeta GAJDA^{*}, Mariusz B. BOGACKI^{**}

LABORATORY SIMULATION OF NICKEL(II) AND COBALT(II) ION SEPARATION IN A CONTINUOUS COUNTER-CURRENT EXTRACTOR

Received March 15, 2006; reviewed; accepted May 15, 2006

In the paper studies were presented related to application of CYANEX 272 (di(2,4,4-trimethylpentyl)phosphine acid) extractant in the extractive separation of nickel(II) and cobalt(II) ions originating from a sulphate solution. Values of $pH_{0.5}$ amounted to 4.6 and 5.7 for cobalt(II) and nickel(II) ions, respectively, which permitted selective separation of the ions. Simulation of the three-stage extraction process, performed in laboratory conditions, permitted to conclude that such a process allows for a selective separation of cobalt(II) and nickel(II) ions although it requires appropriate modification only when pH of the aqueous phase is controlled.

Key words: ions separation, extraction, counter-current extractor, simulation

INTRODUCTION

Various industrial processes water streams contain nickel(II) and cobalt(II) ions at relatively low concentrations. One of the ways in which they are processed involves application of extraction techniques, aimed at their selective separation and isolation. In a counter-current apparatus, such a process can be conducted in a continuous way and such procedure as waste utilization is advantageous since it allows to adjust size of the installation to current needs of the producer.

Literature contains several examples of equilibrium studies on extractive separation of nickel(II) and cobalt(II) using phosphoorganic extractants such as di(2-ethylhexyl)phosphoric acid (D2EHPA), di(2,4,4-trimethyl-pentyl)-phosphinic acid (CYANEX 272) and its sulphuric derivatives, di(2,4,4-trimethylpentyl)dithio-

^{*} Częstochowa University of Technology, Department of Metal Extraction and Recirculation, Armii Krajowej 19, 42-200 Częstochowa, Poland.

^{**} Poznań University of Technology, Institute of Chemical Technology and Engineering, Pl. M. Skłodowskiej-Curie 2, 60-965 Poznań, Poland; E-mail: Mariusz.Bogacki@put.poznan.pl

phosphinic acid (CYANEX 301) and di(2,4,4-trimethylpentyl)thiofosfinic acid (CYANEX 302) (Fu and Golding, 1987; Komasa et al., 1981, 1983, 1984; Gajda and Apostoluk, 2000, 2002; Reddy et al., 2005; Devi et al., 1998). All the above mentioned extractants of the CYANEX series may be used to extraction of both Co(II) and Ni(II) ions but selectivity of separation of the ions decreases in the following order: Cyanex 302 > Cyanex 272 >> Cyanex 30 (Sole and Hiskey, 1992).

Most of presented studies involve equilibrium studies. Their results point to the potential of separation of nickel(II) and cobalt(II) ions at a single stage of extraction. Such results are of high importance in basic studies but manifest restricted applicability in designing multi-step processes running in a continuous manner. In the latter case not only the efficiency of individual extraction stage of 85-95% is important but also progression of several side reactions which may decrease extracting ability of the extractant.

Present study aimed at examining the potential for separation of nickel(II) and cobalt(II) ions in a three-stage counter-current extractor operating in a continuous manner.

EXPERIMENTAL

The raw material involved a sulphate solution containing 0.01 and 0.015 mol/dm³ of nickel(II) and cobalt(II), respectively. Adding appropriate amounts of sodium sulphate, ionic strength of the original solution was adjusted to 0.10 M. The preliminary pH in the starting solution of 8.00 was obtained adding appropriate amounts of 1 M NaOH solution. The reagents were obtained from POCh (Poland). CYANEX 272 (CYTEC, Canada), containing 85 % di(2,4,4-trimethyl)phosphinic acid was used as the extractant. The organic phase was obtained dissolving 0.02 M of the extractant in a kerosene of 0.85 g/dm³ in density (ALDRICH). Flasks, each containing 40 cm³ of aqueous and organic phases, were mechanically agitated at constant temperature of 25±1°C for 15 min. After separation of the phases, metal ion concentrations were estimated in the aqueous phase using AAS Solar 939 spectrophotometer (Unicam). pH of the equilibrium was estimated in the aqueous phase using a combined electrode (type ERH-136, Hydromet) coupled to a pH-meter (CX-731, Elmetron). Concentration of metal ions in the organic phase was calculated from the mass balance.

The multi-step, counter-current extraction was performed in a cascade of apparatuses of a mixer/settler type. Scheme of such a process is shown in Figure 1. The essence of the system involves counter-current type of contact between the aqueous and the organic phases, which assures the maximum loading of the organic phase. The reaction of metal ion transfer from the aqueous to the organic phase was accompanied by increase in acidity of the aqueous phase, in line with the following reaction:



Such a course of the reaction denoted an increasing acid concentration in the aqueous phase after every step of the extraction. Since the extraction process was strongly influenced by acidity of the raw solution the amounts of metal ions transferred at sequential stages of the extraction should be expected to decrease.

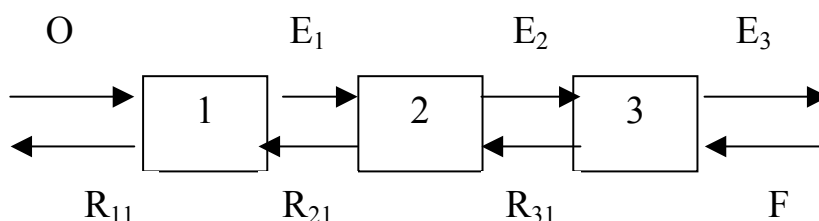


Fig. 1. Scheme of three-step counter-current extraction. O – supplied organic phase; F – supplied aqueous phase; $R_i, E_i, i=1,2,3$ – the consecutively obtained raffinates and extracts following the first, second and third steps of extraction

In laboratory simulation of the multi-step counter-current extraction was conducted in vessels (flasks or separators) subjected to multifold, consecutive mixing and phase separation (Figure 2). As the result of the extraction, the raffinates were obtained (denoted in the scheme as $R_1^I, R_1^{II}, \dots, R_1^{VI}$), and extracts ($E_3^I, E_3^{II}, \dots, E_3^{VI}$). The superscripts indicate consecutive approximations of the final raffinate and extract concentrations following the first, second and third step of extraction (subscript). The process was conducted until properties of the consecutively obtained E and R products stabilized. The scheme of the extraction corresponded to a three-step counter-current extraction performed in a continuous manner, presented in Figure 1. It was assumed that equilibrium was reached at individual steps of the extraction.

The principles of the procedure were as follows (Fig. 2): the measured volume of the raw solution F (aqueous phase containing 0.01 mol/dm^3 of Ni(II) and 0.015 mol/dm^3 Co(II) ions, of $\text{pH} = 8.00$) was mixed at the step 3^I with appropriate volume of the organic phase O (extractant, 0.02 mol/dm^3 solution of CYANEX 272 in kerosene). After settling, the organic phase, E_3^I extract, and the aqueous phase, R_3^I raffinate were separated from each other. The raffinate phase was transferred to step 2^I and mixed with a new dose of the fresh extractant, O . The obtained extraction phase, E_2^I , was mixed at the step 3^{II} with a new dose of the raw solution F , and the R_2^I raffinate with a new dose of the extractant O at the step 1^I , etc. Termination of the extraction process was signified by absence of changes in the composition of $R_1^I, R_1^{II}, \dots, R_1^{VI}$ raffinates.

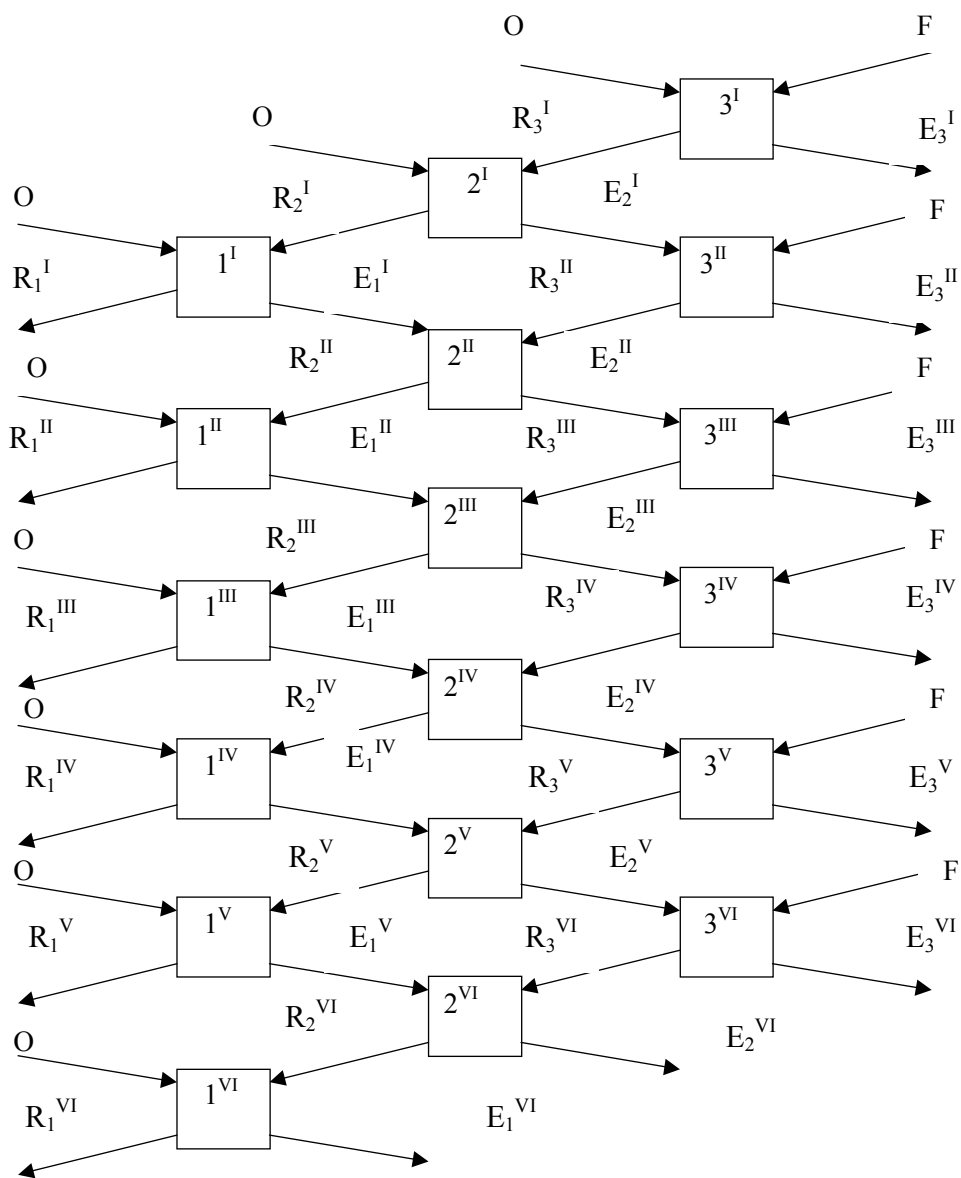


Fig. 2. Scheme of three-step counter-current extraction under laboratory conditions. Six steps of the extraction were assumed. *O*: the supplied organic phase, *F*: the supplied aqueous phase, *R*: raffinate, *E*: extract. Superscripts correspond to consecutive approximations of the extraction system. Subscripts correspond to numbers of steps in the extractor battery

DISCUSSION

Preliminary experiments showed that the extraction equilibrium was reached after 5 min of contact of the phases. Separation of phases was complete. In order to define conditions under which the extraction process of separating nickel(II) from cobalt(II) ions should be conducted, equilibrium experiments were performed. The relationships between $\log D$ and pH for nickel(II) and cobalt(II) ions are shown in Figure 3. The arrangement of lines in the figure was influenced by conditions in which the extraction process was conducted, i.e. by concentration of reagents both in the aqueous and in the organic phases and by the type of solvent. Cobalt(II) ions could be noted to be extracted better than nickel(II) ions. This was indicated by the difference in values of $\text{pH}_{0.5}$, which amounted to 4.6 and 5.7 for cobalt(II) and nickel(II) ions, respectively. This pointed to the potential of separating the two metal cations in the extraction process. However, separation of the studied ions should be strongly dependent upon pH of the raw solution. It should be expected that the lower is pH, the less pronounced will be the separation. Therefore, in the studies on the counter-current extraction process pH of the raw solution was set at 8.

Taking advantage of the preliminary results from extraction studies, the McCabe – Thiele graph was drawn (Fig. 7 and 8). This provided grounds for the conclusion that two extraction steps should be sufficient for separation of the studied metal ions. However, taking into account a lowered efficiency of extraction steps in further studies a three-step counter-current extraction was employed.

Changes in pH and metal ions concentrations in the organic phase, $E_1^I, E_1^{II}, \dots, E_1^{VI}$ at individual steps of the simulation are shown in Figs. 4 and 5. As can be noted, already at the step 4 of the simulation pH of the aqueous phase approximated the value of 4 and did not practically change in the subsequent steps. Similarly, concentrations of cobalt(II) and nickel(II) ions in the organic phase asymptotically approached the values of, respectively, 250 and 100 mg/dm³. The values were reached already in the 4th step of the simulation. This demonstrated that the counter-current extraction process reached a stable condition. Alterations in the separation coefficient in the course of the extraction process are shown in Fig. 6. The separation coefficient stabilized at the level of approximately 5 already at the second step of the extraction.

In the presented here counter-current extraction process of separating nickel(II) from cobalt(II) ions a relatively good coefficient of ion separation was obtained. Nevertheless, the transfer of cobalt(II) ions to the organic phase was accompanied by transfer of small amounts of nickel(II) ions. This was related to the relatively pronounced drop in pH of the aqueous phase, to the level of around 4.0, following consecutive steps of the extraction. Such a result pointed to the need of controlling pH following every step of the extraction.

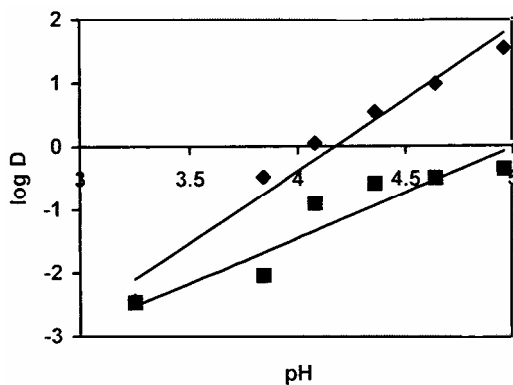


Fig. 3. Cobalt(II) (◆) and nickel(II) (■) separation coefficient between the aqueous and organic phases. Original concentrations of Ni(II) and Co (II): 0.01 mol/L

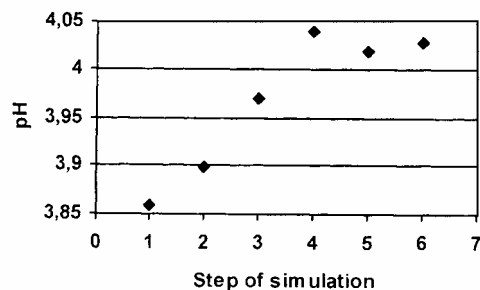


Fig. 4. Change in raffinate pH after third step of the extraction at individual steps of the simulation.

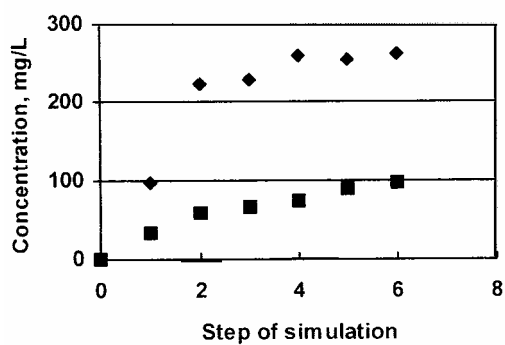


Fig. 5. Changes in concentration of Co(II) (◆) and Ni(II) (■) in the extract after third step of extraction

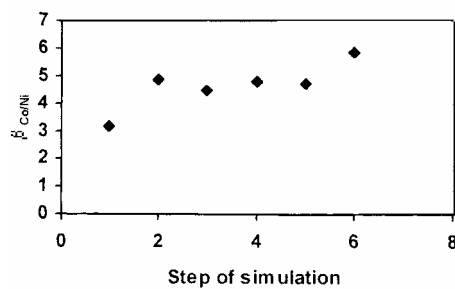


Fig. 6. Separation coefficient $\beta_{Co/Ni}$ for nickel(II) and cobalt(II) ions

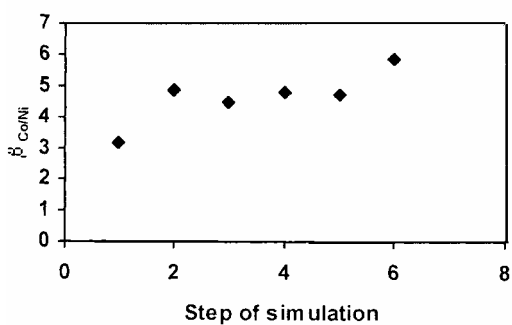


Fig. 7. McCabe – Thiel graph. Nickel(II) extraction

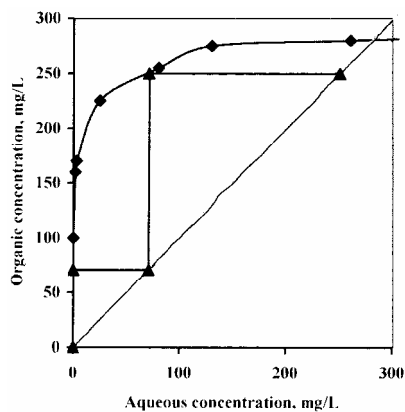


Fig. 8. McCabe – Thiel graph. Cobalt(II) extraction

CONCLUSIONS

Laboratory simulation of the counter-current extraction process points to the potential of using CYANEX 272 extractant for selective separation of cobalt(II) ions in presence of nickel(II) ions from sulphate solutions in the counter-current extraction process. The obtained results indicate the need for pH control following every step of the extraction and for setting it at such a level which prevents against the parallel transfer of nickel(II) ions. The performed studies on the counter-current extraction process on a laboratory scale allow to draw significant technological conclusions related to the way in which the process should be conducted.

ACKNOWLEDGEMENTS

The study was partially subsidized by the grant No. 32-139/06-DS provided by the Poznań University of Technology.

REFERENCES

- DEVI N.B., NATHSARMA K.C., CHAKRAVORTTY V., (1998), *Hydrometallurgy*, (49), 47-61.
FU X, GOLDING JA., (1987), *Solvent Extr. Ion Exch.*;5(2), 205-226.
GAJDA B., APOSTOLUK W., (2000), *Proceedings of the XV International Symposium on Physico-Chem. Methods of Mixtures Separation*, "Ars Separatoria 2000", 78-81.
GAJDA B., W. APOSTOLUK W., (2002), *Ars Separatoria Acta*, Nr 1, 55-60
KOMASAVA I, OTAKE T, HATTORI I., (1983), *J. Chem. Eng. of Japan*, 16(5), 384-388.
KOMASAVA I, OTAKE T, HATTORI I., (1984), *J. of Chem. Eng. of Japan*, 17(4), 410-417.
KOMASAVA I, OTAKE T, HIGAKI Y., (1981), *J. Inorg. Nucl. Chem.*, 43(12), 3351-3356.
REDDY B.R., PRIYJA D.N., RAO S.V., RADHIKA P., (2005), *Hydrometallurgy*, (77), 253-261.
SOLE K. C., HISKEY J.B., (1992), *Hydrometallurgy*, (30) 345-365.

Gajda B., Bogacki M.B., *Laboratoryjna symulacja rozdzielu jonów niklu(II) i kobaltu(II) w przeciwnieprądowym – ciągłym ekstraktorze*, *Physicochemical Problems of Mineral Processing*, 40 (2006), 195-201 (w jęz. ang.).

W pracy przedstawiono badania związane z zastosowaniem ekstrahenta CYANEX 272 (kwas di(2,4,4-trimetylopentylo)fosfinowy) do ekstrakcyjnego rozdzielania jonów niklu(II) i kobaltu(II) z roztworu siarczanowego. Stwierdzono, że wartości $pH_{0.5}$ wynoszą 4.6 i 5.7 odpowiednio dla jonów kobaltu(II) i niklu(II), co pozwala na selektywny rozdział tych jonów. Przeprowadzona symulacja w warunkach laboratoryjnych przeciwnieprądowego trzystopniowego procesu ekstrakcyjnego pozwala stwierdzić, że w procesie takim możliwe jest selektywne rozdzielanie jonów kobaltu(II) od jonów niklu(II) jedynie w przypadku kontroli pH fazy wodnej.

R. KUCEROVA, P. FECKO*

BIODEGRADATION OF PAH, PCB, AND NEL SOIL SAMPLES FROM THE HAZARDOUS WASTE DUMP IN POZD'ÁTKY (CZECH REPUBLIC)

Received March 15, 2006; reviewed; accepted May 15, 2006

The objective of the project was a laboratory check of biodegradation of soil samples contaminated by PAH(s), PCB(s) and NEL from the hazardous waste dump in the Pozd'átky locality. For the laboratory check, pure bacterial cultures of *Rhodococcus sp.* and *Pseudomonas putida* have been used. It is apparent from the laboratory experiments results that after one-month bacterial leaching, applying the bacterium of *Rhodococcus sp.* there is a 66 % removal of NEL, a 67 % removal of PAH(s) and a 14 % removal of PCB(s). Applying a pure culture of *Pseudomonas putida* there is a 76 % removal of NEL, a 25 % removal of PAH(s) and a 14 % removal of PCB(s).

Key words: contamination, biodegradation, organic pollutants

INTRODUCTION

Human activities lead to the contamination of our planet by organic and inorganic pollutants. The pollution is spreading and it represents a real threat to a healthy development of mankind, animals and plants. One of the most questionable is the group of persistent – exceptionally resistant substances which have been produced by man in significant amounts in the course of last 50 years in the form of herbicides, pesticides, insecticides, as well as they are present in many industrial products (e.g. capacitor, transformer or hydraulic charges).

For degradation of classical biogenic compounds, which have been present in the environment for millions of years, microorganisms have developed special mechanisms. Xenobiotics, i.e. synthetic substances produced by man, have been more abundant in the environment only for a few decades. Nevertheless, microorganisms are able to use some of these compounds as the only sources of carbon and energy

* VSB - Technical University of Ostrava. Faculty of Mining and Geology 17 listopadu 15,
708 33 Ostrava-Poruba, Czech Republic.

(Brenner, 2003). The fate and direct removal of extraneous substances from the environment mainly depends on their metabolism intermediated by enzyme systems of organisms forming trophic (food) chains.

Biotechnological processes include mining, dressing and processing methods, during which post reaching the desired qualitative changes of raw materials and refuse, they make use of microorganisms or products of their metabolic activity. Basically, nature develops these systems on her own, and unconsciously people have been using their products since the beginning of their history. Biotechnologies embrace mainly microbiological, biochemical and chemical knowledge.

Biodegradation of hazardous harmful substances in the environment embody significant prospective methods, when complex and ecologically unsound pollutants are decomposed into simpler substances (sound ones) by the action of microorganisms. The principle of biodegradation technologies is an optimization of nutrient ratios (to support the growth of selected microorganisms able to degrade the target contaminants) and an application of suitably selected isolated microorganism strains with relevant degradation abilities.

Previously suggested decontamination technologies were often very costly and severe to the environment. There is though a tendency to propose and apply procedures that are not only cheaper but also more natural. One of the prospective ways is a biological decontamination of the environment by means of microorganisms and plants (Páca, 2003).

Currently, biodegradation technologies, biological methods to remove a variety of pollutions are being improved in an intense way. Biodegradation technologies first proved practical on a wider scale during an oil spill of Exxon Valdez tanker, since then they have been used more frequently in the majority of countries. In the Czech Republic, this trend began to develop after 1989. These are mainly biodegradation technologies designed for the decontamination of soil and water contaminated by oil substances and their derivatives, for the decontamination of coal tar-phenol pollutions and last but not least for the decontamination of persistent organic pollutants (xenobiotics). Since 2000 a number of companies dealing with this issue have been active in the Czech Republic. Already now, some of them reach very good results and they make use of technologies on a worldwide level. For example, in the Czech Republic hundreds of tons of contaminated soils by oil substances are annually treated by the technologies of biological improvement in many decontamination sites.

The application of biological improvement technologies should be preferred to physical and chemical methods as in principal they remove only the share of contamination in question. Moreover, in some cases, these methods harm the environment even more than the very pollution. The advantage of biodegradation of contaminated soils by oil substances is the fact that in the course of microbial degradation no waste materials polluting the environment are formed (the final products are carbon dioxide and water in the last stage).

One of the problems during the application of decontamination technologies based on biological methods in the CR are insufficient valid general rules and missing specific legislation in the aspect of removal of old ecological burdens. At present, biotechnologies fall under the State Health Institute of the CR and the State Hygiene Stations in terms of occupational safety and public health protection.

In the course of application of biodegradation methods it is necessary to keep in mind that it is a complex process. Their success, or failure depend on the following factors:

- chemical (types of contaminant, pH medium, concentration of macro and microbiogenic elements, water content, chemical composition of the contaminated material, chemical composition and concentration of suitable nutrient solutions, etc.),
- microbiological (degradation activity of microorganisms),
- physical (temperature, water solubility, sorption onto solid particles).

Without external interference, the speed of a natural biodegradation process in the improved localities is very low. An appropriate improvement method may increase the speed of biological processes several times.

WAYS OF BIODEGRADATION OF AROMATIC AND POLYAROMATIC HYDROCARBONS

GENERAL PRINCIPLE

Degradation of organic substances by means of microorganisms makes part of the natural carbon cycle in the nature. The process of biodegradation is based on the abilities of microflora to use the present harmful substances as a source of carbon and energy for their own growth. The ability of microorganisms to degrade hydrocarbons has been known since 1895, when a growth of yeast fungus on paraffin was described. Later, the ability of bacteria to use methane as a source of carbon was discovered, and finally in 1969 Davis et. al. (Žebrák, 1997) proved that there are bacteria degrading virtually all component parts of crude oil. Prokaryotes (bacteria and cyanobacteria) as well as eukaryotes (fungi including yeast fungus, algae and protists) assert one selves in these cases. In addition, archaeobacteria play an important role in many cases.

More than 200 microorganism species capable of hydrocarbon degradation have been identified. They follow in the order of importance: heterotrophic bacteria, fungi, aerobic bacteria, actinomycetales, phototrophes and oligotrophic bacteria. The most applied bacteria fall under the genders of *Pseudomonas*, *Arthrobacter*, *Acinetobacter*, *Flavobacterium*, *Alcaligenes*, *Micrococcus* and *Corynebacterium* (Masák, 1992). Intense research in this area confirms that besides bacteria, other microorganisms, including fungi and algae, can be used.

The ability of biodegradation is given by enzymatic make-up of the individual bacterial genders. The enzymatic spectrum of a given cell is given by its genetic

potential. A part of genes coding enzymes utilisable for biodegradation are found in the DNA of plasmids. Plasmids usually carry complement information which is not vital for the cell under normal circumstances and whose loss is not lethal to the cell. However, sometimes it can be an advantage in certain special conditions. In that respect, catabolic plasmids are very important as they permit their cells to use non-traditional sources of energy.

Basically, biochemical processes during which the decay of hydrocarbons occur, can be divided into two fundamental groups, i.e. anaerobic processes taking place with the access of oxygen and anaerobic processes taking place without the access of oxygen. As the anaerobic degradation is very slow, mainly aerobic processes are used in practice.

Benzene and non-substituted polyaromatic hydrocarbons, hereinafter referred to as PAH(s), have a high negative resonance energy, and therefore they are thermodynamically very stable, which reflects in their chemical properties. In practice, usually 16 polycyclic aromatic hydrocarbons are monitored, which are on the list of priority pollutants of US EPA. PAH(s) range among persistent organic pollutants. Their molecules are formed by two or more condensed benzene nuclei. Bonding of other substituents (e.g. halogen-, sulfo-, amino-, nitro-) onto the benzene nucleus, the reactivity of the nucleus resonance structure towards oxygen falls considerably and the circle becomes more resistant to opening (Holoubek, 2000).

CHARACTERISTICS OF PSEUDOMONAS BACTERIA

Pseudomonas bacteria are gram-negative, chemoorganotrophic, aerobe obligate, aerobically respiratory metabolisms. Some species are facultative chemolithotrophic. They are straight or curved rods. Their dimensions range between 0.5 and 1.0 μm x 1.5 – 4.0 μm . They move by one or more polar-located flagella. They are arranged mainly individually or in small clusters or chains. They grow under strict aerobic conditions in common substrates, on which they form irregularly large colonies producing water-soluble exopigment (pyocyanine and fluoresceine), which diffuse into the atmosphere and dyes it yellow or blue-green. Older cultures dye dark brown. The temperature range of their growth is 0 – 42 °C; the optimum temperature is 35 °C. The enzymatic activity is dependent on ecological conditions out of which the individual genders were isolated. They make use of some sugars, out of which they form acids, but not gas. Many genders oxidize glucose into gluconic acid, 2-keto-gluconic and other acids. The majority of the studies genders reduce nitrates down to nitrites. They live saprophytically in soil and water. There appears a high affinity with the *Vibrio* and *Xantomonas* genders. In total, there are approximately 29 genders. Figure 1 shows *Pseudomonas putida* bacteria.

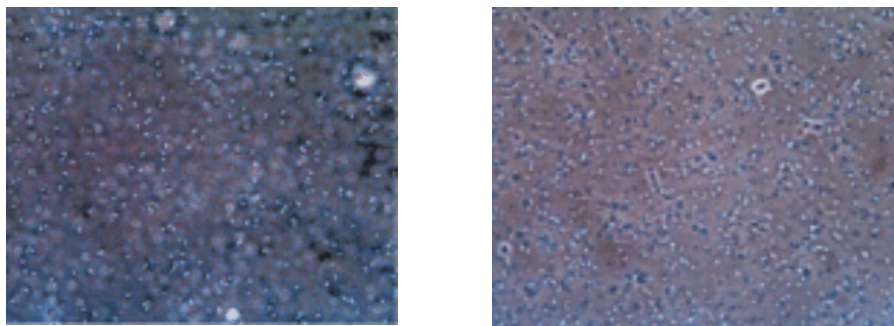


Fig. 1. *Pseudomonas putida*

CHARACTERISTICS OF RHODOCOCCUS SP. BACTERIA

These are gram-negative, chemoorganotrophic, aerobe obligate, aerobically respiratory metabolisms. The cells are of a spheroidal shape. The average size of the cells fluctuate between 0.5 and 3.5 μm ; they appear individually or two and more cells aggregate into irregular clusters, sometimes tetrads or bundles. They grow under aerobic conditions in common substrates, under the optimum temperature of 25 – 35 $^{\circ}\text{C}$. On the substrates they form shiny colonies with the dimensions of 2 – 4 μm . Many colonies precipitate pigments of various colours (pink, yellow, orange). In the nature, they occur as saprophytes. Figure 2 shows *Rhodococcus sp.* bacteria.

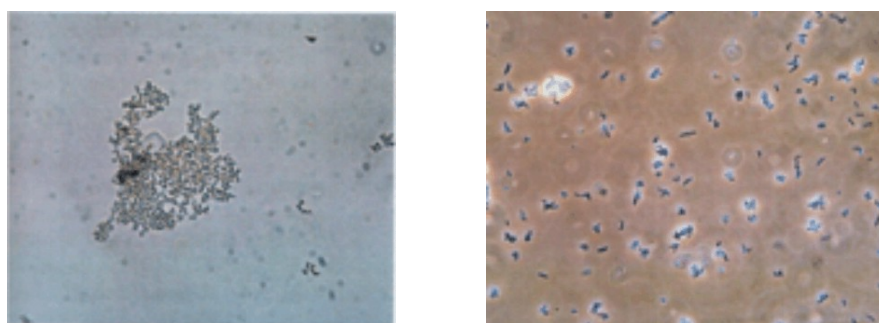


Fig. 2. *Rhodococcus sp.*

METHODS OF THE EXPERIMENTAL WORK

The experimental biodegradation of the selected harmful substances – PAH(s), PCB(s) and NEL - took place with a soil sample from the hazardous waste dump and municipal refuse dump near Pozďátky, Třebíč district. It was carried out by means pure cultures of *Pseudomonas putida* and *Rhodococcus sp.* bacteria. These

microorganism cultures were acquired from the Czech collection of microorganisms with the Natural Science Faculty at the Masaryk University in Brno.

In the course of the cultivation works the following media were made use of:

- liquid medium M1 (Beef extract Broth, peptone, NaCl, distilled water, pH 7.2),
- liquid medium M96 (Mineral Medium with Vitamins, Media, Bacteria, pp. 123),
- liquid medium M65 (Mineral Medium for Chemolitotrophic Growth H-3, Media, Bacteria, pp. 120).

The check of bacteria viability and an approximate determination of their number is done by means of a microscope. For this task we used the Carl Zeiss Jena "Amplival" microscope and Cyrus I cell with a raster for reading the number of bacteria. The enlargement ratio of the microscope ranged from 400 (reading the number of bacteria) up to 1000-fold enlargement (observation of bacteria viability). Post treatment, the mineralogical composition of the sample was determined by an X-ray diffraction analysis in the laboratory of the Institute of Geological Engineering at VŠB – TU Ostrava. The measurement was carried out using a modernized, fully-automated diffractometer URD-6 (Rich. Seifert-FPM, SRN). With the given sample, the following phases were identified: quartz, microcline, plagioclase, amphibole chlorite, biotite, illite – montmorillonite.

The determination of NEL, PAH(s), and PCB(s) was carried out in an accredited laboratory for fuels, waste and water of VÚHU, a.s. Most. In total, the laboratory experiment lasted four weeks. 100 g of soil, 100 ml of bacterial solution and 500 ml of substrate were inserted into 1-litre containers which were following closed. Aeration was secured by means of aquarium pumps. The required volume was gradually filled with distilled water. Samples for analyses were taken after one and four weeks.

THE RESULTS OF BACTERIAL BIODEGRADATION

It is apparent from the results of bacterial leaching using a pure bacterial culture of *Rhodococcus sp.* that after one-month leaching it is possible to remove 66 % of NEL, 67 % of PAH(s) and 14 % of PCB(s) from the sample. The results are shown in Table 1. In the table Σ PAH(s) represents 15 individual polyaromatic hydrocarbons. It is apparent that the application of this bacterial culture is suitable for the degradation of PAH(s) and NEL. However, the degradation of PCB(s) is very low.

Table 1. The course of degradation of the selected harmful substances by means of *Rhodococcus sp.* bacteria (values stated in mg/kg solid)

	NEL	Σ PAH(s)	Σ 7 congeners PCB(s)
Input	255	6.7	0.07
One week	160	5.5	0.06
Four weeks	87	2.2	0.06

The results of bacterial leaching applying a pure bacterial culture of *Pseudomonas putida* imply that after one-month leaching it is possible to remove 76 % of NEL, 25 % of PAH(s) and 14 % of PCB(s) from the sample. The results are displayed in Table 2. In the table, Σ PAH(s) represents 15 individual polyaromatic hydrocarbons. It is apparent from the acquired results that the application of this bacterial culture is suitable for the degradation of NEL and PCB(s), but the degradation of PAH(s) is low.

Table 2. The course of degradation of the selected harmful substances by means of *Pseudomonas putida* bacteria (values stated in mg/kg solid)

	NEL	Σ PAH(s)	Σ 7 congeners PCB(s)
Input	255	6.70	0.07
One week	125	6.10	0.06
Four weeks	60	5.05	0.06

The results imply that for the given sample the most suitable is the application of *Rhodococcus sp.* bacteria with which the best biodegradation results have been acquired.

CONCLUSIONS

The objective of the project was a laboratory check of biodegradation of NEL, PAH(s), and PCB(s) with a soil sample from the Pozd'átky locality. The acquired results show that for the given sample it was more convenient to apply the bacterial culture of *Rhodococcus sp.*, as the removal efficiency of PAH(s) was 67 % and of NEL it was 66 %; though, for the removal of PCB(s) these culture appears inefficient. Better results could be reached by prolonging the period of biodegradation or an application of adapted bacterial cultures.

ACKNOWLEDGEMENT

The authors of the project would like to thank the Grant Agency of the Czech Republic which financially supports this project, under the GAČR No 105/05/0004.

REFERENCES

- BRENNER, V. (2003), *Biodegradace perzistentních xenobiotik*, Biodegradace VI, pp. 45 - 47, Seč.
 HOLOUBEK, I.; VOKOUNOVÁ, Š.; KOMPRDA, J. (2000), *Perzistentní organické polutanty v atmosféře a půdách, těkání z půd*, Ochrana ovzduší č. 3, Praha.
 MASÁK, J. et al. (1992), *Speciální mikrobiální technologie*, VŠCHT Lecture Notes.
 PÁCA, J.; SUCHÁ, V.; MIKŠANOVÁ, M.; STIBOROVÁ, M. (2003), *Enzymy kvasinky Candida tropicalis participující na biodegradaci fenolu*, Biodegradace VI, pp. 9 - 13, Seč.
 SEZIMA, T. (2003), *Biodegradace vybraných škodlivin v půdách a vodách*. Doctoral Thesis, VŠB – TU Ostrava.
 ŽEBRÁK, R. (1997), *Biotechnologické metody sanací kontaminovaných zemin a vod*. Lecture of Biodegradace, spol. s r.o. Ostrava.

Kucerova R., Fecko P., *Biodegradacja PAU, PCB I NEL w próbach gleby pochodzących ze składowiska niebezpiecznych odpadów w Pazdatky (Republika Czech)*, Physicochemical Problems of Mineral Processing, 40 (2006), 203-210 (w jęz. ang.).

Przedmiotem badań było sprawdzenie, w warunkach laboratoryjnych, możliwości przeprowadzenia procesu biodegradacji próbek gleby zawierających PAH, PCB i NEL. Próbki gleby pochodziły z hałdy niebezpiecznych odpadów zlokalizowanej w Pazdatky (Republika Czech). W badaniach laboratoryjnych zostały wykorzystane czyste szczepy bakterii *Rhodococcus* sp. i *Pseudomonas putida*. Przeprowadzone badania biodegradacji wykazały, że po okresie jednego miesiąca, stosując bakterie *Rhodococcus* sp. zostało zbiodegradowanych 66% NEL, 67% PAH i 14% PCB. Stosując czysty szczep *Pseudomonas putida* w analogicznych warunkach, otrzymano następujące wyniki biodegradacji: 76 % NEL, 25 % PAH i 14 % PCB.

Agnieszka SZUBERT, Michał ŁUPIŃSKI, Zygmunt SADOWSKI*

APPLICATION OF SHRINKING CORE MODEL TO BIOLEACHING OF BLACK SHALE PARTICLES

Received June 1, 2006; reviewed; accepted June 30, 2006

Four size fractions of a black shale ore originating from the Lubin Copper Mine (Southwestern Poland) were leached in a small column using autotrophic bacteria (*Acidithiobacillus ferrooxidans*). The best results of bioleaching were obtained for the most fine fraction, where the copper recovery was 84%, and the surface area of the ore increased from 4.50 m²/g to 13.74 m²/g. Based on the shrinking core model, a new model describing bioleaching of the black shale type ore in a column is proposed. The model is based on assumption of dependence of copper recovery and surface area increase during the process.

Key words: bioleaching, shrinking core model, black shale

INTRODUCTION

Much attention was focused on studies of shrinking core models in the last years (Brochot, 2004; Crundwell, 1997; Lapidus, 1992; Pritzker, 1996, 2003; Vegliò, 2001; Velardo, 2002, and others). They adapted earlier model equations to their experiments.

Liddell (2005) remarked that two facts about early development of shrinking core models have been overlooked. The first was focused mostly to gas-solid systems, and it was proposed by Levenspiel (1979). The author finds the shrinking core model as the simplest for reactions of gas with particles of unchanging size. He suggests, it must be a sharp reaction front between a porous product layer called "ash" and the fresh reactant, and shows that the three resistances controlling the shrinkage process are possible: diffusion of the reactant through the gas film surrounding the particle, diffusion of the reactant through the ash layer and a reaction at the unreacted core. Since 1960s, the use of shrinking core model for solid-liquid systems was examined (Chae, Wadsworth 1978, Veglio et al., 2001). The model considers the reaction of the

* Wrocław University of Technology, Faculty of Chemistry, Department of Chemical Engineering, Zygmunt.Sadowski@pwr.wroc.pl

reactant at the surface of the solid particle, which results in both aqueous and solid products which may form on the surface of the particle. As reaction proceeds, the unreacted core of the particle is reduced in size, while more solids and aqueous products are formed (Crundwell, 1995). It is important to notice that most of these models involve the pseudo-steady state (PPS) approximation (Liddell, 2005) to make the reactant concentration across the porous ash layer determination possible.

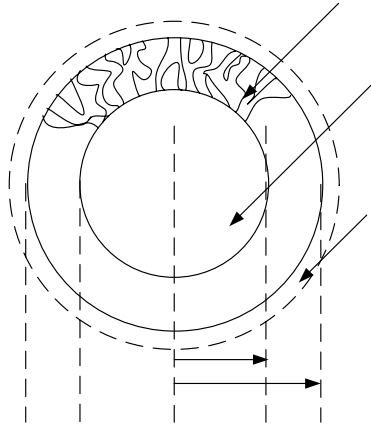


Fig. 1. Shrinking core particle

For a spherical particle (Fig.1) involving the quasi-steady state diffusion of the reactant through the previously reacted portion of the particle, followed by the chemical reaction at the surface of the unreacted core, it is useful to express the reaction rate in terms of fraction reacted (i.e. particle conversion) (Chae, 1979; Burghardt, 2001; Liddell, 2005). Describing the shrinkage process, the authors relate the fraction reacted (α) with reaction time (t) in equations. If the process is controlled by the reactant diffusion through the fluid surrounding the particle (Burghardt, 2001):

$$\frac{t_f}{t_f^*} = 1 - \left(\frac{r_c}{R}\right)^3 = \alpha \quad (1)$$

where, t_f^* is the time required for the particle to react completely, r_c is the unreacted core radius at given time, and R is the initial particle radius. If the reaction is controlled by product layer diffusion (ash diffusion), then:

$$\frac{t_a}{t_a^*} = 1 - 3\left(\frac{r_c}{R}\right)^2 + 2\left(\frac{r_c}{R}\right)^3 = 1 - 3(1-\alpha)^{2/3} + 2(1-\alpha), \quad (2)$$

where, similarly to Eq. 1, t_a^* is the time required for the particle to react completely. When the process is controlled by the chemical reaction:

$$\frac{t_r}{t_r^*} = 1 - \left(\frac{r_c}{R} \right) = 1 - (1 - \alpha)^{1/3}. \quad (3)$$

There are different ways to find out the mechanism controlling the shrinkage process (Eq. 1-3), e.g. experiments using different particles radius (R_1 , R_2) are carry out, regarding different times (t_1 , t_2) necessary to attain the same particle conversion. In the case of the reactant diffusion through the fluid surrounding the particle control:

$$\frac{t_1}{t_2} = \left(\frac{R_1}{R_2} \right)^{1.5-2.0} \quad (4)$$

If the process is controlled by “ash diffusion”:

$$\frac{t_1}{t_2} = \left(\frac{R_1}{R_2} \right)^2 \quad (5)$$

For chemical reaction control:

$$\frac{t_1}{t_2} = \frac{R_1}{R_2} \quad (6)$$

In hydrometallurgy the shrinking core models are generally applied to describe the shrinkage of ore particles during mineral leaching reactions, which are a central unit operation in the hydrometallurgical ores treatment. The model is applied to description of the leaching process both for column or heap leaching (Lizama, 2004, 2005, Chae, 1979) and for stirred-tank reactors, including continuous systems (Crundwell, 1995). There are also literature data on the use of the shrinking core model for modelling of bacterial leaching processes. Most of the data concern sulphide ores bioleaching (Brochot, 2004; Conner, 2005, Leachy, 2005).

Bioleaching of sulphide minerals consists of oxidation of ferric ions, resulting in release of metal ions to the leaching solution, and formation of a sulphur layer (McGuire, 2001). At present, bioleaching processes are based on activity of chemolithotrophic bacteria like *Acidithiobacillus ferrooxidans*, which are able to act in an acid environment, and which convert metal sulphides via biochemical oxidation reactions into water-soluble metal sulphates (Bosecker, 1997). In principle, metal can be released from sulphide minerals by direct and indirect bacterial leaching (Sadowski, 2005).

Heap leaching is usually simulated in columns charged with ore where leaching solution percolates from the top (Lizama, 2004). At steady state conditions, metal leaching has been described as being pore-diffusion controlled by a reacted porous zone surrounding a region of unreacted ore, correlate to shrinking core model (Braun, 1974). However, Lizama (2004, 2005) proved that the shrinking core equation does not apply at the initial stages of bioleaching, which was due to an initial period of bacteria cells colonization on the ore surface.

In this study, a model for column bioleaching of Polish copper-bearing black shale ores is investigated to identify and understand aspects of bacteria in bioleaching applications, which can have implications in heap bioleaching operations. Based on general assumptions of the shrinking core model, new equation describing bioleaching of black shale particles is proposed. The primary assumption for this model equation is that the surface area of the more porous core increases with metal (copper) releasing from it, and that this dependence is constant. The final equation subordinates the black shale surface area from leaching time, taking into account the initial surface area (in m^2/g).

EXPERIMENTAL

The black shale ores used in this study was supplied by the Lubin Copper Mine (KGHM S.A.), Southwestern Poland, and it was in the form of broken core samples consisting of chunks of diameter <5.0 mm. The material was screened into the four size fractions: 5.0 – 4.0 mm, 4.0 - 3.15 mm, 3.15 – 2.5 mm and 2.5 - 1.6 mm. Density (d) of each fraction as well as the results of chemical analyses are presented in Table 1.

Table 1. Chemical analysis of four black shale fractions

Size fraction Chem.analysis	4.0 – 5.0 mm ($d = 2.66 \text{ g/cm}^3$)	4.0 - 3.15 mm ($d = 2.56 \text{ g/cm}^3$)	3.15 – 2.5 mm ($d = 3.16 \text{ g/cm}^3$)	2.5 - 1.6 mm ($d = 3.40 \text{ g/cm}^3$)
Cu [%]	6.02	6.05	6.24	7.03
Fe [%]	1.15	1.07	1.23	1.08
Ni [g/t]	436	440	335	387
V [g/t]	1050	1060	1110	1045
As [%]	0.09	0.085	0.06	0.075
Ag [g/t]	285	223	270	298
C_{tot}^* [%]	11.1	11.3	11.12	11.3
C_{org}^* [%]	7.42	6.85	6.4	7.85

* C_{tot} – total carbon, C_{org} – total organic carbon

Autochthonous bacteria. *Acidithiobacillus ferrooxidans* (F701), obtained from the Practical and Experimental Biology Department of the University of Opole, was used for the bioleaching study. The cultures of 15% *inoculum* were grown at 32°C in shake flasks (170 rpm) at pH = 2.0 in the Silverman and Lundgren 9K nutrient medium (Silverman, 1959). The bioleaching experiments were carried out in small glass column (5/40cm). Figure 2 illustrates the system used in this study. For each experiment, the same weight of each fraction was used. The solid density in all cases was 10% (w/v) provided with 15% of bacterial *inoculum* in mineral medium 0K, containing: KH_2PO_4 : 0.1 g/l and $\text{MgSO}_4 \cdot 7\text{H}_2\text{O}$: 0.1 g/l. The solution was adjusted to pH=2 with 2M H_2SO_4 . Each experiment started in reactors about 3 days before inoculation in order to neutralize carbonates and stabilize leaching solution to pH=2. Solution and solid samples were taken at regular intervals for analysis of copper concentration and the surface area (m^2/g), respectively.

The bacterial growth was checked by Eh (mV), Fe^{2+} and Fe^{3+} measurements. The bacterial activity was found satisfied by observation of Eh changes from 285 mV at the beginning of the process to about 575 mV at the end. Because of relatively low content of iron in the ore, an increase of Fe^{3+} ion concentration and a rapid decrease of Fe^{2+} ions were observed only during 5-6 days of the process.

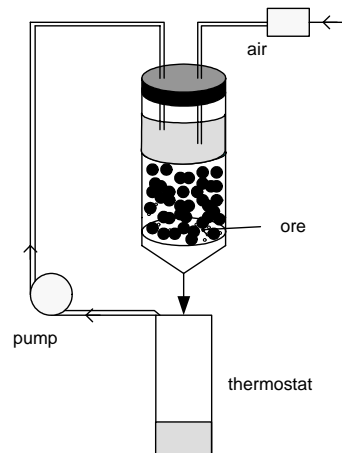


Fig. 2. Schematic representation of apparatus used for black shale ore bioleaching

MATHEMATICAL FORMULATION

Bioleaching of copper-bearing black shale ores is usually described using formulas based on partial differential equation:

$$\frac{\partial c_{Cu}}{\partial t} = -w \frac{\partial c_{Cu}}{\partial x} + r_o, \quad (7)$$

where t denotes time, and x is the column length. In the case when “an ideal mixing” of ore in column is reached, an uniformity of the copper concentration gradient c_{Cu} within the column can be written as:

$$\frac{\partial c_{Cu}}{\partial x} = 0. \quad (8)$$

Based on Eq. 8 we receive a simple differential equation, including the reaction rate r_0 :

$$\frac{\partial c_{Cu}}{\partial t} = -r_0. \quad (9)$$

The fact that the ore surface area [m^2/g] increases during the process, which is due to bacterial penetration into ore particle making the core more porous, is important and helpful for description of the efficiency of copper-bearing ores bioleaching. The primary assumption for our model equation is that the increase of the surface area of the more porous core is directly proportional to decrease of copper concentration in the ore particle:

$$\frac{a - a_0}{c_{Cu}^0 - c_{Cu}} = const = \frac{1}{C}, \quad (10)$$

where a_0 is the initial surface area of ore particles [m^2/g], and c_{Cu}^0 is the initial concentration of copper in the ore particle. By transforming and differentiating Eq. 10:

$$a - a_0 = C \cdot (c_{Cu}^0 - c_{Cu}), \quad (11)$$

$$da = C \cdot (-dc_{Cu}), \quad (12)$$

and by coupling these equations with Eq. 9, we receive:

$$\frac{\partial a}{\partial t} = C \cdot r_0. \quad (13)$$

The core-surface reaction rate is directly proportional to surface area (m^2/g) changes:

$$r_0 = k \cdot a. \quad (14)$$

Substituting Eq. 14 with Eq. 13 we receive the first order differential equation:

$$\frac{\partial a}{\partial t} = C \cdot k \cdot a. \quad (15)$$

In order to make our calculations more simple, a constant B was introduced: $C \cdot k = B$. The solution of this equation for the initial condition: $a(0) = a_0$ can be written as:

$$a(t) = a_0 e^{Bt}. \quad (16)$$

It is known that for an exponential function, as a function of real variable x , the plot of e^x is always positive and continuously increasing. That is why, the function is not useful for describing long-term processes, because going to infinity it assumes values, which don't possess any equivalent in nature. In order to limit the surface area a increasing values, coupled with reaction rate expression, we introduced the "limiting module" $d \cdot (a_K - a)$:

$$r_0 = k \cdot a \cdot d \cdot (a_K - a), \quad (17)$$

and received the new reaction rate equation:

$$\frac{\partial a}{\partial t} = C \cdot k \cdot d \cdot a \cdot (a_K - a). \quad (18)$$

The constants of the equation are included into constant B :

$$\frac{\partial a}{\partial t} = B \cdot a \cdot (a_K - a). \quad (19)$$

For initial condition: $a(0) = a_0$, after the variables separation the solution is:

$$a(t) = \frac{a_0 e^{Bt}}{1 - \frac{a_0}{a_K} (1 - e^{Bt})}. \quad (20)$$

To use Eq. 20 three process parameters have to be known: initial surface area a_0 , reaction conversion parameter B and surface area a_K . The relevance of the parameter a_K , as the maximal surface area of ore increasing during the process can be found by analyses of Eq. 20 for very long periods of time:

$$\lim_{t \rightarrow \infty} \frac{a_0 e^{Bt}}{1 - \frac{a_0}{a_K} (1 - e^{Bt})} = \lim_{t \rightarrow \infty} \frac{a_0}{e^{-Bt} - \frac{a_0}{a_K} (e^{-Bt} - 1)} = \frac{a_0}{0 - \frac{a_0}{a_K} (0 - 1)} = \frac{a_0}{\frac{a_0}{a_K}} = a_K. \quad (21)$$

It is worth to notice that if the time goes to zero $t \rightarrow 0$ we obtain: $e^{Bt} = 1$ (for short periods of time). Thus, the above derived two-parameter Eq. 10 can be useful for determination of B parameter at the beginning of the process.

$$\lim_{t \rightarrow 0} \frac{a_0 e^{Bt}}{1 - \frac{a_0}{a_K} (1 - e^{Bt})} \approx \frac{a_0 e^{Bt}}{1 - \frac{a_0}{a_K} (1 - 1)} = a_0 e^{Bt}. \quad (22)$$

RESULTS and COMMENTS

The overall behavior of copper-bearing shale bioleaching is revealed in Figure 3. As it can be seen there, the best copper recovery (84%) was attained for the most fined (2.5-1.6 mm) fraction. For the 3.15-2.5 mm fraction the percentage of copper recovery was 73%, and for 4.0-3.15 mm and 5.0-4.0 mm fractions the bioleaching yield was almost the same; 66-67%. In comparison to copper recovery, the percentage of Ni bioleaching was very low: the highest recovery of 19% was observed for the most fined fraction. For all fraction very low (about 3%) vanadium extraction was observed. However, in this case a slight decrease of vanadium concentration in leaching solution during the process could be seen. Even the yield of the process was quite low (e.g. in comparison to stirred tank bioleaching). It is worth to notice, that the heap leaching, a very slow process, is usually simulated in columns.

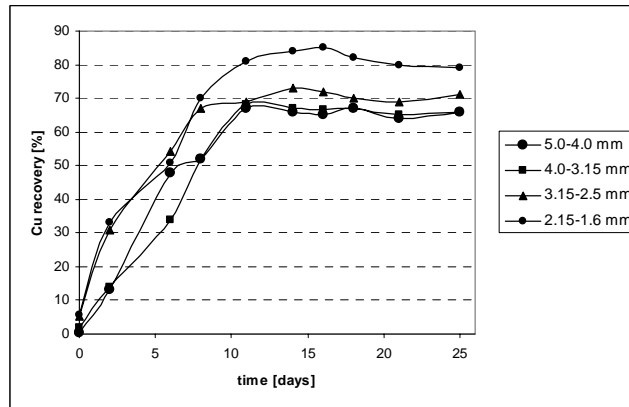


Fig. 3. Copper recovery from Polish black shales bioleaching from different ore size fractions

The kinetics of the process was followed by the iron ions concentration and redox potential Eh [mV] measurements. For the four fractions the increase of Eh from about 256 mV to 565 mV was observed. The most significant changes in Eh were seen during the first 10 days of bioleaching. Also, it was observed that, the Fe^{3+} ions concentration increases and Fe^{2+} ions concentration decreases during first 6-7 days of the process.

Correlating the data of copper recovery and surface area increase (Fig. 4) for all fractions, it is possible to notice that for the most fine fraction, where the copper recovery was the best, the surface area increase was the highest as well. For the others three fractions these values were lower, respectively.

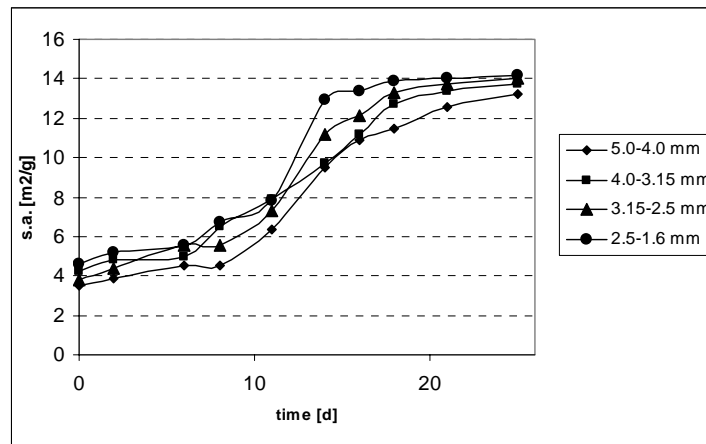


Fig. 4. Black shale surface area increment during bioleaching process

In order to make easier the modelling calculations, the surface area values obtained for all size fractions were averaged and presented in Fig. 5. Equation (14), which is also called the logistic equation, was transformed to the form

$$\ln\left(\frac{a}{a_K - a}\right) = a_K B t + \ln\left(\frac{a_0}{a_K - a_0}\right) = B \cdot a_K \cdot t + D \quad (23)$$

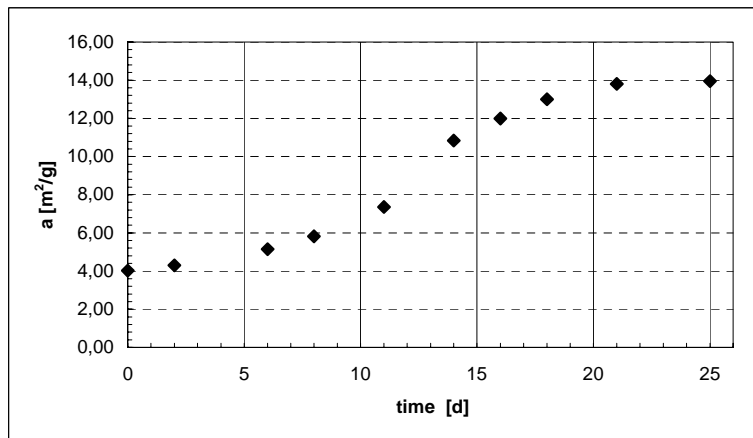


Fig. 5. Average of four size fractions values of surface area obtained during bioleaching process

Assuming $a_K = 14$, the following calculations (Table 2) of process results have been made:

Table 2. Experimental data for logistic equation (23)

l. p.	t	a	$\frac{a}{a_K - a}$	$\ln\left(\frac{a}{a_K - a}\right)$	$D_{theoret} = \ln\left(\frac{a_0}{a_K - a_0}\right)$
1	0	4.02	0.4032	-0.9084	-0.9093
2	2	4.30	0.4433	-0.8135	-0.9093
3	6	5.15	0.5810	-0.5430	-0.9093
4	8	5.83	0.7131	-0.3382	-0.9093
5	11	7.35	1.1061	0.1008	-0.9093
6	14	10.83	3.4164	1.2286	-0.9093
7	16	12.00	6.0000	1.7918	-0.9093
8	18	13.00	13.00	2.5649	-0.9093
9	21	13.80	69.00	4.2341	-0.9093
10	25	13.95	279.00	5.6312	-0.9093

The plotted dependence (Figure 6): $\ln\left(\frac{a}{a_K - a}\right) = f(t)$ is a linear function only in a final stage of the process:

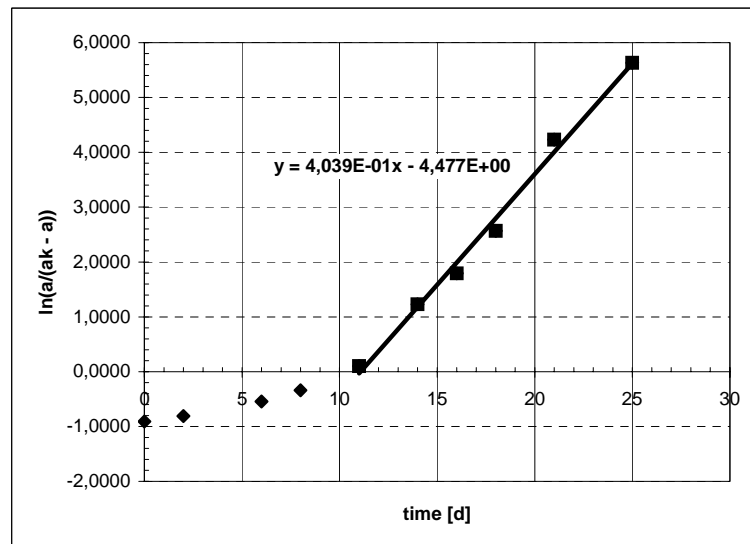


Fig. 6. Linear dependence $\ln\left(\frac{a}{a_K - a}\right) = f(t)$ in the final stage of the process

Based on the correlation line equation (Fig. 6) it is possible to estimate the value of parameter $a_k B$ value: $a_k B=0.4039$, and thus $B=0.0993$ ($\text{g}/(\text{m}^2 \text{ s})$). The value of free-term coefficient $D = -4.477$ differs from those theoretically determined one. It is due to deviations from the ideal model assumptions.

$$a = \frac{a_K}{1 + e^{-(a_K B t + D)}} = \frac{14}{1 + e^{-0,4039t + 4,477}} \quad (24)$$

The model obtained from Eq. (23) is illustrated in Figure 7. As it is seen, it is not possible to describe the first stage of the process using the logistic model due to simplifications assumed. The solution obtained can be useful only to describe the second stage of the black shale column bioleaching. The differences in a character of the two stages of the process can be due to the fact, that the beginning of the process is a period of bacteria cells colonization on the ore surface (Lizama, 2004, 2005).

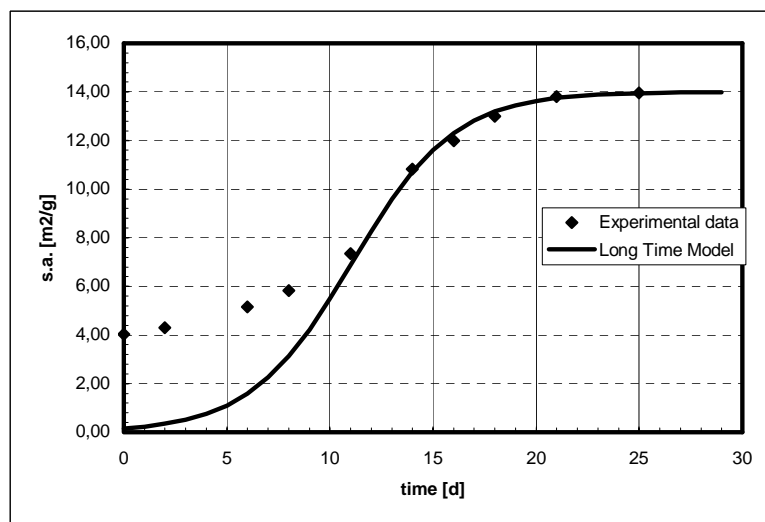


Fig. 7. Relationship between the Long Time Model calculated and experimental surface area data for black shale ore bioleaching

In order to describe the first stage of the process Eq. 16 was used. As above-considered, it is possible to simplify Eq. 16, which after transformation gives the form:

$$\ln(a) = B \cdot t + \ln(a_0) \quad (25)$$

The linear dependence: $\ln(a) = f(t)$, for the first stage process is presented in Fig. 8a. Figure 8b is a magnified Fig. 8a.

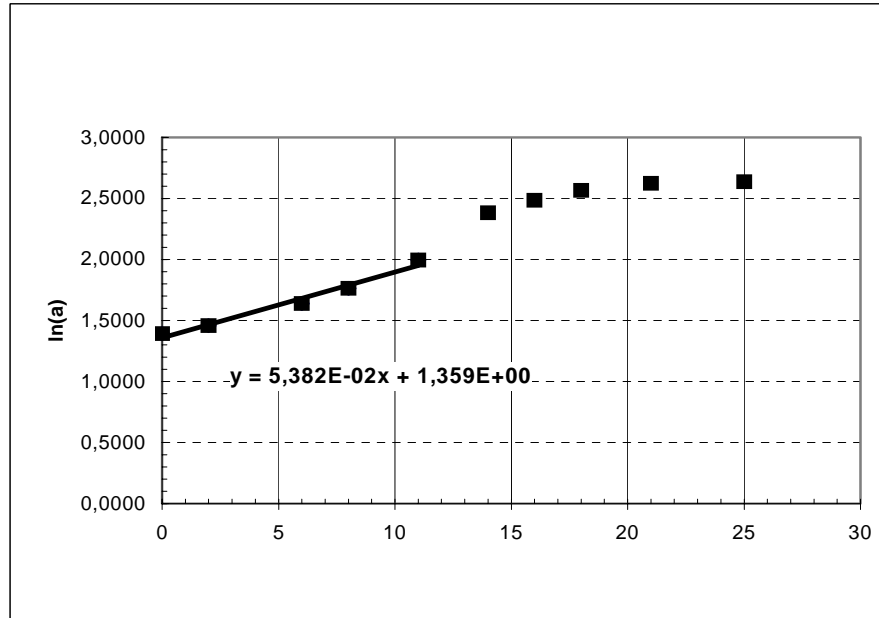


Fig. 8a. Linear dependence at the beginning of bioleaching process: $\ln(a) = B \cdot t + \ln(a_0)$

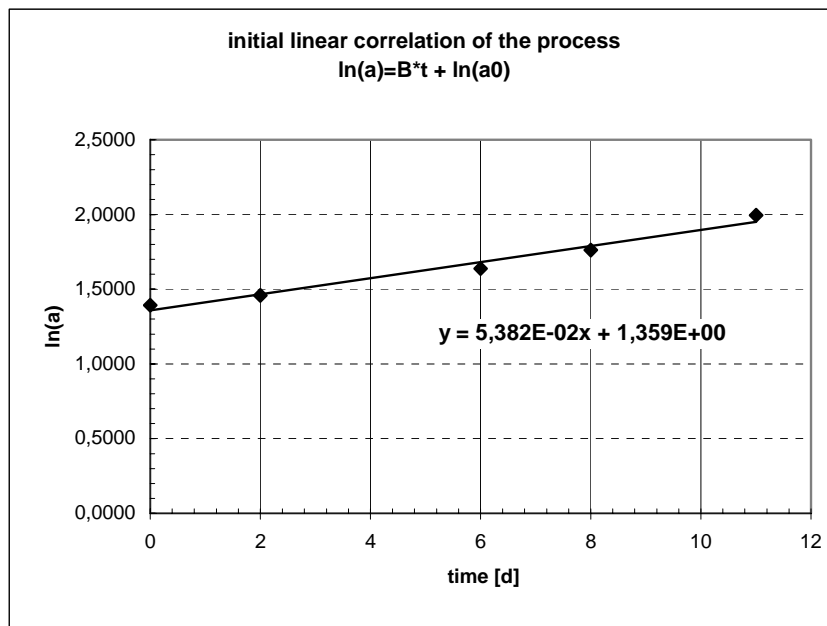


Fig. 8b. Linear dependence at the beginning of the bioleaching process: $\ln(a) = B \cdot t + \ln(a_0)$

Based on the trend line equation (Fig. 8b) we obtained the value of $B = 0.05382$, and a value of the free-term coefficient: $\ln(a_0) = 1,359 \rightarrow a_0 = 3,89$ which is in a great accordance with the experimental data of the initial surface area: $a_0 = 4,02$. It is then possible to assume the simplified model for the first stage of the bioleaching process:

$$a(t) = 3,89e^{0,05382t} \tag{26}$$

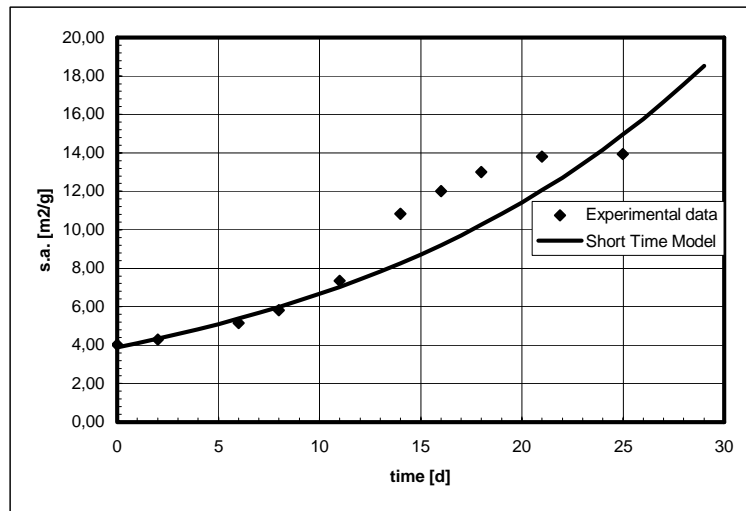


Fig. 9. Relationship between the Short Time Model calculated and experimental surface area data for black shale ore bioleaching

Taking into account both models: for the first and the second stage of the bioleaching process, we receive a correlation presented in Fig. 10.

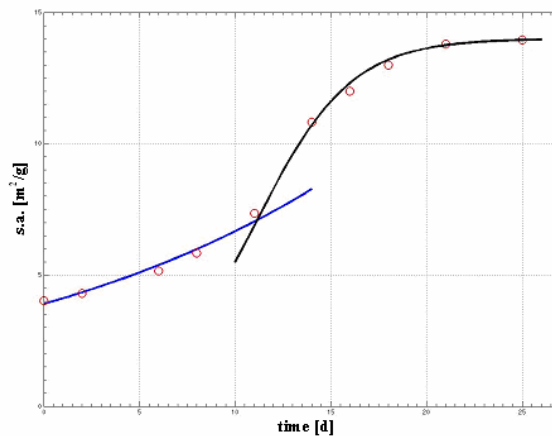


Fig. 10. Relationship between both Short Time and Long Time Models calculated and experimental surface area data for black shale ore bioleaching

CONCLUSIONS

1. The kinetics of bioleaching of the copper-bearing black shale ores can be described using equations based on surface area “ a ” (m^2/g) of the ore.
2. For the beginning of the process description the logistic equation can be used, assuming its simplified form. It is necessary to take into account a separation of the first stage of the process from the second one. For the first stage the kinetics of the process has an exponential character, while the kinetics of the second stage is strongly limited by the character of the system.
3. For the first stage of the bioleaching only one parameter B_1 has to be found. For the second stage two parameters are needed in order to describe the process more precisely: B_2 and corrective factor D . This is due to complications resulting from a two-step transport of substrates (to the surface and through the porous layer). The parameters a_0 and a_k are estimated taking into account the characteristics of the bioleached ore.
4. The assumption of correlation between the percentage of copper recovery and the surface area increase (Eq. 4) is correct.
5. The percentage of Cu recovery was the best for the most fine size fraction: 84%. For the other three fractions the area of the process was lower. The nickel recovery was also low, and no vanadium extraction was observed.
6. Bibliographic studies on simple mathematical models allowed to propose easy bioleaching model equations which can be used in practice.

ACKNOWLEDGEMENTS

The investigations were supported by the BIOSHALE project No. 505710 UE. One of authors (AS) wishes to thank the Ministry of Science and High Education for providing financial assistance in the form of doctoral research scholarship.

REFERENCES

- BRAUN R.L., LEWIS A.E., WADSWORTH M.E., 1974, *In-place leaching of primary sulphide ores: laboratory leaching data and kinetics model*, Metallurgical Transactions, 5, 1717-1726.
- BROCHT S., DURANCE M.V., VILLENEUVE J., d'HUGUES P., MUGABI M., 2004, *Modelling of the bioleaching of sulphide ores: application for the simulation of the bioleaching/gravity section of the Kasese Cobalt Company Ltd process plant*, Minerals Engineering, 17, 253-260
- BURGHARDT A., BARTELMUS G., 2001, *Inżynieria reaktorów chemicznych II – Reaktory dla układów heterogenicznych*, PWN, Warszawa 339-345.
- CHAE D., WADSWORTH M.E., 1979, *Modeling of the Leaching of Oxide Copper Ores*. US Bureau of Mines 1-21.
- CONNER B.D., 2005, *Bioleaching and electrobioleaching of sulphides minerals*, Master of Science in Chemical Engineering, West Virginia University, Morgantown, West Virginia.
- CRUNDWELL F.K., 1995, *Progress in the mathematical modeling of leaching reactors*, Hydrometallurgy, 39, 321-335.
- CRUNDWELL F.K., GODORR S. A., 1997, *A mathematical model of the leaching of gold in cyanide solutions*, Hydrometallurgy, 44, 147-162.

- McGUIRE M.M., EDWARDS K.J., BANFIELD J., HAMERSR R.J., 2001, *Kinetics, surface chemistry, and structural evolution of microbially mediated sulfide mineral dissolution*, *Geochimica et Cosmochimica Acta*, 65, 1243–1258.
- LAPIDUS M., GRETCHEN P., 1992, *Mathematical modelling of metal leaching in nonporous minerals*. *Chem. Eng. Sci.*, 47, 1933–1941.
- LEAHY M. J., DAVIDSON M. R., SCHWARZ M. P., 2005, *A two-dimensional CFD model for heap bioleaching of chalcocite*, *ANZIAM J.* 46(E), C439–C457.
- LEVENSPIEL O. 1979. *The Chemical Reactor Omnibook*, OSU Book Stores. Inc., Corvallis.
- LIDDELL K., NONA C., 2005, *Shrinking core models in hydrometallurgy: What students are not being told about the pseudo-steady approximation*, *Hydrometallurgy*, 79, 62–68.
- LIZAMA H.M., 2004, *A kinetic description of percolation bioleaching*, *Minerals Engineering*, 17, 23–32.
- LIZAMA H.M., HARLAMOVS J.R., McKAY D.J., DAI Z., 2005, *Heap leaching kinetics are proportional to the irrigation rate divided by heap height*, *Minerals Engineering*, 18, 623–630
- PRITZKER M.D., 1996, *Shrinking-core model for systems with facile heterogeneous and homogeneous reactions*. *Chem. Eng. Sci.*, 51, 3631–3645.
- PRITZKER M.D., 2003, *Model for parallel surface and pore diffusion of an adsorbate in a spherical adsorbent particle*, *Chem. Eng. Sci.*, 58 473 – 478.
- SADOWSKI Z., 2005, *Biogeochemia, wybrane zagadnienia*, Oficyna Wydawnicza Politechniki Wrocławskiej.
- SIRVERMAN M.P., LUNDRGREN D.G., 1959, *Studies on the chemoautotrophic iron bacteria *Ferrobacillus ferrooxidans*. An improved medium and harvesting procedure for securing high yields*, *J. Bacteriol.*, 77, 642-647.
- VEGLIO F., TRIFONI M., PAGNANELLI F., TORO L., 2001, *Shrinking core model with variable activation energy: a kinetic model of manganiferous ore leaching with sulphuric acid and lactose*, *Hydrometallurgy*, 60, 167–179.
- VELARDO A., GIONA M, ADROVER A., PAGNANELLI F., TORO L., 2002, *Two-layer shrinking-core model: parameter estimation for the reaction order in leaching processes*, *Chemical Engineering Journal*, 90, 231–240.

Szubert A., Łupiski M., Sadowski Z., *Zastosowanie modelu kurczącego rdzenia do opisu bioługowania ziaren rudy łupkowej*, *Physicochemical Problems of Mineral Processing*, 40 (2006), 211-225 (jęz. ang.).

Cztery klasy ziarnowe rudy łupkowej, otrzymanej z kopalni Lubin (Polska Miedź S.A.), zostały poddane procesowi bioługowania w kolumnie. Do procesu bioługowania wykorzystano autotroficzne bakterie *Acidithiobacillus ferrooxidans*. W wyniku procesu bioługowania odzyskano 84 % miedzi z najdrobniejszej frakcji rudy (2,5-1,6 mm). W trakcie procesu bioługowania nastąpił wyraźny wzrost wielkości powierzchni właściwej ługowanych ziaren mineralnych. Początkowa wartość rozwinięcia powierzchni wynosiła 4,50 m²/g a po procesie bioługowania osiągnęła wartość 13,74 m²/g. Opracowany został nowy model bioługowania rudy łupkowej w kolumnie. Nowy model bazuje na istniejącym i opisanym w literaturze modelu kurczącego się rdzenia. Nowy model poprawnie opisuje otrzymane wyniki eksperymentalne.

Remigiusz MODRZEWSKI, Piotr WODZIŃSKI*

A METHOD OF DESIGNING MEMBRANE SCREENS

Received March 5, 2006; reviewed; accepted June 1, 2006

A model of screening granular materials on a membrane screen is presented in this study. A device which was a subject of research is an experimental frame screen with a membrane sieve used to screen very fine materials. The proposed design method can be used to assess sieve dimensions suitable for the process conditions. Screening efficiency is one of the elements taken into account in the method. A mathematical description of screening is proposed in the form of the simple equation and coefficients of this equation are specified.

Key words: membrane sieve, separation, screening efficiency, mathematical model

INTRODUCTION

The subject of this study is the membrane screens with vibrating sieves. The work is a next step of the research project dealing with the screens that is carried out in the Department of Process Equipment, Lodz Technical University. In general, the project covers two areas: dynamics of membrane sieve motion, and screening of fine granular materials on this sieve. The present study refers to the latter one, i.e. ability to screen granular media. It is a basis for drawing capacity-efficiency diagrams which are used to determine the efficient screening output at basic process parameters.

The authors propose a process description using mass balance equations for individual control volumes into which the granular layer, moving and screened on the membrane sieve, has been divided. The aim of this research was to determine an efficiency function, i.e. a relation that describes changes of screening efficiency along the membrane sieve length. Knowing this function for particular independent variables specific for a given screening case, we can assess and design the membrane sieve surface in a given case.

* Technical University of Łódź, Faculty of Process and Environmental Engineering, Department of Process Equipment, Granular Material Classification Group.

EXPERIMENTAL MEMBRANE SCREEN

The research was carried out in the lab at the Department of Process Equipment, Technical University of Lodz. The tested machine was an experimental frame screen with a membrane sieve, designed and built in the Department of Process Equipment, Technical University of Lodz. It was used to screen fine and very fine materials. The machine was mounted in the experimental set-up shown schematically in Fig. 1.

Supporting structure 1 is the frame of the machine. Riddle 2 with sieve 3 is placed in the frame at different angles. The riddle remains motionless during the screen operation. In the experiments a standard woven wire screen was used. It has rectangular mesh with side length: $l = 0.63$ mm. Flat springs 4 are mounted on the riddle and on these springs drive frame 5 is located. The drive frame is connected to electrovibrators 6. An electromagnetic vibrator or vibrators can also be applied. The drive frame is connected to the sieve by means of rigid push rods 7. Feed is supplied to the screen from tank 8 with valve 9 that controls the inlet size. Oversize fraction is collected in container 10, while undersize fraction goes to container 11. The tested sieve dimensions were $L = 1250$ mm and $B = 480$ mm. The angle of screen inclination to the level is adjusted within the range from 0 to 45° , but the tests were performed at the inclination equal to 15° , 20° and 25° . These are typical angles of sieve inclination used in industrial machines. The side of rectangular mesh of the sieve is 0.63 mm long. In the case of fine screening, this is a typical industrial screen scale. Such are sieve surfaces of the machines applied in fine and very fine screening.

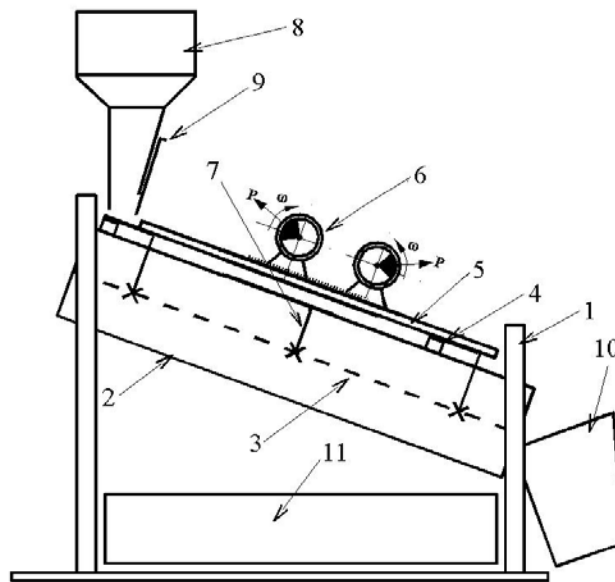


Fig. 1. Schematic diagram of the experimental set-up

Container 11 is divided into 12 sections. In each section there is a tank to collect undersize fraction corresponding to the present sieve length during the screening process, due to which the process can be carried out continuously. Feed is supplied to the sieve from the second section. Once the particles from each section had been weighed, masses of these fractions were obtained which were then converted to the height of material layer on the sieve.

The screen was driven by two electrovibrators operating in backward self-synchronisation. Such a drive system guarantees linear trajectory of vibrations. The trajectory is perpendicular to the sieve surface. The maximum exciting force is $P = 2.574$ kN. Centrifugal forces can be adjusted by changing the location of unbalanced mass on the vibrator shaft.

EXPERIMENTAL MATERIAL

The aim of research carried out at the Technical University of Lodz is to find a relationship between the shapes of particles constituting the screened materials and the process of screening. In general, three different particle shapes considered as model ones, were identified:

- spherical particles (a),
- irregular particles (b),
- sharp-edged particles (c).

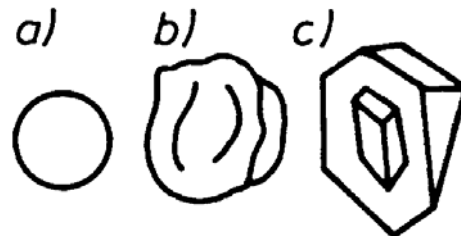


Fig. 2. Model particle shapes

In the experiment, spherical particles, i.e. agalite, irregular – pit sand and sharp-edged particles, i.e. marble aggregate, were screened.

The experimental material was in dry state only, without transient moisture. The material was not used earlier, and as such it was free from industrial contaminants and organic residues; other impurities were insignificant.

ASSUMPTIONS TO THE MODEL OF SCREENING ON A MEMBRANE SIEVE

In the continuous process feed in the form of a granular stream of flow rate Q [g/s] or q [g/s·m²] is supplied to the beginning of the sieve. In this place thickness of the layer on the sieve is H_p and this is the initial material layer height. On the whole, sieve

length L at which the final product of predetermined parameters can be obtained, the process of screening proceeds until reaching the final layer height H_K at the end of the sieve. The initial granular material is composed of two main particle fractions: K_G – oversize fraction, and K_D – undersize fraction. The material is directed to the sieve and divided into two streams: undersize fraction Y and oversize fraction X . Hence, the equations of basic mass balance are as follows:

$$Q = X + Y \quad (1)$$

$$Q = K_G + K_D \quad (2)$$

Assuming full process efficiency, we would have:

$$X = K_G \text{ and } Y = K_D \quad (3)$$

At the end of the sieve two granular streams are observed: K_G – the stream containing the entire oversize fraction and K_D' – the stream containing unscreened part of the undersize fraction, which altogether form the oversize fraction X . Hence, the whole oversize fraction that was in the feed at the beginning of the process, and part of the undersize fraction which did not pass through the sieve and remained in the oversize fraction, fall down from the sieve.

Just this part of the undersize fraction determined screening efficiency which is defined as:

$$\eta = \frac{\text{amount of undersize fraction which passed through the sieve}}{\text{amount of undersize fraction in the feed}} \quad (4)$$

or in the symbol notation

$$\eta = \frac{K_D - K_D'}{K_D} = \frac{Y}{K_D} \quad (5)$$

Here, we assume that the oversize fraction from the layer on the sieve does not pass through the sieve. This assumption holds in the case when mesh size has been adjusted to the intended size distribution and when the sieve is not damaged. In other cases the process of screening is incorrect, and such situation may occur in industrial practice.

The undersize fraction can be screened off only from the near-to-sieve layer which is included in the whole layer – the bed of granular material, moving along the sieve. This is a “discharge” layer. Its characteristic feature is that at every vibration cycle identified with a screening period (process period), the undersize fraction flows out of it totally. The height of this layer depends on many parameters specific for the screening process description (such as particle shape, moisture content and particle size distribution in the material, dynamic factor and others). In this sense of the

process mechanism, screening consists of subsequent discharge of the undersize fractions from the discharge layer and completing the particle size composition each time with smaller portions of undersize fraction which cyclically “flows down” from higher parts of the particle layer. Significant in this process is the earlier mentioned segregation in the bed on the sieve. The rate of this segregation, i.e. the rate at which big particles move from the sieve and small particles move toward it, is of basic importance for the process efficiency. Hence, segregation is a process which causes mixing of particles in the discharge layer.

BALANCE MODEL OF SCREENING

To investigate the rate of changes in the whole material layer thickness on the sieve and shape of the upper edge of the layer, we should consider mass balance of the elementary sieve surfaces (sieve sections). Such a balance is shown in Fig. 3.

According to symbols presented in this Figure, we obtain the height of the layer at the end of the i -th section:

$$Q_i = H_i \cdot B \cdot \rho_n \cdot u_m \Rightarrow H_i = \frac{Q_i}{\rho_n \cdot B \cdot u_m} \quad (6)$$

where:

Q_i [kg/s] – the rate of flow of the layer from the i -th section,

$$Q_i = Q_{i-1} - Q_{KDi} \quad (7)$$

Q_{i-1} [kg/s] – the rate of flow to the i -th section,

$$Q_{KDi} = \frac{m_{Di}}{t_{pl}} \quad (8)$$

Q_{KDi} – flow rate of undersize fraction from the i -th section [kg/s],

m_{Di} [kg] – mass of undersize fraction screened in time t_{pl} from the i -th section [kg],

t_{pl} [s] – process time,

H_i [m] – height of the layer on the sieve at the end of the i -th section,

B [m] – sieve width,

ρ_n [kg/m³] – bulk density of the layer,

u_m [m/s] – mean layer velocity calculated from the relation:

$$u_m = \frac{L}{t} \quad (9)$$

L [m] – sieve length,

t [s] – time in which material passes along the sieve length.

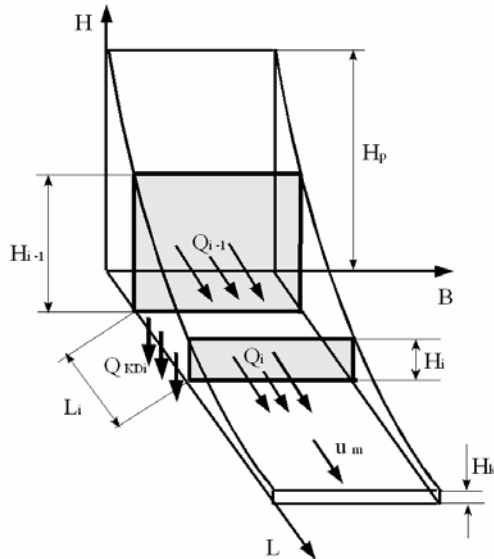


Fig. 3. Mass balance of particular sections of the screen

Here, some values need a comment. Process time t_{pl} is the time in which the feed flows to the screen (the time of feeding material onto the screen). Such definition of this value is related to the assumption that material over each section resides as long as the process takes place. On the other hand, the process lasts as long as feed is supplied to the sieve. This assumption corresponds to the statement that the process is carried out in the steady state at constant values of particular streams. The whole process of screening is always considered as continuous, i.e. lasting infinitely long. In laboratory investigations, however, the process lasts always for some specified period. Hence, it is necessary to introduce some simplifications that would enable interpretation of the process duration as the time in which screening takes place in steady-state conditions. Another value that requires explanation is the mean velocity of material on the sieve (Eq. 10). It can be calculated from available equations presented in literature, but it is most suitable to determine it experimentally for a given screen.

Coming back to the main considerations, the mass balance for the whole screen is given by the formula:

$$Q_0 = \sum Q_{KDi} + Q_K \quad (10)$$

where:

Q_K [kg/s] – flow rate from the last section, equal to the stream of oversize product,

Q_0 [kg/s] – flow rate of the feed.

Basing on the feed stream Q_0 , the initial layer height H_p can be determined:

$$Q_0 = H_p \cdot B \cdot \rho_n \cdot u_m \Rightarrow H_p = \frac{Q_0}{\rho_n \cdot B \cdot u_m} \quad (11)$$

Applying further this procedure, a subsequent height of the layer (on next sections, from $i=1$ to k) is determined by the relations:

$$Q_1 = H_1 \cdot B \cdot \rho_n \cdot u_m \Rightarrow H_1 = \frac{Q_1}{\rho_n \cdot B \cdot u_m} \quad (12)$$

where: $Q_1 = Q_0 - Q_{KD1}$, $Q_{KD1} = \frac{m_{D1}}{t_{p1}}$ similarly to 6.28 and 6.29,

and next:

$$Q_2 = H_2 \cdot B \cdot \rho_n \cdot u_m \Rightarrow H_2 = \frac{Q_2}{\rho_n \cdot B \cdot u_m} \quad (13)$$

$$Q_2 = Q_1 - Q_{KD2}, \quad Q_{KD2} = \frac{m_{D2}}{t_{p1}}$$

layer height at the end of the last section:

$$Q_K = H_K \cdot B \cdot \rho_n \cdot u_m \Rightarrow H_K = \frac{Q_K}{\rho_n \cdot B \cdot u_m} \quad (14)$$

$$Q_K = Q_{K-1} - Q_{KDK}, \quad Q_{KDK} = \frac{m_{DK}}{t_{p1}}$$

where:

Q_{KDK} [kg/s] – rate of flow of the undersize fraction from the k-th (last) section,

m_{DK} [kg] – mass of undersize fraction screened in time t_{p1} from the k-th section [kg].

Final height of the layer on the sieve H_K is closely related to the screening efficiency. On this basis we can estimate whether the process lasted long enough (the sieve length was sufficient) to achieve the expected screening effect, i.e. the desired total stream of undersize fraction.

The above considerations were a starting point to carry out process research, whose aim was to find the relation $H=H(L)$ or $H=H(t)$. This relation is a basis for a mathematical model of the screening process on the frame screen with a membrane sieve. On the basis of this model, and assumed independent variables, we can attain information on process conditions in order to achieve the desired product quality.

SCREENING OF MODEL MATERIALS ON A MEMBRANE SIEVE

In a continuous process, feed in the form of a granular stream Q [g/s] or q [g/s·m²] is supplied to the beginning of the sieve (the place of material input on the sieve). In this place, the layer on the sieve has thickness equal to H_p and this is the initial height of material layer. Along the whole sieve length L , where the final product with

determined parameters can be obtained, the process of screening takes place until reaching final layer height H_K at the end of the sieve. Initially, the granular material was composed of two basic fractions: K_G – oversize fraction, and K_D – undersize fraction, and when supplied to the sieve it is divided into two streams: undersize Y and oversize X . If the process efficiency was full, then the whole undersize fraction would be equal to the oversize stream, while the whole oversize fraction would be equal to oversize stream. However, this is not so and we have efficiency of screening process called also effectiveness, accuracy of separation, etc. It is defined by the formula:

$$\eta = \frac{\text{amount of undersize fraction which passed through the sieve}}{\text{amount of undersize fraction in the feed}} \quad (15)$$

The undersize fraction can be screened off from the near-to-sieve layer which is in the structure of the entire layer – a bed of granular material moving along the sieve. This is a “discharge” layer. Its characteristic property is that at each vibration cycle of the screen, which is identified with the screening period, the undersize fraction flows out of it totally.

The efficiency of screening process is closely related to the thickness of material layer on the sieve, strictly speaking not on the thickness, but a change of this thickness along the sieve length. To investigate the rate of changes of the whole material layer thickness on the sieve mass balance of elementary sieve surfaces (sieve sections) should be considered. Such balance is shown in Fig. 3.

The final layer height on the sieve H_K is strictly related to the assumed (technological) efficiency of screening. On this basis we can assess if the process was long enough (the sieve length was appropriate), to obtain the desired screening effect, i.e. the assumed total stream of undersize fraction. When analysing results of studies on the mass of screened material over subsequent sieve sections and converting them to process efficiency over these sections, we can find that the efficiency changes according to the following relation:

$$\eta = \eta_k - \frac{\eta_k}{1 + \left(\frac{L}{L_0}\right)^p} \quad (16)$$

where: η - screening efficiency [-],

η_k - final efficiency (assumed) [-],

L - sieve length [m],

L_0 - sieve length at which process efficiency reaches 50% η_k [m],

p - coefficient [-].

Process efficiency η is an independent variable which determines screened product quality. The final efficiency η_k is assumed according to material type, and actually the fact if the material is easy or difficult to screen. Parameters L_0 and p are the values that determine how far efficiency η is close to the desired efficiency η_k . Hence, they are the function of independent variables in the process, i.e. particle shape (material type), process yield, and particle size distribution of the screened material.

In this connection the function determined in equation 16 has the form $\eta=f(L)$, i.e. it determines the sieve length at which the efficiency of screening process is satisfactory. The parameters:

$$L_0 = f(\text{particle shape, } y, x_t, \alpha, Q), \tag{17}$$

$$p = f(\text{particle shape, } y, x_t, \alpha, Q), \tag{18}$$

where: y – percentage of undersize fraction in the feed,
 x_t – percentage of particles hard to screen in the feed,
 α – angle of sieve inclination,
 Q – feed flow rate.

Below, only some values of coefficients L_0 and p are compared for particular process conditions for agalite. Similar coefficients were obtained also for other tested materials. Results were obtained using calculations made with the help of Mathcad version 11.0a (Mathsoft Engineering & Education, Inc.). The results are presented as follows:

- type of tested material, angle of sieve inclination, feed flow rate,
- the table presents determined values of L_0 ; rows represent constant values of undersize fraction in the feed, while columns – constant content of hard to screen particles in the feed,
- the table shows determined values of p , the method of presentation is the same as that given above.

Table 1. Agalite, $\alpha = 25^\circ$, $Q = 0.5 \frac{\text{kg}}{\text{s}}$

Lo [mm]	x_t			p	x_t				
	0.1	0.5	0.9		0.1	0.5	0.9		
y	0.1	362	442	541	y	0.1	2.116	2,129	1.828
	0.3	326	374	469		0.3	2.310	2,334	1.958
	0.5	299	366	479		0.5	2.390	1.942	1.792
	0.7	341	401	479		0.7	2.582	2.221	1.797
	0.9	367	483	673		0.9	2.107	1.934	1.611

CONCLUDING REMARKS

The main aim of this study was to propose a model of fine screening on a frame screen with membrane sieve. In this section a mathematical description of screening is proposed (Eq.16), and values of the coefficients in equation 16 are presented. Coefficient L_0 represents the sieve length on which the screening process can be treated as a steady-state one. Since that moment screening proceeds according to the model with discharge function. On the other hand, parameter p shows the rate at which assumed product quality parameters are achieved, i.e. the desired screening efficiency is reached. Both L_0 and p depend on initial process parameters, i.e. type of material, particle size distribution and process conditions.

The proposed model holds for the tested dynamic factor, which determined dynamics of the screening machine, and consequently, the rate of material transport along the sieve. Further research on this model should focus on its verifications for other values of dynamic process parameters.

REFERENCES

- BANASZEWSKI T., (1990), *Przesiewacze*, Śląsk, Katowice.
 SZTABA K., (1993), *Przesiewanie*, Śląsk, Wyd. Techniczne, Katowice.
 SZYMAŃSKI T., WODZIŃSKI P., (2001), *Membrane screens with vibrating sieves*, Physicochemical Problems of Mineral Processing, 35, p. 113-123.
 SZYMAŃSKI T., WODZIŃSKI P., (2002), *Rozkład amplitudy na sicie przesiewacza membranowego z sitem drgającym*, ZN Polit. Śląskiej no. 1564, p. 601-614.
 WODZIŃSKI P., (1997), *Przesiewanie i przesiewacze*, Monografie, Wyd. P.Ł., Łódź.
Modrzewski R., Wodziński P., *Metoda projektowania przesiewaczy membranowych*, Physicochemical Problems of Mineral Processing, 40, (2006) 227-336 (w jęz. ang.).

Niniejsza praca przedstawia model przesiewania materiałów drobnoziarnistych na przesiewaczu membranowym. Urządzeniem, które było przedmiotem pracy badawczej, jest doświadczalny przesiewacz ramowy z sitem membranowym, zaprojektowanym i zbudowanym w Katedrze Aparatury Procesowej Politechniki Łódzkiej. Służy on do przesiewania materiałów drobno i bardzo drobno uziarnionych. Zaproponowana metoda projektowania pozwala oszacować użyteczne wymiary sit (długość i szerokość) dla zadanych warunków procesu w celu osiągnięcia założonych efektów. Metoda ta uwzględnia między innymi skuteczność (efektywność, sprawność) procesu przesiewania, a więc punktem wyjścia do obliczeń jest końcowa zawartość klasy dolnej w produkcji nadsitowym. Jest to ważne dlatego, że technologia procesów przerobczych zakłada „z góry” dopuszczalne zawartości klas ziarnowych innych, niż właściwe dla danego produktu. W niniejszym opracowaniu został zaproponowany opis matematyczny zjawiska odsiewania w postaci prostego równania, jak również przedstawiono wartości współczynników tego równania. Występujący w równaniu podstawowy parametr L_0 wskazuje nam długość sita, powyżej której proces przesiewania możemy traktować jako proces ustalony. Od tego momentu przesiewanie odbywa się zgodnie ze znanym modelem z funkcją odsiewu. Natomiast bezwymiarowy parametr p wskazuje nam szybkość osiągnięcia założonych parametrów jakościowych produktu, czyli osiągnięcia zadanej sprawności odsiewu. Zarówno L_0 , jak i p zależą od parametrów wejściowych procesu, czyli rodzaju materiału, składu ziarnowego oraz od warunków prowadzenia procesu. Zaproponowany model jest słuszny dla określonych, stosowanych w czasie badań wskaźników podrzutu, które określają dynamikę maszyny przesiewającej, a co za tym idzie szybkość transportu materiału po sicie przesiewacza. Dalsze prace badawcze nad tymże modelem powinny iść w kierunku zbadania jego słuszności dla innych wartości parametrów dynamicznych prowadzenia procesu.

Andrzej HEIM, Tadeusz GLUBA, Andrzej OBRANIAK,
Estera GAWOT-MŁYNARCZYK, Michał BŁASZCZYK*

THE EFFECT OF WETTING PARAMETERS ON MECHANICAL STRENGTH OF GRANULATED MATERIAL

Received March 15, 2006; reviewed; accepted May 15, 2006

Results of the investigation of the effect of changes in surface tension, wetting liquid drop size and final moisture content of the bed on the strength of granulated material are presented in the paper. The tested material was silica flour. After each run, representative feed samples were taken from the drum and on their basis the strength of the granulated product was determined by means of abrasion and compression tests. The abrasion tests were conducted in a horizontal drum of diameter $D'=0.2$ m and length $L'=0.14$ m, with perforated walls, where the bed was destroyed during tumbling. Trials were made for steady rotational speed of the drum $n'=26$ r.p.m. and for constant times of testing $t=30$ to 180s. The compression tests were conducted between two pressing plates up to the moment when a single granule was destroyed between the pressing surfaces.

Key words: drum granulation, granulated product strength

INTRODUCTION

Mechanical strength of granulated products is one of the most important features that determine their further processing possibilities. Formation of an agglomerate with specific properties requires a proper granulation method and application of relevant process parameters with special reference to wetting conditions.

The bed of material saturated with liquid, which is a complicated three-phase system, requires that many parameters having an influence on material strength should be taken into account.

Narrow interparticle spaces in the bed of comminuted material are capillary in nature, hence the liquid present in the bed forms characteristic liquid bridges with curved surfaces that are a result of liquid surface tension (Fig. 1).

* Technical University of Lodz, Department of Process Equipment, 90-924 Lodz, Stefanowskiego 12/16, Poland

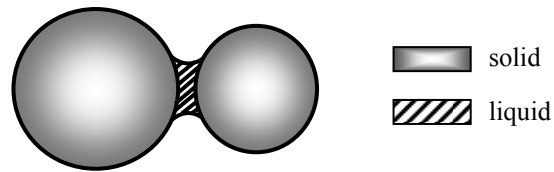


Fig. 1. Schematic of a liquid bridge between two solid surfaces

Conditions of wetting the granulated bed affect the character of capillary interactions in the layer of loose material, which depends on the amount of water in the point of particle contact, type of contact and the number of contacting points in the unit of material volume. Hence, the type of forces that bind particles in the granule depends on liquid content in the interparticle space. Newitt and Conway-Jones (1958) distinguished four basic states of distribution of the liquid present in a granule (Fig. 2):

- pendular – free spaces between particles are only partly filled with liquid, single liquid bridges appear between solid particles. Strength of this agglomerate is induced by the presence of discrete liquid bridges in the points of contact or due to closeness of particles;
- funicular – the number of liquid bridges increases, free space in the granule is partly filled with liquid;
- capillary – all pores between particles are filled with liquid, concave meniscus appears on the outer surface. The granule strength depends on capillary subatmospheric pressure; between particles there are no other substances – particles can interact;
- drop-like – material particles are suspended in the liquid. The strength of granules depends only on liquid surface tension.

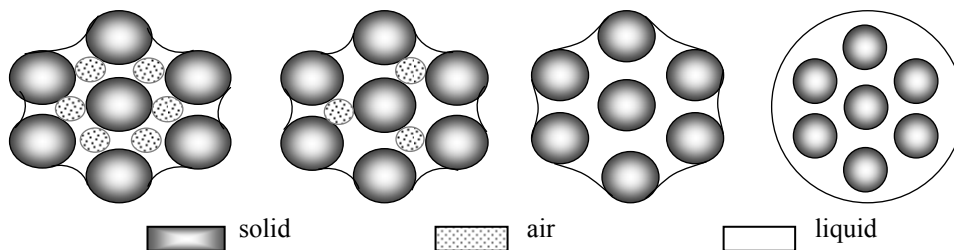


Fig. 2. States of the granule in the presence of the liquid: suspended (pendular), linear (funicular), capillary, drop-like

In literature there are many publications dedicated to studies on granule breakage. From the point of view of granulated product quality, studies on granulated product strength are significant for the processes of transport, storage and applications of these materials.

Pepin et al. (2001) studied the strength of wet granules in relation to the content and type of a binding liquid. Suzuki et al. (2001) analysed the process of micro-crystalline cellulose (MCC) granulation and observed that hardness of the granulated product increased with an increase of water added.

Gluba (2001) tested the compression strength of granulated dolomite flour and found that with an increase of drop size of liquid supplied by the pneumatic nozzles, the strength of the granulated product was increasing. He also observed that the granulated material obtained during drop-wise wetting was characterised by lower strength than in the case of wetting with the biggest drops from the nozzle. Walker et al. (2003) tested the crushing strength of a NPK fertiliser. Based on analyses, they observed that the final product containing a bigger amount of water, prior to drying, was characterised by a higher strength. Bika et al. (2005) studied the crushing strength of granules formed from lactose and mannitol that were wetted with different liquids. They found that addition of a surfactant to a binding liquid caused a significant decrease of strength of the dried granulated product.

AIM OF THE STUDY

The study was aimed at the assessment of the effect of changes in surface tension, wetting liquid drop size and final moisture content of the bed on the strength of granulated product obtained in the process of tumbling agglomeration.

EXPERIMENTAL SET-UP AND METHODS

The granulation process was carried out batch-wise in a horizontal drum granulator of diameter $D = 0.6$ m and length $L = 0.4$ m. The drum was driven by an electric motor via a toothed gear and belt transmission. In the whole experimental cycle constant rotational speed of the granulator $n = 20$ rpm and constant volumetric filling of the drum with raw material $k = 0.1$ (16.125 kg), in relation to bulk density of loosely packed material, were used.

A tested material was silica flour (MK 0.075) produced in Strzeblow Mineral Mine at Sobótka. The mean flour particle size was $d_z = 0.024$ mm. Wetting liquid was distilled water with addition of a surfactant (Rokanol L4P5 – polyoxyalkyl-glycol ether of saturated lauryl alcohol). Changes in water surface tension γ , caused by Rokanol added to the wetting liquid are shown in Table 1.

Table 1. Surface tension of the wetting liquid

	Rokanol L4P5 concentration in the binding liquid [%]		
	0	0.01	0.04
$\gamma \cdot 10^{-3}$ [N/m]	71.97	54.79	35.04

Fine-grained material in the drum was wetted, while tumbling, by means of two pneumatic spray nozzles introduced axially to the drum. Experiments were made at a constant rate of wetting liquid flow through the nozzles $Q_w=12\cdot 10^{-3}$ m³/h and at determined values of air flow rates in the range $Q_p = 2.5$ to 4 m³/h, which enabled different degrees of liquid jet break-up, determined by the coefficient $q = Q_w/Q_p$, and consequently, different values of mean drop size d_k (Table 2). Experiments were carried out at three final moisture contents of the bed in the range $w = 0.19$ to 0.20 [kg water/kg dry material].

Table 2. Spray nozzle operation parameters

Q_p [m ³ /h]	q [-]	d_k [mm]
2.5	0.0048	0.154
3.0	0.0040	0.143
3.5	0.0034	0.134
4.0	0.0030	0.128

Having completed the granulation (32 min), a representative product sample of mass ca. 1 kg was taken from the drum, dried, separated into size fractions on sieves to determine the particle size composition, and then on this basis the strength of granulated product was determined.

In order to test the resistance to attrition, a granulated material sample of mass ca. 0.5 kg was placed in a horizontal drum of diameter $D' = 0.2$ m and length $L' = 0.14$ m equipped with perforated walls (Fig. 3), where during bed tumbling the sample was destroyed. Tests were carried out at determined rotational speed of the drum $n' = 26$ rpm. For each sample the experimental time $t = 30$ to 180s was constant and after every experiment the mass of abraded material was determined ($d_g < 1.5$ mm).

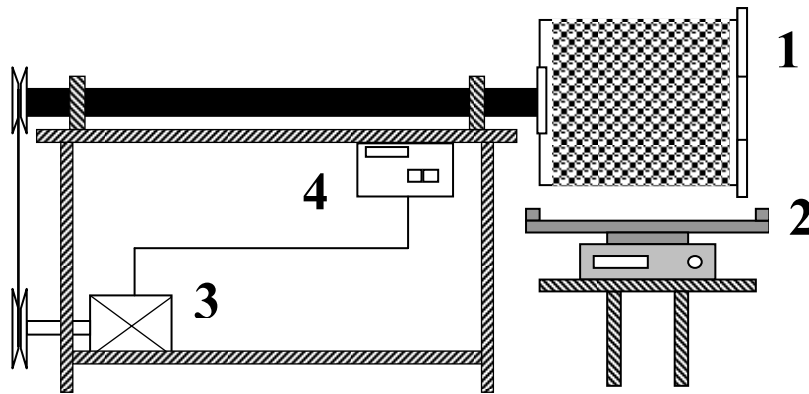


Fig. 3. Set-up for testing attrition resistance of the granulated material: 1- perforated drum, 2- balance, 3-motor, 4- inverter

To investigate compression strength, 10 granules in the shape close to spherical were taken from each fraction, and next each granule was placed separately between parallel compressing plates (mobile and immobile). The test lasted until the moment when the granule was destroyed between the compressing plates (Fig. 4).

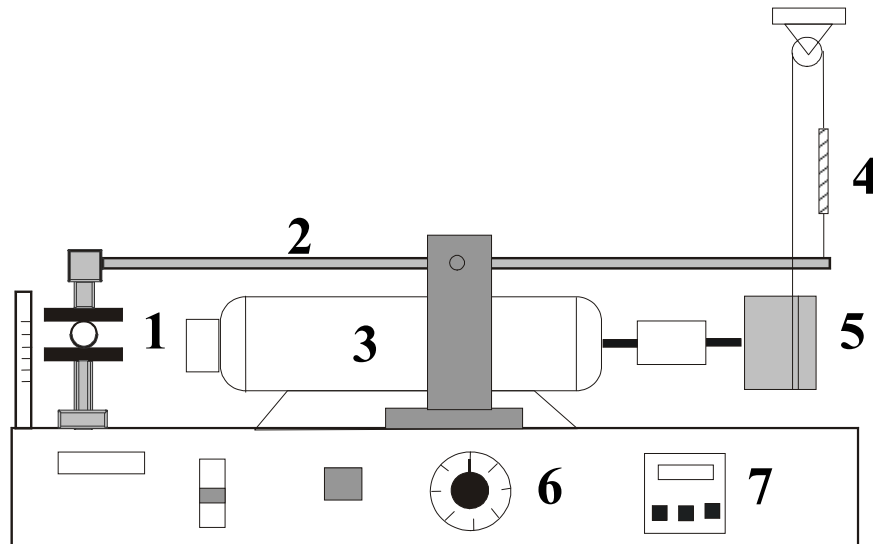


Fig. 4. Experimental set-up for testing compression strength of the granulated product: 1- compressing plates, 2- lever, 3- motor, 4- spring, 5- winding reel, 6- potentiometer, 7- torquemeter.

RESULTS

Abrasion resistance of the granulated product was estimated using the grindability index that represents the loss of material by measuring an increment of the mass of abraded material (particles of diameter $d_g < 1.5\text{mm}$).

The grindability index was determined from the relation:

$$W_{S(t)} = \frac{m_w - m_{S(t)}}{m_w} \cdot 100\% \quad (1)$$

where: $m_{S(t)}$ – mass of abraded material, after time t ,
 m_w – total mass of the sample charged to the drum.

Compression strength of the granulated product was estimated on the basis of the force of granule breakage during compression. The force was calculated by measuring the torque moment on the winding reel shaft, recorded by the torquemeter in the moment of sample destruction. The following relation was used:

$$P = \frac{M_s}{D_{bn}/2} \quad (2)$$

where: D_{bn} – winding reel diameter [m],

M_s – moment recorded in the time of granule destruction [Nm].

The above calculation of the breaking force with reference to the granule size, allowed us to determine the conventional compressive stress described by the formula:

$$\sigma_s = \frac{4P}{\pi d_g^2} \quad (3)$$

where: d_g – granule diameter [m].

Results of the experiments showed a significant influence of the binding liquid drop size (liquid jet break-up) on the abrasion process. Examples of the relations presenting changes in the grindability index W_s during abrasion of granulated product are given in Fig. 5. It follows from this diagram that when the bed is wetted with big drops the strength of granulated product is higher. This can be explained by the mechanisms of granulated product formation. In the case of wetting the bed with big drops, bigger nuclei can be formed which are then transformed into granules. Wetting with small drops leads to the formation of granules by coalescence which causes that sphericity of the obtained agglomerates is lower and air is enclosed inside the formed granules, which much reduces their mechanical strength.

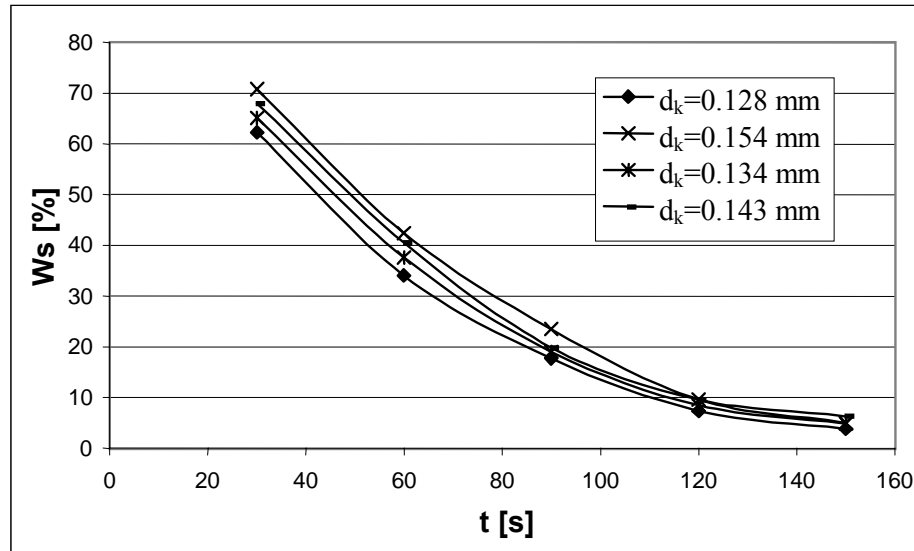


Fig. 5. Change of W_s during attrition for different wetting liquid drop sizes ($w = 0.19$; $\gamma = 71.97 \cdot 10^{-3} \text{ N/m}$)

Figure 6 shows changes in the breakage force for different diameters of granules obtained in tumbling agglomeration. It follows from the figure that the compression strength of the granulated product increases linearly with a mean granule size. Results of experiments show also that even the use of small amounts of a surfactant added to the wetting liquid (0.01%) causes a decrease of compression strength of the granules. Most probably this is caused by formation of weaker liquid bridges (lower surface tension) than in the case of granulated material wetted with distilled water. It was observed also that for bigger granules a further increase of Rokanol concentration in the binding liquid caused only a slight decrease of the tested material strength.

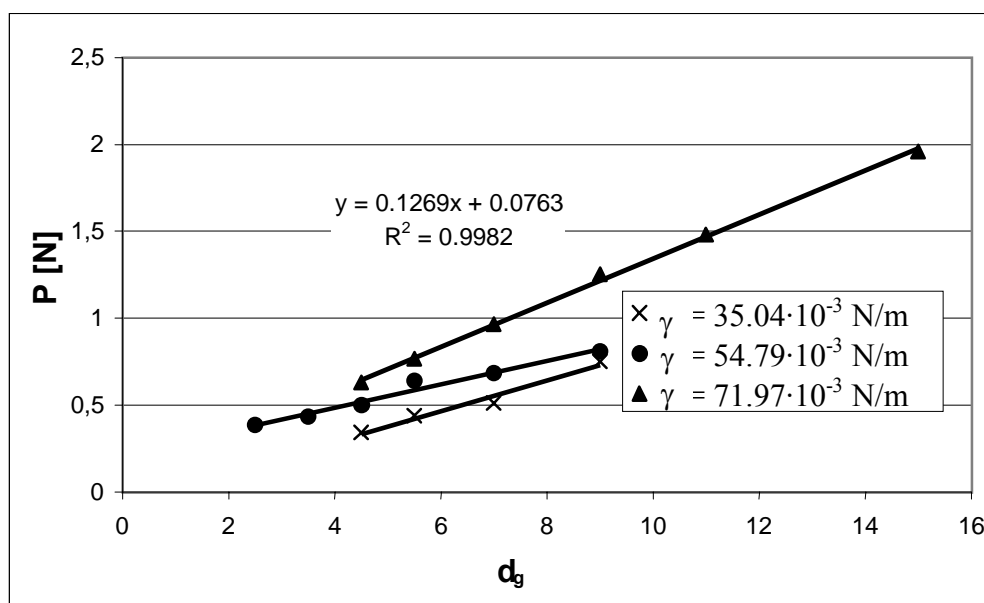


Fig. 6. Comparison of curves $P = f(d_g)$ for different values of surface tension of the binding liquid ($w = 0.195$, $d_k = 0.143$ mm)

To determine the effect of final moisture content of the bed on the strength of tested granulated material, curves $\sigma_s = f(d_g)$, presented in Fig. 7, were compared. When analysing the graph below, we can observe that with an increase of granule size the breaking stress induced by sample compression decreases. It was also found that with an increase of the bed final moisture content the strength of tested material increased. Lower strength of the granulated product formed from less humid bed can be caused by higher non-homogeneity of binding particle structures inside the granules. A reason may be the presence of air bubbles, beside liquid bridges (pendular state), which weaken the granulated product significantly. In the case of granules formed from the bed of higher final moisture content, the air is forced from the granules by the binding

liquid faster (funicular or capillary state), which causes enhancement of interparticle bonds, and consequently, an increase of the tested sample strength. Results of the tests showed also that an increase of the final moisture content of the granulated bed best improved the strength of granules with small diameters, while in the case of bigger granules differences in the breaking stresses that appeared during compression were minimal.

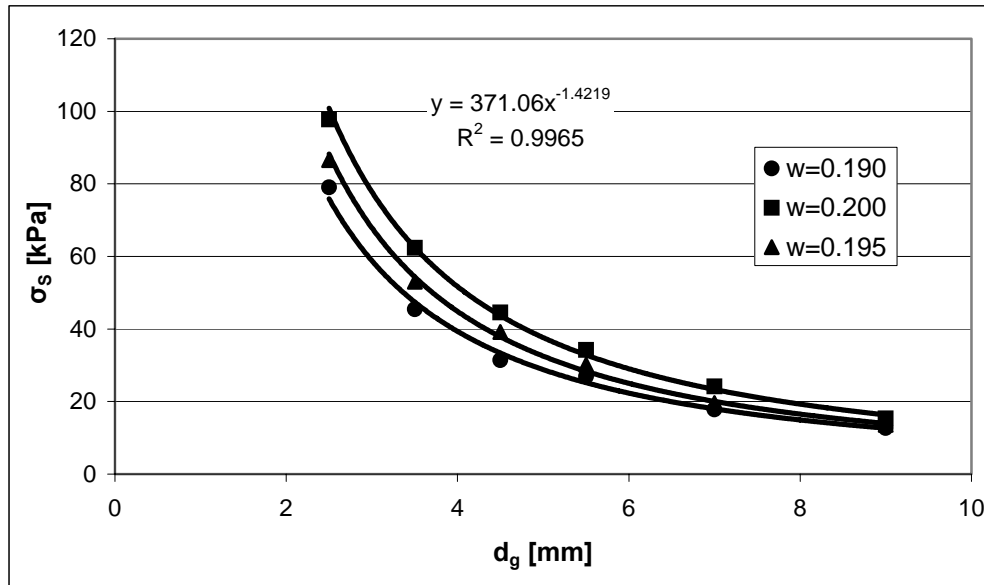


Fig. 7. Comparison of curves $\sigma_s = f(d_g)$ for different final moisture contents of the feed ($d_k=0.143$ mm; $\gamma=54.79 \cdot 10^{-3}$ N/m)

CONCLUSIONS

1. Mechanical strength of a product formed during wet drum granulation depends significantly on wetting parameters. Very important is final moisture content of the granulated bed, wetting liquid drop size (jet break-up) and surface tension.
2. An increase of drop size of the liquid supplied by pneumatic nozzles leads to the formation of a product with higher mechanical strength.
3. A decrease of liquid surface tension causes a decrease of granule strength.
4. An increase of the final moisture content of the bed contributes to the formation of granules with higher mechanical strength.

REFERENCES

- NEWITT D. M., CONWAY-JONES J. M. (1958), *A contribution to the theory and practice of granulation*, Trans. Inst. Chem. Eng., 36, 142.
- PEPIN X., SIMONS S.J.R., BLANCHON S., ROSSETTI D., COUARRAZE G., (2001), *Hardness of moist agglomerates in relation to interparticle friction, granule liquid content and nature*, Powder Technology: 117, (1-2), 123-138.
- SUZUKI T., KIKUCHI H., YAMAMURA S., TERADA K., YAMAMOTO K., (2001), *The change in characteristics of microcrystalline cellulose during wet granulation using a high-shear mixer*, Journal of Pharmacy & Pharmacology, 53, 609-616.
- GLUBA T., (2001), *Badania wytrzymałości granulatu*, Materiały VI Ogólnopolskiego Sympozjum „Stan techniki oraz nowe zastosowania procesów i aparatury do granulacji” (Puławy-Kazimierz Dolny 24-31.05), 877-885.
- WALKER G. M., MOURS Y. H. E. M. N., HOLLAND C. R., AHMAD M. N., (2003) *Effect of process parameters on the crush strength of granular fertilizer*, Powder Technology, 132, 81-84.
- BIKA D., TARDOS G. I., PANMAI S., FARBER L., MICHAELS J., (2005), *Strength and morphology of solid bridges in dry granules of pharmaceutical powders*, Powder Technology, 150, 104-116.

ACKNOWLEDGEMENTS

The study was carried out within project W-10/21/2006/B.W.

Heim A., Gluba T., Obraniak A., Gawot-Młynarczyk E., Błaszczyk M., *Wpływ parametrów nawilżania na wytrzymałość mechaniczną granulatu*, Physicochemical Problems of Mineral Processing, 40 (2006), 237-245 (w jęz. ang.).

W pracy przedstawiono wyniki badań wpływu zmian napięcia powierzchniowego, wielkości kropelek cieczy nawilżającej oraz wilgotności końcowej złoża na wytrzymałość otrzymanego granulatu. Jako materiał badawczy zastosowano mączkę kwarcową pochodzącą ze Strzeblowskiej Kopalni Surowców Mineralnych w Sobótce (MK 0.075). Granulację prowadzono w sposób okresowy w poziomym bębnie o średnicy 0,6m i długości 0,4m, przy stałej prędkości obrotowej $n=15$ obr/min. Złoże materiału sypkiego nawilżano w czasie jego ruchu przesypowego, przy stałym objętościowym natężeniu przepływu cieczy $Q_w = 12 \cdot 10^{-3} \text{ m}^3/\text{h}$ (woda destylowana z dodatkiem Rokanolu L4P5), za pomocą zestawu dwóch pneumatycznych dysz rozpyłowych. W celu uzyskania różnej wielkości kropelek (stopnia rozbicia strugi) stosowano zmienne natężenie przepływu powietrza przez dysze $Q_p = 2.5 \div 4 \text{ m}^3/\text{h}$. Badania prowadzono przy ustalonych wartościach wilgotności końcowej złoża $w=0.19 \div 0.2$ [wag]. Po każdej próbie pobierano z bębna reprezentatywne próbki wsadu, na podstawie których określano wytrzymałość otrzymanego granulatu za pomocą testów na ścieranie oraz ściskanie. Badanie wytrzymałości na ścieranie, prowadzono w poziomym bębnie o średnicy $D'=0,2$ m i długości $L'=0,14$ m zaopatrzonym w perforowane ścianki, gdzie w czasie ruchu przesypowego złoża następowało jego niszczenie. Próby prowadzono dla ustalonej prędkości obrotowej bębna $n'=26$ obr/min. oraz dla stałych czasów prowadzenia testu $t=30 \div 180$ s. Badanie wytrzymałości na ściskanie prowadzono między dwoma płytkami ściskającymi, próba trwała do momentu zniszczenia pojedynczej granulki między ściskającymi ją powierzchniami. Uzyskane wyniki pokazały istotny wpływ zmian warunków nawilżania złoża, podczas aglomeracji bębnowej, na wytrzymałość mechaniczną otrzymanego granulatu.

Tomasz P. OLEJNIK*

GRINDING KINETICS OF SELECTED MINERALS WITH REFERENCE TO THE NUMBER OF CONTACT POINTS

Received March 15, 2006; reviewed; accepted May 15, 2006

Results of experiments whose aim was to determine the rate of grinding of mineral materials with different susceptibility to comminution are discussed in the paper. Experimental materials were gabbro and sandstone. The experiments were carried out in a laboratory ball mill. During grinding the number (mass) of balls of constant diameter at constant feed mass was changed. The main objective of the experiments was to give a specific rate of grinding of particular size fractions of the mineral materials used in road making. An initial equation was the Gardner and Austin formula in a differential form for discrete values of the fractions, assuming an ideal mixing of the ground material. The grinding rate for selected size fractions of the ground material was described by a correlation equation. Parameters of the correlation equation and the effect of ball number (mass) on their values were specified. Additionally, a mathematical relation describing the change of a mean particle diameter in time, was given.

Keywords: ball mill, contact point, grinding rate

INTRODUCTION

Due to a complex character of the motion of feed and grinding elements in the mill, and variable in time contribution of particular grinding mechanisms related to it, the description of process kinetics requires refined mathematical tools. In the Department of Process Equipment researches are carried out on the modelling of grinding kinetics, which will enable to scale them up from laboratory to pilot-plant or industrial scale. One of possible solutions to simplify the description of grinding kinetics in ball mills is the use of a possible relation between the rate of grinding of particular material fractions and the number of contact points between the balls.

The process of grinding proceeds mainly due to a complex interaction between the balls and ground material and additionally by the action of grinding elements on the

* Faculty of Process and Environmental Engineering, Technical, University of Lodz, Wólczajska 213, 90-924 Łódź, Poland.

inner drum surface. Feed, which is between the balls, is subjected to attrition and shearing with a possible addition of crushing [MATTAN 1971, LYNCH 1974]. These mechanisms of comminution appear mainly in a cataracting motion of the balls. At a cascading motion of the balls, there is additionally an impact mechanism involved which is a result of collisions of balls falling on the bed at the bottom of the grinding chamber. This type of motion, at which impacts prevail, occurs for rotations frequency of the mill close to a critical frequency. This is a very desirable phenomenon because of grinding intensity, but dimensions of industrial ball mills and related inertia forces reduce the character of mill operation at velocities close to the critical frequency [SHIPWAY 1993]. Due to this, choosing lower frequencies of the mill rotations, the contribution of particular grinding mechanisms can be changed by changing the size and number of balls. During the grinding process, the mill filling with feed and the number of balls in the drum can be changed. Owing to limited mill dimensions, it is desirable to determine such composition of balls at which grinding of particular size fractions takes place at the highest possible rates. A ground product characterised by very high monodispersivity is obtained. It is also important to obtain a specified mean particle diameter after a possibly shortest grinding time.

An increase of ball sizes determines an increment of a single ball mass and an increase of mutual interaction between the grinding elements. An increasing size of grinding media, at unchanged mill filling with balls, provokes a decrease of the number of contact points. This causes a decrease of mini-regions, where stresses destroying ground material particles can occur in a given moment. Selection of ball diameter depends on the strength of ground material and on particle diameter. In the case of bigger particles that require stronger breaking forces, balls of bigger size should be used, while for smaller particles and weaker materials better effects will be obtained when the number of points of ball contacts will be increased, hence, by increasing their number at the cost of diameter [HEIM et al. 2004].

A simple construction of the mill does not keep up with the efficiency of grinding process. Low process efficiency makes technologists look for such a composition of balls and packing of the mill, at which the mean particle diameter decrease is the fastest. This will enable a more economic use of the mill operating time [HEIM OLEJNIK and PAWLAK 2005].

From this point of view grinding effects in a mill with different number of balls were analysed. Dry grinding process was carried out in a laboratory mill. A feed was a mixture of mineral materials used in road pavement production.

EXPERIMENTAL

Changes in particle size distribution of ground material in time were investigated in a laboratory mill of inner diameter 0.25 m and total water volume of 6 dm³. Grinding was a dry process. Experimental material included gabbro and sandstone. Prior to grinding, the minerals were subjected to preliminary processing that included selection

of particles with diameters ranging from 1 to 2.5 mm. Grinding was performed using four types of drum filling with corundum balls 30 mm in diameter. Process parameters are given in Table 1.

Grinding was carried out until the moment when on the sieve with 1 mm mesh size, less than 2.5 g material remained (this was about 1.4 % mass of input fraction – 180 g). In determined time intervals samples were taken to analyse particle size distribution. The analysis was made using an ANALYSETTE 22 laser particle size analyser (FRITSCH).

Table 1. Equipment and process parameters of grinding

Trial no.	Number/mass of balls [-/kg]	Frequency of mill revolutions [min^{-1}]	Feed type	Feed volume [dm^3]
A	14 / 0.901	90	sandstone	0.6
B	19/1.15			
C	23/ 1.392		gabbro	
D	27 / 1.683			

RESULTS AND DISCUSSION

Table 2 gives examples of particle size analysis of 1 dm^3 ground gabbro at mill filling with the balls of mass 0.901 kg.

Grinding rates for particular size fractions were calculated basing on the particle size analysis. Equation (1) proposed by Gardner and Austin in a differential form for discrete values of fractions, was used in calculations assuming an ideal mixing of the ground material.

$$\frac{dw_i(t)}{dt} = -S_i w_i(t) + \sum_{j=1, i>1}^{i-1} S_j b_{i,j} \cdot w_j(t) \quad (1)$$

To determine the distribution function $b_{i,j}$ the following equation was applied:

$$b_{i,j} = \phi \left(\frac{d_i}{d_j} \right)^\gamma + (1 - \phi) \left(\frac{d_i}{d_j} \right)^\beta \quad (2)$$

Using Statistica® and the software developed at the Department of Process Equipment, Łódź Technical University, correlation equations of changes in the grinding rate as a function of particle size fraction d_i were proposed. In the correlation the effect of particular size fractions as well as filling the mill with feed and grinding elements on the rate S_i was specified. A function in the form was selected:

$$S(i) = K_s \cdot d_s(i)^{n_s} \cdot e^{-b_s \cdot d_s(i)} \quad (3)$$

Table 2. Mass fractions of gabbro particles of various sizes. Ball mass 1.683 kg

d_i	Grinding time [min], fractions w_i [%] of various particle sizes												
	0.5	1	3	5	7	10	15	20	30	40	60	80	110
2	25.8	23.1	20.1	19.1	17.5	14.8	13.1	12.6	10.4	7.7	5.4	3.3	0.5
1.6	13.2	11.5	11.4	8.7	8.2	7.1	6.6	4.9	3.3	2.7	3.3	2.7	0.0
1.4	12.1	12.1	10.9	10.4	8.7	7.7	4.9	4.4	4.4	3.3	2.7	2.2	1.6
1.25	11.5	12.1	10.9	9.8	8.7	8.7	8.2	7.7	6.6	5.5	3.8	3.3	1.6
1	23.1	22.5	20.7	18.0	16.9	15.9	14.8	12.0	10.4	8.7	8.2	4.9	2.2
0.8	8.2	9.3	11.4	13.7	13.1	11.5	10.9	10.4	9.8	9.8	8.7	9.2	10.3
0.63	2.2	2.8	3.3	3.8	3.8	4.4	4.9	5.5	6.0	6.6	6.5	7.1	7.0
0.5	0.6	1.1	2.2	3.3	4.4	5.5	6.0	6.6	7.1	7.7	9.2	10.3	11.4
0.4	1.7	2.2	2.7	3.3	4.4	5.5	6.0	6.0	6.6	7.1	7.1	8.2	9.7
0.315	0.6	0.6	0.5	1.1	1.6	1.6	1.6	1.6	2.2	2.7	3.3	4.4	6.5
0.2	0.0	0.6	1.1	1.6	2.2	2.7	3.8	4.4	4.9	5.5	6.5	7.6	9.2
0.125	0.0	0.6	1.1	1.6	2.7	4.9	6.6	8.2	8.7	9.8	10.3	10.9	12.4
0.09	0.6	1.1	2.2	2.7	4.4	6.0	7.1	8.7	9.8	11.5	12.0	12.5	13.5
0.071	0.0	0.0	0.5	1.1	1.6	2.2	3.3	4.4	6.6	7.7	8.7	9.2	9.7
0.063	0.6	0.6	0.5	0.6	0.6	0.6	0.6	0.6	0.6	0.6	1.1	1.1	1.1
0	0.0	0.0	0.5	1.1	1.1	1.1	1.6	2.2	2.7	3.3	3.3	3.3	3.2

Coefficients K_s , n_s , and b_s for each measuring series are given in Table 3. The obtained values of S_i are also illustrated graphically. For easy interpretation of the results diagrams were prepared separately for gabbro (Fig. 1) and sandstone (Fig. 2).

Table 3. Comparison of coefficients γ , β and ϕ in equation (2) and K_s , b_s and n_s in Eq. 3

Ball load [pcs / kg]	Feed	γ	β	ϕ	K_s	b_s	n_s
14/0.901	Sandstone	0.672	2.233	1.124	6.3	2.55	1.21
19/1.15		0.5625	4.894	1.738	11.9	2.13	2.23
23/1.392		0.752	2.335	1.607	1.06	1.4	0.29
27/1.683		0.8961	4.681	4.802	5.15	1.9	1.52
14/0.901	Gabbro	0.5439	4.592	0.9134	0.0358	1.12	0.645
19/1.15		0.7456	1.03	1.022	0.0234	0.1	-0.319
23/1.392		0.6523	1.647	2.914	1.06	1.59	2.96
27/1.683		0.6834	2.917	3.217	0.23	1.1	0.733

It is interesting to follow the variability of S_i values for ground minerals. Owing to the fact that the grinding balls had a constant diameter, the impact of grinding media on the feed was similar. For gabbro particles (Fig. 1) from the upper size range, exceeding 1.4 mm, the impact of balls was similar. In this connection, the obtained values of comminution S_i depend mainly on the number (mass) of grinding elements. The biggest gabbro particles are characterised by the lowest susceptibility to grinding. So, in the above mentioned range of particle sizes, the number of contact points does not play any important role.

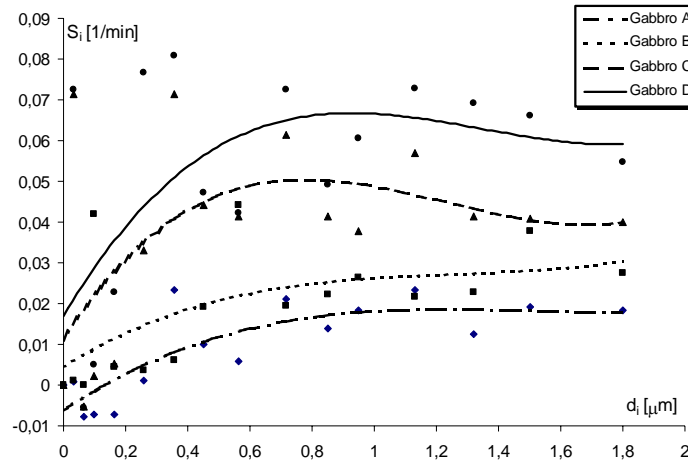


Fig. 1. Change in grinding rate S_i of gabbro for the tested ball composition. Correlation function (Eq. 3)

The mean range of particle diameters (from around 0.5 to ca. 1.4 mm) is characterised by the biggest differentiation of S_i values (Fig. 1). The effect of an increased number of contact points (increased mass of balls) is enhanced by a bigger variety of particles. The rate of grinding of hard inclusions still depends on the number of balls, but disruption of particle structure accelerates the rate of grinding. For very fine fractions low values of S_i were obtained and although differences of absolute values for a different number of balls are small, these absolute values are very significant. Additionally, the process of particle agglomeration causes that the rates of comminution of the smallest particles at a small number of balls (a few contact points) are close to zero, and even at the smallest size fractions the calculated values are negative.

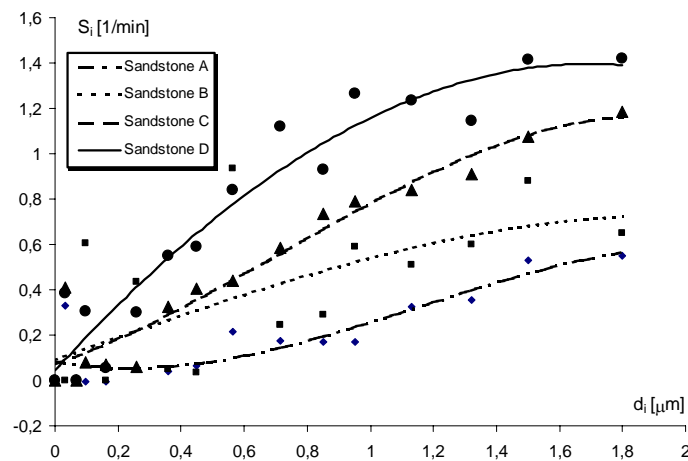


Fig. 2. Change in grinding rate S_i of sandstone for the tested ball composition. Correlation function (Eq. 3)

For sandstone, the rates of grinding S_i are similar to those for gabbro. However, due to different particle structure – bigger fraction of soft inclusions in the matrix, the impact of grinding media on the feed causes a multiple increase of the grinding rate. This is caused by numerous soft calcium inclusions which bond harder particles of iron compounds. In the range of particle size fractions exceeding 1.6 mm, the obtained values of S_i for sandstone are more than 1.4 min^{-1} for the biggest number of balls (series D), and over 0.4 min^{-1} for the smallest number of balls (series A). For a comparable size fraction of gabbro particles the S_i rates are ca. 0.06 min^{-1} (series D) and 0.01 min^{-1} (series A), respectively.

Figures 3 and 4 show additionally changes of mean particle size of ground material in time. However, a comparison of the obtained curves does not allow us to draw conclusions like in the above analysis concerning the effect of the number of balls on the time required to obtain sufficient feed comminution. While for gabbro an increase of the number of balls causes shortening of the grinding time (series D) to ca. 120 minutes, at grinding times for series A and B reaching ca. 200 min, in the case of sandstone the effect of the number of balls is not so obvious any longer. For series B the grinding times were the longest (ca. 16 min), however by several minutes longer as compared to series A. Lack of grinding time increase for series A can be explained by the effect not only of the number of contact points but also a specific feature (non-homogeneity) of sandstone particles. The effect of the number of grinding elements and their mass should be confirmed by further studies and determination of mechanical strength of particular size fractions.

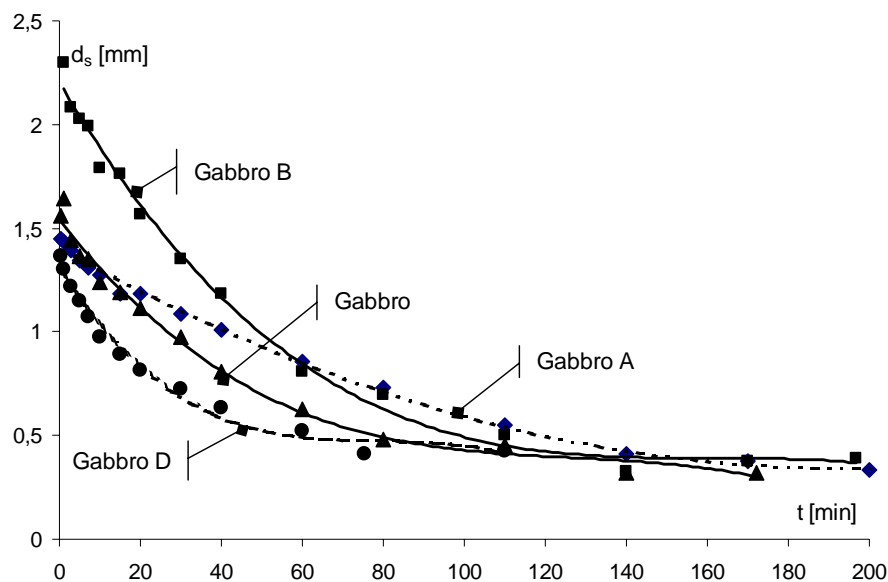


Fig. 3. Change of mean size d_s of gabbro particles

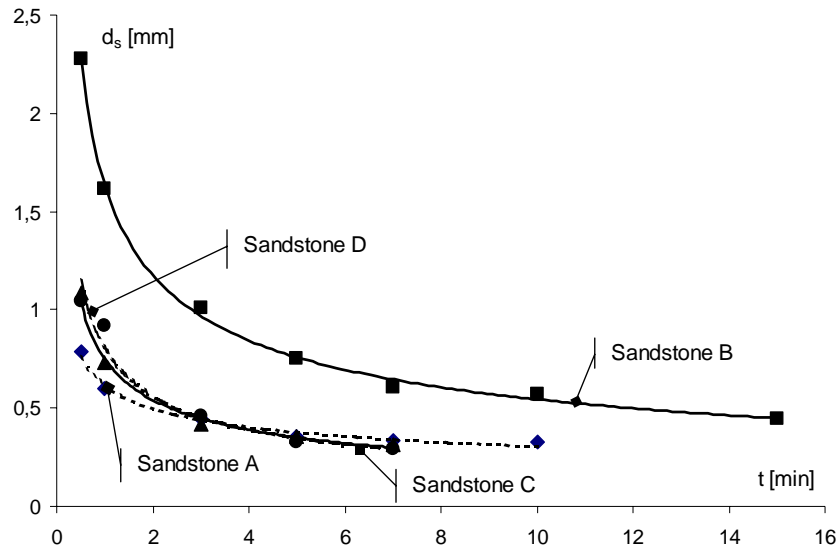


Fig. 4. Change of mean size d_s of sandstone particles

CONCLUSIONS

1. The following conclusions can be drawn from the obtained results:
2. The process of grinding of the tested minerals is determined by material characteristics, mainly particle structure and proportions between hard and soft components of the particles.
3. An increase of the number of balls causes an enhancement of grinding process, especially of mean particle size fractions.
4. The rate of comminution of small particle fractions depends on the number of contact points and particle agglomeration.

NOMENCLATURE

- $d_{s i}$ – mean (arithmetic) particle size in size fraction i
- $b_{i,j}$ – distribution function defined as this part of ground material from size fraction j which is transferred to size fraction i ,
- b_s – coefficient of exponent in equation (3)
- b_s, n_s, K_s – parameters of correlation equation (3)
- d_i, d_j – particle diameters in size fractions i and j , respectively
- S_i, S_j – specific rate of grinding of particles from size fraction i or j called also distribution parameter,
- $w_i(t), w_j(t)$ – weight fraction of particles i or j after grinding time t ,
- β, φ, γ – parameters in equation (2).

REFERENCES

- LYNCH A.J., (1974), *Mineral crushing and grinding circuits*. Amsterdam, Oxford, New York.
- MATTAN J., (1971), *How to step up ball mill efficiency*. Rock Products, Nr 5.
- SHIPWAY P. H., HUTCHINGS I. M., (1993), *Attrition of brittle spheres by fracture under compression and impact loading*. Powder Tech. 76, 23-30.
- HEIM A., OLEJNIK T.P., PAWLAK A., (2004), *Comparision analysis of some industrial ball mill*. KOMEKO.
- HEIM A., OLEJNIK T.P., PAWLAK A., (2005), *Rate of ceramic body grinding in a ball mill*, Physicochemical Problems of Mineral Processing, **39**, s. 189-198.

ACKNOWLEDGEMENTS

This study was carried out within research project no. W-10/21/206 B.W.

Olejnik T.P., *Kinetyka przemiatu wybranych surowców skalnych z uwzględnieniem liczby punktów kontaktu*, Physicochemical Problems of Mineral Processing, 40 (2006), 247-254 (w jęz. ang.).

W artykule przedstawiono wyniki badań, których celem było określenie szybkości przemiatu surowców skalnych o zróżnicowanej podatności na rozdrabnianie. Próby mielenia przeprowadzono na surowcach skalnych, którymi było gąbro oraz piaskowiec. Przemiał prowadzono w młynie kulowym w skali laboratoryjnej. W trakcie przemiatów zmieniano liczbę (masę) kul o stałej średnicy przy stałej masie nadawy. Podstawowym celem prowadzonych badań było określenia szybkości właściwej rozdrabniania poszczególnych frakcji rozmiarowych materiałów skalnych wykorzystywanych w budownictwie drogowym. Jako równanie wyjściowe zastosowano równanie Gardnera i Austina, w formie różniczkowej dla dyskretnych wartości udziałów, zakładając idealne wymieszanie mielonego materiału. Szybkości przemiatu wybranych frakcji rozmiarowych mielonego materiału opisano w formie równania korelacyjnego. Określono parametry tego równania korelacyjnego oraz wpływ liczby (masy) kul na ich wartość. Dodatkowo, określono w postaci zależności matematycznej zmianę w czasie średniego wymiaru ziarna.

Filip CIESIELCZYK, Andrzej KRYSZTAFKIEWICZ, Teofil JESIONOWSKI*

SEDIMENTATION AND WETTABILITY OF SYNTHETIC MAGNESIUM SILICATES

Received March 15, 2006; reviewed; accepted May 15, 2006

In the paper studies were presented which aimed at obtaining synthetic magnesium silicate, which could be applied as a selective adsorbent, polymer filler or a filler of paper-coating masses. Synthetic magnesium silicate was obtained by precipitation using solutions of $MgSO_4 \cdot 7H_2O$ and Na_2SiO_3 (water glass). In view of specific application of the precipitated silicates, the process of their production was broadened by introduction to the reactive system agents which hydrophobically transform silicate surface. Non-ionic surfactants were used for this purpose. The obtained products were subjected to a comprehensive physicochemical analysis. The tested parameters included bulk density, capacities to absorb water (wettability with water), dibutyl phthalate and paraffin oil, particle size distribution, and specific surface area. A significant element of the work involved studies on sedimentation of synthetic magnesium silicates, an important variable which determines directions of their application.

Key words: synthetic magnesium silicate, non-ionic surfactants, specific surface area, sedimentation, wettability

INTRODUCTION

Sedimentation and wettability of surface with various agents belong to most significant parameters which determine application of mesoporous silicate fillers. Due to numerous applications of both natural and synthetic magnesium silicates, their behaviour in various media has to be determined. Considering application of magnesium silicates as selective adsorbents it is necessary to determine their adsorptive properties, i.e. specific surface area and porosity.

Both natural and synthetic magnesium silicates are used as adsorbents with various effects, due to their variable specific surface areas (Kociołek-Balawejder 2006).

* Poznan University of Technology, Institute of Chemical Technology and Engineering,
M. Skłodowskiej-Curie 2 Sq., 60-965 Poznan, Poland,
E-mail: Filip.Ciesielczyk@doctorate.put.poznan.pl, phone:+48(61)6653626, fax:+48(61)6653649.

Promising results have been obtained removing waste As(III) and As(V) ions by application of natural and modified zeolites (Elizalde-Gonzales 2001, Xu 2002), and also laterite - the mineral containing iron and aluminium oxides (Viet 2002).

Literature contains reports on the application of natural zeolites for removal of sewage Cd(II) ions (Dąbrowski 2006). A similar application involved clinoptylolite modified with hexadecyltrimethylammonium cation, which proved to be a selective ion exchanger for Cr(VI) ions in the pH range of 3 to 13 (Li 1997, Haggerty 1994). Zeolites modified with surfactants adsorb non-polar organic substances such as benzene, toluene, xylene, chlorinated aliphatic compounds, inorganic cations (e.g. Pb(II)), by ion exchange and formation of surface complexes (Dąbrowski 2006). Similar results could be expected using synthetic magnesium silicates, which manifest numerous analogies in structure and physicochemical properties with their natural analogues.

Sedimentation and wettability play a significant role, particularly when the precipitated silicates are applied as supplements to protein-coating masses or as carriers of inorganic pigments. In order to fulfil its role, the synthetic silicate should not sediment and its surface should be well wettable with the medium in which the silicate is supposed to be used. An example of such a system is provided by magnesium silicate coated with layers of TiO₂ water gels or by introduction of pure TiO₂ (in the form of a powder) into a silicate matrix (Cardona 2004). After testing, such systems can be safely used as a supplement of paints, in which they have to form a stable dispersion (Brown 1997, Kobayashi 1996).

Synthetic magnesium silicates, precipitated by reaction of inorganic salt solution and water glass solution demonstrate a pronounced sedimentation, particularly in aqueous media. In addition, modification of their surface significantly affects their behaviour in various media (Krysztafkiewicz 2004).

A detailed physicochemical analysis of various MgO-SiO₂ systems has been described in detail in various studies (Wentzcovitch 1995, Karki 1997, Chaplot 2000, Belonoshko 1996). In turn, Temuujin (1998) and co-authors have described studies on the role of water in mechanic-chemical reactions of MgO-SiO₂ systems.

EXPERIMENTAL

MATERIALS

Synthetic magnesium silicate was obtained by precipitation reaction, using 5% MgSO₄·7H₂O solution (5% in respect to MgSO₄) and 5% aqueous solution of Na₂SiO₃ (5% in respect to SiO₂). The sodium metasilicate solution manifested the following parameters: contents of Na₂O - 8.8 %; SiO₂ - 28.5 %, density - 1.38 g/dm³ and modulus 3.33. Surface hydrophobization was conducted using appropriate non-ionic surfactants produced by the PPC „Rokita” S.A. Compounds applied for this purpose included nonylphenylpolyoxyethyleneglycol ethers, Rokafenols N3, N6, N9, of the

general formula $C_9H_{19}C_6H_4O(CH_2CH_2O)_nH$ (where $n_{av}=3$; $n_{av}=6$; $n_{av}=9.7$ for respective Rokafenol) and oxyethylated unsaturated fatty alcohols, Rokanol K3 and K7, of the general formula $RO(CH_2CH_2O)_nH$ $R=C_{16-22}$, where $n_{av}=3$; $n_{av}=7$ for respective Rokanol).

METHODS OF STUDIES

In the earlier performed studies (Ciesielczyk 2004) the process of obtaining synthetic magnesium silicates by chemical reaction was optimised, using 5% waste solutions of magnesium sulphate(VI) and sodium metasilicate. The reaction was conducted in a reactor of 500 cm³ capacity, equipped with top stirrer. Into a reactor containing appropriate amount of magnesium(VI) sulphate, the same amount of water glass solution was dosed. The process was conducted at room temperature.

After obtaining synthetic magnesium silicates, the precipitation process was broadened by introduction to the reactive system of hydrophobicity-inducing agents in the form of non-ionic surfactants: Rokafenols N3, N6 and N9 and Rokanol K3 and K7. Respective surfactants were introduced in the amount of 1; 3; of 5 weight parts, implementing the so called "wet" modification process.

In order to obtain images of the obtained modified and unmodified magnesium silicates, their selected samples were examined in a scanning electron microscope (Philips SEM 515).

For all the samples particle size distributions were established, basing on dynamic light scattering (DLS) technique and using for the purpose ZetaSizer Nano ZS apparatus (Malvern Instruments Co).

A significant element of the studies involved determination for the samples of sedimentation tendency in aqueous media and wettability with water. The studies were performed using K100 tensometer (Krüss).

RESULTS AND DISCUSSION

Particle size distribution and SEM microphotograph of synthetic magnesium silicate obtained with no supplementation of the hydrophobicity-inducing agent are presented in Fig.1.

In the particle size distribution (Fig.1) three bands could be noted. The first occupied the diameter range of 342-396 nm with maximum intensity of 30.9 for particles of 396 nm in diameter. The other band corresponded to particles of diameters in the range of 712-825 nm (maximum intensity of 22.6 corresponded to agglomerates of 825 nm in diameter). The third band, in turn, fitted the range of 2670-3090 nm, with maximum intensity of 25.2 for particles of 2670 nm in diameter. The unmodified sample contained both particles of high diameters (representing agglomerates of magnesium silicate particles, which unfavourably affected physicochemical parameters of the entire sample), and particles of lower diameter.

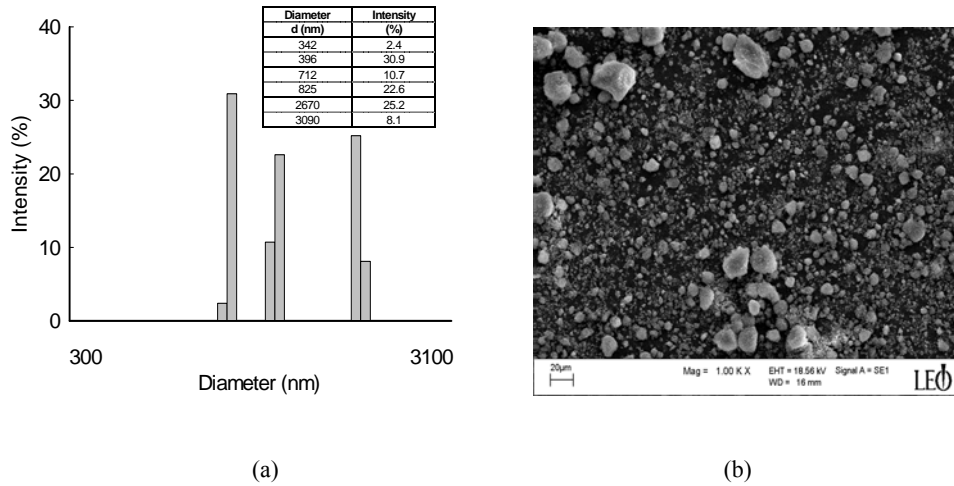


Fig. 1. (a) Particle size distribution and (b) SEM microphotograph of unmodified magnesium silicate

The distribution was confirmed by graphs illustrating input of particles of a given diameter into volume and number of particles in the sample (Fig. 2). The graph illustrating volume input of particles of a given diameter showed that particles of the lowest diameters comprised 37% of sample volume, while particles of the second band and agglomerates comprised each 33% of the volume. Numerical input of the particles in the examined sample was similar: particles of individual bands comprised 36%, 30% and 34% samples particles for the first, second and third band, respectively. The distribution of particle diameters was confirmed by SEM microphotograph of the unmodified sample (Fig. 1b).

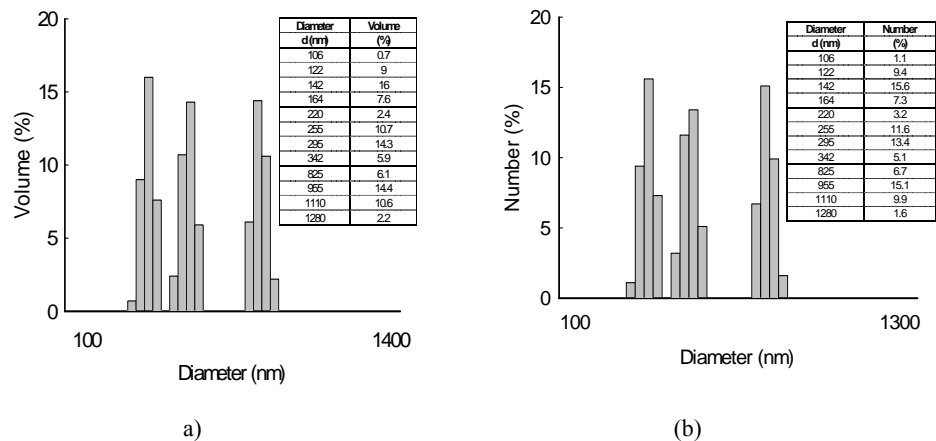


Fig. 2. (a) Volume and (b) numerical input of individual particles of unmodified magnesium silicate

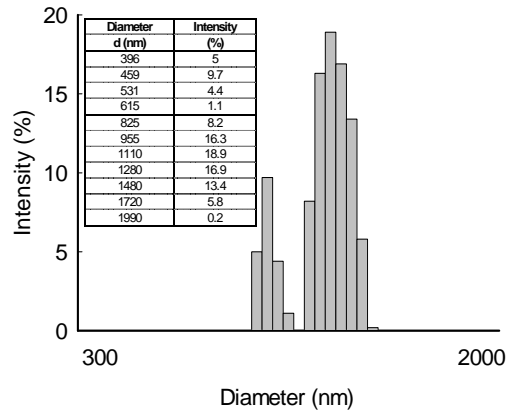


Fig. 3. Particle size distribution of magnesium silicate modified with 3 w/w of Rokanol K7

Application for the modification of 3 weight parts of Rokanol K7 (Fig. 3) insignificantly improved quality of the sample. In the particle size distribution two bands were noted. The most intense band corresponded to particles of 825-1990 nm in diameter (maximum intensity of 18.9 corresponded to the particles of 1110 nm in diameter), while the other band representing the particle diameter range of 396-615 nm was characterized by maximum intensity of 9.7 for the particles of 459 nm in diameter.

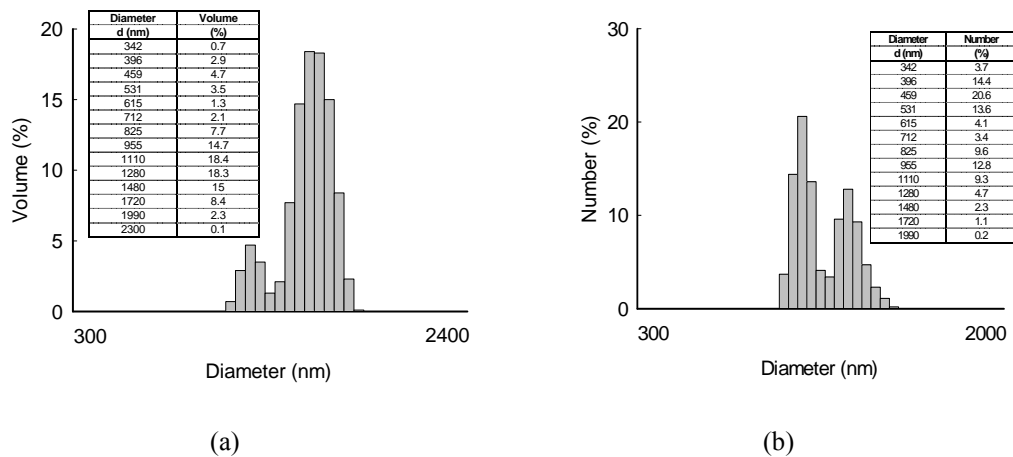


Fig. 4. (a) Volume and (b) numerical input of individual particles of magnesium silicate modified with 3 w/w of Rokanol K7

In analysis of volume input of particles of a given diameter (Fig. 4a) it could be noted, in comparison with the unmodified sample, that the number of agglomerates (the band of particles in the range of 1110-2300 nm) markedly increased. Particles of

lower diameters, i.e. in the range of 300 to 825 nm, comprised only 20% volume of all the particles. In turn, considering numerical input of particles of a given diameter in the sample (Fig. 4b) the difference in numbers of large and small particles could be noted to be much less pronounced: the particles corresponding to the first band comprised 60% and those corresponding to the second band included 40% of all particles. This, however, reflected the applied measuring technique since the larger particles (agglomerates) yielded a definitely stronger signal even if they might be present in lower numbers in the sample. Therefore, to corroborate the presence of particles of a specific diameter in the sample, analysis of particle size distribution had to be performed in respect to band intensity and input into sample volume/numerical force particles. Sedimentation of magnesium silicates unmodified or modified using non-ionic surfactants is presented in Fig. 5.

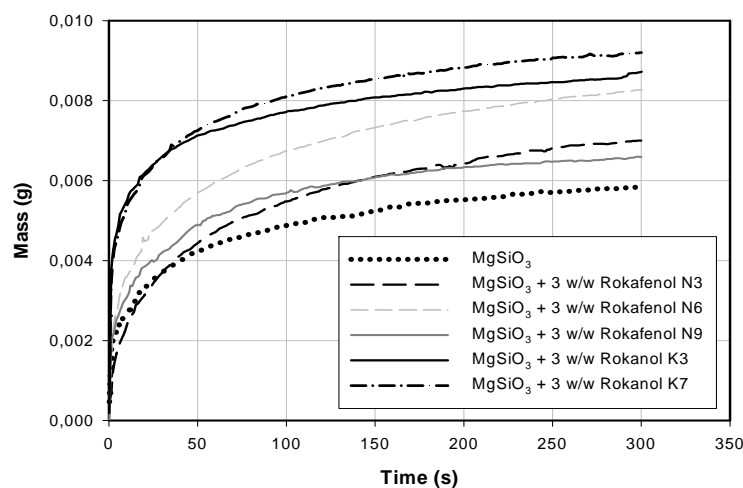


Fig. 5. Curves of sedimentation of magnesium silicate particles, unmodified or modified using non-ionic surfactants

The graph allowed to determine effect of the applied modifying agent on agglomeration tendency of precipitated silicate particles and, thus, on their sedimentation in water solutions. The most pronounced mass increments were recorded in the first 50 s of measurement, which might point to a very good sedimentation of the samples. After subsequent seconds the mass became stable, as shown by the course of the curves. In analysis of the total mass of the sedimented samples at a given time, it could be found to be radically different for the modified and unmodified samples. For the unmodified sample the mass amounted to 0.0059 g being the lowest among all samples tested. For the samples modified with non-ionic surfactants the value amounted, for samples modified with 3 weight parts of Rokafenol N3 to 0.0070 g, for samples modified with 3 weight parts of Rokafenol N6

to 0.0082 g, for samples modified with 3 weight parts of Rokafenol N9 to 0.0065 g, for samples modified with 3 weight parts of Rokanol K3 to 0.0089 g and for samples modified with 3 weight parts of Rokanol K7 to 0.0092 g. This might indicate that supplementation with appropriate non-ionic surfactant induced agglomeration of silicate particles, which was confirmed by the increased volume of the sedimented sample (as compared to the unmodified one) at the same time point. Surface wettability with water of modified and unmodified synthetic magnesium silicates is illustrated in Fig. 6.

Synthetic magnesium silicates belong to substances, which manifest high wettability with water. In view of numerous applications, silicate surface is subjected to surface modifications to increase hydrophobic character of the surface. In the cases of samples modified with non-ionic surfactants every sample manifested a distinct wettability. All the modifiers increased wetting time, as indicated by the character of wetting curves in the course of the first 1000 s. The magnesium silicate sample modified with 3 weight parts of Rokafenol N6 proved to be slowest in wetting, followed by samples modified with 3 weight parts of Rokafenol N3, Rokanol K7, Rokanol K3 and Rokafenol N9. The most rapidly wetted sample was found to be unmodified magnesium silicate. The total amount of adsorbed water for all the samples ranged between 1.5 and 1.8 g. In the same period of time the highest amount of water was adsorbed by the sample modified with 3 weight parts of Rokafenol N3, the lowest amount of water – by the sample modified with 3 weight parts of Rokafenol N6 and by the unmodified sample.

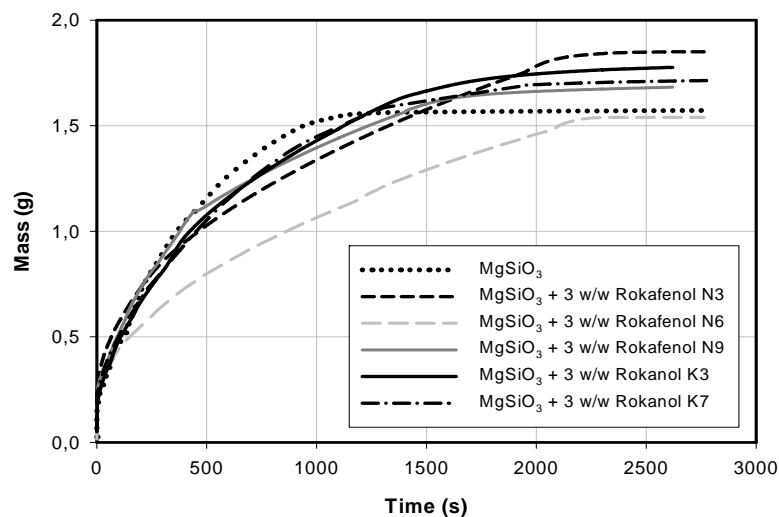


Fig. 6. Curves of wetting with water of the surface of magnesium silicate, unmodified and modified using non-ionic surfactants

CONCLUSIONS

As the result of performed studies synthetic unmodified and modified magnesium silicates were obtained which could successfully be used as selective adsorbents, fillers of polymers and of paper-coating masses. This was indicated first of all by the potential for modification of physicochemical properties of the precipitated silicates using appropriate compounds (in this case this involved hydrophobization of the surface using non-ionic surfactants).

Addition of small amounts of non-ionic surfactants was found to induce no pronounced changes in diameters of magnesium silicate particles. Higher amounts of the agents induced extensive agglomeration of the obtained sample (confirmed by the particle size distribution). In turn, more pronounced agglomeration of the sample intensified sedimentation of synthetic magnesium silicate particles (in particular the modified ones) in water solutions. In the solutions within a defined time period a decisively higher sample mass sedimented as compared to the unmodified silicate. In addition, the samples precipitated in the presence of respective modifying agents manifested lower rate of wetting with water as compared to the unmodified sample. This resulted from the accentuated hydrophobic character of the synthetic magnesium silicate surface, particularly following the modification with higher amounts of non-ionic surfactants.

The simple method for production of synthetic magnesium silicates and for modification of their physicochemical properties causes that the products may successfully compete with their natural equivalents, both in their physicochemical properties and in direction of their application.

REFERENCES

- BELONOSHKO A. B., DUBROVINSKY L. S., (1996), *Molecular and lattice dynamics study of the MgO-SiO₂ system using a transferable interatomic potential*, *Geochemica et Cosmochimica Acta*, 60, 1645-1656
- BROWN R. F. G., CARR CH., TAYLOR M. E., (1997), *Effect of pigment volume concentration and latex particle size on pigment distribution*, *Progress in Organic Coatings*, 30, 185-194
- CARDONA A. I., CANDAL R., SANCHEZ B., AVILA P., REBOLLAR M., (2004), *TiO₂ on magnesium silicate monolith: effects of different preparation techniques on the photocatalytic oxidation of chlorinated hydrocarbons*, *Energy*, 29, 845-852
- CHAPLOT S. L., CHOUDHURY N., (2000), *Phase transitions of enstatite MgSiO₃: a molecular dynamics study*, *Solid State Communications*, 116, 599-603
- CIESIELCZYK F., KRYSZTAFKIEWICZ A., JESIONOWSKI T., (2004), *Influence of precipitation parameters on physicochemical properties of magnesium silicates*, *Physicochemical Problems of Mineral Processing* 38, 197-206
- DĄBROWSKI A., HUBICKI Z., PODKOŚCIELNY P., BARCZAK M., (2006), *Selektywne usuwanie jonów metali ciężkich z wód oraz ścieków przemysłowych poprzez wymianę jonową*, *Przemysł Chemiczny*, 85, 232-241
- ELIZALDE-GONZALES M. P., MATTUSH J., EINICKE W. D., WENNRICH R., (2001), *Sorption of natural solids for arsenic removal*, *Chemical Engineering Journal*, 81, 187-195

- HAGGERTY G. M., BOWMAN R. S., (1994), *Sorption of chromate and other inorganic anions by organo-zeolite*, Environmental Science and Technology, 28, 452-458
- KARKI B. B., STIXRUDE L., CLARK S. J., WARREN W. C., ACKLAND M. C., (1997), *Elastic properties of orthorhombic MgSiO₃ perovskite at lower mantle pressures*, American Mineralogist, 82, 635-638
- KOBAYASHI T., (1996), *Pigment dispersion in water-reducible paints*, Progress in Organic Coatings, 28, 79-87
- KOCIOLEK-BALAWAJDER E., OCIŃSKI D., (2006), *Przegląd metod usuwania arsenu z wód*, Przemysł Chemiczny 85, 19-26
- KRYSZTAFKIEWICZ A., LIPSKA L. K., CIESIELCZYK F., JESIONOWSKI T., (2004), *Amorphous magnesium silicate – synthesis, physicochemical properties and surface morphology*, Advanced Powder Technology, 15, 549-565
- LI Z., BOWMAN R. S., (1997), *Counterion effects on the sorption of cationic surfactant and chromate on natural clinoptilolite*, Environmental Science and Technology, 31, 2407-2412
- TEMUJIN J., OKADA K., MACKENZIE K. J. D., (1998), *Role of water in the mechanochemical reactions of MgO-SiO₂ systems*, Journal of Solid State Chemistry, 138, 169-177
- VIET P. H., CON T. H., HA C. T., HA H. V., BERG M., GIGER W., SCHERTENLEIB R., (2002), *Proceedings of the 5th International Conference on Arsenic exposure and health effects*, San Diego, California
- WENTZCOVITCH R. M., HUGH-JONES D., ANGEL R. J., PRICE G. D., (1995), *Ab initio study of MgSiO₃ C2/c enstatite*, Physics and Chemistry of Minerals, 22, 453-460
- XU Y. H., NAKAJIMA T., OHKI A., (2002), *Adsorption and removal of arsenic(V) from drinking water by aluminium-loaded Shirasu-zeolite*, Journal of Hazardous Materials, B92, 275-287

ACKNOWLEDGEMENTS

This work was supported by the 6th Framework Programme, Contract No INCO-CT-2003-003355, within the project of Scientific Network Surfactants and Dispersed Systems in Theory and Practice (SURUZ), and by the PUT Research Grant No. 32/115/06-DS.

Ciesielczyk F., Krysztafkiewicz A., Jesionowski T., *Sedymentacja i zwilżalność syntetycznych krzemianów magnezu*, Physicochemical Problems of Mineral Processing, 40 255-263, (2006) (w jęz.. ang.).

W pracy przedstawiono badania prowadzone w celu otrzymania syntetycznego krzemianu magnezu, mogącego posłużyć jako selektywny adsorbent, napełniacz polimerów lub wypełniacz do mas powlekających papier. Syntetyczny krzemian magnezu otrzymano w reakcji strącania z użyciem roztworów MgSO₄·7H₂O i Na₂SiO₃ (tzw. szkła wodnego). Ze względu na konkretne aplikacje strącanych krzemianów proces ich otrzymywania rozszerzono o element wprowadzenia do układu reakcyjnego czynników hydrofobizujących powierzchnię. W tym celu zastosowano niejonowe związki powierzchniowo czynne. Otrzymane w ten sposób produkty poddano szerokiej analizie fizykochemicznej. Oznaczono: gęstość nasypową, chłonności wody (zwilżalność wodą), ftalanu dibutyli i oleju parafinowego, rozkłady wielkości cząstek, powierzchnię właściwą. Istotnym elementem pracy były badania nad sedymentacją syntetycznych krzemianów magnezu, ważnym parametrem decydującym o kierunkach zastosowania.

Wojciech MALEWSKI, Andrzej KRYSZTAFKIEWICZ, Teofil JESIONOWSKI*

PREPARATION OF POLYSILIC ACID SOLS BY ION EXCHANGE METHOD

Received March 15, 2006; reviewed; accepted May 15, 2006

In the study application of the macroporous ionite, Amberlyst® 15 (Merck), was tested in the process of production of dilute solutions of silicic acid sols. The process of ion exchange was conducted in a periodic reactor employing batch technique at the temperature of 45°C or 85°C. The products involved clear and stable solutions of sols of mean SiO₂ concentrations of 4.31, 4.72, 6.34 and 6.46 wt.%. A two-stage technique for ionite recovery was also worked out.

Key words: silica sol, sodium silicate solution, cation exchange, Gaussian distribution

INTRODUCTION

Silica sols represent stable dispersions of amorphous silica particles of 4 - 5 nm to 100 nm in diameter. In most of sols silica particles manifest a non-porous structure. The idea of silica sol stability is related both to maintenance of stable particle diameter and to prevention against their aggregation. The counteraction against particle aggregation involves introduction to the system of ionic electric charge or steric stabilization of the particles. Such interactions take place in the course of adsorption on silica surface of non-ionic particles (Iler 1979).

The techniques of obtaining silica sols can be categorized into a few groups, employing, respectively,

- neutralization of alkaline solutions with acids,
- electro dialysis,
- ion exchange,
- peptization of silica gel.

* Poznan University of Technology, Institute of Chemical Technology and Engineering,
M. Sklodowskiej-Curie 2 sq., 60-965 Poznan, Poland,
E-mail address: Teofil.Jesionowski@put.poznan.pl, phone: +48(61)6653720, fax: +48(61)6653649

The neutralizing techniques most frequently involve a reaction of sodium silicate solution performed in this way that pH around 2 results, which warrants momentary stability of silica sol solution. This permitted to precipitate and to separate the sodium salt and, following its separation, to alkalize the sol in order to stabilize it and to cause further increase in the particle size. Teicher (1960) neutralized sodium silicate solution using an acid, in presence of water-soluble organic liquids, e.g., alcohols, the presence of which induced precipitation of sodium salts. White (1942) neutralized sodium silicate solution using sulphuric acid solution, and precipitated sodium sulphate by supplementation of the obtained sol with acetone. Marcheguet and Ganddon (1962) in similar experiments employed compounds forming marginally insoluble sodium salts, e.g., involving reaction of sulphate ion and glyoxal. Sanchez (1959) patented an electro dialysis process, in which alkaline metal was continuously removed until the moment when the sol developed. Such a process permitted to obtain alkalies, oxygen and hydrogen.

The pioneering studies on removal of sodium from sodium silicate solution by ion exchange were conducted by Bird (1941). Subsequent studies of Bechtold and Snyder (1951) permitted to obtain sols of controlled particle size. The technique was termed the process of particle overlapping. It involves separation into two parts of the diluted silica sol, pH >7, warming one of the parts to a temperature >60°C, so that diameters of dispersed phase reach 4 - 6 nm, which is followed by addition of the second part of the sol at a sufficiently slow rate to deposit the introduced silica on particles suspended in the solution.

Dirnberger (1955) passed sodium silicate solution through a fluidal ionite deposit at such a rate that individual ionite grains were suspended in the solution flowing up the column. Alexander (1956) obtained sol clear as water, free of soluble salts, manifesting mean particle diameters of 5 to 8 nm and specific surface area of the silica of 350 to 600 m²/g. A possibility to control the growth of the silica colloidal particles during the preparation of the stabilized silica sols by means of regulating medium pH values has been studied (Hayrapetyan 2005). Brykov evaluated regularities of dissolutions of colloidal SiO₂ particles in the formation of concentrated polysilicate solutions from stabilized silica sols (Brykov 2004). Dirnberger and Nelson (1961) obtained sol of minimum turbidity charging the periodic reactor in parallel with sodium silicate solution and ionite in the hydrogen form (temp. 88 – 90 °C, pH = 8.3 – 8.7).

The techniques taking advantage of peptization have been known for a long time and involved addition to the gel of certain amount of alkalies and warming it in water, so that no evaporation could take place (Ahlberg 1959, Mertz 1971).

EXPERIMENTAL

MATERIALS

Dilute silicic acid sols were obtained from sodium silicate solutions (density at 20°C – 1.252 g/cm³, Na₂O – 6.38 wt.%, SiO₂ – 20.31 wt.%; molar modulus – 3.28). Amberlyst[®] 15 in hydrogen form (particle size 0.3-1.2 mm, ionic exchanging capacity – 1.7 mmol/m²) as an ionic exchanger was applied.

METHODS OF STUDIES

The process of ion exchange was performed in a periodic reactor using the batch technique at the temperature of 45 or 85°C. The pressure-less reactor, made of acid-proof steel had working capacity of 450 cm³. Scheme of the equipment for production of silicic acid sols is presented in Fig.1.

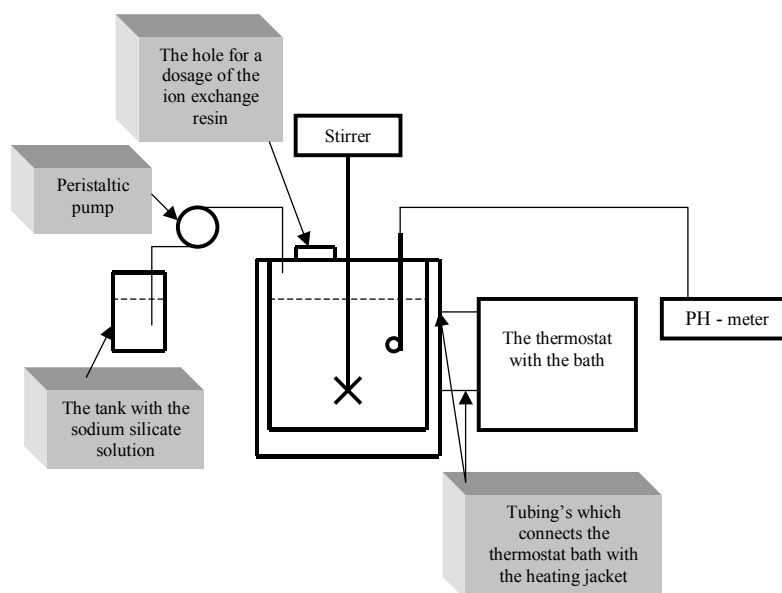


Fig.1. The apparatus for producing of the silica sol by ion exchange method (batch method)

The reactor was charged in parallel with ionite and sodium silicate so that in the sol pH of around 8.5 was maintained.

The ionite was recovered in the column at two stages. At the first stage silica was washed off the deposit using 0.5 wt.% NaOH and, at the subsequent stage, Na⁺ ions were exchanged to H⁺ ions rinsing the deposit with 5 wt.% HCl solution.

In the obtained solutions of silicic acid sols contents of SiO₂, Na₂O, and pH were estimated. The calculated molar modulus is defined as a ratio of SiO₂ mole number per

number of Na₂O moles in any amount of the sol. Exchange capacity of the ionite was established passing 1M NaOH solution through the ionite in its hydrogen form. The number of hydrogen ions exchanged in the deposit was estimated by establishing in the outflow from the deposit the amount of remaining sodium ions, using alkacymetric titration.

For statistical evaluation of the process the normal Gauss'es distribution was applied. The function of probability of density distribution for the normal distribution in the range of (+∞, -∞) has the following form:

$$f(x) = \frac{1}{\sigma\sqrt{2\pi}} e^{-\frac{(x-\mu)^2}{2\sigma^2}},$$

where:

μ – expected value of the random variable x

σ – standard deviation.

Definition of the function of probability density $f(x)$ is linked to the following condition:

$$\int_{-\infty}^{+\infty} f(x)dx = 1 .$$

Moreover, the value of arithmetical mean is assumed to represent an estimator of the unknown value of the distribution's expected variable.

RESULTS AND DISCUSSION

Histograms for molar modulus and pH of diluted solutions of silicic acid sols are presented in Figs. 2 to 5.

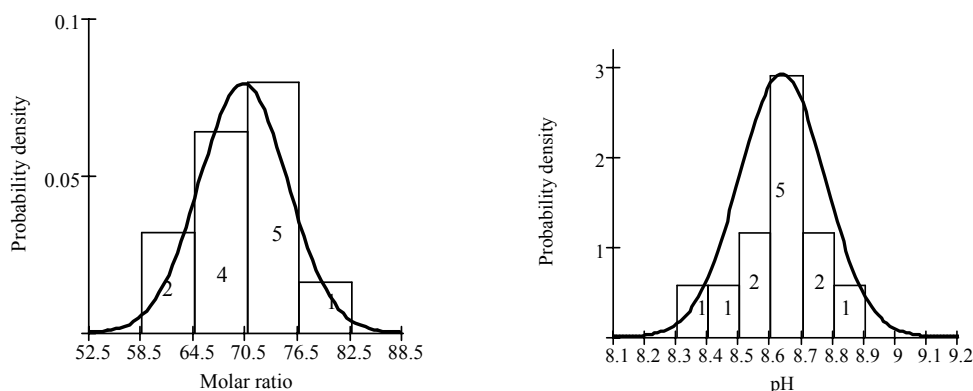


Fig. 2. The probability density functions for molar ratio and pH, concerning silica sols obtained at temperature 45°C, for scheduled SiO₂ concentration of 5 wt.%. The molar ratio probability for the range (77 ; 60) is equal to 0.89. The pH probability for the range (8.86 ; 8.39) is equal to 0.91

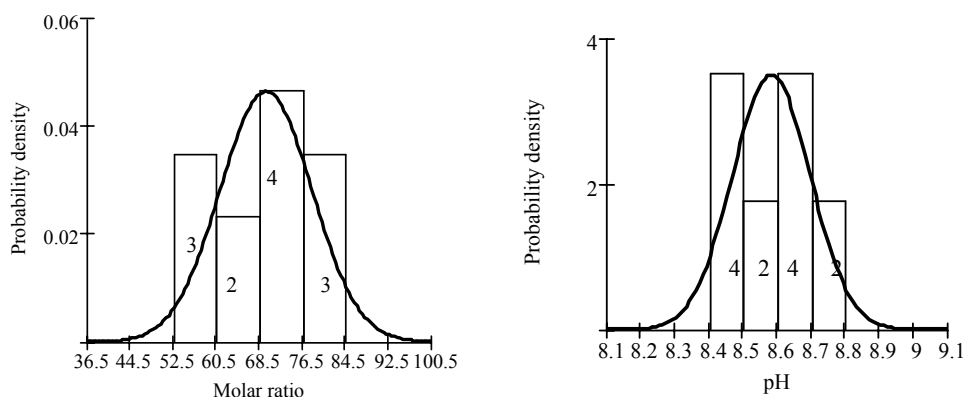


Fig. 3. The probability density functions for molar ratio and pH, concerning silica sols obtained at 45°C for scheduled SiO₂ concentration of 7.5 wt.%. The molar ratio probability for the range (81 ; 55) is equal to 0.86. The pH probability for the range (8.72 ; 8.41) is equal to 0.82

Taking advantage of the function of density distribution probability for pH and molar modulus the probability was estimated of fitting the range defined by threshold values of the variables, obtained in consecutive series of experiments. The numbers in bars denote number of measurements in a given compartment. In the case of histograms of molar modulus, rational values were accepted as limits of consecutive compartments since values of molar modulus were rounded up to integers.

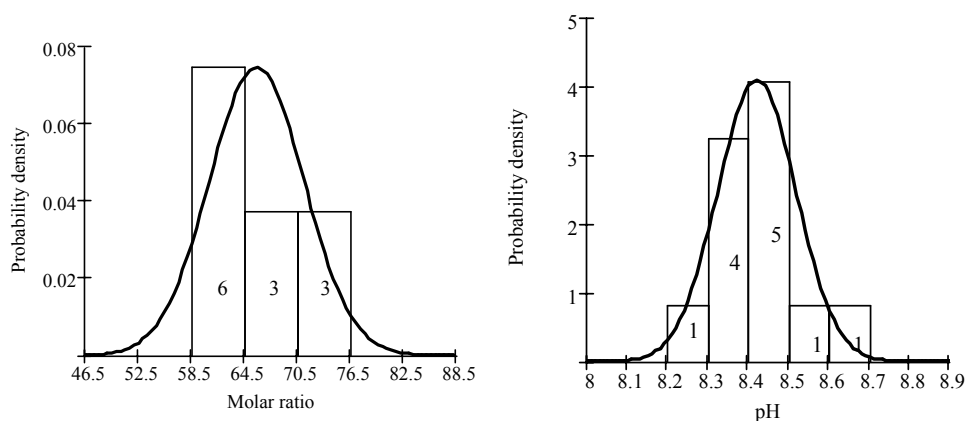


Fig.4. The probability density functions for molar ratio and pH, concerning silica sols obtained at temperature 85°C for scheduled SiO₂ concentration of 5 wt.%. The molar ratio probability for the range (75 ; 59) is equal to 0.86. The pH probability for the range (8.62 ; 8.29) is equal to 0.89

Due to the low number of measurements not all the histograms reflect symmetric nature of the normal distribution in respect to mean value and its unimodal character. Parameters of silicic acid sols obtained at the same temperatures for various planned

SiO₂ concentrations and of sols obtained at various temperatures for the same planned concentrations of SiO₂ are presented in Figs. 6 to 7.

The data of Fig. 6 indicate that at the temperature of 45°C the highest scatter of molar modulus values characterized higher concentrations of SiO₂, while mean values of the modulus were very similar for both concentrations of SiO₂. The small difference between mean values of the two modulus reflected higher content of Na₂O in the sol of higher SiO₂ content and lower content of Na₂O in the sol of lower silica content. Values of pH in two cases demonstrated similar mean values and scatters.

At the temperature of 85°C similar scatters of molar modulus and of Na₂O were obtained for both concentrations of SiO₂. In the case of molar modulus peak of density probability was clearly shifted toward higher values for higher SiO₂ concentration since positions of peak Na₂O content were almost the same. Both peaks of probability density for pH manifested similar scatters and mean values.

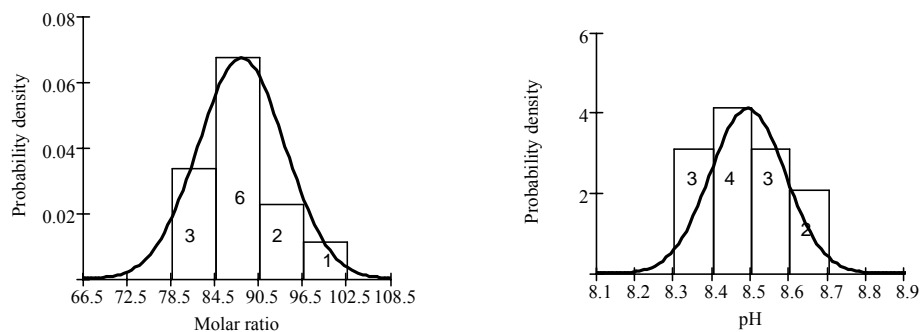


Fig. 5. The probability density functions for molar ratio and pH, concerning silica sols obtained at 85°C for scheduled SiO₂ concentration of 7.5 wt%. The molar ratio probability for the range (102 ; 81) is equal to 0.87. The pH probability for the range (8.67 ; 8.38) is equal to 0.84

As indicated by data of Fig. 7, the peak of probability density for molar modulus at the temperature of 85°C was shifted toward higher modulus, since the peak of probability density of Na₂O content at the temperature of 85°C was present among lower values as compared to the analogous peak at the temperature of 45°C. At the temperature of 85°C lower scatters of molar modulus and of sodium oxide content were obtained. The function courses for probability density distribution for pH were similar at the two tested temperatures.

The evaluation included also the ionite which was sixfold recovered and recycled in the process of sol production. In order to evaluate ionite suitability the exchanging capacity was estimated for each of the samples and compared to exchanging capacity of ionite not used in the process. The ion exchanging capacities of the samples are compared to each other in Table 1. The ion exchanging capacities of samples used in the process were slightly lower than capacity of the not yet used sample. Nevertheless, data of Table 1 documented no significant effect of sol production parameters on ionite exchanging capacity.

Table 1. Exchanging capacity of ionite samples

Estimated parameter	Exchanging capacity of ionite not used in the process	Parameters of sol production process			
		45°C		85°C	
		SiO ₂ (5 wt.%)	SiO ₂ (7.5 wt.%)	SiO ₂ (5 wt.%)	SiO ₂ (7.5 wt.%)
Ion exchanging capacity (mmol/cm ³)	1.677	1.663	1.657	1.653	1.649
		1.658	1.654	1.650	1.651

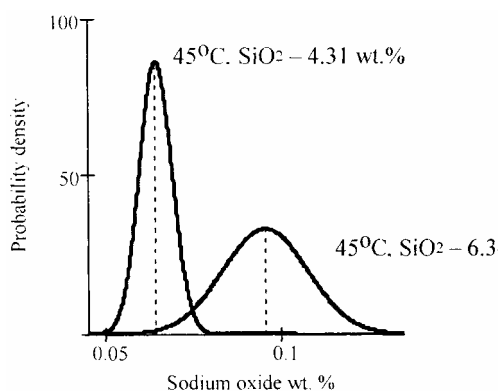
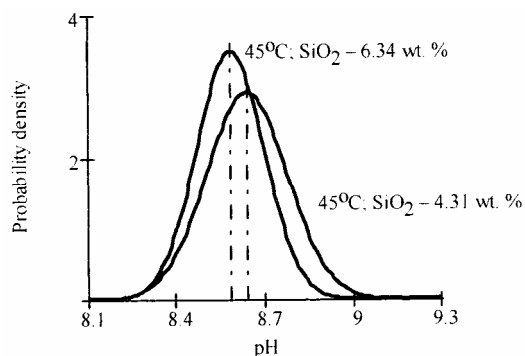
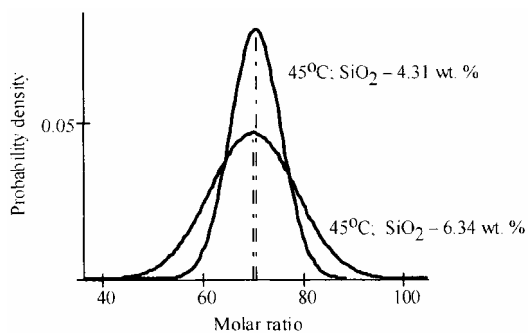


Fig. 6. The confrontation of Gaussian distributions for molar ratio, pH, and Na₂O wt.% for 45°C and scheduled SiO₂ concentrations of 5 wt.% and 7.5 wt.%

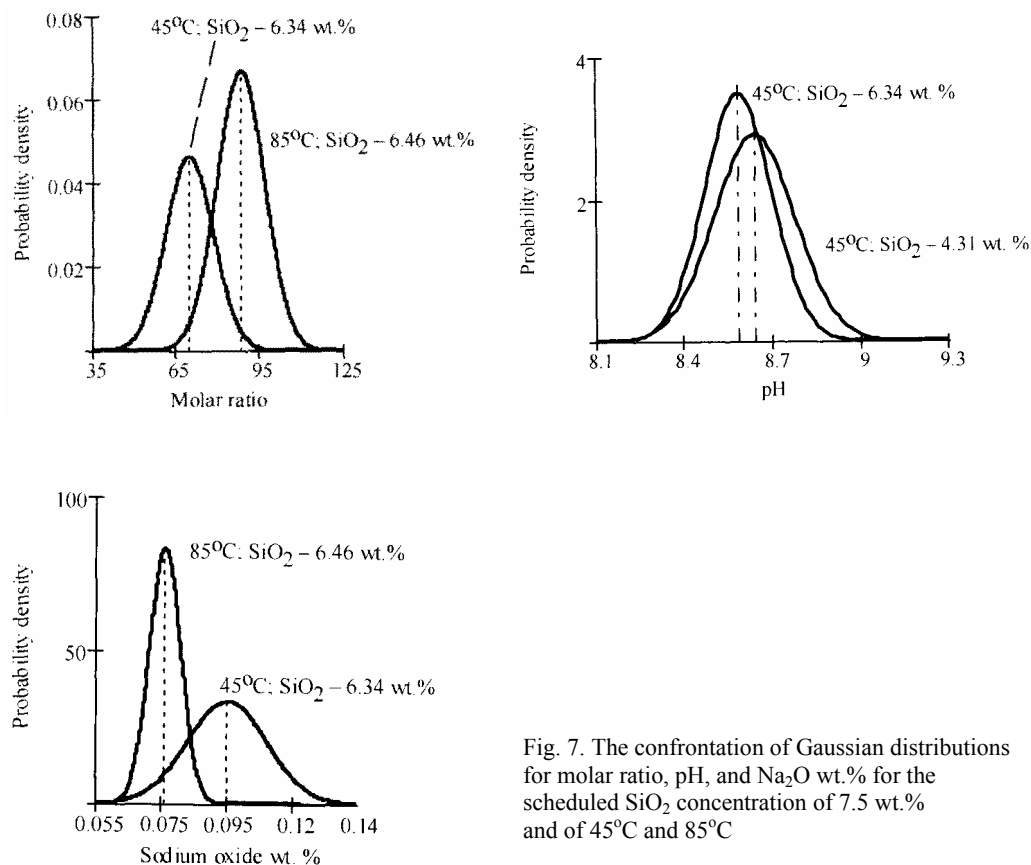


Fig. 7. The confrontation of Gaussian distributions for molar ratio, pH, and Na₂O wt.% for the scheduled SiO₂ concentration of 7.5 wt.% and of 45°C and 85°C

CONCLUSIONS

Silica gels having relatively high modulus (70–90) were obtained. Analysis of statistical data showed that increase in SiO₂ concentration in processes conducted at the temperature of 45°C induced no significant changes in molar modulus while analogous increase in processes conducted at the temperature of 85°C induced an increase in molar modulus. In all solutions of silicic acid sols pH fitted the range of (8.29 – 8.86). All the obtained sol solutions were clear.

From the point of view of ionite suitability evaluation, the batch yielded better results than the column technique. The former technique secured full access of the solution to ionite grains and precisely maintained pH in the entire reactor. Statistical evaluation confirmed high reproducibility of parameters of the obtained sols: probability of hitting the range between threshold values of pH and molar modulus always exceeded 0.8.

REFERENCES

- AHLBERG J.E., SIMPSON E.A., (1959), *Preparation of silica sols*, (W.R. Grace & Co.), US Pat. 2.900.348.
- ALEXANDER G.B., (1956), *Process for producing sols of 5-8 milimicrons silica particles and product*, (Du Pont), US Pat. 2.750.345.
- BECHTOLD M.F., SYNDER O.E., (1951), *Chemical processes and composition*, (Du Pont), US Pat. 2.574.902.
- BIRD P.G., (1941), *Colloidal solutions of inorganic oxides*, (National Aluminate Co). US Pat. 2.244.325
- BRYKOV A.S., (2004), *Formation of concentrated polysilicate solutions from stabilized silica sols*, Colloid Journal, 66, 481-486.
- DIRNBERGER L.A., NELSON R.T., (1961), *Preparation of silica sols of minimum turbidity*, (Du Pont), US Pat. 2.974.109.
- DIRNBERGER L.A., (1955), *Process of preparing an aqueous silica sol*, (Du Pont) US Pat. 2.703.314.
- HAYRAPETYNA S.S., KHACHATRYAN H.G., (2005), *Control of the growth processes of the silica sols colloidal particles*, Microporous and Mesoporous Materials, 78, 151-157.
- ILER R.K., (1979), *The chemistry of silica*, J. Wiley & Sons, New York 1979, 327.
- MARCHEGUET H.G., GADON A.L., (1962), *Process for the preparation of silica sols*, (Nobel – Bozel. Paris. France), US Pat. 3.026.267.
- MERTZ G., (1971), *Verfahren zur herstellung von kieselsauresolen*, (Baudusche Anilin & Soda Fabrik A G.), Ger. Pat. 2.006.021.
- SANCHEZ M.G., (1959), *Process for the preparation of silica sols*, (W.R. Grace & Co.), Can. Pat. 586.261.
- TEICHER H., (1960), *Preparation of silica aqua-sols*, (Monsanto Chemical Co.), Can. Pat. 609.190.
- TEICHER H., (1960), *Silica aqua-sols*, (Monsanto Chemical Co.), Can. Pat. 609.186.
- WHITE J.F., (1942), *Method of producing sols*, (Monsanto Chemical Co.), US Pat. 2.285.477.

ACKNOWLEDGEMENTS

This work was supported by the 6th Framework Programme. Contract No. INCO-CT-2003-003355 within the project of Scientific Network Surfactants and Dispersed Systems in Theory and Practice (SURUZ) and by the PUT Research Grant No. 32/115/06-DS.

Malewski W., Krysztafkiewicz A., Jesionowski T., *Otrzymywanie zoli kwasu krzemowego metodą wymiany jonowej*, Physicochemical Problems of Mineral Processing, 40 265-273, (2006) (w jęz. ang.).

W pracy przetestowano makroporowaty jonit Amberlyst® 15 (prod. Merck) w procesie otrzymywania rozcieńczonych roztworów zolu kwasu krzemowego. Proces wymiany jonowej prowadzono w reaktorze okresowym metodą batch w temp. 45 i 85°C. Produktami były klarowne roztwory zoli o średnich stężeniach SiO₂ 4,31; 4,72; 6,34; 6,46 %wag. Opracowano również dwuetapową metodę regeneracji jonitu.

Katarzyna SIWIŃSKA-STEFAŃSKA, Andrzej KRYSZTAFKIEWICZ,
Teofil JESIONOWSKI*

PHYSICOCHEMICAL ANALYSIS OF SILICAS COATED WITH NATURAL LATEX MILK

Received March 15, 2006; reviewed; accepted May 15, 2006

Studies were presented on the ways surface character of colloidal silica (SYLOID®244) can be altered from a hydrophilic to hydrophobic using natural latex milk. Effects of concentration and volume of the applied latex emulsion, LATEKS KAGETEX®FA, were examined on structure of hydrophobic silicas and their physicochemical properties, including bulk density, capacities to absorb water, dibutyl phthalate and paraffin oil. Sedimentation rate and wettability with water were also examined for the modified and unmodified silicas.

Key words: modification of silica surface, latex milk, sedimentation, particle wettability

INTRODUCTION

Due to the presence on the surface of precipitated silicas, of reactive silanol groups, the silicas find several technological applications, including their use as valuable fillers of elastomers and plastomers. The silica-filled elastomers and plastomers manifest higher tearing and abrasive strength, higher thermic and chemical resistance and improved mechanical parameters.

The inorganic-organic composites represent increasingly interesting materials in technology, due to their unusual properties reflecting parallel manifestation of characters typical for each type of the compounds.

The polymer-inorganic hybrids co-express the characters of inorganic particles, such as mechanical and thermal resistance, stability with processing potential and thermoplasticity of organic compounds. Introduction of inorganic substances to a polymer matrix may induce radical alterations in mechanic, thermal, electrical or magnetic properties as compared to those of pure organic compounds.

* Poznan University of Technology, Institute of Chemical Technology and Engineering.
M. Skłodowskiej-Curie 2 Sq, 60-965 Poznan, Poland.

E-mail: Katarzyna.Siwinska@doctorate.put.poznan.pl, phone:+48(61)6653626, fax:+48(61)6653649.

Polymer-coated inorganic particles such as silica are applied in several branches of industry, including biomedical, optical or microelectronic industries. Their use in cosmetic products, inks and paints improves the dispersion of the products. Fillers coated with macromolecular compounds increase affinity of the filler to a polymer.

Impregnation of silica surface using polymers may proceed in a physicochemical, physical (physical adsorption) or a chemical way (chemical adsorption). In the physicochemical procedure macromolecules are placed on a mineral surface due to evaporation of a solvent or become adsorbed due to chemical, biochemical or electrostatic interactions.

In a chemical process polymerization (i.a., emulsive, radical or suspension polymerization) is conducted directly in the presence of inorganic particles. In either case, the polymer must exhibit specific interactions with the inorganic surface. Various types of interactions may develop between the polymer and the inorganic material, including strong interactions (covalent, coordinate or ionic interactions) or weak ones (van der Waals interactions, hydrogen bonds, or hydrophilic-hydrophobic interactions) or the interactions may be absent (Kickelbick 2003, Luna-Xavier 2001, 2002, Bourgeat-Lami 1995, 1995).

The techniques of obtaining the polymer-inorganic hybrids may be classified into:

- „grafting onto the surface”: attaching the polymer to the mineral surface due to interaction with functional groups present on the surface (most frequently involving a chemical reaction),
- „grafting from the surface”: polymerization of monomers starting at active compounds (initiators, co-monomers) covalently grafted to the inorganic surface.

Polymer grafting onto the surface, involving condensation of polymer functional groups with reactive groups of the solid, does not allow for formation of “polymer brushes of various length”. The adsorbed polymer diminishes diffusion of subsequent chains to the inorganic surface and due to steric hindrance blocks the surface of active centers. The technique of grafting from the surface allows for a more dense packing of polymer on inorganic particles and, thus, for augmentation of their resistance to friction and corrosion (Laruelle 2004, Quingye Zhou 2002).

EXPERIMENTAL

MATERIALS

In the experiments of alteration of silica surface character by coating with the natural latex, poly(cis-isoprene) the commercial precipitated SYLOID[®]244 silica was used (produced by GRACE DAVISON). It was obtained by precipitation from sodium metasilicate solutions using sulphuric acid solution at room temperature in the form of a silica gel. The obtained gel in the form of a thin filtration cake was subsequently washed with water, dried and, then, dispersed and segregated. For the surface modification of silica latex milk was used, with the general formula of $(-\text{CH}_2-\text{C}(\text{CH}_3)=\text{CH}-\text{CH}_2-)_n$, produced by SAMIC-ALCAN GmbH.

METHODS OF STUDIES

The LATEKS KAGETEX[®]FA latex emulsion was used to change the type of surface the SYLOID[®]244 silica. The process of silica surface modification was conducted in a reactor of 500 cm³ capacity, charged before the reaction with 5 g of SYLOID[®]244 silica to which latex milk was dosed of appropriate concentration and in adequate volume. In the prepared reactor the reaction was implemented in 3 h, at the temperature of 100°C under a reflux cooler. The resulting white sediment was washed with water and filtered under a reduced pressure and the filtration cake was subjected to a stationary drying at the temperature of 105°C for 48 h.

For all the samples principal physicochemical parameters were estimated which characterize highly dispersed fillers (including bulk density, capacities to absorb water and appropriate organic agents). Sedimentation rate and wettability were also determined using the TENSIOMETR K100 type apparatus (Krüss). Silica particle size and particle size distribution were documented in the NANO ZS type apparatus (Malvern) using the technique of dynamic light scattering (DLS). Selected samples were subjected to morphological and microstructural analysis using scanning electron microscopy (SEM) and the Philips SEM 515 electron microscope. Particle size distribution allowed to determine polydispersity of the particles (as a measure of uniform character of examined powders).

RESULTS AND DISCUSSION

The relationship between bulk density of the impregnated silicas on one hand and concentration and volume of the applied latex emulsion on the other is presented in Fig. 1. Bulk density of the original, unmodified SYLOID[®]244 silica amounted to 57 g/dm³.

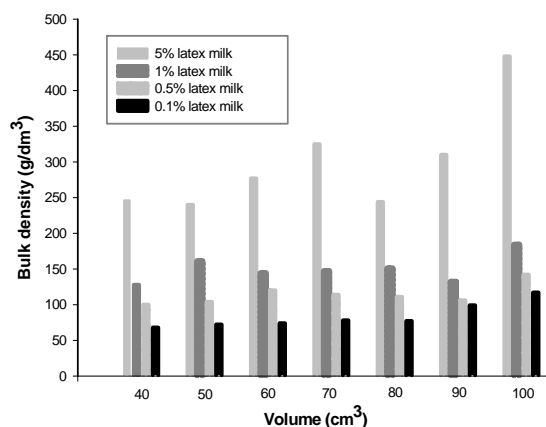


Fig. 1. Bulk density of silicas impregnated with a variable concentration and a defined volume of natural latex milk

The performed studies showed that increase in concentration and volume of latex milk used for modification of SiO₂ surface was accompanied by increasingly high bulk density of the silica.

Alterations in principal physicochemical properties of silicas impregnated with natural latex milk are illustrated in Fig. 2. The original SYLOID[®]244 silica manifested the following physicochemical parameters: capacity to absorb water: 775 cm³/100g, capacity to absorb dibutyl phthalate: 1275 cm³/100g capacity to absorb paraffin oil: 1900 cm³/100g.

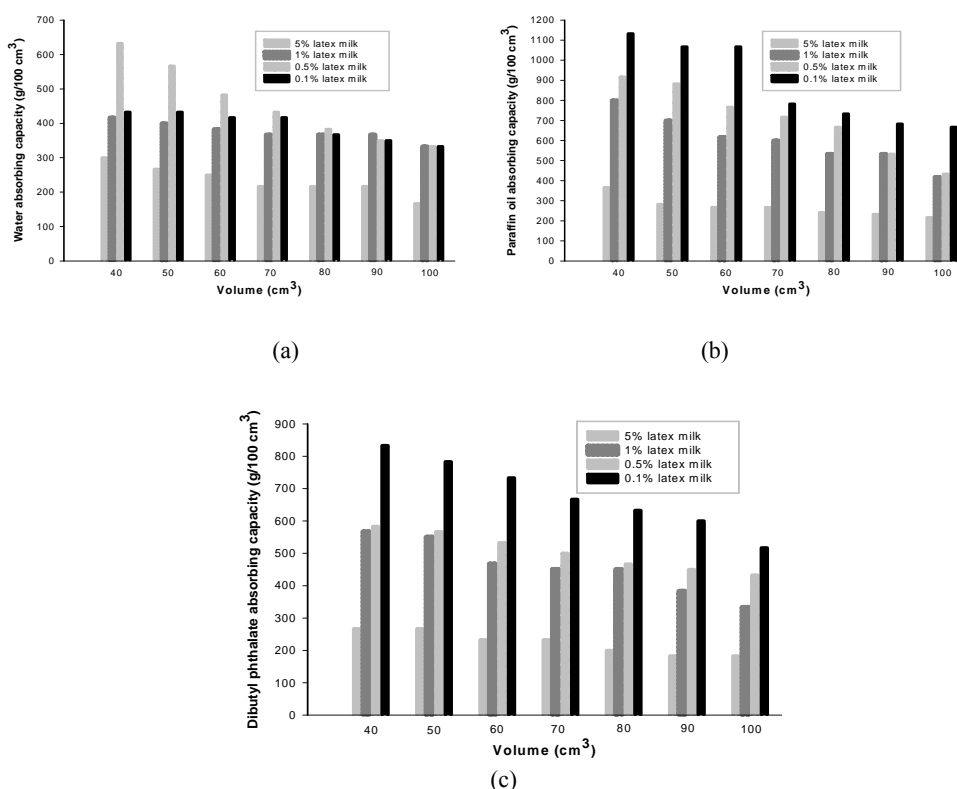


Fig. 2. Capacity to absorb water (a), paraffin oil (b), dibutyl phthalate (c) manifested by silica samples impregnated with natural latex milk of a known concentration and a variable volume

The above data allowed to note that augmented volume and concentration of the latex applied for surface modification resulted in decreasing capacities to absorb paraffin oil, dibutyl phthalate (hydrophobic substances) and even water. In every case impregnation of silica surface with natural latex took place as indicated not only by the low absorbing capacities but also by visual exponents of polymer adsorption. The silica surface showed alteration in its colour intensity: coating of silica with poly(cis-

isoprene) resulted in yellowish shade of the colour. With increasing concentration and volume of the applied latex milk the colour became darker, turning to a dark-yellow colour of the product. On the other hand the unmodified SYLOID[®]244 silica manifested white colour. Monitoring effects of latex milk applied for modification its increased concentrations could be noted to result in increased hydrophobicity of the silicas.

Particle size distribution and SEM microphotograph of silica modified with 100 cm³ 5% latex milk are presented, respectively, in Figs. 3 - 4.

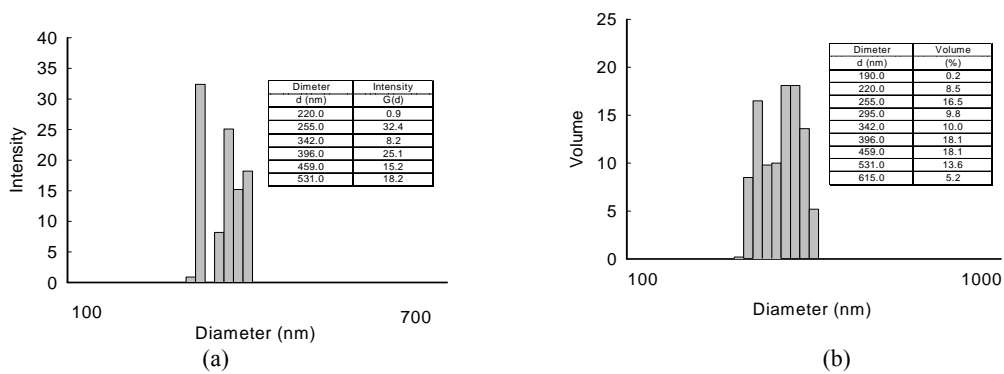


Fig. 3. Particle size distribution of silica modified with 100 cm³ 5% latex milk, as affected by the concentration of the intensity (a) and volume (b)

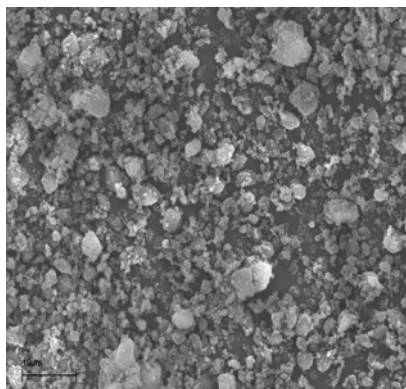


Fig. 4. SEM microphotograph of silica impregnated with 100 cm³ 5% latex milk

The particle size distribution, which reflected intensity of representation, manifested two bands. The first band corresponded to the modified silica particles of lower diameters and fitted the range of 220–255 nm (maximum intensity of 32.4 corresponded to the particle diameter of 255 nm). The other band of the particle size

distribution corresponded to particles of higher diameters and covered the range of 342–531 nm (maximum intensity of 25.1 corresponded to the particles of 396 nm in diameter). The polydispersity index amounted to 0.773. On the other hand, only one band could be observed when volume was taken into account in the particle size distribution. The band corresponded to particles of diameters ranging from 190 to 615 nm, with maximum volume of 18.1 for particles of 396 and 459 nm in diameter. The SEM microphotograph (Fig. 4) confirmed the presence of particles of low diameters, which clumped with each other forming larger aggregates and agglomerates of particles.

Particle size distribution and SEM microphotograph of silica modified with 90 cm³ 1% latex milk are shown in, respectively, Fig. 5 and Fig. 6.

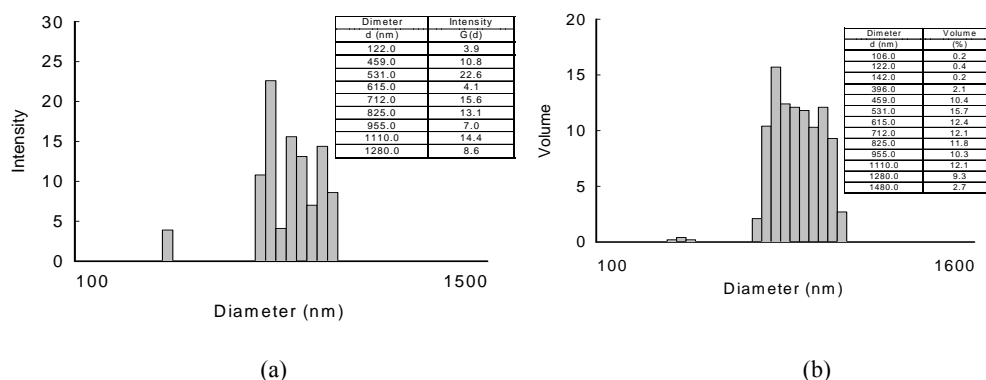


Fig. 5. Particle size distribution of silica modified with 90 cm³ 1% latex milk, as affected by the concentration, of the intensity (a) and volume (b)

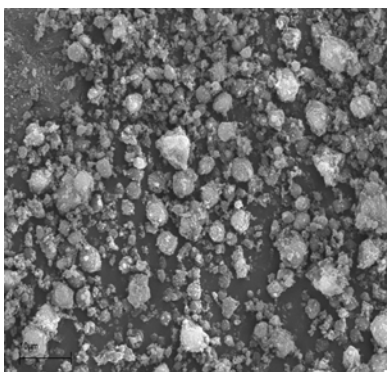


Fig. 6. SEM microphotograph of silica impregnated with 90 cm³ 1% latex milk

As demonstrated by the particle size distribution the sample was not fully uniform. The particle size distribution demonstrated the presence of two bands of distinct intensities. The first band, of a definitely lower intensity, could be ascribed to particles

of 122 nm in diameter, manifesting intensity of 3.9 and polydispersity of 0.357. The other band in the particle size distribution could be ascribed to the presence of secondary agglomerates. The band spanned the range of 459–1280 nm (maximum intensity of 22.6 corresponded to the agglomerates of 531 nm in diameter). Taking into account particle volume distribution also two bands could be distinguished. The first band of a very low intensity could be ascribed to particles of 106–142 nm in diameter, which corresponded to maximum volume of 0.4. On the other hand, the other, more intense band corresponded to particles of higher diameters, ranging from 396 to 1480 nm, with maximum volume of 15.7 for particles of 531 nm in diameter. SEM microphotograph (Fig. 6) confirmed the presence of particles with higher diameters, resulting from clumping of smaller particles into aggregates and agglomerates.

Particle size distribution and SEM microphotograph of silica modified with 60 cm³ 0.5% latex milk are presented in, respectively, Fig. 7 and Fig. 8.

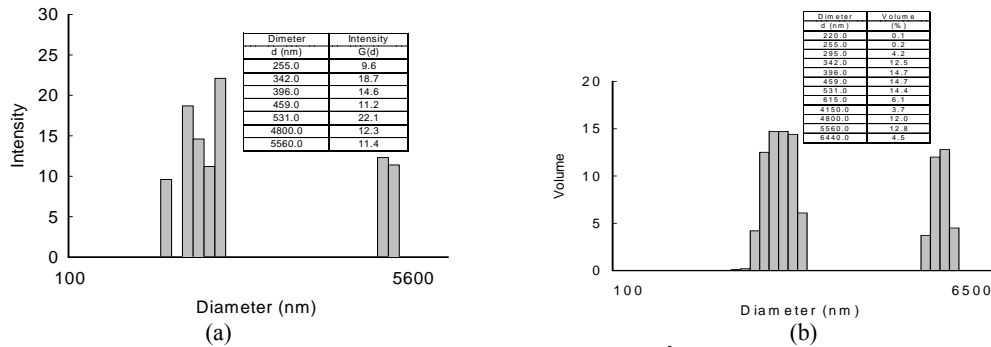


Fig. 7. Particle size distribution of silica modified with 60 cm³ 0.5% latex milk, as affected by concentration, (a) intensity (b) volume

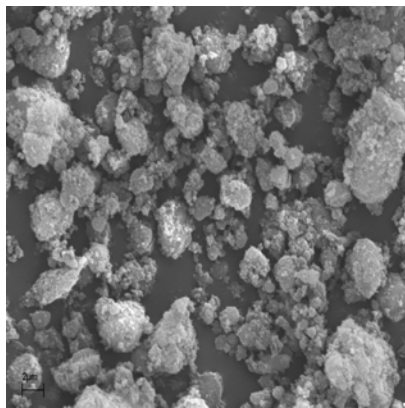


Fig. 8. SEM microphotograph of silica impregnated with 60 cm³ 0.5% latex milk

In this case particle size distribution manifested the presence of three bands of a variable intensity. The first two of them fitted the range of, respectively, 255 nm and 342–531 nm (in the second of them, maximum intensity of 22.1 corresponded to the modified silica particle size diameter of 531 nm). The third band in the particle size distribution could be ascribed to agglomerates of higher diameters. The band spanned the range of 4800–5560 nm (maximum intensity of 12.3 corresponded to particles of 4800 nm in diameter). The polydispersity index amounted to 0.750. On the other hand, taking into account particle volumes two bands could be noted. The first, more intense band was ascribed to particles of lower diameters, ranging from 220 to 615 nm, which corresponded to aggregates (maximum volume of 14.7 corresponded to aggregates of 396 and 459 nm in diameter). The other, less intense band reflected the presence of particles of higher diameters, ranging from 4150 to 6440 nm (with maximum volume of 12.8 for particles of 5560 nm in diameter). The presence of particles of the higher diameters was confirmed by SEM microphotograph (Fig. 8).

Upon modification of silica surface using 50 cm³ 0.1% latex milk the particle size distribution (Fig. 9) demonstrated, as in the previous case, the presence of three bands.

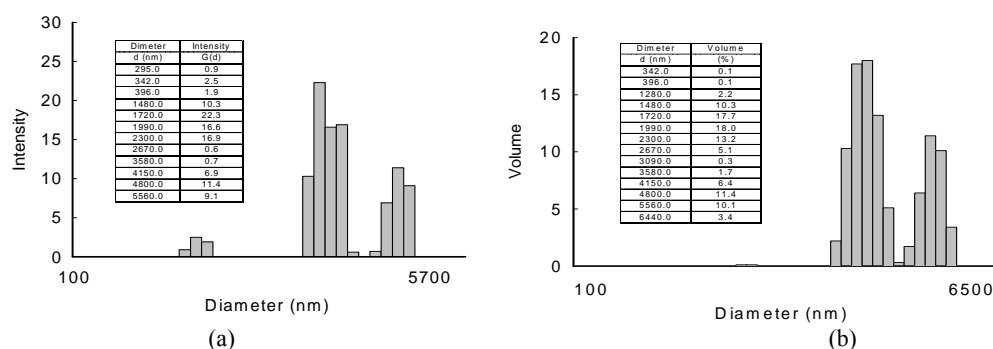


Fig. 9. Particle size distribution of silica modified with 50 cm³ 0.1% latex milk, as affected by the concentration, (a) intensity (b) volume

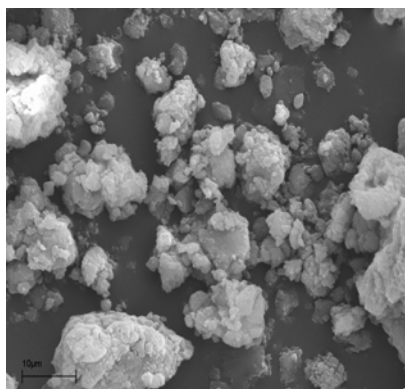


Fig. 10. SEM microphotograph of silica impregnated with 50 cm³ 0.1% latex milk

The first band was linked to the presence of particles of low diameters, in the range of 295–396 nm (maximum intensity of 2.5 corresponded to particles of 342 nm in diameter). The two remaining bands of higher intensities corresponded to particles of higher diameters and to secondary agglomerates in the range of 1480–5560 nm, with maximum intensity of 22.3 for particles of 1720 nm in diameter. The polydispersity index amounted to 0.530. Taking, on the other hand, the volume into account, the particle size distribution manifested the presence of two bands, of which the first manifested minimum intensity in the particle diameter range of 342–396 nm while the other band, spanning the range of 1280–6440 nm, corresponded to particles of higher diameters with maximum volume of 18.0 for the particles of 1990 nm in diameter. The SEM microphotograph (Fig. 10) confirmed the presence of secondary agglomerates.

The rates of wetting with water for silicas modified with 5% latex milk and the unmodified silica are compared to each other in Fig. 11.

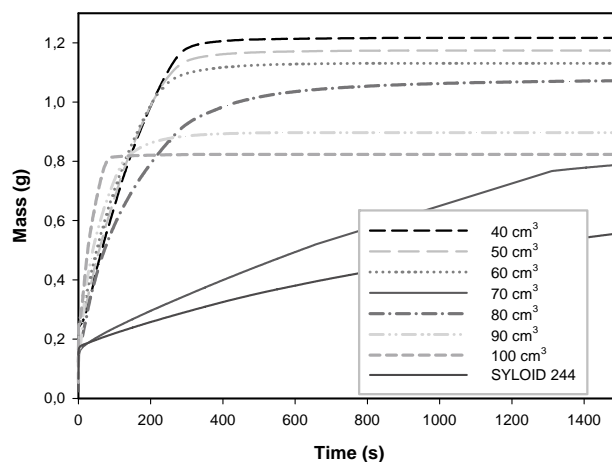


Fig. 11. Rate of wetting with water of the unmodified silica and silica modified with 5% latex milk

The studies documented that increasing bulk density of silica was accompanied by decreasing increments in silica weight in time, reflecting decreasing rates of wetting of the silica sample. For the sample modified with 40 cm³ 5% latex milk bulk density amounted to 246 g/dm³ and the silica demonstrated the highest increments in weight in time. For silicas modified with 60 cm³ and 100 cm³ latex bulk density values amounted to, respectively, 277 g/dm³ and 488 g/dm³. The relationship did not hold in the case of sample modified with 70 cm³ latex milk, which manifested the lowest weight increase but the sample showed higher wettability as compared to that of the original, pure SYLOID[®]244 silica.

Rates of wetting with water of the unmodified silica and silicas modified with 1% latex milk are compared in Fig. 12.

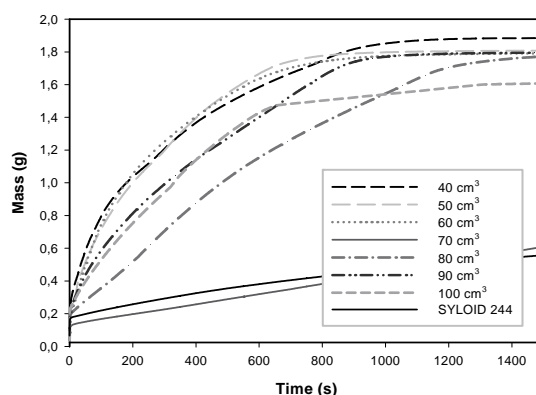


Fig. 12. Rate of wetting with water of the unmodified silica and silica modified with 1% latex milk

In the analysis of wettability with water of silicas modified with 1% latex milk and those modified with 5% latex milk a similar character of their surface could be disclosed. The weight increments in time, determined by the rates of wetting the samples decreased with increase in their bulk density. For the sample modified with 40 cm^3 1% latex milk bulk density amounted to 128 g/dm^3 , while bulk densities of silica samples modified with 80 cm^3 and 100 cm^3 latex amounted to, respectively, 151 g/dm^3 and 184 g/dm^3 . Similarly, the sample modified with 70 cm^3 latex milk manifested the lowest weight increment but the sample showed better wettability as compared to the original SYLOID[®]244 silica.

Rates of sedimentation in water of silicas modified with 1%, 0.1% latex milk and of unmodified silica are compared in Fig. 13, respectively.

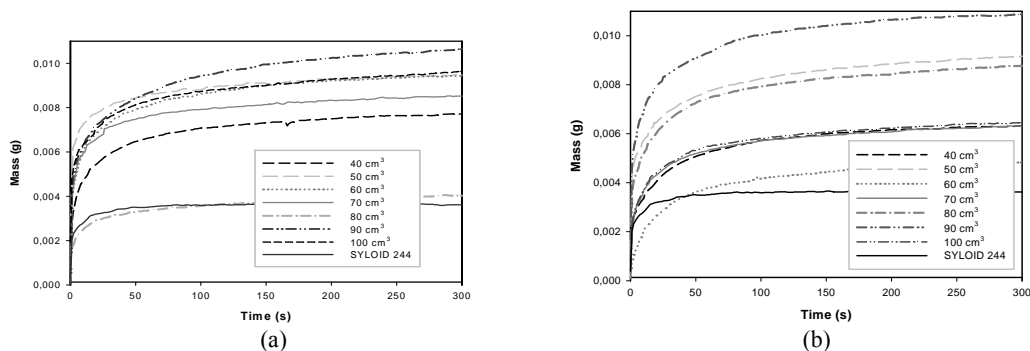


Fig.13. Rates of sedimentation in water of unmodified silica and silica modified with 1% latex milk (a), 0.1% latex milk (b)

The results showed that silicas modified with latex milk manifested sedimentation rates which decreased with increasing amounts of latex milk used for modification and with increasing hydrophobic character of the silica. For the sample modified with 1%

latex milk the situation was as follows: the capacity to absorb water amounted to 400 cm³/100g when silica was modified with 50 cm³ latex milk, 383 cm³/100g when it was modified with 70 cm³ latex milk, 363 cm³/100g when it was modified with 80 cm³ latex milk. As demonstrated by the above values, an increase in silica surface hydrophobicity resulted in decreasing weight increments in time, which determined the rate of sample sedimentation in water. A similar situation was in the case of the sample modified with 0.1% latex milk: the capacity to absorb water amounted to 433 cm³/100g when the sample was modified with 50 cm³ latex milk, 367 cm³/100g when it was modified with 60 cm³ latex milk, 333 cm³/100g when it was modified with 70 cm³ latex milk. The highest weight increment for the studied samples was observed at the beginning of the measurements and the increments decreased in time when the weight of the samples increased.

CONCLUSIONS

The proposed method for silica surface modification using latex emulsions represents a simple technique, which leads to products of interesting physicochemical parameters. Present studies indicate that augmented concentration and amount of the latex milk used for alteration of silica surface increase bulk density and hydrophobicity of SiO₂. Silicas of lower particle diameters are obtained upon surface modification with 5% latex, as demonstrated by SEM microphotographs. The lowest polydispersity (0.357) has been manifested by the silica, which was modified using 1% latex milk.

The experiments have shown that augmented bulk density of the modified samples is accompanied by decreasing weight increments in time, determining the rate of wetting the samples with water. The exception involves samples modified with 70 cm³ latex which show lower weight increments in time but the weight remains more favourable than that of pure SYLOID[®]244 silica.

The rate of silica sedimentation in water measured by the weight increments in time is lower for the samples modified with latex milk (it decreases with increasing amount of latex emulsion used for the modification). The observed effect clearly proves for augmented hydrophobicity of silica following its modification using the polymer emulsion.

REFERENCES

- BOURGEAT-LAMI E., ESPIARD PH., GUYOT A., (1995), *Poly(ethyl acrylate) latexes encapsulating nanoparticles of silica: 1. Functionalization and dispersion of silica*, Polymer, 36, 4385-4389.
- BOURGEAT-LAMI E., ESPIARD PH., GUYOT A., (1995), *Poly(ethyl acrylate) latexes encapsulating nanoparticles of silica: 2. Grafting process onto silica*, Polymer, 36, 4391-4395.
- KICKELBICK G., 2003, *Concepts for the incorporation of inorganic building blocks into organic polymers on a nanoscale*, Progress in Polymer Science, 28, 83-114.
- LARUELLE G., PARVOLE J., FRANCOIS J., BILLON L., (2004), *Block copolymer grafted-silica particles: a core/double shell hybrid inorganic/organic material*, Polymer, 45, 5013-5020.

- LUNA-XAVIER J.L., GUJOT A., BOURGEAT-LAMI E., (2002), *Synthesis and characterization of silica/poly(methyl methacrylate) nanocomposite latex particles through emulsion polymerization using a cationic azo initiator*, Journal of Colloid and Interface Science, 250, 82-92.
- LUNA-XAVIER J.L., GUJOT A., BOURGEAT-LAMI E., (2001), *The role of initiation in the synthesis of silica/poly(methyl methacrylate) nanocomposite latex particles through emulsion polymerization*, Colloid Polym Science, 279, 947-958.
- QUINGYE ZHOU, WANG S., FAN X., ADVINCULA R., (2002), *Living anionic surface-initiated polymerization (LASIP) of a polymer on silica nanoparticles*, Langmuir, 18, 3324-3331.

ACKNOWLEDGEMENTS

This work was supported by the 6th Framework Programme, Contract No INCO-CT-2003-003355, within the project of Scientific Network Surfactants and Dispersed Systems in Theory and Practice (SURUZ), and by the PUT Research Grant No. 32/115/06-DS.

Siwińska-Stefańska K., Krysztafkiewicz A., Jesionowski T., *Analiza fizykochemiczna krzemionek powlekanych naturalnym mleczkiem lateksowym*, Physicochemical Problems of Mineral Processing, 40, (2006), 275-286 (w jęz. ang.).

Przedstawiono badania nad sposobem zmiany charakteru powierzchni krzemionki koloidalnej SYLOID 244 z hydrofilowego na hydrofobowy, wykorzystując naturalne mleczko lateksowe. Badano wpływ stężenia oraz objętości użytej emulsji lateksowej LATEKS KAGETEX®FA na strukturę krzemionek hydrofobowych oraz na właściwości fizykochemiczne, takie jak: gęstość nasypowa, chłonności wody, ftalanu dibutyli i oleju parafinowego. Wykonano również pomiary sedimentacji i zwilżalności wodą modyfikowanych i nie modyfikowanych krzemionek.

Marcin JANCZAREK*, Jan HUPKA*, Horst KISCH**

HYDROPHILICITY OF TiO₂ EXPOSED TO UV AND VIS RADIATION

Received March 15, 2006; reviewed; accepted May 15, 2006

Thin titania films can be used especially as a component of self-cleaning glass, utilizing photoinduced hydrophilic properties of titanium dioxide surfaces. For the first time thin titania layer on the Pilkington Glass ActivTM was modified with ammonia, thiourea and urea to introduce non-metal elements into titania structure to shift absorption spectrum to visible light region. Contact angles for water on Pilkington glass plates were measured for unmodified and modified titania resulting in noticeable shift of absorption spectrum towards lower energy radiation.

Key words: titanium dioxide, thin films, photoinduced hydrophilicity

INTRODUCTION

Titanium dioxide has been widely used, due to its photocatalytic properties, for environmental purification. Another application area pertains to the effect of light on the properties of TiO₂-modified surfaces (e.g. self-cleaning glass). Hydrophilicity of TiO₂ surface can be induced by UV-irradiation (Wang, et al., 1997). Wang *et al.* (1999) examined changes of contact angles for different liquids on TiO₂ single crystals (see Table 1).

Table 1. Contact angles of different liquids on the surface of single TiO₂ crystal (Wang et al., 1999)

TiO ₂ surface	Contact angles [deg]			
	Water	Ethylene glycol	Tetralin	Hexadecane
Before UV irradiation	74	44	12	7
After UV irradiation	0	0	0	0

* Department of Chemical Technology, Gdansk University of Technology, 80-952 Gdansk, ul. Narutowicza 11/12, Poland.

** Institute of Inorganic Chemistry, University of Erlangen-Nürnberg, 91054 Erlangen, Egerlandstr. 1, Germany.

As a result of UV illumination (40 mW/cm² for 30 min) of TiO₂ surfaces, contact angles of even 0° were reported. While the contact angle for oil did not change too much upon UV illumination, the contact angles for water and ethylene glycol changed significantly. The results of investigations reported in the literature show that contact angles for different liquids decrease during UV irradiation and the value of contact angle depends on time and intensity of irradiation. It was also reported that the light-induced hydrophilic surface can be reversed to a hydrophobic one when the catalyst was kept in the dark for a period of time (Wang *et al.*, 1997; 1999; Miyauchi *et al.*, 2000; 2002; Nakajima, *et al.*, 2001, 2002; Sakai *et al.*, 2001, 2003; Nakamura *et al.*, 2002; Irie *et al.*, 2003; Seki *et al.*, 2004).

MECHANISM OF PHOTOINDUCTION OF HYDROPHILIC CONVERSION OF TITANIA SURFACE

Wang *et al.* (1998) and Sakai *et al.* (2001) postulated that electrons and holes produced by UV irradiation are trapped by surface and O²⁻ ions, producing Ti³⁺ and oxygen vacancies, respectively. It results in adsorption of water molecules at the defect sites and hydrophilic domains are formed, whereas the rest of the surface remains oleophilic. On long-term storage in the dark, the chemisorbed hydroxyl groups are replaced with oxygen from air to change back the surface properties of TiO₂ from hydrophilic to hydrophobic. Presence of O₂ blocked the hydrophobic-to-hydrophilic surface wettability conversion. On the other hand, during long-term UV irradiation, when the hydrophilic domain size becomes larger, the oleophilic domain size is smaller. Therefore, the surface becomes relatively hydrophilic and oleophobic when exposed to UV light for a longer time (Wang *et al.*, 1999).

VISIBLE LIGHT-INDUCED HYDROPHILICITY OF TITANIA SURFACE

TiO₂ absorbs only UV light, therefore, it should not be possible to obtain hydrophilic properties of unmodified titania surface using visible light. Asahi *et al.* prepared TiO_{2-x}N_x films on which SiO₂ was deposited to hold adsorbed water (Asahi, 2001). Their results showed hydrophilic surface of the material which maintained contact angle equal to 6° even after 30 days, contrary to SiO₂/TiO₂ film, for which the contact angle gradually increased with time. Irie *et al.* (2003) prepared thin film of TiO_{2-x}N_x without SiO₂ deposition. They observed a decrease of water contact angle from 20° to 7° after 4 h irradiation with visible light. The contact angle for unmodified titania film did not change at such conditions. Thus, the hydrophilic properties were enhanced by increasing the degree of nitrogen substitution. A decrease of water contact angle from 25° to 15° as a result of 30 min irradiation of TiO_{2-x}N_x polycrystalline thin film was observed. The hydrophilic conversion was enhanced by applying high anodic potentials. This could be due to efficient charge separation by the anodic potentials and led to better transformation of holes to the titania surface (Premkumar, 2004).

The availability of commercial TiO₂ nanofilm, in the form of the Pilkington self-cleaning glass, made it possible to examine the visible light photoinduced hydrophilicity of nitrogen-modified titania films. It is still not clear whether visible light irradiation could influence such phenomenon, similarly to photocatalytic properties of titania.

During research presented in this paper, urea, thiourea and ammonia gas were used to modify with nitrogen commercially-available self-cleaning glass covered with a very thin layer (15 µm) of TiO₂. The Pilkington Glass ActivTM represents possible successor to Degussa P-25, especially as a reference for all other photocatalyst films that are being applied for light-enhanced air and water purification, and for self-cleaning purposes (Mills, 2003). Own modification procedure involved dip-coating step (to introduce nitrogen, carbon and sulphur) using urea and thiourea solutions in water and ethanol. Another modification method was calcination in gaseous ammonia atmosphere.

EXPERIMENTAL

Glass plates (20x60x5 mm) with a thin layer of TiO₂ (15 µm) deposited on one side of TiO₂ were obtained from Pilkington (Pilkington ActivTM, self-cleaning glass). Similarly to powder catalyst preparation procedure, thiourea, urea and gaseous ammonia were used as the source of nitrogen. The concentration of these compounds was for thiourea: 0.1 M, 1 M; for urea: 1 M, 3 M; and ammonia gas flow: 10 and 45 dm³/h. Ethanol, water and water-ethanol solutions: 1:1, 1:2, 2:1, 1:9, 9:1 were used. The dip-coating technique with 24, 60, 72 mm/min velocity of dipping was applied for the modification using self-made apparatus. Glass plates were washed thoroughly with 2 M NaOH solution and subsequently with distilled water to remove impurities from glass surface. Glass plates were UV pre-irradiated before the dipping procedure. Catalyst samples were heated in air and argon at 250°C to 500°C – for dip-coating procedure from 500 to 600°C when gaseous ammonia was used. Heating a plate without TiO₂ layer (blank sample) at 60°C in 2 M NaOH solution was carried out and allowed to remove titania layer completely for reference purposes. The contact angles for water on glass plates were measured by optical goniometer. Oriel 1000 W xenon arc lamp equipped with four optical cut-off filters: λ_≥320 nm, 400 nm, 455 nm and 495 nm was the light source. IR radiation was eliminated by water filter which was situated between lamp and cut-off filter. The radiation intensity (power flux) was 800 mW/cm².

RESULTS AND DISCUSSION

In order to activate the Pilkington glass plates in visible light modification were made. All modified samples were not active in visible light with respect to 4-chlorophenol (2.5·10⁻⁵ M). A noticeable shift of absorption spectra of thin titania layer

towards visible light was observed only for a sample modified with 0.1 M thiourea in ethanol/water solution (9:1) - see Figure 1. This sample was used in measurements of water contact angles and signed as “modified”. The velocity of dipping was fixed at 24 mm/min. After dipping the plate was dried and subsequently heated at 400°C for 15 min in limited access of air.

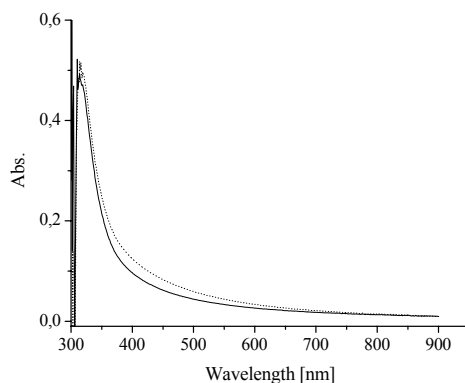


Fig. 1. Absorption spectra of unmodified (solid line) Pilkington titania layer and modified (dotted line)

Glass plates (blank, unmodified and modified) were irradiated for 15 min and 30 min using four cut-off filters: $\lambda \geq 320$ nm, $\lambda \geq 400$ nm, $\lambda \geq 455$ nm and $\lambda \geq 495$ nm. Immediately after irradiation water contact angles were measured. The samples were stored in a dark place for 1 day and water contact angles were measured again. The results of the measurements are shown in Tables 2-5.

Table 2. Results of water contact angle measurements for $\lambda \geq 320$ nm cut-off filter

Sample	Contact angle [deg]			
	Initial	Irradiation 15 min	Irradiation 30 min	Storage in dark - 24 h
Blank	61	58	59	58
Unmodified	58	0	0	54
Modified	53	0	0	50

Table 3. Results of water contact angle measurements for $\lambda \geq 400$ nm cut-off filter

Sample	Contact angle for water [deg]			
	Initial	Irradiation 15 min	Irradiation 30 min	Storage in dark - 24 h
Blank	61	58	57	60
Unmodified	58	36	25	55
Modified	53	27	19	53

Table 4. Results of water contact angle measurements for $\lambda \geq 455$ nm cut-off filter

Sample	Contact angle for water [deg]			
	Initial	Irradiation 15 min	Irradiation 30 min	Storage in dark - 24 h
Blank	61	60	57	60
Unmodified	58	40	36	56
Modified	53	31	28	51

Table 5. Results of water contact angle measurements for $\lambda \geq 495$ nm cut-off filter

Sample	Contact angle for water [deg]			
	Initial	Irradiation 15 min	Irradiation 30 min	Storage in dark - 24 h
Blank	61	60	57	60
Unmodified	58	52	50	54
Modified	53	45	41	50

For both samples (unmodified and modified), after UV illumination ($\lambda \geq 320$ nm) the contact angles decreased to 0° for two irradiation times contrary to glass plate without titania layer (blank sample), which is consistent with data available in the literature, pertaining to the Pilkington glass (Mills, 2003). Therefore, strong photoinduced hydrophilic effects of titania surface has a strong evidence for such a range of irradiation. After 1-day storage in dark the contact angles returned to almost initial values. The elimination of UV range using $\lambda \geq 400$ nm cut-off filter resulted in significantly greater values of water contact angle after irradiation. For unmodified titania layer the contact angle decreased from 58° to 36° (28 % of contact angle decrease) and 25° (57 %) after 15 and 30 min of irradiation. For the modified sample, a clear improvement was observed, not resulting from the experimental error: 53° to 27° (49 %) and 19° (64 %). For $\lambda \geq 455$ nm cut-off filter the hydrophilic effect was smaller, especially the difference between 15 and 30 min of irradiation contained in experimental error. After 15 min of irradiation contact angles were comparable to that obtained for the cut-off filter used previously. Modification of catalysts did not result in a significant increase of the hydrophilic effect in this case. Restriction of light range to 495 nm resulted in a very small decrease of contact angles for both samples. For the modified sample contact angle decreased from 53° to 41° (23 %), and for unmodified from 58° to 51° (12 %) after 30 min of irradiation.

CONCLUDING REMARKS

For the first time titania coating on the Pilkington Glass ActivTM was modified with non-metal elements (nitrogen, carbon, sulphur) using thiourea as precursor. A small shift in the absorption spectrum was observed. The change in optical properties of the thin film is probably responsible for improvement of hydrophilic properties in comparison with unmodified sample under visible light irradiation.

REFERENCES

- IRIE, H.; WASHIZUKA, S.; YOSHINO, N.; HASHIMOTO, K. (2003), *Visible-light induced hydrophilicity on nitrogen-substituted titanium dioxide films*, Chem. Comm., 1298-1299
- MILLS, A.; LEPRE, A.; ELLIOTT, N.; BHOPAL, S.; PARKIN, I.P.; O'NEILL, S.A. (2003), *Characterisation of the photocatalyst Pilkington Activ (TM): a reference film photocatalyst?*, J. Photochem. Photobiol. A: Chem, 160, 213-224
- MIYAUCHI, M.; NAKAJIMA, A.; FUJISHIMA, A.; HASHIMOTO, K.; WATANABE, T. (2000), *Photoinduced surface reactions on TiO₂ and SrTiO₃ films: photocatalytic oxidation and photoinduced hydrophilicity*, Chem. Mater., 12, 3-5
- MIYAUCHI, M.; KIEDA, N.; HISHITA, S.; MITSUHASHI, T.; NAKAJIMA, A.; WATANABE, T.; HASHIMOTO, K. (2002), *Reversible wettability control of TiO₂ surface by light irradiation*, Surf. Sci., 511, 401-407
- NAKAJIMA, A.; KOIZUMI, S.; WATANABE, T.; HASHIMOTO, K. (2001), *Effect of repeated photo-illumination on the wettability conversion of titanium dioxide*, J. Photochem. Photobiol. A:Chem., 146, 129-132
- NAKAMURA, M.; SIRGHI, L.; AOKI, T.; HATANAKA, Y. (2002), *Study on hydrophilic property of hydroxy-oxygenated amorphous TiO_x:OH thin films*, Surf. Sci., 507-510, 778-782
- PREMKUMAR, J. (2004), *Development of super-hydrophilicity on nitrogen-doped TiO₂ thin film surface by photoelectrochemical method under visible light*, Chem. Mater., 16, 3980-3981
- SAKAI, N.; FUJISHIMA, A.; WATANABE, T.; HASHIMOTO, K. (2001), *Enhancement of the photoinduced conversion rate of TiO₂ film electrode surfaces by anodic polarization*, J. Phys. Chem. B, 105, 3023-3026
- SAKAI, N.; FUJISHIMA, A.; WATANABE, T.; HASHIMOTO, K. (2003), *Quantitative evaluation of the photoinduced hydrophilic conversion properties of TiO₂ thin film surfaces by the reciprocal of contact angle*, J. Phys. Chem. B, 107, 1028-1035
- SEKI, K.; TACHIYA, M. (2004), *Kinetics of photoinduced hydrophilic conversion processes of TiO₂ surfaces*, J. Phys. Chem. B, 108, 4806-4810
- WANG, R.; HASHIMOTO, K.; FUJISHIMA, A. (1997), *Light-induced amphiphilic surfaces*, Nature, 388, 431-432
- WANG, R.; SAKAI, N.; FUJISHIMA, A.; WATANABE, T.; HASHIMOTO, K. (1999), *Studies of surface wettability conversion on TiO₂ single-crystals surfaces*, J. Phys. Chem. B, 103, 2188-2194
- Janczarek M., Hupka J., Kisch H.**, *Hydrofilowość powierzchni TiO₂ naświetlanej promieniowaniem UV i VIS*. Physicochemical Problems of Mineral Processing, 40 (2006), 287-292 (w jęz. ang.).

Cienkie filmy tlenku tytanu (IV) mogą być używane szczególnie jako komponent szkieł samoczyszczących wykorzystując zjawisko fotoindukowanej hydrofilowości powierzchni TiO₂. Po raz pierwszy cienka warstwa TiO₂ znajdująca się na powierzchni Pilkington Glass ActivTM została poddana modyfikacji za pomocą amoniaku, tiomocznika i mocznika w celu wprowadzenia pierwiastków niemetalicznych do struktury TiO₂ aby przesunąć widmo absorpcji w kierunku światła widzialnego. Kąty zwilżania dla wody zdemineralizowanej płytek szklanych Pilkington zostały zmierzone dla próbek niezmodyfikowanej i zmodyfikowanej, która odznaczała się zauważalnym przesunięciem spektrum absorpcyjnego w kierunku promieniowania o mniejszej energii.

Marta KRASOWSKA^{1*}, Konrad TERPILOWSKI², Emil CHIBOWSKI²,
Kazimierz MALYSA¹

APPARENT CONTACT ANGLES AND TIME OF THE THREE PHASE CONTACT FORMATION BY THE BUBBLE COLLIDING WITH TEFLON SURFACES OF DIFFERENT ROUGHNESS

Received March 15, 2006; reviewed; accepted May 15, 2006

The paper presents results and analysis of influence of hydrophobic surface roughness on apparent contact angle values (equilibrium conditions) and time of the bubble attachment (dynamic conditions) to hydrophobic solid surfaces (Teflon) of different roughness. The surface roughness of Teflon plates was modified in a mechanical way using abrasive papers and/or diamond paste of different grid numbers. Measurements of contact angles were carried out by the sessile drop technique, while the time of three phase contact (TPC) formation and the bubble attachment were determined in a course of the bubble collisions with Teflon plates, using a high speed camera (1182 Hz). It was found that the surface roughness is an important parameter affecting both quantities determined. With increasing surface roughness the static contact angle was increasing, while the time needed for TPC formation and the bubble attachment was significantly shortened, from ca. 80 to 3 ms. Air entrapped inside surface scratches seems to be a reason of these effects. With increasing roughness a larger amount of air can be entrapped inside the scratches. This hypothesis is confirmed by measurements of the diameters of contact perimeter of the attached bubble, where it was found that the perimeter increases with the surface roughness.

Key words: hydrophobic solids, Teflon, surface roughness, three phase contact, bubble collision, bubble attachment, time of attachment, sessile drop, contact angle

INTRODUCTION

The hydrophobic/hydrophilic characteristic of solids is known to play a key role in many processes such as: wetting, flotation, enhanced oil recovery, cleaning technologies, superhydrophobicity, liquid spreading, plants protection, etc. Wettability is quantified in terms of the contact angle (θ) values, and it is generally, but rather

¹ Institute of Catalysis and Surface Chemistry Polish Academy of Sciences, Cracow, Poland.

² Maria Curie-Skłodowska University Department of Physical Chemistry – Interfacial Phenomena Faculty of Chemistry, Lublin, Poland.

* Corresponding author: nckrasow@cyf-kr.edu.pl.

arbitrarily assumed that $\theta < 90^\circ$ indicates that the solid is partially wetted by a liquid (for example water). Surfaces characterized by the contact angle of water smaller than 90° are usually termed hydrophilic, and if the contact angle $\theta > 90^\circ$ they are called hydrophobic. On the other hand, if the contact angle of water is higher than zero, then the work of spreading, W_s , is negative.

$$W_s = W_A + W_C \quad (1)$$

where: W_A is the work of adhesion and W_C is the work of cohesion. The works of adhesion and cohesion are related to solution surface tension as follows:

$$W_A = \sigma_{LV}(1 + \cos\theta) \quad (2)$$

$$W_C = 2\sigma_{LV} \quad (3)$$

Hence:

$$W_s = \sigma_{LV}(1 + \cos\theta) - 2\sigma_{LV} = \sigma_{LV}(\cos\theta - 1) \quad (4)$$

Negative value of W_s is the necessary condition for the flotation process to occur. So, theoretically at any contact angle higher than zero flotation of a mineral can proceed (Leja, 1982; Drzymala, 2001) and therefore in flotation the surfaces having contact angles below 90° are termed as weakly hydrophobic (Leja, 1982), while that of $\theta > 90^\circ$ are called strongly hydrophobic. Recently it was also showed (Chibowski and Hołysz, 1999/2000) in laboratory flotation experiments (Halimond's tube) that for a 50% floatability of a mineral, the negative work of spreading should amount to minimum -20mJ/m^2 . It means that for an efficient flotation the contact angle of water has to be at least 48° and more. Solids showing the contact angles of an order 140° are termed as the superhydrophobic ones and are of rapidly increasing importance in many applications (contamination prevention, enhanced lubricity and durability of materials, biocompatibility and many others). Roughness modification of a hydrophobic solid surface is one of ways for obtaining the superhydrophobic surfaces.

The first approach to characterize the equilibrium in a solid/liquid/vapor system was introduced by Young (1805) and his equation describes the mechanical balance at the line of the three phase contact (TPC) on an ideal (smooth, homogeneous, rigid and insoluble) solid (see Fig. 1A) as:

$$\sigma_{SV} = \sigma_{SL} + \sigma_{LV} \cos\theta \quad (5)$$

where: σ_{LV} is the liquid/vapor surface energy, σ_{SL} is the solid/liquid surface energy, and σ_{SV} is the solid/ vapor surface energy. The fundamental problem associated with the equilibrium contact angle is related to the structure and topography of the solid

surface, as the real solids are rough. Surface roughness can affect strongly wettability and values of the apparent contact angles. To characterize the non-geometrical ideality of a surface, roughness parameter r was introduced and defined as:

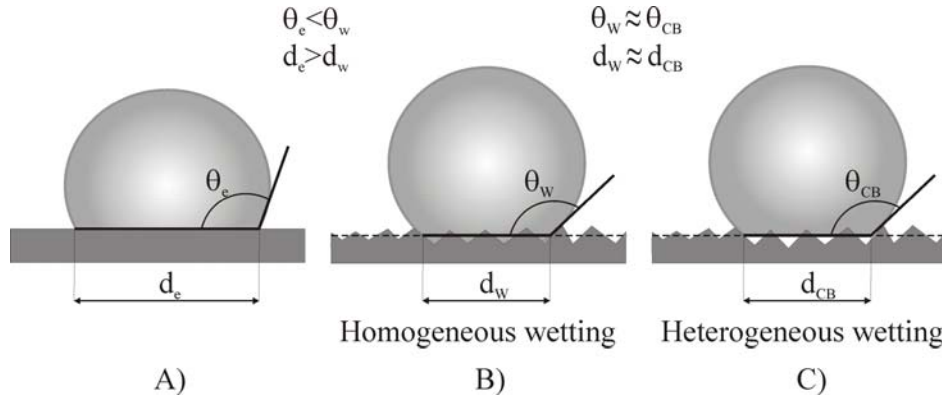


Fig. 1. Schematic of the effect of surface roughness of the hydrophobic solid on contact angle measurements by the sessile drop method

$$r = \frac{A_{real}}{A_{geometrical}} \tag{6}$$

where: (A_{real}) and ($A_{geometrical}$) are the geometrical and real areas of the surface. For $r > 1$ Young equation (5) was modified by Wenzel (1936). The Wenzel equation:

$$\cos \theta_w = r \cdot \cos \theta \tag{7}$$

is a generalization of the Young equation where: θ_w is the Wenzel contact angle. The Wenzel equation refers to so-called homogeneous wetting regime (Marmur, 2003; 2004), i.e. when the liquid completely penetrates scratches, grooves and cavities (Fig. 1B). Another situation, when air is entrapped inside the grooves underneath the liquid, is termed the heterogeneous wetting (see Fig.1C), and is described by the Cassie-Baxter equation (Cassie and Baxter, (1944):

$$\cos \theta_{CB} = r_f f \cos \theta + f - 1 \tag{8}$$

where: θ_{CS} is Cassie-Baxter contact angle, f is a fraction of the projected area that is wet by a liquid and r_f is the roughness ratio of the wet area. When $f=1$ then r_f is equal r and Cassie-Baxter equation (8) turns into Wenzel equation (7). As recently discussed by Extrand (2004) and Sedev et al. (2004), the phenomenon of higher values of contact angle on modified (roughened, micro patterned, machined or etched (Veeramasuneni et al. (1997); Oner and McCarthy (2000); Nakajima et al. (2001))

hydrophobic surfaces is caused by inhibition of the liquid spreading into grooves, scratches and/or cavities on the rough surface. Moreover, a spreading of such drop can be “arrested” by the edges of the grooves.

Differences in wettability are the factor governing possibility of separation of various components of ores during flotation. When air bubble collides with hydrophobic mineral particle inside a flotation chamber, then a thin liquid film (TLF) separating them ruptures and the particle can be attached. A stable bubble-grain aggregate formed follows up to the froth layer where grains of useful component are concentrated. Grains of the waste material (hydrophilic in their nature) do not undergo attachment to the air bubbles and settle to the bottom of the flotation tank.

During a bubble collision, which is dynamic and complex phenomenon, with hydrophobic particle following steps must take place (Leja, 1982; Nguen and Schulze, 2004): i) the film drainage until its critical thickness of rupture is obtained, ii) the film ruptures and the “nuclei” of the TPC is formed and iii) TPC expansion until perimeter ensuring the bubble-grain aggregate stability is created. Time needed for the drainage, rupture of the TLF and the bubble-particle attachment is called time of the TPC formation (t_{TPC}). Magnitude of the t_{TPC} depends strongly on hydrophilic/hydrophobic properties (Schulze et al., 2001; Stöckelheuber et al., 2001) and surface roughness (Krasowska and Malysa, 2005; Krasowska and Malysa, 2006), as well.

This paper reports results on influence of roughness of the hydrophobic solid surface on the apparent contact angle values (static conditions) and the time of the three phase contact formation by the colliding bubble (dynamic conditions). The results are discussed in terms both of the surface roughness and presence of submicroscopic gas bubbles at the hydrophobic rough surfaces being in contact with water.

EXPERIMENTAL

The contact angle measurements were carried out using Digidrop apparatus of GBX (France). To measure the contact angle hysteresis, 6 μl doubly distilled water droplet was settled on the Teflon surface and the advancing contact angle was measured. Then, 2 μl of water was sucked-off and the receding contact angle was measured. Both temperature ($22^\circ \pm 2^\circ$) and humidity (50%) were constant.

The set-up for monitoring the bubble collision with Teflon plates consists of the following parts: i) a square glass column filled with four-fold distilled water (conductivity 0.2-0.4 μS), ii) capillary of inner diameter of 0.075 mm mounted at the bottom of the column, iii) syringe pump for high precision gas supplying, iv) high-speed camera for recording the bubble collisions with the Teflon plates, v) PC with image analysis software. For monitoring and recording the bubble collisions with studied surfaces the high-speed camera (SpeedCam 512+) was mounted at the same level as the Teflon plate. All movies recorded during bubble collision with the Teflon plates were transformed into *.bmp files and carefully analyzed using the Sigma Scan

Pro 5.0 software. All other details of the experimental procedure were described elsewhere (Krasowska et al., 2003; Malysa et al., 2005). Teflon plates were mounted horizontally inside the column at the distance ca. 300 mm from the capillary orifice, just beneath the water surface. The diameter of the rising bubble was constant ($d_b = 1.5$ mm).

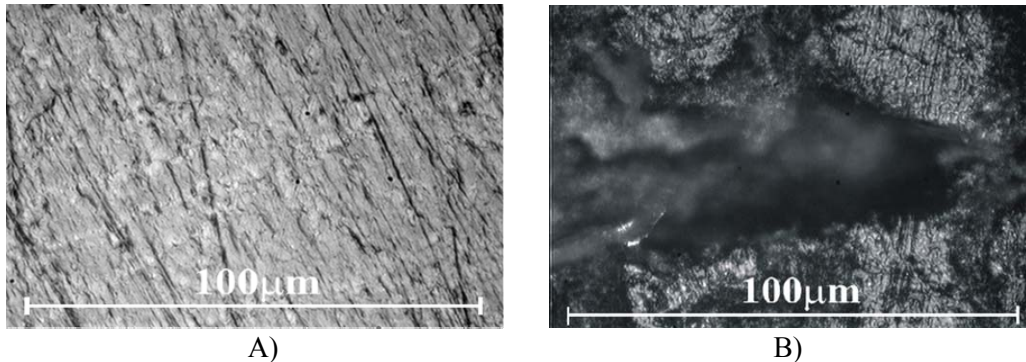


Fig. 2. Microscopic photos of the Teflon plates surfaces. A) - "Teflon I", B) - "Teflon V"

Five plates (20x20x3mm) were prepared from the same piece of Teflon, but their surface roughness was modified in a mechanical way using abrasive papers of different grid numbers. Figure 2 presents the microscopic photos of the smoothest (Fig. 2A) and the roughest (Fig. 2B) surfaces of the Teflon plates used in the experiments. First plate, called "Teflon I", had the surface modified using the abrasive paper No. 2400 and then, the diamond grinding DP-Paste $\frac{1}{4}$ μm . The second one, called "Teflon II" was tailored by using the abrasive paper No. 2400, the third one – "Teflon III" – was a Teflon plate as received from the manufacturer shop. The fourth plate, called "Teflon IV", was roughened with the abrasive paper No. 220, and the "Teflon V" was roughened using the abrasive paper No. 100. Cavities dimensions determined from the microscopic photos are listed in Table 1. As can be seen there the scratches dimensions at the "Teflon I" and "Teflon II" plates were below $1 \mu\text{m}$, for "Teflon III" – ca. 30 – 60 μm , "Teflon IV" – ca. 50-80 μm , "Teflon V" – ca. 80-100 μm .

For the contact angle measurements the plates were washed in methanol and three times in water from a Milli-Q 185 system. Then, they were boiled in the distilled water to remove air which could be entrapped between scratches, cavities etc at the Teflon surface. Next, they were put for 15 min to ultrasonic bath, rinsed with doubly distilled water and dried at 100°C . For the dynamic bubble collision measurements all Teflon plates were cleaned with a chromic mixture to avoid organic contaminants, which would strongly affect mobility of the rising bubble because of their adsorption at the bubble surface. Then, all plates were carefully washed-out with four-fold distilled water and boiled in four-time distilled water.

The experiments were carried out at room temperature ($22 \pm 2^\circ\text{C}$).

RESULTS AND DISCUSSION

Variation of the advancing and receding contact angles values as a function of Teflon surface roughness are presented in Fig.3 and in Table 1. As can be seen there the contact angle values depend on the surface roughness. For the smoothest “Teflon I” and “Teflon II” the advancing contact angles were the smallest and did not reach 100°. With increasing the Teflon surface roughness an increase in values of the measured contact angles was observed. For the roughest “Teflon V” surface the advancing contact angle was over 128 degree. As the surface modified in mechanical way is not homogenous and size of the scratches, grooves, cavities varied in a quite wide range (see Table 1), therefore some scatter in the measured values was observed. To avoid inappropriate data interpretation every contact angle measurement was repeated 20-30 times on each Teflon plate. The obtained results clearly indicate that there is a correlation between roughness of the hydrophobic (Teflon) surface and the contact angle values.

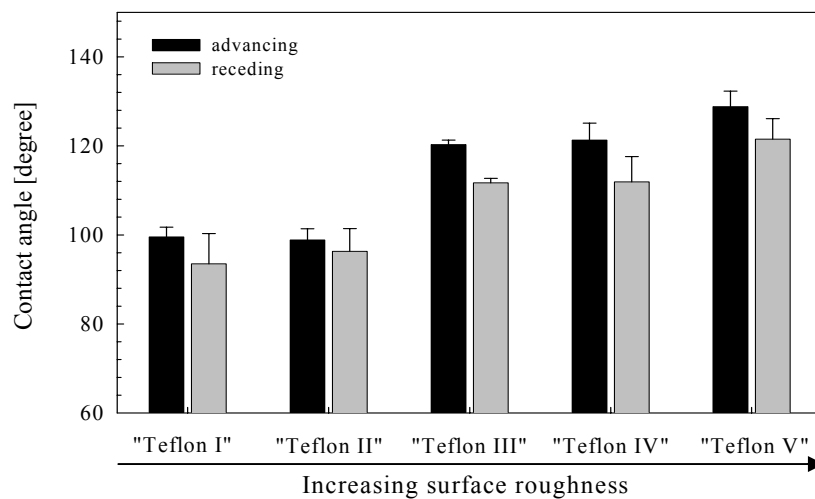


Fig. 3. Diagram of advancing and receding contact angles on Teflon surfaces of different roughness

Table 1 Advancing and receding contact angles, and roughness of the Teflon plates surfaces

Plate	Surface roughness	Contact angle	
		Advancing	Receding
Teflon I	Below 1 μm	99.6 ± 2.2	93.5 ± 6.8
Teflon II	Below 1 μm	98.9 ± 2.5	96.3 ± 5.1
Teflon III	30 – 60 μm	120.3 ± 1.0	111.7 ± 1.0
Teflon IV	50-80 μm	121.3 ± 3.8	111.9 ± 5.7
Teflon V	80-100 μm	128.8 ± 3.5	121.5 ± 4.6

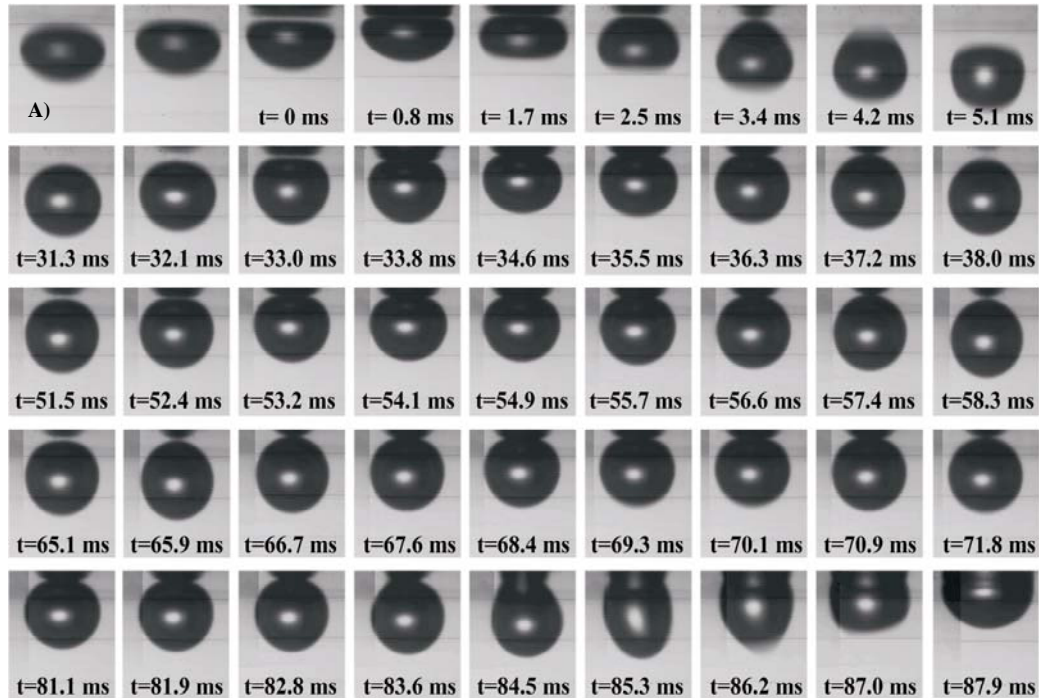


Fig. 4. Sequences of photos of the bubble colliding with “Teflon I” (A) and “Teflon V” (B) plates in distilled water

Figures 4A and 4B present two sets of photos illustrating sequence of the bubble collisions with the smoothest “Teflon I” (Fig. 4A, contact angle ca. 100°) and the roughest “Teflon V” (Fig. 4B, contact angle ca. 130°) surfaces. It is commonly assumed that when the solid surface is hydrophobic then the bubble colliding with such solid should be attached at once. Data presented in Fig.4 show clearly how surface roughness strongly affects the time of the TPC formation (t_{TPC}) and bubble attachment. It can be immediately noted that in the case of the smoothest (roughness below $1\ \mu\text{m}$) “Teflon I” surface (Fig. 4A) the attachment did not occur during the first collision but the bubble bounced a few times, despite that the surface was highly hydrophobic (contact angle ca. 100°). In the case of much more rough “Teflon V” surfaces (cavities of $80\text{-}100\ \mu\text{m}$) the bubble was attached during the first collision – there was no bouncing (see Fig. 4B). Thus, with increasing roughness of the Teflon surface the t_{TPC} was significantly shortened. As can be noted in Fig.4 the time needed for formation of the first “spot” of the TPC contact (i.e. the moment when rupture of the wetting film (WF) occurred) was $t_{TPC} = 83.6\ \text{ms}$ in the case of the smoothest surface (“Teflon I”), while for the rough “Teflon V” surface it was of an order of 2.5 ms only, i.e., 20 - 25 times shorter. However it should be stressed that the zero time on the time scale of the TPC formation and the bubble attachment had to be settled. To

avoid any arbitrariness as the zero time, called $t_{TPC} = 0$ ms it was chosen as the moment (first frames of the recordings) at which the horizontal diameter of the colliding bubble started to increase. This means that the bubble was already in contact with the solid, what stopped its upwards motion.

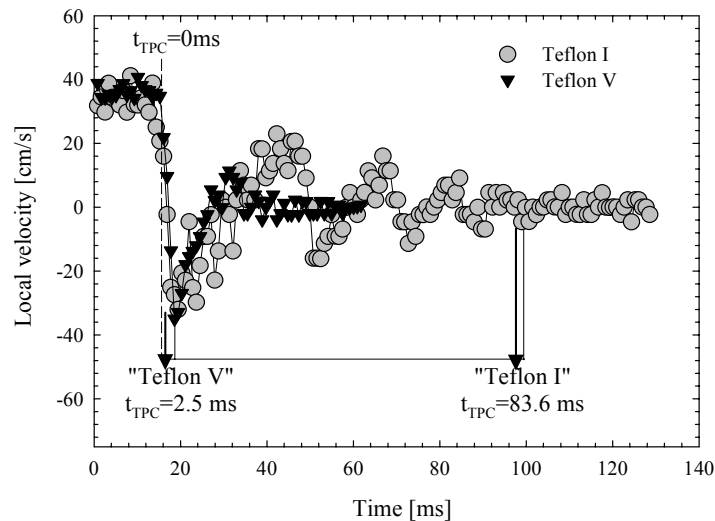


Fig. 5. Variations of the bubble local velocity during collisions (“approach-bounce” cycles) with “Teflon I” and “Teflon V” surfaces in distilled water

Quantitative data on variations of the bubble velocity during collisions with the “Teflon I” and “Teflon V” plates are presented in Fig 5. As seen there prior to the first collision the local velocity of the bubble was constant and equal to ca. 35cm/s. During the first collision the bubble was attached to the “Teflon V” surface ($t_{TPC} = 2.5$ ms). In the case of the smoothest “Teflon I” surface the bubble bounced and five “approach-bouncing” cycles can be clearly noted (see Fig. 5) prior to the TPC formation ($t_{TPC} = 83.6$ ms) and the bubble attachment. Due to energy dissipation the bubble velocity was decreasing in every subsequent cycle. Values of the t_{TPC} refer to the moment of the first “spot” of the TPC formation (see Fig. 4). As can be seen in Fig. 4 the diameter of the TPC is increasing after the t_{TPC} , but after next few milliseconds a constant perimeter was always achieved.

Contact angles can be determined using sessile drop technique or in a reverse system, i.e. by the captive bubble method. In both techniques, values of the contact angle are measured through the liquid phase. In the sessile drop method the drop settled on a highly hydrophobic surface remains almost spherical. The higher value of the contact angle is the more spherical shape of the bubble can be observed. Thus, the length of perimeter and/or the diameter of the three phase contact (TPC) are the parameters related to the contact angle values. With increasing contact angle (hydrophobicity) the diameter of TPC perimeter will decrease. The opposite is true in the case of the captive bubble method, i.e., in the case of the attached bubble.

Table 2. Photos and the three phase contact (TPC) diameters of the sessile drop and the bubble attached to different Teflon plates

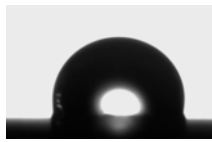
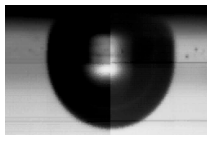
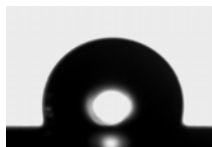
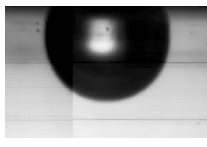
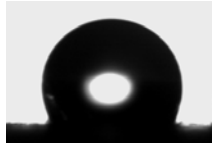
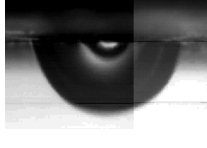
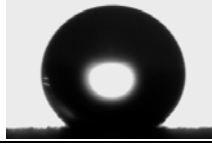
Plate	Sessile drop	Sessile drop - TPC diameter [mm]	Bubble attached	Bubble attached - TPC diameter [mm]
Teflon I		2.64		1.71
Teflon II		2.67		1.72
Teflon III		2.15		1.76
Teflon IV		2.05		2.04
Teflon V		1.88		2.29

Table 2 presents photos of the sessile drops and bubbles attached to the Teflon surfaces. As can be noticed there both TPC diameters (the sessile drop and the bubble attached to Teflon surface) depend on the surface roughness. Figure 6 presents the diameters of the TPC formed at equilibrium (contact angle measurements) and dynamic conditions (bubble attachment to the Teflon surface) as a function of the Teflon surface roughness. For the sessile drop method the diameter of the TPC becomes smaller with increasing Teflon surface roughness (see Fig. 6 and Table 2). The diameter varies from 2.64-2.67 mm for the smoothest “Teflon I” and “Teflon II” surfaces to 1.88 mm for roughest “Teflon V”. Opposite relationship can be observed for the TPC diameter of the bubble attached to the Teflon surfaces studied. Here, the

diameter of the TPC increases within the range with increasing the surface roughness (see Fig. 6 and Table 2). The smallest value of the TPC diameter was determined for "Teflon I" (1.71 mm) and the largest one for "Teflon V" (2.29 mm). Let us discuss reasons of the variations with Teflon surface roughness both the sessile drop and the attached bubble diameters. The rougher surface is the bigger scratches, grooves and gaps are on the surface. When a drop of water is settled on such surface a motion of the edge of the TPC is "restricted" by the scratches and cavities (Marmur (2004)).

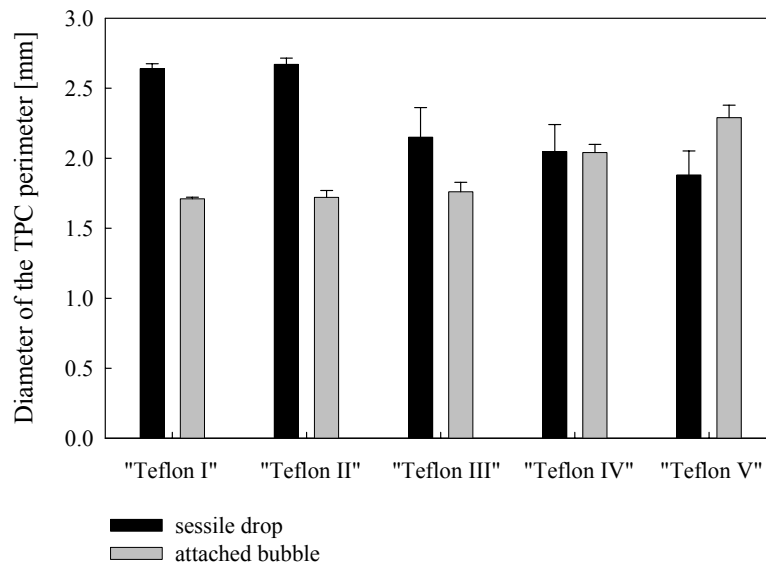


Fig. 6. Diameters of the three phase contact (TPC) perimeter for Teflon plates of different roughness

Therefore, water can not spread further over the solid surface and the diameter of the TPC becomes smaller with the increase in the surface roughness (drop remains more spherical). In the reverse system (i.e. bubble at the hydrophobic Teflon surface) the increase of the attached bubble diameter with surface roughness is related, in our opinion, to the number and size of submicroscopic bubbles adhered to the hydrophobic Teflon surface. It was reported by Ryan and Hemmingsen (1998) and Snoswell et al (2003) that during immersion of dry hydrophobic surface into solution there can be some microscopic air bubble entrapped in the grooves, scratches and gaps. In our previous papers (Malysa et al., 2005; Krasowska and Malysa, 2006) it was also showed that the presence of a micro-bubble at the hydrophobic solid surface can be one of most important parameters facilitating attachment of the colliding bubble. Because higher roughness is the bigger cavities are and more gas is entrapped. Therefore, the needed perimeter of the TPC for the bubble attachment is faster formed

there. The results presented in this paper again support this hypothesis. In the experiments the bubble size was always the same ($d_b = 1.5$ mm). Therefore, the fact that the diameter of the three phase contact of the attached bubble varied with the surface roughness (Fig. 6 and Table 2) shows that the volumes of air adhered to the Teflon plates were different. The largest diameters of the attached bubbles were found for the roughest surfaces and this is a strong evidence that this is due to larger volumes of the gas entrapped in larger cavities of the rough surface.

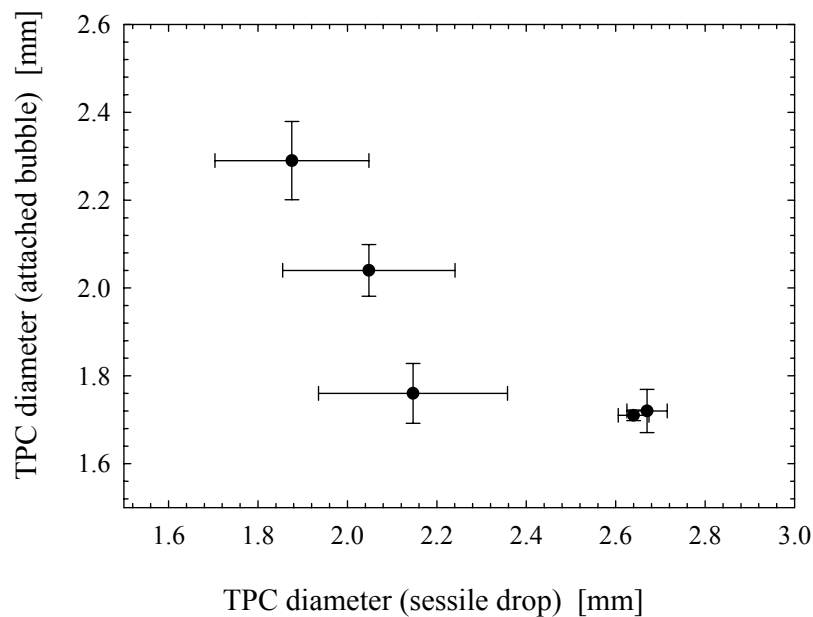


Fig. 7. Three phase contact (TPC) diameter of the attached bubble versus the TPC diameter of the sessile drop

The relationship between diameters of the TPC perimeters formed under dynamic (attached bubbles) and static (sessile drops) conditions is presented in Figure 7. It is clearly seen there that both magnitudes are inversely proportional. The contact angles are always measured through the liquid phase, i.e. smaller diameter of the sessile drop and larger diameter of the attached bubble indicate that the contact angle was larger. When the water drop is settled on the hydrophobic solid, cohesive forces between water molecules are stronger than interaction with the solid and the water tends to form a drop rather than to spread over the surface. In the case where the air bubble attached to the hydrophobic solid, such a system tends to minimize the area of the hydrophobic surface contacted with water and this is why the bubble seems to “spread” at the surface thus increasing the TPC diameter.

CONCLUSIONS

Roughness of hydrophobic Teflon surface affects both the static contact angle and the kinetics of the bubble attachment. With increasing roughness, the static contact angles at the Teflon surfaces were increasing, while the time needed for the TPC formation and attachment of the colliding bubble was decreasing (from ca. 80 to 3 ms). An appropriate modification of surfaces of the hydrophobic solids (for example through roughening) makes obtaining the superhydrophobic surfaces, i.e., the surfaces showing contact angle (for water) of 150° and larger (up to almost 180°) possible.

Air entrapped inside the scratches and cavities of Teflon surface is responsible for both the increase in contact angle and facilitation of the bubble attachment. This hypothesis is confirmed by measurements of the diameters of three phase contact perimeters of the sessile drops and the attached bubbles. In the case of sessile drop, the TPC diameter was decreasing with increasing the surface roughness because the scratches and grooves caused an energetic barrier for the water drop to spread. An opposite effect was observed for the bubble attached to the Teflon surfaces studied. The diameter of the TPC perimeter of the attached bubble was increasing with the Teflon surface roughness. As higher roughness means that more air was entrapped inside the surface cavities, therefore the diameter of the attached bubble increased.

ACKNOWLEDGEMENTS

Partial financial support of the work by Scientific Network "SURUZ" – INCO-CT-2003-003355 project is gratefully acknowledged.

LIST OF SYMBOLS AND ABBREVIATIONS

ABBREVIATIONS

TLF	Thin liquid film
TPC	Three phase contact
WF	Wetting film

SYMBOLS

$A_{\text{geometrical}}$	Geometrical area of the surface
A_{real}	Real area of the surface
d_b	Bubble diameter
f	Fraction of the projected area that is wet by a liquid
r	Roughness ratio
r_f	Roughness ratio of the wet area
t_{TPC}	Time of the TPC formation
W_A	Work of adhesion
W_C	Work of cohesion

W_S	Work of spreading
σ_{LV}	Liquid/vapor surface energy
σ_{SL}	Solid/liquid surface energy
σ_{SV}	Solid/vapor surface energy
θ	Contact angle
θ_{CS}	Cassie-Baxter contact angle
θ	Equilibrium (Young) contact angle
θ_W	Wenzel contact angle

REFERENCES

- CASSIE A. B. D., BARTER S., (1944), *Trans. Faraday Soc.*, 40, 546-551.
- CHIBOWSKI E., HOŁYSZ L., (1999/2000), *Annales UMCS*, LIV/LV8, 117-131.
- DRZYMALA J., (2001), "Podstawy mineralurgii", Oficyna Wydawnicza Politechniki Wrocławskiej (in Polish).
- EXTRAND C. W., (2004), *Langmuir* 20, 5013-5018.
- MALYSA K., KRASOWSKA M., KRZAN M., (2005), *Advances Coll. Interface Sci.* 114-115, 205-225.
- MARMUR A., (2003), *Langmuir* 19, 8343-8348.
- MARMUR A., (2004), *Langmuir* 20, 3517-3519.
- NGUYEN A.V., SCHULZE H.J., (2004), "Colloidal Science in Flotation", Marcel Dekker.
- KRASOWSKA M., KRZAN M., MALYSA K. (2003), *Physicochem. Problems Mineral Process.*, 37, 37-50.
- KRASOWSKA M., MALYSA K., (2005), *Physicochem. Problems Mineral Process.*, 39, 21-32.
- KRASOWSKA M., MALYSA K., (2006), *Intern. J. Mineral Process.* (accepted).
- LEJA J., (1982), "Surface Chemistry of Froth Flotation", Plenum Press, New York and London
- ONER D, MCCARTHY T. J., (2000), *Langmuir* 16, 7777-7782.
- SEDEV R., FABRETTO M., RALSTON J., (2004), *The J. Adhesion*, 80, 497-520.
- SHULZE H. J., STÖCKELHEUBER K. W., WENGER A., (2001), *Colloids & Surfaces A*: 192, 61-72
- SNOSWELL D. R. E., DUAN J., FORNASIERO D., RALSTON J., (2003), *J. Phys. Chem. B*, 1007, 2986-2994.
- STÖCKELHEUBER K. W., SCHULZE H. J., WENGER A., (2001), *Progr. Colloid Polym. Sci.*, 118, 11-16.
- RYAN W. L., HEMMINGSEN E. A., (1998), *J. Colloid. Interface Sci.*, 197, 1001-107.
- VEERAMASUNENI S., DRELICH J., MILLER J.D., YAMAUCHI G. (1997), *Prog. Org. Coat.* 31, 265-270.
- WENZEL N. R., (1936), *Industrial and Engineering Chemistry*, Vol.28, No. 8, 988-994.
- YOUNG T., (1805), *Phil. Trans. Roy. Soc.*, 95, 65-87.

Krasowska M., Terpilowski K., Chibowski E., Malysa K., *Kąty zwilżania a czas powstawania kontaktu trójfazowego podczas kolizji bańki z powierzchniami teflonu o różnej szorstkości*, *Physicochemical Problems of Mineral Processing*, 40 293-306, (2006) (w jęz. ang.).

W pracy przedstawiono wyniki i analizę wpływu szorstkości powierzchni hydrofobowej na wielkości wstępujących kątów zwilżania (warunki równowagowe) oraz na czas potrzebny do przyczepienia bańki (warunki dynamiczne) do hydrofobowej powierzchni ciała stałego (teflon). Szorstkość powierzchni płytek teflonowych była modyfikowana mechanicznie przy użyciu papieru ściernego o różnym

uziarnieniu oraz pasty diamentowej. Pomiarów kątów zwilżania wykonano metodą “siedzącej” kropli (sessile drop) a czas powstawania kontaktu trójfazowego (TPC) i przyczepienia bańki był wyznaczany przy zastosowaniu szybkiej kamery (1182 Hz). Wykazano, że szorstkość powierzchni jest parametrem mającym olbrzymi wpływ na obie badane wielkości. Ze wzrostem szorstkości powierzchni wzrastały wartości kąta zwilżania, a czas potrzebny do utworzenia TPC i przyczepienia bańki ulegał znacznemu skróceniu, od ok. 80 ms do 3 ms. Ponieważ ze wzrostem szorstkości zwiększa się ilość powietrza “uwięzionego” wewnątrz nierówności powierzchniowych dlatego wydaje się, że jest to czynnik decydujący o zmianach wielkości kąta zwilżania i wartości czasu potrzebnego do utworzenia TPC. Potwierdzeniem poprawności tej hipotezy są także przedstawione w pracy wyniki pomiarów średnic perymetru przyczepionej bańki. W pomiarach tych wykazano, że ze wzrostem szorstkości wzrasta średnica perymetru bańki przyczepionej do powierzchni teflonu.

Andrzej HEIM, Tadeusz GLUBA, Andrzej OBRANIAK,
Ester GAWOT-MŁYNNARCZYK, Michał BŁASZCZYK*

THE EFFECT OF WETTING ON SILICA FLOUR GRANULATION

Received March 15, 2006; reviewed; accepted May 15, 2006

The effect of changes in surface tension and degree of liquid jet break-up as well as final moisture content of the bed on changes in particle size distribution during wet drum granulation was described in the paper. The tumbling bed of loose material (silica flour) was wetted at a constant volumetric flow rate, using a system of two pneumatic spray nozzles. Different values of surface tension of the binding liquid (distilled water) were obtained due to the application of a surfactant Rokanol L4P5. In every trial samples of the feed were taken from the drum at specified time intervals and on this basis particle size composition was determined.

Key words: drum granulation, surface tension, granulation kinetics

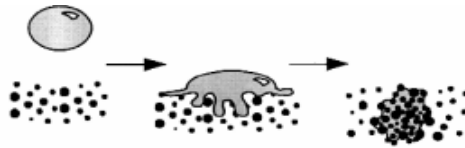
INTRODUCTION

Granulation is one of the methods of processing powder materials into granulated products which are more suitable for storage, transport and further processing. The process consists in the formation and growth of particles in a mobile bed of material. When the wetted material tumbles in the drum, interactions occur between solid particles and liquid droplets depending on the properties of particular media. In the case of granulation, important parameters are both particle size composition of the tested material, physicochemical properties of the liquid wetting the bed, the method of its dosing and mutual quantitative relations (moisture content).

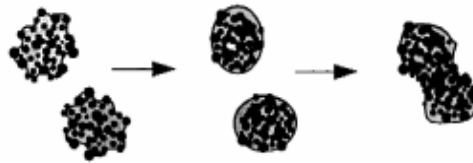
Iverson et al. (2001) assumed that properties of the tested product depended on three stages of granulation (Fig. 1). The authors defined dimensionless numbers that determined the course of two first stages and developed a so-called map of granulation regimes useful in the assessment of the process mechanism. However, such maps are not suitable to predict properties of the granules, in particular their size distribution.

* Technical University of Lodz, Department of Process Equipment, 90-924 Lodz, Stefanowskiego 12/16, Poland

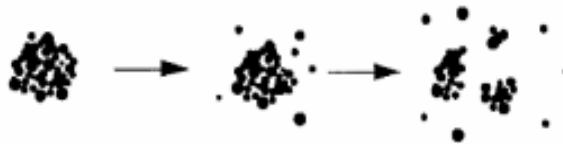
Wetting and nucleation



Growth and consolidation



Disintegration and grinding of granules



According to Newitt and Conway-Jones (1958), granules can appear in four states, depending on the amount of liquid present in the intraparticle spaces:

- pendular – single liquid bridges between particles,
- funicular – with free space in the granule filled partly with air,
- capillary – with free space between granules filled entirely with liquid, however with dry outer surface,
- drop-like – with particles enclosed totally in liquid.

All these states can occur during a single granulation process. During wetting of the material a drop falling onto the bed causes local overwetting and forms a drop-like state with material particles. As a result of bed tumbling and attaching new not wetted particles to the formed nucleus, the newly formed granule is transformed into a porous, loosely packed agglutination of material particles in the pendular state. Next, as a result of collisions of particles against each other and drum walls in the tumbling bed, the air is gradually removed from the granule which makes that it is transferred into funicular and next capillary state. As a result of a further condensation of particles in the granule, the liquid is pressed out from the granule which causes formation of big unstable agglomerates and determines the end of the process.

While analysing silica flour, Gluba et al. (2004) found that particle size distribution of the material subjected to granulation had a significant effect on the process. They observed that the bigger is the grain diameter, the smaller is the granulation rate and that mean granule diameter increased with an increase of the mean droplet diameter.

When searching for a binding agent, Ennis et al. (2000) analysed the forces that occurred during collisions of two spherical particles. They proposed a viscosity Stokes number whose value is inversely proportional to binding liquid viscosity and does not depend on its surface tension. On the other hand, Nienow (2005) modified this theory and proved that surface tension of the liquid phase should be introduced into it. Basing on experiments, he declared that the surface tension had a bigger influence on the granulation process than viscosity itself.

Due to complexity of problems related to the effect of wetting parameters on the granulation process, further studies are necessary on the kinetics of granulation of raw materials with different physical properties in various wetting conditions and then some generalisation should be searched for.

THE AIM OF RESEARCH

The aim of research was to describe the effect of changes in surface tension and degree of wetting liquid jet break-up as well as final moisture content of the bed on tumbling agglomeration kinetics in a horizontal drum granulator.

CHARACTERISTICS OF TESTED MATERIALS

The tested material was a commercially available fraction of silica flour MK 0.075, produced in Strzeblow Mineral Mine at Sobotka. The particle size composition of this material was determined using a laser particle size analyser ANALYSETTE 22. The mean flour particle size $d_z = 0.024$ mm was determined on the basis its size distribution.

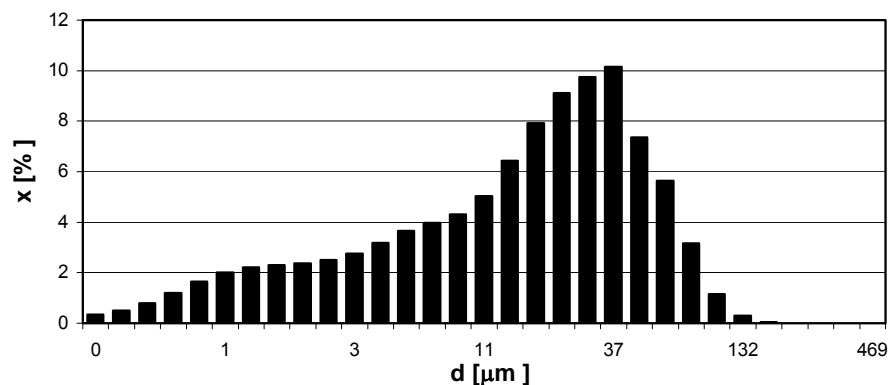


Fig. 1. Particle size distribution of silica flour MK 0.075

Wetting liquids used in the experiments were distilled water and two water solutions of Rokanol L4P5 at different concentrations. Rokanol L4P5 is a trade name of polyoxyalkyl-glycol ether of saturated lauryl alcohol, produced by PCC ROKITA S.A. in Brzeź Dolny. This compound was used to decrease the surface tension of

distilled water (Table 1). A small concentration of Rokanol in the solution and its properties similar to water (e.g. density $\rho = 0.99 \text{ g/cm}^3$), cause that other features of distilled water do not change significantly.

Table 1. Liquid surface tension

	Tested liquid		
	Distilled water	Water solution of Rokanol	
		0.01%	0.03%
Surface tension $\sigma \cdot 10^{-3} \text{ [N/m]}$	71.97	54.79	37.61

THE SCOPE OF INVESTIGATIONS AND MEASURING METHODS

In the whole experimental cycle the rate of wetting liquid flow through nozzles was constant and equal to $Q_w = 12 \cdot 10^{-3} \text{ m}^3/\text{h}$. Changes in the liquid jet break-up (drop size) were caused by changes in the rate of air flow through the nozzles in the range $Q_p = 2.5$ to $4 \text{ m}^3/\text{h}$ which provided four different coefficients of jet break-up q defined as the ratio of liquid flow rate Q_w to air flow rate Q_p (Table 2). The drop size distribution in the broken-up jet at specified parameters of nozzle operation, was measured by a laser drop size analyser DANTEC. Investigations were made for defined final moisture content of the bed $w = 0.19, 0.195, 0.2$ and 0.205 (kg water/kg dry material).

Table 2. Parameters of spray nozzle operation

Q_w	Q_p	q
$[\text{m}^3/\text{h}]$	$[\text{m}^3/\text{h}]$	$[-]$
0.012	2.5	0.0048
0.012	3	0.004
0.012	3.5	0.0034
0.012	4	0.003

The process of granulation was carried out batch-wise in a horizontal drum with longitudinal baffles (1), of diameter $D = 0.5 \text{ m}$ and length $L = 0.4 \text{ m}$. In the whole experimental cycle the rotational speed of the granulator was constant and equal to $n = 0.25 \text{ s}^{-1}$. The mass degree of drum filling with raw material $k = 0.1$ was also constant and determined in reference to bulk density of loosely packed material. The drum was driven by an electric motor (3) through a cogbelt and coupling. For adjustment and control of the rotational speed, an inverter (4) and revolution meter were used, respectively. The granular bed in the drum was wetted by two pneumatic nozzles, Spraying System Deutschland GmbH (2). They were mounted on a separate stand (5) and introduced axially to the apparatus through a hole in the cover. The flow rate of liquid supplied from the tank (7) placed at the height 3.5 m on the drum axis, was set

by a liquid flow controller COLE-PARMER LC-500 (6a), while the flow rate of air supplied by an air compressor (8) was set by a mass air flow controller AALBORG GFc47 (6b).

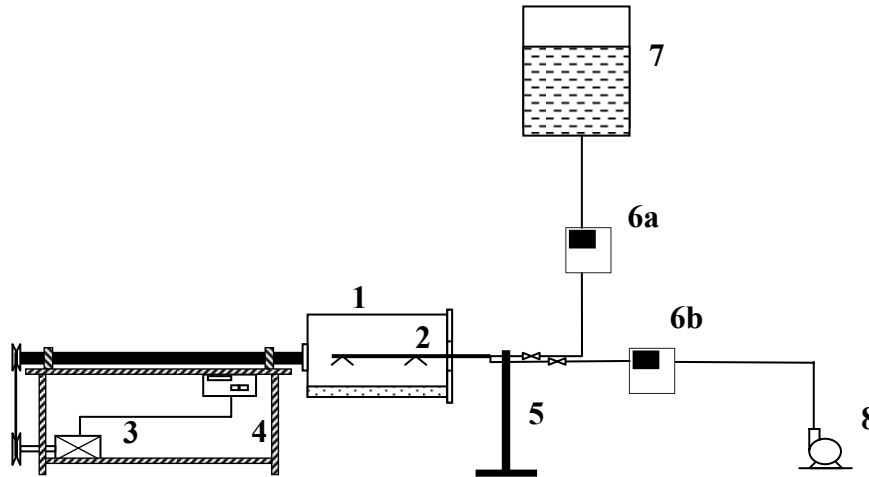


Fig. 2. Diagram of the measuring station. 1- drum, 2- spray nozzles, 3- motor, 4- inverter, 5- stand, 6a- liquid flow controller, 6b- air flow controller, 7- water tank, 8- air compressor

At the initial stage of experiments, the flour was dried in order to remove moisture from it. After supplying a proper amount of flour to the drum, the first stage of the process, i.e. wetting, started. After dosing the whole wetting liquid on the tumbling bed at assumed operation parameters of the spray nozzles, the second stage proceeded, i.e. granulation. In time intervals ($t = 0, 4, 8, 16, 24$ and 32 [min]) constant for each trial, representative samples were taken from the drum by means of a specially constructed device. The samples were subjected to a particle size analysis. The first sample was taken immediately after finishing the wetting process, and the last one at the moment when the process was completed ($t = 32$ min). The samples were dried at the temperature 338 K for 24 hours, and next they were weighed, which enabled the analysis of granulation kinetics.

RESULTS

Based on the analysis of the samples taken immediately after finishing the wetting process, it was found that the bed contained both not granulated raw material and a specified fraction of nuclei and weak granules. The amount and size of particles obtained at this stage of the process depend mainly on the size of liquid drops and final moisture content of the bed (U_s – total share of particular granule fractions; D_{mean} – mean granule diameter).

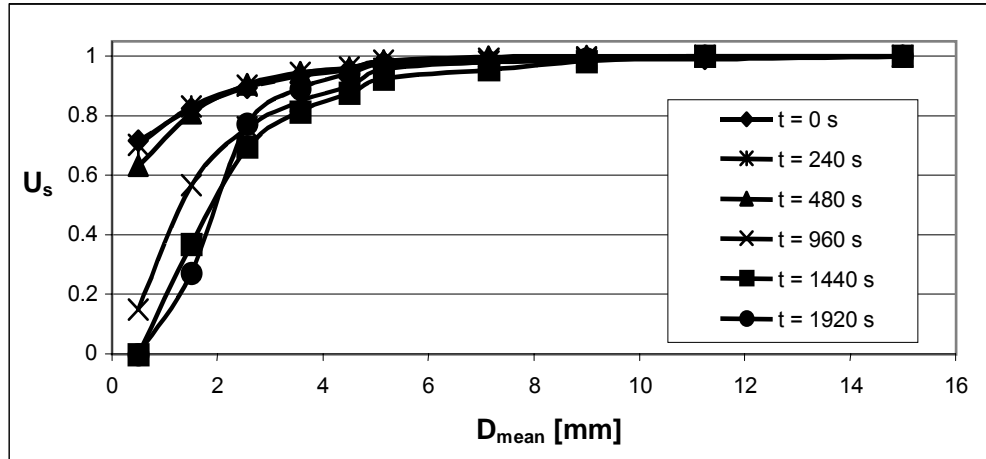


Fig. 3. Change in the particle size composition of the feed during granulation for $q = 0.002$; $w = 0.19\text{kg/kg}$; $\sigma = 54.79 \cdot 10^{-3} \text{ N/m}$

When analysing the change of particle size composition (Fig. 3) one can find that the process of granulated material formation is not uniform in time. During the wetting process and at the initial stage of granulation the increase of mean granule size is due mainly to the nucleation and aggregation of not granulated feed mass on earlier formed nuclei. In this period the rate of changes in the average granule size increases. At subsequent stages of the granulation the smallest fraction is reduced until its absolute exhaustion. In this period of the granulation process a maximum rate of the granule size increment is observed. Then, due to collisions the granules gradually condense which causes that water is pressed out of the granules to their surface. When water appears on the surface, a further growth of granule size is observed. A dominating mechanism of granule growth at this stage is consolidation and coalescence. This is a period in which the rate of changes of mean granule size decreases.

It was found that the rate of changes taking place in the granulated bed depended on wetting conditions. Figure 4 shows a change in the mean granule size during the process for different degrees of wetting liquid jet break-up. It follows from this Figure that with an increase of the jet break-up the rate of agglomerate growth decreases. This process can be affected by both the size of nuclei formed during the nucleation and capillary forces in liquid bridges that connected particles in the granules. It was also observed that the effect of liquid jet break-up on the granule size diminished with a decrease of liquid surface tension.

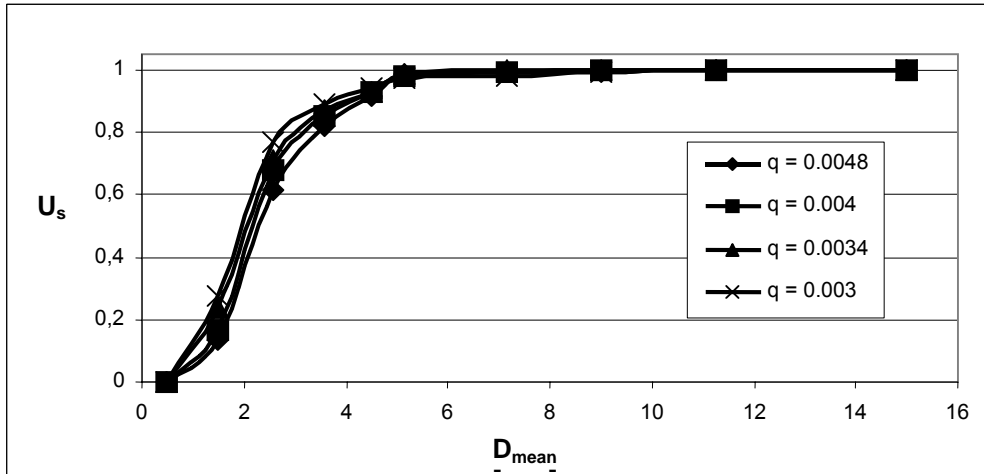


Fig. 4. The effect of liquid jet break-up on the change of particle size composition of the tested material at $t = 1440$ s; $w = 0.2$ kg/kg; $\sigma = 54.79 \cdot 10^{-3}$ N/m

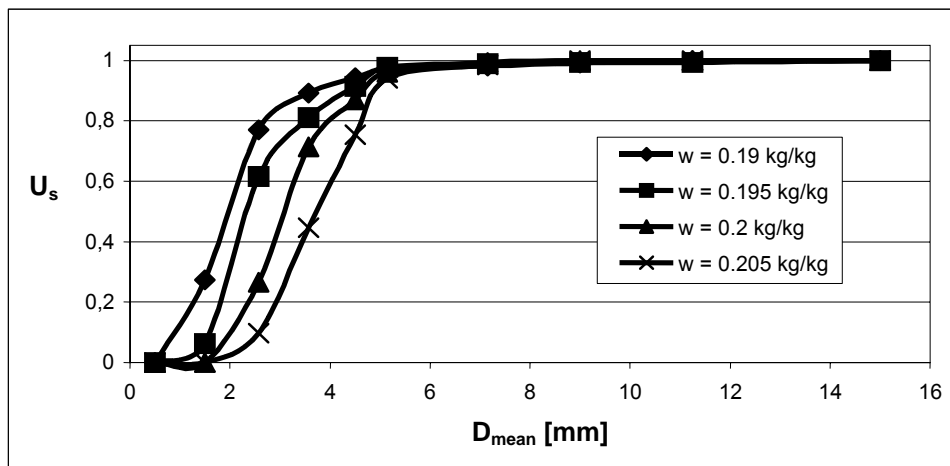


Fig. 5. The effect of final moisture content of the bed on changes in the particle size composition of the tested material at $t = 960$ s; $q = 0.0032$; $\sigma = 37.61 \cdot 10^{-3}$ N/m

The higher final moisture content of the granulated bed causes a significant increase of mean particle diameter of the granulated product (Fig. 5). This result is determined by two mechanisms: at the initial stage of granulation a bigger amount of water in the bed causes higher elasticity of the nuclei and makes that their collisions result in the formation of big agglomerates, further during the granulation, excess moisture which is pressed much faster from the granules causes that material which is still not granulated quickly agglomerates.

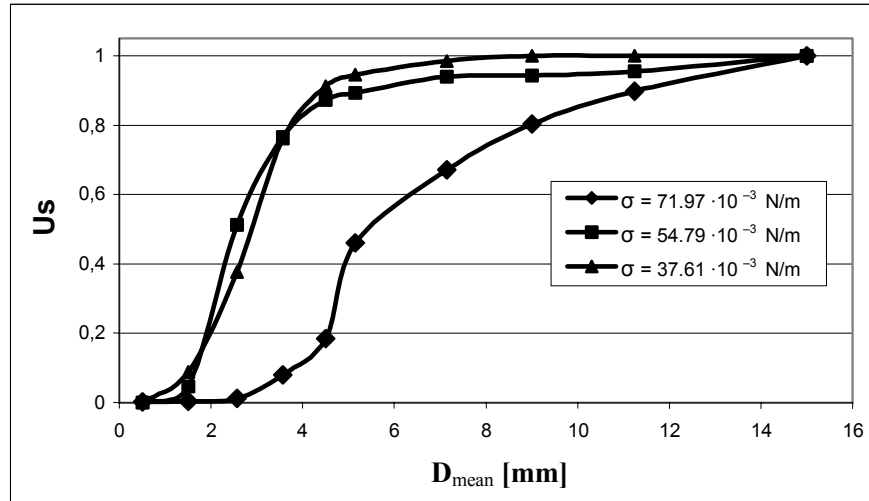


Fig. 6. The effect of changes in surface tension on particle size composition of the feed at $q = 0.0048$; $w = 0.2$ kg/kg; $t = 1920$ s

As shown in Figure 6, the decrease of wetting liquid surface tension has a significant effect on the size of formed granules. It was observed that an increase of Rokanol concentration in the wetting liquid solution results in a remarkable decrease of the agglomerate growth rate. This relation follows most probably from a lower resistance of the agglomerates and domination of the mechanisms of granule breaking and attrition over growth and consolidation. Of special importance is the fact that an increase of Rokanol concentration in the solution, and consequently a decrease of its surface tension, does not cause such a big change in the particle size composition of the product. Probably, for smaller granules the decomposition processes are balanced with the processes of their growth and consolidation.

CONCLUSIONS

1. Results of experiments show a significant effect of bed wetting parameters on the kinetics of wet drum granulation.
2. With an increase of mean liquid drop diameter the mean granule diameter in the bed decreases. The effect of liquid jet break-up on granule size decreases with a decrease of the liquid surface tension.
3. A decrease of the liquid surface tension causes a decrease of the rate of agglomerate growth and unification of the particle size composition in the bed.
4. With an increase of feed moisture content an increase of the process rate and granule size was observed.

REFERENCES

- ENNIS B.B., LI J., TARDOS G.I., PFEFFER R., (1991), *A microlevel-based characterization of granulation phenomena*, Powder Technology, 65, 257-272.
- ENNIS B.B., LI J., TARDOS G.I., PFEFFER R., *The influence of viscosity on the strength of an axially strained pendular liquid bridge*, (1990), Chem. Engng Sci. 45, 3071-3088.
- GLUBA T., OBRANIAK A., BŁASZCZYK M., (2004), *Kinetics of wet drum granulation – by example of silica flour*, Inż. i Aparat. Chem. 3, 45-46, (in Polish).
- IVERSON S.M., LITSTER J.D., HAPGOOD K., ENNIS B.J., (2001), *Nucleation, growth and breakage phenomena in agitated wet granulation processes: a review*, Powder Technology, 117, 3-39.
- NEWITT D.M., CONWAY-JONES J.M. (1958), *A contribution to the theory and practice of granulation*, Trans. Inst. Chem. Eng., 36, 142.
- NIENOW A.W. *Fluidised bed granulation and coating application to materials agriculture and biotechnology*, (1995), Chem. Eng. Comm. 139, 233-253.

ACKNOWLEDGEMENTS

The study was carried out within project W-10/21/2006/B.W.

Heim A., Gluba T., Obraniak A., Gawot-Młynarczyk E., Błaszczuk M., *Wpływ nawilżania na granulację mączki kwarcowej*, Physicochemical Problems of Mineral Processing, 40 307-315, (2006) (w jęz. ang.).

Celem pracy było zbadanie wpływu zmian napięcia powierzchniowego cieczy nawilżającej, wielkości kropeł oraz wilgotności końcowej złoza na właściwości granulowanego złoza otrzymanego w procesie mokrej granulacji bębnowej. Materiałem badawczym była mączka kwarcowa pochodząca ze Strzeblowskiej Kopalni Surowców Mineralnych w Sobótce. Wykorzystano frakcję oznaczoną symbolem MK 0,075 dla której skład ziarnowy frakcji określono za pomocą laserowego analizatora wielkości ziaren „ANALYSETTE 22”. Proces granulacji prowadzono w sposób okresowy w poziomym bębnie o średnicy $D = 0,6$ m i długości $L = 0,4$ m obracającym się ze stałą prędkością obrotową $n = 15$ obr/min. W przeprowadzonych doświadczeniach jako ciecz nawilżającą zastosowano wodę destylowaną z dodatkiem Rokanolu L4P5. W całym procesie nawilżania natężenie dopływającej cieczy, ustalane za pomocą regulatora przepływu cieczy COLE-PARMER LC-500, było stałe i wynosiło $Q_w = 12 \cdot 10^{-3}$ m³/h. W celu uzyskania różnych wielkości kropeł nawilżających stosowano zmienne natężenia przepływu powietrza przez dysze, ustalone za pomocą masowego regulatora przepływu powietrza AALBORG GFc47, w zakresie $Q_p = 2,5 \div 4$ m³/h. Badania prowadzono przy ustalonych wartościach wilgotności $w = 0,19; 0,195; 0,20; 0,205$ [kg/kg]. W stałych dla każdej próby momentach czasowych pobierano z bębna reprezentatywne próbki które poddawane były analizie sitowej, a następnie suszeniu i ważeniu co umożliwiło wykonanie analizy kinetyki granulacji. Uzyskane wyniki wykazały istotny wpływ warunków nawilżania na właściwości granulatu otrzymanego w wyniku granulacji bębnowej.

Teresa FARBISZEWSKA^{*}, Jadwiga FARBISZEWSKA-KICZMA^{*},
Ewa JAŹDŹYK^{**}, Zygmunt SADOWSKI^{**}, Agnieszka SZUBERT^{**}

KINETIC STUDY OF BIODEGRADATION OF ORGANIC MATTER EXTRACTED FROM BLACK SHALE ORE

Received March 15, 2006; reviewed; accepted May 15, 2006

Microbial degradation of organic matter extracted from black shale ores was investigated. The kinetic models of biodegradation of organic compounds were discussed. The effect of chloroform on the rate of biomass growth was described. Our results suggested that the process of biodegradation of organic matter is rather slow. The Haldane kinetic model could be available to describe the kinetic of biodegradation of organic matter.

Keywords; biodegradation, black shale, heterotrophic macroorganism, kinetic, organic matter

INTRODUCTION

The *in situ* biodegradation of organic compounds is a function of the catabolic activity of bacteria. Some toxic organic compounds are chemoattractant for different bacteria species, which can lead to improved biodegradation of these compounds. For instance, crude oil is a complex mixture of hydrocarbons, basically composed of aliphatic, aromatic and asphaltene fractions. Many microbes have ability to utilize hydrocarbons as a sole source of carbon and to transform them to a less toxic form (Kunar et al., 2005).

Asphaltenes is a group of organic compounds extracted from crude oil samples. Their composition is close to the organic matter extracted from black shale. Biodegradation of asphaltenes through the used of a microbial consortium or mixed

^{*} University of Opole, Faculty of Natural and Technical Sciences, ul. Dmowskiego 7/9,
45-365 Opole, Poland.

^{**} Technical University of Wrocław, Faculty of Chemistry, ul. Wybrzeże Wspiańskiego 27,
50-370 Wrocław, Poland.

cultures isolated from soil samples has been described (Pineda-Flores et al., 2004). However, the extent of biodegradation was from 0.55 to 35 %.

There have been relatively few studies on the bacterial degradation of metallorganic compounds. Several strains of *Pseudomonas fluorescens* were used to degrade tetracyanonickelate (TCN) as a sole nitrogen source (Baxter Cummings, 2006). An *Acinetobacter* sp. strain isolated from gold mine was cable for degrading gold, silver, cadmium, zinc, copper, cobalt, and iron cyanide complexes.

Microbial degradation of complex organic compounds such as phtalic acid was investigated using bacteria cultures isolated from sewage sludge. More than 99% of phthalic acid at the initial concentration of 4000 mg/dm³ was degraded within 5 days (Fan et al., 2004).

A biological decolourisation process was used for azo dyes (Beydilli Pavlostathis 2005). The kinetic modelling of azo decolourisation was performed using the data obtained from the tests where the effect of different initial dye concentrations on the decolourisation process was examined. Up to now, some research dealing with the mineralogical analysis showed that very important compounds of organic matter are metalloporphyrins. However, lake petroporphirins, metalloporphyrins from black shale are highly resistance towards biodegradation (Grosjean et al., 2004).

The goal of this research is to understand better biodegradation of complex chemical mixtures such as organic matter by microbial consortium.

KINETICS OF BIODEGRADATION

The mathematical model of homogeneous substrate consumption (biodegradation) should take in consideration the microbial growth, competitive inhibition and the formation of toxic intermediates. Most models have been tested with single or two substrates (Reardon et al., 2002). The initial stapes in model creation was used the simple model for cell growth kinetics and substrate depletion.

$$\frac{dS}{dt} = -\frac{\mu X}{Y_{X/S}} \quad (1)$$

where S is the substrate concentration, t is time, μ is specific growth rate, $Y_{X/S}$ is the biomass yield, and X is biomass concentration. To determine the yield, $Y_{X/S}$ the concentration of cells produced (cells/cm³) was divided by the concentration of substrate consumed (mM). In the case of single substrate, the growth kinetics is well fitted by the Monod equation:

$$\mu = \frac{1}{X} \left(\frac{dX}{dt} \right) = \frac{\mu_{\max} S_L}{K_S + S_L} \quad (2)$$

in which μ_m is the maximum specific growth rate and K_S is the Monod half-saturation constant. However, in some cases, the substrate inhibition effect has been observed (Andrews 1968). Haldane has proposed a substrate inhibition model:

$$\mu = \frac{1}{X} \left(\frac{dX}{dt} \right) = \frac{\mu_{\max} S_L}{K_S + S_L + \left(\frac{S_L^2}{K_i} \right)} \quad (3)$$

where K_i is an inhibition parameter.

MATERIALS AND METHODS

ORGANIC MATTER

The organic matter was extracted from black shale sample (middling) from Lubin mine. This material was collected from the flotation circuits. The mineral sample was treated with HCl solution to remove carbonate components, than it was treated with HF solution to decompose clay minerals. The organic matter was extracted in Socslet. The conditions of extraction were as follows: the solid fraction 300 g; chloroform 600 cm³, temperature 70°C, time of extraction 24 h. The composition of both “middlings” and organic matter is presented in Table 1.

Table 1. Concentration of metals and organic matter in middlings

Metal concentration [ppm or %]	Cu	Co	Ag	Fe	Ni	V	C _{org}
Lubin middlings	1.96[%]	498	-	1.75 [%]	304	897	8.84
Organic matter	254	31.5	1.1	198	450	259	-

MICROORGANISMS

Microbial degradation of organic matter was investigated using culture of heterotrophic bacteria enriched from solid samples collected with waste heap. A mixture of bacteria (Consortium C) containing *Pseudomonas fluorescens*, *Areomonas hydrophilia*, *Oligella* sp. *Bacillus megaterium*, *Streptomonas maltophilia*, *Stenotrophomonas maltophilia*, *Bacillus amyloliquefaciens*, *Bacillus circulans*, *Bacillus pumilus* and *Burkholderia capacia* was used for the biodegradation experiments. The media used in this study contained (g/dm³): (NH₄)₂SO₄ – 2g; K₂HPO₄ – 3g; KH₂PO₄-2g; MgSO₄ 7H₂O 0.5g. The pH value of the medium was adjusted to about 7.0.

ORGANIC MATTER EXTRACTION

The powdered black shale ore samples were exhaustively extracted with chloroform in Soxhlet. The conditions of organic matter extraction were as follows: solid samples –300g; volume of chloroform 600 cm³; temperature 70⁰C; time of extraction 24 h.

BIODEGRADATION EXPERIMENT

A series of 250 ml sterile Erlenmeyer flasks were used in biodegradation study. Each flask contained 100 cm³ of sterile mineral salt medium. 20 cm³ of the water emulsion, contains the organic matter dissolved in chloroform, was added to the flask. Also, 0.2 cm³ of inoculum was added. The biodegradation of organic matter experiments was carried out in a shaker and the temperature was 30⁰C.

RESULTS AND DISCUSSION

Fresh shale contains approximately from 1 to 10 wt. % organic carbon (Fischer and Gaupp, 2005). Table 2 shows the concentration of organic carbon bleached and unbleached black shale.

Table 2. Total organic carbons content of bleached and unbleached black shale ores (Fischer, Gaupp, 2005)

Sample	black	dark grey	pole grey	whitish yello
Total organic carbon [wt%]	8.08	2.42	1.55	1.35

EFFECT OF CHLOROFORM ON THE BACTERIA GROWTH

The rate at which microorganism cells grows during the biodegradation process can be depended on the reagent used for organic mater extraction (chloroform). The effect of the presence of chloroform on the microbial growth was investigated. Figures 1 and 2 show the effect of the addition of 15 % of chloroform on the kinetic of *Bacillus cereus* and *Bacillus laterosporus* growth.

The experimental results indicated that the presence of chloroform could greatly decrease the kinetics of growth of bacteria. The population of bacterial cells dramatically decreased. For support of this conclusion photographs of bacterial colonies have been taken. The surface colonies of *Bacillus cereus* after 6 hours growth with and without chloroform are presented in Figure 3.

BIODEGRADATION OF ORGANIC MATTER

The recommended procedure for estimating biodegradation of organic matter would be to use mixtures of microorganisms. The biodegradation of organic matter was carried out for up to 69 and 76 days for the Lubin and Mansfeld samples, respectively. A special prepared bacteria consortium (consortium C) was used.

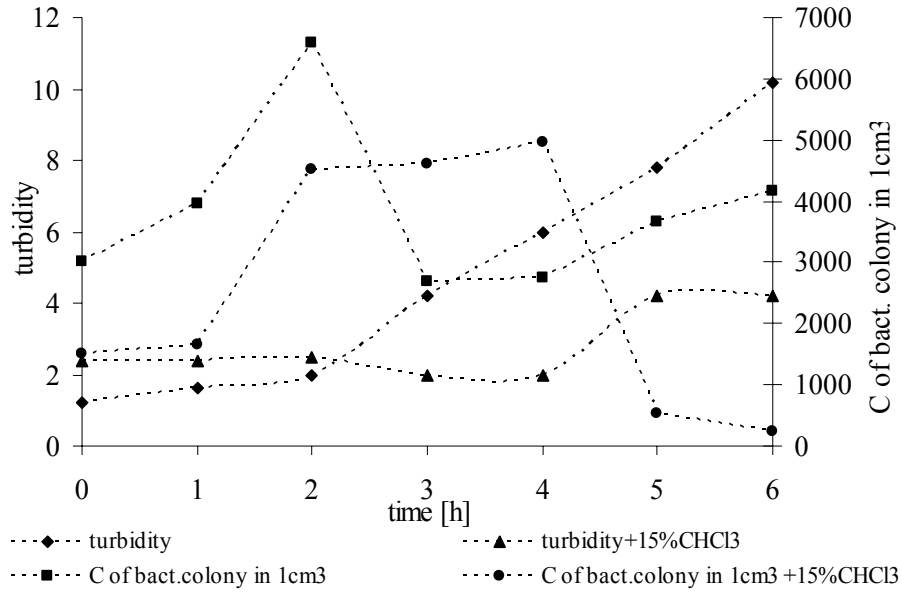


Fig. 1 The growth of *Bacillus cereus* with the presence and absence of chloroform

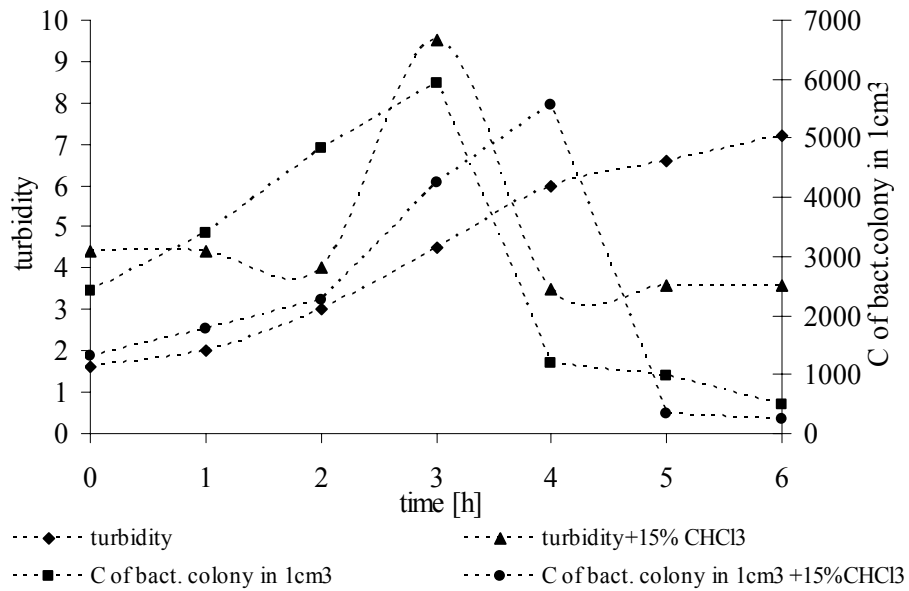


Fig. 2. The growth of *Bacillus laterosporus* in the presence and absence of chloroform



Fig. 3. The colony of *Bacillus cereus* in the presence of chloroform (left) and its absence (right)

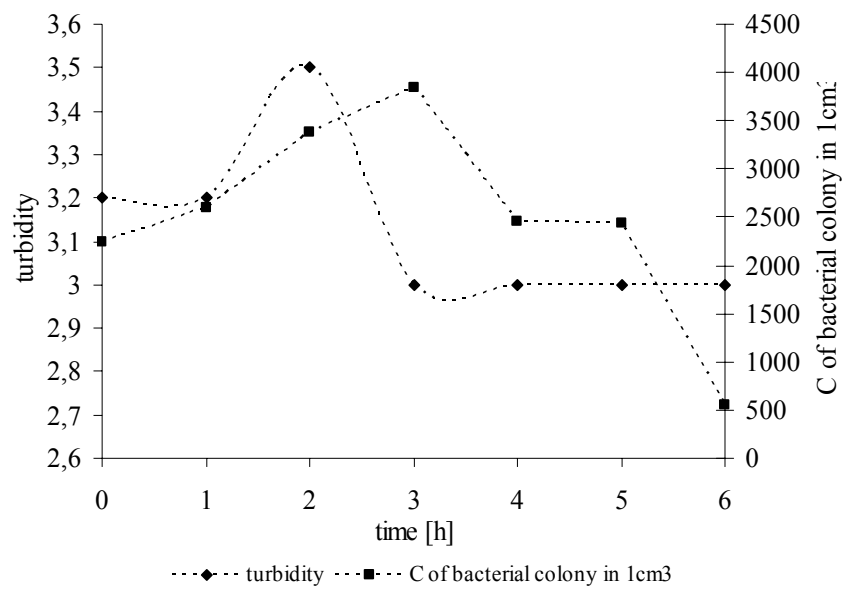


Fig. 4. The growth of *Bacillus cereus* in the presence of organic matter

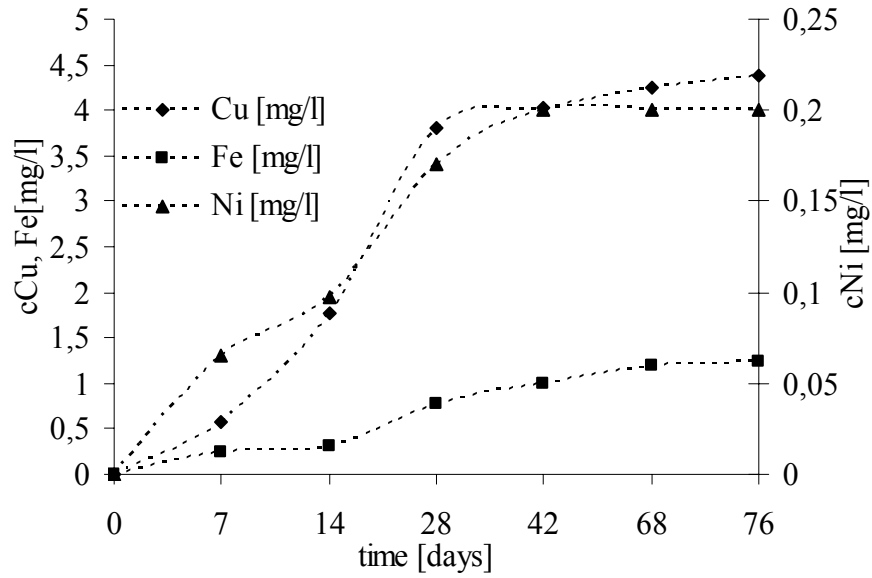


Fig. 5. Biodegradation of organic matter extracted from black shale (Lubin, Poland)

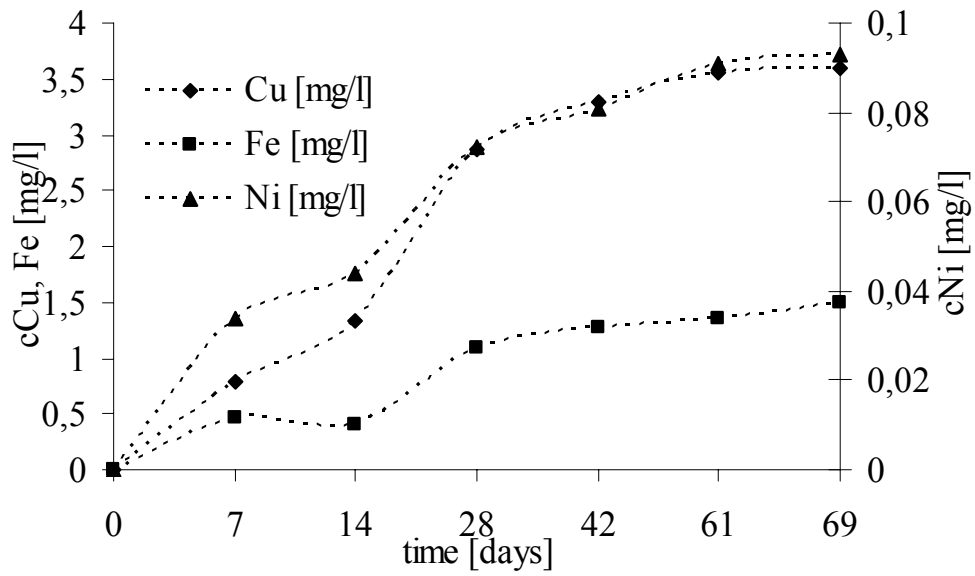


Fig. 6. Biodegradation of organic matter extracted from black shale (Mansfeld, Germany)

The rate of ions production can be involved in biodegradation of organic matter. The biological degradation of metal-organic compounds, contained in organic matter, produced metal ions. The rate of increase of the metal ions concentration should correlate with the biodegradation rate. However, the theory of biodegradation single or mixed organic compounds bases on the rate of substrate decrease. A model biodegradation based on changes of product rate should be developed. The above reported results showed that the biodegradation of organic matter was quite slow. Initial analysis showed that modified Haldane equation would be responsible for biodegradation described. The concentration of substrate should be exchanged for the concentration of products. Further investigations of mechanism of organic matter biodegradation should be done for a discovery of correlation between substrate and product during an organic matter biodegradation process.

CONCLUSIONS

The investigations revealed that organic matter dissolved in chloroform and suspended in water solution could be degraded by bacteria. The presence of chloroform caused a decrease of microbial growth kinetics. Preliminary study showed that a modified kinetic model could be used to describe the biodegradation of organic matter extracted from the black shale ore samples.

ACKNOWLEDGEMENTS

The authors wish to acknowledge support received from EU project BIOSHALE STRR NMP2-CT-2004 No 507710.

REFERENCES

- ANDREWS J.F., 1968, *A mathematical model for the continuous culture of microorganisms utilized inhibitory substrate*, Biotech. Bioeng., 10,707-723.
- BAXTER J., CUMMINGS P.S., 2006, *The impact of bioaugmentation on metal cyanide degradation and soil bacteria community structure*, Biodegradation, 17, 207-217.
- BEYDILLI I.M., PAVLOSTATHIS G.S., 2005, *Decolorization kinetics of the azo dye Reactive Red 2 under methanogenic conditions: effect of long-term culture acclimation*, Biodegradation 16, 135-146.
- FAN Y., WANG Y., QIAN Y-P., JI-DING GU D-J., 2004, *Optimization of phtalic acid batch biodegradation and use of modified Richards model for modelling degradation*, Intr. Biodeterioration Biodegradation, 53, 57-63.
- FISCHER C., GAUPP R., 2005, *Change a black shale organic material surface area during oxidative weathering implications for rock-water surface evolution*, Geochimica Cosmochimica Acta, 69,1213-1224.
- GROSJEAN E., ADAM P., CONNAN J., ALBRECHT P., 2004, *Effects of weathering on nickel and vanadyl porphyrins of a Lower Toarcian shale of the Paris basin*, Geochimica Cosmochimica Acta, 68, 789-804.
- KUNAR R.J., KAPUR M., LABANA S., LAL B., SARMA M.P., BHATTACHARYA D., THAKUR S.I., 2005, *Microbial diversity: Application of microorganisms for the biodegradation of xenobiotics*, Current Sci., 89, 101-112.

- PINEDA-FLORES G., BALL-ARGUELLO G., LIRA-GALEANA C., MESTA-HOWARD M.A., 2004, *A microbial consortia isolated from a crude oil sample that uses asphaltenes as a carbon and energy source*, Biodegradation, 15, 145-151.
- REARDON F.K., MOSTELLER C.D., ROGER B.J., DUTEAU M.N., KIM K-H., 2002, *Biodegradation kinetics of aromatic hydrocarbon mixtures by pure and mixed bacteria cultures*, Environ. Health Persp., 110, 1005-1011.
- WHITE E.V., KNOWLES J.C., 2003, *Degradation of copper-NTA by Mesorhizobium sp. NCI MB 13524*, Inter. Biodeterioration Biodegradation, 52, 143-150.

Farbiszewska T., Farbiszewska-Kiczma J. Jażdżyk E., Sadowski Z. Szubert A., Badania kinetyki procesu biodegradacji matrycy organicznej ekstrahowanej z rudy łupkowej, Physicochemical Problems of Mineral Processing, 40 (2006), 317-325 (w jęz. ang.).

Matryca organiczna, ekstrahowana z próbek mineralnych rudy łupkowej, poddana została procesowi biodegradacji. Do procesu biodegradacji użyto specjalnie przygotowanej mieszaniny bakterii. Na podstawie danych literaturowych przeanalizowano istniejące modele kinetyki procesu biodegradacji i uznano, że zmodyfikowany model zaproponowany przez Haldane będzie najlepszym dla opisu procesu. Modyfikacja wymaga zastąpienie stężenia substratu stężeniem produktu reakcji biodegradacji. To, czy jest możliwe, jako produkty użyć stężeni jonów metali, odpowiedź dadzą następne badania. Zbadano wpływ obecności chloroformu na proces biodegradacji i wzrostu mikroorganizmów. Wykazano, że obecność chloroformu pogarsza kinetykę procesu biodegradacji. Proces biodegradacji jest procesem powolnym.

Our books are available in *Tech* bookstore
plac Grunwaldzki 13
50-377 Wrocław, D-1 PWr, tel. (071) 320 32 52
Orders can also be sent by post

ISSN 0137-1282
Physicochemical Problems of Mineral Processing, 40 (2006)